THERMAL ELASTIC PLASTIC BEHAVIOUR AND MODELLING OF SATURATED CLAYS

by

NAOTO TANAKA

A Thesis
Submitted to the Faculty of Graduated Studies
in Partial Fulfillment of the Requirements for the Degree of

DOCTOR OF PHILOSOPHY

Department of Civil and Geological Engineering
University of Manitoba
Winnipeg, Manitoba
Canada

October, 1995

Canada

Name _____

Dissertation Abstracts International is arranged by broad, general subject categories. Please select the one subject which most nearly describes the content of your dissertation. Enter the corresponding four-digit code in the spaces provided.

$\mathcal{GEOTECHNOLOGY}$

SUBJECT TERM

| 0 | 4 | 2 | 8 | U·M·I

SUBJECT CODE

Subject Categories

THE HUMANITIES AND SOCIAL SCIENCES

COMMUNICATIONS AND THE ARTS
Architecture 0729
Art History 0377
Cinema 0900
Dance 0378
Fine Arts 0357
Information Science 0723
Journalism 0391
Library Science 0399
Mass Communications 0708
Music 0413
Speech Communication 0459
Theater 0465

EDUCATION
General 0515
Administration 0514
Adult and Continuing 0516
Agricultural 0517
Art 0273
Bilingual and Multicultural 0282
Business 0688
Community College 0275
Curriculum and Instruction 0727
Early Childhood 0518
Elementary 0524
Finance 0277
Guidance and Counseling 0519
Health 0680
Higher 0745
History of 0520
Home Economics 0278
Industrial 0521
Language and Literature 0279
Mathematics 0280
Music 0522
Philosophy of 0998
Physical 0523

Psychology 0525
Reading 0535
Religious 0527
Sciences 0714
Secondary 0533
Social Sciences 0534
Sociology of 0340
Special 0529
Teacher Training 0530
Technology 0710
Tests and Measurements 0288
Vocational 0747

LANGUAGE, LITERATURE AND LINGUISTICS
Language
  General 0679
  Ancient 0289
  Linguistics 0290
  Modern 0291
Literature
  General 0401
  Classical 0294
  Comparative 0295
  Medieval 0297
  Modern 0298
  African 0316
  American 0591
  Asian 0305
  Canadian (English) 0352
  Canadian (French) 0355
  English 0593
  Germanic 0311
  Latin American 0312
  Middle Eastern 0315
  Romance 0313
  Slavic and East European 0314

PHILOSOPHY, RELIGION AND THEOLOGY
Philosophy 0422
Religion
  General 0318
  Biblical Studies 0321
  Clergy 0319
  History of 0320
  Philosophy of 0322
Theology 0469

SOCIAL SCIENCES
American Studies 0323
Anthropology
  Archaeology 0324
  Cultural 0326
  Physical 0327
Business Administration
  General 0310
  Accounting 0272
  Banking 0770
  Management 0454
  Marketing 0338
Canadian Studies 0385
Economics
  General 0501
  Agricultural 0503
  Commerce-Business 0505
  Finance 0508
  History 0509
  Labor 0510
  Theory 0511
Folklore 0358
Geography 0366
Gerontology 0351
History
  General 0578

  Ancient 0579
  Medieval 0581
  Modern 0582
  Black 0328
  African 0331
  Asia, Australia and Oceania 0332
  Canadian 0334
  European 0335
  Latin American 0336
  Middle Eastern 0333
  United States 0337
History of Science 0585
Law 0398
Political Science
  General 0615
  International Law and
    Relations 0616
  Public Administration 0617
Recreation 0814
Social Work 0452
Sociology
  General 0626
  Criminology and Penology ... 0627
  Demography 0938
  Ethnic and Racial Studies 0631
  Individual and Family
    Studies 0628
  Industrial and Labor
    Relations 0629
  Public and Social Welfare 0630
  Social Structure and
    Development 0700
  Theory and Methods 0344
Transportation 0709
Urban and Regional Planning 0999
Women's Studies 0453

THE SCIENCES AND ENGINEERING

BIOLOGICAL SCIENCES
Agriculture
  General 0473
  Agronomy 0285
  Animal Culture and
    Nutrition 0475
  Animal Pathology 0476
  Food Science and
    Technology 0359
  Forestry and Wildlife 0478
  Plant Culture 0479
  Plant Pathology 0480
  Plant Physiology 0817
  Range Management 0777
  Wood Technology 0746
Biology
  General 0306
  Anatomy 0287
  Biostatistics 0308
  Botany 0309
  Cell 0379
  Ecology 0329
  Entomology 0353
  Genetics 0369
  Limnology 0793
  Microbiology 0410
  Molecular 0307
  Neuroscience 0317
  Oceanography 0416
  Physiology 0433
  Radiation 0821
  Veterinary Science 0778
  Zoology 0472
Biophysics
  General 0786
  Medical 0760

EARTH SCIENCES
Biogeochemistry 0425
Geochemistry 0996

Geodesy 0370
Geology 0372
Geophysics 0373
Hydrology 0388
Mineralogy 0411
Paleobotany 0345
Paleoecology 0426
Paleontology 0418
Paleozoology 0985
Palynology 0427
Physical Geography 0368
Physical Oceanography 0415

HEALTH AND ENVIRONMENTAL SCIENCES
Environmental Sciences 0768
Health Sciences
  General 0566
  Audiology 0300
  Chemotherapy 0992
  Dentistry 0567
  Education 0350
  Hospital Management 0769
  Human Development 0758
  Immunology 0982
  Medicine and Surgery 0564
  Mental Health 0347
  Nursing 0569
  Nutrition 0570
  Obstetrics and Gynecology .. 0380
  Occupational Health and
    Therapy 0354
  Ophthalmology 0381
  Pathology 0571
  Pharmacology 0419
  Pharmacy 0572
  Physical Therapy 0382
  Public Health 0573
  Radiology 0574
  Recreation 0575

  Speech Pathology 0460
  Toxicology 0383
Home Economics 0386

PHYSICAL SCIENCES
Pure Sciences
Chemistry
  General 0485
  Agricultural 0749
  Analytical 0486
  Biochemistry 0487
  Inorganic 0488
  Nuclear 0738
  Organic 0490
  Pharmaceutical 0491
  Physical 0494
  Polymer 0495
  Radiation 0754
Mathematics 0405
Physics
  General 0605
  Acoustics 0986
  Astronomy and
    Astrophysics 0606
  Atmospheric Science 0608
  Atomic 0748
  Electronics and Electricity 0607
  Elementary Particles and
    High Energy 0798
  Fluid and Plasma 0759
  Molecular 0609
  Nuclear 0610
  Optics 0752
  Radiation 0756
  Solid State 0611
Statistics 0463

Applied Sciences
Applied Mechanics 0346
Computer Science 0984

Engineering
  General 0537
  Aerospace 0538
  Agricultural 0539
  Automotive 0540
  Biomedical 0541
  Chemical 0542
  Civil 0543
  Electronics and Electrical 0544
  Heat and Thermodynamics ... 0348
  Hydraulic 0545
  Industrial 0546
  Marine 0547
  Materials Science 0794
  Mechanical 0548
  Metallurgy 0743
  Mining 0551
  Nuclear 0552
  Packaging 0549
  Petroleum 0765
  Sanitary and Municipal 0554
  System Science 0790
Geotechnology 0428
Operations Research 0796
Plastics Technology 0795
Textile Technology 0994

PSYCHOLOGY
General 0621
Behavioral 0384
Clinical 0622
Developmental 0620
Experimental 0623
Industrial 0624
Personality 0625
Physiological 0989
Psychobiology 0349
Psychometrics 0632
Social 0451

THERMAL ELASTIC PLASTIC BEHAVIOUR AND MODELLING

OF SATURATED CLAYS

BY

NAOTO TANAKA

A Thesis submitted to the Faculty of Graduate Studies of the University of Manitoba
in partial fulfillment of the requirements of the degree of

DOCTOR OF PHILOSOPHY

© 1995

ABSTRACT

This research presents an investigation into effects of temperature (up to 100°C) on clay soil behaviour. Specimens tested in the laboratory consisted of reconstituted illite, compacted illite, and compacted sand-bentonite. Drained triaxial compression tests were performed along assigned stress paths to examine stress-strain relationships, yield loci, hardening law, flow rule and plastic potential, and failure criterion for the illite specimens. Undrained triaxial compression tests were performed to examine stress-strain relationship, pore water pressure generation, and failure criterion for all three types of clay specimens.

The thesis presents for the first time experimental evidence that yield loci shrink with temperature. It appears that effective stress strength of clays is independent of temperature, while volume changes, pore water pressures, stress-strain behaviour and yield loci all depend on temperature.

A proposed model which can describe soil behaviour subjected to temperature changes was developed, calibrated, and verified using experimental data in this study. The model needs only a few additional parameters to those in a conventional elastic-plastic model for isotropically consolidated clays. The model may be used for compacted clays with few modifications.

i

TABLE OF CONTENTS

vi

LIST OF FIGURES

xix

LIST OF TABLES

LIST OF SYMBOLS AND ABBREVIATIONS

CSL   Critical state line

E   Elastic Young's modulus

G   Elastic shear modulus

I_p Plasticity index (w_L-w_P)

K   Elastic bulk modulus

Λ $= (\lambda-\kappa)/\lambda$

LSSV   Length of the stress vector

M   stress ratio at critical state

m   pore water pressure parameter $\Delta u/\Delta p$

N   Equilibrium specific volume corresponding to unit effective mean stress

NCL   Normal consolidation line

OCR   Overconsolidation ratio

p   Total mean stress $(\sigma_1+2\sigma_3)/3$

p′   Effective mean stress $(\sigma_1'+2\sigma_3')/3$

q   Deviator stress $(\sigma_1-\sigma_3)$

SEL   Swelling equilibrium line

SBS   State boundary surface

T   Temperature

URL   Unload-reload line

u   Pore water pressure

V   Specific volume

V Volume

W   Work

w	Water content
β	Coefficient of thermal expansion
ρ_d	Dry density
ε	Strain
η	Stress ratio (q/p')
κ	Slope of unload/reload line in V $vs.$ p' space
κ'	Quasi-slope of unload-reload line in V $vs.$ p' space
ν	Poison's ratio
s	strength $(\sigma_1 - \sigma_3)/2$
σ	Stress
ϕ'	Effective Mohr-Coulomb friction angle

Subscripts

1,2,3	Principle, intermediate and minor (stresses)
c	Preconsolidation pressure (for example, p_c')
c	Clay fraction (for example, V_c)
D	Drained
e	Equivalent (for example, p_e')
p	Plastic (normal cosolidation line)
L,P	Liquid, plastic (limits)
o	Initial condition (prior to shear, for example, p_o')
s,v	Shear, volume (strains)
T	Temperature
u	Undrained
y	Yield

Superscripts

e,p   Elastic, plastic (stresses and strains)

CHAPTER 1 INTRODUCTION

1.1 Statement of Problem

Heat from nuclear waste canisters in underground boreholes or in the sea bed will raise the temperature of adjacent soil. Such applications are of considerable importance in relation to public safety, and raise difficult technical questions for geotechnical engineers. Until recently there was no good framework for understanding temperature effects in soils. Some researches concluded that heating caused decreased strengths, while others reported increased strengths. Heating may also cause significant changes in compressibility, stiffness in shear, and pore water pressure generation. In addition, thermal properties such as thermal expansion, thermal conductivity, and thermal diffusivity; and physical properties such as hydraulic conductivity may also be significantly altered by changes in temperature. In nuclear waste disposal, initial heating will be followed by subsequent cooling, and it is known that temperature effects may not be reversible if drainage is permitted.

Because the range of temperatures and the time period associated with the permanent storage of high-level radioactive waste are so large, a need has developed for the extension of current knowledge of engineering properties of soils under elevated temperatures. Clay failure may increase permeability and enhance the migration of radionuclides in the presence of groundwater flow.

1

Therefore, it is necessary to understand soil behaviour subjected to temperature changes, and make a useful predictive model under various stress and boundary conditions.

1.2 Research Objectives

A laboratory investigation of the thermo-mechanical response of clay specimens is presented in this thesis. The study is limited to thermal and pressure loadings in a range of interest for the emplacement of radioactive waste in the deep underground.

The purpose of the laboratory testing program is to determine the engineering properties and characterize the behaviour of clays subjected to thermo-mechanical loadings, and to examine hypotheses and assumptions made in this study for constructing a model which describes soil behaviour under temperature change. The laboratory testing program included (1) mechanical and thermal consolidation, (2) drained stress path compression tests, and (3) undrained triaxial compression tests with pore water pressure measurement.

The objective of the research program is to explain the observed behaviour in terms of a constitutive model which takes temperature effects into account. The proposed model is based on an elastic-plastic model for clay, namely the Modified Cam clay model, and is therefore called a thermo-elastic-plastic model. The assumptions used in constructing the new model are based in part on results from

the research literature, and on the experimental data presented in the thesis.

1.3 Scope of Thesis

Three types of specimens, that is, reconstituted illite, compacted illite, and compacted sand-bentonite, are used in laboratory tests. Illite is less active clay than sand-bentonite. Comparisons between compacted and reconstituted clays are made in terms of volume change, stress-strain behaviour, pore water pressure development, and strength characteristics under conditions of temperature changes. The temperatures and pressures that have been used in the testing are up to 100°C and 3.0 MPa, respectively.

Effects of temperature on volume changes are investigated under both drained and undrained conditions with isotropic stress applied. Thermally induced pore water pressures are examined under undrained conditions with and without deviator stresses being applied. Effects of temperature on yield loci are one of the main purposes in the laboratory testing in this research program. Drained stress path tests are assigned for this purpose. Stress-strain behaviour and strength characteristics are investigated in drained and undrained compression tests.

Development of a new thermo-elastic-plastic model is attempted to describe clay behaviour under a temperature field. Calibration and verification of the model is made using experimental data. The

3

model allows prediction of how heating and cooling affect volume changes, pore water pressures, stress-strain behaviour, and strengths for both normally consolidated and overconsolidated clays.

1.4 Organization of Thesis

Identification of problems in understanding the effects of temperature in soils is made in Chapter 2 through a detailed literature review.

A possible thermo-mechanical model for describing soil behaviour is proposed in Chapter 3. It is based on what appears to be a number of reasonable hypotheses and assumptions, though not all of them have been adequately examined in the existing research literature. An experimental program is proposed that examine these hypotheses and assumptions. Its results are subsequently used to examine the validity of the proposed model.

The materials, apparatuses, and testing procedures used in this study are described in Chapter 4. Results of the experimental study are given in Chapters 5 through 8.

Findings from the experiments are used for detailed development of a thermo-elastic-plastic model in Chapter 9. Calibration and validation of the model are presented in Chapter 10.

Discussion of the effects of temperature on soil behaviour is made in Chapter 11.

Conclusions and suggestion for future work are presented in Chapter 12.

CHAPTER 2 LITERATURE REVIEW

2.1 Introduction

Effects of temperature on materials subjected to temperature changes

The behaviour of materials subjected to thermal loading has been discussed in many publications on metals and rubbers in the last two decades. Solutions from these projects have been applied in such area as laser technology, nuclear reactor design, turbine analysis, and aerospace design. (for example, Kammash *et al.* 1960, Levy 1981, Sharifi and Yates 1974).

The effect of heating on the geotechnical properties of soils and rocks has been under investigation for many years. This work has been published in many conferences, journals, and in special publications of the Highway Research Board (1969); ASTM Special Technical Publication 869 (1983); and in the Proceedings of an International Workshop on Thermo-mechanics of Clays and Clay Barriers held in Bergamo, Italy, in 1993. Early research concentrated on the influence of temperature increases on soil properties with particular reference to construction in permafrost, highway design and soil stabilization (for example, Barata 1969, Chandrasekharan *et al.* 1969, Takashi 1969). In recent years attention has focused primarily on the areas of high-level radioactive waste disposal and energy resource development.

Introduction of nuclear waste canisters into underground boreholes
or the sea bed will form a heat source that raises the temperature
of the soil adjacent to the canister. These applications are of
great importance for public safety, and raise difficult technical
questions for geotechnical engineers. Therefore, it is necessary to
have a sound framework of engineering in which the effects of
temperature on soil behaviour are well understood.

However, until recently there was no good understanding of
temperature effects on soils. For example, some researchers
concluded that temperature increase caused decreasing strength of
soils. On the contrary, others reported that temperature increase
caused increasing strength. These two positions are contradictory
and cannot provide a sound basis for design.

Effects of temperature may also cause a significant change in other
mechanical properties such as compressibility, stiffness in shear,
and pore water pressure generation. In addition, thermal properties
such as thermal expansion, thermal conductivity, and thermal
diffusivity; and physical properties such as hydraulic conductivity,
may also be significantly altered due to changes in temperature.

The dependence of the mechanical behaviour of rocks on temperature
and pressure has been studied extensively by geologists,
geophysicists, mining engineers, and petroleum engineers.
Temperatures to 800°C and pressures as great as 2.1 GPa in

conjunction with extremely low rates of loading have been used in geological studies. Laboratory experiments have been conducted to approximate conditions in the earth's crust to depths of 20 km for studies of faulting and folding. In mining and petroleum engineering, pressures and temperatures rarely exceed 140 MPa and 150°C, respectively (Cheatham 1968). These temperature and pressure conditions are high compared to those encountered in soils.

It is necessary first to review how temperatures affect soil characteristics and behaviour even though the available information is limited. This chapter will examine only temperatures above the freezing point of water (0°C), mostly below the boiling point (100°C), and a pressure range up to 10 MPa. (Testing performed by the author was in the range 28°C to 100°C, and pressures up to 2.5 MPa.)

Variations of temperature can cause several important changes in soil characteristics and behaviour. Decreases and increases in temperature are both possible occurrences, though it should be pointed out at once that the resulting effects on soil properties are in general not simply mirror images of one another. That is, temperature effects may or may not be reversible.

8

2.2 Review

2.2.1 Thermal Stability of Minerals

One important consideration that must be taken into account when reviewing the effects of temperature on soil properties is the thermal stability of the clay minerals present. Clay mineral transformations depend on temperature, pressure and most importantly, on the chemical composition of percolating groundwater solutions. Hydrothermal reactions on minerals have been extensively studied in the geological literature.

One issue that has received considerable attention is the possibility that field conditions might promote the illitization of smectite clay minerals. This is primarily of interest in relation to the performance of bentonite barriers for nuclear waste containment (Pusch 1985), but is also relevant to the field behaviour of other clays. The main concern is that the transport properties (hydraulic conductivity, sorption capacity, etc.) might be adversely affected by hydrothermal reactions, resulting in increased field radionuclide mobility (Pusch and Karnland 1988). Montmorillonite is gradually converted to illite (mica) and then to kaolinite under elevated temperatures and pressures. Details of these reactions are summarized in Pirajno (1992) and Güven (1990).

As do temperature and pressure, pore fluid chemistry plays an important role in clay mineral transformations under hydrothermal conditions. Most of the reactions occur when the temperature

exceeds 150°C to 200°C (Hoffman and Hower 1979). The reaction rate is slower at lower temperature. As a consequence, at temperatures below 100°C, interlayer cations (controlled by pore fluid chemistry) and not temperature, become the dominating influence controlling mineral transformations (Pusch and Karnland 1988).

The mechanism of clay mineral transformations is thought to occur in three stages (Pusch and Karnland 1988): (a) the creation of high lattice charge through the removal of Si^{4+} and replacement by Al^{3+} or Mg^{2+} which are locally available from accessory minerals or supplied by dissolved smectite, (b) the influx of K^+ from local solutions of potassium-bearing minerals or percolating groundwater which saturates the exchange capacity of the highly charged smectite and, (c) collapse of the lattice to the non-expansive illite form. The rate-limiting stage in bentonite used for nuclear waste containment may be the production of a highly charged smectite lattice by progressive substitution. The temperature must be high enough to allow ions to diffuse in and out of the lattice. The process is thought to be exceedingly slow at low temperatures, possibly significant over performance assessment time-scales at T > 60°C, and relatively more rapid at T > 100°C (Hoffman and Hower 1979). Although there is some dissension on the kinetics of this process, it is possible that, at 100°C, smectites could collapse to non-expansive illites over a 10^5-10^6 year time-scale (Pytte 1982), depending on the availability of potassium. Based on the potassium content of the pore waters of two Swiss mudrocks, McKinley (1989)

10

estimates that total conversion of backfill bentonite to illite will occur in about 10^7 years. The kinetics of other clay mineral transformations (for example, chloritization) are generally less well known (Pusch and Karnland 1988), but are thought to be less significant.

Comprehensive hydrothermal testing in recent years, for example as part of the Stripa Project in Sweden, has demonstrated that smectite in the form of soft gels of montmorillonite with pore water consisting of seawater, strongly brackish water, or distilled water, undergoes insignificant alteration even at 200°C heating for one year (Pusch *et al.* 1991). Furthermore, hydrothermal tests of denser clay, saturated with weakly brackish water and exposed to a temperature gradient of almost 0.6°C/mm (130°C and 90°C at the boundaries) for one year showed that the smectite content was practically unchanged (Pusch *et al.* 1993). However, drying/wetting of K-montmorillonite shows that a significant amount of non-expanding 10 Å minerals is formed, which suggests that such conversion requires contraction of the stacks of flakes, by drying or alternatively, by increase of the effective stress through compaction.

Hence dehydration seems to be a major factor in smectite-illite or other mineral-to-mineral conversion. Effect of dehydration can be seen in results from differential thermal analysis (DTA) in which a

clay mineral type is identified using clay mineral-temperature response characteristics (Mitchell 1976).

2.2.2 Volume Change due to Temperature Change

The volume change characteristics of soils subjected to temperature change have been investigated by many researchers (Campanella and Mitchell 1968, Plum and Esrig 1969, and others). A number of test programs have come to somewhat surprising conclusion that temperature increases cause a decrease in soil volume as long as the drainage of pore water is permitted under constant effective stress conditions (Fig.2.1). Temperature-induced volume changes of this type have been reported by a number of researchers (for example, Gray 1936, Mitchell and Campanella 1963, Paaswell 1967, Campanella and Mitchell 1968, Plum and Esrig 1969, Demars and Charles 1982, Green 1984, Baldi *et al.* 1988, Tidförs and Sällfors 1989, Kuntiwattanakul 1991). Temperature increases cause expansion of the minerals and the water. However, they may also change the way in which the minerals support the applied stresses under drained conditions. The net effect is a decrease in volume (Campanella and Mitchell 1968, Dixon *et al* 1993). Reasons for these decreases in volume will be discussed in a later section. The effect of temperature decrease has also been reported by several researchers (for example, Campanella and Mitchell 1968, Baldi *et al.* 1985, Tidförs and Sällfors 1989, Kuntiwattanakul 1991) As long as drainage of pore water is permitted under the constant effective

stresses, the volume of soil increases (Fig.2.1). In other words, the volumetric strains are expansive under cooling.

The effect of temperature cycles (combinations of increases and decreases in temperature) has also been reported by a number of researchers (Campanella and Mitchell 1968, Demars and Charles 1982, Baldi et al. 1985, Tidförs and Sällfors 1989, Kuntiwattanakul 1991). In some circumstances, the changes in volume are not reversible under temperature cycling. Campanella and Mitchell (1968) showed that a significant irrecoverable volume of water was drained from the specimen during the first heating/cooling cycle. The irrecoverable portion of the water expelled upon heating is attributed to a permanent change in the soil microstructure that is reflected as a reduction in void ratio. The authors suggested that volume changes were reversible in cycles of decreasing-increasing temperature after the first heating. The initial temperature cycles remove most of the irreversible volume change, and subsequent temperature cycles of the same magnitude and range produce almost no further permanent volume change. The reversible portion of the volume change is due to water being expelled upon heating and re-absorbed upon cooling. This reversible portion may be called thermo-elastic volumetric strain. It has been suggested (Campanella and Mitchell 1968, Plum and Esrig 1969) that cooling the soil causes it to behave as if it were overconsolidated. "Normally consolidated" means a clay has never previously experienced higher stress than its current stress. "Overconsolidated" means that it

13

did experience a higher stress than at present. The ratio of past highest stress to current stress is the "overconsolidation ratio, OCR".

Demars and Charles (1982) showed that the magnitude of irreversible volume changes due to a heating-cooling cycle is approximately independent of stress level. In a given soil, irreversible volume changes are independent of stresses in the normally consolidated range (Campanella and Mitchell 1968, Tidförs and Sällfors 1989). However, the magnitude of the irreversible volume change differs significantly from soil to soil. It is greatest for clays, less in silts, and not measurable for sands (Demars and Charles 1982). Figure 2.2 (Demars and Charles 1982) shows that the irreversible volume change increases with the plasticity of the soil. Each soil has a unique value of this permanent reduction in void ratio, that is a thermo-plastic volumetric strain, for a given imposed temperature cycle.

The magnitude of strains induced by temperature changes depends on the magnitude of the temperature increase, the stress level, and stress history. The effect of past stress history, (described for example by the overconsolidation ratio, OCR), on the observed volume changes was reported by Plum and Esrig (1969), Baldi et al. (1988), and Kuntiwattanakul (1991). Demars and Charles (1982) showed that overconsolidated soils exhibit a permanent reduction in void ratio due to temperature cycling along a reloading path. A similar

14

observation has been reported by Kuntiwattanakul (1991). Volume changes due to changes in temperature decrease with increasing OCR in Fig.2.3 (Baldi *et al.* 1988). Hueckel *et al.* (1987) stated that volumetric strains caused by heating were reversible upon cooling in the overconsolidated range of stresses. As the OCR gets higher, volumetric strains caused by heating are less compressive, and may become expansive (Fig.2.3). Kuntiwattanakul (1991) reported that in the overconsolidated state, volume changes depend on the direction of loading. For unloading, heating causes expansion in high OCR specimens, and small contraction in low OCR specimen. On the other hand, reloaded specimens exhibit contraction during heating. As an added complexity, Paaswell (1967) suggested that the volume changes may depend on the rate of temperature increase.

2.2.3 Mechanism of Volume Change Induced by Temperature

Direct measurements of changes in particle spacing with variations in temperature in a montmorillonite slurry subjected to low stresses were reported by Yong *et al.* (1962). They observed volume increases when sodium montmorillonite was heated at constant externally applied stresses of less than one atmosphere. One might expect that the increase in energy associated with heating a soil would cause the expansion of the electric double layer proposed in Gouy-Chapman theory (Lambe 1958).

However, in dense clay-water mixtures like clay soils, previous paragraphs have shown that drained heating causes compressions, not expansions. Lambe (1958) also used the diffuse double layer equations to explain the decrease in volume of cohesive soils on heating. The development of these·equations includes the assumption that the dielectric constant of the pore water is decreased with temperature. In this form, the equations suggest that an increase in temperature depresses the electro-chemical double layer and permits the soil particles to move together. Under constant load, Lambe observed that the clay compressed with heating and expanded with cooling. He explained that these volume changes are exactly those expected from the effect of temperature on the double layer. That is, an increase in temperature depresses the double layer, and a decrease in temperature expands the double layer.

In the overconsolidated range, volume changes caused by temperature cycling were found to be reversible (Hueckel et al. 1987). Baldi et al. (1988) developed a physics-based expression of the volume change caused by heating and cooling of low porosity clays for both normally consolidated and overconsolidated ranges. However, extensive (and perhaps impossible) tests are needed to determine the parameters in this relationship.

The experiments outlined earlier indicate that heating causes compression rather than expansion of the clay skeleton in normally consolidated clays. The reduction of volume is a well-known effect

16

at much higher temperatures in brick technology (Borwmnell 1976)
The mechanism of reduction of volume during heating can be explained
as dehydration due to evaporation when ceramics are in contact with
air at a free surface (Grim 1962). This mechanism is not likely to
occur under the conditions of interest in both laboratory
experiments and nuclear waste disposal sites. The principal
microstructural mechanism for shrinkage on heating under fully
saturated conditions seems to be the water phase exchange. Of the
four phases of water in clay, that is, structural, firmly adsorbed
and loosely adsorbed, and free pore water (Rosenquist 1995), only
the last two can leave the soil when heated. It is most probable
that volume reduction is caused by changes of configuration of
loosely adsorbed water (Paaswell 1967, Demars and Charles 1982) due
to a reduction of its density and its partial transformation into
free pore water. A more complete description of the states of water
in soils has been given by D.A.Dixon (1995).

2.2.4 Pore Water Pressure Changes Induced by Temperature

It is self-evident that soil behaviour mainly depends on the
effective stress (total stress minus pore pressure) even in dense
sand-bentonite mixtures (Graham *et al.* 1992). Therefore, pore water
pressure plays an important role in soil behaviour. The fact that
when heated, water expands more than the mineral particles (Dixon *et
al.* 1993), leads to the conclusion that excess pore water pressures
will develop whenever drainage is restricted. This is noted
frequently in the research literature (Henkel and Sowa 1960,

17

Campanella and Mitchell 1968, Noble and Demirel 1969, Plum and Esrig 1969, Houston and Lin 1987). On the other hand, under constant deviator stresses, pore water pressure changes induced by temperature are not always reversible. Hueckel and Pellegrini (1992) reported that cycles of undrained heating and cooling on saturated clays under constant deviator stress can cause substantial decreases of pore water pressure, resulting in corresponding increases in effective stress. Thermally induced pore water pressure changes may eventually lead to failure under constant deviator stress because the mean effective stresses reduce (Fig.2.4).

Pore water pressure changes induced by temperature are essentially reversible under constant isotropic total confining pressures. Fig.2.5 shows that temperature cycling results in the reversibility of pore pressure generated by temperature under undrained conditions (Campanella and Mitchell 1968, Plum and Esrig 1969). It can be seen that the pore water pressure induced by temperature rise is substantial and as a result the reduction of effective stress can be significant.

As pointed out earlier, the pore water pressures induced by temperature greatly affect soil behaviour. Close attention must be paid to this effect.

The magnitude of pore water pressure changes accompanying temperature changes under undrained conditions depends on the thermal expansion of the pore water, the compressibility of the soil structure, and the initial effective stress. The lower the compressibility, the greater the pore pressure increase for a given temperature increment under undrained conditions (Campanella and Mitchell 1968, Plum and Esrig 1969).

Pore water pressure induced by temperature change depends on the initial effective stress, and this is important in evaluating soil behaviour. The pore pressure induced by temperature rise under undrained conditions is a non-linear function of temperature under constant isotropic total confining pressure conditions (Agar *et al.* 1986, Houston and Lin 1987). Figure 2.6 shows the non-linear relationship of pore water pressure induced by temperature and its dependence on initial effective stress.

2.2.5 Thermal Expansion

In thermodynamics, the thermal expansion of a volume is defined as the magnitude of volume change under constant pressure. However, there are several definitions for thermal expansion of soils reported in the literature. In general, volume changes corresponding to temperature change are defined as thermal expansion in the following discussion, independent of accompanying effective stress changes.

Baldi *et al.* (1988) examined how thermal volumetric strains depend on the stress history (OCR) of a clay under constant effective stress conditions (Fig.2.3). The double-layer bound water was taken into account in calculating the thermal expansion of water for clay with low water content. Figure 2.7 shows that the coefficient of thermal expansion of water in clay pores is smaller than that of free water (Baldi *et al.* 1988, Kuntiwattanakul 1991, Dixon *et al.* 1993). The differences in the coefficients are larger at low temperatures, but gradually decrease as temperatures increase. It is likely that the coefficients are of the same magnitude at temperatures higher than about 70°C. These studies indicate that not all the pore fluid in the very small pore spaces of active clays behaves as normal unstructured water, but is more like the structured, crystalline type of water seen in ice. Transition between these two types of water appears to occur between 70°C to 90°C (Khitarov and Pugin 1966, Derjaguin *et al.* 1986, Pusch and Güven 1990, Pusch *et al.* 1991, Dixon *et al.* 1993).

As mentioned previously, the volume of a soil specimen changes when temperature changes under undrained conditions (Campanella and Mitchell 1969, Hueckel and Pellegrini 1992, Agar *et al.* 1986). This volume change was defined as undrained thermal expansion in order to separate it from the drained thermal compression observed under constant effective stress. Changes in height during undrained heating are shown in Fig.2.8. Undrained thermal expansion is always accompanied by pore water pressure changes caused by temperature

changes (Fig.2.4). Reversibility of volume change under isotropic stress conditions has been reported during temperature cycling, with increases and decreases in volume accompanying heating and cooling, respectively, (Campanella and Mitchell 1968). Under non-isotropic stresses, expansion has been observed (Fig.2.4) in a small temperature increase of 10°C-20°C, but compression in a large temperature increase of more than 30°C (Hueckel and Pellegrini 1992).

2.2.6 Stress-strain Properties

The stress-strain properties of most engineering materials (for example, metals, rubbers, and rocks) are temperature-dependent, and similar behaviour can be expected in clay soils. In clays, compressibility during consolidation and stiffness during shear are important parameters to be evaluated for design purposes.

It has been reported that compressibility of normally consolidated soils is not affected by temperature changes (Gray 1936, Finn 1951, Campanella and Mitchell 1968, Demars and Charles 1982, Tidförs and Sällfors 1989). Campanella and Mitchell (1968) reported equal compression indices (C_c) for three temperatures of 24.7°C, 37.8°C, and 51.4°C at pressures greater than 200 kPa in the normally consolidated range of illitic clay (Fig.2.9). Similar results have been reported in other clays (Demars and Charles 1982, Tidförs and Sällfors 1989).

The effect of temperature on compressibility of overconsolidated soils has not been clear until recently. In the oedometer test results in Fig.2.10, the recompression curves plotted as volume strain *vs* vertical stress show that at higher temperature soil tends to compress more that at lower temperature for the same load increment (Eriksson 1989, Tidförs and Sällfors 1989, Boudali *et al.* 1994).

Murayama (1969) used a visco-elastic model to investigate the temperature-dependence of the elasticity of clays (Fig.2.11). If the stiffnesses shown in this figure are taken to represent the elastic modulus of the material, then it may be seen that an increase in temperature causes a significant decrease in modulus. The temperature effects on shear wave velocity (which is related to shear modulus G) have been shown by Anderson and Richart (1974). They showed that the shear modulus G decreased with undrained heating. They explained that because these tests performed by Murayama (1969) and Anderson and Richart (1974) were performed under undrained heating conditions, the effective stress decreased upon heating so that the stiffness of soil decreased. However, if drainage is permitted and the excess pore water pressures dissipate, effective stresses approach their original values and finally the shear wave velocity is the same as the original shear wave velocity (Anderson and Richart 1974). Decreasing the testing temperature increased the shear wave velocity. In the overconsolidated region

22

of stressing, the stiffness of soil decreases with increasing temperature in drained tests (Hueckel and Baldi 1990).

The literature presents conflicting evidence on how the stiffness of clay in shear depends on temperature. Increasing stiffness with increasing temperature has been observed by Kuntiwattanakul 1991, and Wong et al. 1993. On the other hand, decreasing stiffness with increasing temperature has also been reported (Murayama 1969, Anderson and Richart 1974, Hueckel and Baldi 1990)

Changes in the size and shape of yield loci with temperatures are of importance in understanding elastic-plastic behaviour in engineering materials. Obvious changes in the size of yield loci have been reported in metals as shown for example in Fig.2.12 (Phillips 1968). Some observations on the thermal sensitivity of the yield surface in soils may be obtained from heating experiments either under drained unload-reloading, or under undrained conditions at constant total stresses (Hueckel and Baldi 1990, Hueckel and Pellegrini 1992, Kuntiwattanakul 1991). Hueckel and Baldi (1990) showed that consolidation tests with unload-reloading cycles at elevated temperatures showed a strong dependence on the preconsolidation pressure. In other words, the extent of the elastic domain depends strongly on temperature (Fig.2.13). However, it has still not been shown how the shape and size of yield loci change in q-p' space with temperature, and this will form one of the main objectives of the experimental work reported here.

2.2.7 Strength

Available descriptions of the effects of temperature on the strength of soils are confusing. On one hand, there have been many experimental results which show that increases in temperature cause weakening of soils (Mitchell 1964, Murayama 1969, Sherif and Burrous 1969, Hueckel and Baldi 1990, Kuntiwattanakul 1991). On the other hand, there have also been many test results which clearly show the reverse, that increasing temperatures cause strengthening (Laguros 1969, Noble and Demirel 1969, Houston et al. 1985, Kuntiwattanakul 1991, Lingnau 1993). Each group of researchers has tried to explain their results using currently available theories. However, the current state of knowledge at the beginning of this research seemed unable to explain the conflicting results that are observed. Until the modelling that will be presented later in this thesis, no coherent understanding has been available to explain why some soils weaken and others strengthen.

Explanations will be proposed why these differences in shear strength exist in the literature. Careful examination of test conditions reveals that after drained heating, undrained shear strength of soil increases (Laguros 1969, Noble and Demirel 1969, Houston et al. 1985, Hueckel and Baldi 1990, Kuntiwattanakul 1991, Lingnau 1993). In contrast, under undrained heating, undrained shear strength decreases (Mitchell 1964, Murayama 1969, Sherif and Burrous 1969, Agar et al. 1987, Hueckel et al. 1987, Kuntiwattanakul 1991). As mentioned in the previous section, drained heating keeps

24

the effective stress constant, whereas undrained heating causes an increase in pore water pressure, resulting in decreased effective stress, and hence decreased strength. It can be concluded that drained heating before undrained shearing causes soil to compress thermally, resulting in a strengthening of normally consolidated soils. Undrained heating causes a reduction in effective stress, resulting in weakened soil. Drained heating has little effect on the strength of overconsolidated soil because the thermally induced volume changes are small. Derjaguin *et al.* (1987) suggested that increases of strength with temperature can be explained by the thermal disruption of the special water structure in fine pores. Depending on the circumstances, heating a saturated clay specimen can cause either a decrease or increase in its void ratio, and independently, a decrease or an increase in its pore water pressure, with consequent changes in effective stress. Thus, heating or cooling individual specimens can cause strength increases or strength decreases.

However, when we come to examine strength envelopes in q-p' space at different temperatures, they seem to be independent of temperature in Fig.2.14, Kuntiwattanakul (1991) shows three specimens consolidated to the same pressure of 200 kPa. One specimen was sheared undrained at 28°C. The other two specimens were heated to 60°C and 90°C, respectively, under drained conditions before undrained shearing. Figure 2.14 shows the stress paths for each specimen in q-p' space. As mentioned previously, the heated

25

specimens have higher strength at failure. However, the strength envelopes at all temperatures appear to be identical.

2.3 Modelling of Temperature Effects

2.3.1 Model for Materials Subjected to Temperature Changes

Theoretical models for representing the behaviour of elastic-plastic materials subjected to thermal loading have been discussed in many works on metals and rubbers in the last two decades. Solutions are available in the areas of laser technology, nuclear reactor design, turbine analysis,and aerospace design, to name but a few (for example, Kammash, *et al* 1960, Levy 1981, Sharifi and Yates 1974). The thermo-mechanical behaviour of clays in relation to their use as natural and artificial barriers for heat-emitting waste repositories was discussed at the recent International Workshop on Thermo-mechanics of Clays and Clay Barriers (Bergamos, Italy 1993) which focused mainly on interpretation and modelling of temperature effects in geomechanical media

A good summary of investigations on thermo-elastic-plastic analysis has been discussed by Perzyna and Sawczuk (1973). There are two main approaches for thermal analysis: thermodynamics and thermomechanics. Rational thermodynamics approaches were initiated by Coleman and Noll (1963) and developed further by Green and Naghdi (1965).   Onsager (1931) developed another approach to the thermodynamics of continua called the classical thermodynamics of irreversible processes. It is important to stress that classical

26

and rational thermodynamics approaches both have shortcomings and neither is universally accepted.

In uncoupled thermo-mechanical approaches, temperature enters the stress-strain relations only through thermal dilation (Boley and Weiner 1969, Nowacki 1962). The heat conduction boundary value problem is solved first. Once, the temperature field has been calculated, the mechanical boundary value problem is formulated and solved. The solution is therefore sequentially coupled rather than fully coupled.

Applications using thermo-mechanics have been successfully made in the areas of nuclear reactor design, turbine analysis,and aerospace design (Kammash, et al 1960, Levy 1981, Sharifi and Yates 1974).

Following sections mainly discuss models for soils subjected to temperature changes because the main purpose of the thesis is to deal with clays. Importantly, it should be noted that compared with most materials, clay soils can experience large volume changes of the order 10% of the initial volume or greater. First, important features of soil behaviour such as pore water pressure and volume change induced by temperature changes are reviewed. Second, more general models and analyses are presented with a concentration on thermo-mechanical models since they are more applicable to soil behaviour.

2.3.2 Prediction of Volume Change Induced by Temperature

A framework for predicting volume changes in soils resulting from temperature variations and pore water pressure changes due to undrained heating has been developed by Campanella and Mitchell (1968), (see also Mitchell 1976). Under fully drained conditions the volume change of a soil subjected to increases in temperature arises from the expansion of the individual mineral grains, thermal expansion of the water, and structural changes in the soil matrix. Under completely undrained conditions the volume change of a fully saturated soil experiencing a temperature increase results from the expansion of the individual mineral grains and pore fluid. Pore water pressure response depends on both the thermal expansion of the components and the tendency for volume change in the soil matrix. The material properties required in the Mitchell and Campanella analysis are coefficients of thermal volume change and the coefficients of compressibility for the soil structure.

Campanella and Mitchell (1968) showed that under fully drained conditions and constant isotropic confining pressure, a volume of water (ΔV_{dr}) will drain from a saturated soil as a result of a temperature increase (ΔT).

$$(\Delta V_{dr})_{\Delta T} = \alpha_w V_w \Delta T + \alpha_s V_s \Delta T - \alpha_s V_m \Delta T - (\Delta V_{st})_{\Delta T}$$

where

α_s : coefficient of thermal expansion of mineral solids (or soil particles),

α_w : coefficient of thermal expansion of soil water,

ΔV_w : volume of pore water,

ΔV_s : volume of mineral solids,

ΔV_{st} : change in volume of soil structure due to temperature-induced changes in interparticle forces.

A major disadvantage of this model is that the equation does not include the effect of stress history (OCR). It is difficult to evaluate the change in volume of the soil structure caused by temperature induced changes in interparticle forces.

Relationships between permanent changes in void ratio and the plasticity index were proposed by Campanella and Mitchell (1968) and used by Demars and Charles (1982).

$$\Delta e^{Tp} = (0.00048 + 0.0000088 I_p) \ \Delta T$$

where

Δe^{Tp} : permanent change on void ratio (thermo plastic strain)

I_p : plasticity index

ΔT : temperature changes

Baldi *et al.* (1988) developed an expression for volume changes caused by temperature changes in low porosity clays for both normally consolidated and overconsolidated stress ranges. Volume changes that depend on stress history can therefore be calculated. However, extensive test data are needed to determine the required parameters and the extrapolation technique that is used is sensitive to small changes in temperature and stress history.

2.3.3 Prediction of Pore Water Pressure Changes Induced by Temperature

Temperature-induced pore water pressure changes have been reported by many researchers (for example, Gray 1936, Seed *et al.* 1960, Mitchell and Campanella 1963, Campanella and Mitchell 1968). Pore water pressure changes induced by temperature changes depend on the initial effective stress, initial temperature, and on non-linearity with temperature as shown in Fig.2.6 (Houston and Lin 1985).

Several expressions have been developed to permit prediction of the temperature-induced pore water pressure in undrained clays, for example by Campanella and Mitchell (1968). The expressions generally take account of the volume changes in soil and water due to temperature changes, but do not consider any changes in soil compressibility with temperature, the effects of secondary compression, or effective stress. The expression proposed by Campanella and Mitchell (1968) uses the thermal expansion of the soil particle and water, compressibility of the soil, and takes

30

account of physico-chemical effects. Under constant isotropic confining pressure, the change in pore water pressure can be expressed as:

$$\Delta u = \frac{n\Delta T(\alpha_s - \alpha_w) + \alpha_{st}\Delta T}{m_v + nm_w}$$

where

α_s : coefficient of cubical thermal expansion of mineral solids (or soil particles),

α_w : coefficient of thermal expansion of soil water,

α_{st}: physico-chemical temperature coefficient of volume change on soil structure,

m_v : compressibility of soil structure,

m_w : compressibility of water,

n : porosity.

There is a disadvantage in using this model because the equation does not include the effect of initial effective stresses.

2.3.4 Thermo-elastic Model

Elasticity is an important tool that can be used under certain conditions for predicting deformations in soil. Thermo-elasticity is an extension of elasticity that introduces a reversible thermal isotropic strain and allows for thermal changes of bulk modulus. The latter assumption leads to a coupled thermo-elasticity (Nowacki

31

1962). By definition, thermo-elastic strain and energy should be recoverable for any closed-stress temperature cycle. On the other hand, at least in clays, the thermal reversal expansion coefficient was found to depend on the effective stress (Baldi *et al*. 1988).

Curve fitting of experimental data indicates that the hyperbolic model (hypo-elasticity) may be a useful empirical technique for modelling non-linear stress-strain behaviour of oil sand (Agar *et al*. 1987). The hyperbolic model presented by Duncan and Chang (1970) is a useful technique for modelling the non-linear stress-strain behaviour of soils within the framework of incremental elasticity, but needs extensive development and calibration for thermal effects. Calibrations are highly sensitive to initial temperatures, stresses and stress histories.

Numerical modelling has been performed using thermo-elasticity to simulate the consolidation and pore water pressure around hot cylinders buried in clay (Booker and Savvidou 1985, Aboustit *et al*. 1985, Booker and Smith 1989, Britto *et al*. 1989). These results showed that pore water pressures generated by heating around the cylinder depend on the ratio of the coefficient of consolidation and the diffusivity of the soil. The lower the hydraulic conductivity, the higher the generated pore water pressures. These thermo-elasticity models consider only volume changes of soil minerals, pore water, and soil skeleton that are reversible with temperature changes.

The greatest disadvantage of thermo-elastic models is that they cannot describe soil behaviour accurately once non-recoverable behaviour appears, and such behaviour is readily observed in the laboratory.

2.3.5 Thermo-elastic-plastic Model

The most useful model for soils appears to be a phenomenological elastic-plastic model which can describe both elastic (recoverable) and plastic (non-recoverable) behaviours. A constitutive model for oil sand under triaxial stress condition and different thermal conditions has been presented by Wan *et al.* (1991). A Ramberg-Osgood function was used to describe a hardening/softening law, while Matsuoka-Nakai (1982) failure criterion and Rowe's stress dilatancy equation were adopted to describe the mechanical behaviour of the oil sand. Temperature effects were included in the model by changes in the assigned material properties. This model is a non-associated generalized plasticity model for 3-D stress conditions. Many identifiable behavioural aspects such as hardening, softening, plastic volumetric expansion and contraction are incorporated in the formulation.

Hueckel and Borsetto (1990) and Hueckel and Baldi (1990) proposed a useful thermo-elastic-plastic model of clay behaviour based on the critical state model (Schofield and Wroth 1960, Roscoe and Burland 1968). They defined rules for the dependence of elastic states and the yield surface on temperature (Fig.2.15). The elastic domain is

33

assumed to shrink during undrained heating (thermal softening) and to expand during cooling, when the stress state is elastic. At a constant stress state, thermal softening may entirely be compensated by plastic strain hardening leading to thermal consolidation. The focus in this work was on thermo-mechanical behaviour of the soil skeleton in drained conditions.

Other aspects of soil heating have been dealt with by Hueckel with a variety of co-authors. They include thermal expansion of water in clay, including adsorbed water (Baldi *et al.* 1988), failure of saturated clay specimens in triaxial undrained conditions due to heating (Hueckel and Pellegrini 1989), coupling of hydraulic and mechanical fields in clay mass under thermal conditions (Baldi *et al.* 1987, Hueckel *et al.* 1987), coupling of clay solid water and water response to heating through the adsorbed water, and the mixture theory aspects of clay response to heat (Hueckel 1989). These tend to be highly mathematical in nature and are presented principally in q,p',T plots. They have not extended significantly the understanding of soil behaviour in the compression space (V,ln p') that is such an important feature of Cam clay modelling. Rules for elastic and plastic straining in (V,ln p') space have not been clearly identified, and this forms one of the principal features of work discussed later in the thesis.

2.4 Review on Sealbond and Buffer Research

The safe disposal of nuclear fuel waste requires the isolation of the waste from the biosphere for a sufficient period of time. The Canadian concept for nuclear waste disposal is to emplace the waste, packaged in corrosion-resistance containers, in a vault mined deep into plutonic rock of the Canadian Shield. It is proposed that the vault will comprise a number of mined chambers some 500-1000 m below the ground surface. The preliminary layout of the disposal vault consists of a single-level vault, approximately 1700 m × 3600 m. A total are of 822 rooms, 195 m long, 7.5 m wide, and 5-6.2 m high, will be arranged within 16 rectangular panels. In the Canadian reference design for a nuclear fuel waste vault, the near-field ambient temperature is estimated to be about 100°C for several hundred years following waste emplacement.

Because nuclear waste emits heat long after being disposed of underground, the effects of temperature on soil properties require attention. Thermal properties such as thermal expansion, thermal conductivity, and thermal diffusivity are among those of interest. Thermal conductivity is a measure of the rate at which heat will flow through a material, and thermal diffusivity a measure of the rate of internal heat transfer within a substance.

Research on buffer has been conducted for about 10 years at the University of Manitoba and AECL's Whiteshell Laboratory, Pinawa, MB. The properties of the buffer material that determine its ability to

inhibit or retard radionuclide migration are its hydraulic conductivity and its ion exchange and sorption capacities. Similarly, its ability to support the containers and maintain its structural integrity is determined by its physical properties, namely its compressive strength, compressibility or deformability, and swelling potential. The rate of heat dissipation from the waste containers depends on the thermal properties of the buffer and associated moisture migration phenomena.

For the buffer to fulfill its function, its required material properties must be sustained over very long periods of time (thousands of years) under changing vault environments (for example, temperature, pressure, and groundwater chemistry). Highly compacted bentonite or bentonite-based mixtures have been proposed for vault and borehole sealing because of their capacity to swell upon wetting and thus retard the movement of water (Pusch 1980). Bentonite has also been found to retard the mobility of various species of radionuclides (Allard *et al.* 1977).

Extensive research has been conducted in Canada to obtain the relevant properties of buffer materials. The physical and mechanical properties of the buffer materials were studied by Gray *et al.* (1984), Dixon and Gray (1985), Gray (1984), Graham *et al.* (1986), and Yong *et al.* (1986). The thermal and transport characteristics of the buffer materials have also been determined by

Radhakrishna (1982), Westski *et al.* (1982), Selvadurai *et al.* (1985, 1986), and Dixon (1995).

Bentonite clay barriers proposed for use in nuclear fuel waste facilities are expected to be placed at unusually high dry densities. Reference Buffer Material (RBM) is a mixture of 50:50 sand-bentonite by dry weight. Clay densities greater than 1.25 Mg/m^3 have been suggested, and the dry density of RBM would then be 1.67 Mg/m^3 corresponding to 95% ASTM Modified Maximum Dry Density. Illitic clay (Sealbond) has been tested at various densities as high as 2.25 Mg/m^3 to examine its engineering properties, and to compare with data from the more active sand-bentonite buffer.

Considerable research has examined the hydraulic properties of buffer material in conjunction with its use as a sealing material against advective transportation of radioactive nuclide. In common with lower density clays, the hydraulic conductivity decreases with increasing dry densities of the clay (Dixon *et al.* 1987). In these tests, the material was confined in a rigid-walled cell, similar to the conditions expected in a nuclear-fuel-waste disposal vault. The behaviour of illitic Sealbond specimens at low applied hydraulic gradients has been discussed in detail by Dixon *et al.* (1992). The values of hydraulic conductivity for the two clays are generally less than 10^{-10} m/s. The dependence of hydraulic conductivity on temperature is less pronounced in the range of 25°C to 100°C. An

37

increase in hydraulic conductivities for dry density of 0.2 and 1.0 Mg/m^3 at concentration of 10^{-4} M is about three times at 100°C than at 25°C (Fig.2.16).

Thermal expansions of buffer, illitic clay, and quartz were examined at various densities and temperatures by Dixon et al. (1993) . In Fig.2.17a, low density bentonite clay exhibits thermal expansion coefficients of pore water that are significantly lower than those of free water. The thermal expansions of illitic clay were broadly similar to those for quartz and free water (Fig.2.17b).

Thermal conductivities of the candidate materials have also been measured and the effects of clay type, clay content, dry density, moisture content, and temperature examined (Radhakrishna et al. 1989). The thermal conductivity of compacted crushed granite-clay mixtures generally decreases with increased clay content. Bentonite-based mixtures exhibit the lowest thermal conductivity values compared with other mixtures. This was attributed to the low interparticle density and poor conductance at the interparticle contacts. The thermal conductivity of clay-based buffers is highly dependent on moisture content in the low moisture region and the relationship is nonlinear. A significant drop in the thermal conductivity by about 50 % was measured at water contents below 4-5 % for bentonite-based and Sealbond-based buffers and of course this could have a major influence on temperature fields round fuel-waste containers.

Significant improvements can be achieved in thermal conductivity of clay-based buffers by increasing their interparticle density, and/or by adding coarse-grained fractions such as silica or crushed granite. The thermal conductivity of the buffer samples did not show a strong dependence on the ambient temperature up to 100°C as long as samples were pressurized to prevent moisture loss. Kaolin and Sealbond materials exhibited thermal conductivities superior to those shown by the bentonites and bentonite mixtures.

Attention has also been paid to the stress-strain relationship of buffer. In early stages of the research, both undrained and drained behaviour of buffer was investigated only at ambient temperature at pressures up to 10 MPa (Sun 1986, Wan 1988, Saadat 1989, and Oswell 1991). More recently, high temperature tests (up to 100°C) have been performed in both drained and undrained conditions (Yarechewski 1993, and Lingnau 1993) and a conceptual model was proposed to explain the complex buffer behaviour at elevated temperatures (Lingnau 1993). The results of those programs were given elsewhere (Oswell 1991, Lingnau 1993) and only the major findings are discussed here.

The applicability of the effective stress concept to dense, compacted, plastic clays has been examined (Graham et al. 1992) under conditions of constant volume, constant pore fluid chemistry, and constant temperature. Even in dense buffer material (initial dry density ρ_d = 1.67 Mg/cm^3), it was found that the effective stress

concept originally proposed by Terzaghi can be applied to the buffer behaviour at ambient temperature. A small amount of similar testing by Yarechewski supports the idea that effective stresses can also be used at elevated temperatures. In general, the buffer behaves like highly plastic compacted clay (Oswell 1991). Previous reports and publications presented stress-strain for dense active clays and data interpreted using effective stresses (Graham *et al.* 1989, 1990). The yield locus and plastic potential of buffer material were investigated by Oswell (1991). Yield loci were strongly hook-shaped in q-p' space (Fig.2.18). Oswell suggested that the hook-shaped yield locus is a result of one-dimensional compaction that produced anisotropic particle structure in the buffer.

Recently, the effects of temperature on stress-strain relationships of buffer material have been investigated by Yarechewski (1993), and Lingnau (1993). They found that the behaviour of the buffer is not significantly changed by temperature changes. At elevated temperatures, buffer generally behaves like it does at ambient temperature with some minor exceptions. Under undrained conditions, excess pore water pressures generated during shear are greater at elevated temperature than at ambient temperature. Values of shear moduli G_{50} tend to decrease with pressure, and increase with temperature. Strength envelopes in q-p' space depend on temperature, with higher envelopes at higher temperature (Fig.2.19). As has been seen elsewhere in highly plastic clays, the strength envelopes are curved. Compression lines or Swelling Equilibrium

Lines (SEL) seem also to depend on temperature, having lower specific volume in V-*ln* p' space at higher temperatures (Fig.2.20). Figures 2.20 also shows that critical state lines in V-*ln* p' space depend on temperature. From Fig.2.20, swelling pressures in buffer may be expected to decrease from 1.5-2.0 MPa at 26°C to 0.35-0.5 MPa at 100°C (Lingnau *et al.* 1993). Loss of swelling pressure has also been reported through exposure to steam upon heating (Couture 1985). This has been explained by reductions in interparticle/interlayer forces of repulsion, although the effect may be largely attributed to silica cementation (Pusch 1987).

Constitutive models for buffer material have been developed by several researchers, for example Yin (1990), Oswell (1991), and Lingnau (1993). Because of time-dependent behaviour, the elastic-visco-plastic model proposed by Yin (1990) seems to be a reasonable and useful tool and predicts the buffer behaviour better than other models, such as anisotropic hypoelasticity. Analysis of *in situ* modelling was made by Saadat (1989) using the finite element method. However, all this work was at isothermal temperatures.

In a nuclear waste disposal vault and in other conditions encountered in geotechnical engineering, temperature changes will likely not to be simply monotonic, but will include cycles of heating and cooling. To understand soil behaviour more fully, it is necessary to examine the effect of temperature cycling. No experimental work on this topic has been done on buffer material

41

before the tests described later in this thesis. In addition, this understanding must be incorporated into a useful model for analysing and designing safe and economical nuclear waste disposal structures.

2.5 Summary from Literature on Effects of Temperature on Soil Behaviour

The following conclusions can be drawn from the literature review presented in preceding sections.

Knowns

(1) During drained heating under constant effective confining stress soils compress. The magnitude of the compression increases with increasing temperature.

(2) Undrained heating caused the pore fluid pressure to increase, the magnitude of the increase depending on the level of effective stress and the soil type.

(3) Undrained heating also causes soil volume to increase.

(4) Yield stresses decrease with increasing temperature in isotropic consolidation.

(5) Failure strengths seem to be independent of temperature as long as the soil mineralogy does not change significantly. This probably requires the temperature to be below 150°C – 200°C, temperatures considerably higher than those proposed in the Canadian nuclear fuel management program..

(6) Soil stiffnesses depend on stress level and on temperature. For the normally consolidated range, drained heating causes increases in undrained shear stiffness.

Unknowns

(1) For the overconsolidated range it seems that drained shear stiffnesses decrease, but undrained stiffnesses increase with increasing temperature.

(2) It is not clear how the size and shape of yield loci vary with temperature.

(3) The dependence of compressibility and stiffness on temperature are not clear.

(4) The effects of effective stress level, and the magnitude of temperature increase on pore water pressure changes are not clear.

(5) Models are required that can explain as many as possible of these features for clay soils subjected to temperature changes.

(6) The effects of temperature cycling on soils, especially buffer, have not yet been examined.

As it may be seen from this list of unknowns, it is necessary to examine the effects of temperature cycling under both drained and undrained condition in terms of stress-strain relationship, strength, pore pressure, thermal expansion, etc.

Drained tests along carefully controlled stress path give useful information for understanding soil behaviour, particularly yield stresses, stress-strain behaviour, and strengths. To the author's knowledge, no one has previously run stress path tests at different temperatures to examine how yield loci change with temperature. In addition, undrained triaxial compression tests also give additional information which drained tests cannot provide, for example, pore water pressure generation, and undrained stress-strain relationships. To cover all conditions expected in real situation, both drained and undrained tests need to be performed.

As mentioned earlier, no temperature cycling tests have yet been performed on buffer. Because of the possible application of buffer material to nuclear waste disposal, it also necessary to investigate soil behaviour not only at elevated temperatures but also at ramped temperature under various boundary and pressure conditions. However, because the hydraulic conductivity of buffer is low and physico-chemical effects are dominant in soil behaviour, only undrained compression tests will be performed. This will minimize uncertainties resulting from other factors, such as test duration, and membrane leakage or diffusion.

It can be seen that there are still many aspects of soil behaviour that remain to be investigated when the soil is subjected to changes in temperature. Most previous work on modelling is based on limited experimental data, and sometimes the simulated results are not good.

None of the existing experimental work involved comprehensive testing at elevated and ramped temperatures to investigate soil behaviour on the highly expansive clay that forms the main contribution of this thesis. No unique thermo-elastic-plastic model is yet available which can conveniently describe such features of soil behaviour as volume change, pore water pressure, stress-strain relationships, yield loci, and strength characteristics of clays subjected to temperature changes under various mechanical and thermal loading conditions and different hydraulic flux boundary conditions. It was therefore thought necessary to perform a comprehensive testing program at elevated and ramping temperatures to investigate the effects of temperature on soil behaviour. This was then used to supplement and develop more realistic thermo-elastic-plastic models for simulating soil behaviour.

In addition, a thermo-elastic-plastic model which can be used to describe the complex behaviour of clays subjected to temperature changes has been proposed.

CHAPTER 3   A POSSIBLE THERMO-MECHANICAL MODEL

3.1   Hypotheses and Assumptions

As discussed in Chapter 2, the effects of temperature on soil behaviour are complicated and difficult to understand in a simple framework of soil behaviour. This chapter presents several hypotheses based on what appear to be reasonable assumptions derived from the literature. The remainder of the thesis examines these hypothesis on the basis of a detailed experimental program and develops an accessible model for understanding soil behaviour.

Hypothesis 1:   Under drained conditions, volume changes of normally consolidated specimens are always compressive upon heating, and expansive upon cooling.   Volume changes are not completely recoverable when a normally consolidated specimen is first heated and later cooled.   For overconsolidated specimens, volume changes depend on the stress history and may be either expansive or compressive upon heating depending on the applied levels of mean stress and shear stress.   Volume changes are fully recoverable in a temperature cycle when mean effective stresses are less than yield stresses at the highest temperature in the cycle.

There is ample evidence supporting the proposed volume change relationships for normally consolidated clays (Campanella and Mitchell 1968, Plum and Esrig 1969, Hueckel and Baldi 1990, Kuntiwattanakul 1991, among others). Although less data are

available for overconsolidated clays, the effects of temperature on volume changes are reasonably well supported by existing literature (Plum and Esrig 1969, Baldi *et al.* 1988, Kuntiwattanakul 1991). This hypothesis has been expressed in terms of general stress states. However, it has typically been investigated in terms of isotropic stress states, and this practice has been continued in this thesis.

Hypothesis 2: *Under undrained conditions, heating normally consolidated and overconsolidated clays produces increased pore water pressures. Cooling produces reduced pore water pressures. Thermally induced pore water pressures are reversible in a temperature cycle as long as drainage is not permitted.*

Thermally induced pore water pressures mainly depend on the difference between the thermal expansion of the soil minerals and pore water (Campanella and Mitchell 1968, Plum and Esrig 1969, Agar *et al.* 1986). Changes in the soil structure also affect these thermally induced pore water pressures (Campanella and Mitchell 1968). The magnitude of thermally induced pore water pressures depends on the temperature increment and the consolidation pressures (Houston and Lin 1987).

Hypothesis 3:   The size of yield loci depends on temperature.   Yield loci shrink due to heating when specimens are overconsolidated or undrained.   However, the shapes of yield loci do not change with temperature.

It has been shown that yield stresses depend on temperature (Sallförs and Tidförs 1989, Hueckel and Baldi 1990).   Under a given deviator stress in undrained tests, heating produced thermally induced pore water pressures, and decreased mean effective stresses. At times, this could produce failure (Hueckel and Pellegrini 1991). Hueckel and Pellegrini (1991) suggested that this can be explained if the sizes of yield loci decrease with heating.   However, actual yielding behaviour and changes in the size and shape of the yield loci were not fully examined.   Reduction of the mean effective stresses might be attributable only to thermally induced pore water pressures, and in this case, shrinkage of the yield loci would be a secondary effect.   It is clear that an examination is needed to provide better understanding of the mechanism that produces changes in the size and shape of yield loci upon heating and cooling.

When yield loci shrink and expand on heating and cooling, care has to be taken with the terms "normally consolidated" and "overconsolidated".   Strictly the terms should refer to current stress-strain-temperature states, rather than to the specimens themselves.   For example, when a specimen having an overconsolidated state is heated, its yield locus may shrink sufficiently that its

48

stress state may now lie on the new yield locus and become normally consolidated.

Hypothesis 4: The strength envelope in (q,p') space at critical states is independent of temperatures. More generally, peak strengths depend on temperature, stress history, and the boundary conditions imposed by the tests.

Although there is not a large body of data available to support this hypothesis, it can be inferred from results provided by Hueckel and Baldi (1990), and Kuntiwattanakul (1991).

Hypothesis 5: Strengths and elastic parameters are affected by temperature changes. The effects of temperature depend on the boundary conditions of the tests and the stress history of the specimen. First loading (λ) lines are parallel at elevated temperature in (V,ln p') plots. However, the slopes (κ) of unload-reload lines depend on temperature.

Evidence for parallel λ-lines is fairly strong (Campanella and Mitchell 1968, Demars and Charles 1982, Eriksson 1989, Sallförs and Tidförs 1989, Hueckel and Baldi 1990, Kuntiwattanakul 1991). However, on the basis of some initial qualitative modelling, the author decided that unload-reload (κ) lines must be affected by temperature. The higher the temperature, the higher is the slope of the κ-lines. Until recently this assumption has not been well

supported by laboratory data. Some experimental evidence (Sallförs and Tidförs 1989, Hueckel and Baldi 1990, Kuntiwattanakul 1991, Boudali *et al.* 1994) suggest the dependency of κ-lines on temperature, but the phenomenon does not seem to have been noted previously in a formal way. This is an important new assumption that needs to be examined.

Hypothesis 6: Compacted soils behave broadly like overconsolidated soil, irrespective of soil type.

Evidence supporting this hypothesis is rare. There are few data available that compacted soils show apparent preconsolidation pressures during reloading in oedometer tests (Yang and Barbour 1992). However, this hypothesis also needs to be carefully examined in terms of both consolidation and shear behaviour.

These six hypotheses are examined in Chapter 5 through Chapter 8 on the basis of data from carefully controlled laboratory tests.

3.2 Outline of a Proposed Model

The hypotheses and assumptions made in Sec. 3.1 allow a new thermo-elastic-plastic model to be proposed. In this section, only a brief outline of the model is presented. Full details and applications of the model will be discussed in later chapter with experimental results from the testing program. The model is applicable to reconstituted isotropically consolidated soils at temperatures below

50

which soil minerals experience reversible changes. For compacted soil, the model needs some modifications to incorporate anisotropy induced by the compaction process. These modifications are also discussed later in Chapter 10.

The proposed model is based on the Modified Cam Clay (Schofield and Wroth 1968, Roscoe and Burland 1968) which has been adapted to take into account temperature effects. Assumptions made in the model are as follows:

(1) Strength envelopes in q *vs.* p′ space are independent of temperature with a constant slope M.

(2) Yield loci are elliptical and depend on temperature. They do not change in shape, but decrease in size with higher temperatures.

(3) The slopes λ of first-time consolidation lines are independent of temperature. However, the slopes κ of unload-reload lines increase with temperature. The assumptions of constant λ-lines, varying κ-lines, and elliptical yield loci, result in corresponding range of critical state lines (CSL) in V *vs. ln* p′ plots.

(4) The elasticity of the material is assumed to be isotropic. Elastic parameters (κ, K, G, etc.) depend on temperature, generally showing decreasing values with temperature.

(5) The flow rule is assumed to be "associated" at all temperatures, that is, yield functions and the corresponding plastic potentials coincide.

3.3 Required Research Program for Validating a Model

The majority of tests in the program were done on reconstituted illitic specimens. Reconstituted soils are often used in test programs because, in comparison with natural specimens, they can be made as ideal isotropic, homogeneous specimens. This has the advantage that stress history and initial specific volumes can be controlled.

Triaxial testing was selected because of its several advantages in comparison with other tests. In a triaxial test, a cylindrical specimen is separated by flexible membranes from a cell fluid that applies all-round pressures used during isotropic consolidation. Compression and extension shear tests can be performed by changing the axial loading through the piston mounted in the top of the cell. Drained or undrained tests can be carried out if drainage lines from the specimen are respectively open or closed. Stress conditions during consolidation are isotropic, which means that the mean effective stress is the same as the effective consolidation pressure (= total cell pressure - pore water pressure). However, this is not the case in one-dimensional oedometer testing which is often more popular in common geotechnical practice. In oedometer tests, the specimen is confined laterally while axial stresses are applied. In

52

most cases, the lateral stress is not measured, so the mean effective stress (and hence the stress state) can not be determined accurately unless assumptions are made for the coefficient of earth pressure at rest (K_o). For this reason, the oedometer was not used in this study. More importantly, triaxial testing allows axial and lateral stresses to be controlled separately, allowing stress paths during tests to be selected and controlled.

In order to calibrate and validate the proposed model, a program of laboratory tests was designed to examine each of the hypotheses and assumptions in turn. Tests were done at temperatures of room temperature (28°C), 65°C, and 100°C. Consolidation pressures were varied mainly in the range 0.5 MPa to 1.5 MPa, with one test 3.0 MPa. An overconsolidation ratio of 2 was chosen for the stress-path tests used to measure yield loci because the stress state of the specimen would be centrally placed inside yield loci in q *vs.* p' space. Compacted illite and sand-bentonite specimens were used to examine how the effects of compaction can be incorporated into the proposed model.

3.3.1 Mechanical and Thermal Consolidation Tests

To examine consolidation behaviour in terms of λ and κ values, reconstituted specimens were isotropically consolidated from low pressure (0.1 MPa) to high pressure (1.0 MPa). Normally consolidated λ-lines can be obtained from these tests. After first loading to 1.0 MPa, the specimens were generally unloaded to 0.5 MPa

giving an overconsolidation ratio (OCR) of 2. This process allows the reloading behaviour to be examined and κ-lines to be obtained. Compacted illite specimens were mostly also consolidated 1.0 MPa and then unloaded to 0.5 MPa. The compacted sand-bentonite specimens were consolidated to 1.5 MPa.

In order to examine the thermally induced volume changes, temperatures were changed after mechanical loading had been completed at different temperatures, pressure levels, and stress history. Thermal consolidation was performed under drained conditions in which the effective stress is maintained constant while temperatures are change in a controlled way. For the tests on reconstituted illite, thermal consolidation was performed at pressures ranging from 0.5 MPa for overconsolidated specimens to 1.5 MPa for normally consolidated specimens. For compacted illite, thermal consolidation was performed at 0.5 MPa and 1.0 MPa; and for compacted sand-bentonite specimens at 1.5 MPa. Volume changes during thermal consolidation were measured. In some cases, height changes of specimens were measured independetly for thermal expansion calculations.

3.3.2 Undrained Temperature-changed Tests

Undrained temperature-changed tests were performed at different temperatures, pressure levels, and stress history to examine thermally induced pore water pressure under isotropic stress conditions. In these tests, drainage is not permitted during

54

temperature changes. Resulting thermally induced pore water pressures were measured under constant total stress conditions so that the characteristics of thermally induced pore water pressure could be determined. In addition to the thermally induced pore water pressure, height changes of the specimens were measured for thermal expansion calculation.

For the reconstituted illite specimens, both normally consolidated and overconsolidated specimens were subjected to undrained temperature changes. The confining pressures ranged from 0.5 MPa to 1.5 MPa. For compacted illite, one undrained temperature-changed test was performed at 1.0 MPa; and one test was done on compacted sand-bentonite specimen at 1.5 MPa.

3.3.3 Drained Stress-path Tests

The main purpose of this part of the program was to determine how yield loci change in both size and shape at elevated temperatures. In order to examine yield loci in q *vs.* p' stress space at elevated temperatures, controlled stress-path tests are needed from which individual yield stresses can be determined. Results from these stress-path tests also contribute an understanding of how elastic parameters vary with temperature. They also permit examination of an appropriate flow rule, and critical state conditions may be determined. Temperature was maintained constant throughout these tests.

Five different stress paths were pre-selected in stress (q, p') space to examine yield loci at each of the chosen temperatures (28°C, 65°C, and 100°C). One of the stress paths is simply reloading along the p'-axis under isotropic stress conditions with no deviator stress. The other stress paths were defined by $dq/dp' = -8$, -1.5, 0.72, 3. These results can also be used to analyze the dependency of κ- and λ-lines on temperature. More complete tests for this purpose have been designed in a parallel Masters degree program conducted by T.Crilly. Details of his results will be published later in 1995.

Specimens of both reconstituted and compacted illites were first consolidated to 1.0 MPa and then unloaded to 0.5 MPa, to give an OCR of 2. Specimens were sheared along pre-assigned stress paths using constant increments of deviator stress and/or mean effective stress.

3.3.4 Undrained Triaxial Compression Tests

Because a sudden failure is frequently observed in drained stress-path tests where stresses are controlled, the critical state or large-strain strength of the specimen cannot be determined. However, the controlled straining in undrained triaxial compression tests has the advantage that critical state strength can be easily obtained. Therefore, in order to determine the failure envelope in q *vs.* p' space at each temperature, *isothermal undrained compression tests* have been performed. In some cases, the temperatures were changed under undrained condition so that the effects of temperature

on thermally induced pore water pressure and yield loci could be observed.

After thermal consolidation for both normally consolidated and overconsolidated illite specimens were complete, isothermal strain-controlled undrained loading was performed. The stress path for normally consolidated specimens during undrained testing can be defined as a state boundary surface, that is, a boundary on which the soil can exist in terms of (q,p',V) three dimensional plots. The tests allowed examination of undrained elastic parameters at three temeperatures. For compacted soils, undrained compression tests were performed on illite at 0.5 MPa and 1.0 MPa at 65°C; and on sand-bentonite at 1.0 MPa and 1.5 MPa, at 28°C, 65°C, and 100°C.

For some reconstituted illite specimens, temperatures were changed in both normally consolidated and overconsolidated specimens at a given deviator stress q, while maintaining a constant q (*non-isothermal undrained test*). The temperature was increased from 28°C to 65°C at a given deviator stress on one of the compacted illite specimens consolidated at 1.0 Ma. Similarly the temperature was increase from 28°C to 100°C on a compacted sand-bentonite specimen consolidated at 1.5 MPa. Thermally induced pore water pressures were monitored during heating. Some specimens were sheared again after temperature was changed to examine the resulting stress-strain behaviour. Changes of yield loci following undrained heating can be examined by these tests.

57

CHAPTER 4   TEST EQUIPMENT, MATERIALS, AND PROCEDURES

4.1   Introduction

Geotechnical investigations often use the so-called triaxial apparatus to examine stress-strain behaviour in soil. The triaxial apparatus allows independent control of axial and radial principal stresses on cylindrical specimens. Tests can be done using stress-controlled or strain-controlled conditions. While this research program used several types of testing equipment to investigate soil behaviour at different temperatures up to 100°C, the majority of the tests were performed in a triaxial testing apparatus. The remainder of the tests used a pressure chamber to carry out isotropic consolidation tests with no shear stress applied. This chapter discusses technologies and procedures involved in the experiments. It is organized as follows. Following a description of the equipment used in this study, attention is given to work done on producing better membranes for use in the tests. Technologies for specimen preparation and the test procedure are then presented. Information is given about the materials that have been used in the program. The chapter ends with detailed description of the conditions used in the testing program.

4.2   Test Equipment

Four different types of triaxial cells have been used in this program. Tests at room temperature were performed using a Geotechnical Digital Systems (GDS) pressure control system with a

Bishop and Wesley (1975) triaxial cell, and a system using Brainerd-Kilman (B-K) triaxial cell. Tests under elevated temperatures (65°C and 100°C) and ramped temperatures used the High Temperature and High Pressure (HITEP) triaxial cells developed by Lingnau (1993) for consolidated-shear tests, and the High Temperature and High Pressure Consolidation (HITEPC) cell developed by Oswell (1991) for tests involving only consolidation. A one-dimensional consolidometer was used to prepare reconstituted specimens from slurry. A rigid compaction mold allowed form compacted specimens to be formed from pre-mixed materials. Compressed nitrogen was used to supply high pressures for both cell and back pressure during testing. It was used because of its lower solubility in water compared with air.

4.2.1 GDS System

The GDS system is a computer-controlled apparatus (Fig. 4.1). The system consists of five components: an IBM-AT compatible computer, three hydraulic controllers that operate using microprocessor controlled electric stepper motors, and a Bishop and Wesley (1975) "stress-path" triaxial cell (manufactured by Wykeham Farrance). The triaxial cell has a pressure capacity up to 1.7 MPa. Additional equipment was added by Oswell (1991) to permit measurement of pore water pressures at the base of the specimen and measurement of deviator stresses using a submersible load cell (3000 N capacity) inside the pressure cell. In order to automate the system, the GDS software program was modified in this study so the additional reading from a voltmeter can be achieved. This modification of the

59

GDS software program allows all instrument readings to store data automatically. Full details of the system and equipment were given by Oswell (1991), and the modification of the equipment is presented in Appendix A.

4.2.2 Brainerd Kilman (B-K) Triaxial Cell

The B-K cells and testing system were fully described by Oswell (1991), and therefore only a brief description of is needed here. Figure 4.2 shows the B-K cell and its control system. The B-K cell has aluminum cell walls and can operate to a maximum confining pressure of 3.5 MPa. Axial loads are applied by a 12.7 mm stainless steel ram passing through the top of the cell. A linear bearing maintains ram alignment and reduces friction resistance. Carefully designed seals stop cell fluid leakage through the linear bearings. Drainage and pore water pressure generated by the specimen can be measured at the cell base. Tests using the B-K cells were performed either under undrained conditions with the drainage line closed, or under drained conditions with the drainage lines open to a constant, elevated, back pressure that ensures saturation..

4.2.3 High Pressure and High Temperature (HITEP) Triaxial Cells

Three High Temperature High pressure triaxial compression cells (HITEP cells) are available at the University of Manitoba. The HITEP system is shown schematically in Fig. 4.3. In this test program, two cells were used for drained and undrained triaxial tests. The third cell has been used by T.Crilly in a parallel

research program to investigate consolidation behaviour at different temperatures. The author used one of the two HITEP cells mainly for undrained strain-controlled compression tests, and the second for drained stress-controlled compression tests. Details of the design and fabrication of the HITEP cells were presented by Lingnau (1993) and Yarechewski (1993), and will not be described further here. The major components of the cell are made from nickel-plated mild steel because of its favourable thermal properties and resistance to corrosion. The cell was designed to test soil specimens of about 50 mm diameter and 100 mm height at temperatures from 20°C to 100°C and confining pressures up to 10 MPa. Axial loading may be applied to the specimen through the piston which carries a load transducer inside the pressurized chamber of the test cell. This eliminates the need for correction for piston friction on calculating axial stresses. Volume change, axial displacement, specimen temperature, temperature difference along the specimen, cell pressure and pore water pressure can all be measured and recorded. Only a slight modification on the cells will be discussed.

The only modification made to Lingnau's cells has been redesign of the specimen pedestal which had been suspected of leakage through the O-ring seals at high temperatures. The new pedestals were designed using stainless steel and connected directly through the cell base to stainless steel tubings to reduce the possibility of leakage.

4.2.4 High Pressure/ High Temperature Isotropic Consolidation (HITEPC) Cell

The HITEPC cell was originally designed for consolidation tests on sand-bentonite mixture by Oswell (1991), and modified for high temperature research by Yarechewski (1993). In this program, the HITEPC cell was used for consolidation tests at elevated temperature, and for diffusion tests on membranes. Basic features of the HITEPC cell are similar to the HITEP cells, except that no axial stress can be applied (Fig. 4.4). Drainage connected to the base of the cell was used for back-pressurizing and volume change measurements.

4.2.5 Compaction Equipment

The compaction frame designed by Yarechewski (1987) was used to form compacted specimens for testing. The compaction equipment consists of a compaction frame, piston, a rigid split-mold, and hydraulic pump. The compaction force is applied statically through the piston using a hand-pumped oil jack. The mold has inside diameter of about 50 mm and has enough height to make a 100 mm height specimen (Fig. 4.5). It can be split into two so that a compacted specimen can be easily removed. The maximum compaction force corresponds approximately to 5000 psi (35 MPa) vertical pressure.

4.2.6 One-dimensional Consolidometer

For preparing reconstituted soil specimens, a large diameter, one-dimensional consolidometer used by Kwok (1984), Ambrosie (1985), Lau

(1986), and Jamieson (1989) was utilized to produce large cakes of homogeneous clay (Fig. 4.6). Full details of the system were given by Lau (1986). The vertical load on the samples is applied through a lever system using dead weights. Porous stones were used at both the top and bottom of the tank. No side drains were used to eliminate non-uniformity of the water content after consolidation (Lau 1989, Graham et al. 1987, and Atkinson et al. 1985).

4.2.7 Cell and Pore Fluids

Distilled-deaired water was used as pore fluid in the entire testing program. Chapter 2 showed that clay mineral transformation is unlikely occurred under the testing conditions that were used. For the room temperature tests, distilled-deaired water was used as cell fluid. For the elevated temperature and ramped temperature tests, silicon oil was used as cell fluid to prevent potential boiling of fluid at the expected temperature of 100°C. In addition, the submersible load transducers inside the cells required silicone oil rather than water as the cell fluid.

4.2.8 Calibrations of Instruments

All electronic devices were calibrated against reliable sources to ensure their precision and accuracy. Because both pressure and temperature are factors affecting the devices' performance, care was taken towards reliability and calibration under elevated pressures and temperatures. Extensive calibrations were performed under the pressures and temperatures in the program. Periodic calibration

checks of the devices were conducted to eliminate any errors and calibration shifts. It was found that the effect of temperature on measuring devices was insignificant.

Since temperature changes cause significant changes in the dimensions of all components of the apparatus as well as in the test specimen, calibrations are required prior to each test to provide a reference for strain measurements. In order to calculate actual volume changes and height changes in specimens during temperature changes, calibration tests were performed to determine the system compliance. A dummy aluminum specimen (Lingnau 1993) instead of a real clay specimen was used for system compliance calibration. Test set-ups were identical to that for a real specimen; namely two porous stones, two filter papers, six strips of geotexile side drains, and membranes. Calibration data allow calculation of actual measurements by subtracting or adding the system compliance from total measurements of volume and height.

4.3 Membranes

It must be emphasized that all elements of the apparatus were very carefully checked to be sure that any water pressure drop was due to the behaviour of the specimen and not due to the equipment itself. Major membrane leaks or diffusion can be excluded. The least sensitive membrane (butyl) was selected for 100°C tests. A leak would lead to an inverse liquid flow, i.e. towards the specimen, and thus would increase the pore pressure. The cell liquid was silicone

64

oil, and no trace of this liquid was found in the specimen after completion of the test. Finally, in isotropic undrained heating no water pressure drop has been observed.

It was noticed in some early tests in this test program and by others (Lingnau 1993, Yarechewski 1993) that silicone membranes have high diffusivity at higher temperature, especially at 100°C. Therefore, it was felt that new types of membranes were needed to ensure the elimination of possible leaks at 100°C.

Various kinds of membranes were tested and used to seal the soil specimen from the cell fluid. Basically, two different types of membranes (latex and silicone membrane) had been used to seal the soil specimen for tests. Latex membranes were used as an inside membrane for tests at both 28°C and 65°C. It has been found from leakage tests that the latex membrane performs satisfactorily at these temperatures. However, latex membranes melt at 100°C and no longer maintain their original shape and stiffness. Therefore, latex cannot be used for tests at 100°C. Similarly, the silicone rubber membranes also showed unacceptably high leakage/diffusion rates at 100°C Among other membranes tested were EPDM, Butyl, Santoprene (Advance Elastomer System), Viton (Du Pont), Krayton (Shell Chemical). Results have been presented in Graham et. al. (1993). As a result of extensive leakage tests, three membrane types such as latex, butyl, and silicone, were used in this test program.

The selection of the possible membranes are based on the their stiffness, resistance against chemical, temperature, and diffusion. The advantage of the latex membrane is that it displays a lower Young's modulus and is more resilient than the other membrane materials tested. It was found that latex membrane performed well at 65°C, but not at 100°C. No change in strength was observed at 65°C and diffusion rate are less than 0.2 ml/day. As expected at 100°C, latex membrane melted and had no strength. It also stuck to the side drains and porous stones so that it might clog the drainage.

Silicone rubber was used only as an outside membrane which acts as a barrier to avoid direct contact of the inside membrane to silicone oil in the cell.

Butyl membranes performed well at 100°C, with diffusion rate less than 0.3 ml/day. This is a substantial reduction of diffusion rate from about 1.00 ml/day on silicone and other membranes reported by Yarechewski (1993), and Graham *et al.* (1993). As can be seen, the butyl membranes are still not perfect in terms of zero diffusion, but they are reasonable. They can be used as long as the diffusion rates are known and can be corrected for if necessary. From the diffusion tests, butyl membranes were chosen for use at 100°C because of their lower diffusivity, proper stiffness, and successful application (ISMES Report 1990).

4.4 Test Materials

Two types of soils were tested to determine the effects of temperature on their engineering properties: illitic clay and a sand-bentonite mixture. As mentioned earlier, the sand-bentonite mixture is a potential buffer material for nuclear waste disposal technology.

The illitic clay is a commercially available material called Sealbond, a crushed illitic shale. The dominant mineral of the sediments is illite. Grain size analyses (Fig.4.7) show approximately 22% of the particles at less than 0.002 mm (clay size) with very little sand. X-ray analysis of the Sealbond material shows that it is dominated by illite, but contains significant quantities of kaolin, chlorite, and quartz (Quigley 1984). Atterberg limits for the illitic clay used in this program showed liquid limit = 30, plastic limit = 21, and plasticity index = 9. The activity (plasticity index divided by % clay fraction) is 0.40. Dixon *et al.* (1985) reported the specific surface area = 43 m^2/g and cation exchange capacity (CEC) = 16 meq/100g. Physical properties are summarized in Table 4.1.

Table 4.1 Physical properties of clays

		Illitic clay	Na$^+$benotnite
(1)	Specific Gravity	2.72	2.75
(2)	Mineralogy (dominant)	Illite	Smectite
(3)	Specific surface area (m^2/g)	43	519
(4)	Cation exchange capacity (meq/100g)	16	71
(5)	Liquid limit (%)	30	222
(6)	Plastic limit (%)	21	40
(7)	Plasticity index (%)	9	182

Note: (2), (3), (4) were from Dixon and Woodcock (1986).

The sand used in the program is a subangular crushed quartz. It is a blended mix with D_{10} = 0.2 mm and D_{85} = 1.3 mm. A sieve analysis of the blended sand is shown in Fig. 4.7. Specification of the sand was reported by Gray *et al.* (1984).

The sand-bentonite used in this program is a 50:50 mixture by dry weight of quartz sand and bentonite, commonly called reference buffer material (RBM). The soil mixture used in this research program was a 50:50 mix by dry weight of quartz sand and bentonite. The sand was a blended mix with D_{10} = 0.2 mm and D_{85} = 1.3 mm. A sieve analysis of the blended sand is shown in Fig. 4.7 (Dixon *et al.* 1985). The specification of the sand was reported by Gray *et al.* (1984). The bentonite was sodium rich smectite commercially available from Avonlea Mineral Industries Ltd., Saskatchewan. Composition and mineralogy were reported by Dixon and Woodcock (1986) and Quigley (1984). The liquid limit was in the order of

225% to 250% with a plasticity index of about 200%. Distilled, de-aired water was used in the preparation of all compacted specimens.

4.5 Test Procedure

4.5.1 Specimen Preparation

Reconstituted Specimens: Illitic clay (Sealbond) was first oven-dried at a temperature of 110°C for one day, and then cooled in a temperature-humidity-controlled room for few hours while covered to prevent moisture absorption from the atmosphere.   The clay was then mixed with distilled water.   The first 11 specimens were prepared by mixing to a water content twice the liquid limit.   Early in the test program, it was found convenient for scheduling purpose to mix the rest of the specimens at 1.7 times as the liquid limit.   Mixing was first performed by hand to make sure that large lumps in the clay slurry were destroyed and the mixture was uniform.   After the mixing by hand, the container was transferred to a vertical drilling machine, and mechanical mixing was done for three days under a vacuum to remove any air from the slurry.

After three days, the slurry was poured into a one-dimensional consolidometer which was either an acrylic plastic cylinder, or a steel tank (Kwok 1984, Ambrosie 1985, Lau 1986, Jamieson 1989). The diameters of the cylinder and the tank are 101 mm and 256 mm, respectively.   Measurement of water content was done to determine the initial water content.   Consolidation in the acrylic plastic cylinder was done using a hanger system in which vertical dead loads

69

were applied.   The steel tank had a lever-arm which applied the vertical load through a piston to the slurry.   The majority of the specimens except three early specimens were formed in the larger steel tank.   Consolidation was done by step loading to a maximum vertical stress of 0.07 MPa for the first three specimens and 0.14 MPa for the remaining specimens.   These pressures were chosen to produce samples with adequate strength for trimming suitable triaxial specimens and installing them in the test cells.   Vertical compression of the slurry was measured with a dial gauge.   The end of consolidation was determined when sufficient time was allowed to be sure that secondary consolidation had started.

Once consolidation ended, the consolidated sample of clay was extruded from the consolidometer and cut into twelve pie-shaped blocks that were trimmed for storage in a temperature and humidity controlled room.   The blocks were first wrapped with Saran wrap, then with aluminum foil, and finally wax-coated to prevent moisture loss during storage.

Procedures for forming and trimming the specimens are the same as those used by Kwok (1984), Ambrosie (1985), Lau (1986), and Jamieson (1989).   Detailed description of these processes will therefore not be repeated here.   From the pie-shaped blocks, cylindrical specimens (50 mm diameter and 100 mm height) were trimmed using a special trimming device designed to minimize torsion disturbance during trimming (Lau 1986).   After trimming, five measurements were taken

70

of the diameter and the height of the specimens. The specimen was weighed and water content measurements were also done on excess pieces trimmed from the larger block.

Compacted Specimens: Sun (1986), Wan (1987), Yarechewski (1988, 1993), Saadat (1989), Oswell (1991), and Lingnau (1993) detailed the methods and equipment used to prepare compacted specimens by "static" compaction in a rigid cylindrical mold. Once again, only a brief description will be given of specimen preparation procedures.

Target dry densities were 1.93 Mg/m^3 for the illitic clay and 1.67 Mg/m^3 for the sand-bentonite mixture (Dixon and Gray 1985). These dry densities correspond to Modified Dry Densities of approximately 95 %.

Illitic clay (Sealbond), silica sand, and bentonite components for compacted specimens were first oven-dried (temperature of 110°C) for one day, and then allowed to cool in a temperature-controlled room for some hours having been covered to prevent moisture absorption from the atmosphere. Based on the maximum dry density measured in compaction tests. Calculated the amounts of dry soil particles and de-aired water were mixed by hand in a temperature-humidity-controlled room for 10 minutes. After this initial mixing, illite or sand-bentonite samples were kept in air-tight plastic bags for curing and storage. Illitic samples were kept for a minimum of one day, and sand-samples bentonite for three days to distribute the

71

moisture uniformly through the entire clay mass. After curing in the temperature-humidity-controlled room, the mixture was compacted using the rigid compaction frame described earlier, and the method developed by Yarechewski (1993) using non-uniform layer compaction to get uniform density distribution in the specimens.

4.5.2 Installation of Specimens

The methods and techniques for specimen installation described by Oswell (1993), Yarechewski (1993), and Lingnau (1994) were closely followed in this study.

Before a specimen was mounted in a triaxial cell, all drainage lines of the system were flushed with distilled de-aired water to eliminate entrapped air. Distilled and de-aired water was used throughout this program. The specimen was placed on the pedestal of the cell with a filter paper and a porous stone at its both bottom and top. Whatman No.54 was used as filter paper. Side drains of six strips were placed spirally around all specimens to facilitate drainage. This arrangement allows accelerated consolidation and avoids the need to make corrections in the specimen strength for side drain stiffness. A geotexile (Miraf #132 140NS nonwoven geotexile, initial thickness Miraf #132 140NS nonwoven geotexile, initial thickness) was used for side drains to avoid collapse compression of the drains under high pressure (Oswell *et al.* 1991). Once the porous stones and filter papers were in place, a loading cap was placed on the top porous stone.

All specimens in the B-K cell were covered with two latex membranes, separated by a light coating of silicone grease to minimize the problem of osmotic flow through the membranes. For room temperature tests, two latex membranes (0.685 mm thick) were used. To reduce water absorption by the membranes during tests. They were soaked overnight in de-aired water before being used. (Leroueil *et al.* 1988). For 28°C and 65°C tests in the HITEP cells, a combination of an inner latex membrane an outer silicone membrane was used. Several combinations of membrane setting were examined during the research and details are discussed in a later section. In some cases, Saran film was wrapped around the specimen between two membranes for extra protection against diffusion of silicone oil and pore water. A total of 8 O-rings was used on the membranes: 4 on the inside membrane and 4 on the outside membrane. After installation of the membranes and O-rings, the thermocouples and RTD (Resistance Temperature Device) shown in Fig.4.8 were installed on the specimens. In early tests on buffer, a lateral strain gauge was also installed on the specimens. At later stages of the program it malfunctioned at higher temperatures and since then it was not used. After all the measuring instruments were installed, the cell sleeve was mounted and the cell filled with silicone oil as the cell fluid.

4.5.3 Consolidation

Consolidation was begun under an initial pressure of 0.10 MPa without applying a back pressure. To ensure complete saturation, back pressures of 0.2 MPa for B-K cell and 1.0 MPa for HITEP cell

were then applied in at least 20 increments through a burette volume change system. This was done by increasing the cell pressure and pore water pressure simultaneously by the same amount, so that their difference (the effective cell pressure) remained constant. Back pressurizing usually took an hour to reach a desired pressure.

After back-pressuring for about one day, the pore water pressure B-parameter was measured with a base-mounted pressure transducer while the specimen was subjected to an additional undrained increment of confining pressure. B-parameters of 0.98 or better were required to assure saturation and there was no difficulty obtaining saturation by this definition in reconstituted specimens.

When the sepcimen volume had stabilized under a previous loading, the next load was added. Most specimens were consolidated to the desired final pressure (generally 1.0 MPa or 1.5 MPa) using a load increment ratio $(\Delta p'/p') = 1.0$. For the stress-probe tests, the effective isotropic confining pressure was increased in steps to 0.3 MPa, 0.6 MPa, and 1.0 MPa, and then unloaded in steps to 0.75 MPa and 0.5 MPa. This gives an overconsolidation ratio (OCR) of 2. Specimen temperatures were monitored by RTD. The temperature of the specimen and the laboratory were controlled in HITEP testing, but not in B-K testing which experienced room temperature variations of ± 2°C.

74

Temperature changing was done as follows. For heating tests (65°C and 100°C), the temperature was increased with the drainage valve open, giving what has been called "drained heating." The height change and volume change of the specimen were recorded. In some cases the temperature was increased with the drainage valve closed, so-called "undrained heating." Height changes and pore water pressure changes were recorded. For temperature cycling (heating and cooling) tests, an open drainage valve gave "drained temperature cycling", and a closed drainage valve "undrained temperature cycling." The time for heating and cooling was approximately 6 hours from 28°C to 65°C, and 12 hours for 100°C, giving a rate of heating 6°C/hr. For investigation of volume change behaviour due to temperature changes, specimens were first consolidated at 28°C. At a chosen stress level, volume change measurements were then made as the specimen expelled water following periods of heating. Once temperature became constant, the specimen was allowed to reach volume equilibrium under the new temperature. For temperature cycling, the specimen was cooled similar volume measurements taken. These procedures were followed for temperature changes in both normally consolidated and overconsolidated specimens.

4.5.4 Shear

For the stress-probe tests at temperatures of 65°C and 100°C, drained compression shear tests were performed with various predetermined stress paths: $dq/dp' = 3.0$, 0.72, -8.1, -1.5, and isotropic reloading with no shear stress ($dq/dp' = 0$). The stress

paths were controlled by adding dead weights and regulating the cell pressure as necessary. At room temperature (28°C), tests were done along the same stress paths using both the GDS equipment and the B-K system. The GDS equipment was not suitable for tests at elevated temperature. Throughout the shear tests, volume change, displacement, cell temperature, axial load, cell pressure, back pressure, and temperature difference along the specimen were recorded. Step loading for the stress-probe tests was performed as follows. Load increments were determined in such a way that 4 increments were applied before the expected yield stress was reached. A following load increment was added when no volume change was recorded or the axial strain rate became constant under the previous loading (Yarechewski 1993).

For undrained tests, constant strain shear tests were performed. The rate of strain through the shear program was 0.004 mm/min in strain-controlled tests. Undrained tests involved the same measurements as the drained shear tests, but in this case the drainage valve was closed.

4.5.5 Post-test Procedures

In all tests, the shear test was considered finished when large axial displacement took place and there was no sign of decreasing rates of axial strain with time. For the high temperature tests, the cell temperature was first brought down to the room temperature (28°C) either with drainage open in drained shear tests, or without

drainage in undrained shear tests. At this stage, the back pressure valve was closed and piston was clamped. The cell pressure was released to zero and the cell fluid was drained. The specimen was then dismounted from the triaxial cell as quickly as possible to minimize absorption of water from the system. Photographs and sketches of the specimen were taken, and measurements of its diameter, height, and weight carried out. Water content measurement was carried out by cutting the specimens into five layers, and the core and outside of each layer measured for water content by oven drying.

Table 4.2 shows test numbers and the corresponding hypotheses from Chapter 3 examined in the tests. Further details of each of the tests are given in Appendix 2, 3, and 4.

Table 4.2   Test Numbers and hypotheses examined

Soil Type	Temperature	Test No.	Comment	Hypothesis
Reconstituted illite	28-65°C	T1460	N.C	1,4,5
		T1440,T1441, T1442,T1443 T1444,T1445	O.C	1,3,5
	28-65-28°C	T1463	N.C	1,4,5
		T1464,T1468	N.C	2,4,5
	28-65°C	T1465	O.C	2,4,5
		T1466		1,3,4,5,
		T1467	N.C	2,4,5
	28-100°C	T1461	N.C	1,4
		T1450,T1451, T1452,T1453	O.C	1,3,5
		T1472	N.C	2,4,5
		T1473	O.C	2,3,4,5
		T1474	O.C/N.C	1,3,4,5
	28°C	T1490,T1491, T1492	N.C	1,4,5
		T1420	O.C	3,4,5
		T1421,T1422		3,5
		T1480,T1481 T1482,T1483	O.C	1,3,5
		T1486		3,4,5
Compacted illite	28°C	T1485,T1487 T1488,T1489 T1495		3,4,5
	28-65°C	T1446,T1447, T1448		1,3,4,5
		T1469,T1470 T1471		1,2,4,5
Compacted S/B	28°C	T1401,T1403, T1404		3,4,5
	28-65°C	T1402		1,3,4,5
	28-100°C	T1406		1,3,4,5
		T1475		2,3,4,5

4.6 Corrections on Test Data

Due to the remaining leakage or diffusion through the membranes, the measured volume changes of the specimens were corrected on the basis of calibration data from the leakage/diffusion tests mentioned earlier in Section 4.3. At constant temperatures of 65°C or 100°C, the water level in the burette decreased with time during tests. The diffusion rate is constant at a given temperature, so corrections to volume change can be made by adding the loss of water calculated from the measured diffusion rate for a given test duration.

The testing system itself contains some water, for example, in the drainage lines, porous stones, and side drains. The volume of this water increases/decreases depending on heating/cooling due to expansion/contraction of the water. These changes in volume have nothing to do with the actual change in volume of the specimen. Therefore, corrections to measured volume changes must be made to determine the real volume change of the specimen. Calibrations were made using steel dummy specimens with the same set-up as the real soil specimen, that is, top cap, membranes, two porous stones, two filter papers, and side drains. A calculated volume of water was added when specimens were cooled, and subtracted when they were heated.

Height changes were measured in some specimens after temperature changes. Calibrations were again performed using the steel dummy

79

specimens and the system compliance determined. It was felt that these calibrations were not fully accurate, but could be reasonably used to determine the system compliance due to temperature changes. Changes in height were calculated by subtracting/adding the calibrated system compliance from measured height changes depending on heating/cooling.

Membrane stiffness corrections were not applied in this study mainly because Lingnau (1993) showed they were not significant in terms of stress calculations for stiff specimens such as those used in this study.

CHAPTER 5 CONSOLIDATION

As outlined earlier, a series of consolidation tests has been conducted to investigate both the mechanical and the thermal consolidation behaviour of reconstituted illite, compacted illite, and a compacted sand-bentonite mixture. The consolidation tests comprised two stages: (1) mechanical consolidation and (2) thermal consolidation. In mechanical consolidation, the cell temperature was maintained constant during the tests while the pressures were changed. In thermal consolidation on the other hand, the pressures were maintained constant while cell temperature was changed. All specimens were isotropically consolidated. Figure 5.1 shows typical temperatures, pressures, and volume strains during mechanical consolidation of one of the reconstituted illite specimens. Similar results are shown in Fig.5.2 for thermal consolidations. In Fig.5.2(b), the dotted line represents 'raw' readings of volume change while the solid line represents data that have been corrected for diffusion through the membrane. These two figures show that good control was achieved for the applied pressures and temperatures during test periods of about two days.

5.1 Reconstituted Illite

5.1.1 Mechanical Consolidation

Normal consolidation behaviour: Figure 5.3 shows a typical consolidation test result for first loading plotted in volume strain *vs.* time for T1481 at various pressure levels. It can be seen that

the primary consolidation was complete within two hundred minutes and secondary consolidation is small. The end of primary consolidation seems to be independent of pressure level at between 100 and 200 minutes. At the end of consolidation at an effective stress of 1.0 MPa, the volume change is very small (less than 0.1 %/day in volume strain, a criterion used extensively in other programs at the University of Manitoba) so that it can be said that sufficient time was allowed to eliminate the secondary consolidation effect on clay behaviour. For all other specimens, primarily consolidation was complete within 5 hours irrespective of pressure levels.

The effect of back pressure u_b on consolidation behaviour can be seen in Fig.5.4 where effects of two different back pressures, 0.2 MPa and 1.0 MPa, are compared for the same increment of mean effective stress 0.3 MPa-1.0 MPa on two specimens T1443 and T1483. The magnitudes of the volume strains in the two tests are closely similar. The time to the end of primarily consolidation is again about 100-300 minutes, and the shapes of the consolidation curves are similar to those in Fig.5.3. As a result, the figure suggests that changes in back pressure do not produce significant changes in volume change behaviour provided the effective stresses are the same.

Unloading-Reloading behaviour

Specimens were unloaded from 1.0 MPa to 0.5 MPa in two steps of decrement of pressure from 1.0 MPa to 0.75 MPa, and then to 0.5 MPa to give an overconsolidation ratio (OCR) of 2. Typical relationships in the volume change behaviour with time for tests having back pressures of 0.2 and 1.0 MPa respectively are shown in Fig.5.5. Smaller volume strains are recovered during unloading than during equivalent loading (compare Figs.5.3 and 5.4), and the effect of back pressure is again negligible. The curves of volume change with time in unloading are totally different from those in the normally consolidated first loading stage. In the normally consolidated range, the shapes of consolidation curves are S-shaped in ε_v *vs. log*(time) plots, but no such curves are observed in unloading. S-shaped curves are necessary to determine the times of consolidation and hence to calculate the hydraulic conductivities. Because of the different shape of the curves, hydraulic conductivity cannot be evaluated from unloading stages.

In order to examine the dependency of reloading behaviour on temperature, specimens T1460, T1461, and T1474 were reloaded isotropically from 0.5 MPa to 1.5 MPa at elevated temperatures of 28°C, 65°C, and 100°C, respectively. The consolidation behaviour during loading from 1.25 MPa to 1.5 MPa for three temperatures is shown in Fig.5.6. The small volume increases after about 1000 minutes may be due to (a) some leakage or diffusion rates through the membrane, or (b) some uncertainties in pressure control. In all

cases the rate of volume straining at the end of the loading period was close to or below the value $\dot{\varepsilon}_v > 0.1\%$/day that has been used extensively in the University of Manitoba. The volume strain under the same pressure change seem to be independent of temperature. Similar behaviour has been reported in other clays (Finn 1961, Campanella and Mitchell 1968, Tidförs and Sällfors 1989). It is not clear from Fig 5.6, but other tests show that time to complete primary consolidation reduced at higher temperature. Similar results were obtained in a different soil by Kuntiwattanakul (1991).

At the end of consolidation, the B-value, the ratio of an increase of pore water pressure to an increase of cell pressure under isotropic pressure undrained conditions, was evaluated by way of applying a small increment of cell pressure of about 0.1 MPa with the back pressure valve closed. The resulting change in pore water pressure was measured. Values of $B = \Delta u / \Delta \sigma_{cell}$ were always close to unity indicating the specimens were saturated.

5.1.2. Thermal Consolidation

In order to investigate the effect of temperature on specimen volume during consolidation, heating was performed at 0.5 MPa for overconsolidated specimens, and 1.5 MPa for normally consolidated specimens, respectively. Drainage was allowed throughout heating. As a result, the effective stress (here defined by $\sigma_{cell} - u_b$) was kept constant.

Typical experimental results of thermally induced volume changes of specimens as a function of time are presented in Fig.5.7. The volume strains were calculated from water expelled from the specimens at the constant effective stress of 0.5 MPa during heating from 28°C to 65°C and from 28°C to 100°C, respectively. In general, the curves in Fig.5.7 are similar to those obtained from mechanical consolidation, although the equalization times (around 600-800 minutes) appear somewhat longer (compared Figs.5.2 and 5.3). The duration of heating from 28°C to 100°C at the selected rate of 6°C/hr is 720 minutes. This is about equal to the equalization times for mechanical loading, and may explain the slightly longer times required for thermal equalization. The heating rates are about 3 to 5 times larger than were used in similar tests at ISMES. The apparently increasing volumes after about 1000 minutes may be due to some effects of thermal changes on interparticle reactions, to leakage and diffusion through the membranes, or to thermal compliance of the system. The data in Fig.5.7 have not been corrected for diffusion rates, though these corrections will be applied in later discussions (Chapter 6). Thermal consolidation seem to be complete in about 1000 minutes. The volume of water expelled during heating is larger at higher temperature. The shapes of the volume change curves are similar at both temperatures.

Figure 5.8 shows similar results from drained thermal consolidation at 1.5 MPa. Again, water was expelled from the specimen during heating, and the volume of water expelled depends on temperature,

85

with a higher magnitude of volume change being observed at higher temperature.

In order to investigate the effects of a temperature reversal, temperatures were cycled by heating followed by cooling under constant effective pressure. Results of such a test are shown in Figs.5.9 and 5.10. In Fig.5.10, results from monotonic heatings are also shown for comparison purposes, and arrows only indicate the process of heating, not the actual temperature-volume strain path.

Thermally induced volume strain upon cooling is apparently less than that upon heating, implying a reduction in specific volume after the temperature has been through a heating-cooling cycle. Thus, a temperature cycle produces irreversible volumetric strain in soil. As mentioned in Chapter 2, similar results were obtained in other soils (Campanella and Mitchell 1968, Demars and Charles 1982, Hueckel *et al*. 1987, Kuntiwattanakul 1991). This observation can be interpreted in a mechanical sense that the soil becomes overconsolidated due to an irreversible volume strain upon a temperature cycle of heating-cooling, even though there has been no physical change in effective stress loading. Generally however, strains produced by heating or cooling appear to be smaller than those produced by loading or unloading.

5.1.3. Summary of Consolidation on Reconstituted Illite

The graphs shown in Figs.5.7 and 5.8 for thermal consolidation were not corrected for membrane diffusion or system compliance. Subsequently, corrections for these effects were applied to volume measurements at the end of each of the load increments. These corrected consolidation results are summarized in the specific volume V *vs.* mean effective stress p' relationships shown in Fig.5.11. The figure shows specific volumes decreasing with temperature at a given pressure. At 28°C, the data at pressures above 1.0 MPa indicate a compression index similar to the average value (dotted) from all other tests in the program. (The 1.0 MPa pressure was the previous highest loading experienced by the specimen before unloading and reloading.) At elevated temperatures, the curves approach the same slope as the 28°C data, but at successively lower specific volumes. This supports the Hypotheses 1 and 5 in Chapter 3 that normal consolidation lines at different temperatures are parallel. The separation of normal consolidation lines for the temperature differences 28°C-65°C, and 65°C-100°C becomes approximately independent of pressure levels. For both normally consolidated and overconsolidated illite specimens, monotonic heating produces compressive volume change. However, as noted in Fig.5.9, if a specimen is cooled after heating, not all of the volume change is recoverable. It will be shown later that this will produce overconsolidated behaviour.

These tests also lend some support to the idea mentioned in Chapter 3 that the slopes κ of unload/reload lines increase with temperature (Hypothesis 5). It is accepted that the data are not conclusive on this point. The variation of the slope κ of the unload/reload line can probably be explained by changes in the structure of adsorbed water surrounding the clay particles.

5.2. Compacted Illite

5.2.1. Mechanical Consolidation

Consolidation is here taken to mean isotropic loading with open drainage. Compressive and expansive volume changes may be observed depending on stress level.

All but one of the compacted illite specimens were loaded directly to $p' = 1.0$ MPa at beginning of the tests. The remaining specimen (T1485) started from $p' = 0.1$ MPa. The solid line in Fig.5.12 shows a typical relationship of volume strain *vs.* time for the loading $p' = 1.0$ MPa. Characteristic curves for volume change of compacted illitic clay are different from those for reconstituted illite (compare Figs.5.3 and 5.12). Even at a high effective pressure of $p' = 1.0$ MPa, the specimens expanded, suggesting that compaction had produced the equivalent of a preconsolidation pressure that must be higher than 1.0 MPa. After consolidation at 1.0 MPa was complete, specimens were unloaded to 0.5 MPa and further expansion was observed. These unloading relationships are similar to those during unloading of reconstituted illitic clay.

88

5.2.2. Thermal Consolidation

In a way similar to that used for reconstituted illite, thermal consolidation was performed on the compacted illite specimens once mechanical consolidation was complete.

Fig.5.13 shows the thermal consolidation behaviour of two compacted illite specimens at effective pressured of 0.5 MPa and 1.0 MPa during heating from 28°C-65°C. As in reconstituted illite, the curves of volume strain vs.time are again generally similar to those for mechanical consolidation. Corrections for system compliance, diffusion, etc. have not been applied in Fig.5.13. The varying behaviour after 1000 minutes is due to variations in pressure control. Water was expelled from the specimens due to the net effect of compression of adsorbed water (Chapter 2), and thermal expansion of the clay particles and the pore water. This will be discussed more fully in Chapter 6.

5.2.3 Summary of Consolidation on Compacted Illite

Plots of specific volume V vs. mean effective stress p' are shown in Fig.5.14 for an unload-reload cycle on compacted illite specimens at 28°C. The slope of the unloading segment is almost equal to that of the reloading segment and can be considered reversible. The figure also shows the NCL and URL for reconstituted illite for comparison purposes. The consolidation curve (V vs. log p', where V is specific volume and p' mean effective pressure) for the statically compacted specimen (Fig.5.14) has flatter slope than that for

89

specimens consolidated from slurry (Fig.5.11), indicating development of an apparent preconsolidation pressure as a result of compaction. The slope of the unload-reload line in the V-$\ln$ p′ plots in Fig.5.14 is about 0.02, which is close to the value for the unload-reload line for reconstituted illitic clay. These observations support the suggestion in the previous section that the compacted illitic clay was initially overconsolidated during the compaction process. The measured compaction pressure of the piston ram during compaction was approximately 5 MPa, although whether all of this was experienced by the soil particles during the short period of compaction must be considered doubtful. This produced the soil to be overconsolidated. Similar observations have been reported in highly plastic Regina clay (Yang and Barbour 1992).

5.3. Sand-bentonite Mixture (Buffer Material)

5.3.1. Mechanical Consolidation

Three tests were done on buffer under conditions where consolidation was performed at room temperature under a succession of isotropic pressures. (A much larger series of such tests was reported by Lingnau 1993). The tests were done to examine the influence of stress history on volume change behaviour and shear behaviour, and in particular to examine the uniqueness of the swelling equilibrium line (SEL). The results of these tests are compared with results of a single-increment loading test in which a given effective pressure was applied at the beginning of consolidation.

Figure 5.15 shows results from specimen T1403 which was initially consolidated to 0.5 MPa. As always in this work, compressive volume strain is considered positive. Once initial consolidation was complete ($\dot{\varepsilon}_v < 0.1\%$/day) the effective pressure was reduced to 0.29 MPa which would usually be considered to give an overconsolidation ratio (OCR) p_1'/p_2', of 1.72. When the volume change rate criterion was again satisfied, the effective pressure was returned to its original value of 0.5 MPa. Subsequent loading took the consolidation pressure to 1 MPa, then to 0.69 MPa ($p_3'/p_4' = 1.44$), and finally back to 1 MPa. After consolidation was complete, the specimen was sheared undrained in the usual way with pore water pressure measurement.

The loading sequences for the three specimens tested in this way can be summarized as follows.

T1403 – isotropic consolidation: 0.5 MPa, 0.29 MPa, 0.5 MPa, 1.0 MPa, 0.69 MPa, 1.0 MPa.

T1404 – isotropic consolidation: 1.0 MPa, 0.67 MPa, 1.0 MPa.

T1405 – isotropic consolidation: 1.0 MPa, 0.58 MPa, 1.0 MPa, 1.5 MPa, 0.87 MPa, 1.5 MPa.

Results are shown in Fig.5.16 for T1404; and in Fig.5.17 for T1405.

These three tests were done at room temperature in the Brainerd-Kilman (B-K) cells described in Chapter 4 (also see Graham *et al.*

91

1992). The room temperature was not well controlled during these tests (average of 23°C with a variation of about ±2°C). However, it has been shown that this should not produce noticeable change in the results for buffer (Lingnau 1993).

The consolidation results from these three specimens are summarized in Fig.5.18 which shows $ln\ p'_{cons}$ vs. V_c, the specific volume of the clay-water phase. Some additional results are also included from single-increment specimens. The data have been drawn with two sets of symbols, with closed symbols representing "equilibrium" ($\dot{\varepsilon}_v < 0.1\%$/day) at the end of loading increments, and open symbols representing conditions at the end of loading decrements. The result in V vs. ln p′ relationship can be expressed by the equation:

[5.1] $$ln\ V_c = 1.346 - 0.071\ ln\ p'_{cons}\ :\ R^2 = 0.90$$

Saadat (1989) obtained similar results on sand-bentonite specimens.

Two things are immediately apparent from this figure. One, scatter in these data appears to be rather less than from the main program of single-increment specimens that typically start from slightly different initial specific volumes following compaction (for example, Graham et al. 1992). Two, although not shown in the figure closely spaced parallel lines could be drawn to represent results

coming respectively from the end of "compression" increments, and from "swelling' decrements in pressure. The difference in V_c between the two lines is not large (about $\Delta V_c = 0.005$) compared with the scatter that has been seen in the larger program managed by Dr.Graham at the University of Manitoba. This suggests that the concept of a Swelling Equilibrium Line" (SEL) that has been a feature of publications on buffer from the University of Manitoba has a reasonable basis in experimental evidence. The SEL has been thought of as similar in many ways to a normal consolidation line NCL.

However, it is also fair to comment that a specimen whose volume strain rate $\dot{\varepsilon}_v$ is less than the arbitrarily chosen value of 0.1%/day is still not fully equilibrated. Graphs of ε_v vs. elapsed time such as those shown in Figs.5.15, 5.16, and 5.17 can be extrapolated to lower values of ε_v for compression cycles, and to higher values of ε_v for expansion cycles. After conversion to specific volumes, the extrapolated values (representing true equilibrium conditions) lie between the two lines drawn in Fig.5.18. The fact that the specimens are not fully equilibrated at volume strain rates of 0.1%/day means that some differences of stress-strain and pore pressure behaviour can be expected during shear, depending on whether the specimens have been loaded or unloaded to their stress state at the end of consolidation (that is, the beginning of shear). Shear behaviour of buffer will be discussed in later section.

The expansive/compressive behaviour of these specimens is also related to swelling pressure, which is currently thought to be in the range of 1.5 - 2.0 MPa for high density buffer (ρ_d = 1.67 Mg/cm^3). Earlier testing has shown that specimens tested at consolidation pressures lower than the swelling pressure are still swelling slowly at the end of consolidation ($\dot{\varepsilon}_v$ = 0.1%/day), and tend to show dilative behaviour in shear. Conversely, specimens tested at higher pressure, are still compressing at the end of consolidation, and show compressive behaviour in shear.

Although the idea of a Swelling Equilibrium Line is attractive, the picture it represents may be oversimplified. Plots of specific volume V *vs.* mean effective stress p' for compacted illitic clay were shown in Fig.5.14. They show good reversibility, and suggest that the compacted illite specimen behaves much like an elastic material. It was suggested earlier that compaction may have produced the effects of overconsolidation. The slope of the unload-reload line in V-*ln* p' space is about 0.02, which is close to equivalent value for reconstituted illitic clay, but less than the first-loading curve for reconstituted illite from slurry.

Despite previous emphasis on the "Swelling Equilibrium Line" being much like a normal consolidation line, the author believes that the consolidation of compacted sand-bentonite mixtures may need to be reconsidered as an unload-reload phenomenon. Upon unload-reloading in Fig.5.18, the consolidation behaviour has been seen as a

94

reversible process in a range of consolidation pressure of 0.25 MPa to 1.5 MPa. The slope of the consolidation line in Fig.5.18 is 0.11, a value that is very much smaller than measured by Olson and Mesri (1970) values of $\lambda \geq 1.43$ and $\kappa \geq 0.619$ for Wyoming bentonite at pressures ranging from 0.5 MPa to 5.0 MPa. A similar conclusion may be drawn from the survey by Dixon *et al.* (1991) of different methods of measuring swelling pressure.

5.3.2. Thermal Consolidation

After mechanical consolidation to 1.5 MPa, the sand–bentonite specimens were heated with the drainage leads open, and the cell pressure and back pressure held constant to keep mean effective stress constant. The rate of heating was about 6°C/h. Figure 5.19 shows volume of water expelled during heating with time. Curves of reconstituted and compacted illites were shown in Figs. 5.7, 5.8, and 5.13. The volume of water expelled from the specimen during heating form 28°C to 100°C is greater than that for heating to 65°C. Less water was expelled from the sand–bentonite mixture during heating than from reconstituted or compacted illites. The curves for thermal consolidation of sand–bentonite buffer in Fig.5.19 are different from those in mechanical consolidation.

5.3.3. Summary of Consolidation on Sand–bentonite Mixture

It may be noted from the ramped pressure tests summarized in Fig.5.18 that compacted sand–bentonite shows a high level of reversible volume change behaviour when the loading is reversed.

95

Two reason may be suggested to explain this reversibility. One, the material may be 'elastic' in the way that all overconsolidated soils are elastic. This would imply that compression loads during compaction have the effect of pre-consolidating the material. Two, the pronounced swelling/compression behaviour of the bentonite component may mean that the concept of "overconsolidation" in sand-bentonite is not relevant, and all specimens are essentially normally consolidated in the way suggested for example by Oswell (1991). This question will be discussed further when the behaviour in shear is being examined in Chapter 7.

Thermally induced volume strains are compressive, with higher temperatures producing larger thermally induced volume changes.

5.4 Discussion and Conclusion

Graphs of ε_v vs. elapsed time for sand-bentonite mixtures (Figs.5.15, 5.16, and 5.17) show the volume change behaviour is quite different from reconstituted and compacted illite specimens, respectively. This is due to the high surface activity of the sand-bentonite mixture reflected by its high plasticity ($w_L = 112\%$, $I_p = 92\%$) compared with the illitic clay ($w_L = 30\%$, $I_p = 9\%$). As a result of the high surface activity, time dependent behaviour is dominant in the sand-bentonite mixture, and it does not behave like more usual soils. The consolidation behaviour is due mainly to a time-dependent creep mechanism rather than the more usual process of dissipation of excess pore water pressure.

Saadat (1989) showed that V_c depends on the consolidation pressure p'_{cons}, the initial compaction density V_{ci} and the duration of consolidation t.

[5.2] $ln\ V_c = 1.609 - 0.099\ ln\ p'_{cons}$: $R^2 = 0.95$

[5.3] $ln\ V_c = 1.367 - 0.075\ ln\ p'_{cons}$: $R^2 = 0.89$

The above two equations for consolidation behaviour for low and high density buffer show that if these relationships are taken as elastic behaviour, the slopes of reload/unload relationship are 0.099 for lower density and 0.075 for higher density. It is likely that the lower density buffer behaves like a normally consolidated common clay in terms of its volume-pressure relationship.

From all data in consolidation, the virgin compression line and unload/reload line are tabulated in Table 5.1 in which the slope of unload-reloading line for compacted sand-bentonite specimens is taken as κ.

Table 5.1 Consolidation parameters

Soil Type	λ			κ		
	28°C	65°C	100°C	28°C	65°C	100°C
Reconstituted illite	0.087	0.087	0.087	0.021	0.029	0.035
Compacted illite	–	–	–	0.019	–	–
Compacted buffer	–	–	–	0.084	–	–

97

CHAPTER 6   THERMAL EXPANSION AND THERMALLY INDUCED PORE WATER PRESSURE UNDER ISOTROPIC STRESS CONDITIONS

Temperature changes cause soils to contract or expand. These volume changes can be expressed using the idea of a coefficient of thermal expansion. However, since soil behaviour is noticeably non-linear, thermal expansion coefficients will not be constant, but will vary with temperature. The coefficient of thermal expansion of soil is an important parameter for the prediction of thermally induced stress changes and ground deformations. It is also known that pore water pressures are changed by temperature change, and that this can result in effective stress changes defined as total stress minus pore water pressure. Thus, thermally generated changes in pore water pressure may have a major impact in determining soil behaviour which is controlled by effective stresses. This chapter discusses fundamental definitions of coefficients of thermal expansion, and presents results from the experimental program.

It must be recognized at once that the results in this chapter are sparse and do not constitute fully convincing experimental evidence for the statements that will be made. The experimental program was primarily designed to examine the hypotheses listed in Chapter 3. This work on thermal expansion arose as a complementary way of analyzing data collected for different purposes. However, the results have been reviewed in light of other data reported in the literature, and the conclusions that have been drawn are believed to be supportable.

6.1 Definition of Thermal Expansion

In thermodynamics, volumetric thermal expansion is defined by

$$(6.1) \qquad \beta = \frac{1}{V} \left(\frac{\partial V}{\partial T} \right)_{\sigma}$$

where V is the initial volume, ∂V the volume change due to temperature change, ∂T the magnitude of temperature change. The differential coefficient is found under conditions of constant applied stress σ. The value of the coefficient of thermal expansion is taken as positive when the material expands. In soil, however, two different boundary conditions can be encountered. One is thermal expansion under undrained conditions, while the other is thermal expansion under drained conditions. A lower bound value of the volumetric thermal expansion may be determined by performing drained heating experiments in which the effective stress is kept constant during heating (Agar *et al.* 1986). A constant pore water pressure is maintained during drained experiments by heating sufficiently slowly to permit excess fluid pressures to dissipate continuously by drainage. The drained thermal expansion coefficient β_{DT} can be defined as

$$(6.2) \qquad \beta_{DT} = \frac{1}{\Delta T} \left(\frac{\Delta V}{V} \right)_{D} = \frac{1}{\Delta T} \, \varepsilon_{vDT}$$

where ΔV is the volume of water drained from specimen and accounts for both thermal expansion of the water phase, and changes in volume (expansion or contraction) of the particle skeleton; and ε_{vDT} is the volume strain induced by temperature change under drained

99

conditions. This definition of β_{DT} differs in some respects from that used by Campanella and Mitchell (1968), and is an alternative to the expression for thermal expansion coefficient given in eqn. (6.1).

An upper bound for the magnitude of thermal expansion can be determined by conducting undrained heating experiments in which pore fluid drainage is prevented (Agar *et al.* 1986). The magnitude of undrained thermal expansion depends on the volumetric expansion of both the matrix of mineral solids and the pore fluids. The undrained coefficient of thermal expansion β_{UT} may be expressed as

$$(6.3) \qquad \beta_{UT} = \frac{1}{\Delta T} \left(\frac{\Delta V}{V} \right)_U = \frac{1}{\Delta T} \varepsilon_{vUT}$$

where ε_{vUT} is the volume strain induced by temperature change under undrained conditions. Strictly speaking, a coefficient of undrained thermal expansion is not same as the thermal expansion defined in thermodynamics because effective stresses change with temperature. However, the term "undrained thermal expansion" will be used in the following discussion because it provide insight into the effects of temperature on volume change, and the relationship between β_{UT} and thermally induced pore water pressures Δu_T. All data for drained thermal expansion presented in this sections were corrected for the expansion of water contained in the testing system outside of the specimen, that is, in the porous stones, drainage tubes, filter

100

papers, side drains, etc., and for diffusion through the membranes. For undrained thermal expansion calculations, corrections were applied for thermal expansion of the testing system.

6.2 Drained Thermal Expansion β_{DT}

Figure 6.1 shows coefficients of drained thermal expansion β_{DT} calculated using eqn.(6.2) for both normally consolidated and overconsolidated reconstituted illite. Values of thermal expansion coefficients in this chapter have been calculated from measured volume changes ΔV for a temperature change ΔT from T_1 to T_2. In each case, T_1 has been taken as 28°C, and the values at T_2 are therefore average values in the range T_1 to T_2. The data are relatively limited, and so the lines fitted through the data points should be considered as guidelines. Because water is expelled from specimens during heating and the specimens actually compress, the coefficient of drained thermal expansion is taken as negative according to the definitions discussed previously. Figure 6.1 indicates that drained thermal expansion coefficients of normally consolidated specimens seem to decrease nonlinearly and become increasingly negative with temperature. Similar results have been reported by Campanella and Mitchell (1968) and Hueckel et al. (1987) for other soils. Values of the coefficients of drained thermal expansion for normally consolidated specimens are -2.2×10^{-4} (°C^{-1}) at 65°C and -3.4×10^{-4} (°C^{-1}) at 100°C, taking a reference temperature as 28°C.

On the other hand, drained thermal expansion coefficients for overconsolidated specimens seem to be approximately the same at 65°C and 100°C in Fig. 6.1, although some scatter is evident in the data. The thermal expansion coefficients for overconsolidated specimens seem to be larger (less negative) than those for normally consolidated specimens. An average value of -1.5×10^{-4} (°C^{-1}) was obtained with reference to the volume at 28°C.

As can be seen from Fig. 5.10, thermally induced strains upon cooling after first heating are less than those generated by first heating. Coefficients of drained thermal expansion upon cooling can be calculated with the same way as for heating. Figure 5.10 shows straight dotted lines joining data for 28°C and 65°C. This should not be taken as the true relationship, since the other specimen heated from 28°C to 65°C and then 100°C shows non-linear behaviour. It should be remembered that volumetric equilibrium was really only established at the three temperatures used in the program, namely 28°C, 65°C, and 100°C. A single result is shown in Fig.6.1 for a normally consolidated specimen. (This specimen expanded upon cooling: the sign of the volume change has been changed to assist comparison.) The value shown in Fig.6.1 is less than upon the first heating, and is approximately similar to those obtained from overconsolidated specimens. This suggests that upon cooling, specimens might be overconsolidated in terms of their mechanical behaviour. Similar results have been reported by Campanella and

Mitchell (1968), and Hueckel *et al.* (1987). The effect of cooling on overconsolidation will be discussed further in Chapter 8.

Figure 6.2 shows coefficients of thermal expansion of compacted illite specimens at two different consolidation pressures of 0.5 MPa and 1.0 MPa. Data are in this case only available for tests heated from 28°C to 65°C. For comparison purposes, the lines in Fig.6.1 describing the coefficients of drained thermal expansion for normally consolidated and overconsolidated reconstituted illites have been replotted in Fig.6.2 as dotted lines. The values are broadly similar to those for overconsolidated reconstituted illite, but there may be some indication of stress dependency in the results. At 0.5 MPa, values of drained thermal expansion seem to be smaller (more negative) than the average for results at 1.0 MPa. The observation that (negative) thermal expansions vary with temperature and pressure support hypothesis No.5 in Chapter 3 that the slope κ of unload-reload lines depend on temperature.

Figure 6.3 shows results of coefficients of drained thermal expansion of sand-bentonite buffer from 28°C to 65°C and to 100°C. The results for thermal expansion of reconstituted illite in Fig.6.1 are again shown in the figure for comparison purposes. Figure 6.3 clearly shows that coefficients of drained thermal expansion of the sand-bentonite buffer is much larger (less negative) than those of both reconstituted and compacted illite specimens.

6.3 Thermal Expansion of Pore Water β_w

Section 6.2 discussed the drained thermal expansion of bulk soil consisting of a combination of pore water and soil particles. This section examines the thermal expansion of pore water by considering the volume change of pore water in soil. The coefficient of thermal expansion of pore water in drained heating can be calculated as

$$(6.4) \qquad \beta_w = \frac{1}{\Delta T} \left(\frac{\Delta V_w}{V_w} \right)_D$$

where ΔV_w is a corrected volume of drained water during heating, V_w is the volume of pore water before heating, and ΔT is the magnitude of the temperature increase. This calculation allows estimation of coefficients of thermal expansion of pore water in the soil, and hence comparison with those of free (pure) water.

Figure 6.4 shows results of coefficients of thermal expansion of pore water calculated for both normally consolidated and overconsolidated reconstituted illite specimens. Figure 6.4 also shows coefficients of thermal expansion of free water (Dixon *et al.* 1993) for comparison purpose. For normally consolidated specimens, the coefficients of thermal expansion of pore water appear to have values that are broadly similar to those of free water at both 65°C and 100°C. Similar results has been reported on pore water of other soils (Kuntiwattanakul 1991, Dixon *et al.* 1993). It has also been reported that at about 70°C the special structure of adsorbed water

104

is gradually destroyed (Derjaguin *et al.* 1986, Dixon *et al.* 1993). This is compatible with Fig.6.4 where pore water in normally consolidated illite may have similar characteristics to those of pure water at temperatures of both 65°C and 100°C.

On the other hand, Fig. 6.4 clearly shows thermal expansions of pore water in overconsolidated illite that are less than those of pore water in normally consolidated illite and of pure water, even at 100°C. Campanella and Mitchell (1968) showed that the first temperature cycle of heating-cooling produced irrecoverable volume changes on illite specimens. Volume changes during the second heating were much less than those during the first heating, and close to those during the first cooling. This indicates that the thermal expansion of pore water depends on the history of temperature cycling. It can be concluded from Campanella and Mitchells' data that after the first temperature cycle of heating-cooling, specimens behave as if lightly overconsolidated in a mechanical sense. Calculated values for thermal expansion of water taken from Campanella and Mitchell (1968), show clearly that the second heating produces less thermal expansion than the first heating, 4.0×10^{-4} ($°C^{-1}$) compared with 9.0×10^{-4}($°C^{-1}$). These values are in good agreement with the author's data in Fig. 6.4 and confirm that thermal expansion of pore water in overconsolidated specimens is less than in normally consolidated specimens. Figure 6.4 also shows that coefficients of thermal expansion of pore water in overconsolidated illite are independent of temperature.

Coefficients of thermal expansion of pore water in compacted illite are shown in Fig. 6.5. Although there is again scatter in the data, values of thermal expansion coefficients of pore water in compacted illite are less than those for both free water and for the pore water in normally consolidated illite. Pressure level may affect the value of thermal expansion of pore water in compacted illite. The single measured value for a consolidation pressure of 1.0 MPa is higher than the average (and towards the upper end of the range) from 4 tests at 0.5 MPa. Values of thermal expansion of pore water in compacted illite at 0.5 MPa and 1.0 MPa in Fig.6.5 are close to the values for reconstituted overconsolidated illite (OCR = 2) in Fig. 6.4. This may indicate that the specimens of compacted illite are also overconsolidated at 0.5 MPa and 1.0 MPa, perhaps due to compaction process, as mentioned previously.

Figure 6.6 shows results that have been calculated for the thermal expansion of the pore water in sand-bentonite mixture at a consolidation pressure of 1.5 MPa. The resulting thermal expansions of pore water are much less than those of pure water, and even less than those in compacted illite. In contrast, Dixon *et al.* (1993) showed that the coefficients of thermal expansion of pore water in compacted sand-bentonite are close to those of pure water at temperatures above 80°C. However, their tests were done in a confined cell under the constant volume conditions which are different from the constant effective stresses in the triaxial tests performed in this study. Palciauskas and Domenico (1982) suggested

that under constant volume conditions, much higher pore water pressures are generated by heating than under constant total stress conditions. This indicates that the amounts of water drained form the specimens during drained heating under the constant volume conditions in the tests by Dixon *et al.* (1993) are larger than under the constant stress conditions in this study, which allow thermally induced pore water pressure to dissipate. In this way, it is reasonable to expect the coefficient of thermal expansion of pore water under constant volume conditions to be larger than that under constant stress conditions. The constant volume conditions in Dixon's tests are probably a better representation of likely conditions in a nuclear waste disposal vault.

6.4 Undrained Thermal Expansion β_{UT}

Approximate values for coefficients of undrained thermal expansion of reconstituted illite, compacted illite, and compacted sand-bentonite buffer have been calculated from changes in the measured height of specimens after temperature change, assuming that the thermal volumetric expansion strain is three times the axial strain induced by temperature change, that is, that thermally induced straining is isotropic. Experiments were carried out at effective mean pressures ranging from 0.5 MPa to 1.5 MPa, with OCR's of 1.0 and 2.0, with cell pressure being kept constant during heating or cooling. Drainage of pore water from the specimens was not permitted during undrained heating (*bulk undrained heating*). In some cases after bulk undrained heating, the calibrated mass of

water in the measurement system due to temperature changes was released by opening the drainage valve. The specimen mass, therefore, can be said to have remained constant (*constant mass heating*) during heating, although the specimen volume will have changed. Cooling after heating was also done under undrained conditions. For constant-mass tests, a mass of water required by system calibration was injected after cooling in order to keep the mass of the specimen constant. In other tests, no drainage was permitted during a heating-cooling cycle, and the resulting coefficient will be referred to as a "bulk expansion" coefficient. Changes in both pore pressure and height of specimen were measured during heating-cooling cycles.

Figure 6.7 shows coefficients of undrained thermal expansion of reconstituted illite plotted against the temperature at the end of heating. The figure shows a combination of coefficients of undrained thermal expansion for both normally consolidated and overconsolidated specimens from both constant-mass and bulk undrained tests. It can be expected that undrained thermal expansion coefficients for constant-mass tests will be less than for bulk undrained thermal expansion due to the release of water after heating in the former case. The sparse data in Fig. 6.7 provide insufficient evidence to decide whether coefficients of undrained thermal expansion decrease or increase with temperature. However, knowledge of the results from oil sands reported by Agar *et al.* (1986), make it reasonable to assume that the coefficient of

undrained thermal expansion is essentially independent of temperature and stress history. The approximate value of the coefficient of undrained thermal expansion for reconstituted illite is about 2.0×10^{-4} (°C^{-1}), a value similar to that obtained by Agar and his colleagues for oil sands.

Figure 6.8 shows these results for the coefficient of undrained thermal expansion of compacted illite and compacted sand-bentonite. Again, the scatter is considerable, and the data sparse. However, the coefficients of undrained thermal expansion of compacted illite and compacted sand-bentonite seem to be broadly similar, independent of temperature, and of the same order as those for reconstituted illite (Fig.6.7).

6.5 Thermally Induced Pore Water Pressure Δu_T

A study has also been made of pore water pressures induced by temperature change under constant isotropic total stress conditions. Specimens were initially consolidated at room temperature (28°C) under various pressures ranging from 0.5 MPa to 1.5 MPa. After mechanical consolidation was complete, the drainage valve was closed. The temperature was then increased to a desired value, and in some cases, decreased afterwards. The process of heating and/or cooling usually took 12 hours for 65°C and 24 hours for 100°C. After the temperature stabilized, changes in pore water pressure and specimen height were measured.

Figure 6.9 shows the results of pore water pressure induced by temperature changes in reconstituted illite. The figure shows that increases in temperature cause increases in pore water pressure during undrained heating. These result in reductions of effective stress defined as constant total stress minus pore water pressure. The magnitude of the observed reductions is significant and can be expected to affect the soil behaviour in shear. This topic will be discussed in Chapter 8. Thermally induced pore water pressures for constant-mass heating tests are less than those for bulk-undrained heating tests. (The dotted lines in Fig.6.9(b) have been imported from Fig.6.9(a) to represent bulk-undrained behaviour.) This is due to the release of water in the former procedure to take account of system compliance upon heating.

The effects of pressure level on thermally induced pore water pressure are also shown in Fig. 6.9. Higher consolidation pressures produce higher pore water pressure increases than lower consolidation pressures for a given temperature increase. Similar results have been reported for other soils (Borsetto *et al.* 1984, Agar *et al.* 1986, Houston and Lin 1987). The rate of increase of thermally induced pore water pressure Δu_T with temperature is clearly nonlinear in Fig.6.9.

The test program also investigated the effect of stress history on thermally induced pore water pressure in terms of overconsolidation ratio OCR. Results for both normally consolidated and

overconsolidated specimens are presented in Fig. 6.10. Normalization of thermally induced pore water pressure Δu_T with respect to preconsolidation pressure p'_c is shown in Fig. 6.10(a), and with respect to consolidation pressure p'_0 in Fig. 6.10(b). It will be remembered that $p'_0 = p'_c$ for normally consolidated specimens. As expected, differences between results from normally consolidated and overconsolidated specimens diminish considerably in the normalization by p'_0 in Fig.6.10(b). Despite this, there are some advantages to using the preconsolidation pressure p'_c. Calling upon the effective stress concept, $\Delta u = -\Delta p'$, so Fig.6.10 also shows how much reductions of effective stress is produced upon heating. At 100°C, for example, the effective stress in normally consolidated specimens is reduced to 55% of the initial effective stress at 28°C. For overconsolidated specimens, similar reductions of effective stress can be predicted as long as the preconsolidation pressure is known before heating.

Figure 6.10(a) also shows that thermally induced pore water pressures for normally consolidated specimens are broadly reversible upon a temperature cycle of heating followed by cooling. However, this is not true for overconsolidated specimens which appear not to be reversible. This is consistent with data by Campanella and Mitchell (1968) where a hysteresis loop was found upon temperature cycling in lightly overconsolidated specimens. In the illite specimens, pore water pressures upon cooling to the original temperature were lower than they were before heating. However, upon

111

re-heating, the pore water pressure recovered to its original value before the temperature was cycled.

Figure 6.11 shows results of normalized pore water pressures induced by heating specimens of compacted illite. Normalization was performed in this case using the consolidation pressure p_0'. As in reconstituted illite, heating caused increases in pore water pressure in compacted illite, and corresponding reductions in effective stress. The magnitudes of the increases in pore water pressure, and hence the reductions of effective stress, in compacted illite specimens, are similar to those for overconsolidated illite specimens. This again suggests that compacted illite specimen are overconsolidated.

Figure 6.11 also includes one result of normalized pore water pressure change induced by heating for compacted sand-bentonite. Consolidation pressure p_0' was again used for normalization. The figure shows that heating sand-bentonite to 100°C produces smaller reduction of effective stress than the same heating in illite specimens. Irreversibility of pore water pressure was again observed upon cooling to 28°C.

112

6.6 Discussion and Conclusion

Figure 6.12 summarizes results of thermal expansion coefficient measurements for both drained and undrained specimens of illite and sand-bentonite. Several conclusions can be drawn from these results.

For normally consolidated clay, coefficients of drained thermal expansion (DTE) depend on temperature, stress history, and soil type. The absolute value of the coefficient of drained thermal expansion increases with temperature, but is independent of pressure levels. However, in overconsolidated specimens, the coefficient of thermal expansion depends on stress levels. At higher OCR values (lower stress levels in these tests where p'_c = constant), the value of β_{DT} tends to be smaller. In all cases, β_{DT} is negative. That is the volumes of specimens decrease upon drained heating. The magnitude of β_{DT} seems to be approximately constant with temperature for overconsolidated specimens. Higher plasticity soil such as the compacted sand-bentonite mixture has lower coefficient of drained thermal expansion than lower plasticity soil such as illite.

Coefficients of thermal expansion of the pore water depend on pressure level, stress history, magnitude of the increase in temperature, and soil type. The boundary conditions during testing, for example whether the tests are run at constant volume or constant effective stress, are important factors, so attention has been paid to these conditions when using values of thermal expansion. It has

113

also been reported that most pore water in high plastic clay is adsorbed to clay particles, and that the characteristics of adsorbed water are different from those of free water (Low 1979). At about 70°C the special structure of adsorbed water appears to be gradually destroyed (Derjaguin *et al.* 1986, Dixon *et al.* 1993). The complex characteristics of pore water may explain the lower coefficients of thermal expansion that have been measured.

Interestingly, the coefficient of undrained thermal expansion β_{UT} seems to be independent of stress level, stress history, temperature change, and soil type. An average value of 2.0×10^{-4} (°C^{-1}) has been obtained from both the illite and the sand-bentonite specimens that have been tested. Values of thermal expansion for soil minerals and for free water are respectively about 0.35×10^{-4} (°C^{-1}) and greater than 5.0×10^{-4} (°C^{-1}), respectively. These values explain how the results for undrained thermal expansion shown in Fig.6.13 result from the volumetric expansion of both the matrix of mineral solids and the pore fluids.

As has been seen in the previous section, the magnitudes of thermally induced pore water pressures depend on pressure level and stress history. It has been reported that thermally induced pore water pressures depend on the compressibility of the soils (Campanella and Mitchell 1968), and on the magnitude of the temperature increase (Houston and Lin 1987). These features are also been seen in results reported in this chapter. The unload-

114

reload compression parameter κ (in V-$ln\ p'$ space) is about 0.02, which is lower than the value 0.07 measured for compacted sand-bentonite. The non-linearity and reversibility of thermally induced pore water pressures reported in this study (and also by Campanella and Mitchell 1968, and Houston and Lin 1987), can be explained by the results from constant undrained heating. Predictions and further discussion of thermally induced pore water pressures will be presented later in Chapter 10.

CHAPTER 7   DRAINED STRESS-PATH TESTS AND YIELDING BEHAVIOUR

The series of tests for examining yielding behaviour consisted of 5 different stress paths on reconstituted illite specimens at each of 28°C, 65°C, and 100°C, and 3 different stress paths on compacted illite specimens at each of 28°C and 65°C. In all cases, specimens were consolidated initially to 1.0 MPa at 28°C and then unloaded to 0.5 MPa. Following unloading, the temperature was increased to 65°C or 100°C at 0.5 MPa for the tests at elevated temperature. The tests were all done at constant temperature. The stress paths used for reconstituted illite specimens at 28°C are shown in Fig.7.1, with θ = $arctan(dq/dp')$ representing the inclination from the p'-axis of the stress probe originating from the end-of-consolidation pressure p_o'.

7.1   Reconstituted Illite

7.1.1   Stress-strain Behaviour

Relationships for deviator stress and for volumetric strain *versus* axial strain for the ambient temperature (28°C) tests are shown in Figs.7.2a and 7.2b. Each stress path is designated by the angle θ the stress path makes with the p'-axis in Fig.7.1. It can be implied from Fig. 7.2a that failure stresses at large strains decrease with increasing θ. The stress path for θ = 36° did not intersect the failure envelope, so failure was not reached. In general, as θ increased, the specimen failed at smaller axial strain ε_{af}. For example, axial failure strains for θ = 72°, 96°, and 124°

116

are   about ε_{af} = 10%, 4%, and 2%, respectively.   The initial

portions of the q-ε_a curves in Fig.7.2(a) seem to be independent of

the inclination of the stress path.

Corresponding volume change behaviour is shown in Fig.7.2b.

Specimens with higher θ-values tend to dilate with shear, while

specimens with lower θ-values tend to compress .   This can be

explained as follows.   It is well-known that volumetric strains ε_v

are closely related to a change in mean effective stress

$p' = (\sigma_1' + 2\sigma_3')/3$.   In general, as the mean effective stress

increases, the volumetric strain increases.   For lower θ-value tests

the mean effective stresses decrease during shearing, so the

volumetric strains are expansion (negative).   Isotropic elastic

theory suggests there would be no volume change where θ = 90°, that

is, where p' = constant.   For θ = 96° in Fig.7.2, p' slightly

decreased during shearing.   The resulting volumetric strains were

small and negative (expansive) about ε_v = -0.5%.   The volume change

characteristics shown in Fig.7.2 are in accordance with those

commonly seen for isotropically consolidated soils in drained stress

path tests.

The stress-strain paths in Fig.7.2 are step-shaped due to the

incremental   loading test procedure that was used.   Continuous

stress-strain relationships can only be obtained from strain-control

tests done in the GDS equipment.   Comparison between load-control

and strain-control tests is made in Fig.7.3 which presents results

from two different stress paths with $\theta = 72°$ and $96°$, respectively. This figure shows that stress-strain curves in the strain-control tests closely parallel stress-strain curves defined by the end of each increment in the load-control tests. This suggests that a smooth curve can be drawn on stress-strain curves from load-control test through data points at the end of each load increment. Failure strengths seem not to be significantly affected by different loading procedures along the same stress path.

Results of stress-paths and stress-strain relationships are shown in Figs.7.4 and 7.5 for 65°C; and in Figs.7.6 and 7.7 for 100°C. The observed stress-strain behaviours are in all cases essentially similar to those observed at 28°C. Specimens with a high θ-value tend to dilate during shearing. Failure stresses and strains to failure decrease with increasing θ-values. The abrupt drops in q and decreases in ε_v at the end of tests resulted from the procedures used (described in Chapter 4) during cooling from elevated temperature to the build-out temperature of 28°C.

After shearing was terminated, the axial piston was clamped to the cell. During cooling, both the specimen and the whole system shrink in size due to negative thermal expansion. The internal load cell was made of aluminum and the piston made of steel both which have larger thermal expansion coefficient than that for soil. Therefore, the load could not be kept constant during cooling, and decreased, resulting in a reduction of deviator stress.

7.1.2 Yielding Behaviour

Graham *et al.* (1988) showed that if test results are examined using suitable stress-strain parameters, then linear behaviour can be observed over a significant range of pressures from the end-of-consolidation stresses towards yielding. In this study, yield stresses were identified using the techniques proposed by Graham *et al.* (1988)..

Fig.7.8 shows typical test results at room temperature in terms of the tendency to change volume (p' *vs.* ε_v curve in Fig.7.8a), to distort or change shape (q *vs.* ε_s in Fig.7.8b), and to absorbed energy W during straining (W *vs.* LSSV in Fig.7.8c). In the last case the energy W absorbed per unit volume by a specimen during stressing and the length of the stress vector, LSSV, as the specimen moves towards yield, are given by

[7.1] $$W = \Sigma \; (\bar{p} \; d\varepsilon_v + \bar{q} \; d\varepsilon_s)$$

[7.2] $$LSSV = \sqrt{(p' - p_0')^2 + (q - q_o)^2}$$

where $\bar{p}$ and $\bar{q}$ are respectively the average values of the mean effective and deviator stresses in a loading increment, $d\varepsilon_v$ and $d\varepsilon_s$ are the corresponding volumetric and shear strain increments, p and q are the current stresses, and p_0' and q_o are the initial values at the beginning of the stress path. This plotting in Fig.7.8c uses two scalar quantities to provide a yield criterion that is

119

independent of stress path direction (Crooks and Graham 1976, Tavenas *et al.* 1979).

Figure 7.8 also shows that in common with some other lightly overconsolidated clays the post-yield behaviour of reconstituted illitic clay is often linear over a measurable range of stresses. The stress path for T1480 in Fig.7.8 has $\theta = 72°$. Compared with the pre-yield behaviour, larger nonrecoverable plastic strains are experienced that are markedly stress-path dependent. Depending on the value of θ and the parameters being examined, the post yield behaviour may be straight, hardening (usually in tests with low θ-values), or softening (usually in tests with high θ-values where the specimen is moving towards shear failure). Linear post-yield behaviour causes some conceptual difficulties. It might be expected that the soil should exhibit the exponential behaviour that is observed as straight lines in semi logarithm plots of oedometer and triaxial test results (for example, by Roscoe and Burland 1968). The evidence for post-yield linearity over a limited range of stresses comes from a wide variety of lightly overconsolidated or cemented clays (Mitchell 1970, Crooks and Graham 1976, Graham *et al.* 1983) and can also be used as an approximation for reconstituted soils. In the reconstituted illite specimens described here, the post-yield behaviour in tests with $\theta = 36°$ and $72°$ became exponential at stresses just after the last data points shown. Similar trends were reported by Graham *et al.* (1983) for Winnipeg clay.

Yield stresses determined from stress-path tests using above method using the above methods are plotted in p'-q space in Fig.7.9 for room temperature (28°C), 65°C, and 100°C. The original preconsolidation pressure was 1.0 MPa at 28°C, and the specimen were then unloaded to 0.5 MPa before stress-path testing was begun. Although there is some scatter in the data, it seems reasonable to approximate them by ellipses in the way suggested by Modified Cam clay modelling.

It is clear from Fig.7.9 that the yield points move inwards towards the consolidation stress state (0.5 MPa) as the temperature increases. The shapes of the yield loci are not affected by temperature, though their sizes decrease with temperature. In other words, the yield loci have been shown to shrink with temperature, keeping an elliptical shape. Although the data in Fig.7.9 are limited, they represent a considerable amount of research effort. They are believed to be the first to show explicit support for the assumptions made previously that yield envelopes associated with varying temperatures homologous with smaller sizes of yield envelope being associated with higher temperatures.

7.1.3. Failure Modes

Distinct visible shear surfaces were observed on most of the reconstituted specimens for all temperatures of 28°C, 65°C, and 100°C tests after load-controlled drained shearing. Specimens at failure shows well-developed shear planes. Observation of the shear

surfaces on the specimens showed that they were not planar, but curved. At both the top and bottom of the specimen, the slope of the shear surfaces is relatively flatter (from the horizontal), and in the middle it is more steeper. This change in slope of the failure plane may be caused by constraints at both ends of the specimen by friction from the porous stones. The measured angles of the shear surfaces varied in the range 65° to 76.5° to the horizontal. These results suggest an angle of friction of the specimen in a range of 27° to 50°. It was sometimes difficult to identify the shear surface when it intersected the spirally-mounted side drains. In any case, it is well known that calculation of the angle of friction of specimens from measurements of the failure surface is very sensitive to the measured angles. This is usually thought of as an ineffective way of measuring soil friction angles.

7.2 Compacted Illite

7.2.1 Stress-strain Behaviour

To investigate the yielding behaviour of compacted illite (as opposed to the reconstituted illite in Section 7.1), three stress-path tests were performed at temperatures of both 28°C and 65°C. The resulting stress paths are shown in Fig.7.10 for the 28°C tests, and in Fig.7.12 for the 65°C tests. Corresponding stress-strain behaviour is shown in Fig.7.11 for 28°C; and in Fig.7.13 for 65°C. The behaviour is generally similar to that shown earlier obtained for reconstituted illite, though it will be shown that the yield stresses are rather different. As before, tests with lower angles

122

of the stress direction θ have higher failure stresses. Along the stress path with $\theta = 36°$, failure could not be reached. The strains at failure again tend to decrease with increasing θ. The volumetric strain behaviour for compacted illite is also similar in nature to that for reconstituted illite. The higher the angle θ of stress path, the more the specimen tends to dilate with strain; while at low angles, the specimen tends to compress. However, closer examination of the volume change behaviour leads to an understanding that reconstituted and compacted specimens have rather different volume change behaviour in detail. These differences will be discussed in a following section.

7.2.2 Yielding Behaviour

The same techniques were used to determine yield stresses in compacted illite as were used for reconstituted illite. Yield stresses determined for the compacted illite are shown in p'-q space in Fig.7.14 which also shows for comparison, yield loci for reconstituted illite at elevated temperatures shown in Fig.7.9. Although data are sparse, approximate yield loci can be drawn for 28°C and 65°C, using as a guide, the shapes of yield loci for natural (anisotropic) clays published in the literature.

Published data on natural clays show that their yield loci are not elliptical as in Modified Cam clay (Fig.7.9), but appear to be symmetrical about the K_o line in s'-t plots. However, since the mapping of s'-t into p'-q is not conformal, the symmetry about the

123

K_o line which is seen in s'-t plots is not observed in p'-q plots. The vertical preconsolidation stress ($\sigma'_v = \sigma'_a$ in case of triaxial test) can be determined by drawing a line having slope of $-2(H):3(V)$ to the p'-axis from the intersection of the η_o line. This gives a value of about 1.6 MPa, which is greater than the isotropic consolidation pressure of 1.0 MPa. This is thought to be due to transient, unequilibrated axial stresses in recompacted specimens during 1-D compaction. It is thought that the isotropic yield stress p'_{iso} in anisotropic specimens will be less than the major principal preconsolidation pressure σ'_{1c}, and probably in the range 0.4-$0.7 \times p'_{iso}$ (Graham et al. 1988). It is therefore reasonable to draw the yield loci shown in Fig.7.14 merging with data from reconstituted specimens at corresponding temperatures. Figure 7.14 clearly shows that the yield loci are distorted from elliptical shape in q-p' space. At 65°C the yield locus has become smaller in size than the 28°C locus, though the shape has not changed greatly. It may be seen that heating causes yield stresses to be displaced towards the origin, in a similar way to what was observed for reconstituted illite. There is no apparent reason why heating should causes a different effect on the yield locus when only the microstructure is changed (here though compaction as opposed to isotropic consolidation from a slurry), and all other conditions are unchanged. Therefore, it is again reasonable to say that heating causes the yield locus to decrease homologously in size towards the origin, independent of the processes that formed the soil microstructure.

7.2.3. Failure Modes

No visible shear surfaces were observed in the six compacted specimens at temperatures of 28°C and 65°C. Some wrinkles appeared in the membranes on specimens that were sheared to large strains of more than $\varepsilon_a = 15\%$. One specimen with a stress path of $\theta = 122°$, showed some indication of a shear plane with an angle of 70° to the horizontal. This value is in the range of values measured on reconstituted specimens, suggesting that reconstituted and compacted specimens may have essentially the same friction angle. This is reasonable because the major component of both sets of specimens is the same material. At large strains the original microstructures are altered by strains during shearing until they are essentially similar. At critical state ($\partial p'/\partial \varepsilon_s = \partial q/\partial \varepsilon_s = \partial u/\partial \varepsilon_s = \partial \varepsilon_v/\partial \varepsilon_s = 0$), strengths and friction angle will be controlled by the mineralogy of the material regardless of the initial differences in microstructure.

7.3 Discussion

7.3.1 Effect of Temperature on Pre-Yield Elasticity

The evidence for pre-yield linearity in soils comes largely from monotonically increasing stress systems such as the test results reported here. Evidence of reversibility is less strong, although some information on the reversibility of stress-strain relationship in soil is available from cyclic loading tests (Pappin and Brown 1980) or with small strain measurement with small q increments (Shibuya *et al.* 1992). Thus bulk and shear moduli that can be

interpreted from stress-strain plots such as those shown in Fig.7.8 are best thought of as pseudo-elastic parameters (Graham and Houlsby 1983) at medium strain levels, say 0-1%. An initial range of elastic behaviour is a central feature of the critical state family of constitutive relationships (Schofield and Wroth 1968, Roscoe and Burland 1968, Wroth and Houlsby 1985).

Clay materials are not ideally elastic, however, since measurable components of irrecoverable strains may occur during initial loading. There is also a components of hysteretic behaviour, with corresponding energy absorption. As a first approximation, however, the illitic clay, especially the reconstituted specimens, may be treated as an isotropic quasi-elastic material whose constitutive behaviour can be described by a linear deformation theory involving only two independent parameters. The two effective parameters (E', ν') or (K', G') required to describe the deformation characteristics of the soil prior to yielding have been evaluated from drained test results along different stress paths. Because the axial stress σ_1 and radial stress σ_3 both change along the assigned stress paths in the drained tests, Young's modulus E and Poisson's ratio ν can not be evaluated simply from stress strain measurements, but must be calculated through the shear modulus G and bulk modulus K. The G and K moduli are easily evaluated from relations of $q-\varepsilon_s$ and $p'-\varepsilon_v$, respectively, using the procedures described by Graham and Houlsby (1983). The pre-yield linear behaviour shown in Figs.7.8a, 7.8b, and 7.8c permit evaluation of pseudo-elastic bulk and shear moduli,

K and G, from graphs of p' vs. ε_v and q vs. ε_s for each specimen. An isotropic lightly overconsolidated specimen can be expected to have constant values of K/p'_o and G/p'_o. However, tests on anisotropic Winnipeg clay, Graham *et al.* (1983) found these parameters are not constant, but depend on the stress path direction, defined by $\theta = arctan$ (dq/dp').

While the pre-yield behaviour typified by Figs.7.8(a),(b),(c) was interpreted as being linear for the purposes of evaluating yield stresses, closer examination shows that the shear stiffness in particular varies with shear strain. Similar observations have been found by Richardson (1988) and Atkinson *et al.* (1990). Figure 7.15 shows values of tangent and secant shear moduli plotted against logarithm of shear strain ε_s for three stress paths at 28°C. The shear stiffness appears to vary to some extent with stress path direction θ. At elevated temperatures of 65°C and 100°C, the shear stiffnesses are lower than at 28°C, though similar trends have been observed (Fig.7.16a). Figure 7.16a shows values of secant shear modulus up to yield stress.

Values of the bulk modulus K at elevated temperatures are shown in Figs.7.16b for reconstituted illite. There is again a reduction of K with temperature, though it is smaller than that for the shear modulus G. Similar trends of these elastic properties have been reported by Date (1969) for steels. The values of G and K shown in Fig.7.16 allow calculation of corresponding values of Young's

127

modulus E and Poisson's ratio μ (Fig.7.17). Young's modulus decreases with temperature (Fig.7.17a), while Poisson's ratio increases with increasing temperature (Fig.7.17b).

Now turning to compacted illite, Fig.7.14 showed that the effect of compaction on yield loci at 28°C and 65°C. Graham and Houlsby (1983) proposed an approximate procedure (called the K,G,J model) for evaluating and predicting soil behaviour using anisotropic elasticity. The (K,G,J) model takes into account anisotropy of soil behaviour by introducing the coupling modulus J which allows the coupling of shear strain with mean effective stress and volume strain with shear stress. Values of the parameters, K^*, G^*, and the coupling modulus J are presented in Table 7.1 which also shows values of K and G evaluated on the basis of an isotropic elastic soil model. Similar trends to those have been observed in reconstituted illite in these elastic properties can also be seen in compacted illite (Figs.7.18 and 7.19).

Table 7.1 Anisotropic and isotropic elasticity moduli for compacted illite

Anisotropic		Isotropic	
K^* (MPa)	39.9	K (MPa)	51.6
G^* (MPa)	23.0	G (MPa)	23.9
J^* (MPa)	12.4	E (MPa)	62.1
		ν	0.30

Apart from the anisotropy shown in Table.7.1, the compacted illite shows generally similar trends to those shown earlier for reconstituted illite. Figures 7.18 and 7.19 show elastic stiffnesses G, K, and E decreasing with temperature and increasing with θ. In Fig.7.19(b), Poisson's ratio increases slightly with temperature for $\theta = 36°$ and $72°$, but decreases for $\theta = 124°$. These stiffnesses come from specimens that were initially consolidated to 1.0 MPa, unloaded to 0.5 MPa, and then heated where necessary. It is sometimes helpful to present such data normalized by the preconsolidation pressure. This has not been done here because (a) the preconsolidation pressure is uncertain in compacted illite, and (b) the preconsolidation pressure changes with temperature.

7.3.2 Effect of Temperature on Yield loci

Figures 7.20 and 7.21 show yield data for reconstituted and compacted illite specimens that have been normalized by division by p'_{cT}, the isotropic preconsolidation pressure in Fig.7.9 for the corresponding temperature. A single locus can be drawn through the normalized data showing that the yield loci for the three temperatures (28°C, 65°C, and 100°C) that have been tested have essentially the same shape. That is, the ratio of the minor to major axes of the ellipses is constant. This implies uniqueness of the yield locus when it is normalized by an appropriate parameter such as the preconsolidation pressure for the appropriate temperature.

Figures 7.20 and 7.21 confirm the results, obtained in the previous section that the shape of yield loci are different for reconstituted and compacted illites. Yield loci for reconstituted illite are elliptical, but yield loci for compacted illite are distorted towards to the K_o-consolidation line due to the compaction process.

Normalization shows that the shape and the size of the yield loci can be presented by unique function for a given soil in q-p' stress space.

7.3.3 Effect of Temperature on Plastic Potentials

One of the important concepts in describing the elastic-plastic response of soils is the mode of plastic deformation that occurs after the soil reaches yielding. This is commonly done by defining the 'plastic potential' as the locus to which plastic strain increment vectors $\delta\varepsilon_v^p$, $\delta\varepsilon_s^p$ are orthogonal in p' *vs*. q stress space (Wood 1990). The direction of nonrecoverable strain increment vectors should depend on the absolute stress level at yielding, and not on the incremental stress change (Graham *et al*. 1983, Wood 1990). Post-yield straining comprises an elastic recoverable component, and plastic nonrecoverable component:

[7.3] $$d\varepsilon_v^{tot} = d\varepsilon_v^e + d\varepsilon_v^p$$

[7.4] $$d\varepsilon_s^{tot} = d\varepsilon_s^e + d\varepsilon_s^p$$

130

where $d\varepsilon_v^{tot}$ is the total volumetric strain increment, $d\varepsilon_v^e$ is the elastic volumetric strain component, $d\varepsilon_v^p$ is the plastic volumetric strain component, $d\varepsilon_s^{tot}$ is the total shear strain increment, $d\varepsilon_s^e$ elastic shear strain component, and $d\varepsilon_s^p$ is the plastic shear strain component. If plastic strains ($d\varepsilon_v^p$ and $d\varepsilon_s^p$) are to be examined, the elastic strains $d\varepsilon_v^e$ and $d\varepsilon_s^e$ associated with post-yield stress increments must be subtracted from measured total strains. In isotropic soils, the elastic volume and shear strain increments can be calculated from the measured bulk and shear moduli described earlier, for example, in Fig.7.16 and 7.17.

[7.5]
$$d\varepsilon_v^e = dp'/K$$

[7.6]
$$d\varepsilon_s^e = dq/3G$$

Figures 7.22a and 7.22b show diagrammatically how each component can be determined from graphs of p' *vs.* ε_v and q *vs.* ε_s. The initial, transitional, and secondary sections observed in real specimens have in each case been approximated by bilinear curve fitting (Graham *et al*. 1983). For a standardized resultant stress change of $0.1 \times p_c'$, corresponding value of dp' and dq can be evaluated for the each stress path. Resulting values of $d\varepsilon_v^p$ and $d\varepsilon_s^p$ can then be found from the abscissa differences between the post-yield lines and the extrapolated pre-yield lines.

131

This study follows the determination techniques used by Graham *et al.* (1983). The increment of post yield stress was taken as $0.1 \times p_c'$ along the respective stress path directions in all tests, where p_c' is the pre-consolidation pressure. The technique of projecting pre-yield elastic behaviour into the post-yield plastic region is common in metal plasticity, and appears to be valid, in principle, for clay soils (Graham *et al.* 1983, Wood 1990). It is common to examine normality by aligning the $d\varepsilon_v^p$ and p' axes; and also the $d\varepsilon_s$ and q axes, and then plotting plastic strain increments $d\varepsilon_v$ and $d\varepsilon_s$ as a strain vector from the corresponding yield stress. Resultant plastic strain increment vectors and plastic potential at room temperature (28°C), 65°C, and 100°C are shown in Figs.7.23a, 7.23b, and 7.23c. From these figures, approximate normality of the plastic strain vectors to the yield locus at 28°C, 65°C and 100°C can be inferred, although some deviation of normality can be seen at lower p' stress levels, where the specimens failed in such a way that the specimen expands during straining. The rate at which the increases in volume can actually occur is controlled by the hydraulic conductivity of the material, and often cannot follow those required by the rate of shear straining in load controlled tests. Some uncertainty therefore exists in determining the plastic volumetric strain components and the resultants may therefore appear steeper than they should be. Larger plastic volumetric strains can be derived if real measurement can be made along the shear plane (Atkinson and Richardson 1987).

132

Figure 7.23 suggests it is reasonable to say that the yield locus and plastic potential coincide at each of the temperatures that have been tested. Thus an associated flow rule may be applied to isotropically reconstituted illite at any temperature. It can be easily accepted that the effects of temperature on anisotropic yield locus should be isotropic in terms of mechanical behaviour. Only the size of the yield locus is changed by temperature, but not its shape. The plastic strain vectors, and therefore the corresponding plastic potential, are not affected.

For compacted illite, the plastic strain increment vectors measured at 28°C and 65°C are shown in Figs.7.24a and 7.24b, respectively and related to the corresponding yield loci. Although the results are available for only three stress paths, it can be clearly seen that deviations of the plastic strain vectors from normality can be seen at both temperatures. This suggests that the yield loci and the plastic potentials do not coincide, indicating that the flow rule for compacted illite may be non-associated. However, the data are sparse. Similar behaviour can be seen in results from compacted sand-bentonite mixture reported by Oswell (1991). It can be tentatively concluded that the flow rule in statically compacted soil may be non-associated due to the anisotropic microstructure founded by one-dimensional compaction.

CHAPTER 8 UNDRAINED STRESS-STRAIN BEHAVIOUR IN SHEAR

8.1 Reconstituted Illite

8.1.1 Shear Behaviour at Elevated Back Pressure

Effect of back pressure: The concept of effective stress states that soil behaviour is controlled by effective stresses.   In other words, if the effective stress is the same in two specimens, but the back pressure is different, then soil behaviour in terms of compression and shear should be the same.   This is illustrated in Figs.8.1a and 8.1b which shows results from three undrained triaxial compression tests.   All three specimens were normally consolidated at 1.5 MPa mean effective pressure.   The back pressures in the three specimens were respectively 0.5 MPa,   1.0 MPa,   and   1.0 MPa.   All three specimens exhibit very similar behaviour when results are plotted as deviator stress q *versus* axial strain ε_a (Fig.8.1a); pore pressure du *versus* axial strain ε_a (Fig.8.1b); and mean effective pressure p' *versus* deviator stress q (Fig.8.2).

Similar effects of back pressure on stress-strain relationships in overconsolidated specimens are shown in Figs.8.3a, 8.3b, and stress paths in Fig.8.4.   The back pressure u_b = 0.2 MPa was used for T1420, while u_b = 1.0 MPa was used for T1486.   Due to some computer software difficulties, initial portions of the stress-strain curves were not recorded for T1420.   Despite this, rather similar behaviour is seen in the stress-strain relationships in both specimens, though the results in this case are not as convincing as in the normally consolidated specimens shown previously.

134

From Figs.8.1-8.4, it can be concluded that the effects of the level of back pressure on the behaviour of reconstituted specimens are negligible in both normally and overconsolidated specimens.

8.1.2 Shear Behaviour at Elevated Temperature

Effect of elevated temperature: the effects of elevated temperatures on undrained triaxial compression stress-strain behaviour are shown in Figs.8.5a and 8.5b. Figure 8.5 shows test results on normally consolidated specimens at 28°C, 65°C, and 100°C. (The initial offset for T1492 indicates lack of contact between the piston on the top of the specimen at the beginning of the test.) Specimens with higher temperatures show higher shear strengths (Fig.8.5a), and lower pore water pressures (Fig.8.5b). That is, they show less compressive behaviour, and indeed some tendency to dilative behaviour at higher temperature. Corresponding stress paths in p'-q space (Fig.8.6) show different stress paths at different temperatures, though the strength envelopes (usually taken as straight lines through the origin) at the end of the tests seem to be independent of temperature. That is, the normally consolidated strength envelope does not vary with temperature.

Figures 8.7a and 8.7b shows similar results for overconsolidated specimens (isotropic OCR = 2) at 28°C and 65°C. Similar behaviour was observed at both temperatures. At 65°C the strength was slightly the higher than at 28°C, and a slight dilative behaviour produced a decrease in pore water pressure with strain. The stress

135

paths in the p'-q plots in Fig.8.8 again show that failure envelopes at large strains seem not be affected by drained heating.

8.1.3 Effect of Ramped Temperature

Effect of drainage condition upon temperature change: In order to investigate the effect of drainage conditions and ramped temperatures, a specimen was heated undrained under the isotropic consolidation stress, and then sheared undrained at the same elevated temperature. Figure 8.9 shows a stress path of this type for the test T1467 in which the specimen was initially normally consolidated at 0.98 MPa at 28°C, and then heated to 65°C under undrained conditions. As discussed in Chapter 6, excess pore pressure was developed during undrained heating, resulting in a reduction of effective stress defined by total stress minus pore pressure. The specimen was maintained under constant mass conditions after heating (see Chapter 6), by allowing a calibrated amount of water to be released from the system. Thermally induced pore pressures were 0.45 MPa under bulk-undrained conditions, and 0.37 MPa under the constant-mass conditions. The stress-strain behaviour during subsequent shearing is shown in Fig.8.10. For comparison purposes, undrained stress-strain curves and stress paths for drained-heated overconsolidated specimens at 28°C (T1486) and 65°C (T1466) are also shown in the Figs.8.9 and 8.10. It is clearly shown that the undrained heated specimen (T1467) has similar failure strength as an overconsolidated, drained heated specimen (T1466) consolidated at 0.5 MPa, with a preconsolidation pressure of

136

1.0 MPa.   The stress-strain behaviour and stress paths suggest that the specimen behaves as if overconsolidated, although before heating it was normally consolidated at 1.0 MPa and 28°C.

Similar ideas have been proposed by others (for example, Campanella and Mitchell 1968, Plum and Esrig 1969), although it was not extensively investigated by them in terms of stress-strain relationships.   Kuntiwattanakul (1991) showed similar behaviour for kaolinite.   According to the observations in this study and in other research, it can be concluded that undrained heating causes soil to behave as if it is overconsolidated in a mechanical sense. This is mainly due to thermally induced pore water pressures and the resulting reduction in effective stress.   The stress-strain behaviour and undrained shear strength of reconstituted illite are simply controlled by the current effective stress at the end of the consolidation phase even at elevated temperature, irrespective of the drainage conditions.

Effects of ramping temperature under a given deviator stress q: The previous section reported the effect of ramping temperatures under isotropic stresses and undrained conditions.   This section investigates the effect of ramping temperature under given deviator stresses in undrained tests.   Figure 8.11, 8.12, and 8.13 show stress paths from three specimens T1464, T1468, and T1472 respectively, in which two normally consolidated specimens were heated undrained from 28°C to 65°C or to 100°C at several different

137

levels of deviator stress q. Corresponding values of deviator stress, pore water pressure and temperature are shown in Figs.8.14, 8.15, and 8.16 respectively. Numbered points on the two sets of figures corresponding with the same stage of testing.

Test T1464 was first sheared undrained to q = 0.3 MPa at 28°C (Points 1-2 in Figs.8.11 and 8.14). It was then heated undrained to 65°C (Pts.2-3) under bulk-undrained conditions, when p′ decreased from 1.12 MPa to 0.74 MPa, corresponding to a pore water pressure increase of 0.38 MPa. Release of pore water to achieve constant mass (Pts.2-4) gave p′ = 0.88 MPa, a pore water pressure reduction of 0.24 MPa from Pt.2. Subsequently this specimen was cooled to Pts.5-6; sheared at 28°C to Pt.7; heated undrained to 65°C to Pts.8-9; sheared at 65°C to Pt.10; and cooled to 28°C to Pt.11 where the test terminated. Further discussion of the behaviour from Pt.4 to Pt.11 will be given later.

Chapter 6 showed that heating from 28°C to 65°C under bulk-undrained isotropic stress conditions produced pore water pressure of 0.4 MPa and 0.6 MPa respectively at isotropic consolidation pressures of 1.0 MPa and 1.5 MPa. Under constant mass conditions, the induced pore water pressures were 0.3 MPa and 0.4 MPa respectively. From 28°C to 100°C under bulk-undrained and isotropic stress conditions, the corresponding thermally induced pore water pressure was 0.85 MPa (Fig.6.9). As shown in Chapter 6, normalization of thermally induced pore water pressures with respect to consolidation pressure

138

p'_o provides consistent modelling for both normally consolidated and overconsolidated specimens. Taking values of $(\Delta u_T/p'_o) = 0.4$ and 0.3 respectively for bulk-undrained and constant-mass heating from 28°C to 65°C, together with the consolidation pressure of 1.3 MPa for Test T1464, provides predicted thermally induced pore water pressures of 0.52 MPa and 0.39 MPa, respectively. The corresponding measured changes were rather less, 0.38 MPa and 0.24 MPa, respectively. For Test T1468 with consolidation pressure $p'_o = 1.44$ MPa, predicted thermally induced pore pressure were 0.58 MPa and 0.43 MPa for bulk-undrained and constant-mass heating, respectively. These values are slightly larger in Test T1464 than those actually measured, but similar in Test T1468. With a measured value of $(\Delta u_T/p'_o) = 0.5$ from isotropic heating and $p'_o = 1.43$ MPa, the predicted pore water pressure change is $\Delta u_T = 0.72$ MPa, close to that measured.

The results shown in Figs.8.11-8.16 suggest that during undrained heating from 28°C to 65°C or 100°C under a constant given deviator stress q, the thermally induced pore water pressure change generated in normally consolidated specimens are similar to those generated under isotropic stress conditions, although it is recognized there is some scatter in the data. There appears to be no reason why undrained thermal expansions in clay should be different at different deviator stresses under otherwise identical conditions. On this basis, one might expect the magnitude of thermally induced pore water pressure changes in clay (which are directly related to

139

undrained thermal expansion) to be independent of deviator stress unless the clay is actually failing.

Specimen T1464 was subjected to a further heating cycle from 28°C to 65°C when the deviator stress q was 0.18 MPa (Pts.7-9) in Figs.8.11 and 8.14. An effort was made to maintain q constant, but the specimen could not sustain the loading. The resulting stress path during heating suggests that the specimen underwent a reduction in both q and p', possibly corresponding with the failure envelope.

After initial shearing to q = 0.3 MPa at 28°C, specimen T1468 was heated to 65°C (Pts.2-4 in Figs.8.12 and 8.15), and then shearing was continued (Pts.4-5). The stress-strain relationships after heating were quite different from those during the earlier period of shearing at lower temperature. They suggest that linear elastic behaviour was initially observed from q = 0.3 MPa to q = 0.5 MPa, and the corresponding changes in pore water pressure during shear were small. The stress path (Pts.4-5) in Fig.8.12 and stress-strain relationships (Pts.4-5) in Fig.8.15 support the idea that the specimen was overconsolidated by undrained heating. In Test T1468 (Figs.8.11 and 8.14), after pore water pressure induced by heating from 28°C to 65°C had equilibrated (Pts.7-8), the calibrated water was released in order to perform constant-mass conditions (Pts.8-9). The specimen was then loaded further at constant strain rate at 65°C. The curve of deviator stress-axial strain (Fig.8.14a, Pts.9-10) shows an initial linear portion with a distinct change in slope

at ε_a = 6.3%. This change in slope is also seen along the path 9-10 in Fig.8.11. Further loading caused larger increases in axial strain. On the other hand, the resulting pore water pressure decreased slightly with axial strain. The thermally induced pore water pressure, Δu_T = 0.1 MPa from Pts.7-9, substantially lower than the equivalent value Δu_T = 0.24 MPa measured at q = 0.3 MPa in this test (Pts.2-4).

Similar behaviour was reported in a previous section on specimen T1467 during undrained heating under isotropic stress conditions. The specimen was sheared undrained at 65°C after undrained heating to 65°C (Figs.8.9 and 8.10). The stress-strain behaviour and resulting stress path are similar to those for overconsolidated specimens.

As previously shown in Figs.8.13 and 8.16, T1472 was heated undrained to 100°C at q = 0.3 MPa and substantial pore water pressures were induced (Pts.2-3). Following this, the specimen was sheared undrained at 100°C from Pts.3-4. The specimen behaved like a dilative overconsolidated material showing increases in q and decreases in u with further straining. These complex mechanisms are discussed in terms of the concept of a state boundary surface in a later section.

Similar tests were performed on two overconsolidated illite specimens (OCR = 2 with preconsolidation pressure p'_c = 1.0 MPa).

141

Under a given deviator stress q = 0.3 MPa, the specimens were heated undrained to 65°C (T1465) or to 100°C (T1473), respectively. The resulting stress paths are shown in Figs.8.17 and 8.18; and corresponding stress-strain-temperature relationships in Figs.8.19 and 8.20, respectively. Specimen T1465 was initially sheared undrained at 28°C to q = 0.35 MPa (Pts.1-2) during which it displayed isotropic elastic behaviour ($\Delta p' = 0$ in Fig.8.17). It was then heated undrained to 65°C (Pts.2-3-4); cooled undrained to 28°C (Pts.4-5); and then sheared undrained to failure at 28°C (Pts.5-6-7). Thermally induced pore water pressures during heating to 65°C were 0.16 MPa for bulk undrained heating (Pts.2-3), and 0.10 MPa for constant-mass conditions (Pts.2-4).

A similar heating cycle was performed on T1473 (Figs.8.18 and 8.20) except that the temperature was 100°C instead of 65°C. In this case, the specimen could not sustain the constant q = 0.3 MPa during undrained heating, and the deviator stress q dropped from 0.3 MPa to 0.2 MPa. The specimen was then sheared undrained to q = 0.3 MPa (Pts.3-4) when it showed dilative behaviour with steady decreases in pore water pressure. The slope of the $q-\varepsilon_a$ relationship at 100°C is less than at 28°C, suggesting the specimen was less strong (further along the stress-strain curve) after heating. Figure 8.18 suggests that the undrained stress path (Pts.3-4) after undrained heating to 100°C in this overconsolidated specimen follows the critical state line, that is, the large strain failure envelope. After cooling to

142

28°C (Pt.5), the specimen was able to carry higher shear stresses (Pts.5-6).

Cooling Behaviour

After pore water pressures had reached equilibrium, the normally consolidated specimens (Tests T1464, T1467, and T1472) and overconsolidated specimens (Tests T1465 and T1473) were cooled to 28°C under undrained conditions. The specimens experienced shrinkage during cooling that was expressed in part as shortening. Due to this shortening and the way in which the loading piston was controlled, the deviator stress was not controlled at a constant value but reduced towards zero during cooling. Subsequently, undrained shear was performed at 28°C. The stress paths and stress-strain relationships measured at 28°C after cooling show initially linear behaviour that can be considered elastic (see Figs.8.11, 8.14; and Figs.8.13, 8.16 for normally consolidated specimens, and Figs.8.17, 8.19; and Figs.8.18, 8.20 for overconsolidated specimens). This is due to the unloading that took place during cooling, and possibly also to some recovery in the size of yield loci upon cooling. The original strength of the material was recovered after the temperature cycle even though it had been lower while the specimen was still hot (see for example Fig.8.18, 8,20). The stress-strain relationships and stress paths in these figures show that the elastic behaviour and the failure strength was not changed irreversibly by one cycle of temperature change under undrained conditions.

143

8.1.4 Discussion

Isotropy or anisotropy of soil specimens may be examined using undrained test data plotted as du *vs.* dp, where du is the pore water pressure generated during shear, and dp is corresponding total mean stress increment. If the specimen is isotropically elastic, the slope of $m = (du/dp) = 1.00$. In tests T1486 and T1466 on overconsolidated reconstituted illite at 28°C and 65°C respectively, the value of m was close to unity (Fig.8.21a and Table.8.1), indicating isotropy. On the other hand, results from the normally consolidated isotropic specimens in Fig.8.21b showed no linear portion of the slope (du/dp). That is, end-of-consolidation conditions were already on the yield locus, and only non-elastic behaviour was observed. In contrast, Graham and Lau (1988) showed marked regions of linear behaviour when normally consolidated specimens had been formed by 1-D anisotropic consolidation.

Table 8.1 m values for reconstituted illite

Temperature(°C)	m-value	Consolidation pressure p′ (MPa)
28	1.00	0.5 (OCR=2)
65	1.07	0.5 (OCR=2)

where OCR = overconsolidation ratio.

After one cycle of heating-cooling, the initial du-dp relationships from normally consolidated specimens after a temperature cycle behave as if the material is overconsolidated in terms of stress-strain relationships (Pts.5-6 in Figs.8.13, 8.16). Overconsolidated

specimens still behave as isotropic overconsolidated materials with the same (du/dp) = 1.0 as before heating (Pts.5-6 in Figs.8.18, 8.20, 8.22b).

Some indications of reversibility in the volume strains induced by temperature changes have been seen under undrained conditions. After the specimens were cooled, the stress states returned to similar values to those before undrained heating (see Figs.8.6, 8.8, 8.11, 8.13,, 8.17 and 8.18). The reconstituted illite specimens can be considered in general as isotropic and so axial and radial strains are equal during consolidation and heating-cooling processes. In normally consolidated specimens, the stress state comes back after cooling to the same state as before heating even though the specimens exhibit dilative behaviour during shear at 100°C (Figs.8.5 and 8.13). However, in overconsolidated specimens which exhibit dilative behaviour at 100°C the stress state after cooling was somewhat greater than before undrained heating (Fig.8.18). Some irreversibility is therefore experienced by overconsolidated specimens during a temperature cycle of heating-cooling. This may be explained as follows. Since the specimen at 100°C (T1473, Pts.3-4, Figs.8.20, 8.22b) exhibits dilative behaviour in which both mean effective stress p' and the deviator stress q increase with straining, the final mean effective stress p' at 100°C is higher than it was just after heating. However, Chapter 6 showed that the undrained thermal expansion in the specimen was unchanged. This means that the thermal contraction during cooling was the same

145

magnitude but opposite sign as the thermal expansion during heating. As a result, the thermally induced pore water pressure was the same. However, the new mean effective stress p′ at 28°C is higher than before heating because the effective stress before cooling had increased during the period of undrained dilative shearing. A reduction in q of $\Delta q = 0.7$ MPa and an increase in pore water pressure of $\Delta u_T = 0.10$ MPa were observed in normally consolidated specimen (T1460) upon cooling from 65°C to 28°C after shearing was terminated (Figs.8.5 and 8.6).

It is interesting to compare the results from Tests T1472 and T1473 because both specimens exhibit generally similar behaviour at 100°C even though T1472 was normally consolidated and T1473 was overconsolidated. The thermally induced pore water pressure in the normally consolidated specimen was larger than that in the overconsolidated specimen during undrained heating at $q = 0.3$ MPa (Figs.8.13 and 8.18). However, both specimens seem to reach the same failure envelope after undrained heating. During further loading under undrained conditions at 100°C, both specimen showed dilative behaviour despite their different initial stress histories. However, the failure envelopes seem to be independent of temperature.

8.2 Compacted Illite

8.2.1 Effect of Elevated Temperature

Four specimens were tested to investigate the effect of elevated temperature on compacted illite. Two unheated specimens (T1495 and T1485) were consolidated to 0.56 MPa and 1.04 MPa at 28°C, respectively. Two further specimens (T1469, T1470) were initially consolidated at 28°C to at 0.41 MPa and 1.00 MPa respectively, and then heated from 28°C to 65°C at these pressures with drainage leads open. After consolidation at 28°C or drained heating at 65°C, the specimens were sheared undrained at constant temperature and constant strain rate. Stress-strain relationships and stress paths for the compacted illite specimens consolidated at 28°C are shown in Figs.8.23 and 8.24, respectively. Results for compacted illite at 65°C are shown in Figs.8.25 and 8.26.

The specimens consolidated to 1.0 MPa at both temperatures both show shearing resistances that increase rapidly in the early stages of testing with corresponding increases in pore water pressure. As peak shearing is approached at large strains, the shearing resistance increases much more slowly and pore water pressures reduce. The corresponding stress states appear to be moving up the critical state line (CSL). This is typical behaviour of dilative materials, and is clearly related to overconsolidation caused by the compaction process. These same characteristics of slowly increasing shearing resistance and decreasing pore water pressure towards the end of testing are more pronounced at both 28°C and 65°C for the

147

specimens consolidated at about 0.5 MPa. The stress paths for all
the illite specimens show that the large strain failure envelopes
(CSLs) seem to be independent of temperature, consolidation
pressure, and whether the specimens were formed by isotropic
consolidation from slurry or by 1-D static compaction (see Figs.8.5,
8.7, 8.9, 8.11-8.13, 8.17-8.18).

Table 8.2 shows pore water pressure parameters defined by $m = \Delta u / \Delta p$
from the tests on compacted illite at each temperature. It is
evident from the table that the m values depend on temperature and
pressure. At both 28°C and 65°C, the m value increased with
pressure (0.84 to 1.43 at 28°C and 1.16 to 1.79 at 65°C). At a
given pressure, the m value increases with temperature. This is
similar to observations reported by Lingnau (1993) for a compacted
sand-bentonite mixture.

Table 8.2 m values for compacted illite

Temperature(°C)	m-value	Consolidation pressure p'(MPa)
28	0.84	0.55
	1.43	1.43
65	1.16	0.40
	1.79	1.05

8.2.2 Effect of Ramping Temperature

Only one ramping temperature test (Test T1471) was performed on
compacted illite (Figs.8.27-8.29). The specimen was initially
consolidated to 1.0 MPa and sheared undrained at 28°C to about

148

0.45 MPa (Pts.1-2). Undrained heating from 28°C to 65°C was performed at constant $q = 0.45$ MPa (Pts.2-3). After heating the specimen was maintained at constant bulk volume conditions, and then undrained shearing was continued at 65°C (Pts.3-4). The thermally induced pore pressure (Pts.2-3) was 0.33 MPa which is close to those obtained under isotropic stresses on the p'-axis under undrained heating conditions. The deviator stress-axial strain relationship in Fig.8.28a shows that the transition of q-ε_a between 28°C and 65°C is smooth. Further loading at 65°C proceeded in q-ε_a with initially the same stiffness as at 28°C up to about $q = 0.65$ MPa, followed by continuously increasing q with with less stiff response up to large strains at the end of the test. Pore water pressure during shear at 65°C decreased slightly with strain, whereas the pore water pressure increased with strain at 28°C. The stress-strain and stress path at 65°C show that the behaviour after undrained heating is similar to that of specimen T1495 which was consolidated to lower pressure of 0.55 MPa at 28°C. This indicates that undrained heating causes the specimen to behave as if it is more overconsolidated, that is, as if the actual effective stress is reduced. However, the failure envelope in p'-q space seems not to be affected by temperature change.

8.2.3 Discussion

As discussed in Chapter 7, compacted illite exhibits anisotropic behaviour in drained shear due to the anisotropy produced by the compaction process. Similar characteristics have now been

149

demonstrated in undrained shear. Pore water pressure-mean total

pressure relationships show that for p_0' = 1.0 MPa, $m = (\Delta u/\Delta p)$

values are 1.43 and 1.79 respectively at 28°C and 65°C (Fig.8.29 and

Table 8.2). This confirms that the anisotropic structure in

compacted illite is caused by the compaction process and not simply

by testing procedures. However, values of m = 0.84 at 28°C, and

1.16 at 65°C were obtained at p_0' = 0.5 and 0.4 MPa, respectively.

The m-values less than unity suggest that the vertical stiffness is

greater than horizontal stiffness in these specimens (Graham and

Houlsby 1983). This may possibly be explained that during unloading

from 1.0 MPa to 0.5 MPa, the initially stiff horizontal structure

is diminished, and eventually the vertical stiffness overcomes the

horizontal stiffness. That is, the specimen becomes more dilative

horizontally. Wan (1988) and Oswell (1991) also observed that any

tendency to expansion rapidly moved the soil response towards

isotropy (m = 1).

Higher pore water pressures during undrained shear on drained heated

compacted specimens at elevated temperatures have been reported

previously by Mitchell (1964), and Lingnau (1993). Dilative

behaviour exhibited as continuous increases in shearing resistance

with no maximum, and decreases in pore water pressure resistance

after an early peak value, was observed by Mitchell (1964) in

compacted San Francisco Bay mud. However, Lingnau (1993) observed

shearing after reaching an early peak value was constant or

decreased slightly, and pore water pressures decreased slightly

150

after reaching an early peak value. These tests were done on compacted sand-bentonite mixture at a low confining pressure of 0.6 MPa (Lingnau 1993). In the current test series, the undrained heated specimen (T1471) shows dilative behaviour at 65°C (Pts.3-4 in Figs.8.27, 8.28, and 8.29b). The relationship in Fig.8.29b between du and dp is no longer linear, indicating plastic, post-yielding behaviour.

This study has shown that normally consolidated reconstituted illite specimens produce lower pore water pressures during shearing at higher elevated temperature. However, in overconsolidated specimens, the pore water pressures during shear exhibit similar behaviour to tests at lower pressures and temperature. In the compacted illite specimens, the behaviour is more complex (Fig.8.28a). At a consolidation pressure of 1.0 MPa, the pore water pressures generated during shear at a higher temperature are higher than at lower temperature. However, when the consolidation pressure was lower (0.5 MPa), the pore water pressures were also lower, but now they were more markedly dilative. The magnitudes of the pore water pressures were similar until they reached their maximums, though the hotter specimen was more dilative. The increases in shearing resistance q with straining were more pronounced at lower consolidation pressures (Figs.8.25 and 8.26).

After the end of shearing, the specimens tested at 65°C were cooled to 28°C under undrained conditions without controlling q. The

resulting stress paths in Figs.8.26 and 8.27 show that similar reductions in q and increases in p′ during cooling were obtained from specimens consolidated at both 0.5 MPa and 1.0 MPa. The stress state following cooling in Test T1469 (0.4 MPa, 65°C) was close to that in Test T1485 (1.0 MPa, 28°C). In addition, for T1471 which had ramped temperatures, the stress state upon cooling after shearing and cooling was almost the same as the stress state before heating.

In Test T1470 (Fig.8.26), if the final stress state at 28°C after cooling from 65°C is taken as the same as the stress state at 28°C for an unheated specimen, the thermally induced pore pressure would be 0.28 MPa at q = 0.3 MPa. This value is the same as the value, 0.28 MPa, calculated from $(\Delta u/p'_0)$ = 0.4, reported earlier, with p'_0 = 0.7 MPa. Also, in Test T1471 (Fig.8.27) the stress state after cooling from 65°C to 28°C was close to the stress state before heating at q = 0.45 MPa. Again, the calculated thermally induced pore pressure was 0.37 MPa, close to what was actually measured during heating. The stress paths for Tests T1470 and T1471 show similar stress paths at 65°C, and similar failure stresses in terms of p′ and q. It appears reasonable to say that specimens at the same stress and volume behave similarly in terms of their stress-strain relationships and stress paths. The specimens in Tests T1470 and T1471 can be said to have similar volumes and stresses at failure, that is, the same p′, q, V-states. This assumption allows explanation of the cooling behaviour. In Test T1471, undrained

152

heating to 65°C was performed at q = 0.45 MPa. During bulk-undrained heating, the volume of the specimen increased, producing higher specific volume V. On the other hand, the specimen in Test T1470 was heated before shearing from 28°C to 65°C with drainage lines open. This specimen was sheared undrained at 65°C. Shearing started from two different end-of-consolidation states with different κ-lines and specific volumes. However, at the end of shearing, both specimens were at the same temperature, and essentially the same values of p' and q. The two specific volumes are essentially the same, at failure, and so the cooling behaviour was also the same in terms of its final stress state.

The initial specific volumes in Tests T1470 and T1471 are different, with T1470 having the lower value. This produces lower thermal expansion and contraction for T1470, based on the calculation $\Delta V_{uT} = V\beta_{UT}\Delta T$ where both specimens have the same β_{uT} and ΔT. This shows that the lower thermally induced pore water pressures can not only be described and explained, but expected.

8.3 Compacted Sand-bentonite Mixture

8.3.1 Effect of Elevated Temperature

Three specimens of sand-bentonite (T1401, T1402, and T1406) were consolidated to 1.5 MPa at 28°C, and two of them (T1402 and T1406) were heated drained to 65°C and 100°C respectively. They were then sheared undrained at constant temperature (Fig.8.30). The deviator stresses in T1401 and T1402 rise gradually and reach approximately

153

constant values at about 5% axial strain. (For reasons discussed later, the results for T1406 in Fig.8.30 are considered non-typical.) Some small amount of strain softening is observed after peak deviator stress, but the effect is not marked. Pore water pressures increased initially to about 1% to 2% strain, and then decreased through to the end of the tests. No shear planes were observed in these specimens. The resulting stress paths are shown in Fig.8.31, and indicate that similar stress paths are followed at each temperature. It may be seen that the higher temperature (T1406) produces higher peak strength (and more especially higher η_f), but the critical state strengths (the large-strain failure envelope) appear to be independent of temperature. Similar observations reported by Lingnau (1993) for the same material.

Due to some testing difficulties in Test T1406, the specimen was initially presheared undrained. It is not known how much axial deformation occurred during this pre-sheared loading. The general pattern of behaviour from this specimen is like that observed at 28°C and 65°C, although more marked dilatancy and stain softening are evident.

Pore water pressure parameters defined by $m = \Delta u/\Delta p$ are shown in Table 8.3 for the compacted sand-bentonite mixture at each temperature. It is not clear how m values change with temperature at a given pressure. Figure 8.31 and 8.34a give some indication that m may decrease with temperature at a consolidation pressure of

154

1.5 MPa. A more extensive set of tests by Lingnau (1993) reported, however, that m increases with temperature at 1.6 MPa. The peak pore water pressure seems to be largely independent of temperature, though after the peak value has been reached, pore water pressures decrease more rapidly at higher temperatures.

Table 8.3 m values for compacted sand-bentonite mixture

Temperature(°C)	m-value	Consolidation pressure p′(MPa)
28	1.67	1.5
65	1.06	1.5
100	1.00	1.5

8.3.2 Effect of Ramping Temperature

The specimen (T1475) was sheared undrained at 28°C at 1.5 MPa to a deviator stress of q = 0.5 MPa (Pts.1-2 in Figs 8.32 and 8.33), and was then heated under bulk undrained conditions to 100°C with q, held constant (Pts.2-3). After the pore water pressure reached equilibrium, the specimen was sheared undrained at 100°C (Pts.3-4). After undrained heating, the specimen was able to sustain only a small increase in shear stress with further straining (Pts.3-4). During this phase, the pore water pressure decreased with straining. After cooling from 100°C to 28°C, the specimen was sheared undrained at 28°C (Pts.5-6) It was able to carry greater shear stress than at 100°C. The stress-strain curve show slight softening with further straining and almost constant pore water pressure.

Previous research at 26°C to 28°C (Saadat 1989, Lingnau 1993) suggests that a consolidation pressure of about 1.5 MPa, the sand-bentonite buffer material expresses ductile behaviour. On the other hand, at lower pressures of about 0.6 MPa-0.8 MPa, it exhibits more dilatant behaviour. This is similar to the behaviour observed in this study. Undrained heating from Pt.2 to Pt.3 caused a reduction of mean effective stress p'. The behaviour after undrained heating is governed mainly by this effective stress. Yield loci shrink due to heating. However in this case, the reduction of effective stress through the generation of thermally induced pore water pressure is larger than the reduction of preconsolidation pressure caused by the heating. The overall stress-strain behaviour is controlled by the effective stress, and the material now appears to be more heavily overconsolidated. Similarly, upon cooling, the effective stress increases and the resulting behaviour became more ductile.

8.3.3 Discussion

Figure 8.34 shows relationships between du and dp for constant elevated temperatures (Fig.8.34a) and for ramped temperatures (Fig.8.34b). As mentioned earlier, there is some indication that $m = du/dp$ decreases with temperature (Fig.8.34a), and for reversibility of thermally induced pore water pressures following a temperature cycle (Fig.8.34b).

In Test T1475 (Figs.8.32 and 8.33), after undrained heating there was some evidence of dilative behaviour decreasing in u (Pts.3-4).

However the effect was not as significant as in the illite specimens. Considered earlier, and the deviator stress q did not actually decrease during this phase of the test. This may be due to the high plasticity of the sand-bentonite specimen. As is well-known, strongly dilative behaviour is often encountered in less plastic clays, silts, or sand. The sand-bentonite mixture used in this study has a plasticity index of 92 and can be classified as highly plastic clay. (The clay phase alone has a plasticity index of about 200. The material is clay-dominated.) One can reasonably expect that dilative behaviour is less pronounced in this sand-bentonite specimen than in the less plastic illite.

8.4 Discussion

Generally, the three types of clay materials that have been tested, reconstituted illite, compacted illite, and a compacted sand-bentonite mixture, show generally similar behaviour. However, differences in detail are noticeable. Even between the two types of illite specimens, the compacted illite has different characteristics in both drained and undrained tests when compared with data from the reconstituted illite. The compacted illite behaves like an overconsolidated soil and exhibits strong anisotropy and dilatancy. When compared with other compacted clays, similar behaviour has been obtained in this study, and some general conclusions can perhaps be drawn about the behaviour of compacted clays. The general behaviour of the compacted sand-bentonite mixture is basically similar to that of the compacted illite. Because of different mineral composition,

their strengths (particularly their large-strain strengths) are totally dominated by their original clay material. The following discussion presents more details of these relationships, and compares the undrained results in this chapter with data obtained from the drained tests discussed in a previous chapter.

8.4.1 Elasticity

Comparison between undrained and drained test results: The results obtained from reconstituted illite specimens in tests at 28°C (T1486 and T1482) and at 65°C (T1466 and T1443) are of interest because the stress paths followed in these tests are more or less similar in $p'-q$ space (approximately p' = constant), but they were under different temperature and drainage conditions. In each case one was drained and the other undrained (Figs.8.35 and 8.36). Thus they should provide evidence of any influence of temperature and drainage conditions on shear behaviour. As can be seen from Figs.8.37a and 8.38b, the stress-strain behaviour in terms of shear stress-shear strain plots are also very similar. In Figs.8.37b and 8.38b, the volumetric strains in the drained tests (T1482 and T1443) are small during shear, and of course there are no volume changes in the undrained tests (T1486 and T1466). One might expect that in these two tests at a given temperature, the stiffness and strength of the specimens should also be similar. This is clearly shown in Figs.8.35-8.38.

Similarly, comparisons are possible between two undrained tests (T1495 and T1470) and two drained tests (T1487 and T1446) on compacted illite with stress paths close to those in conventional drained tests ($\Delta q/\Delta p = 0$, $\Delta\sigma_3 = 0$). Tests T1495 and T1487 were done at 28°C, while T1470 and T1446 were at 65°C. Once again stress-strain relationships are similar between undrained and drained tests at both temperatures (Figs.8.41 and 8.42). This indicates that Poisson's ratio μ in compacted illite in conventional drained test ($\Delta q/\Delta p = 3$) must be fairly close to 0.5 which is the case in the undrained test. This suggests that the radial stiffness in compacted illite consolidated at 0.5 MPa is less than in reconstituted illite which has a Poisson's ratio of about 0.3.

Contours of shear strains for reconstituted illite at temperatures of 28°C, 65°C, and 100°C in p'–q space are shown in Fig.8.43. It seems there may be something approaching a unique relationship between shear strain ε_s and deviator stress q in p', q stress space in reconstituted illite. Similar contours were obtained on compacted illite (Fig.8.44) and compacted sand-bentonite mixture (Fig.8.45) at all temperatures. The differences between the relationships for all three soils and all three temperatures are remarkably small.

8.4.2 State Boundary Surface

Displays of information about triaxial states of stress (p',q) and about specific volume V requires two two-dimensional plots of the

159

stress plane (q,p′) and the compression plane (V, p′) or one three-dimensional plot (q,p′, V). The Cam clay model can point the way to two-dimensional devices for displaying this information..

A way of inter-relating information about mean effective stresses p′ and deviator stresses q obtained at different specific volumes is to project these data on to a constant volume section. This can be done by normalizing the stresses (p′, q) with respect to the so-called equivalent consolidation pressure p_e'. This equivalent consolidation pressure is the pressure which, in isotropic normal compression, would give the soil its current specific volume. Full details of this concept were described by Wood (1990), and, will not be repeated here. Some important aspects of the concept are shown below.

For stress states on the current yield locus,

[8.4.1]
$$\frac{p'}{p_o'} = \frac{M^2}{M^2 + \eta^2}$$

[8.4.2]
$$\frac{p'}{p_e'} = \left(\frac{M^2}{M^2 + \eta^2} \right)^{\Lambda}$$

where p_o' = consolidation pressure, M = critical state strength parameter, η = current stress state (q/p′) and $\Lambda = 1-(\kappa/\lambda)$ in which κ = slope of unload-reloading line and λ = slope of normal consolidation line. Evidently,

[8.4.3]
$$\frac{q}{p'_e} = \frac{\eta p'}{p'_e}$$

and the pair of expressions [8.4.1] and [8.4.2] can be used to generate the curve in the (p'/p'_e) vs. (q/p'_e) plane corresponding to the Cam clay yield locus. The composite envelope in a plot of (p'/p'_e) vs. (q/p'_e), consisting of the Roscoe yielding surface, the Hvorslev rupture surface, and the tensile fracture surface $(\sigma'_3 = 0)$, can be called a state boundary surface (SBS). Because p'_e remains unchanged during a constant volume undrained test, undrained effective stress paths map directly into the (p'_e/p') vs. (q/p'_e) diagram.

Stress paths in both undrained and drained tests at 28°C, normalized by equivalent pressure, are shown in Fig.8.46. (Here the tensile fracture surface is drawn as a straight line with a slope of 3(V): 1(H) from the origin. The Hvorslev rupture surface that describes overconsolidated strengths may be seen in Figs 8.46 as the straight line drawn between tensile fracture and the Roscoe yield surface. The data for this line were taken from anisotropically consolidated illite tested by Graham et al. (1983) for comparison purposes.) Equivalent pressures were determined from the normal consolidation curve at each stage in the tests (Fig.5.11) at the specific volume of the specimen at 28°C. In undrained tests, the equivalent pressure is equal to the consolidation pressure for normally

161

consolidated specimens, and stress path forms the yield surface (Roscoe yield surface). This is the limit state of the specimen. As can be seen, the shape of the yield surface in the plot of (p'_e/p') vs. (q/p'_e) is no longer elliptical as in Cam clay. Similar results were reported for reconstituted isotropically-consolidated soils (Roscoe et al. 1963), but only at room temperature.

In drained tests in which the specimens were overconsolidated, stress paths can be normalized by the known equivalent pressure derived from the current specific volume of the specimen. Once the specimen yields, the subsequent stress states lie on the state boundary surface and do not go beyond it. Stress paths for the drained tests in Fig.8.46 show that after yielding (shown by open circles in the figure) subsequent stress paths lie close to the SBS determined from undrained tests in which boundary conditions are different. It should also be noted that the slopes of stress paths in (p'_e/p') vs. (q/p'_e) plots are not the same as those in p' vs. q plots, because V and hence p'_e vary systematically through the tests. It can be seen that end-of-test data in the present study on isotropically consolidated illite lie close to the envelope determined by Graham and his colleagues.

These two-dimensional SBS representations bring drained and undrained responses together into a single diagram in terms of effective stresses. They help to emphasize the fact that different

modes of testing are merely probing different parts of a single unified picture of soil behaviour.

One might expect that similar treatment could be applied to test data for elevated temperatures. Results for reconstituted illite at 65°C and 100°C are shown in Figs.8.47 and 8.48. The stress paths for normally consolidated undrained tests form the Roscoe yield surface, and stress paths from the drained tests after yielding follow the SBS determined from the undrained tests. (In this treatment of the data, p'_e has been determined throughout from the NCL for 28°C. A later section will consider the effect of evaluating p'_e from the NCL for the temperature at which the test was performed.) The Roscoe yielding surfaces at 65°C and 100°C are reasonably similar in shape, but smaller in size at higher temperature. That is, the state boundary surface shrinks at higher temperature. Close examination of Roscoe yield surface reveals that the shape of the SBS at higher temperature is slightly different from that at lower temperature. This can be attributed to the higher κ-value found in Chapter 5 (Fig.5.8) at higher temperature. The Hvorslev rupture surfaces at 28°C, 65°C and 100°C all seem to have similar slope, although it is fair to note that the data do not provide a strong control on whether they are indeed the same.

Figures 8.49 and 8.50 respectively show state boundary surfaces evaluated in the same way for compacted illite specimens at 28°C and

65°C. Both p′ and q were once again normalized with the equivalent pressure p'_e from the 28°C NCL.

Although only one set of data is available to specify the state boundary surface below the critical state line, (for example, T1448 in Fig.8.50), it is reasonable to assume the shape of the SBS is distorted by compaction and no longer elliptical. Interestingly, the size of SBS for compacted illite is smaller compared with that for reconstituted illite (Figs.8.46-8.48) when the figures are drawn using the used equivalent pressure of reconstituted illite. One might expect from this that compacted illite has lower strength. However, usually the specific volume of compacted illite is smaller than for reconstituted illite at the same pressure, and then its strength would be higher. It appears that the slopes of the Hvorslev surfaces for reconstituted and compacted illite are similar. Inside the SBS, soil behaves elastically in theory, but not necessarily isotropically. This was shown earlier to be the case in compacted illite.

Graham *et al.* (1988) reported that state boundary surface normalized by equivalent pressure p'_e(1-D) determined from one-dimensional consolidation gave an elliptical shape rather than the "hooked" shape shown in Fig.8.44 and 8.50. This hooked shape is due to some difficulties involved in determining yield stresses along the isotropic reconsolidation line, that is, the p′-axis. As p′ increases isotropically, the specimen obviously yields at some

164

point.   Thereafter, continuous increase in p′ does not produce
distinctive increases in volume (shown in Fig.7.11) because further
stressing   causes   the   specimen   to   approach   the   isotropic
consolidation   line   (NCL).   Sometimes,   therefore,   yield   stresses
determined   from   volume   strains   may   be   misleading   and   do   not
represent the real value.

A principal advantage of the state boundary surface approach is that
tests with different boundary conditions can be treated in a single
surface.   This work has also shown the existence of separate state
boundary surfaces for different temperatures.   When a soil specimen
is yielding, (that is, it is existing outside its range of elastic
behaviour), it lies on   the state boundary surface (SBS) for its
current temperature.   While the soil is behaving elastically, its
stress state is located inside the SBS.   The shapes of the SBS at
different temperature seem to be slightly different due to different
slopes κ of the corresponding unload-reload lines.   As κ-values
become larger at higher temperatures, the curvature of the SBS from
the p′-axis becomes steeper and its size becomes smaller.

8.4.3 Strength

Comparison between reconstituted and compacted illite specimens in
both drained and undrained tests shows that the large-strain failure
envelopes in p′-q space for both sets of specimens are independent
of testing temperature (Fig.8.51)   Data from both undrained and
drained tests show that the failure envelope has slope of M = 1.07

corresponding to $\phi' = 27.0°$. These are typical values for illite and low plastic clays.

At large-strain failure, the strength of a soil depends mainly on its mineralogy (illite), and not on how it was formed, (for example by isotropic consolidation from slurry or by static compaction). Reconstituted and compacted specimens both have similar slope in failure envelopes (M = 1.07, $\phi' = 27.0°$, Fig.8.51). Earlier research by Graham *et al.* (1983) showed that a different anisotropically consolidated illitic clay had similar strength parameters (M = 1.05).

The undrained tests on compacted sand-bentonite mixtures produced the curved failure envelope shown in Fig.8.52. This can be approximately modelled in the range 0 to 2.5 MPa by a straight failure envelope with M = 0.65, $\phi = 17.1$. These are typical values for montmorillonite and high plastic clays. In Fig.8.52 the failure envelope is shown to be independent of temperature in tests with elevated and ramped temperatures. A similar conclusion was reached by Lingnau (1993) for the large-strain normally consolidated envelope in his tests. This work suggested that the failure envelope depends of course on soil type, but is independent of initial soil structure and temperature.

166

CHAPTER 9 DEVELOPMENT OF THERMO-ELASTIC-PLASTIC (TEP) MODEL FOR SOIL

This chapter describes a new thermo-elastic-plastic (TEP) model based on the constant-temperature Critical State model (Schofield and Wroth 1960, Roscoe and Burland 1968). The new model can describe soil behaviour at different temperatures under various boundary conditions with only a few modifications to the Critical State model. As outlined in Chapter 3, a complete elastic-plastic model requires identification of the following requirements

(1) Elastic properties

(2) Yield surface

(3) Hardening rule

(4) Plastic potential

(5) Failure mode

Following paragraphs present the assumptions that have been made in the proposed model. These assumptions arise from the studies of the effects of temperature on real soil behaviour described in preceding chapters. After this, details will be given of the theory of the thermo-elastic-plastic model. Chapter 10 will identify the material parameters that have been selected from the experimental results shown in Chapters 5 to 8 for drained and undrained tests. These parameters will then be used to compare predicted and measured stress-strain behaviour in tests that were not used in forming the model.

The TEP model that has been developed is for isotropically consolidated soils under axially symmetric $(\sigma_2'=\sigma_3')$ conditions such as those encountered in 'triaxial' stress states. Generalization in terms of stresses and strains for the case when $\sigma_2' = \sigma_3'$ is possible if some further assumptions are adopted (Zhang 1992). The model considers only rate independent soil in which creep behaviour is unimportant (Yin 1990).

Under the triaxial stress conditions that have been adopted here, the locus of the state boundary surface for saturated soils may be described by a surface in a three-dimensional space, having specific volume (or water content) as one axis, and two effective stress components

[9.1] $$p' = (\sigma_1' + \sigma_2' + \sigma_3')/3$$

and

[9.2] $$q = \sigma_1' - \sigma_3'$$

as the remaining two axes.

As in preceding chapters, the following definitions have been employed for the volume strain (ε_v) and deviator strain (ε_s) invariants:

[9.3a] $$\varepsilon_v = (\varepsilon_1 + \varepsilon_2 + \varepsilon_3)$$

[9.3b] $$\varepsilon_s = \frac{1}{3} \sqrt{2\{(\varepsilon_1 - \varepsilon_2)^2 + (\varepsilon_2 - \varepsilon_3)^2 + (\varepsilon_3 - \varepsilon_1)^2\}}$$

In case of triaxial test, $\varepsilon_2 = \varepsilon_3$ so that

[9.4a] $$\varepsilon_v = (\varepsilon_1 + 2\varepsilon_3)$$

[9.4a] $$\varepsilon_s = \frac{2}{3} (\varepsilon_1 - \varepsilon_3)$$

9.1 Framework for the TEP Model

9.1.1 Assumptions

On the basis of experimental data published in the literature, Chapter 3 outlined some assumptions that would be needed for the thermo-elastic-plastic modelling. The experiments performed for this thesis (Chapter 5 to 8) show that these assumptions are reasonably valid for isotropically consolidated saturated clay. The assumptions may be restated as follows.

(1) Elastic properties such as shear modulus G and bulk modulus K depend on temperature. More specifically, modulus value are lower at higher temperatures. This leads to the slope κ of unload-reload lines in V-$ln\ p'$ space increasing with increasing temperature.

169

(2) Yield loci shrink with increasing temperature, but their shapes remain elliptical in p'-q space.

(3) First-time compression curves (the normal consolidation lines) have slopes λ that are independent of temperature, though the lines themselves are at successively lower values of specific volume at higher temperatures.

(4) Large-strain strength envelopes are independent of temperature in p'-q space. Their slope $M = (q_f/p'_f)$ is a unique value in p'-q space at all temperatures.

(5) The flow rule is associated at all temperatures.

One additional assumption has been made here from the experimental observations described in Chapter 6:

(6) The coefficient of undrained thermal expansion of soil is independent of temperature.

As mentioned earlier, the material is assumed to be isotropic and rate-independent. The stress-strain relationship during unloading and reloading is considered to be linearly elastic, although the bulk modulus K ($= Vp'/\kappa$) and the shear modulus G depend on stress level. For the sake of brevity, the basic features of the Critical State theory, and specifically the Cam Clay model proposed by

Schofield and Wroth (1968), and Roscoe and Burland (1968), will not be repeated here. Specifically the form of the Modified Cam clay model (in contrast with the original Cam clay model) will be adopted here (Wood 1990). Following comments will be confined to modifications and adjustments needed to expand the capabilities of the Cam Clay model so that effects of temperature on soil behaviour can be incorporated.

One deficiency of the model, as of all Cam Clay models, is that it assumes perfectly elastic behaviour inside the yield locus. Despite this deficiency, its relative simplicity and reasonable assumptions make the model an attractive approach for predicting the effects of temperature on soil behaviour.

9.1.2 Elasticity

As can be seen in chapter 7, yield loci can be considered as defining elastic domains that vary with temperature. In the following discussion, incremental strains and stresses will be used to facilitate a possible later application of the model in numerical modelling, for example using the finite element method (FEM). Infinitesimal differential components of stresses and strains are denoted by the symbol 'd', while the symbol 'Δ' represents finite difference.

Elastic volumetric strains $d\varepsilon_v^e$ are composed of a volumetric strain component ε_v^{se} and a shear strain component $d\varepsilon_s^{se}$. Because as

discussed earlier, elastic volumetric strains are not only mechanically induced, but also thermally induced, the volumetric strains can be written as

[9.5] $$d\varepsilon_v^e = d\varepsilon_v^{se} + d\varepsilon_v^{Te}$$

where $d\varepsilon_v^{se}$ = stress-induced elastic volumetric strain, and $d\varepsilon_v^{Te}$ = thermally induced elastic volumetric strain.

It appears reasonable to assume that the elastic shear strain is purely mechanical and has no component that is thermally induced. That is,

[9.6] $$d\varepsilon_s^e = d\varepsilon_s^{se}, \text{ and } d\varepsilon_s^{Te} = 0$$

where $d\varepsilon_s^{se}$ = stress-induced elastic shear strain and $d\varepsilon_s^{Te}$ = thermally induced elastic shear strain.

The stress-induced elastic volumetric strain is related to the bulk modulus in such a way that

[9.7] $$d\varepsilon_v^{se} = \frac{dp'}{K_T}$$

where dp' = increment of mean effective stress, and K_T = isothermal bulk modulus that depends on temperature. From Cam Clay modelling,

there is also a relationship between the elastic bulk modulus K_T and the slope κ_T of the corresponding unload-reload line which here depends on temperature:

[9.8]
$$K_T = \frac{Vp'}{\kappa_T}$$

where V = specific volume, p' = mean effective stress.   Equation [9.7] therefore becomes

[9.9]
$$d\varepsilon_v^{se} = \frac{\kappa_T}{Vp'}\, dp'$$

The assumption $\kappa = \kappa_T$ allows calculation of $d\varepsilon_v^{Te}$.   Figure 9.1 illustrates different κ lines which intersect at a certain consolidation pressure p_o' at which the overconsolidation ratio OCR is specified as OCR_{To} and the thermal elastic volume strain becomes zero.   In the remainder of this chapter the subscripts $(_1)$ and $(_2)$ represent temperatures T_1 and T_2 where $T_1 < T_2$.   The value of OCR_{To} can be determined as

[9.10a]
$$OCR_{To} = \frac{p_{c_1}'}{p_o'}$$

where p_c' = preconsolidation pressure.   If values of p_{c1}' and p_{c2}' are known at temperatures T_1 and T_2 at the same specific volume, then

$$[9.10b] \qquad OCR_{T_0} = \left(\frac{p'_{c1}}{p'_{c2}} \right)^{\left(\frac{\kappa_2}{\kappa_2 - \kappa_1} \right)}$$

The thermo-elastic volumetric strain $d\varepsilon_v^{Te}$ for heating at an isotropic consolidation pressure p'_A can be defined from the difference between the modelled specific volumes (at A and A') at different temperatures, as illustrated in Fig.9.1. The relationship between the thermally induced volumetric strain and specific volume is given by

$$[9.11] \qquad d\varepsilon_v^{Te} = \frac{dV^{Te}}{V}$$

The κ line is defined as

$$[9.12a] \qquad \kappa = \frac{dV}{d\ln p'}$$

It is assumed from experimental data described in Chapter 5 that the variation of κ with temperature can be expressed

$$[9.12b] \qquad \kappa = \kappa_0 \left[1 + B \ln (T/T_0) \right]$$

where κ_0 = the value of κ at a selected reference temperature, B = constant, T_0 = reference temperature (°C), and T = temperature (°C).

174

With the aid of Fig.9.1, the thermo-elastic volumetric strain becomes

[9.13a]
$$d\varepsilon_v^{Te} = \frac{\kappa_2 - \kappa_1}{V} \ln \left(\frac{OCR_{To}}{OCR} \right)$$

Therefore, using [9.10]

[9.13b]
$$d\varepsilon_v^{Te} = \frac{\kappa_2 - \kappa_1}{V} \ln \left\{ p' \times \left(\frac{(p_{c_1}')^{\kappa_1}}{(p_{c_2}')^{\kappa_2}} \right)^{\left(\frac{1}{\kappa_2 - \kappa_1} \right)} \right\}$$

where p' = consolidation pressure, p_{c1}' = preconsolidation pressure at T_1, and p_{c2}' = preconsolidation pressure at T_2.

As in the usual manner in isothermal elasticity, the elastic shear strain $d\varepsilon_s^{se}$ can be expressed by a shear modulus that depends on temperature:

[9.14]
$$d\varepsilon_s^{se} = \frac{dq}{3G_T}$$

where dq = increment of shear stress, and G_T = shear modulus that depends on temperature.

It is also assumed that the shear modulus G is related to the consolidation pressure p_o' and the overconsolidation ratio (OCR) in the way proposed by Wroth and Houlsby (1985):

[9.15a]
$$\left(\frac{G}{p_o'} \right)_{oc} = \left(\frac{G}{p_o'} \right)_{nc} [\ 1 + C\ ln\ (OCR)\ ]$$

where C = dimensionless constant, and OCR = overconsolidation ratio at reference temperature. This has been extended by the author to include the effect of temperature change

[9.15b]
$$\left(\frac{G}{p_o'} \right)_{oc} = \left(\frac{G}{p_o'} \right)_{nc} [\ 1 + C\ ln\ (OCR)\ ] \{\ 1 + D\ (T-T_o)\ \}$$

where D = constant, and $(T-T_o)$ = change in temperature (°C).

9.1.3 Flow Rule, Hardening Rule, Yield Function, and Plasticity.

For the sake of simplicity, the model assumes an associated flow rule in which the yield function and plastic potential coincide in stress space. That is, the resultant of $d\varepsilon_v^p$ and $d\varepsilon_s^p$ is normal to the local yield locus. This assumption is also used in Cam Clay modelling. Total strains are composed of both elastic strain components and plastic strain components. In a similar way as was done earlier for total elastic strains, total plastic strains are taken as comprising plastic volumetric strain components and plastic shear strain components.

Because, as has been discussed earlier, plastic volumetric strains $d\varepsilon_v^p$ are not only mechanically induced, but also thermally induced. These strains can be written:

176

[9.16]
$$d\varepsilon_v^p = d\varepsilon_v^{sp} + d\varepsilon_v^{Tp}$$

where $d\varepsilon_v^{sp}$ = stress-induced plastic volumetric strain and $d\varepsilon_v^{Tp}$ = thermally induced plastic volumetric strain. Again, the plastic shear strain is assumed to be purely mechanical and independent of temperature. That is,

[9.17]
$$d\varepsilon_s^p = d\varepsilon_s^{sp}, \text{ and } d\varepsilon_s^{Tp} = 0$$

where $d\varepsilon_s^{sp}$ = stress-induced plastic shear strain and $d\varepsilon_s^{Tp}$ = thermally induced plastic shear strain.

The stress-induced plastic volumetric strain can be derived from the consolidation behaviour of the soil, that is the hardening rule. Figure 9.2a illustrates the normal consolidation NCL line and an unload-reload URL line for a soil at a single temperature. The consolidation characteristics of the soil are assumed to be adequately represented in V *vs.* *ln* p′ space by the normal consolidation line

[9.18a]
$$V = N - \lambda \, ln \, p'$$

and the family of swelling lines

[9.18b]
$$V = V_o - \kappa \, ln \, p'$$

177

where V = specific volume, λ = slope of the normal consolidation line, κ = slope of the unload-reloading lines and N = normal consolidation specific volume at unit pressure. The parameters λ, κ, and N are material properties, while V_o is the specific volume at unit pressure on the current unload-reloading line and is therefore not a material property. The current specific volume at any pressure can be defined as

[9.18c]
$$V = N - \lambda \ ln \ p_c' + \kappa \ ln \ \frac{p_c'}{p_o'}$$

where p_c' = preconsolidation pressure, p_o' = consolidation pressure.

Because the plastic strain is nonrecoverable, it can be defined for a general temperature T as

[9.19]
$$d\varepsilon_v^{sp} = \frac{(\lambda - \kappa_T)}{Vp'} \ dp'$$

This relation implies that stress-induced plastic volumetric strains depend on κ_T, that is, on temperature. Remember that λ is independent of T.

Thermally induced plastic volumetric strains can be determined by dividing $d\varepsilon_v^T$ into two components:

[9.20a]
$$d\varepsilon_v^T = d\varepsilon_v^{Te} + d\varepsilon_v^{Tp}$$

178

where $d\varepsilon_v^{Tp}$ = thermally induced plastic volumetric strain. From the separation of the normal consolidation lines (NCL) as a function of elevated temperature (Fig.9.2b), thermally induced volumetric strain may be approximated as in Fig.9.3

[9.20b]
$$d\varepsilon_v^T = E (T - T_o)$$

where E = constant. Therefore, using the thermally induced elastic volumetric strain $d\varepsilon_v^{Te}$ determined previously by eqn.[9.13a], the plastic component of thermally induced volume strain $d\varepsilon_v^{Tp}$ becomes

[9.21]
$$d\varepsilon_v^{Tp} = E \, dT - \frac{\kappa_2 - \kappa_1}{V} \, ln \left(\frac{OCR_{To}}{OCR} \right) \quad .$$

Description of all the strain components is now complete and can be calculated using an appropriate yield function and material parameters.

The model assumes the shape of yield locus to be elliptical. In this case the yield function f may be expressed:

[9.22]
$$f = q^2 - M^2 [p' (p_c' - p')]$$

The yield function f in Cam Clay is known to vary with the past highest isotropic consolidation pressure. It also varies with the Coulomb-Mohr strength parameter M, and hence with the mineralogy of the clay. The particular contribution from this thesis is that f also varies with temperature through its effect on p_{cT}' (see Fig. 7.9).

179

Isotropic yield stresses p_T' at elevated temperatures and constant specific volume (Fig.9.2b) now can be determined from:

[9.23a] $$p_T' = p_1' \ / \ exp \ (d\varepsilon_v^T/\lambda)$$

Therefore, from [9.20b]

[9.23b] $$p_T' = p_1' \ / \ exp \ (EdT/\lambda)$$

It was assumed earlier that the soil obeys the normality condition, that is, an associated flow rule. In this case, the plastic potential and the yield surface coincide, so

[9.24] $$d\varepsilon_v^p = \chi \ \frac{\partial f}{\partial p'}$$

[9.25] $$d\varepsilon_s^p = \chi \ \frac{\partial f}{\partial q}$$

where χ is a scalar multiplier whose value will be derived subsequently from the assumed hardening characteristics of the soil. Based on the assumed flow rule, the vector of plastic strain increments $d\varepsilon_v^p$ and $d\varepsilon_s^p$ is in the direction of the outward normal to the yield locus. Therefore, by differentiating yield function f [9.22] with respect to the stresses p' and q,

[9.26a] $$\frac{d\varepsilon_s^{sp}}{d\varepsilon_v^{sp}} = \frac{(\partial f/\partial q)}{(\partial f/\partial p')}$$

[9.26b] $$\frac{d\varepsilon_s^{sp}}{d\varepsilon_v^{sp}} = \frac{2q}{M^2 \ (2p' - p_c')} = \frac{2\eta}{M^2 - \eta^2}$$

180

where $\eta = q/p'$. The plastic shear strain can therefore be written as

[9.27]
$$d\varepsilon_s^{sp} = d\varepsilon_v^{sp} \frac{2\eta}{M^2 - \eta^2}$$

All the strain components, $d\varepsilon_v^{se}$, $d\varepsilon_v^{Te}$, $d\varepsilon_v^{sp}$, $d\varepsilon_v^{Te}$, $d\varepsilon_s^{se}$, and $d\varepsilon_s^{sp}$, have now been defined and values can be calculated using the equations shown in the preceding paragraphs.

Coupling of the elastic modulus with temperature and preconsolidation pressure p_c' relates it to plastic straining. This has been observed experimentally, but adds complexity in defining the flow rule for numerical modelling.

9.1.4 Failure Condition

Figure 9.4 illustrates the failure criteria that have been used in the model in different stress ranges. They include the Mohr-Coulomb (Critical state) line for normally consolidated states, the peak strength failure line for overconsolidated states, and the no-tension line. In p'-q space for triaxial compression tests, the Mohr-Coulomb criterion can be expressed as

[9.28]
$$q_f = M \, p_f'$$

where M = critical state strength parameter, q_f = deviator stress at failure, and p_f' = effective mean stress at failure.

181

For peak strengths on overconsolidated specimens, the peak strength line is introduced.

[9.29]
$$q_p = H (F + p_p')$$

where F = constant, H = slope of the line in p'-q space, q_p = peak deviator stress, and p_p' = peak effective mean stress. The slope of the peak strength line can be determined as

[9.30]
$$H = \frac{M (p_c'/2) - q_p}{(p_c'/2) - p_p'}$$

where p_c' = preconsolidation pressure. It is assumed here that the slope H of the peak strength line is independent of temperature.

The no-tension line assumes that the soil can withstand no tensile effective stresses. The condition of zero effective radial stress then defines a limiting line in triaxial compression,

[9.31]
$$q = 3 p'$$

Peak strength failure lines for different preconsolidation pressures then span between the corresponding critical state points and the no-tension line.

The intersection (p'_t, q_t) between the overconsolidated peak strength line and the no-tension line can be expressed as

$$[9.32] \qquad p'_t = \frac{(M - H)\,(p'_c/2)}{3 - H} \; ; \; q_t = 3\,p'_t$$

A complete state boundary surface is determined by (1) the Roscoe surface, (2) the Hvorslev surface which is the projection of peak strength lines at a constant specific volume, and (3) the no-tension line.

Once M, H, and p'_c have been identified, all three components of the strength and yielding behaviour have been defined.

Based on Critical State soil mechanics, undrained shear strength s_u can be expressed as

$$[9.33] \qquad \frac{s_u}{p'_o} = \frac{M}{2} \left(\frac{OCR}{r} \right)^\Lambda$$

where r = spacing ratio between the CSL and NCL at constant specific volume (r = 2 in the Modified Cam Clay model), and $\Lambda = 1 - (\kappa/\lambda)$. For normally consolidated specimens in which OCR = 1, the value of Λ varies with temperature because $\kappa = \kappa(T)$. Therefore, from eqn [9.33] with constant values of p'_o, M and r , the undrained strength s_u varies with temperature. Since κ increases with T, s_u should increase with temperature under a constant p'_o condition.

9.2 Thermal Expansion and Pore Water Pressures

9.2.1 Coefficients of Drained and Undrained Thermal Expansions

As discussed in Chapter 6, it is assumed that the limits of thermal expansions of soil are defined by undrained thermal expansion as an upper bound and by drained thermal expansion as a lower bound.

Coefficients of drained thermal expansion β_{DT} can be calculated using the relative spacing of the λ- and κ-lines with temperature in the new TEP model. By definition:

[9.34a]
$$\beta_{DT} = \frac{(dV^T/V)}{dT} \quad \frac{d\varepsilon_v^T}{dT}$$

Therefore, for overconsolidated specimens using [9.13b]

[9.34b]
$$\beta_{DT}(OC) = \frac{\kappa_2 - \kappa_1}{V\ dT}\ ln\left\{ p' \times \left(\frac{p_{c1}'^{\kappa_1}}{p_{c2}'^{\kappa_2}} \right)^{\left(\frac{\kappa_2}{\kappa_2 - \kappa_1} \right)} \right\}$$

Similarly, for normally consolidated specimens using [9.20b],

[9.34c]
$$\beta_{DT}\ (NC) = E$$

Equation [9.34b] shows that the coefficient of drained thermal expansion for overconsolidated specimens depends on both temperature and stress level, and therefore on overconsolidation ratio. On the

other hand, in [9.34c] the coefficient of drained thermal expansion for normally consolidated specimens is independent of temperature and pressure.

It was shown in Chapter 6 that the coefficients of undrained thermal expansion β_{uT} for normally consolidated and overconsolidated specimens are independent of pressure, and temperature for the three soil types that were tested, with a value of about 2.0×10^{-4} ($°C^{-1}$). This value has been assumed in the subsequent modelling.

9.2.2 Thermally Induced Pore Water Pressure Under Undrained Conditions

Prediction of thermally induced pore water pressure Δu_T under undrained heating conditions can be done using the model described above. The preconsolidation pressure at higher temperature (p'_{c_2}) is determined by using eqn. [9.23b]

[9.35] $$p'_{c_2} = p'_{c_1} \, / \, exp \, (\, EdT/\lambda \,)$$

In the case of normally consolidated specimens, Fig.9.5 shows that the unload-reload line at higher temperature is given by:

[9.36] $$\kappa_2 = \frac{\Delta V_{uT}}{ln \, (p'_{c_1}/p'_2)}$$

where ΔV_{uT} = undrained thermal expansion (= β_{uT} V ΔT), and p'_2 = mean effective stress after undrained heating. Therefore, thermally induced pore water pressure results from the change in p'_c with temperature:

[9.37a] $$\Delta u_{uT} = p'_{c_1} - p'_2$$

[9.37b] $$\Delta u_{uT} = p'_{c_1} \left(1 - exp \left(- \frac{\Delta V_{uT}}{\kappa_2} - \frac{EdT}{\lambda} \right) \right)$$

This equation can be used for both normally consolidated and overconsolidated specimens. For overconsolidated specimens, p'_{c_1} becomes the consolidation pressure p'_o at temperature T_1.

If the model is to be used to evaluate stress-strain behaviour as a function of temperature, values of the following parameters are required; N, λ, κ, $(G/p'_o)_{NC}$, M, C, D, E, H, and β_{UT}. All of these can be easily obtained using the conventional soil tests described in Chapters 5 to 8. The model will permit prediction of stresses, strains, pore water pressures, or volume change behaviour in undrained or drained tests along generalized stress path and at different temperatures. The only restriction here is the assumption of axial symmetry.

9.3 Discussion

Using the proposed thermo-elastic-plastic (TEP) model, valuable qualitative understanding can be obtained about the effects of temperature on soil behaviour. This approach has been shown in the contract research report by Graham *et al.* (1993), and subsequently in a series of papers by Graham *et al.*1993, Lingnau *et al.* 1995, and Tanaka *et al.* 1995). Behaviour of soil under both drained and undrained conditions, whether the stress history is, normally consolidated, lightly overconsolidated, or heavily overconsolidated specimens, can be examined and simulated. The framework of the TEP model has been already prepared for publications by Tanaka *et al.* (1995). The following chapter takes this qualitative approach as a starting point, and develops it further to produce quantitative results.

CHAPTER 10   CALIBRATION AND VERIFICATION OF TEP MODEL

Chapter 9 presented a new framework for a TEP model. Calibration and validation of the model now needs to be established using data from the laboratory tests. In this chapter, the model is calibrated using the results of assigned laboratory tests. Following calibration, predictions using the model will be compared with measured results which had not been previously used in the calibration.

10.1   Evaluation of Parameters for the TEP Model

This section describes how parameters needed for the TEP model can be determined . The required parameters described in Chapter 9 are:

(1) Elastic parameters: κ_T (or B), $(G/p_0')_{NC}$, C and D

(2) Yield function: $f = f$ (p',q,T), chosen to be elliptical

(3) Hardening parameters: N, λ, E

(4) Peak and failure strength parameters: H and M

(5) Undrained thermal expansion coefficients: β_{uT}

Because of its simplicity and the numerical significance in most practical applications, a graphical approach is used to determine the needed parameters.

The isotropic consolidation tests results shown in Fig.5.11 allow the normal consolidation line (λ line) during first loading and the

unload-reload line (κ line) to be obtained for the reference temperature of 28°C. The resulting values of λ and κ are 0.087 and 0.017, respectively. Once the λ-value is determined, the value of N can be calculated knowing a specific volume V at a pressure p′ as

[10.1]
$$N = V + \lambda \ln p'$$

The value of B can be obtained by performing unload-reloading tests at several temperatures and then plotting the values of κ versus temperature (Fig.10.1). The resulting value of B in [9.12b] is given by B = 0.825.

Two methods are available for determining the value of E which specifies the separation of normal consolidation lines at various temperatures. The first method is to perform drained heating tests at constant isotropic effective stress. The resulting volumetric strains can then be directly plotted against temperature and E can be determined as

[10.2]
$$E = \frac{d\varepsilon_v}{dT}$$

where

$d\varepsilon_v$ = thermal volume strain

dT = temperature change

A second method is to perform reloading tests for overconsolidated specimens at elevated temperatures. In reloading tests, the isotropic consolidation pressure should be well above the preconsolidation pressure at lower temperatures so that the normal consolidation line at elevated temperature can be well defined in V-ln p' plot. Once the relationship between V and ln p' is defined, at elevated temperatures the parameter E can be calculated from

[10.3]
$$E = \frac{\Delta V_{DT}}{V}$$

where

ΔV_{DT} = separation of normal consolidation lines at elevated temperatures under constant pressure in a V-ln p' plot,

V = specific volume at lower temperature.

In this research, the first method has been used to determine E, see for example Fig.5.18. The value that has been obtained is E = 2.77 × 10^{-4}.

For normally consolidated clay, it is often assumed that the shear modulus G is proportional to consolidation stress. Wroth and Houlsby (1985) reported that a reasonable fit to the variation of G for clays could be obtained by using the expression [9.15a]

[9.15a bis]
$$\left(\frac{G}{P_o'} \right)_{OC} = \left(\frac{G}{P_o'} \right)_{NC} [\ 1 + C\ ln\ (OCR)\ ]$$

In Wroth's work, non-linear normally consolidated behaviour was approximated by equivalent linear behaviour in restricted stress ranges. However, [9.15a] provides a convenient way of estimating both absolute values of shear modulus G and a trend of behaviour at different pressures and overconsolidation ratios. The relationship is well supported by experimental evidence (see also Ladd *et al.* 1977). A method for determining the shear modulus G is to present stress-strain behaviour in q-ε_s plots which give the value of 3G. This study provides values of (G/p'_0) at OCRs of only 1 (normally consolidated) and 2 (overconsolidated). Averaging the available data suggests a value of C = 0.656.

The degradation of shear modulus with temperature is described by the parameter D which can be determined by plotting G modulus with temperature (Fig.7.17). This gives a value of D = -0.0091 in [9.15b] (Fig.10.2).

As in many research projects, the shear modulus is one which is relatively weakly defined from the test results. To specify failure, the peak and failure strength parameters H and M (Fig.9.4) have to be determined using plots of p'_f *vs.* q_f as shown in Fig.8.46. Critical state strength and peak strength parameters as defined in Fig.9.4 can be expressed by the parameters H and M. The values are M = 1.07, and H = 0.087.

As shown in Fig.7.9, it is reasonable to assume that yield loci are elliptical and can be expressed as

[10.4]
$$f = q^2 - M^2 [p' (p'_o - p')] = 0$$

where

q = current deviator stress,

p′ = current mean effective stress,

M = critical strength parameter, and

p'_o = one half of isotropic preconsolidation pressure p'_c, that is $(p'_o = p'_c/2)$.

In summation of the preceding section, Table 9.1 shows calibration constants used in the TEP model for illite.

TABLE 10.1 Parameters in the TEP model for reconstituted illite

Constant	Value
B	0.825
C	1.51
D	-0.091
E	2.77×10^{-4}
H	0.75
λ	0.087
κ	0.017
$(G/p')_{NC}$	27
M	1.07
N	2.105
β_{uT}	2.0×10^{-4}

10.2 Application to Reconstituted Illite

Preceding sections (Chapter 9 and Section 10.2) formulated and calibrated the TEP model for reconstituted illite material.   Now the model   will   be   used   to   predict   soil   behaviour   under   various

conditions of testing which were not used to provide calibration information.

The model developed in Chapter 9 is of course general in the sense that it can be applied to any stress path and drainage conditions. With the assumptions made at the beginning of this chapter, the model can be used to simulate behaviour of specimens under various stresses and boundary conditions under triaxial loading, provided the model parameters and the initial state of the specimen are known. In following sections, the model has been used to predict yield stresses depending on temperature, thermal volume changes for various OCRs, and thermally induced pore water pressures. Two different types of tests have been simulated. One type consists of drained tests on a lightly overconsolidated specimen (OCR = 2), and on a heavily overconsolidated specimen (OCR = 7.5). The second type consists of undrained heating tests (a) under isotropic stress conditions; and (b) under a given constant deviator stress q.

10.2.1 Prediction of Changes in Yield Stress with Temperature

Equation [9.23 bis] allows prediction of yield stress degradation with temperature at constant specific volume.

[9.23 bis]
$$p_2' = p_1' \, / \, exp \, (EdT/\lambda)$$

Calculated values are shown in Fig.10.3 and compared with measured experimental results for isotropic compression. It can be seen that the yield stresses decrease with temperature and there is fairly

193

good agreement between the prediction using [9.23b] and the data points.

10.2.2 Prediction of Thermal (Volume) Strains

As shown in Section 9.1, thermal strains can be said to be comprised of elastic and plastic components as

[9.17 bis] $$d\varepsilon_v^T = d\varepsilon_v^{Te} + d\varepsilon_v^{Tp}$$

The total thermal volumetric strain for normally consolidated specimen can be calculated as

[9.20 bis] $$d\varepsilon_v^T = E\ dT$$

and this can be used as an estimate of $d\varepsilon_v^{Tp}$.

The elastic component of thermal volumetric strain can be calculated

[9.13 bis] $$d\varepsilon_v^{Te} = \frac{\kappa_2 - \kappa_1}{V}\ ln\left\{ p' \times \left(\frac{(p'_{c1})^{\kappa_1}}{(p'_{c2})^{\kappa_2}} \right)^{\left(\frac{1}{\kappa_2 - \kappa_1} \right)} \right\}$$

Results from these predictions for thermal volume strains are shown in Fig.10.4. Figure 10.4 shows that the thermal volume strains depend on temperature and stress history (OCR). The trend of the thermal volume strains shown in Fig.10.4 is similar to that reported by Hueckel and Baldi (1990) and shown in Fig.2.3. Figures 10.4 and 2.3 suggest that volume strain in drained heating may be compressive or expansive depending on OCR and temperature. This observation should be related to the results presented in Fig.6.12. There,

194

drained thermal expansion coefficients were shown to be compressive. However, it should be remembered that the data in Fig.6.12 are only for specimens with OCR = 2. Higher OCRs can be expected to produce expansions.

10.2.3 Prediction of Thermally Induced Pore Water Pressures

Figure 10.5 shows predicted thermally induced pore water pressures during undrained heating for normally consolidated and overconsolidated illite specimens. Calculations of pore water pressures were made using the constant undrained thermal expansion coefficient β_{uT} (discussed in Chapter 6 and 9). Separate calculations for normally consolidated and overconsolidated specimens were made using consolidation pressures. For normally consolidated specimens, consolidation pressures are equal to preconsolidation pressures, but for overconsolidated specimens consolidation pressures were less than preconsolidation pressures. Values of measured and predicted pore water pressures were normalized with respect to consolidation pressures at 28°C.

Figure 10.5 shows that the TEP model underestimates the thermally induced pore water pressure under bulk undrained conditions for normally consolidated specimens. However, measured values of pore water pressures under constant mass conditions seem to agree well with predicted values at 65°C. For overconsolidated specimens, Fig.10.5 shows that the model overestimates thermally induced pore water pressures.

10.2.4 Stress-strain Relationships

Perhaps more significant are predictions from the TEP model for stress-strain relationships at elevated and ramped temperatures. Calculations for stress-strain predictions from the model were done by personal computer using a BASIC program developed by the author. The program solves the model for all components of needed stresses and strains. Appendix 5 presents the listing of the program. The program has been developed at this stage to allow only calculations for conventional drained triaxial compression tests where the slope of stress path $dq/dp' = 3.0$ and for undrained compression tests where $\Delta V = 0$. It is of course possible to modify the program for other stress paths.

10.2.4.1 Drained Behaviour

Figure 10.6 compares measured and predicted stress-strain relationships for drained triaxial compression stress paths with slope $dq/dp' = 3.0$ tests. The model predicted the experimental linear elastic region and the yield stresses very closely. However, in the plastic region, both the deviator stresses and the volumetric strains are underestimated by the model predictions. This may be due to deficiencies in the modified Cam Clay model in which shear strain is usually not accurately estimated. Despite this, it is reasonable to state that the model predicts the general trend of soil behaviour at elevated temperature.

Simulations were also performed for a heavily overconsolidated illite specimen (Fig.10.7). The specimen was isotropically consolidated to 3.0 MPa, and isotropically unloaded to 0.4 MPa giving OCR = 7.5 at 28°C. After drained heating to 65°C, the specimen was sheared in drained triaxial compression $dq/dp' = 3.0$.

Figure 10.7 compares measured and calculated stress-strain relationships. As expected, the simulated values in Fig.10.7(a) show strain softening after peak deviator stress was reached. However, as is common in all modelling based on Cam clay, the amount if strain softening is usually underestimated. The relationships between volume strain and shear strain show dilative behaviour with large shear strains. Again, the simulated values follow similar manner as measured values, but the post-yield volume expansions are underestimated. The under-prediction of dilatancy in Fig.10.7(b) probably controls the underestimation of strain softening in Fig.10.7(a).

10.2.4.2 Undrained Behaviour

Undrained triaxial compression on normally consolidated specimens subjected to drained heating under isotropic pressure

Figures 10.8(a) and (b) show computed and observed shear stresses q and pore water pressures u as a function of shear strain ε_s. Corresponding predicted and observed stress paths are shown in Fig.10.9. The predictions for q continuing to increase to $\varepsilon_1 = 20\%$ in Fig.10.8 are a result of the particular numerical procedures that

have been adopted. The agreement between model and experimental results is fair, especially for the stress paths shown in Fig.10.9.

The model shows that under undrained compression after drained heating for normally consolidated specimens, the specimens become stronger, generated pore water pressures become smaller, and the specimens become stiffer. This agrees with the experimental data, although once again the model under-predicts the changes that have been observed in the testing program.

The model assumes the shear modulus G depends on consolidation pressure p', having assumed a constant Poisson's ratio μ. Houlsby (1982) has shown that this violates the conditions for the second law of thermodynamics. However, this is believed to be a small price in view of the generally successful simulation. Alternatively, a constant value of G can be employed to overcome this problem .

Undrained heating under a given deviator stress

Consideration is now given to the case of changes in temperature under undrained conditions, where specimens are subject to a given deviator stress. Figure 10.10 shows conditions where a specimen consolidated to 1.47 MPa is sheared to a non-failing stress q = 0.35 MPa at 28°C, and then heated undrained to 100°C.

Because the undrained thermal expansion coefficient β_{UT} is positive (Chapter 5), specimens expand during undrained heating under isotropic conditions. It appears reasonable to assume that the same amount of undrained thermal expansion occurs where a specimen with the same specific volume carries a given deviator stress. However, the "state" of the specimen changes from that at lower temperature to that at higher temperature. Therefore, it may be possible for a non-failing specimen at lower temperature to reach critical state failure when heated. In such cases, the state of the specimens moves along the SBS to the critical state during undrained heating even though the deviator stress kept constant (Fig. 10.10).

Overall, the agreement between test results and model predictions is reasonable in view of the fact that the behaviour of overconsolidated clay is difficult to model. Generally, the slope discontinuities in the computed curves occur close to where the stress paths hit the cap of the SBS.

10.2.4.3 Application of the TEP Model to Compacted Soils

The model and the computer program were originally developed for calculating stress and strain components for isotropically consolidated soil. It was not initially intended to apply the model to compacted soils. However, it was thought useful to attempt comparisons between model predictions and measured values for the tests in compacted soils described earlier in the thesis. It was necessary to make some modifications and different assumptions when

applying it to compacted soils. The experimental results suggest that compacted soils might be treated as overconsolidated, and the following predictions were based on this assumption.

For the compacted illite specimen, most parameters used in the predictions are the same as those for reconstituted illite specimens. A preconsolidation pressure of 2.0 MPa for the compacted illite specimen was used in the model. This value was derived from results of yield locus at 28°C in Fig.7.22. Parameters used for predictions are listed in Table.10.2.

TABLE 10.2 Parameters in the TEP model for compacted illite

Constant	Value
B	0.825
C	1.51
D	-0.091
E	2.77×10^{-4}
H	0.75
λ	0.087
κ	0.017
$(G/p')_{NC}$	38
M	1.07
N	2.055
β_{uT}	2.0×10^{-4}

Figures 10.11 and 10.12 shows predictions and measured values for undrained heating under a controlled deviator stress condition. The predicted stress path (O-A in Fig.10.11) deviates from the actual stress path (1-2 in Fig.10.11). This is probably due to compaction-

induced anisotropy in the specimen, whereas the model assumes isotropy. However, the model predicts the overall trend of the test results. Predictions generally underestimate the actual stress-strain behaviour (Fig.10.12), although the prediction of the thermally induced pore water pressure seems to agree reasonably well with measured values.

The disagreement between predictions and measured values may be due to (1) the assumption of a preconsolidation pressure of 2 MPa does not represent the actual behaviour of the compacted specimen; (2) the specimen was subjected to a heating-cooling cycle before shearing; and (3) an anisotropy of the compacted soil.

The behaviour of the sand-bentonite specimen for undrained heating under a given deviator stress was also simulated using the same concept used for the compacted illite specimen. The specimen was assumed to have a preconsolidation pressure $p_c' = 3.0$ MPa, and to be overconsolidated at the consolidation pressure $p' = 1.55$ MPa. Parameters used for modelling the sand-bentonite specimen are shown in Table.10.3. The values of the parameters in Table 10.3 are taken from test results described in Chapter 5,6,8 for compacted sand-bentonite specimens, and are therefore different from those for illite specimens.

TABLE 10.3   Parameters   in   the   TEP   model   for   compacted   sand-
bentonite mixture

Constant	Value
λ	0.12
κ	0.084
$(G/p')_{NC}$	11
M	0.52
N	2.536
β_{uT}	2.0×10^{-4}
p'_c (MPa)	3.0
p'	1.55

Comparisons of measured and predicted results are shown in Figs.10.13 and 10.14. Figure 10.13 shows the predicted and measured stress paths, and Fig.10.14 shows the stress-strain relationships. The predicted stress path (O-A-B in Fig.10.13) simulates the actual stress path (1-2-3 in Fig.10.13) quite well. However, the stress-strain relationships are not predicted well. The thermally induced pore water pressure was overestimated and the shear strain was underestimated in prediction.

As mentioned earlier, factors affecting these differences in stress-strain relationships are the anisotropy of the sand-bentonite, the assumption of overconsolidation, and the temperature cycle of heating-cooling before shearing.

10.4 Discussion

The verification of the TEP model in Section 10.1-10.3 showed that the model gives reasonable simulations of the actual soil behaviour at elevated and ramped temperatures under various boundary conditions. Some fine-tuning of the numerical procedures and modelling assumptions can be expected to produce improved results, but the author decided not to do this.

Predictions for thermally induced pore pressures using the assumption of the constant undrained thermal expansion coefficient indicate that the model simulates pore water pressure generation quite well under ramping temperatures and constant mass conditions (Figs.10.5). One of the important advantages of the model is that only a small number of parameters such as κ_T, β_{uT}, and E are needed to predict the thermally induced pore water pressures. These parameters are easily measured in triaxial testing, or can be estimated from other soil data. For example, the coefficient of undrained thermal expansion β_{uT} used here was assumed to be constant (2.0×10^{-4} $^\circ C^{-1}$) and the value is similar to that obtained from oil sands (Agar *et al*. 1986). No complicated procedures such as an evaluation of the thermal expansion of water at different temperatures and interactions of soil particles, pore water, and soil mass are necessary.

To summarize, the proposed model for isotropic material presented in the preceding section gives a reasonable fit to the test data for

various kinds of stress paths and boundary conditions and presents a simple and consistent picture of the behaviour of clay. Improvements to numerical modelling procedures can be expected to improve the modelling of shear strains and strain softening. The model can predict thermally induced volume changes, thermally induced pore water pressures, stress-strain relationships, and strengths at different temperatures. In addition, the theoretical model is in a form that allows it to be implemented easily into a finite element analysis.

Comparisons with test data indicate that the model provides generally reasonable predictions. The model indicates the effect of drainage conditions during temperature changes on the behaviour of clay specimen. A normally consolidated specimen heated with drainage open is likely to become stronger subsequently in undrained shear. On the other hand, a overconsolidated specimen heated drained is likely to become weaker. However, undrained heating certainly causes normally consolidated specimens to become weaker.

These results have a direct impact on the behaviour of geotechnical structures subjected to temperature changes. If such structures are constructed in normally consolidated or overconsolidated clay, then rapid heating without allowing dissipation of thermally induced pore water pressures will cause loss of strength and may lead to failure of the structure.

CHAPTER 11   DISCUSSION

Preceding chapters have shown how temperature affects the behaviour of clay soils under the conditions in the test program, and how the TEP model predicts the behaviour.   This chapter discusses some more general features of the effects of temperature on soil behaviour.

11.1 Microstructural   Aspects   of   Pore   Water-Clay   Particles Interaction on Volume Change

Volume changes induced by temperature changes are complex.   For example,   normally   consolidated   and   lightly   overconsolidated specimens   have   shown   compressive   volume   strains   under   drained heating,   while   expansive   volume   strains   have   been   observed   under undrained heating conditions.

The   effects   of   temperature   on   the   strength   of   clays   are   also complex.   For   example,   the   undrained   strength   of   a   specimen   after drained heating during the application of the consolidation pressure is   greater   than   for   a   comparable   unheated   specimen.   A   specimen subjected   to   a   heating-cooling   cycle   has   greater   undrained   strength than   an   unheated   specimen,   but   less   undrained   strength   than   a drained heated specimen.

These complicated patterns of behaviour are difficult to understand without   a   conceptual   framework   which   can   handle   the   behaviour   of soil from both the microscopic and macroscopic points of view.   The

observations listed previously were made only by macroscopic experiments. It was, therefore, thought useful to discuss the effects of temperature on soil behaviour from the microscopic point of view, and that this might help the macroscopic observations. No detailed microscopic examinations have been made in the thesis and so reference will have to be made on the research literature and work done at AECL Research Laboratory by A.Wan.

It has been stated that there are four phases of water in clay. That is, structural, firmly adsorbed, loosely adsorbed, and free water (Rosenquist 1959). It is most probable that compressive strains in most clays are associated with changes of configuration of the loosely adsorbed water (Passwell 1967, Demars and Charles 1982), producing a reduction of its density and its partial transformation into pore water. Thus, reversible and irreversible straining of a clay soil can be considered as the reversibility or irreversibility of diffuse double layer (DDL).

Akagi *et al.* (1992) examined the pore fluid expelled from a normally consolidated bentonitic clay during consolidation at 20°C and 70°C. Their results showed that the concentration of cations in the pore fluid was higher at 70°C than at 28°C. They suggested that at higher temperature cations are more easily expelled from the clay particles. That is, the thickness of the diffuse double layer decreases, (adsorbed water is released into pore water solution) at elevated temperature so that more movable ions are available under

206

the same stress conditions.   In this way, drained heating causes the thickness of the DDL to decrease, resulting in a reduction of volume for normally consolidated clay under constant effective stress.

It has been reported that in general, as clay decreases in volume, its strength increases.   This was seen for drained-heated normally consolidated specimens under constant mean effective stress (Fig.8.6 $T = 28°C$, $65°C$, and $100°C$).   Observed changes in volume and strength can be related to each other with the aid of the discussion of microstructure in the previous paragraphs.

A specimen which is initially normally consolidated at $28°C$ and then subjected to a heating-cooling cycle under drained conditions shows a specific volume at the end of the temperature cycle that is smaller than that before heating, but larger than that at the end of the heating phase.   Its undrained strength is greater than that for an equivalent unheated specimen, but less than that for a hot specimen.   These observations can also be explained using the earlier discussion of the changes in the thickness of DDL brought about by temperature changes.   Part of the free pore water in a heated specimen which is released from the adsorbed water by heating can be recovered as adsorbed water upon cooling.   However, the process may be not fully reversible.   As a result, the soil experiences irreversible volume change, that is, a net reduction of volume during a heating-cooling temperature cycle.   The specimen,

therefore, behaves like a lightly overconsolidated soil with higher undrained shear strength due to the lower specific volume .

For overconsolidated specimens, the interaction between pore water and clay particles play a large role in controlling soil behaviour, for example, diffuse double layers developed in pore water, though clay particle-to-particle interactions are still important.   In general, it can be considered that in normally consolidated clay diffuse double layers are more developed than in overconsolidated clay under the condition of the same specific volume.   Therefore, it can be expected that the effects of temperature on diffuse double layer are larger for normally consolidated specimens than for overconsolidated specimens.   This can be seen in Fig.6.12 and Fig.8.8.   Figure 6.12 showed that volume strains accompanying drained-heating, that is, the effects of temperature on diffuse double layer, for lightly overconsolidated specimens are less those for normally consolidated specimens.   Figure 8.8 showed the undrained strengths for 28°C and 65°C specimens in which particle-to-particle interactions are more dominated than pore water-to-particle interaction, have a similar relationship.

However for heavily overconsolidated clays, the particle-to-particle interactions are more dominant than pore water to clay particle interactions.   For example, imagine two specimens, one normally consolidated and the other heavily overconsolidated, with both having identical water contents, that is, the same specific volumes.

The same temperature changes are then applied to the specimens under drained conditions. As mentioned previously, compressive volume strains can be expected for the normally consolidated specimen because more movable cations exist and the soil must compress to sustain the applied pressure. However, the heavily overconsolidated specimen has experienced a larger preconsolidation pressure in the p' constant, and now sustains less pressure. Therefore, it appears reasonable to state (as we do in elastic-plastic modelling) that the system of the soil structure is more rigid than that for the normally consolidated specimen. As a result of drained heating, the soil structure can easily sustain the pressure, and as clay particles expands the total volume of soil increase.

The volume increases are accompanied with an absorption of water from the system outside, resulting in an expansive volume change. These discussion can be seen in the data presented by Baldi *et al.* (1988) and Hueckel and Baldi (1990). They showed that volume strains under drained conditions become more expansive with higher OCR, and that the specimen for higher OCR value (OCR = 15) subjected to drained heating had smaller peak strength than that for the unheated specimen in drained compression tests.

In addition, expansive volume strains observed for overconsolidated specimens upon drained heating might be explained as follows. During unloading to produce overconsolidation the clay specimen has nor reached equilibrium in volume at the end-of-consolidation, and

209

still has a potential to expand further. The following heating, that is, the input of the high level of energy into the specimen, accelerates the expansion. Similar observations had been reported by Kuntiwattanakul (1991) that the unloaded specimens always showed expansive volume strains during drained heating, but the reloaded specimens always showed compressive volume strains during drained heating even at high OCR values.

11.2 Microstructural Aspects of Pore Water-Clay Particles Interaction on Thermally Induced Pore Water Pressure

In contrast to drained heating, undrained heating produces thermally induced pore water pressures. These pore water pressures result from the expansions of pore water and solid particles, and the constraint of volume change. As discussed in previous section, the thickness of diffuse double layer decreases with heating. However, the volume changes are restricted under undrained conditions (not necessary as under constant volume conditions), so the excess pore water pressures generated by undrained heating cannot be dissipated under these conditions.

Now imagine that there are two specimens which have the same specific volume, but one is normally consolidated, and the other overconsolidated. The overconsolidated specimen can be expected to have more mineral-to-mineral contact than the normally consolidated specimen due to the preconsolidation pressure. This indicates less pore water structure exists in the overconsolidated specimen than in

the normally consolidated specimen. Therefore, the amounts of adsorbed water and free pore water which produce DDL are larger in the normally consolidated specimen than in overconsolidated specimen. As mentioned earlier, the adsorbed water and free pore water are most likely affected by temperature changes. As a result, the thermally induced pore water pressures for normally consolidated specimen can be anticipated to be larger than for overconsolidated specimen though the same specific volume or water content.

As been seen in previous chapters, the yield loci shrink with temperature. Drained heating can be considered as the process which is combinations of undrained heating and drained consolidation. For normally consolidated specimen, thermally induced pore water pressures by undrained heating dissipate under drained conditions. However, due to heating the yield locus shrinks but the soil structure under the drained conditions must support the original effective stress, resulting with more volume changes than for overconsolidated specimen.

11.3 Temperature Effects and Time Effects on Soil Behaviour

Consolidation: In Fig.5.52 the normal consolidation lines for 28°C, 65°C, and 100°C are parallel each other with lower specific volume at higher temperature. Similar results have been reported on different soil (Campanella and Mitchell 1968, Demars and Charles 1982, Eriksson 1989, Tidförs and Salförs 1989, Hueckel and Baldi 1990, Kuntiwattanakul 1991). It can be seen that these

relationships are very similar to those proposed by Bjerrum (1967) and Yin (1990) for time dependent behaviour of soil. Aged soil has lower specific volume at constant pressure and greater strength. These are similar to results from the drained heated specimen originally normally consolidated where the heated specimen had higher strength than the unheated specimen which has higher specific volume. The effects of strain rate are also similar to those of time, therefore, can be expected of temperature on volume and strength.

Moreover, the effects of temperature on yield stresses and yield loci are also similar to those of time and strain rate. Tavenas *et al.* (1978) and Graham *et al.* (1983) shows that the preconsolidation pressures and the size of yield loci depend on time for consolidation and strain rate. They showed that as the strain rates decrease, the preconsolidation pressures decrease and therefore, so does the size of yield loci. These observations are similar to what has been reported in the thesis. As the temperatures increase, the yield stresses and the size of yield loci decrease. Therefore, it is reasonable to correlate the effects of temperature and those of time or strain rate.

Boudali *et al.* (1994) showed results from one-dimensional consolidation tests at elevated temperatures and different strain rates. They proposed the following equation in which both temperature and strain rates are taken into account

[11.1] $\sigma'_p (\dot{\varepsilon}_v, T) = \sigma'_p (\dot{\varepsilon}_{vo}, T_o) [\dot{\varepsilon}_v / \dot{\varepsilon}_{vo}]^A [1 + CT_o - CT]$

where

$\sigma'_p (\dot{\varepsilon}_v, T)$ = preconsolidation pressure at $\dot{\varepsilon}_v$ and T

$\sigma'_p (\dot{\varepsilon}_{vo}, T_o)$ = preconsolidation pressure at $\dot{\varepsilon}_{vo}$ and T_o

$\dot{\varepsilon}_v$ = strain rate

$\dot{\varepsilon}_{vo}$ = reference strain rate

C = constant

T = temperature

T_o = reference temperature

Knowing parameters A and C the use of the equation allows the determination of the one-dimensional behaviour of a clay for any temperature and strain rate history.   In general, they derived the values of A and C equal to 0.04-0.05, 0.009°C^{-1}, respectively.

This relationship can be applied for general stress-strain relationships.   Yield function f can be expressed as:

[11.2] $f = q^2 - M^2 [p' (p'_o - p')] = 0$

where

q = shear stress

M = critical state parameter

p'= mean effective stress

p'_o= preconsolidation pressure

213

If a relationship like [11.1] is known for a given clay, the yield function at any temperature and strain rate can be determined. Therefore, stress-strain relationship can also be predicted using the model discussed in Chapter 10.

11.4 Temperature Effects and Chemical Effects on Soil Behaviour

It is well-known that soil behaviour can be affected by changes in both the concentration, pH, and the type of the pore fluid. Behaviours of consolidation show that lower specific volume for higher concentration, lower pH, and more inert fluid.   These relationships are similar to those for the effects of temperature.

Although it has not been well reported how stress-strain behaviour and strength are affected by these factors, it may be related somehow to those observed on the effects of temperature.

The effects of chemical, time and strain rate on soil behaviour may be interrelated each other, especially between temperature and time or strain rate, although it has not yet been clear relationships between chemical effects and temperature effects.

11.5 Necessary Modifications of TEP Model for Compacted Soils

As noted in the previous chapter, additional parameters are needed in order to describe anisotropic behaviour of compacted soils.   A number of workers have been proposing models which can handle anisotropic behaviour of soil.   Davies and Newson (1992) presented

the development of a constitutive model for anisotropically consolidated clay, based on critical state soil mechanics concept. The model requires only one additional parameter α_o, rotation of plastic potential surface, and the hardening rule is non-associated. The TEP model can be incorporated into the anisotropic model for describing fully anisotropic stress-strain relationship without any difficulty to improve more previous predictions.

CHAPTER 12 CONCLUSIONS AND FURTHER WORK

12.1 Summary and Conclusions

Attempts have been made to investigate the effects of temperature on mechanical behaviour for both normally consolidated and overconsolidated clays and compacted clays. The investigation has been carried out to fulfill the following aims:

1. To examine the hypotheses and assumptions made in Chapter 3, and
2. To develop a possible model which takes into account the effects of temperature

Topics examined during the study were:

1. thermally induced volume changes
2. thermally induced pore water pressures
3. effects of temperatures on stress-strain behaviour
4. effects of temperatures on yield loci
5. effects of temperature on strength

The experimental investigation was performed on two types of clay materials: illite (a low plastic clay) and sand-bentonite mixture (a high plastic clay). Reconstituted and compacted illite specimens were tested in order to investigate the effects of specimen preparation.

The thesis has demonstrated that many previous observations relating to the effects of temperatures on the strength characteristics of clays, which formerly appeared to be isolated pieces of information and to be contradictory, may now be fitted into a consistent pattern. They can be used to predict the probable behaviour of various types of clays under different loading conditions using the thermo-elastic-plastic (TEP) model. The effects of drainage conditions during changes in temperature are one of the most important factors on soil behaviour.

The following conclusions can be drawn from the research:

(1) For normally consolidated specimens, drained heating during the consolidation phase causes the undrained shear strength to increase and less pore water pressure to be generated during shearing compared with lower temperature tests. Yield loci do not change in size and shape throughout drained heating, though they move to lower values of specific volume. The changes in slope of unloading-reloading lines upon heating cause changes in stress paths during undrained shearing.

(2) For overconsolidated specimens (OCR = 2), drained heating during consolidation causes no large changes in undrained shear strength, but introduces slightly more dilatant behaviour when the temperature is higher. It may be understood that shrinkage of yield loci at higher temperature causes specimens to become more dilatant.

(3) Undrained heating under isotropic stress conditions for normally consolidated specimens causes the undrained shear strength to decrease and more pore water pressure to be generated during shearing compared with lower temperature tests. This can be explained as a decrease in the effective stress upon undrained heating so that the soil would appear to be overconsolidated at the beginning of shearing. As well, the size of the yield locus at higher temperature is smaller than at lower temperature.

(3) The critical state strengths in drained shear tests are not affected by temperature. This applies for both reconstituted and compacted specimens.

(4) The stress-strain characteristics of compacted specimens are broadly similar to those of overconsolidated specimens made from slurry, in terms of their volume changes, stress-strain behaviour, pore water pressure generation, and strengths. However, they display anisotropic, rather than isotropic behaviour.

(5) Undrained heating under a constant deviator stress can produce a reduction of effective stress, and may result in specimens reaching their failure envelope. Continuing shearing after undrained heating shows that specimens become more dilatant. They generate increasing shear resistance and decreasing pore water pressure with further straining.

(6) Normal consolidation lines and critical state lines in V-ln p' space depend on temperature, with lower specific volumes at higher temperature for the same pressure. For compacted illite specimens, critical state lines are parallel to those for reconstituted illite specimens, but at lower specific volumes.

(7) Volume changes due to temperature may be examined using drained thermal expansion and undrained thermal expansion as lower and upper limits, respectively. Undrained thermal expansion coefficients appear to be unique for all soils. Drained thermal expansion coefficients depend on temperature, stress history, and soil type.

(8) Thermally induced pore water pressures for illite specimens can be normalized by the consolidation pressure, but not by the preconsolidation pressure.

(9) A relatively simple thermal elastic plastic model has been developed which is similar in nature to the elastic plastic Cam Clay model. It permits easy visualization of the likely influence of temperature, pressure, and test type on the behaviour of lean (low plastic) clays. A proposed elastic-plastic model in which temperature effects are taken in to account allows prediction of many of the features observed in the experimental work.

(10) Successful applications of the model were made to reconstituted specimens, but modifications and improvements are necessary if it is

to be applied to compacted and anisotropically consolidated specimens. Specifically, the elasticity needs to be anisotropic, and the flow rule non-associated.

Convincing evidence has been presented for the influence of temperature on soil behaviour. A simple model has been proposed that is based on reasonable assumptions supported by experimental evidence. As a consequence, many previous, apparently contradictory observations relating to the stress-strain, pore water pressure, yield locus, and strength characteristics of clays subjected to change in temperature may now be fitted into a consistent pattern. The resulting soil model may be used to predict the probable behaviour of the various types of clays under different thermal and mechanical loading.

12.2 Further Work

As a result of the findings from this study, the following suggestions are proposed for further work.

Careful examination of soil stiffness at small strain levels such as shear strain ε_s = 0.00001 to 0.001 is recommended. This is because the Canadian nuclear waste disposal program will use buffer material compacted around canisters containing bundles of nuclear fuel waste and confined by surrounding rock. Deformation due to temperature changes will be small.

Hydrothermal effects of soils should also be examined. The design period for a nuclear waste disposal system is well beyond 500 years, and up to 10000 years has been suggested. It should be known how pressure and temperature changes affect the soil properties in the long term. The experimental work in this study has been done using only distilled-deaired water. Generally, constituents of ground water are not the same as those in distilled-deaired water.

As has been discussed, the effects of time and strain rate are related to those of temperature. It is necessary to perform more detailed examinations to better define these relationships.

Because of the procedures of compaction for buffer material and the conditions underground for nuclear waste disposal system, the buffer will be unsaturated during much of its emplacement. The effects of unsaturation must be examined in the near future.

The characteristics of compacted soils are similar to those for anisotropically consolidated soils. It would therefore be worthwhile to examine the behaviour of compacted and anisotropically consolidated soils.

The TEP model requires further development and modification to take account of the anisotropy of compacted or anisotropically consolidated soils.

REFERENCES

Aboustit, B.L., Advani, S.H. and Lee, J.K. 1985. Variational principles and finite element simulations for thermo-elastic consolidation. International Journal of Numerical and Analytical Methods in Geomechanics 9 pp.49-65.

Ambrosie, A.W. 1985. Effects of stress-release disturbance on the shear behaviour of simulated offshore normally-consolidated clay samples. M.Sc. Thesis, University of Manitoba, Department of Civil Engineering, Winnipeg, Manitoba, Canada.

Agar, J.G., Morgenstern, N.R., and Scott, J.D. 1986. Thermal expansion and pore pressure generation in oil sands. Canadian Geotechnical Journal, 23, pp.327-333.

Agar, J.G., Morgenstern, N.R., and Scott, J.D. 1987. Shear strength and stress-strain behaviour of Athabasca oil sand at elevated temperatures and pressures. Canadian Geotechnical Journal 24 pp.1-10.

Akagi, H., Nakahara, T., and Ninomiya, M. 1992. Micro-structural change of saturated clay during high temperature consolidation from the viewpoint of chemical analysis of drained pore water. Proceedings 27th Annual Meeting of Japanese Society of Soil Mechanics and Foundation Engineering, pp.413-416.

Allard, B., Kippatsi, H., and Rydbert, J. 1977. Sorption of long lived radionuclides in clay and rock. Kaernbraenslesaekerhet, KBS Technical Report 55.

Anderson, D.G., and Richart, F.E. 1974. Temperature effect on shear wave velocity in clays, ASCE Journal Geotechnical Engineering Div. 100 GT12 pp.1316-1320

ASTM STP 869. 1983. Measurement of rock properties at elevated pressures and temperatures. H.J.Pincus and E.R.Hoskins, Eds, ASTM, Philadelphia.

Atkinson, J.H., Evans, J.S., and Ho, E.W.L. 1985. Non-uniformity of triaxial sample due to consolidation with radial drainage. Géotechnique 35 pp.353-355.

Atkinson, J.H. and Richardson, D. 1987. The effect of local drainage in shear zones on the undrained strength of overconsolidated clays. Géotechnique 37 pp.393-403.

Atkinson, J.H., Richardson, D., and Stallebrass, S.E. 1990. Effect of recent stress history on the stiffness of overconsolidated soil. Géotechnique 40 pp.531-540.

222

Baldi, G., Borsetto, M., Hueckel, T., Peano, A. and Tassoni, E. 1985. Hard clay as host medium thermo-mechanical experiments and model. Material Research Society Symposium Proceeding 50

Baldi, G., Borsetto, M., Hueckel, T., Peano, A. 1987. Thermally induced strain and pore pressures in clays, Proceedings International Symposium on Environmental Geotechnology, Allentownm Penn.

Baldi, G, Hueckel, T., and Pellegrini, R. 1988. Thermal volume change of mineral-water system in low porosity clay soils. Canadian Geotechnical Journal, 25, pp.807-825.

Barata, F.E. 1969. Effect of heating on bearing capacity of highway subgrades. HRB SR103, pp.141-149.

Bjerrum, L. 1967. Engineering geology of Norwegian normally-consolidated marine clays as related to settlements of buildings. Géotechnique 17 Seventh Rankine Lecture pp.81-118.

Boley, B.A., and Weiner, J.H. 1969. Theory of Thermal Stress. Wiley, New York.

Booker, J.R., and Savvidou, C. 1985. Consolidation around point heat source. International Journal for Numerical and Analytical Methods in Geomechanics 9 pp.173-184.

Booker, J.R., and Smith, D.W. 1989. Behaviour of a heat source in a fully coupled saturated thermoelastic soil. 3rd International Symposium on Numerical Models in Geomechanics (NUMOG 3), Niagara Falls, Canada, Edited by St.Pietruszczak and G.N.Pande, pp.399-406.

Boudali, M., Lerouil, S., and Srinivasa Murthy, B.R. 1994. Viscous behaviour of natural clays. 13th ICSMFE, New Delni, India. pp.411-416.

Britto, A.M., Savvidou, C., Maddocks, D.V., Gunn, M.J., and Booker, J.R. 1989. Numerical and centrifuge modelling of coupled heat flow and consolidation around hot cylinders buried in clay. Géotechnique 39 pp.13-25.

Borwmnell, W.E. 1976. Structural Clay Products. Springer-Verlag, Wien, Austria. 231pp.

Campanella, R.G., and Mitchell, J.K. 1968. Influence of temperature variations on soil behaviour. Journal of Soil Mechanics and Foundations Division, ASCE, Vol.94, No.SM3, pp.709-734.

Chandrasekharan, E.C., Boominathan, S., Sadayan, E., and Setty, K.R. 1969. Influence of heat treatment on the pulverization and stabilization of characteristics of typical tropical soils. HRB SR103, pp.161-172.

Cheatham Jr., J.B. 1968. The effect of pressure, temperature, and loading rate on the mechanical properties of rocks. Mechanical Behaviour of Materials under Dynamic Loads, U.S.Lindholm Eds, Springer-Verlag, N.Y.

Cheung, S.C.H., Gray, M.N., and Dixon, D.A. 1987. Hydraulic and ionic diffusion properties of bentonite-sand buffer materials. Coupled Processes Associated with Nuclear Waste Repositories, Chin-Fu Tsang, ed., Academic Press, Orland, Florida, pp.393-407.

Coleman, B.D., and Noll, W. 1963. The thermodynamics of elastic materials with heat conduction and viscosity, Arch. Ration. Mech. Anal., 13, pp.167.

Couture, R.A. 1985. Steam rapidly reduces the swelling capacity of bentonite. Nature, 318, pp.50-52.

Crookss, J.H.A., and Graham, J. 1976. Geotechnical properties of the Belfast deposits. Géotechinique 26 pp.293-315.

Date, E.H.F. 1969. Elastic properties of steels. Journal of The Iron and Steel Institute, pp.988-991.

Davies, T.G., and Benerjee, P.L. 1980. Constitutive relationships for ocean sediments subjected to stress and temperature gradients. AERE Harwell Rep. No. HL 80/2604 (C22), August.

Davies, M.C.R. and Newson, T.A. 1992. A critical state constitutive model for anisotropic soil. Proceedings, Wroth Memorial Symposium, "Predictive Soil Mechanics", pp.128-139.

Demars, K.R., and Charles, R.D. 1982. Soil volume changes induced by temperature cycling. Canadian Geotechnical Journal, pp.188-194.

Derjaguin, B.V., Churaev, N.V., and Muller, V.M. 1987. Surface forces, Consultants Bureau, New York.

Dixon,D.A., and Gray, M.N. 1985. The engineering properties of buffer material. Research at Whiteshell Nuclear Research Establishment. Proceedings, 19th Information Meeting of the Nuclear Fuel Waste Management Program, Toronto, Atomic Energy of Canada Limited, Technical Report TR-350, Vol.3, pp.513-530.

Dixon,D.A., Cheung, S.C.H., Gray, M.N.,and Davidson, B. 1987. The hydraulic conductivity of dense clay soils. Proceedings, 40th Canadian Geotechnical Conference, Regina, Sask. pp.389-396.

Dixon,D.A., Wan, A.W.L., Graham, J., and Kjartanson, B.H. 1991. Assessing the swelling characteristics of bentonite-based materials. Proceedinfs 44th Canadian Geotechnical Conference, Calgary, AB, pp.61-1 to 61-7.

Dixon,D.A., Sri Ranjan,R., and Graham, J. 1992. Applicability of Darcy's law in laboratory measurement of water flow through low permeability clays. Proceedings, 45th Canadian Geotechnical Conference, Toronto, Ont., pp.87/1-87/7.

Dixon,D.A., Gray, M.N., Lingnau, B.E., Graham, J., and Campbell, S.L. 1993. Thermal expansion testing to determine the influence of pore water structure on water flow through dense clays. Proceedings, 46th Canadian Geotechnical Conference, Saskatoon, Sask, p.p.177-183.

Duncan, J.M., and Campanella, R.G. 1965. The effects of temperature changes during undrained creep tests. Report No.TE65-10, University of California, Berkeley, California.

Duncan, J.M., and Chang, C.Y. 1970. Non-linear analysis of stress and strain in soils. ASCE Journal of the Soil Mechanics and Foundation Division 96(SM5) pp.1629-1651.

Eriksson, L.G. 1989. Temperature effects on consolidation properties of sulphide clays. Proceedings 12th International Conference Soil Mechanics and Foundation, Rio de Janeiro 3 pp.2087-2090.

Finn, F.N. 1951. The effect of temperature on the consolidation characteristics of remolded clay. ASTM STP 126 pp.65-72.

Graham, J., Pinkney, R.B., Lew, K.V., and Trainor, P.G.S. 1982. Curve-fitting and laboratory data. Canadian Geotechnical Journal 19 pp.201-205.

Graham, J., and Houlsby, G.T. 1983. Anisotropic elasticity of a natural clay. Géotechnique, 33, pp.165-180.

Graham, J., Crooks, J.H.A., and Bell, A.L. 1983. Time effects on the stress-strain behaviour of natural soft clays. Géotechnique 33 pp.327-340.

Graham, J., Kwok, C.K., and Ambrosie, R.W. 1987. Stress release, undrained storage, and reconsolidation in simulated underwater clay. Canadian Geotechnical Journal 24 pp.279-288.

Graham, J., Crooks, J.H.A., and Lau, S.L.K. 1988. Yield envelopes: identification and geometric properties. Géotechnique 38 pp.125-134.

Graham, J., and Lau, S.L.K. 1988. Influence of stress-release disturbance storage, and reconsolidation procedures on the shear behaviour of reconstituted underwater clay. Géotechnique 38 pp.279-300.

Graham, J., Saadat, F., Gray, M.N., Dixon, D.A., and Zhang, Q.-Y. 1989. Strength and volume change characteristics of sand-bentonite mixture. Canadian Geotechnical Journal 26 pp.292-305.

Graham, J., Saadat, F., Gray, M.N. 1990. High-pressure triaxial testing on the Canadian Reference Buffer Material. Engineering Geology 28 pp.391-403.

Graham, J., Oswell, L.M., and Gray, M.N. 1992. The effective stress concept in saturated active clays. Canadian Geotechnical Journal 29, pp.1033-1043.

Graham, J., Lingnau, B.E., Yarechweski, D.S., Tanaka, N., and Crilly, T. 1993. Thermo-elastic-plastic-modelling of sand-bentonite buffer for use in underground disposal of nuclear fuel waste - Final report on contract No. WS-30J-79981. Department of Civil Engineering, University of Manitoba, Winnipeg, Manitoba.

Gray, H. 1936. Progress report on research on the consolidation of fine-grained soils. Proc. 1st ICSMFE Vol.2 pp.138-141.

Gray, M.N. 1984. Compaction of Na-bentonite-sand mixtures and creep tests. Atomic Energy of Canada Limited, Communication FW TB-84-16.

Gray, M.N., Cheung, S.C.H., and Dixon, D.A. 1984. Influence of sand content on swelling pressures developed in statically compacted Na-bentonite. Atomic Energy of Canada Limited, Report AECL-7825.

Gray, M.N. 1984. Compaction of Na-bentonite-sand mixtures and creep tests. Atomic Energy of Canada Limited, Communication FW TB-84-16.

Gray, M.N., Cheung, S.C.H., and Dixon, D.A. 1984. Influence of sand content on swelling pressures developed in statically compacted Na-bentonite. Atomic Energy of Canada Limited, Report AECL-7825.

Green, S.L. 1984. The behaviour of deep ocean sediments in response to thermo-mechanical loading. Ph.D Thesis, University of California, Berkeley.

Green, A.E., and Naghdi, P.M. 1965. A general theory of an elastic-plastic continuum, Arch. Ration. Mech. Anal., 18, pp.251.

Grim, R.E. 1962. Applied Clay Mineralogy. McGraw Hill, N.Y. 422pp.

Güven, N. 1990. Longevity of bentonite as buffer material in a nuclear-waste repository. Engineering Geology 28, pp.233-247.

HRB Report. 1969. Highway Research Board: Effects of temperature and heat on engineering behaviour of soils. Special Report 103.

Henkel, D.J. and Sowa, V.A. 1963. Discussion on Symposium on Laboratory Shear Testing of Soils, ASTM STP 361, Ottawa, Canada, pp.104-107.

Hoffman, J., and Hower, J. 1979. Clay mineral assemblages as low grade metamorphic geothermometers: Application to the thrust faulted disturbed belt of Montana, USA. SEPM Special Publ. No.26, 1979.

Horseman, S.T., and McEwen, T.J. 1993. Thermal constraints on disposal of heat-emitting waste in argillaceous rocks. Bergamo Workshop.

Houlsby, G.T. 1982. A derivation of the small-strain incremental theory of plasticity from thermomechanics. IUTAM Conference of Deformation and Failure of Granular Materials, Delft pp.109-118.

Houston, S.L., Houston, W.N., and Williams, N.D. 1985. Thermo-mechanical behaviour of seafloor sediments. Journal of Geotechnical Engineering, ASCE, Vol.111, No.11, pp.1249-1263.

Houston,S.L., and Lin, H-D. 1987. A thermal consolidation model for Pelagic clays. Marine Geotechnology 7 pp.79-98.

Hueckel, T. 1989. Constraints in numerical simulation of thermomechanical behaviour of clay-water system subjected to nuclear waste heat, Nuclear Science and Technology, Commission of European Communities, Luxembourg.

Hueckel, T., and Peano, A. 1987. Some geotechnical aspects of radioactive waste isolation in continental clays. Computers and Geotechnology, 3(2,3), pp.157-182.

Hueckel, T., Borsetto, M., and Peano, A. 1987. Modelling of coupled thermo-elastoplastic-hydraulic response of clays subjected to nuclear waste heat. Numerical Methods in Transient and Coupled Problems, R.W. Lewis et al., eds., John Wiley and Sons, Chichester, U.K.

227

Hueckel, T., and Pellegrini, R. 1989. Modeling of thermal failure of saturated clay. In Numerical Models in Geomechanics, eds. S. Pietruszczak and G.N. Pande, Elsevier, pp.81-90.

Hueckel, T., and Baldi, G. 1990. Thermoplasticity of saturated clays: Experimental constitutive study. ASCE Journal of Geotechnical Engineering 116 pp.1778-1796.

Hueckel, T., and Borsetto, M. 1990. Thermoplasticity of saturated soils and shales: Constitutive equations. Journal of Geotechnical Engineering, ASCE, Vol.116, pp.1705-1777.

Hueckel, T., and Pellegrini, R. 1992. Effective stress and water pressure in saturated clays during heating-cooling cycles. Canadian Geotechnical Journal, 29, pp.1095-1102.

International Workshop on Thermo-mechanics of Clays and Clay Barriers. 1993. Bergamo, Italy.

ISMES Report 1990. Developments in modelling of thermo-hydro-geomechanical behaviour of Boom clay based buffer materials, Commission of European Communities Project ASP-4361, Document No.RAT-DMM-149.

Jamieson, M.R. 1989. Effects of moderate stress-release disturbance on the shear behaviour of lightly overconsolidated simulated marine clay. M.Sc. Thesis, University of Manitoba, Department of Civil Engineering, Winnipeg, Manitoba, Canada.

Kammash, T.B., Murch, S.A., and Naghdi, P.M. 1960. The elastic-plastic cylinder subjected to radially disturbed heat source, lateral pressure and axial force with application to nuclear reactor fuel elements, J. Mech. Phys. Solids, Vol. 8, pp.1-25

Khitarov, N.I.,and Pugin, V.A. 1966. Behaviour of montmorillonite under elevated temperatures and pressures., Geochem. Int., 3(4) pp.621-628.

Kuntiwattanakul, P. 1991. effects of high temperature on mechanical behavior of clays. Ph.D Thesis, Department of Civil Engineering, University of Tokyo

Kwok, C.K. 1984. Effects of stress-release disturbance on the shear behaviour of simulated overconsolidated clay samples. M.Sc. Thesis, University of Manitoba, Department of Civil Engineering, Winnipeg, Manitoba, Canada.

Ladd, C.C., Foott, R., Ishihara, K, Schlosser, F., and Poulos, H.G. 1977. Stress deformation and strength characteristics. State-of-the-art report, Proc. 9th Int. Conf. Soil Mech. Fdn Engng, Tokyo, Vol.2, pp.421-494.

Laguros, J.G. 1969. Effect of temperature on some engineering properties of clay soils. Highway Research Board, Special Report No. 103 pp.186-193

Lambe, T.W. 1958. The engineering behaviour of compacted clays. ASCE Journal of Soil Mechanics and Foundation Division 84(SM2) pp.718-741.

Lau, S. L.-K. 1986. Effects of stress-release disturbance on the shear behaviour of simulated offshore clays subjected to drained storage. M.Sc. Thesis, University of Manitoba, Department of Civil Engineering, Winnipeg, MAnitoba, Canada.

Levy, A. 1981. High-temperature inelastic analysis. Computers & Structures, Vol.13, pp.249-256.

Lingnau, B.E. 1993. Consolidated undrained triaxial behaviour of a sand-bentonite mixture at elevated temperature. Ph.D. Thesis, Department of Civil Engineering, University of Manitoba, Winnipeg, Manitoba, Canada.

Lingnau, B.E., Graham, J., and Tanaka, N. 1995. Isothermal modeling of sand-bentonite mixtures at elevated temperatures. Canadian Geotechnical Journal 32, pp.899-105.

Low, P.F. 1987. Structural component of the swelling pressure of clays. Langmuir, 3, pp.18-25.

Matsuoka, H., and Nakai, I. 1982. A new failure criterion for soils in three-dimensional stresses. IUTAM Conference on Deformation and Failure of Granular Materials, Delft, The Netherlands, pp.253-263.

McKinley, I.G. 1989. The near-field geochemistry of HLW disposal in an argillaceous host rock. Nagra Technical Report NTB-88-26, Baden, Switzerland, 57 pp.

Mitchell, J.K. 1964. Shearing resistance of soils as a rate process. Journal of Soil Mechanics and Foundations Division, Proceedings American Society of Civil Engineers 90 SM1 p.29-61.

Mitchell, J.K. 1976. Fundamentals of soil behavior. John Wiley & Sons Inc. N.Y, 422pp.

Mitchell, J.K., and Campanella, R.G. 1963. Creep studies on saturated clays. Symposium on Laboratory Shear Testing of Soils, ASTM STP 361 pp.91-103.

Mitchell, J.K., *et al.* 1982. Thermal backfill materials. Underground Cable Thermal Backfill, S.A. Boggs, *et al.*, eds., Pergamon Press, New York, N.Y., pp.19-33.

Mitchell, J.K. 1985. Hazardous waste containment. In Groundwater in Engineering Geology, Geological Society of London Engineering Geology Special Publication, 3, pp.145-157.

Noble,C.A. and Demirel, T. 1969. Effect of temperature on strength behavior of cohesive soil, Highway Research Board, Special Report 103, pp.204-219.

Nowacki, W. 1962. Thermoelasticity. Pergamon Press, London.

Onsager, L. 1931. Reciprocal relations in irreversible processes. 1. Phys. Rev. 37, pp.405.

Oswell, J.M. 1991. Elastic plastic behaviour of a sand-bentonite mixture. Ph.D. Thesis, Department of Civil Engineering, University of Manitoba, Winnipeg, Manitoba, Canada.

Paaswell, R.E. 1967. Temperature effects on clay soil consolidation. ASCE Journal of Soil Mechanics and Foundation Division 93(SM3) pp.9-22.

Perzyna, P., and Sawczuk, A. 1973. Problems of thermoplasticity. Nuclear Engineering and Design 24, pp.1-55. North-Holland Publishing Company.

Phillips, A, and Tang, J.-L. 1972. The effect of loading path on the yield surface at elevated temperatures. Int. J. Solids Structures, Vol.8, pp.463-474.

Phillips, A., Liu, C.S., and Justusson, J.W. 1972. An experimental investigation of yield surfaces at elevated temperatures. Acta Mechanics 14, pp.119-146.

Pirajno, F. 1992. Hydrothermal Mineral Deposits: Principles and Fundamental Concepts for the Exploration Geologist, Springer-Verlag.

Plum, R.L., and Esrig, M.I. 1969. Some temperature effects on soil compressibility and pore water pressure. Highway Research Board, SR 103, pp.231-242.

Pusch, R. 1980. Permeability of highly compacted bentonite. Kaernbraenslesaekerhet, KBS Technical Report 16.

Pusch, R. 1985. Final report of the buffer mass test: 3 - chemical and physical stabilities of the buffer materials. Nagra Technical Report NTB 85-60, Baden, Switzerland.

Pusch, R. 1987. Permanent crystal lattice contraction, a primary mechanism in thermally induced alternation of Na bentonite. In Scientific Basis for Nuclear Waste Management X, J.K. Bates and W.B. Seefeldt, ed., MRS, Vol.84, pp.791-802.

Pusch, R., and Güven, N. 1988. Electron microscopic examination of hydrothermally treated bentonite clay. Proc. Workshop on Artificial Clay Barriers for High Level Radioactive Waste Repositories, Lund, Sweden, pp.35-45.

Pusch, R., and Karnland, O. 1988. Hydrothermal effects on montmorillonite: a preliminary study. SKB Technical Report 88-15.

Pusch, R., and Güven, N. 1990. Electron microscopic examination of hydrothermally treated bentonite clay. Engineering Geology 28 pp.303-314

Pusch, R., Karnland, O., Hökmark, H., Sandén, T., and Börgesson, L. 1991. Final Report of the Rock Sealing Project - Sealing Properties and Longevity of Smectite Clay Grouts. Stripa Project, Technical Report 91-30, SKB, Stockholm.

Pusch, R., and Karnland, O. 1993. Physico/chemical stability of smectite clays. Bergamo Workshop.

Pusch, R., Karnland, O., Lajudie, A., and Decarreauu, M. 1993. MX-80 Clay exposed to high temperatures and gamma radiation. SKB Technical Report TR 90-43, SKB, Stockholm.

Pytte, A.M. 1982. The kinetics of the smectite to illite reaction in contact metamorphic shales. Thesis M.A., Dartmouth College, N.H.

Quigley, R.M. 1984. Quantitative mineralogy and preliminary pore-water fluid chemistry of candidate buffer and backfill materials for a nuclear fuel waste disposal vault, Atomic Energy of Canada Limited, Report AECL-7827.

Radhakrishna, H.S. 1982. Evaluation of the thermal properties of buffer materials for a deep underground nuclear waste disposal vault. Atomic Energy of Canada Limited, Technical Record TR-183.

Radhakrishna, H.S., Chan, H.T., Crawford, A.M., and Lau, K.C. 1989. Thermal and physical properties of candidate buffer-backfill materials for a nuclear fuel waste disposal vault. Canadian Geotechnical Journal 26, pp.629-639.

Robinet, J.C., Al-Mukhtar, M., and Rahbaoui, A. 1992. Thermomechanical modeling of non active, low porosity and saturated clays. Franco-American Workshop.

Robinet, J.C., Rahbaoui, A. 1994. A thermo-elastoplastic model with thermal hardening for saturated clay barriers. Proceedings 1st International Congress on Environmental Geotechnics, Edomonton, Canada.

231

Roscoe, K.H., Schofield, A.N., and Thurairajah, A. 1963. Yielding of clays in states wetter than critical. Géotechnique 13, pp.211-240.

Roscoe, K.H., and Burland, J.B. 1968. On the generalized stress-strain behaviour of 'wet' clay. Engineering Plasticity (J. Heyman and F.A. Leckie, eds.), pp.535-609.

Rosenqvist, I.Th. 1959. Physico-chemical properties of soils: Soil-water systems. Journal of Soil Mechanics and Foundation Division, ASCE 85(2) pp.31-53.

Saadat, F. 1989. Constitutive modeling of the behaviour of a sand-bentonite mixture. Ph.D thesis, Department of Civil Engineering, University of Manitoba, Winnipeg, Manitoba, Canada.

Schofield, A.N., and Wroth, C.P. 1968. Critical state soil mechanics. McGraw Hill, London, U.K., 310pp.

Seed, H.B., Mitchell, J.K., and Chan, C.K. 1960. The strength of compacted cohesive soils. Proc. ASCE Research Conf. on Shear Strength of Cohesive Soils, Boulder, Colorado, pp.877-964.

Selvadurai, A.P.S., Lopez, R.S., and Hartley, G.A. 1985. Geotechnical modelling of buffer-container-rockmass interaction in a nuclear waste disposal vault. Proceedings, 11th International Conference on Soil Mechanics and Foundation Engineering, San Francisco, Vol.3, pp.1299-1305.

Selvadurai, A.P.S., McMartin, K.C., and Conley, S. 1986. A computer-aided experimental technique for the study of heat transfer processes in buffer regions of a nuclear waste disposal vault. Proceedings, 1st Canadian Conference on Computer Applications in Civil Engineering/Micro-computers, Hamilton, Ont., Vol.2, pp.212-228.

Sharifi, P., and Yates, D.N. 1974. Nonlinear thermo-elastic-plastic and creep analysis by the finite-element method. American Institute of Aeronautics and Astronautics Journal, Vol.12, No.9, pp.1210-1215.,

Sherif, M. and Burrows,C. 1969. Temperature effects on the unconfined shear strength of saturated cohesive soil. Highway Research Board, Special Report 103 pp.267-272.

Shibuya, S., Tatsuoka, F, Teachavorasinskun, S., Kong, X.J., Abe, F., Kim, Y.-S., and Park, C.-S. 1992. Elastic deformation properties of geomaterials. Soils and Foundations, Vol.32, No.3, pp.26-46.

Sun, B.C.-C. 1986. Stress-strain properties in sand-clay buffer

materials. M.Sc. thesis, Department of Civil Engineering, University of Manitoba, Winnipeg, Manitoba, Canada.

Takashi, T. 1969. Influence of seepage stream on the joining of frozen soil zones in artificial soil freezing. HRB SR103, pp.273-286.

Tanaka, N., Graham, J., and Lingnau, B.E. 1995. A thermal elastic plastic model based on Modified Cam Clay. Accepted for publication, Proc. 10th Pananmerican Conference on SOil Mechanics and Foundattions Engineering, Guadalajara, Mexico, October, 1995.

Tassoni, E. 1980. An experiment on the heat transmission in a clay rock. Proc. Workshop, The Use of Argillaceous Materials for the Isolation of Radioactive Waste, OECD Paris, pp.23-45.

Tavenas, F., Leroueil, S., La Rochelle, P., and Roy, M. 1978. Creep behaviour of an undisturbed lightly overconsolidated clay. Canadian Geotechnical Journal 15 pp.402-123.

Tavenas, F., Des Rosiers, J.-P., Leroueil, S., La Rochelle, P., and Roy, M. 1979. The use of strain energy as a yield and creep criterion for lightly overconsolidated clays. Géotechnique 29 pp.285-303.

Tidförs, M., and Sällfors, G. 1989. Temperature effect on preconsolidation pressure. Geotechnical Testing Journal 12 pp.93-97.

Tsuchida, T., Kobayashi, M., and Mizukami, J. 1991. Effect of aging of marine clay and its duplication by high temperature consolidation, Soils and Foundations 31 pp.133-147.

Wan, A.W. 1988. Compaction and strength characteristics of sand-clay buffer material formed at swelling pressure-water content equilibrium. M.Sc. Thesis, Department of Civil Engineering, University of Manitoba, Winnipeg, Manitoba, Canada.

Wan, R.G., Chan, D.H., and Kosar, K.M. 1991. A constitutive model for effective stress-strain behaviour of oil sands. Journal of Canadian Petroleum Technology 30 pp.89-98.

Westski, J.H., Bray, L.A., Lodges, F.N., and Wheelwright, E.J. 1982. Permeability, swelling and radionuclides retardation properties of candidate backfill materials. Pacific Northwest laboratory, Technical Report PNL-SA-9645.

Wong, R.C.K., Barr, W.E. and Kry, P.R. 1993. Stress-strain response of Cold Lake oil sands, Canadian Geptechnical Journal, 30, pp.220-235.

Wood, D.M.   1990 Soil behaviour and critical state soil mechanics, Cambridge.

Wroth,C.P., and Houlsby,G.T.   1985.   Soil mechanics – Property characterization and analysis procedures, Proc. 11th ICSMFE, San Francisco, Vol.1, pp.1-54.

Yarechewski, D.S.   1993.   Constant mean effective stress tests on sand bentonite specimens at elevated temperature.   M.Sc. Thesis, Department of Civil Engineering, University of Manitoba, Winnipeg, Manitoba, Canada.

Yin, J.-H.   1990.   Constitutive modelling of time-dependent stress-strain behaviour of soils.   Ph.D Thesis, Department of Civil Engineering, University of Manitoba, Winnipeg, Canada.

Yang, N. and Barbour, S.L.   1992.   The impact of soil structure and confining stress on the hydraulic conductivity of clays in brine environments.   Canadian Geotechnical Journal, 29, pp.730-739.

Yong, R., Taylor, L.O., and Warkentin, B.P. 1962.   Swelling pressures of sodium montmorillonite at depressed temperatures. Proceedings 11th National Conference on Clay and Clay Minerals pp.268-281.

Yong, R.N., Boonsinsuk, P., and Wong, G.   1986.   Formulation of backfill material for a nuclear fuel waste disposal vault. Canadian Geotechnical Journal, 23, pp.216-228.

Zhang, R.   1992.   Implementation of KGJ hypoelastic model in finite element program.   M.SC.   Thesis, Department of Civil Engineering, University of Manitoba, Winnipeg, Manitoba, Canada.

APPENDIX 1 Modification of GDS System

In order to take additional readings from an electric device during a test, the GDS system was modified. A voltmeter was connected to the host computer through IEEE interconnecter. The voltmeter was originally made for taking one channel reading from an electrical instrument. In this study, a relay-type device was made for the voltmeter to take two channel readings with a certain interval. By using this device, additional readings from load cell and pore pressure transducer could be automatically stored on the computer diskette while tests are running.

The computer program for the GDS system was also modified to store additional channel data during tests.

APPENDIX 2 Initial Test Conditions

Test No.	w_o(%)	ρ_d(Mg/m^3)	p_c'(MPa)	p_o'(MPa)	Soil Type
T1401	22.50	1.660	1.52	1.52	S.B.
T1402	22.31	1.659	1.34	1.34	S.B.
T1403	22.24	1.663	1.06	1.06	S.B.
T1404	22.00	1.670	1.01	1.01	S.B.
T1405	22.66	1.655	1.56	1.56	S.B.
T1406	22.20	1.666	1.48	1.48	S.B.
T1410	27.45		2.01	2.01	R.I.
T1420	27.63		1.00	0.50	R.I.
T1421	27.87		1.00	0.50	R.I.
T1422	28.00		1.00	0.50	R.I.
T1440	28.15		1.03	0.51	R.I.
T1441	27.22		1.06	0.55	R.I.
T1442	27.59		1.10	0.54	R.I.
T1443	27.55		0.97	0.50	R.I.
T1444	27.86		0.98	0.55	R.I.
T1445	26.78		3.05	0.40	R.I.
T1446	13.31	1.887		0.63	C.I.
T1447	13.30	1.920		0.55	C.I.
T1448	13.62	1.888		0.58	C.I.
T1450	27.17		1.05	0.56	R.I.
T1451	27.63		1.03	0.54	R.I.
T1452	27.92		1.00	0.49	R.I.
T1453	27.69		1.05	0.53	R.I.
T1460	28.02		1.57	1.57	R.I.
T1461	27.19		1.51	1.51	R.I.
T1462	27.79		1.19	1.19	R.I.
T1463	26.85		1.50	1.50	R.I.
T1464	26.74		1.55	1.29	R.I.
T1465	26.63		0.95	0.51	R.I.
T1466	26.83		1.00	0.49	R.I.
T1467	26.54		0.97	0.60	R.I.
T1468	27.41		1.46	1.46	R.I.
T1469	13.25	1.865	1.04	1.04	C.I.
T1470	12.27	1.916	1.01	0.43	C.I.
T1471	13.20	1.906	1.05	1.05	C.I.
T1472	27.58		1.47	1.47	R.I.
T1473	27.81		0.98	0.55	R.I.
T1474	27.13		1.00	0.53	R.I.
T1475	22.40	1.671	1.57	1.57	S.B.

Appendix 2   Initial and Test Conditions (continued)

Test No.	w_o(%)	ρ_d(Mg/m^3)	p_c'(MPa)	p_o'(MPa)	Soil Type
T1480	27.68		·1.00	0.52	R.I.
T1481	27.04		1.02	0.52	R.I.
T1482	27.95		1.00	0.52	R.I.
T1483	27.69		1.00	0.51	R.I.
T1484	27.47		1.56	1.56	R.I.
T1485	13.13	1.952	1.05	1.05	C.I.
T1486	27.05		1.01	0.49	R.I.
T1487	13.19	1.907	1.05	0.52	C.I.
T1488	12.48	1.895	1.07	0.57	C.I.
T1489	13.14	1.922	1.06	0.55	C.I.
T1490	28.65		1.54	1.49	R.I.
T1491	29.97		1.51	1.51	R.I.
T1492	29.96		1.51	1.48	R.I.
T1495	13.25	1.930	1.08	0.57	C.I.

where
  R.I. = Reconstituted Illite
  C.I. = Compacted Illite
  S.B. = Sand-Bentonite
  p_c' = preconsolidation pressure for reconstituted illite, or maximum consolidation pressure for compacted illite and sand-benonite.

APPENDIX 3 Test Data at EOC and EOT

Test No.	V(EOC)	T_c(°C)	T_s(°C)	p'_f(MPa)	q_f(MPa)	V(EOT)	Comments
T1401	1.609	28	28	1.590	0.995	1.609	US
T1402	1.607	28/65	65	1.683	0.966	1.607	DTC/US
T1403	1.667	28	28	1.010	0.624	1.667	US
T1404	1.641	28	28	1.131	0.733	1.641	US
T1405	1.623	28	28	1.402	0.587	1.623	US
T1406	1.681	28/100	100	1.550	0.916	1.560	DTC/US
T1410	1.449	28/100	--	---	---	1.449	
T1420	1.532	28	28	0.448	0.491	1.553	US
T1421	1.555	28	28	0.765	0.753	1.505	DS
T1422	1.510	28	28	0.438	0.390	1.637	DS
T1440	1.510	28/100/65	65	0.738	0.681	1.498	DTC/DS
T1441	1.496	28/65	65	0.726	0.622	1.486	DTC/DS
T1442	1.507	28/65	65	0.244	0.340	1.529	DTC/DS
T1443	1.507	28/65	65	0.416	0.387	1.520	DTC/DS
T1444	1.489	28/65	65	0.557	0.594	1.465	DTC/DS
T1445	1.471	28/100/65	65	0.622	0.661	1.463	DTC/DS
T1446	1.414	28/65	65	0.913	0.784	1.413	DTC/DS
T1447	1.434	28/65	65	0.208	0.267	1.502	DTC/DS
T1448	1.455	28/65	65	1.145	0.000	1.403	DTC/DS
T1450	1.501	28/100	100	0.675	0.550	1.464	DTC/DS
T1451	1.506	28/100	100	0.257	0.260	1.540	DTC/DS
T1452	1.511	28/100	100	0.458	0.473	1.498	DTC/DS
T1453	1.532	28/100	100	1.039	0.000	1.481	DTC/DS
T1460	1.452	28/65	65	1.152	1.065	1.452	DTC/US
T1461	1.414	28/100	100	1.546	1.245	1.414	DTC/US
T1462	1.559	28	--	---	---	1.559	
T1463	1.452	28/65/28	28	1.028	0.914	1.452	DTC/US
T1464	1.461	28	28/65/28	0.880	0.794	1.461	UTS
T1465	1.507	28	28/65/28	0.307	0.309	1.507	UTS
T1466	1.491	28	28/65/28	0.501	0.577	1.491	UTS
T1467	1.496	28/65	65	0.503	0.579	1.496	UTC/US
T1468	1.473	28/65	65	0.787	0.373	1.473	UTS
T1469	1.409	28/65	65	0.905	0.910	1.409	DTC/US
T1470	1.425	28/65	65	0.714	0.373	1.425	DTC/US
T1471	1.416	28	28/65	0.853	0.930	1.416	UTS
T1472	1.466	28	28/100	0.824	0.852	1.465	UTS
T1473	1.513	28	28/100	0.471	0.521	1.500	DS
T1474	1.437	28/100	100	1.264	1.152	1.437	DTC/US
T1475	1.614	28	28/100/28	1.789	0.838	1.614	US

APPENDIX 3 Test Data at EOC and EOT (Continued)

Test No.	V(EOC)	T_c(°C)	T_s(°C)	p'_f(MPa)	q_f(MPa)	V(EOT)	Comments
T1480	1.532	28	28	0.771	0.773	1.500	DS
T1481	1.530	28	28	-0.241	0.349	1.573	DS
T1482	1.520	28	28	0.420	0.480	1.529	DS
T1483	1.526	28	28	0.679	0.717	1.491	DS
T1484	1.421	28	28	---	---	1.421	DS
T1485	1.419	28	28	1.087	1.126	1.401	DS
T1486	1.466	28	28	0.446	0.413	1.519	US
T1487	1.423	28	28	0.851	0.973	1.421	DS
T1488	1.438	28	28	0.256	0.342	1.494	DS
T1489	1.396	28	28	1.858	0.975	1.383	DS
T1490	1.468	28	28	0.856	0.920	1.468	US
T1491	1.469	28	28	0.900	0.974	1.469	US
T1492	1.465	28	28	0.859	0.931	1.481	US
T1495	1.421	28	28	0.846	0.851	1.424	US

where
DTC = Drained Temeprature change in Consolidation
UTC = Undrained Temperature change in Consolidation
DS = Drained Shear
US = Undrained Shear
UTS = Undrained Temperature change in Shear

APPENDIX 4 Table of Test Steps for Temperature-change Tests

T1402 (Compacted sand-bentonite mixture)
  1. Back pressured at $p_0' = 0$ to 1.5 MPa, $T = 28°C$
  2. Isotropic consolidation at $p_0' = 1.5$ MPa, $T = 28°C$
  3. Heating to $T = 65°C$, at $p_0' = 1.5$ MPa, Drained
  4. Sheared undrained, $T = 65°C$
  5. Cooling to $T = 28°C$, Undrained

T1406 (Compacted sand-bentonite mixture)
  1. Back pressured at $p_0' = 0$ to 1.5 MPa, $T = 28°C$
  2. Isotropic consolidation at $p_0' = 1.5$ MPa, $T = 28°C$
  3. Heating to $T = 100°C$, at $p_0' = 1.5$ MPa, Drained
  4. Sheared undrained, $T = 100°C$
  5. Cooling to $T = 28°C$, Undrained

T1440 (Reconstituted illite)
  1. Back pressured at $p_0' = 0$ to 0.1 MPa, $T = 28°C$
  2. Isotropic consolidation at $p_0' = 0.1$ to 1.0 MPa , $T = 28°C$
  3. Isotropic unloading to $p_0' = 0.5$ MPa, $T = 28°C$
  4. Heating to $T = 100°C$, at $p_0' = 0.5$ MPa, Drained
  5. Cooling to $T = 65°C$, at $p_0' = 0.5$ MPa, Drained
  6. Sheared drained, $T = 65°C$
  7. Cooling to $T = 28°C$, Drained

T1441, T1442, T1443, T1444 (Reconstituted illite)
  1. Back pressured at $p_0' = 0$ to 0.1 MPa, $T = 28°C$
  2. Isotropic consolidation at $p_0' = 0.1$ to 1.0 MPa , $T = 28°C$
  3. Isotropic unloading to $p_0' = 0.5$ MPa, $T = 28°C$
  4. Heating to $T = 65°C$, at $p_0' = 0.5$ MPa, Drained
  5. Sheared drained, $T = 65°C$
  6. Cooling to $T = 28°C$, Drained

T1445 (Reconstituted illite)
  1. Back pressured at $p_0' = 0$ to 0.1 MPa, $T = 28°C$
  2. Isotropic consolidation at $p_0' = 0.1$ to 1.0 MPa , $T = 28°C$
  3. Isotropic unloading to $p_0' = 0.5$ MPa, $T = 28°C$
  4. Heating to $T = 100°C$, at $p_0' = 0.5$ MPa, Drained
  5. Isotropic reloading at $p_0' = 0.5$ to 1.0 MPa, $T = 100°C$
  6. Cooling to $T = 65°C$, at $p_0' = 1.0$ MPa, Drained
  7. Isotropic consolidation $p_0' = 1.0$ to 3.0 MPa, $T = 65°C$
  8. Isotropic reloading $p_0' = 3.0$ to 0.35 MPa, $T = 65°C$
  6. Sheared drained, $T = 65°C$
  7. Cooling to $T = 28°C$, Drained

T1446, T1447, T1448 (Compacted illite)
  1. Back pressured at $p_0' = 0$ to 0.1 MPa, $T = 28°C$
  2. Isotropic consolidation at $p_0' = 0.1$ to 1.0 MPa , $T = 28°C$
  3. Isotropic unloading to $p_0' = 0.5$ MPa, $T = 28°C$
  4. Heating to $T = 65°C$, at $p_0' = 0.5$ MPa, Drained
  5. Sheared drained, $T = 65°C$

6. Cooling to T = 28°C, Drained

T1450, T1451, T1452, T1453 (Reconstituted illite)
        1. Back pressured at p_0' = 0 to 0.1 MPa, T = 28°C
        2. Isotropic consolidation at p_0' = 0.1 to 1.0 MPa , T = 28°C
        3. Isotropic unloading to p_0' = 0.5 MPa, T = 28°C
        4. Heating to T = 100°C, at p_0' = 0.5 MPa, Drained
        5. Sheared drained, T = 100°C
        6. Cooling to T = 28°C, Drained

T1460, T1461 (Reconstituted illite)
        1. Back pressured at p_0' = 0 to 0.1 MPa, T = 28°C
        2. Isotropic consolidation at p_0' = 0.1 to 1.0 MPa , T = 28°C
        3. Isotropic unloading to p_0' = 0.5 MPa, T = 28°C
        4. Isotropic reloading to p_0' = 1.5 MPa, T = 28°C
        5. Heating to T=65°C(T1460), 100°C(T1461),at p_0' =1.5MPa,
            Drained
        6. Sheared undrained, T = 65°C (T1460), 100°C (T1461)
        7. Cooling to T = 28°C (T1460), Undrained

T1463 (Reconstituted illite)
        1. Back pressured at p_0' = 0 to 0.1 MPa, T = 28°C
        2. Isotropic consolidation at p_0' = 0.1 to 1.5 MPa , T = 28°C
        3. Heating to T = 65°C, at p_0' = 1.5 MPa, Drained
        4. Cooling to T = 28°C, at p_0' = 1.5 MPa, Drained
        5. Sheared undrained, T = 28°C

T1464 (Reconstituted illite)
        1. Back pressured at p_0' = 0 to 0.1 MPa, T = 28°C
        2. Isotropic consolidation at p_0' = 0.1 to 1.0 MPa , T = 28°C
        3. Heating to T = 65°C, at p_0' = 1.5 MPa, Undrained
        4. Cooling to T = 28°C, at p_0' = 1.5 MPa, Undrained
        5. Sheared undrained to q = 0.35 MPa, T = 28°C
        6. Heating to T = 65°C, at q = 0.35 MPa, Undrained
        7. Releasing water for system compliance
        8. Cooing to T = 28°C, to q = 0 MPa, Undrained
        9. Injecting water for system compliance
        10. Sheared undrained, T = 28°C
        11. Heating to T = 65°C, at q = 0.83 MPa, Undrained
        12. Sheared undrained, T = 65°C
        13. Cooling to T = 28°C, Undrained

T1465 (Reconstituted illite)
        1. Back pressured at p_0' = 0 to 0.1 MPa, T = 28°C
        2. Isotropic consolidation at p_0' = 0.1 to 1.0 MPa , T = 28°C
        3. Isotropic unloading to p_0' = 0.5 MPa, T = 28°C
        3. Heating to T = 65°C, at p_0' = 0.5 MPa, Undrained
        4. Cooling to T = 28°C, at p_0' = 0.5 MPa, Undrained
        5. Sheared undrained to q = 0.35 MPa, T = 28°C
        6. Heating to T = 65°C, at q = 0.35 MPa, Undrained
        7. Releasing water for system compliance
        8. Cooing to T = 28°C, at q = 0.2 MPa, Undrained

9. Injecting water for system compliance
        10. Sheared undrained to q = 0.55 MPa, T = 28°C

  T1466   (Reconstituted illite)
        1. Back pressured at p_0' = 0 to 0.1 MPa, T = 28°C
        2. Isotropic consolidation at p_0' = 0.1 to 1.0 MPa , T = 28°C
        3. Isotropic unloading to p_0' = 0.5 MPa, T = 28°C
        3. Heating to T = 65°C, at p_0' = 0.5 MPa, Drained
        4. Sheared undrained, at T = 65°C
        5. Cooling to T = 28°C, Undrained

  T1467   (Reconstituted illite)
        1. Back pressured at p_0' = 0 to 0.1 MPa, T = 28°C
        2. Isotropic consolidation at p_0' = 0.1 to 1.0 MPa , T = 28°C
        3. Heating to T = 65°C, at p_0' = 1.0 MPa, Undrained
        3. Releasing water for system compliance
        4. Sheared undrained, at T = 65°C
        5. Cooling to T = 28°C, Undrained

  T1468   (Reconstituted illite)
        1. Back pressured at p_0' = 0 to 0.1 MPa, T = 28°C
        2. Isotropic consolidation at p_0' = 0.1 to 1.5 MPa , T = 28°C
        3. Heating to T = 65°C, at p_0' = 1.5 MPa, Undrained
        4. Cooling to T = 28°C, at p_0' = 1.5 MPa, Undrained
        5. Sheared undrained to q = 0.30 MPa, T = 28°C
        6. Heating to T = 65°C, at q = 0.30 MPa, Undrained
        7. Releasing water for system compliance
        8. Sheared undrained to q = 0.55 MPa, T = 65°C
        9. Cooling to T = 28°C, at q = 0, Undrained

  T1469   (Compacted illite)
        1. Back pressured at p_0' = 0 to 1.0 MPa, T = 28°C
        2. Isotropic consolidation at p_0' = 1.0 MPa , T = 28°C
        3. Heating to T = 65°C, at p_0' = 1.0 MPa, Undrained
        4. Releasing water for system compliance
        5. Cooling to T = 28°C, Undrained
        6. Injecting water for system compliance
        7. Heating to T = 65°C, at p_0' = 1.0 MPa, Drained
        8. Sheared undrained, at T = 65°C
        9. Cooling to T = 28°C, Undrained

  T1470   (Compacted illite)
        1. Back pressured at p_0' = 0 to 1.0 MPa, T = 28°C
        2. Isotropic consolidation at p_0' = 1.0 MPa , T = 28°C
        3. Isotropic unloading to p_0' = 0.5 MPa, at T = 28°C
        4. Heating to T = 65°C, at p_0' = 0.5 MPa, Drained
        5. Sheared undrained, at T = 65°C
        6. Cooling to T = 28°C, Undrained

  T1471   (Compacted illite)
        1. Back pressured at p_0' = 0 to 1.0 MPa, T = 28°C
        2. Isotropic consolidation at p_0' = 1.0 MPa , T = 28°C

3. Heating to T = 65°C, Undrained
4. Cooling to T = 28°C, Undrained
5. Sheared undrained to q = 0.45 MPa, at T = 28°C
6. Heating to T = 65°C, at q = 0.45 MPa, Undrained
7. Sheared undrained to q = 0.9 MPa, at T = 65°C
8. Cooling to T = 28°C, Undrained

T1472 (Reconstituted illite)
1. Back pressured at $p_o' = 0$ to 0.1 MPa, T = 28°C
2. Isotropic consolidation at $p_o' = 0.1$ to 1.5 MPa , T = 28°C
3. Heating to T = 100°C, at $p_o' = 1.5$ MPa, Undrained
4. Cooling to T = 100°C, at $p_o' = 1.5$ MPa, Undrained
5. Sheared undrained to q = 0.35 MPa, T = 28°C
6. Heating to T = 100°C, at q = 0.35 MPa, Undrained
7. Sheared undrained to q = 0.6 MPa, T = 100°C
8. Cooling to T = 28°C, at q = 0, Undrained

T1473 (Reconstituted illite)
1. Back pressured at $p_o' = 0$ to 0.1 MPa, T = 28°C
2. Isotropic consolidation at $p_o' = 0.1$ to 1.0 MPa , T = 28°C
3. Isotropic unloading to $p_o' = 0.5$ MPa, T = 28°C
3. Heating to T = 100°C, at $p_o' = 0.5$ MPa, Undrained
4. Cooling to T = 28°C, at $p_o' = 0.5$ MPa, Undrained
5. Sheared undrained to q = 0.33 MPa, T = 28°C
6. Heating to T = 100°C, at q = 0.33 MPa, Undrained
7. Sheared undrained to q = 0.35 MPa, T = 100°C
8. Cooing to T = 28°C, at q = 0 MPa, Undrained
9. Sheared undrained to q = 0.52 MPa, T 28°C

T1474 (Reconstituted illite)
1. Back pressured at $p_o' = 0$ to 0.1 MPa, T = 28°C
2. Isotropic consolidation at $p_o' = 0.1$ to 1.0 MPa , T = 28°C
3. Isotropic unloading to $p_o' = 0.5$ MPa, T = 28°C
3. Heating to T = 100°C, at $p_o' = 0.5$ MPa, Drained
4. Isotropic reloading to $p_o' = 1.5$ MPa, at T = 100°C
5. Sheared undrained, T = 100°C
6. Cooling to T = 28°C, Undrained

T1475 (Compacted sand-bentonite mixture)
1. Back pressured at $p_o' = 1.5$ MPa, T = 28°C
2. Isotropic consolidation at $p_o' = 1.5$ MPa , T = 28°C
3. Heating to T = 100°C, Undrained
3. Cooling to T = 28°C, Undrained
4. Sheared undrained to q = 0.5 MPa, at T = 28°C, Undrained
5. Heating to T = 100°C, at q = 0.5 MPa, Undrained
6. Sheared undrained to q = 0.77 MPa, at T = 100°C,
7. Cooling to T = 28°C, at q = 0, Undrained
8. Sheared undrained, at T = 28°C

APPENDIX 5 Computer Program for Modified Cam-clay Modelling

```
10 PRINT "-------------------------------------------"
15 PRINT "Date : 26 August 1994
20 PRINT "  Cam-Clay Modelling
30 PRINT "           by Naoto Tanaka, 1994"
40 PRINT "-------------------------------------------"
50 INPUT "file name ??";A$
60 A$="D:\naoto2\tepmodel\chap10\"+A$
70 OPEN A$+".PRN" FOR OUTPUT AS #1
80 '---------------------------------
90 '------INPUT INITIAL DATA---------
100 '---------------------------------
110 INPUT "M = ?";M
120 INPUT "lamda = ?";L
130 INPUT "kappa = ?";K
140 INPUT "G/p' = ?";GP
150 INPUT "Pc = ?";PC0 : 'initial preconsolidation pressure
160 INPUT "initial p = ?";P0 : 'initial pressure
170 INPUT "N = ?";N : 'PARAMETER
180 INPUT "HVORSLEV SURFACE SLOPE = ?";HS
190 'INPUT "V = ?";V0 : 'initial specific volume
200 ' M=1.07 : L=.087 : GP=70.6 : PC0=888.9 : P0=500 : N=20 :
    HS=0.7:' V0=1.48
205 IF PC0>P0 THEN GOTO 215 ELSE GOTO 210
210 V0=N-L*LOG(PC0)/LOG(2.71828) : GOTO 220
215 V0=N-L*LOG(PC0)/LOG(2.71828)+K*LOG(PC0/P0)/LOG(2.71828)
220 PRINT #1,"M= ";M;"LAMDA= ";L;"KAPPA= ";K;"G/P= ";GP;"PC0=
    ";PC0;"P0= ";P0;"N= ";N;"HS = ";HS: '"V0= ";V0
230 IF P0>PC0 THEN GOTO 150 ELSE GOTO 250
240 '
250 '------INCREMENTS FOR CALCULATIONS-------
260 '
270 INPUT "HOW MANY DECREMENTS/INCREMENTS FOR P = ?";INC
280 '
290 '-----Test conditions : CIU, CID, or Others ? ---
300 '
310 INPUT "CIU or CID test ? : CIU = U, CID = D, Others = S";TST$
320 'TST$="D"
330 IF TST$="U" GOTO 350
340 IF TST$="D" GOTO 370 ELSE 310
350 PRINT #1,"CIU"
360 PRINT "CIU" : GOTO 400
370 PRINT #1,"CID"
380 PRINT "CID" : GOTO 480
390 '
400 '--------- UNDRAINED TESTS ---------
410 '
420 IF PC0>P0 THEN GOTO 440 : 'overconsolidated case
430 PF=PC0*2^(K/L-1) : DP=(PC0-PF)/INC : FLG=1 : SH=1: GOTO 610
    :'UNDRAINED NC CASE
440 PF=(PC0/2)*(2*P0/PC0)^(K/L) : DP=(P0-PF)/INC : FLG=2 : SH=2
    :'UNDRAINED OC CASE
```

```
450 PCS=PCO/2 : IF PF<PCS THEN HOC=1
455 'PY=PO : QY=HS*(-PCO/2+PO)+M*PCO/2 : PRINT
    "PY=";PY;"QY=";QY;"HOC=";HOC
460 GOTO 610
470 '
480 '---------- DRAINED TESTS -----------
490 '
500 IF PCO>PO THEN GOTO 520 ELSE GOTO 510 : 'HEAVILY
    OVERCONSOLIDATED CASE
510 PF=3*PO/(3-M) : DP=(PF-PCO)/INC : FLG=3 : SH=1 : GOTO 610
    :'DRAINED NC CASE
520 PF=3*PO/(3-M) : DP=(PF-PO)/INC : FLG=4 : SH=2
    :'DRAINED OC CASE
530 PCS=PCO/2
540 QY1=M*(PCO*PCS-PCS^2)^.5 : IF PF<PCS THEN GOTO 580 ELSE GOTO 550
550 AA=(M^2*PCO+18*PO) : BB=(AA^2-4*(M^2+9)*(9*PO^2))^.5 :
    CC=2*(M^2+9)
560 PY=(AA+BB)/CC :PF=3*PO/(3-M): DP=(PF-PY)/INC
    :'DRAINED LIGHTLY OC CASE
565 GOTO 610
570 'Q2=3*(P2-PO) : FLG=3
580 HOC=1 : PZT=(QY1-HS*PCS)/(3-HS) : QZT=3*PZT : 'DRAINED HEAVILY
    OC CASE
590 PF=3*PO/(3-M) : PY=(3*PO-HS*PCS+QY1)/(3-HS) : DP=(PF-PY)/INC
600 '
610 N=0 : PRINT "DP= ";DP;"PF= ";PF
620 '-----initial conditions-----
630 P1=PO : Q1=0 : PCN=PCO : PCO=PCO: 'initial stresses
640 V1=VO : 'initial specific volume
650 EVT=0 : 'INITIAL VOLUME CHANGE
660 IF SH=2 THEN INC=INC+1
670 '
680 FOR Z=N TO INC
690 PRINT "FLG= ";FLG;"SH= ";SH;"POLE = ";POLE;"HOC=";HOC
700 IF Z=0 THEN GOTO 710 ELSE GOTO 720
710 P2=P1 : Q2=0 : V2=V1 : I=0 : GOTO 1040
720 P1=P2 : Q1=Q2 : PCO=PCN
730 IF FLG=1 OR FLG=3 THEN GOTO 750 ELSE GOTO 740
740 IF SH=2 THEN GOTO 830 ELSE GOTO 790
750 IF FLG=1 THEN GOTO 760 ELSE GOTO 790
760 IF SH=2 THEN GOTO 780 ELSE GOTO 770
770 'P2=P1-DP : PCN=(PCO^L/P2^K)^(1/(L-K)) :  GOTO 700
780 P2=P1-DP : PCN=PCO*(P1/P2)^(K/(L-K)) : GOTO 840 :'NC CASE
790 'IF FLG=3 THEN GOTO 620 ELSE GOTO 630
800 IF SH=1 THEN GOTO 810 ELSE GOTO 820
810 print"p1= ";p1,"dp= ";dp: P2=P1+DP : Q2=3*(P2-PO) : print "p2=
    ";p2,"q2= "q2: PCN=(Q2^2/M^2+P2^2)/P2 : V2=VO-
    L*LOG(PCN/PCO)+K*LOG(PCN/P2) :GOTO 890
820 P2=P1+DP : Q2=3*(P2-PO) : PCN=(Q2^2/M^2+P2^2)/P2 : V2=VO-
    K*LOG(P2/PO)-(L-K)*LOG(PCN/PCO) : GOTO 890
830 IF FLG=2 THEN GOTO 840 ELSE GOTO 850 :'OC CASE
840 'IF HOC=1 THEN GOTO 847 ELSE GOTO 845
845 FLG=1 : Q2=M*(P2*PCN-P2^2)^(1/2): GOTO 890
847 'FLG=1 : Q2=QY : GOTO 890
```

```
850 IF HOC=1 THEN GOTO 910 ELSE GOTO 860
860 AA=(M^2*PCO+18*PO) : BB=(AA^2-4*(M^2+9)*(9*PO^2))^.5 :
    CC=2*(M^2+9)
870 P2=(AA+BB)/CC : PY=P2
880 Q2=3*(P2-PO) : FLG=3 : pole =2
890 DQ=Q2-Q1 : I=Q2/P2 : print "dq=";dq
893 IF FLG=3 OR FLG=4 THEN GOTO 895 ELSE GOTO 990
895 IF HOC=1 THEN GOTO 920 ELSE GOTO 896
896 IF POLE=2 THEN GOTO 990 ELSE GOTO 930
900 '
910 '
920 PRINT "pole=";POLE : IF POLE=2 THEN GOTO 950 ELSE GOTO 930
930 QY=3*(PY-PO) : P2=PY : Q2=QY : SH=1: POLE=1 :   V2=VO-(L-
    K)*LOG(PCN/PCO)-K*LOG(P2/PO)
940 PRINT "q2= ";Q2,"p2= ";P2 : GOTO 990
950 'PRINT P1,DP
960 P2=P1+DP : Q2=3*(P2-PO) : PCN=2*((Q2-HS*P2)/(M-HS)) : V2=VO-(L-
    K)*LOG(PCN/PCO)-K*LOG(P2/PO)
970 DQ=Q2-Q1 : I=Q2/P2 : POLE=2 : 'PRINT P2,Q2
980 '
990 PRINT "Z= ";Z;"pco= ";PCO;"pcn= ";PCN;"P1= ";P1;"p2= ";P2;"q2=
    ";Q2;"I= ";I
1000 'PRINT "Press ENTER key to continue"
1010 'INPUT A$
1020 '
1030 IF Z>0 THEN GOTO 1070
1040 EVT=0 : DEVT=0 : DEVE=0 : DESE=0 : DEVP=0 : DESP=0 : EST=0 :
    E1=0 : KK=VO*PO/K/1000
1050 DEVTO=DEVT : DEVEO=DEVE : DESEO=DESE : DEVPO=DEVP : DESPO=DESP
    : ESTO=EST : E10=E1 : GOTO 1180
1060 '
1070 DEVT=DEVTO : DEVE=DEVEO : DESE=DESEO : DEVP=DEVPO : DESP=DESPO
    : EST=ESTO
1080 PRINT V1,V2 : GOSUB 1330 : 'calculation of total strains
1090 'GOSUB 1370
1100 IF FLG=3 OR FLG=4 THEN GOTO 1110 ELSE GOTO 1120
1110 GOSUB 1380 : 'calculation of bulk modulus
1120 GOSUB 1420 : 'calculation of incremantal total strains
1130 GOSUB 1470 : 'calculation of incremental elastic strains
1140 GOSUB 1610 : 'calculation of incremental plastic strains
1150 GOSUB 1770 : 'calculation of total shear strains
1160 GOSUB 1840 : 'calculation of axial strains
1170 '
1180 PRINT " f=0 " : 'on yield locus
1190 '
1200 IF Z=0 THEN GOTO 1210 ELSE GOTO 1240
1210 IF FLG=3 OR FLG=4 THEN GOTO 1220 ELSE GOTO 1230
1220 PRINT #1,"      Point ";"    q     ";"  P2   ";"    PCN ";"
    V2 ";"       EVT   ";"    KK    ";"   DEVT ";" DEVE  ";"     DESE
    ";"   DEVP  ";"   DESP  ";"   EST  ";" E1": GOTO 1250
1230 PRINT #1,"      Point ";"    q     ";"  P2   ";"    PCN ";"
    V2 ";"       EVT   ";"   DEVT  ";"  DEVE  ";" DESE  ";"   DEVP
    ";"   DESP  ";"   EST  ";"  E1   ": GOTO 1270
1240 IF FLG=3 OR FLG=4 THEN GOTO 1250 ELSE GOTO 1270
```

```
1250 'PRINT EVTN;EVTO;evtn*100;KK
1260 PRINT #1,USING
     "#####.###";Z;Q2;P2;PCN;V2;EVTN;KK;DEVTO;DEVEO;DESEO;DEVPO;DESPO
     ;ESTO;E1: GOTO 1280
1270 PRINT #1,USING
     "#####.###";Z;Q2;P2;PCN;V2;EVTO;DEVTO;DEVEO;DESEO;DEVPO;DESPO;ES
     TO;E1 : GOTO 1280
1280 GOTO 1310
1290 '----------------------------------------------
1300 'PRINT "FLG= ";FLG;"SH= ";SH
1310 NEXT
1320 CLOSE : END
1330 '------------------------------
1340 'calculation for total strains
1350 EVTO=EVT
1360 EVT=(VO-V2)/VO*100
1370 RETURN
1380 '------------------------------
1390 'calculation for bulk modulus
1400 KK=V2*P2/K/1000 : 'unit MPA
1410 RETURN
1420 '------------------------------
1430 'calculation for increment of total strains
1440 EVTN=EVT
1450 DEVTO=(EVTN-EVTO)
1460 RETURN
1470 '------------------------------
1480 'calculation for elastic strains
1490 'elastic volumetric strains
1500 'BEEP
1510 DEVE=(K/(V2*P1)*(P2-P1))*100
1520 DEVEO=(DEVE+DEVEO)
1530 'PRINT DEVEO
1540 'elastic shear strains
1550 G=GP*P1
1560 PRINT "pole = ";POLE,"HOC=";HOC :IF POLE=1 AND HOC=1 THEN GOTO
1570 ELSE 1580
1570 BEEP : DESE=(1/(3*G)*Q2)*100 : POLE=2 : GOTO 1590
1580 DESE=(1/(3*G)*DQ)*100
1590 DESEO=DESE+DESEO
1600 RETURN
1610 '------------------------------
1620 'calculation for plastic strains
1630 'plastic volumetric strains
1640 'DEVP=(L-K)/(V2*P2*(M^2+I^2))*((M^2-I^2)*DP+2*I*DQ)
1650 DEVP=((L-K)/(V2*PCO)*(PCN-PCO))*100    .
1660 DEVPO=DEVP+DEVPO
1670 'plastic shear strains
1680 IF HOC=1 THEN GOTO 1700 ELSE GOTO 1730 :'PRINT DEVPO
1690 'IF HOC=1 THEN GOTO 1630 ELSE GOTO 1650
1700 'IF I>=M THEN I=M-.001 ELSE 1610
1710 DESP=DEVPO*(2*I)/(M^2-I^2) : GOTO 1750
1720 'DESP=(L-K)/(V2*P2*(M^2+I^2))*(2*I*DP+4*I^2/(M^2-I^2)*DQ) :
     GOTO 1470
```

```
1730 IF I>=M THEN I=M-.001 ELSE GOTO 1740
1740 DESP=DEVPO*(2*I)/(M^2-I^2)
1750 DESPO=(DESP+DESPO)
1760 RETURN
1770 '-----------------------------
1780 'calculation of total shear strains
1790 DESEN=DESE
1800 DESPN=DESP
1810 EST=ESTO+DESEN+DESPN
1820 ESTO=EST
1830 RETURN
1840 '-----------------------------
1850 'calculation of axial strain
1860 E1=EST+EVT/3
1870 RETURN
```
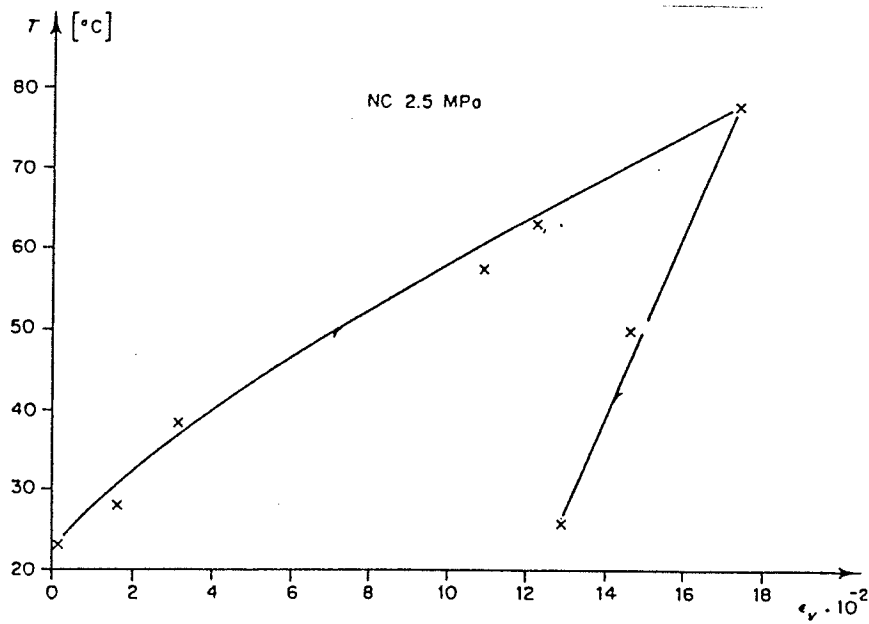
Figure 2.1 Volumetric changes with temperature at constant isotropic stress [After Hueckel *et al.* (1987)]
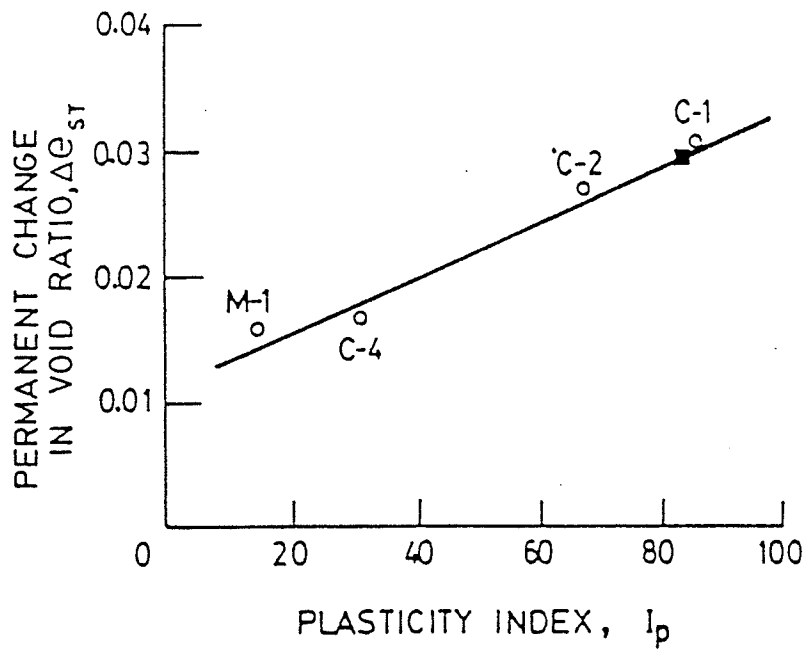
Figure 2.2 Relationship between plasticity index and irreversible volume change. [After Demars and Charles (1985)]
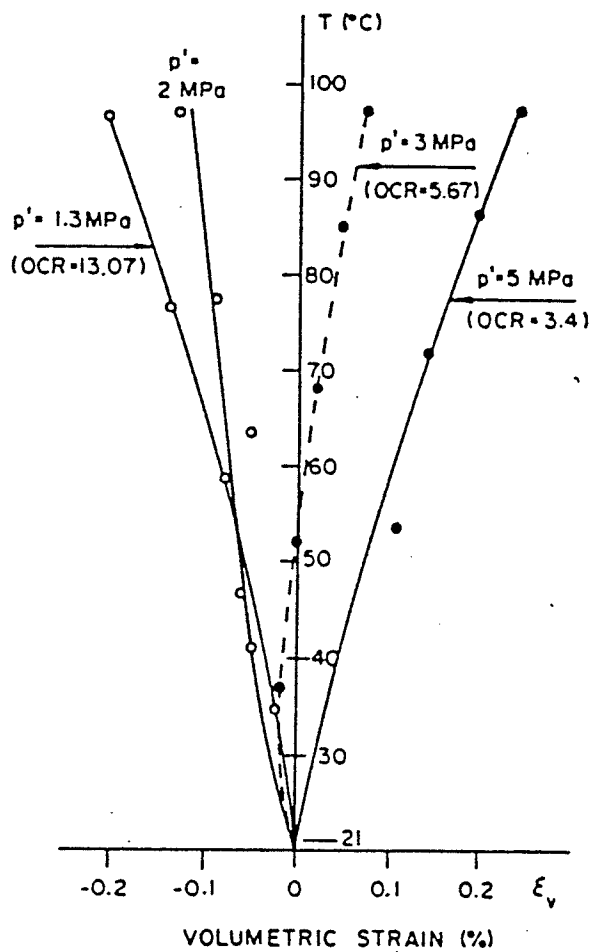
Figure 2.3 Dependency of volumetric strain on overconsolidation ratio (OCR). [After Hueckel and Baldi (1990b)]
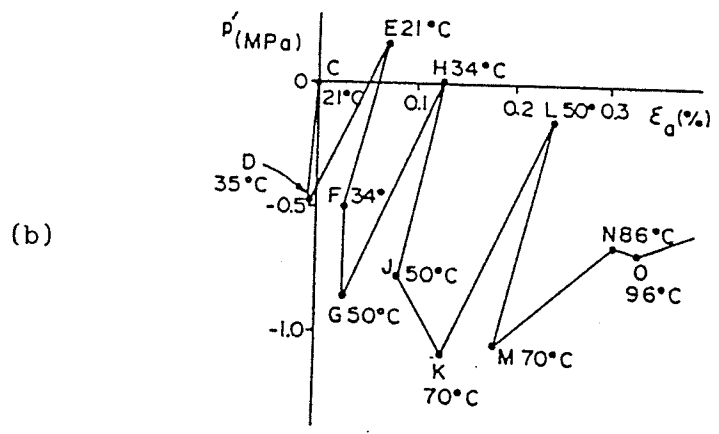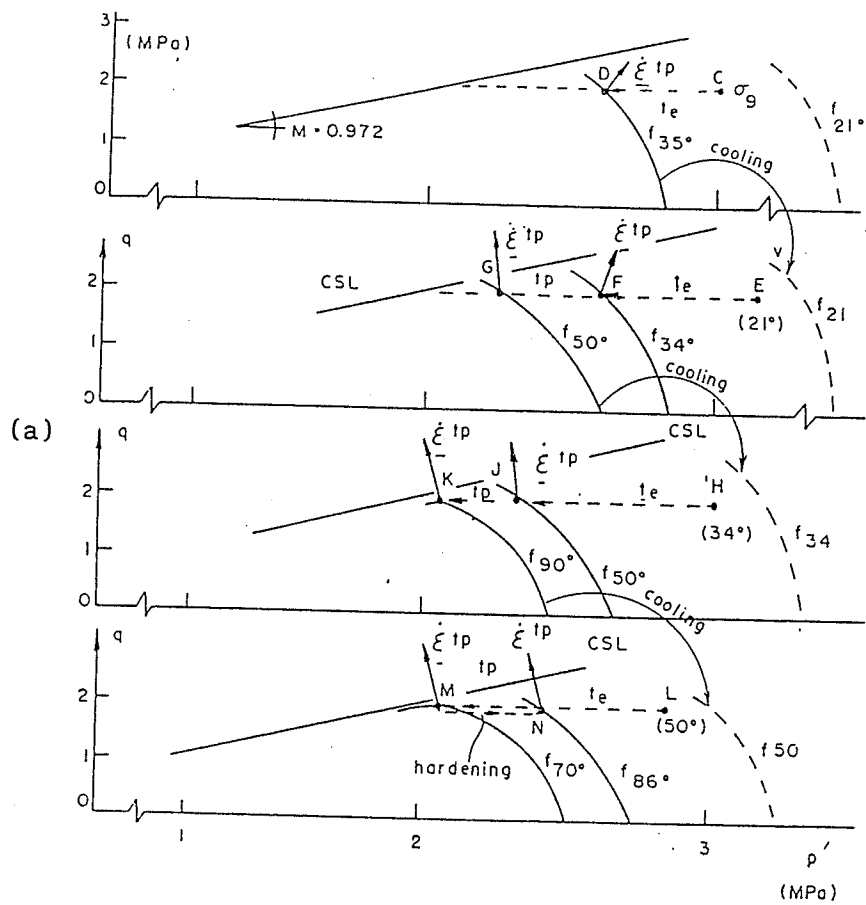
Figure 2.4 Effects of temperature cycle on (a) yield loci, (b) mean effective stress and axial strain under undrained heating conditions.
[After Hueckel and Pellegrini (1992)]
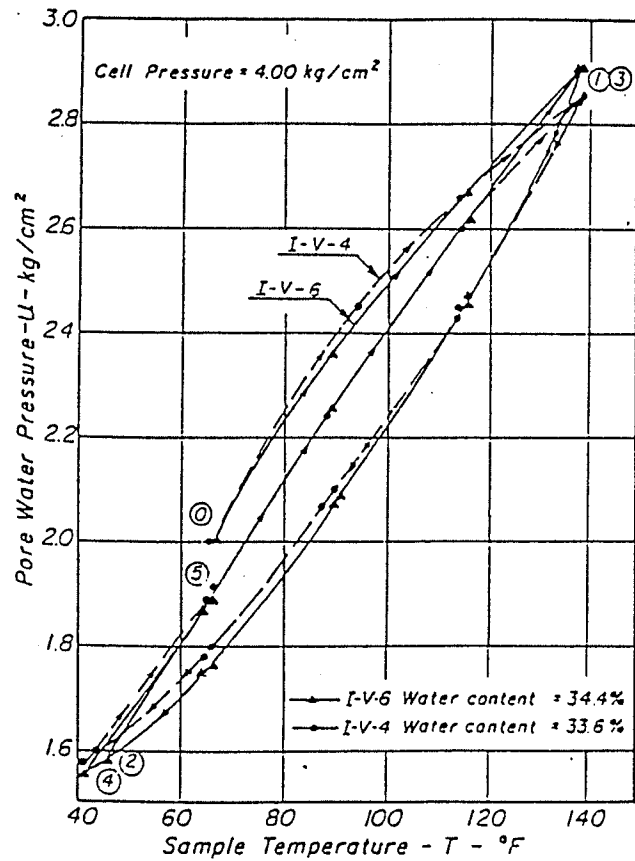
Figure 2.5 Effect of temperature on pore water
        pressure.
        [After Campanella and Mitchell (1968)]
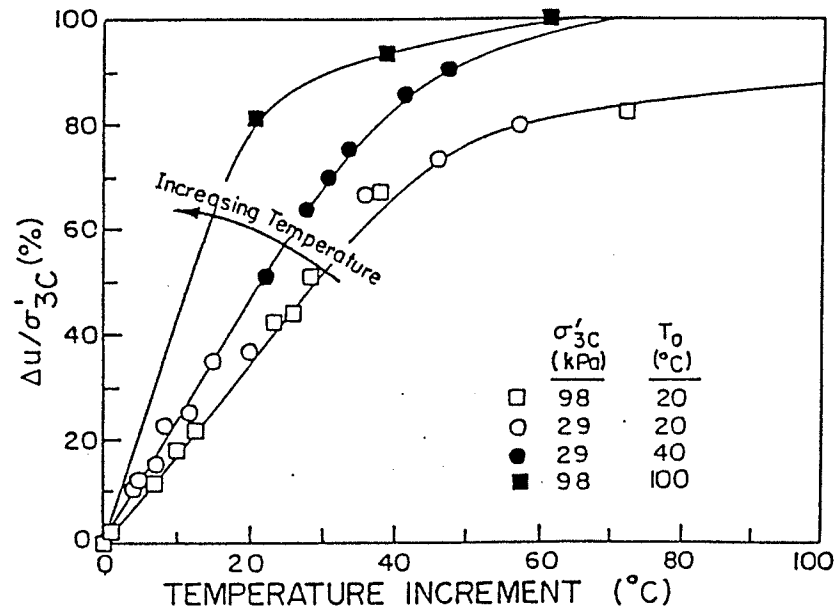
Figure 2.6 Normalized pore water pressure changes
        with temperature.
        [After Houston *et al.* (1985)]
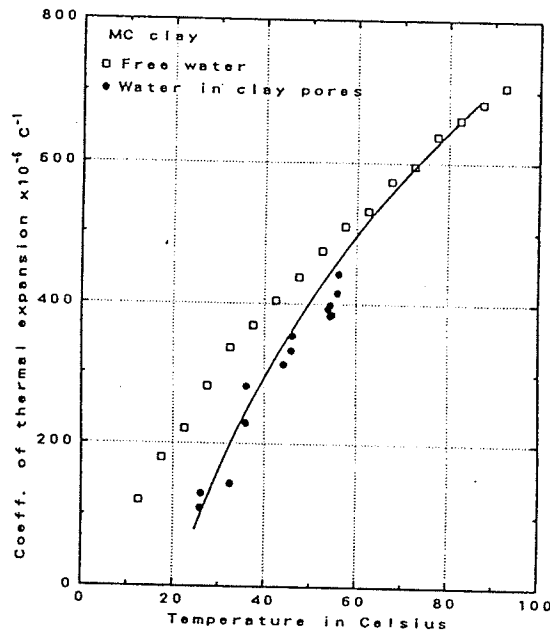
Figure 2.7 Comparison between thermal expansions of water in clay
pores and of pure water. [After Kuntiwattanakul
(1991)]
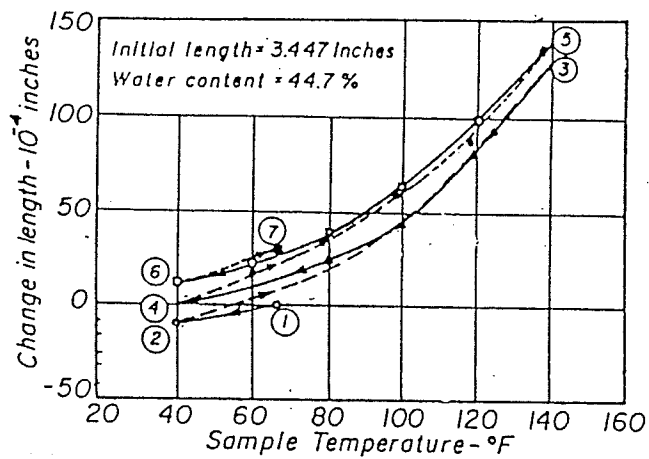
Figure 2.8 Height change with temperature under undrained heating
conditions. [After Campanella and Mithcell (1968)]
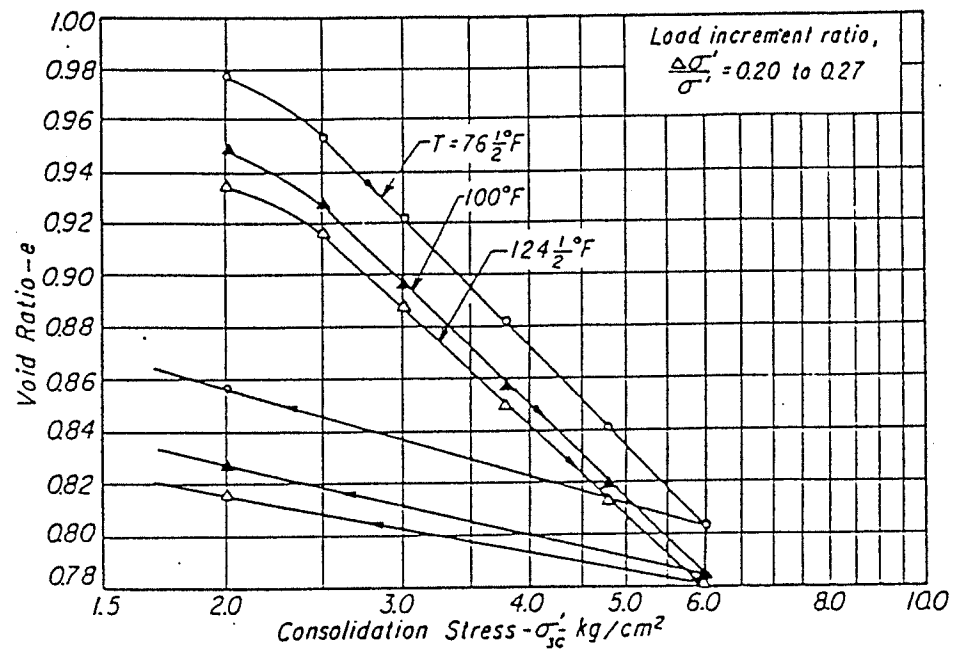
Figure 2.9 Effect of temperature on isotropic
          consolidation behaviour of saturated
          illite. [After Campanella and Mitchell (1968)]
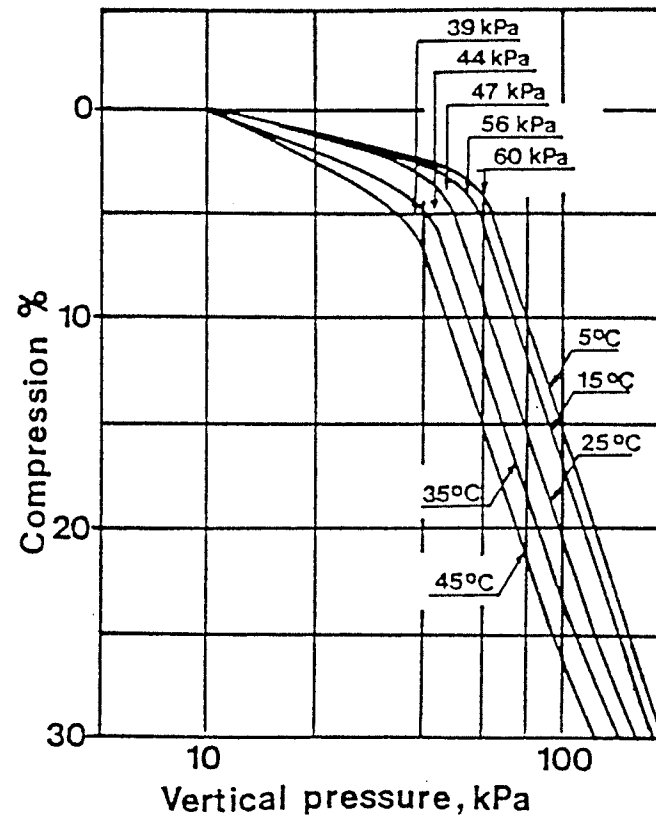
Figure 2.10 Stress-strain behaviour in
          oedometer tests at different
          temperatures. [After Eriksson (1989)]
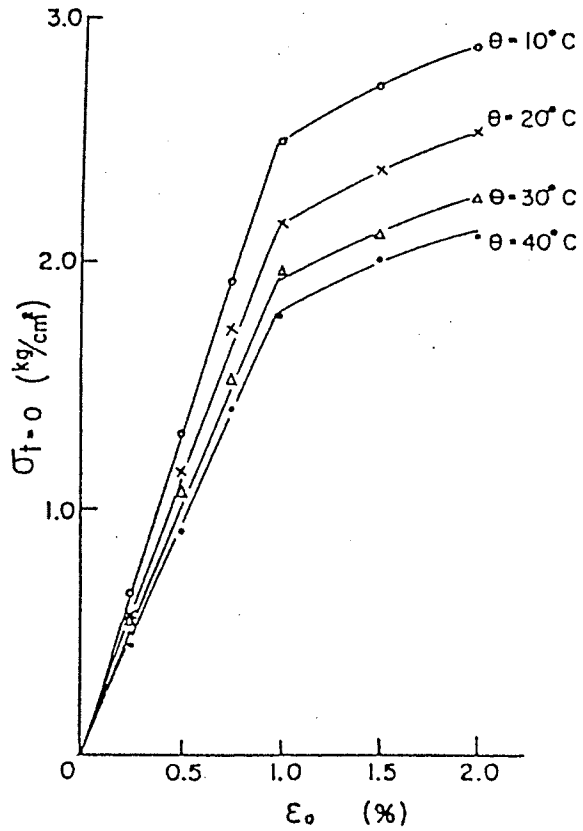
Figure 2.11 Relationship between axial stress
and axial strain for different
temperatures. [After Murayama (1969)]
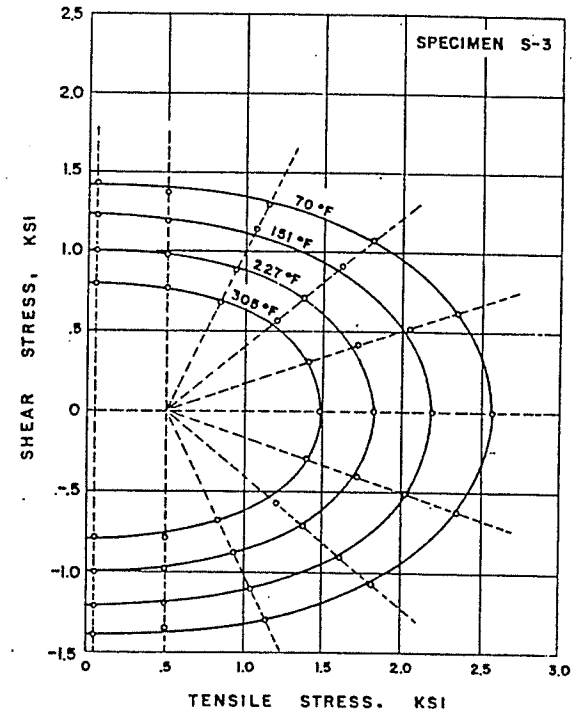
Figure 2.12 Yield loci for pure aluminum at
elevated temperatures.
[After Phillips and Tang (1972)]
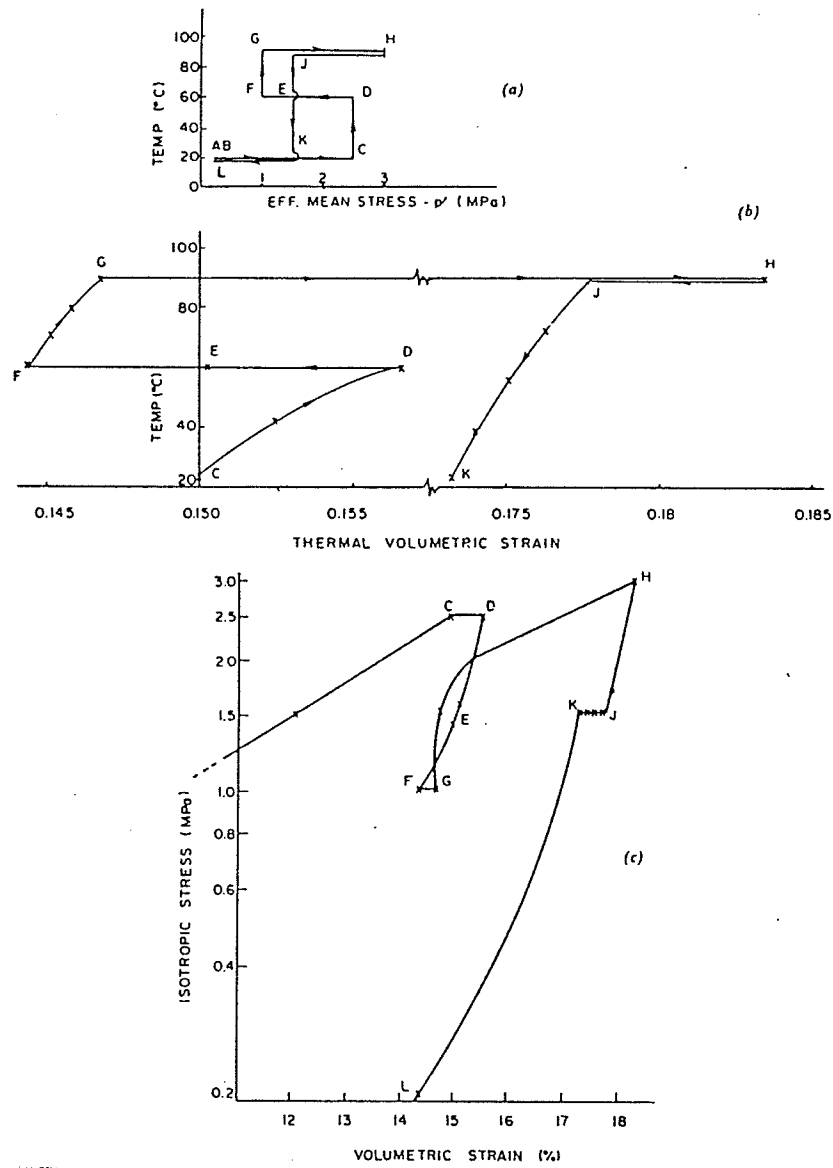
Figure 2.13 Unload-reloading behaviour at elevated temperatures.
[After Hueckel and Baldi (1990)]
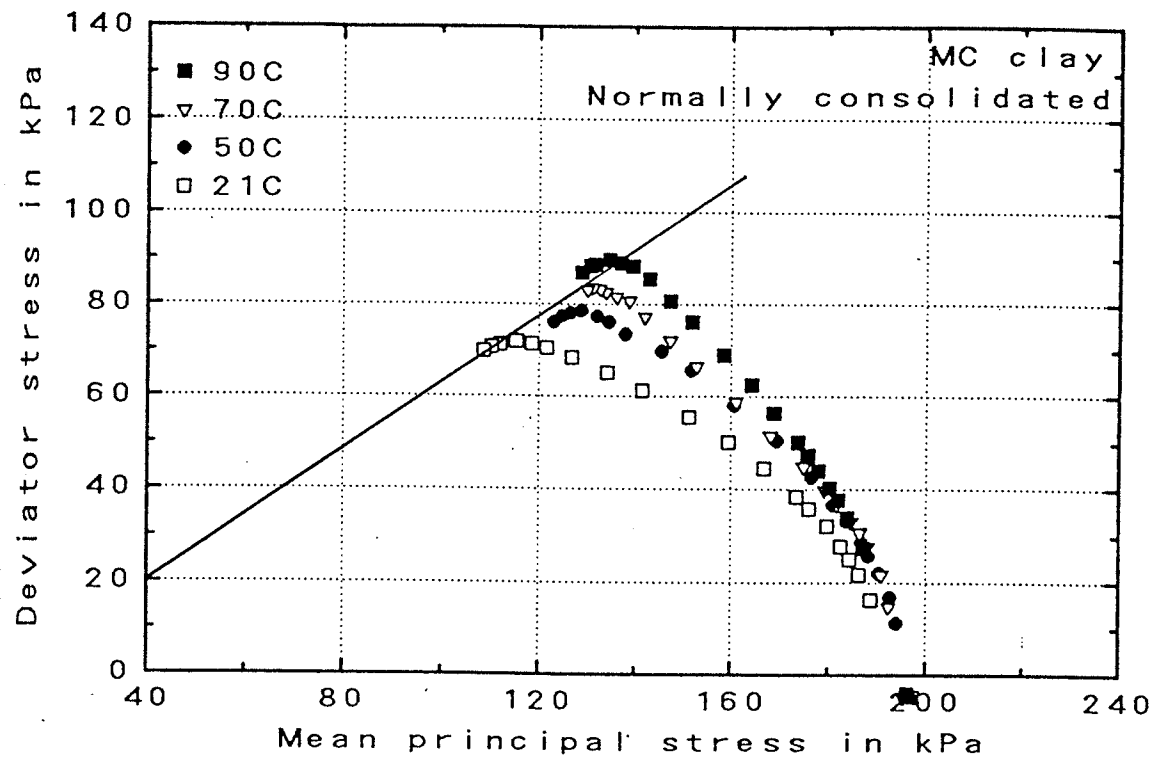
Figure 2.14 Undrained behaviour at elevated temperatures for normally consolidated specimens prepared under drained heating conditions. [After Kuntiwattanakul (1991)]
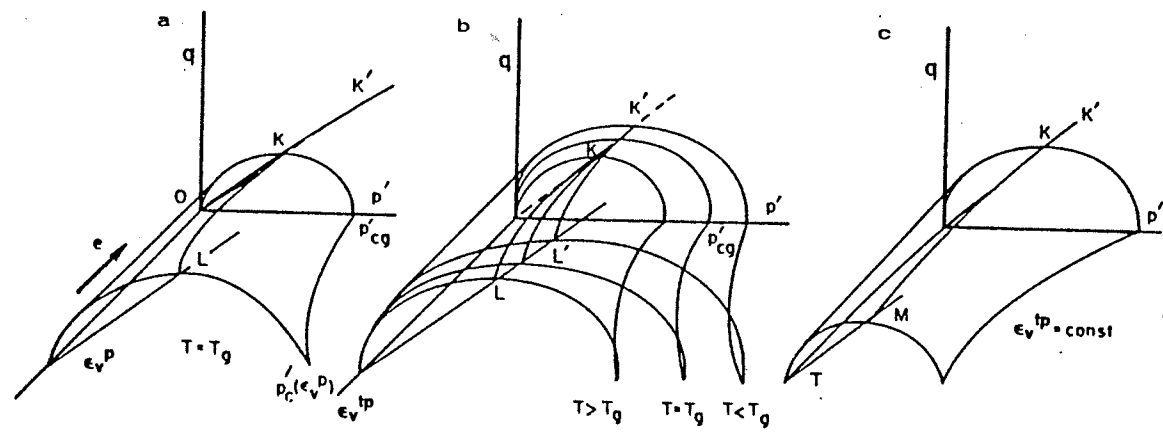
Figure 2.15 Concept of yield loci depending on temperature. [After Hueckel and Baldi (1990)]
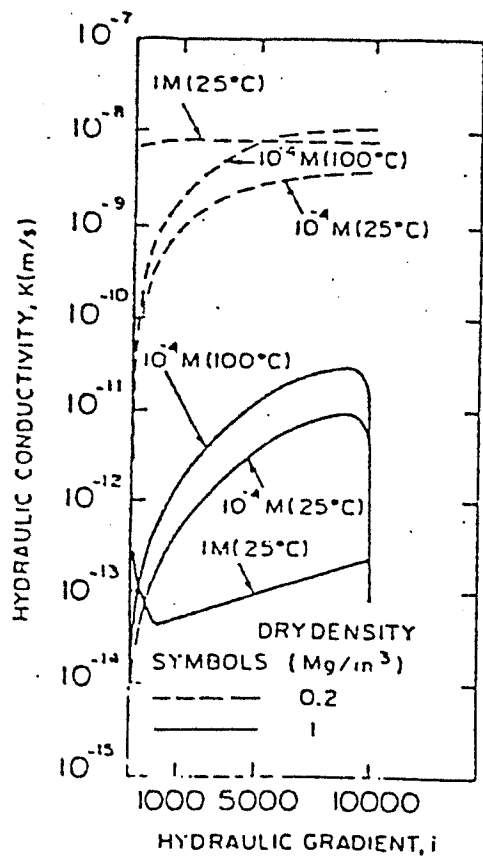
Figure 2.16 Effects of temperature on hydraulic conductivity at different concentrations, hydraulic gradients, and dry densities. [After Dixon *et al.* (1987)]
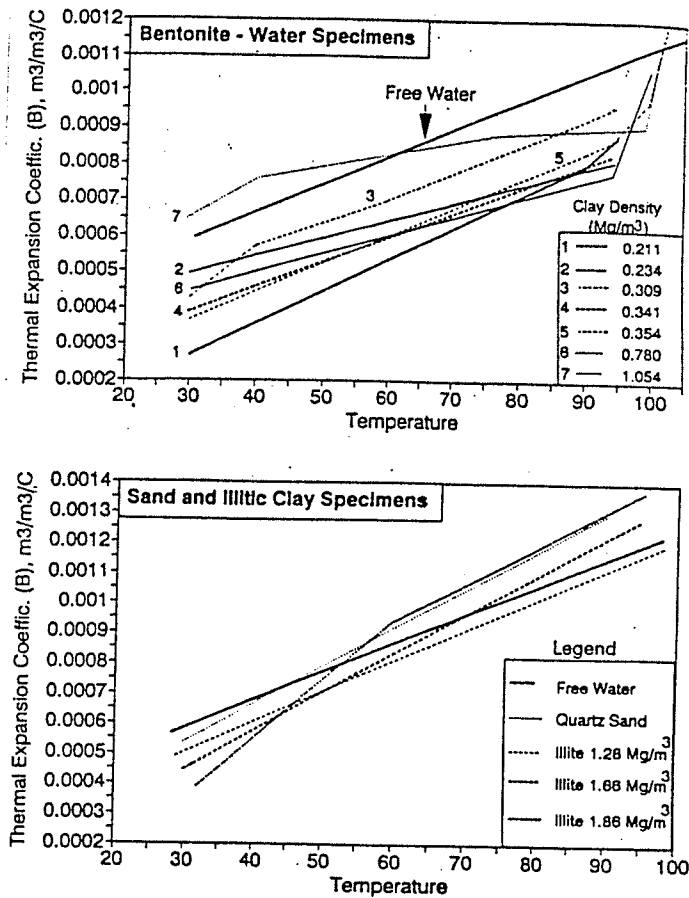
Figure 2.17 Thermal expnasions for sand, illitic clay, and bentonitic clay. [After Dixon *et al.* (1993)]
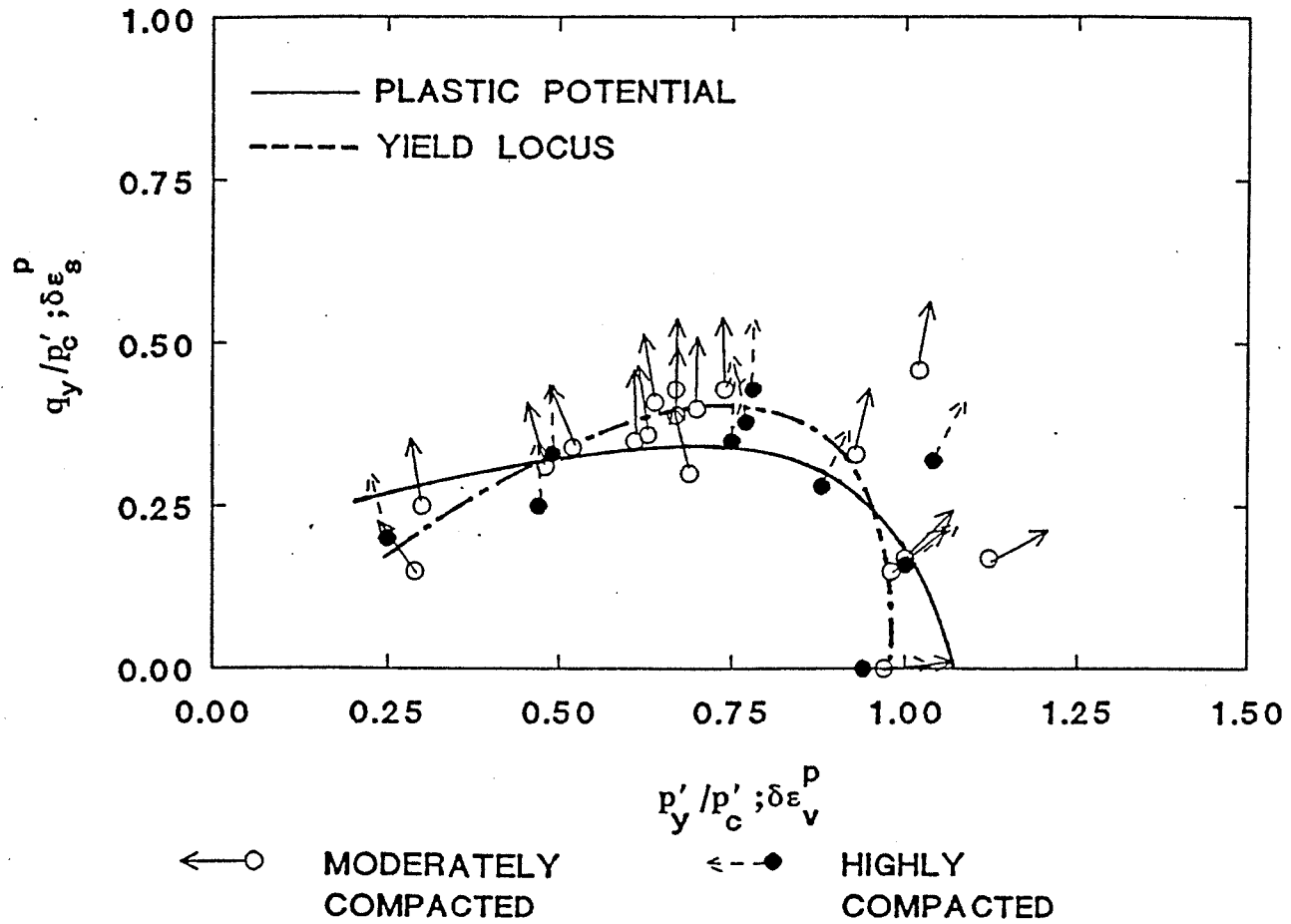
Figures 2.18 Normalized yield locus and plastic potentials for compacted sand-bentonite mixture. [After Oswell (1991)]
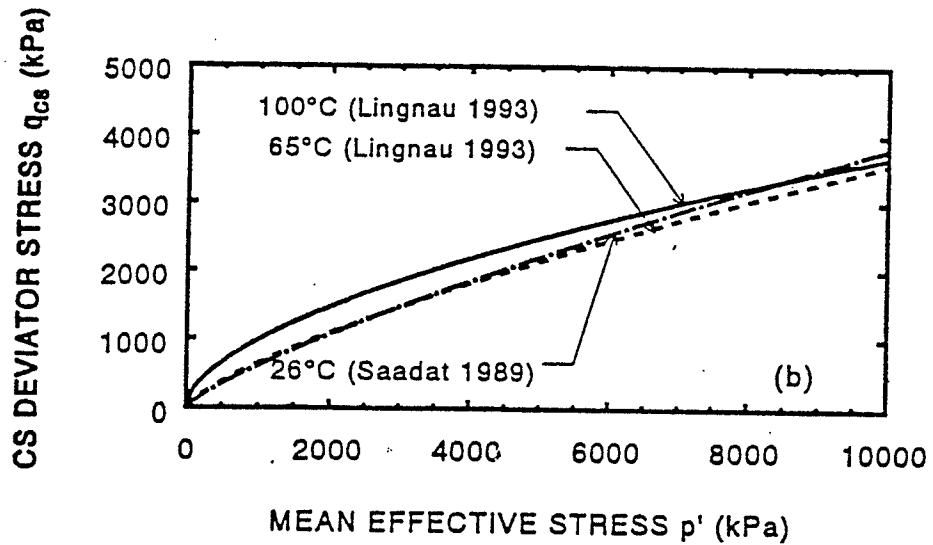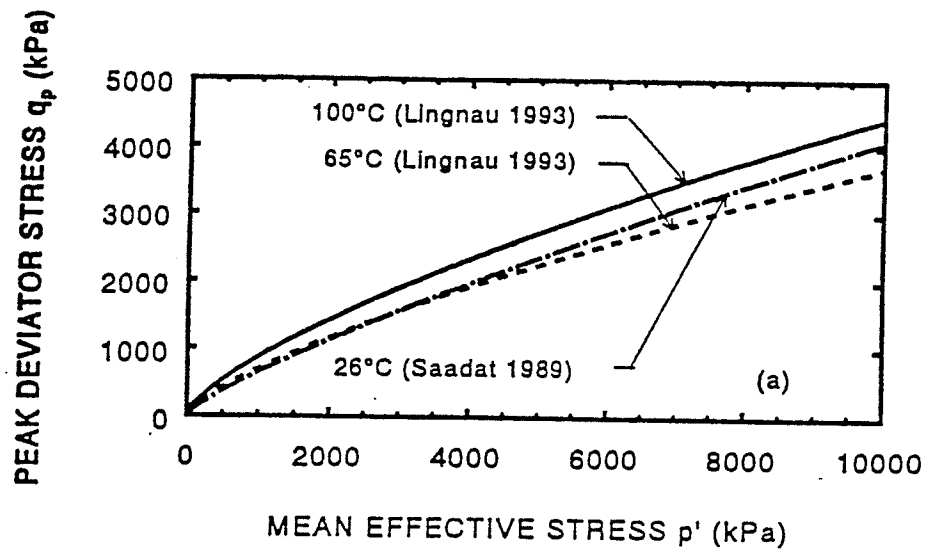
Figure 2.19 Strength envelopes at elevated temperature for compacted sand-bentonite mixture. [After Lingnau (1993)]
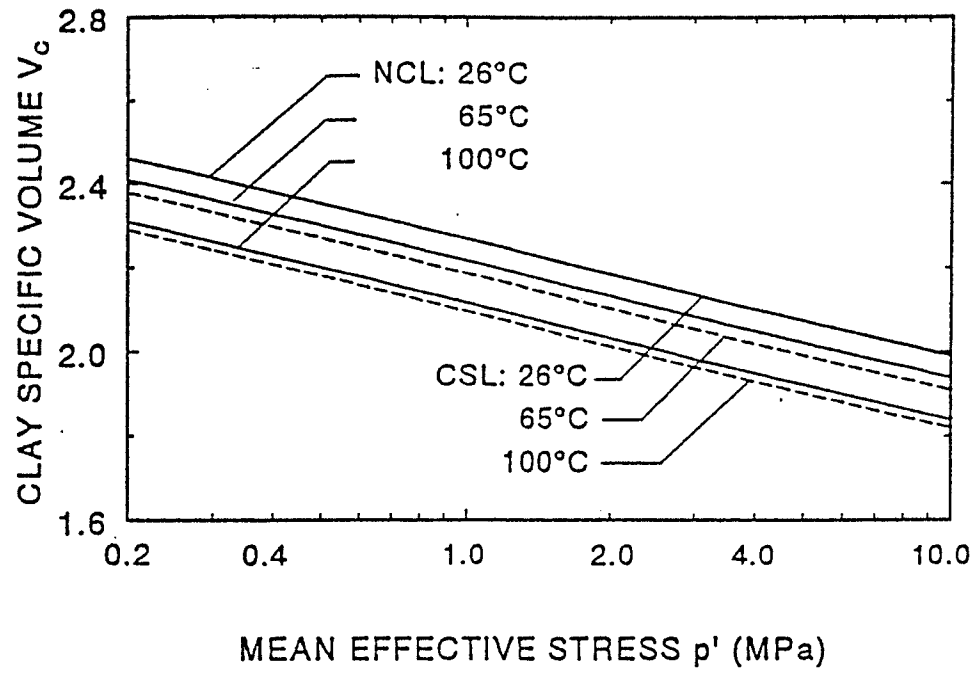
Figure 2.20 Normal consolidation line (NCL) and Critical state line (CSL) at elevated temperatures.
[After Lingnau(1993)]
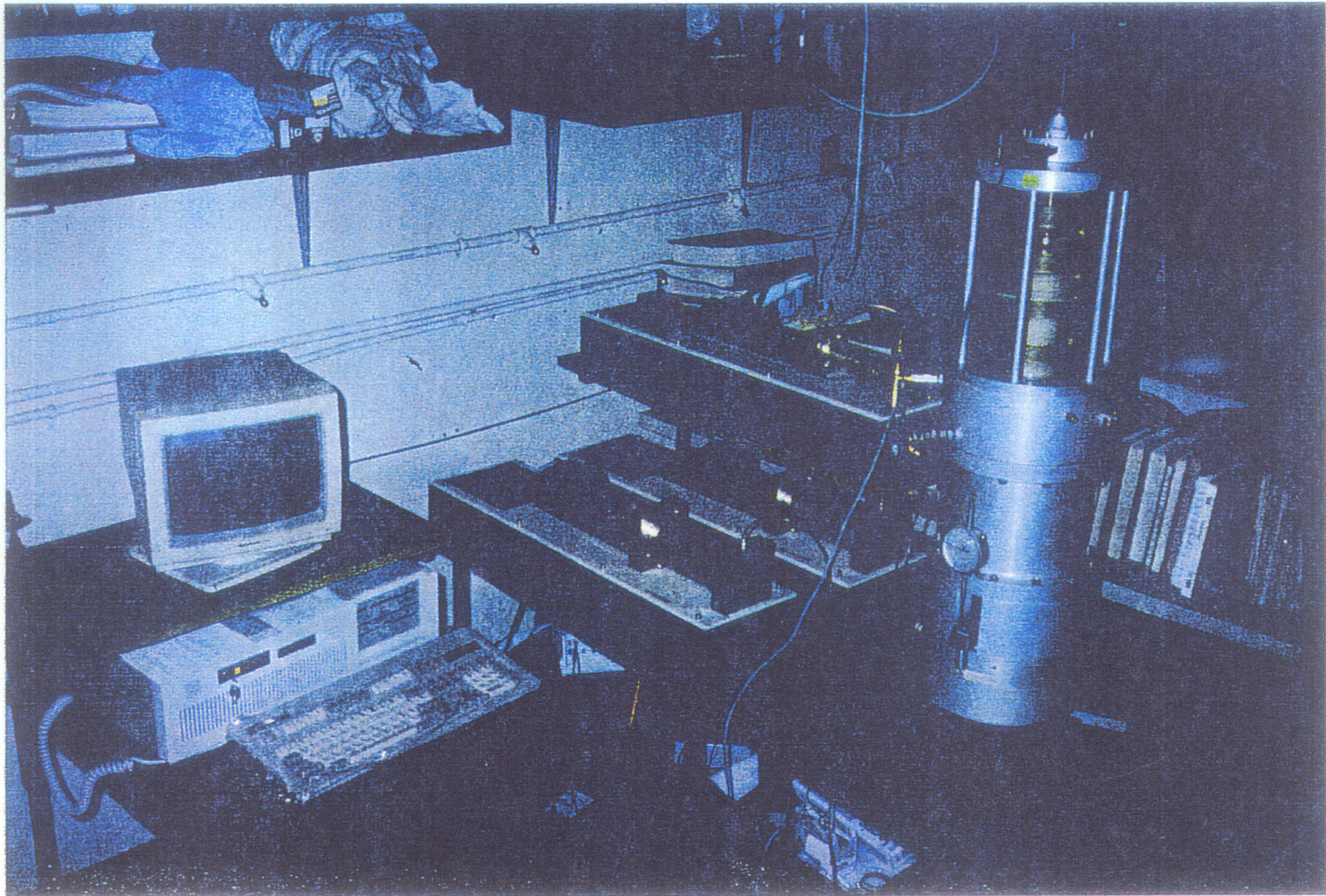
Figure 4.1   The GDS system.
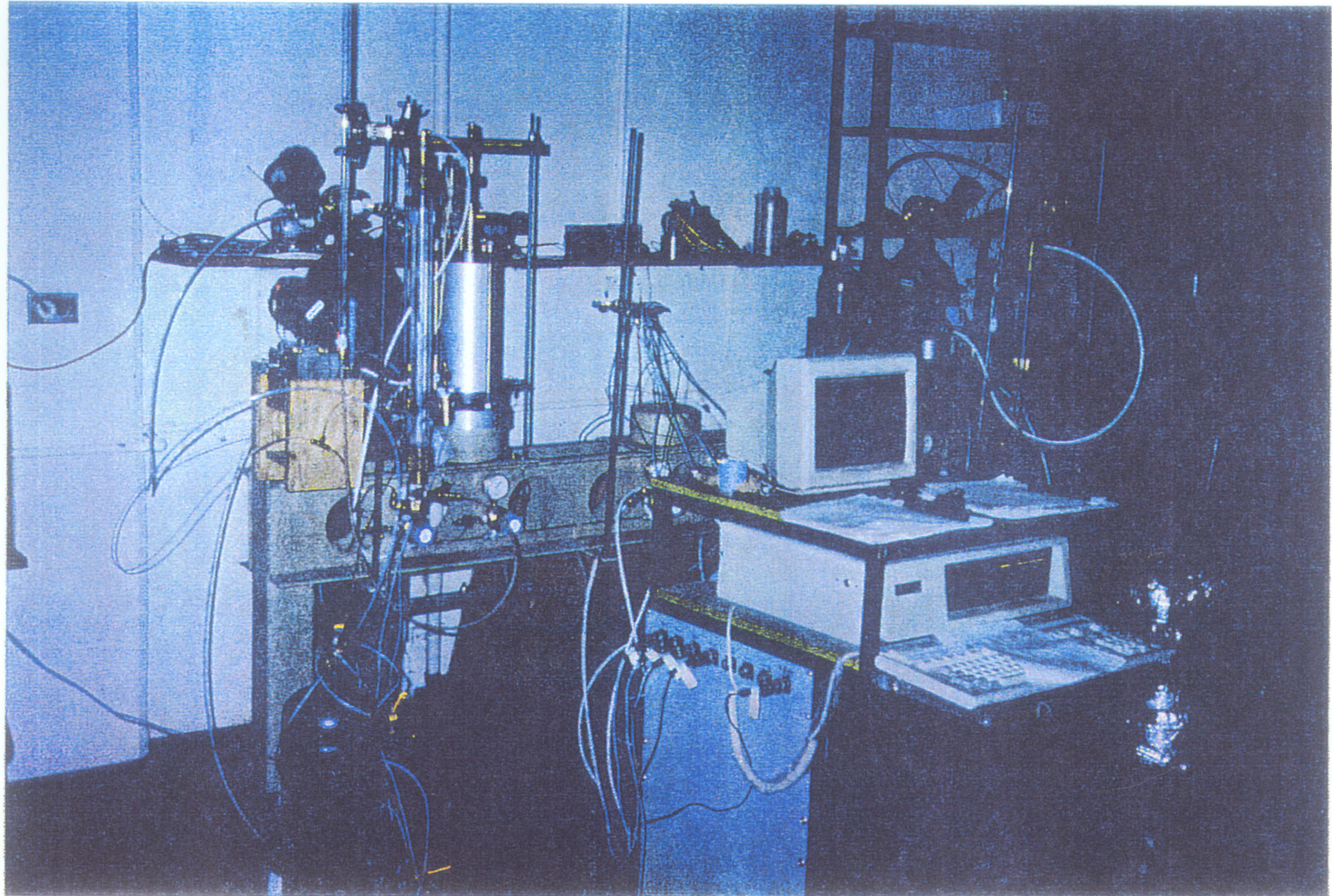
Figure 4.2 The Brainerd Kilman cells and testing system.
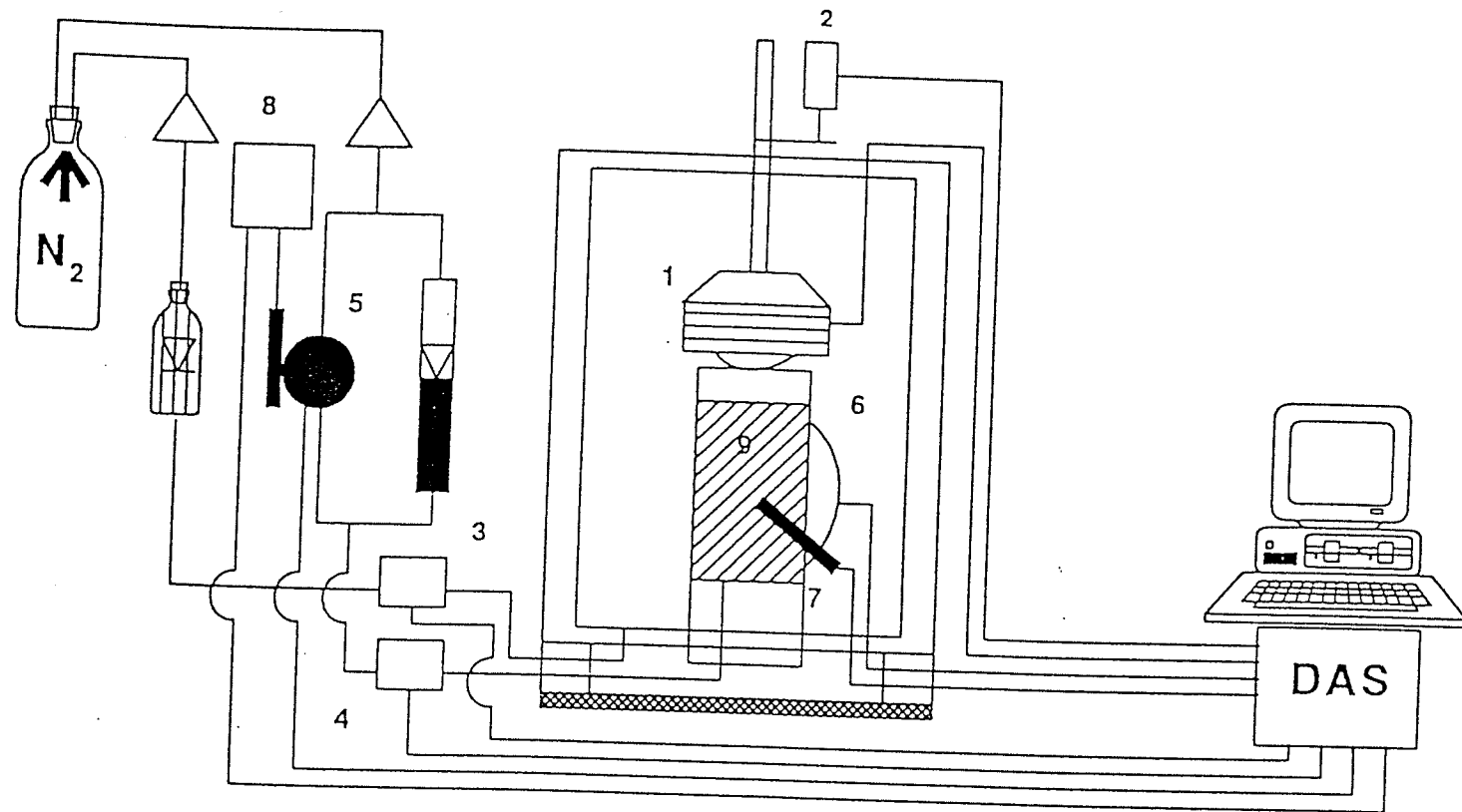
1:load cell	5:DPT	9:specimen
2:LVDT	6:thermocouples	
3:C.P.transducer	7:RTD	
4:B.P.transducer	8:room temp.	

Figure 4.3   Diagram of HITEP triaxial cell system.
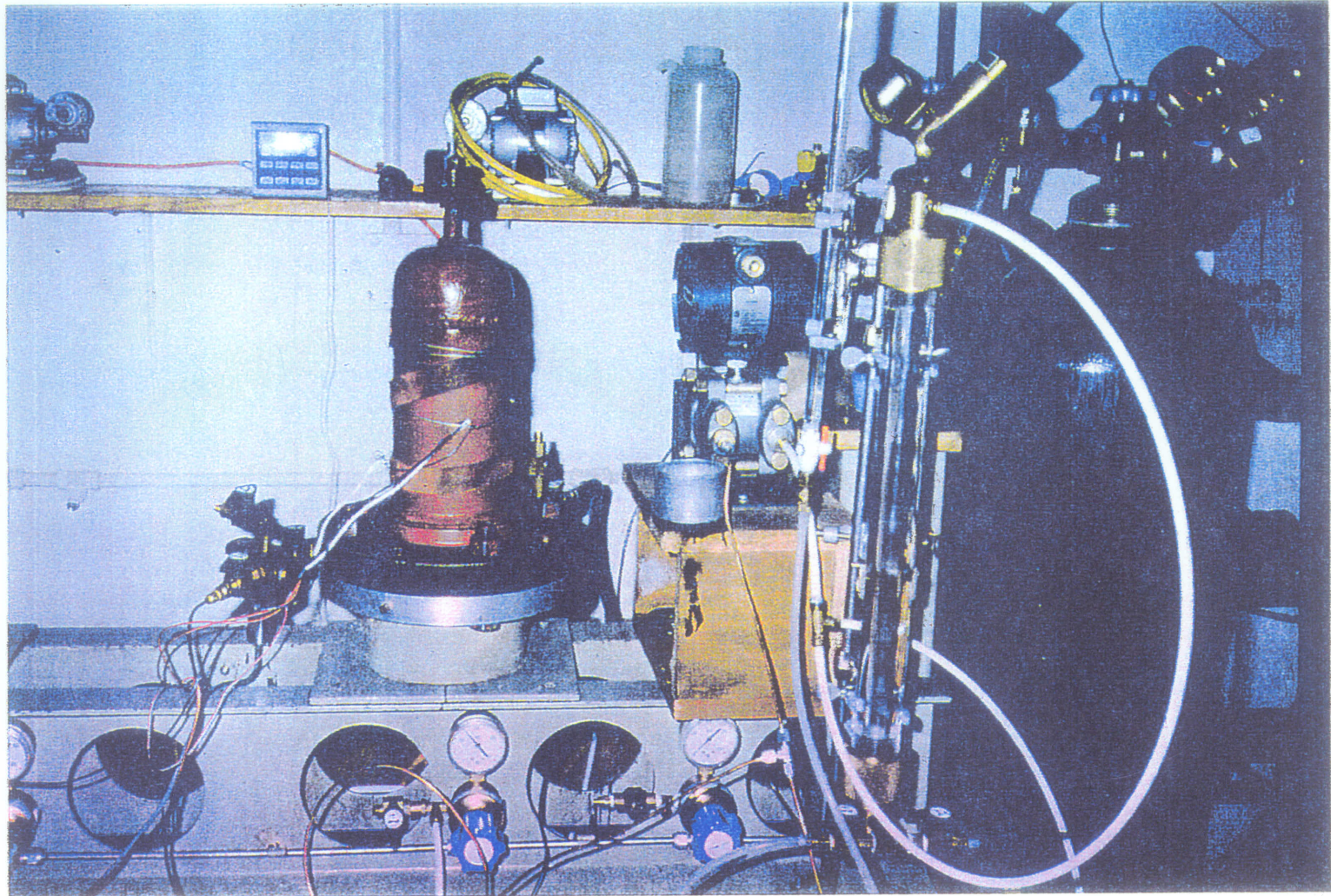
Figure 4.4   The HITEPC cell and testing system.

TOP VIEW

SUPPLY PRESSURE PORT

TOP CAP

PLUG

MEMBRANE

SPLIT MOULD

PRY SLOT

GASKET

BOTTOM

SIDE VIEW
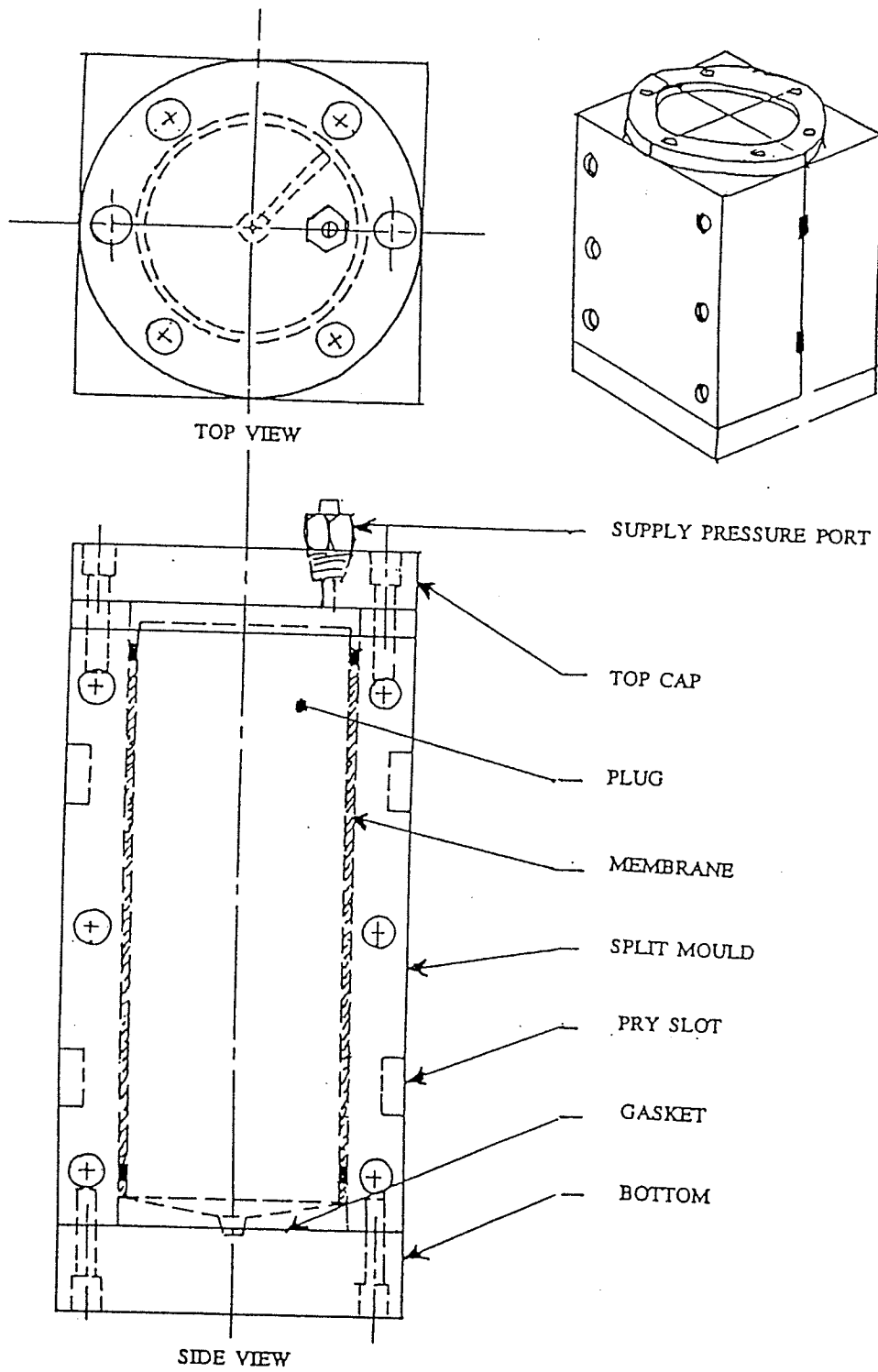
Figure 4.5 Compaction mould [After Yarechewski (1993)].
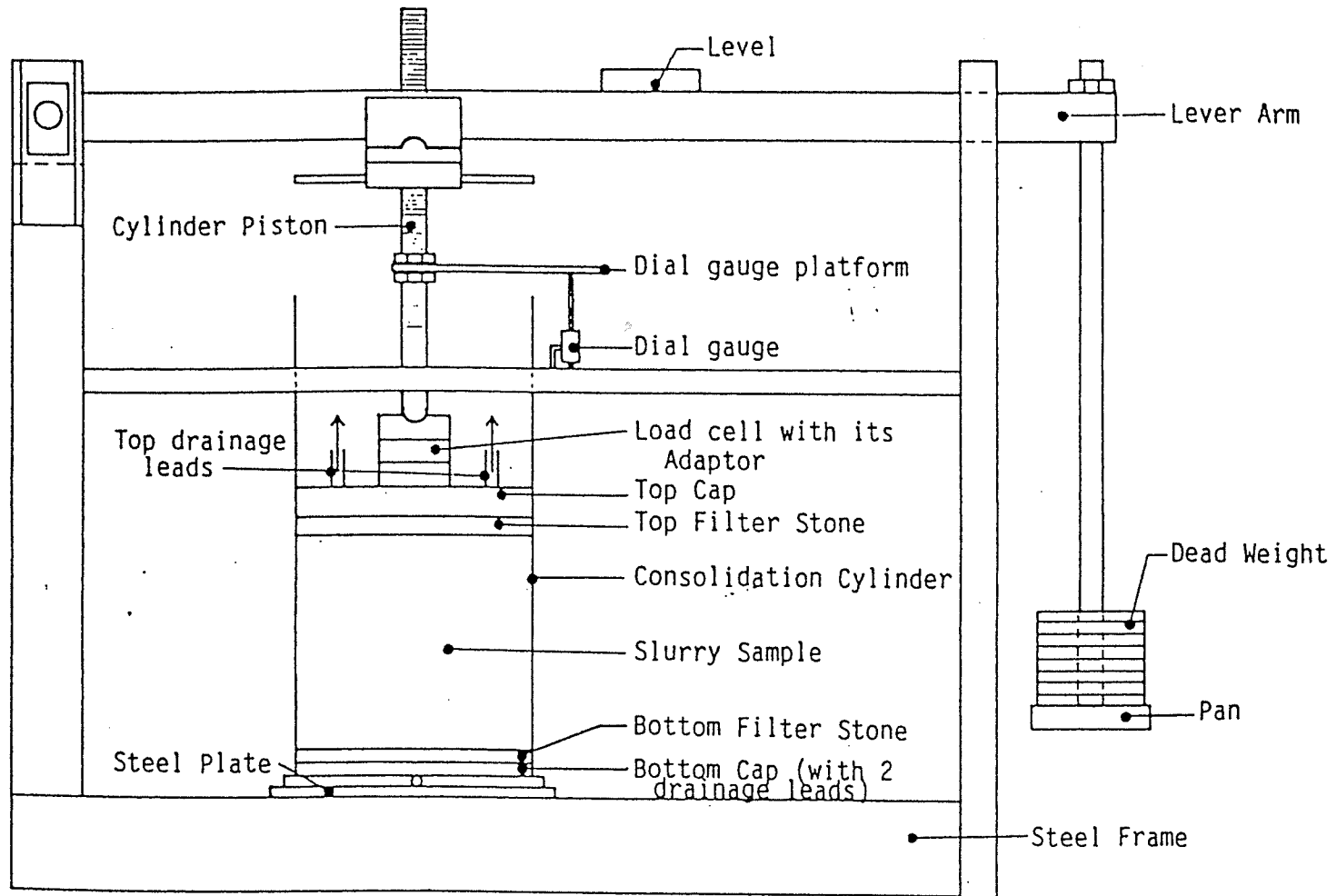
Figure 4.6 Schematic diagram of a lever-loading system for one-dimensional consolidation [After Lau (1989)].
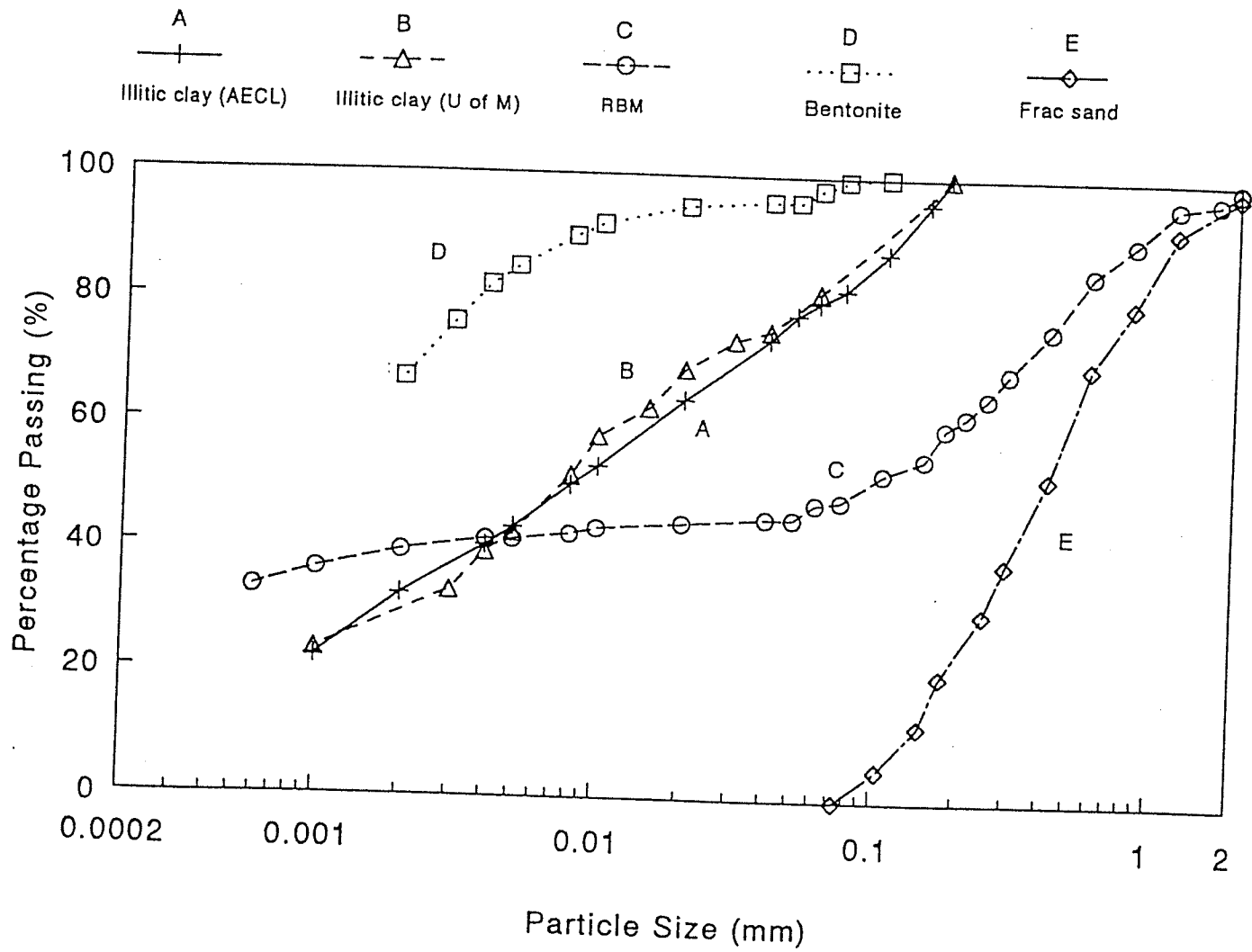
Figure 4.7   Particle size distributions of soils.
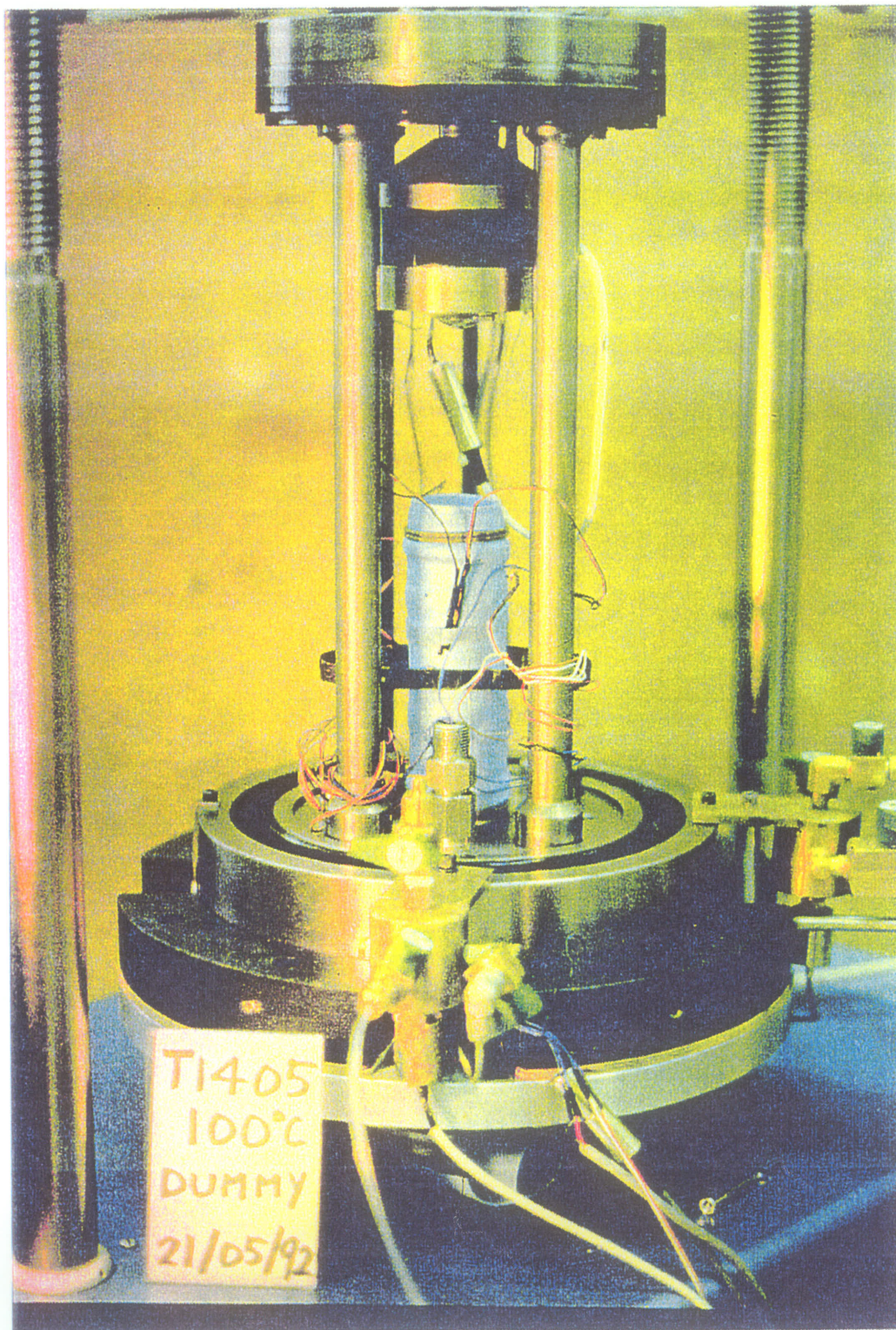
Figure 4.8 Specimen set-up for triaxial compression test.

T1480 : CONSOLIDATION
ILLITE, T=ROOM TEMP.
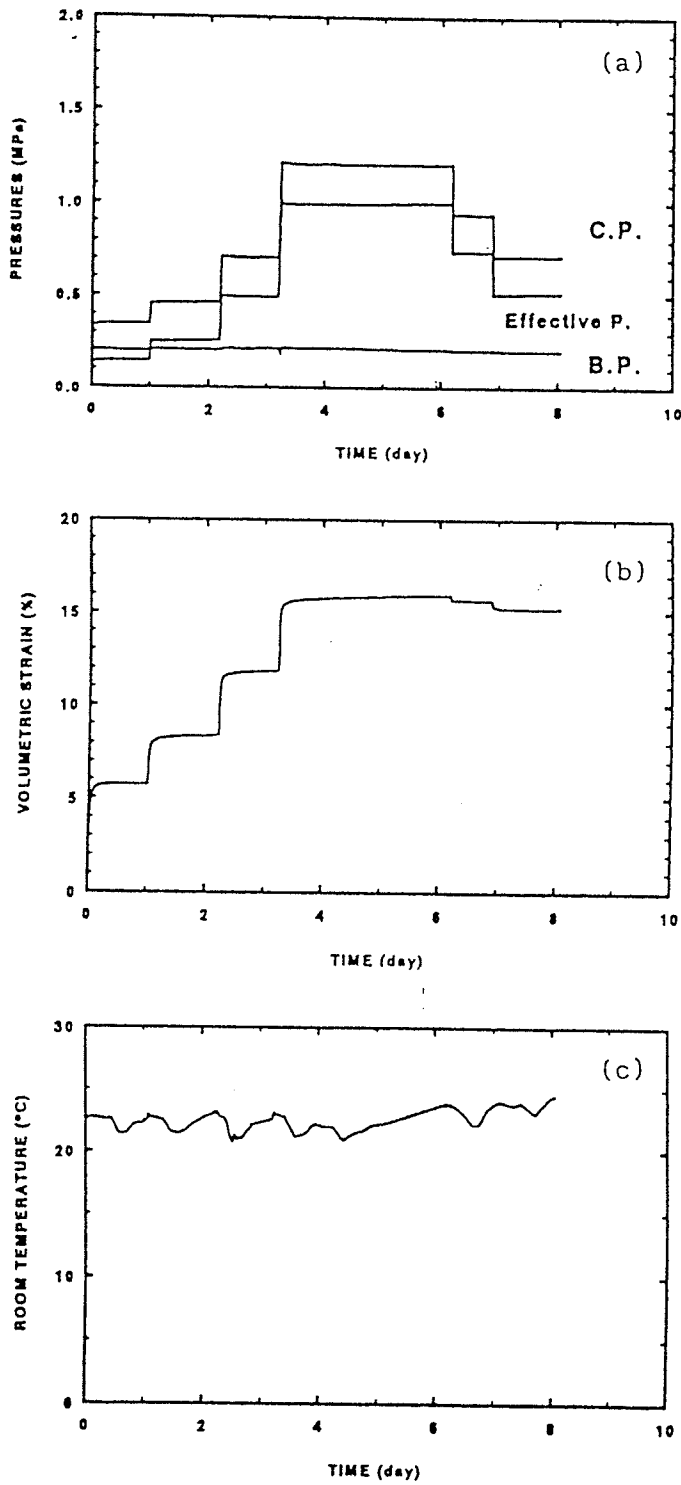
Figure 5.1 Mechanical consolidation (T1480). (a) pressure and time. (b) volume strain and time. (c) temperature and time.
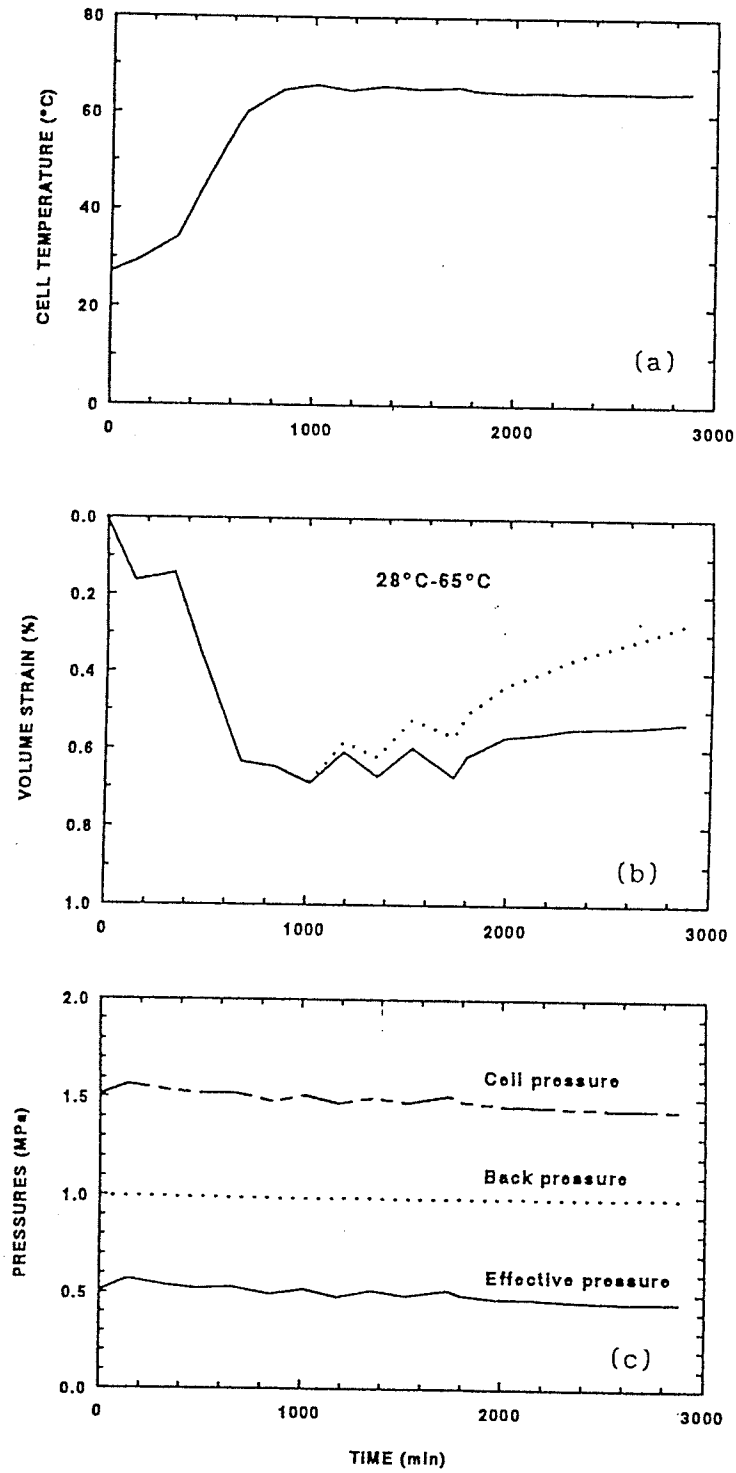
Figure 5.2 Thermal consolidation (T1442). (a) cell temperature and time. (b) volume strain and time. (c) pressures and time.
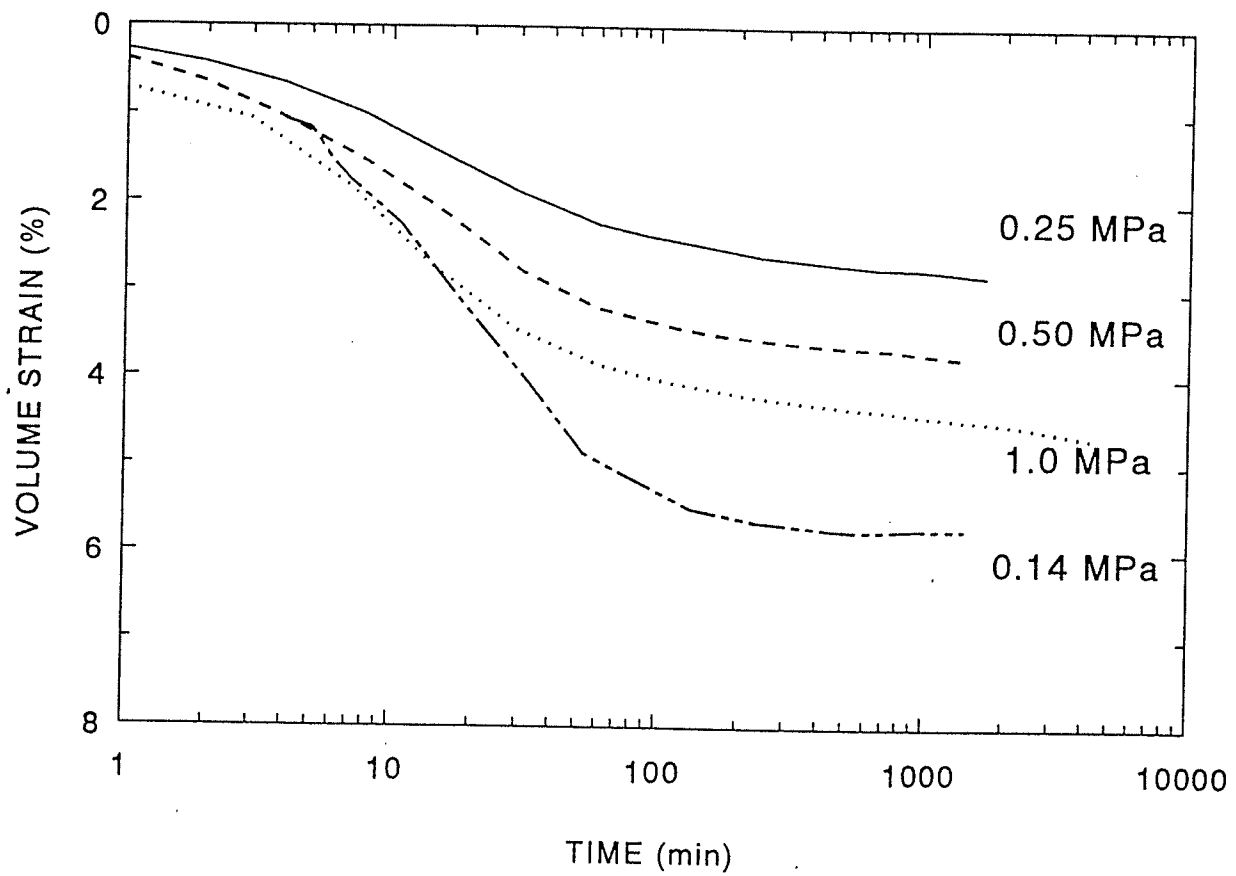
Figure 5.3   Volume strains for various pressures at 28°C (T1480).
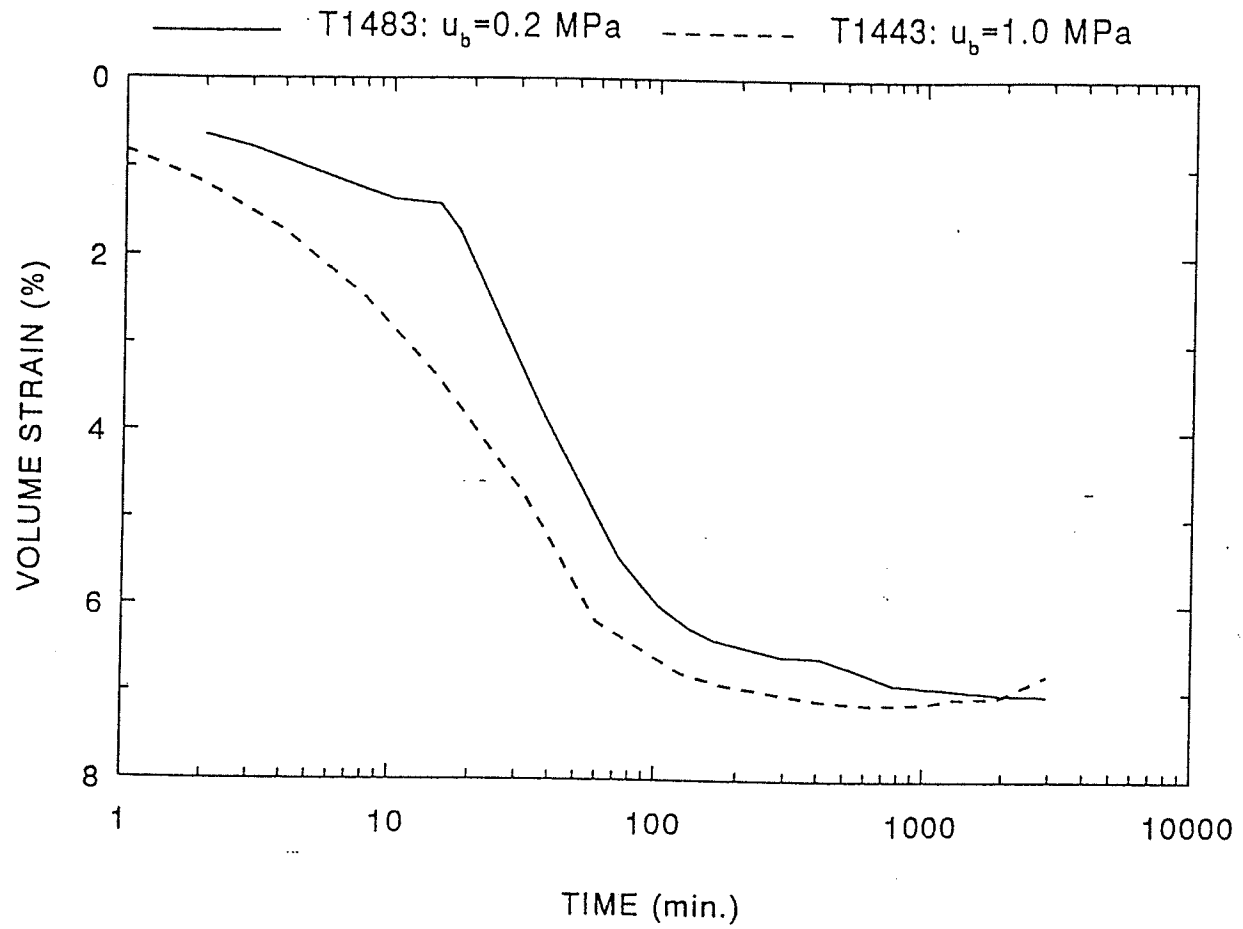
Figure 5.4 Effects of back pressure on volume changes at 28°C (T1483 and T1443).
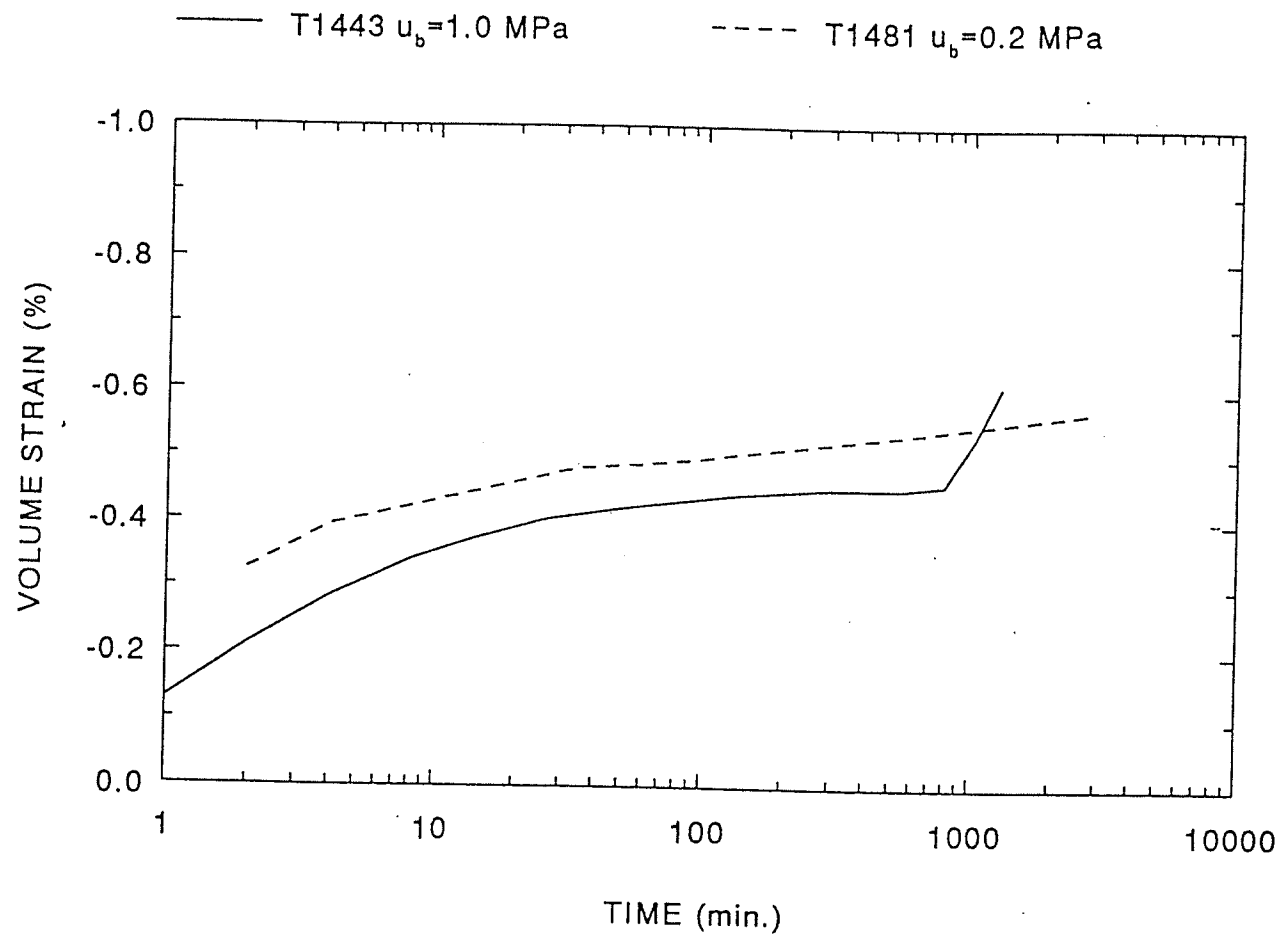
Figure 5.5 Volume strains *vs*. time during unloading under different back pressures (T1481 and T1443).
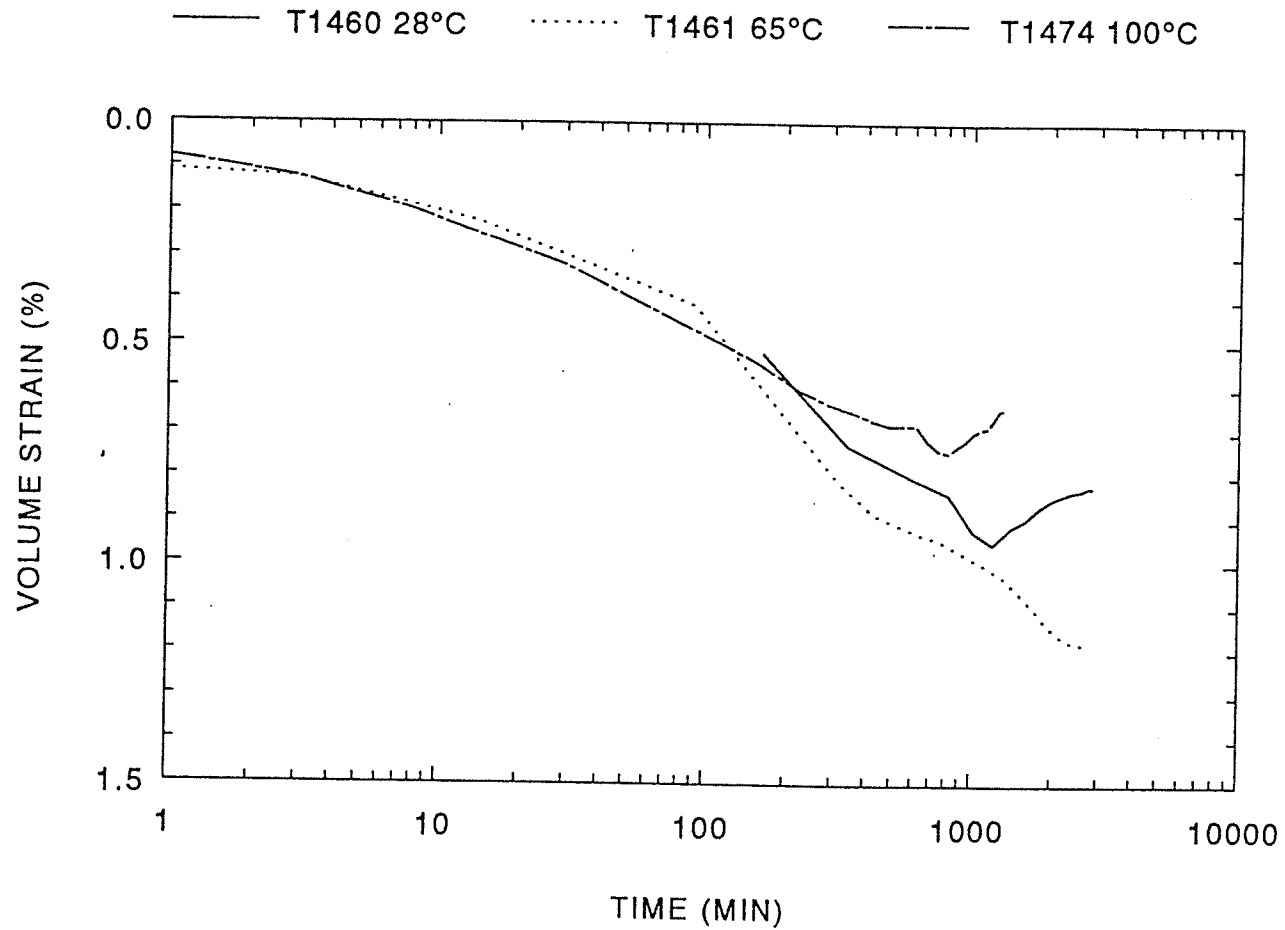
Figure 5.6   Mechanical consolidation from p′ = 1.25 MPa to 1.50 MPa at elevated temperatures of 28°C(T1460), 65°C(T1461), and 100°C(T1461).
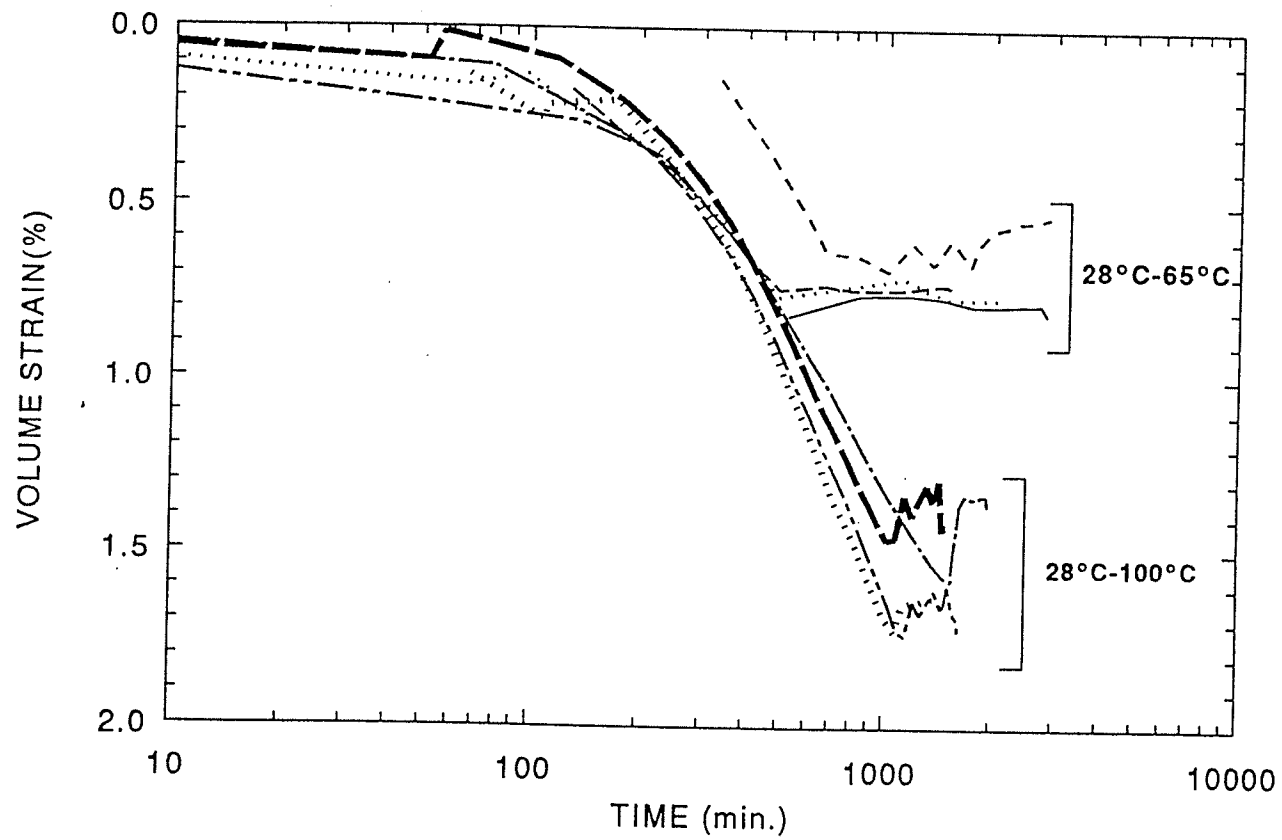
Figure 5.7   Thermal   consolidation   at   p′ = 0.5 MPa   for   overconsolidated   specimen   (OCR = 2):
T = 28°C-65°C and T = 28°C-100°C.
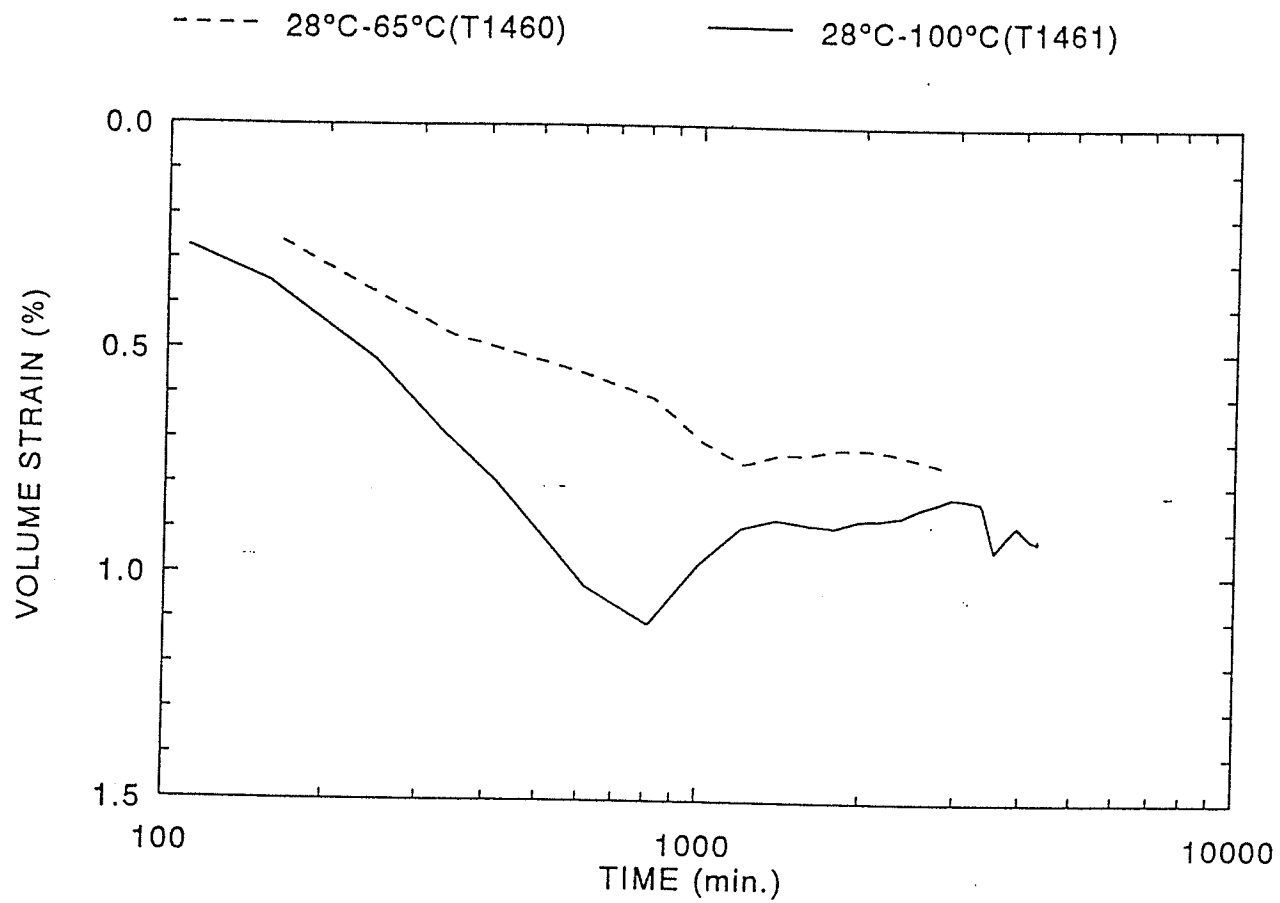
Figure 5.8   Thermal consolidation at p' = 1.5 MPa for normally consolidated specimens. T = 28°C-65°C and T = 65°C-100°C
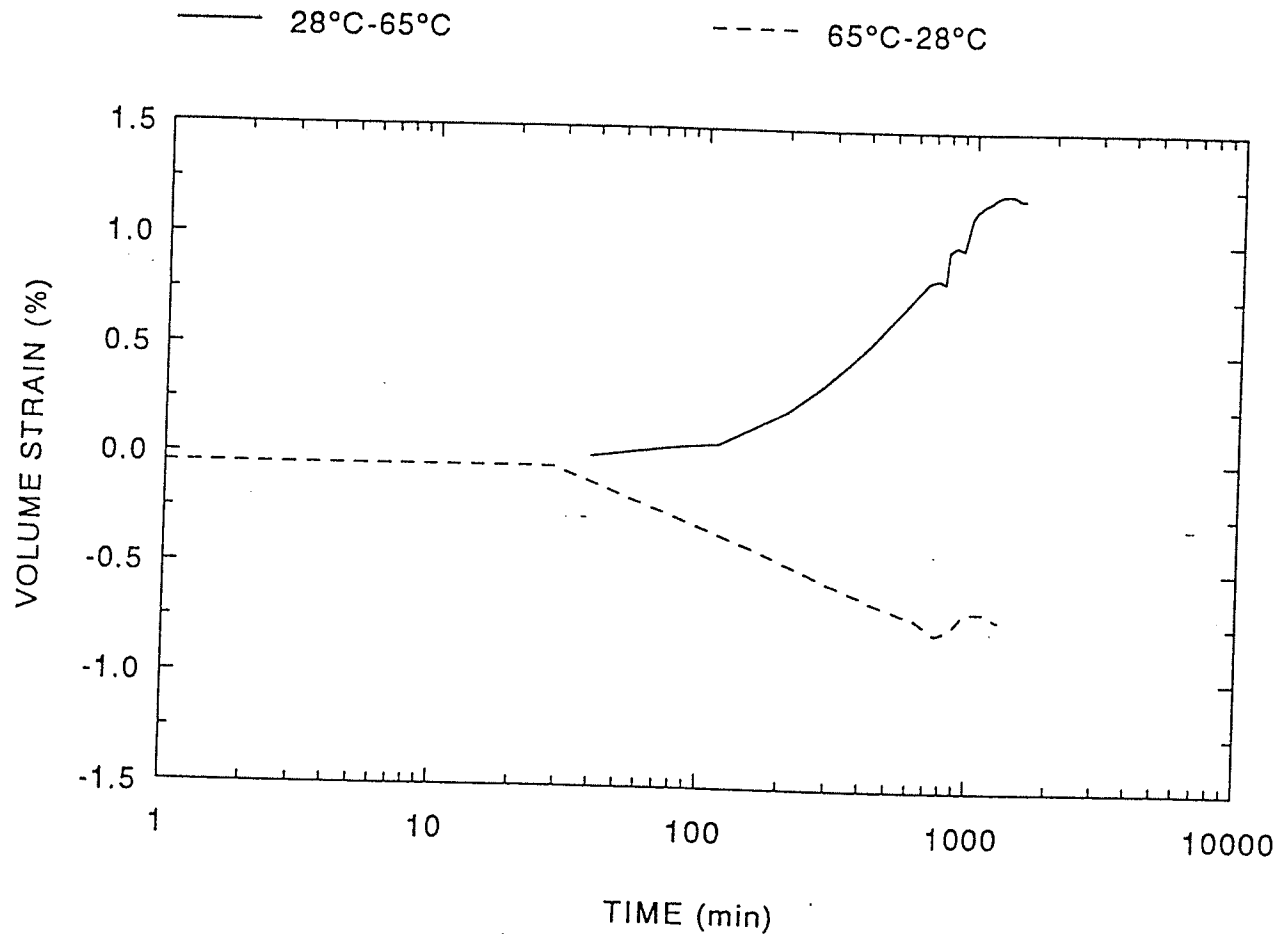
Figure 5.9   Volume strain *vs.* time during temperature cycle (28°C-65°C-28°C) on volume strains at 1.5 MPa for originally normally consolidated specimen
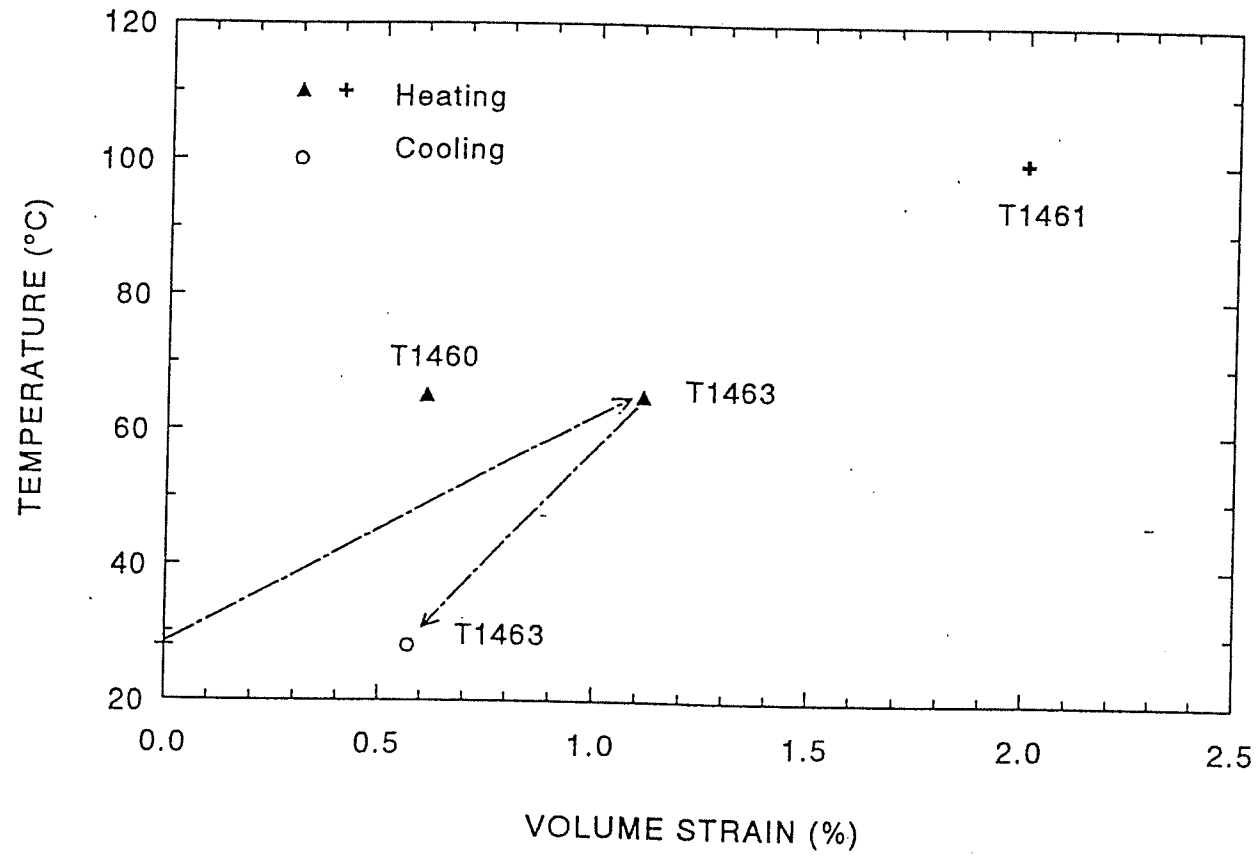
Figure 5.10 Thermal consolidation: Reconstituted illite (normally consolidated specimens); monotonic heating (T1460and T1461), and a temperature cycle of heating-cooling (T1463)
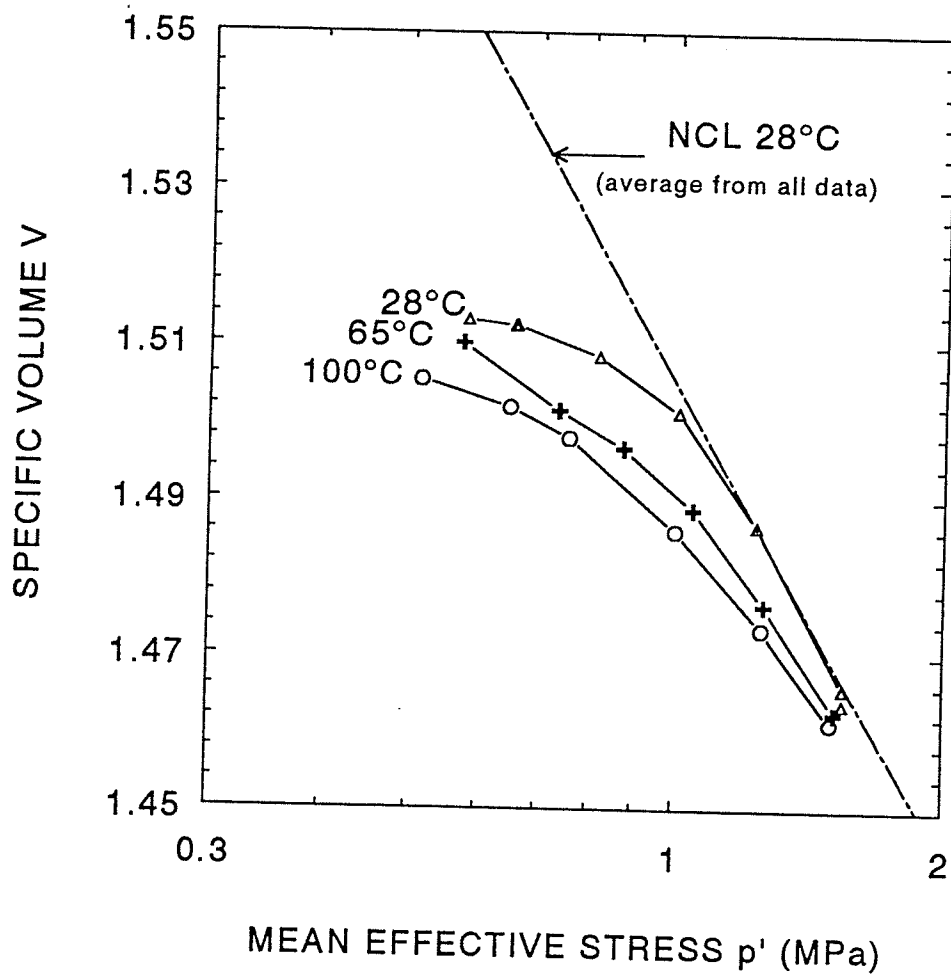
Figure 5.11   Isotropic reloading at elevated temperatures for
    reconstituted illite. (T1460, T1461, T1475)
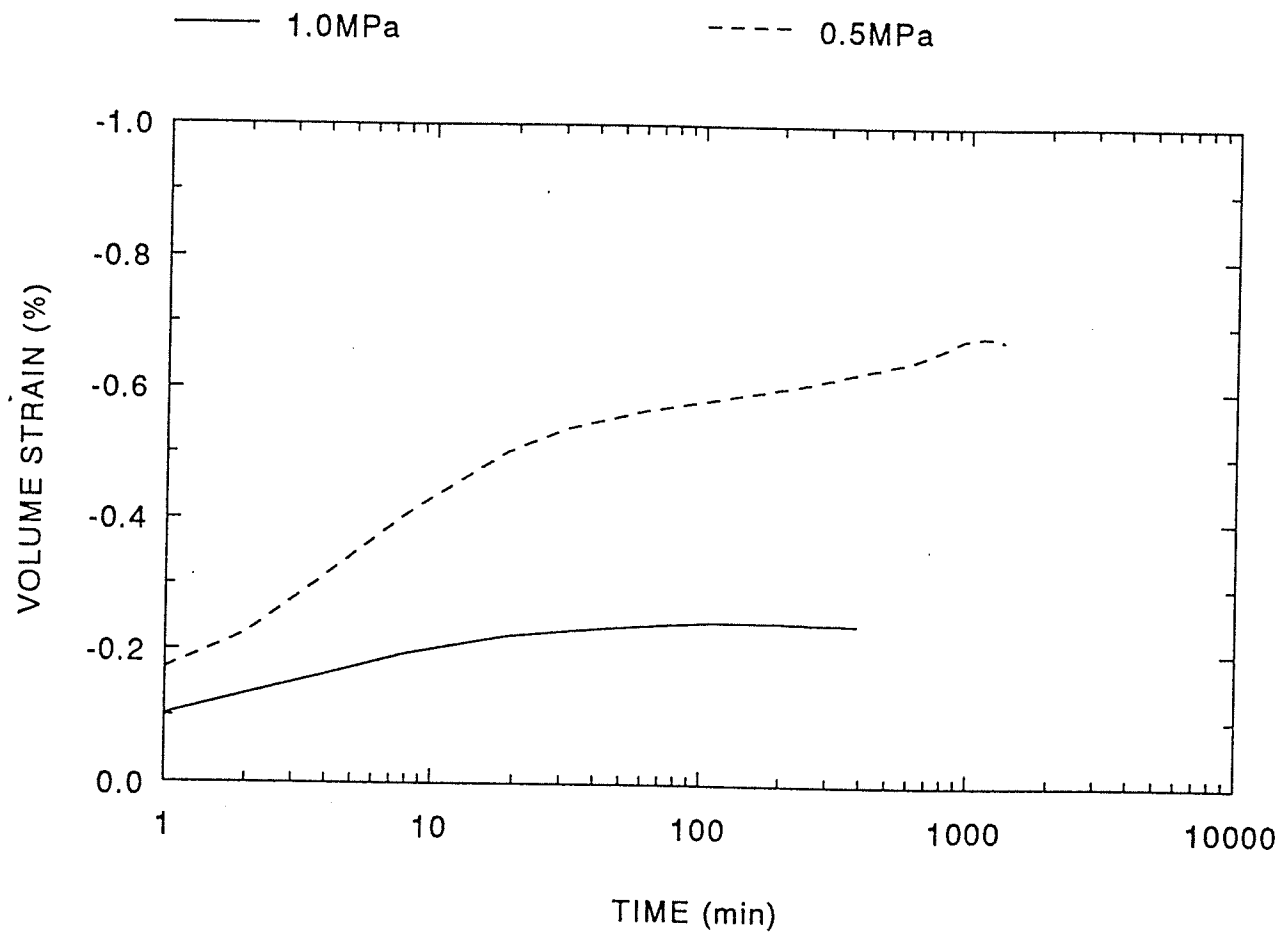
Figure 5.12   Mechanical consolidation for compacted illite at 28°C.
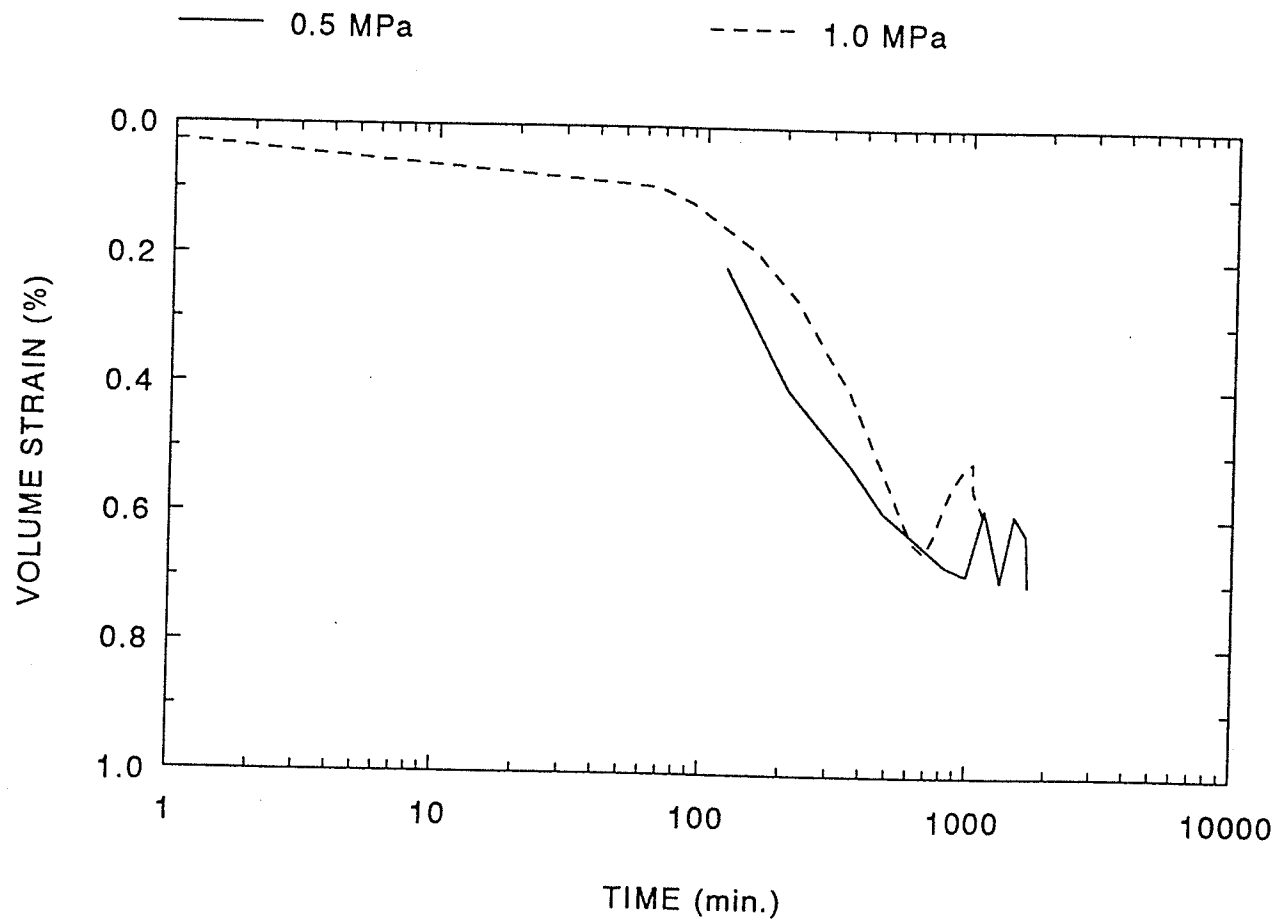
Figure 5.13   Thermal consolidation of compacted illite at elevated pressures (p' = 0.5 MPa and 1.0 MPa).   T = 28°C-65°C.
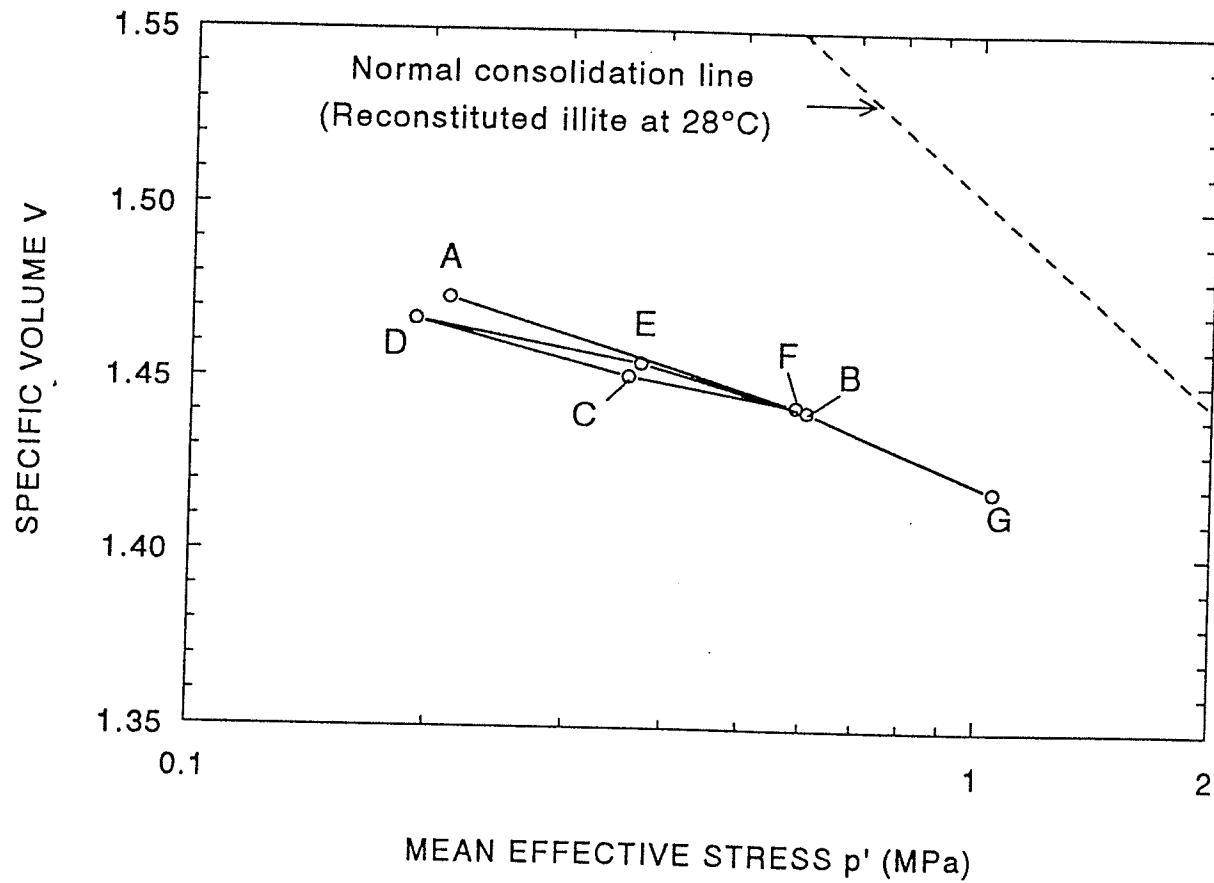
Figure 5.14   Isotropic consolidation results for compacted illite at 28°C.

**T1403: CONSOLIDATION
BUFFER, T-26 C**

(a)

```
— -  B.P.          ———  C.P.          —·-  EFFECT.P.
```

**T1403: CONSOLIDATION
BUFFER, T-26 C**

(b)
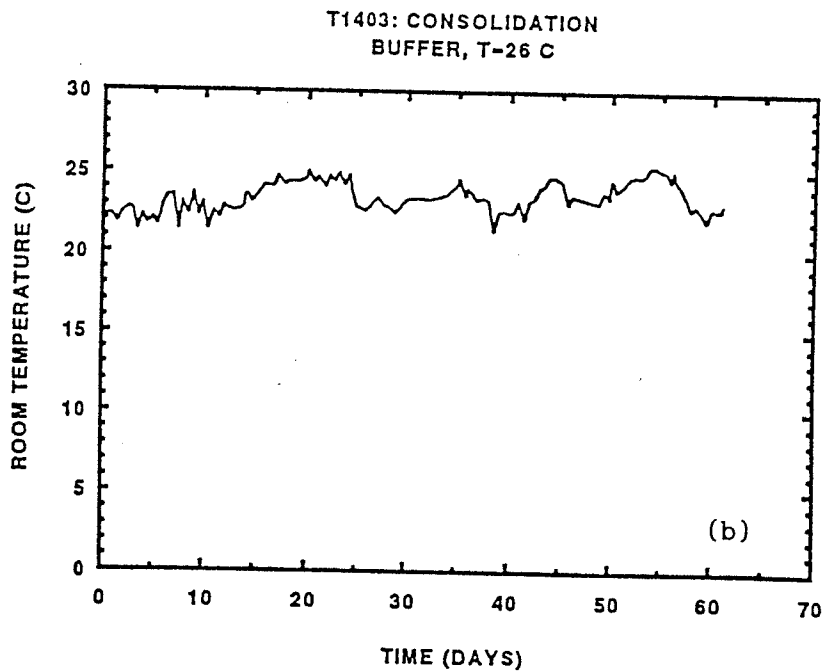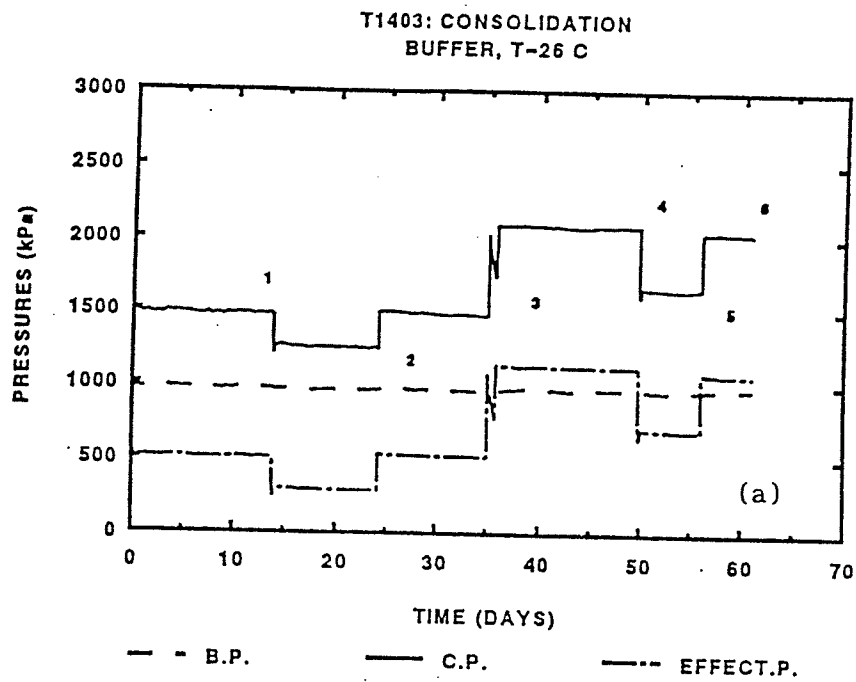
Figure 5.15   Pressure ramping test during consolidation, T1403, 26°C, (a) pressure, and (b) room temperature *vs.*elapsed time.

T1403: CONSOLIDATION
BUFFER, T-26 C

VOLUME STRAIN (%) vs **TIME (DAYS)**

(c)

T1403: CONSOLIDATION
BUFFER, T-26 C

STRAIN RATE (%/DAY) vs **TIME (DAYS)**

(d)
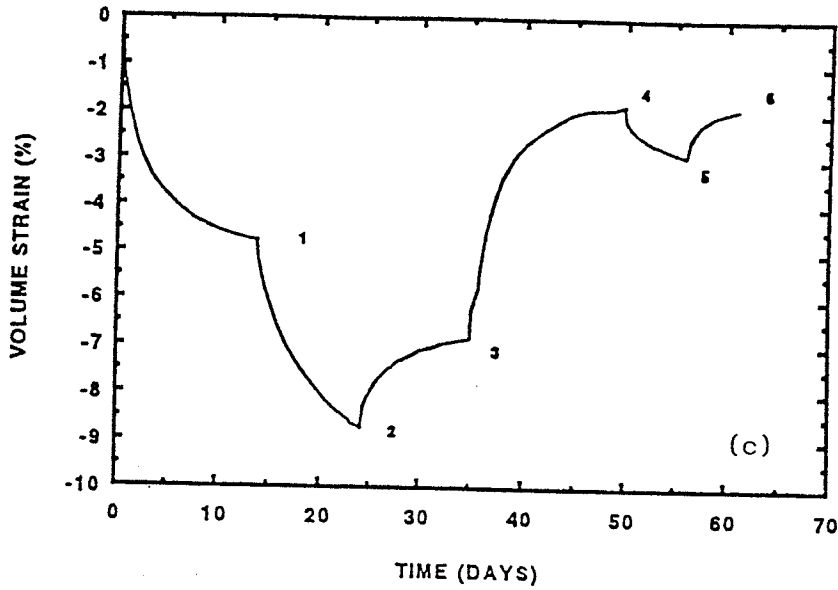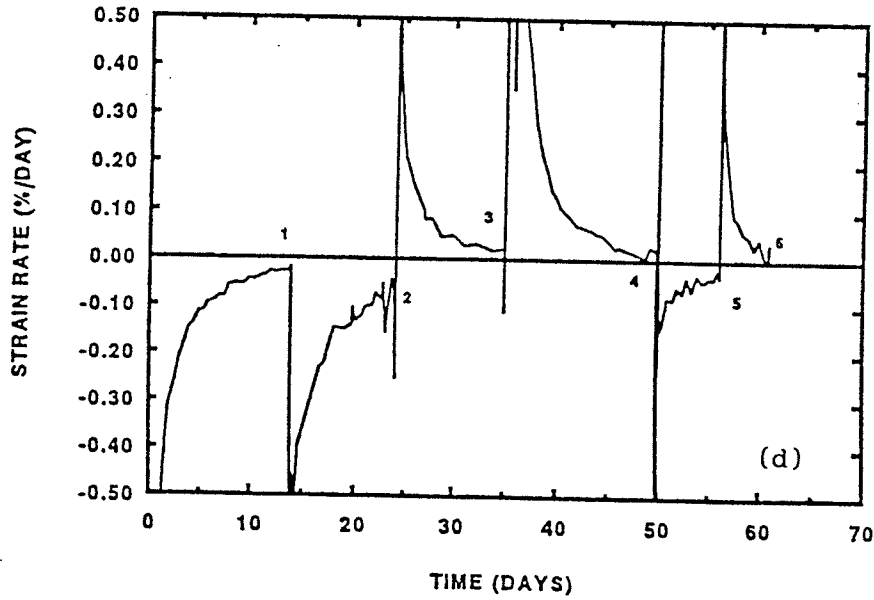
Figure 5.15 (continued) Pressure ramping test during consolidation, T1403, 26°C, (c) volume strain and (d) volume strain rate *vs.* elapsed time.

T1404: CONSOLIDATION
BUFFER, T-26 C

(a)

— - B.P.   —— C.P.   —--- EFFECT.P.

T1404: CONSOLIDATION
BUFFER, T-26 C

(b)
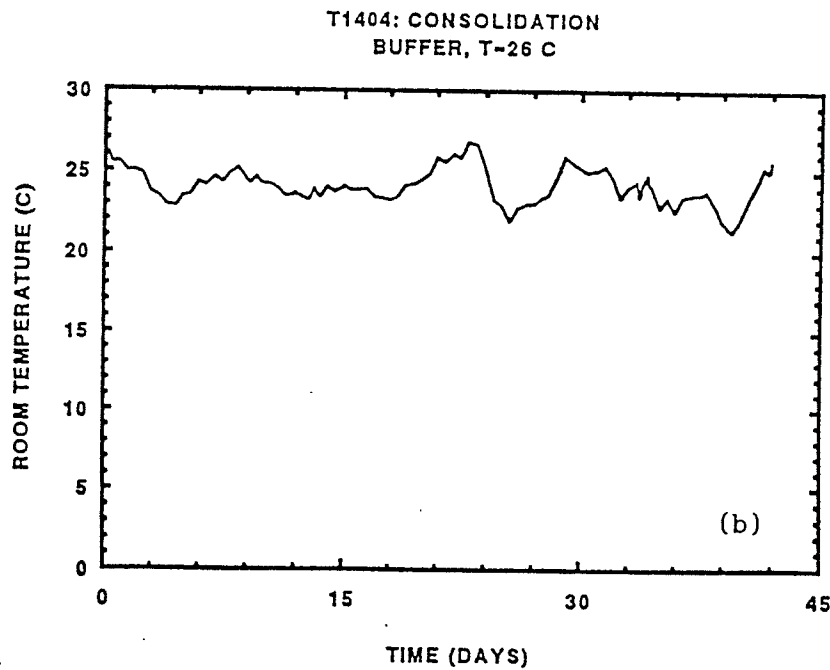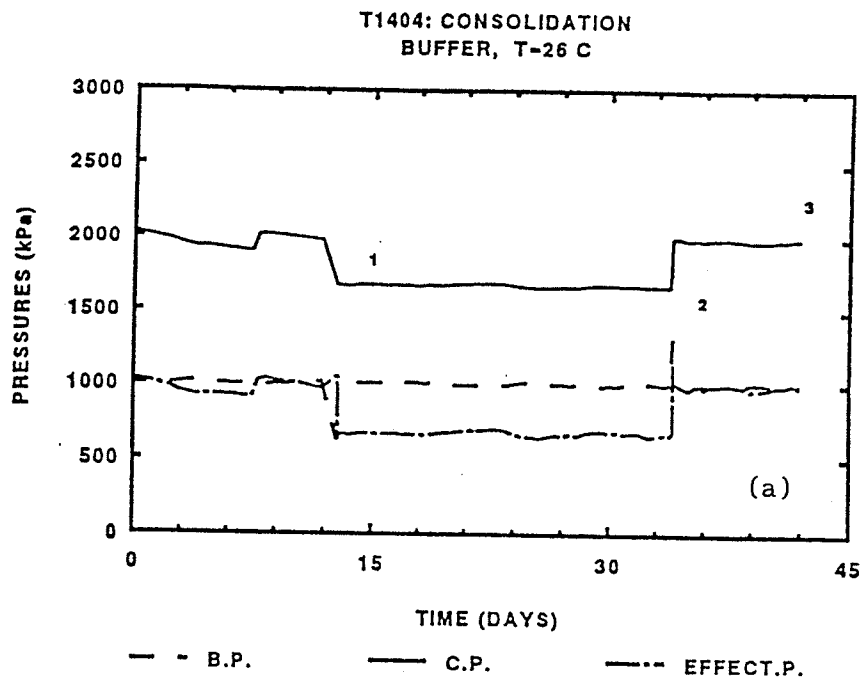
Figure 5.16 Pressure ramping test during consolidatiion, T1404,
26°C, (a) pressure, and (b) room temperature *vs.*
elapsed time.
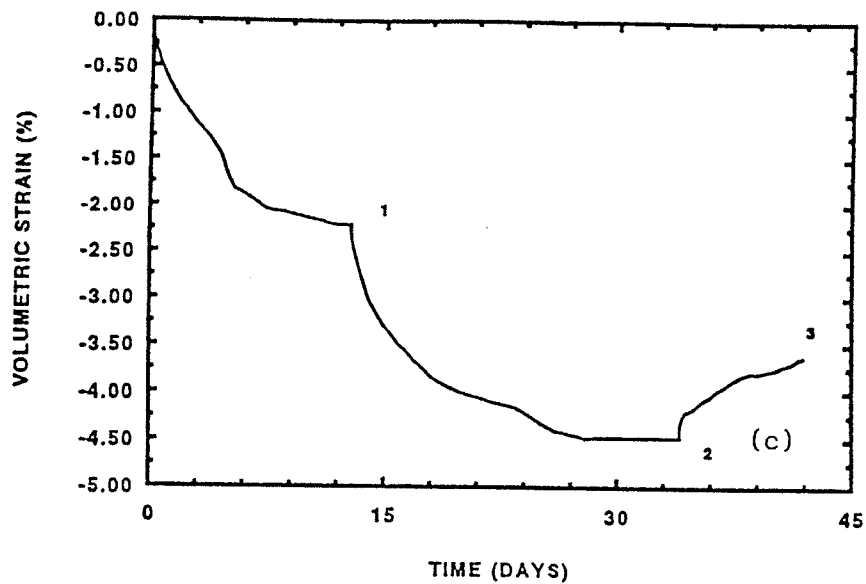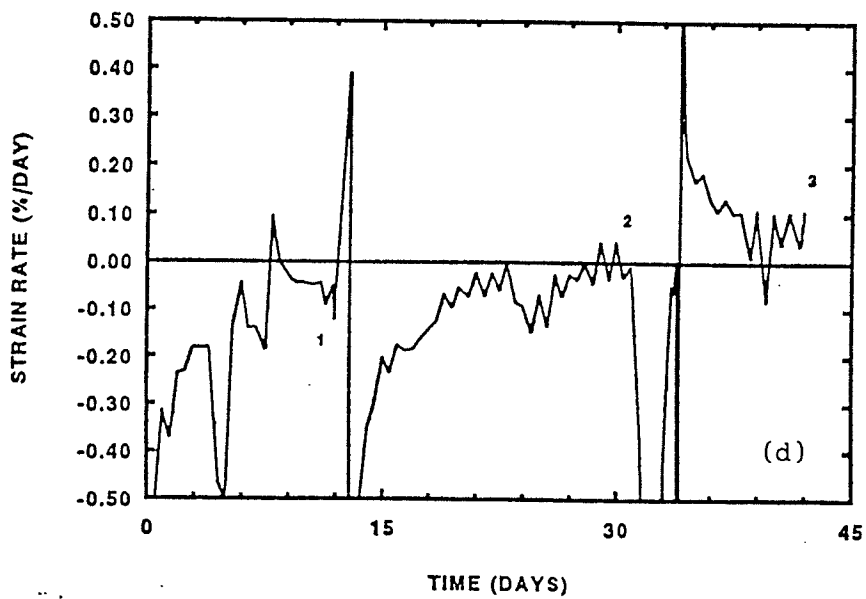
Figure 5.16 (continued) Pressure ramping test during consolidation, T1404, 26°C, (c) volume strain and (d) volume strain rate *vs*. elapsed time.

T1405: CONSOLIDATION
BUFFER, T-26 C

(a)

B.P.   C.P.   EFFECT.P.

T1405: CONSOLIDATION
BUFFER, T-26 C

(b)
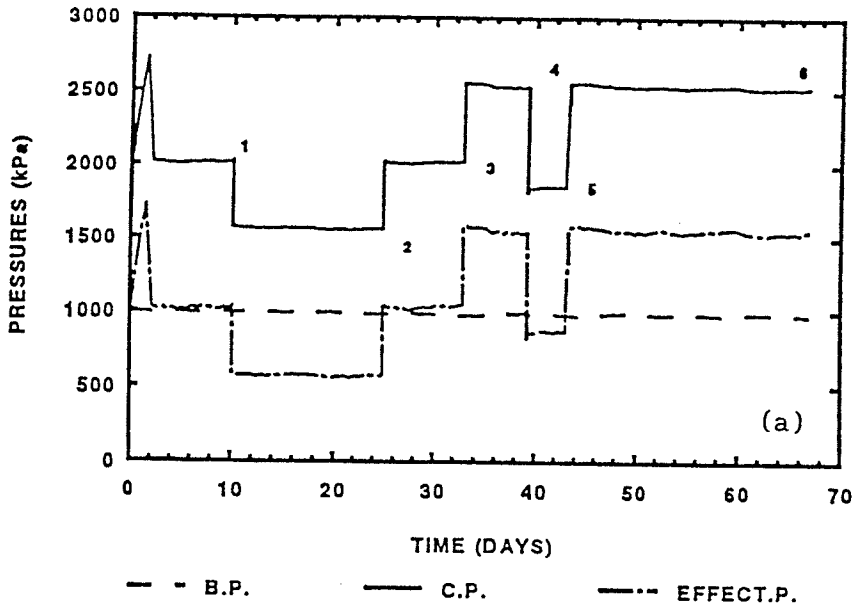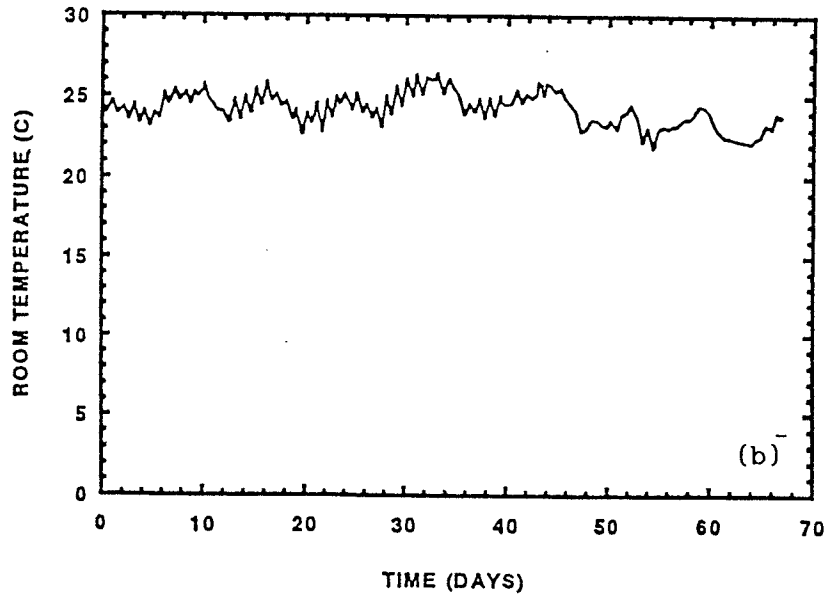
Figure 5.17   Pressure ramping test during consolidatiion, T1405, 26°C, (a) pressure, and (b) room temperature *vs.* elapsed time.

T1405: CONSOLIDATION
BUFFER, T-26C

(c)

TIME (DAYS)
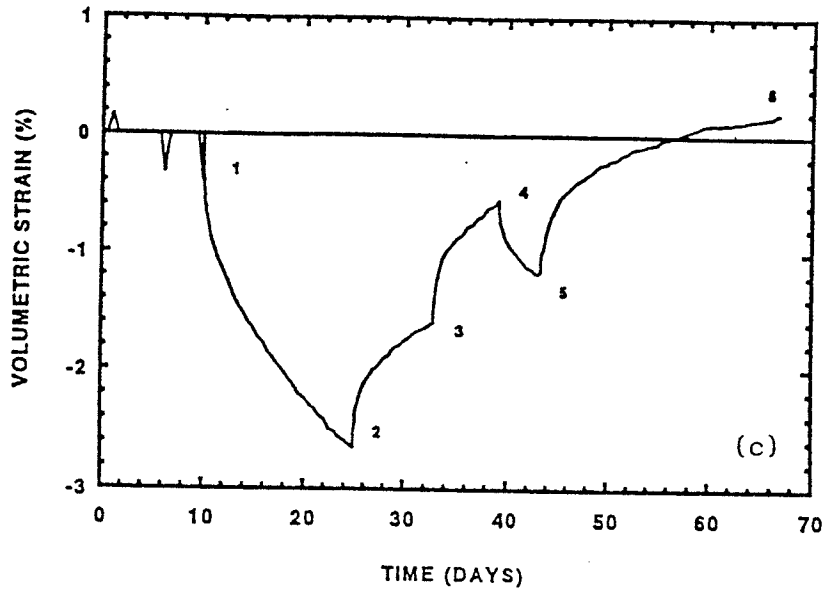
BK1403: CONSOLIDATION
BUFFER, T=26C

(d)

TIME (DAYS)
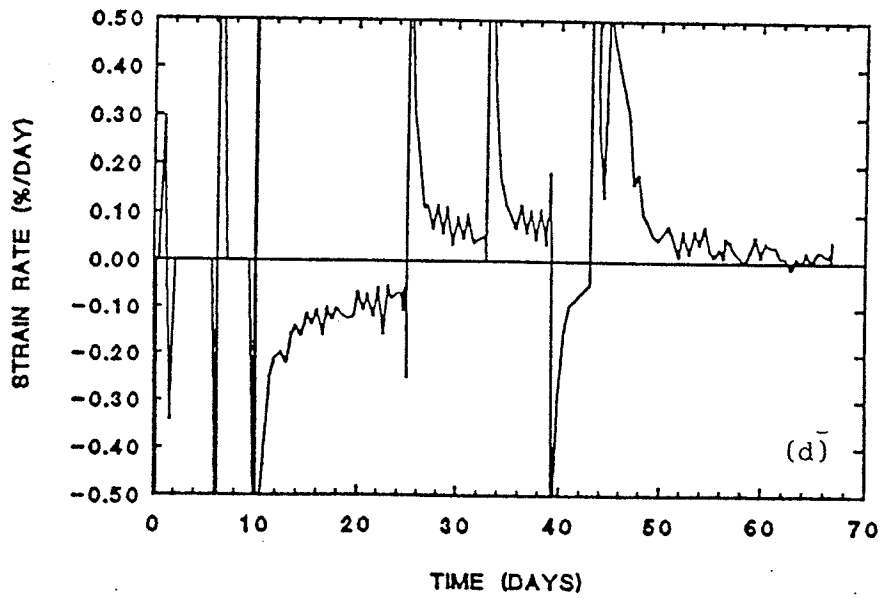
Figure 5.17 (continued) Pressure ramping test during consolidation, T1405, 26°C, (c) volume strain and (d) volume strain rate *vs.* elapsed time.
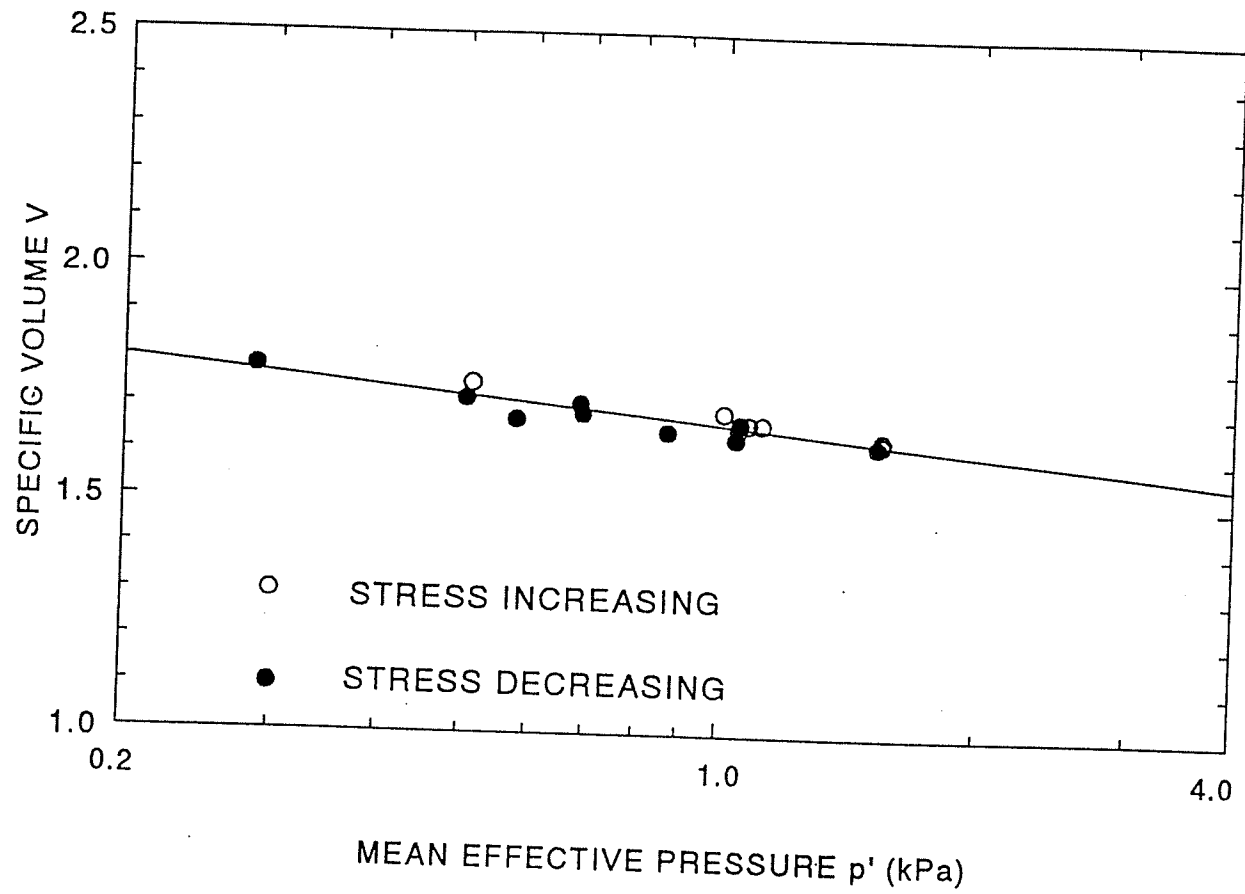
Figure 5.18   Isotropic consolidation for sand-bentonite mixture
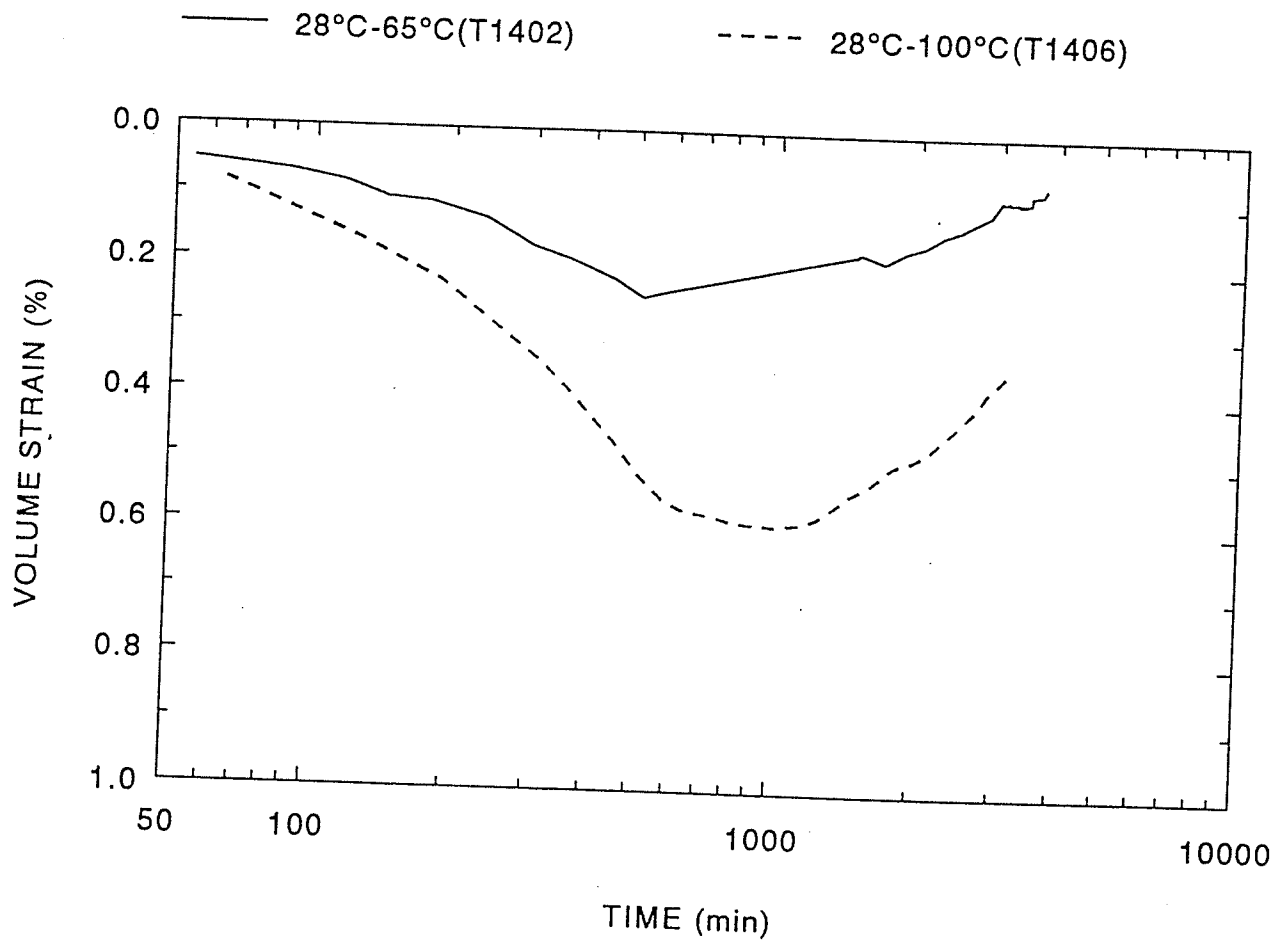
Figure 5.19   Thermal consolidation at 1.5 MPa for compacted sand–bentonite mixture.   T = 28°C–65°C, and 28°C–100°C.
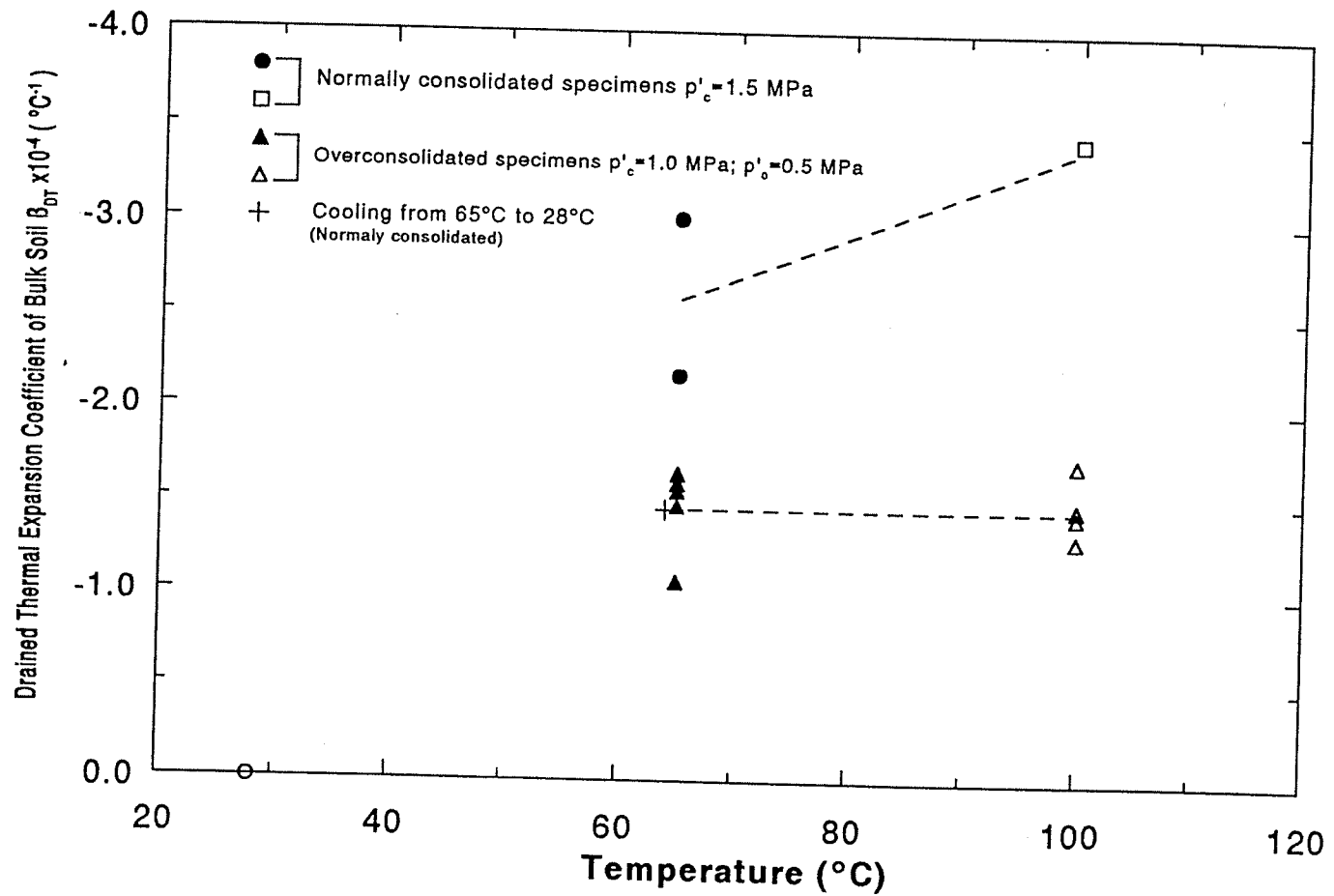
Figure 6.1   Drained thermal expansion coefficient of bulk soil: Reconstituted illite (normally consolidated and overconsolidated specimens).
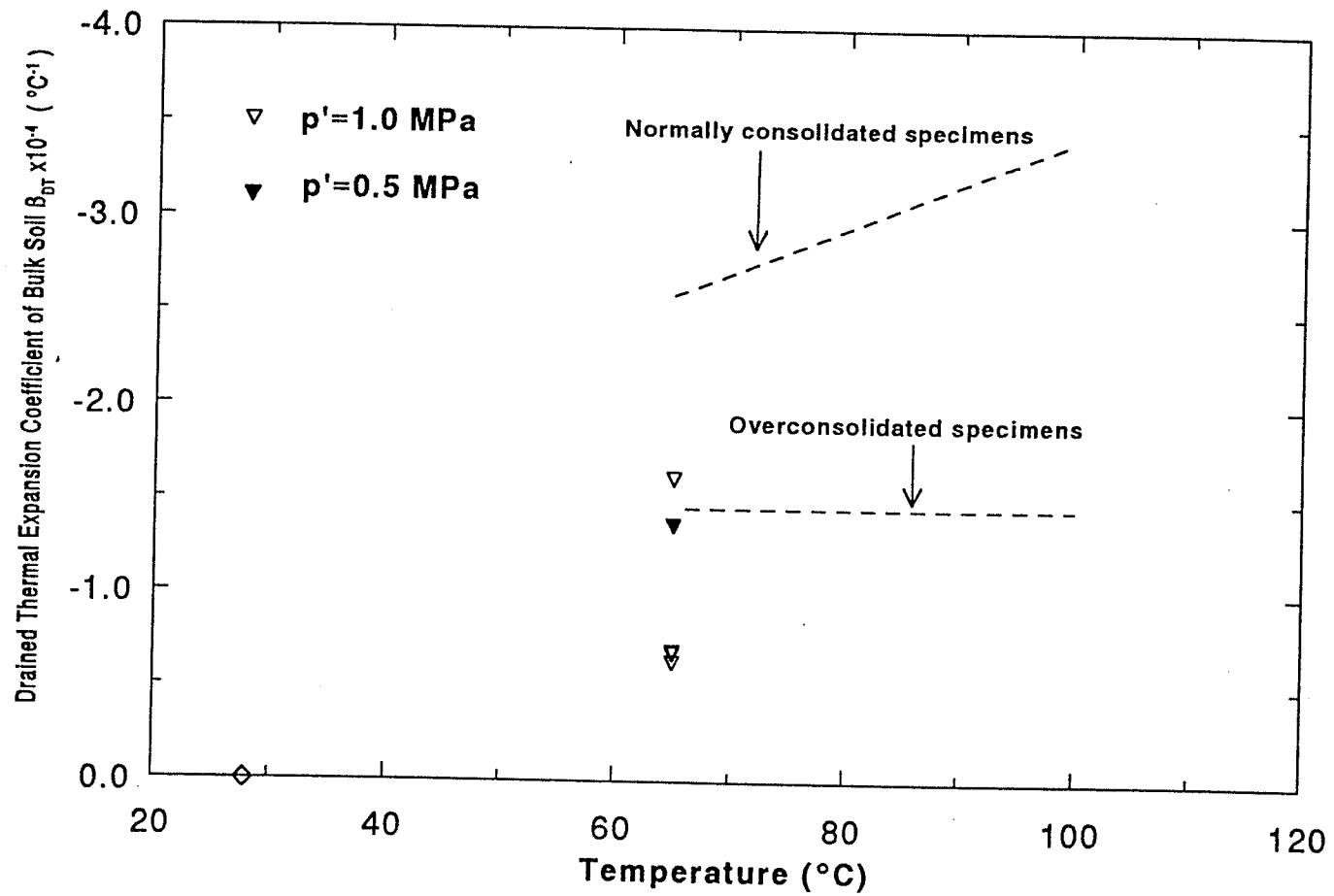
Figure 6.2   Drained thermal expansion coefficient of bulk soil: Compacted illite specimens at p_o' = 0.5 MPa and 1.0 MPa.
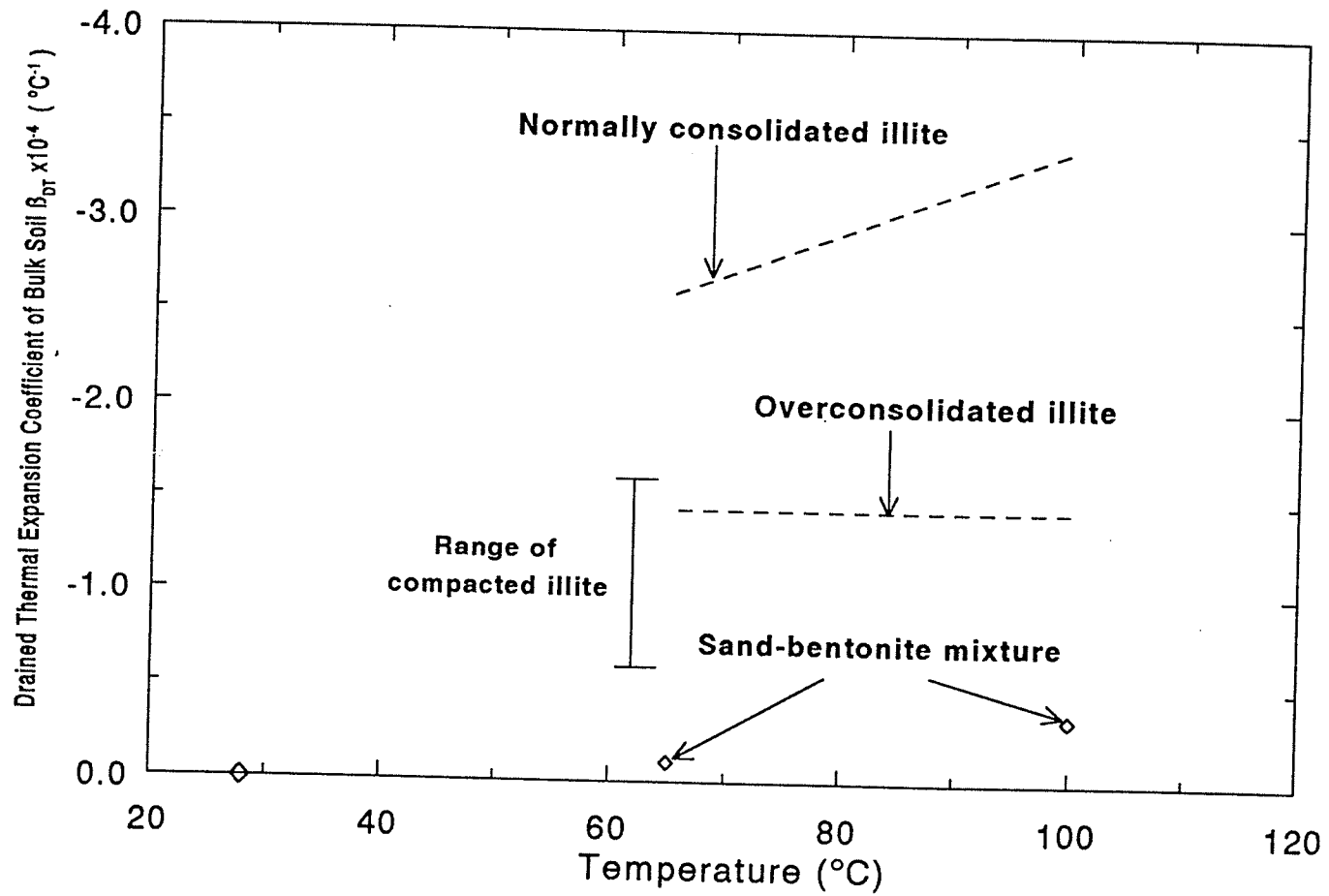
Figure 6.3   Drained thermal expansion coefficient of bulk soil: Compacted sand-bentonite mixture at $p_o' = 1.5$ MPa.
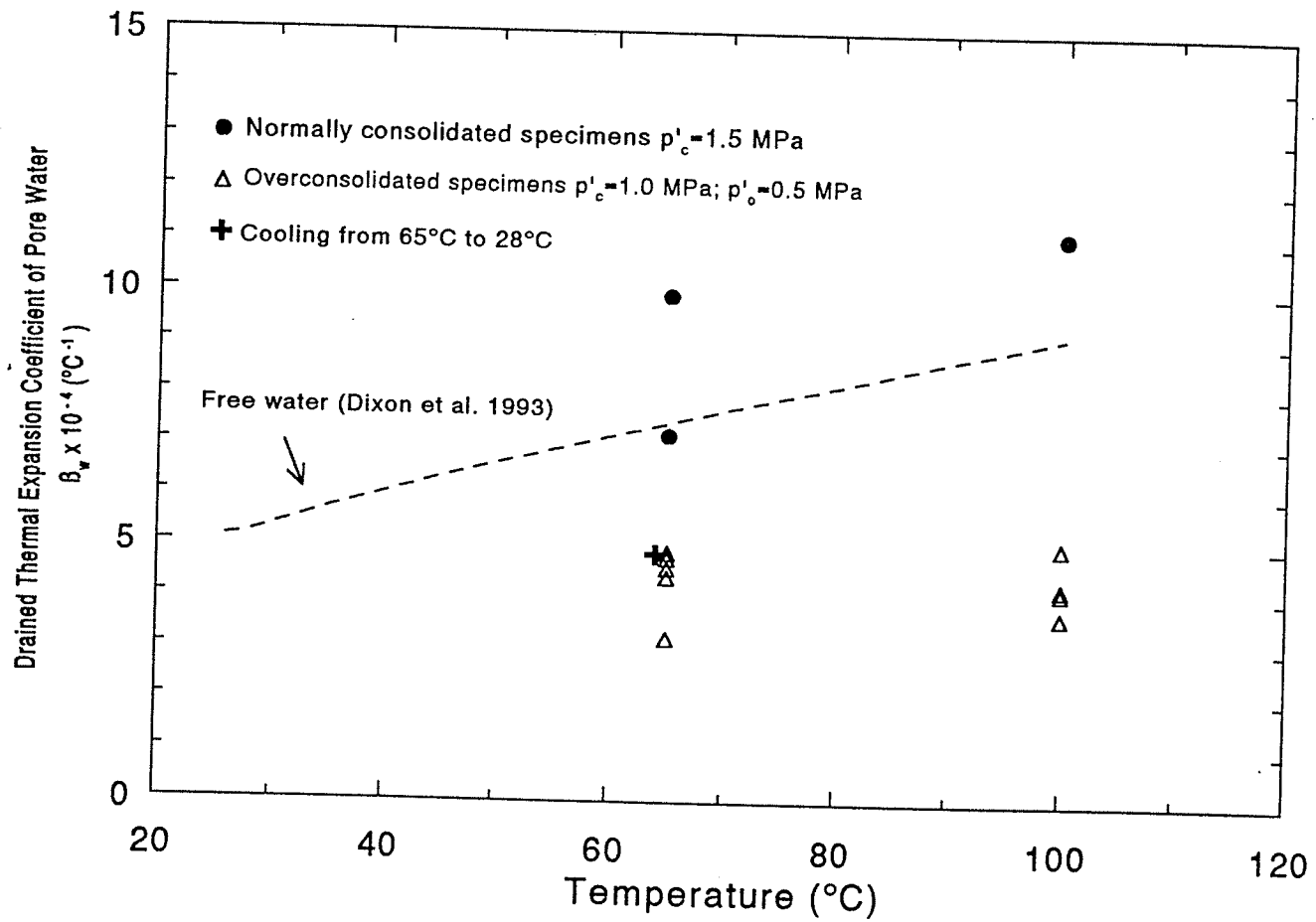
Figure 6.4   Drained thermal expansion coefficient of pore water: Reconstituted illite (normally consolidated and overconsolidated specimens).
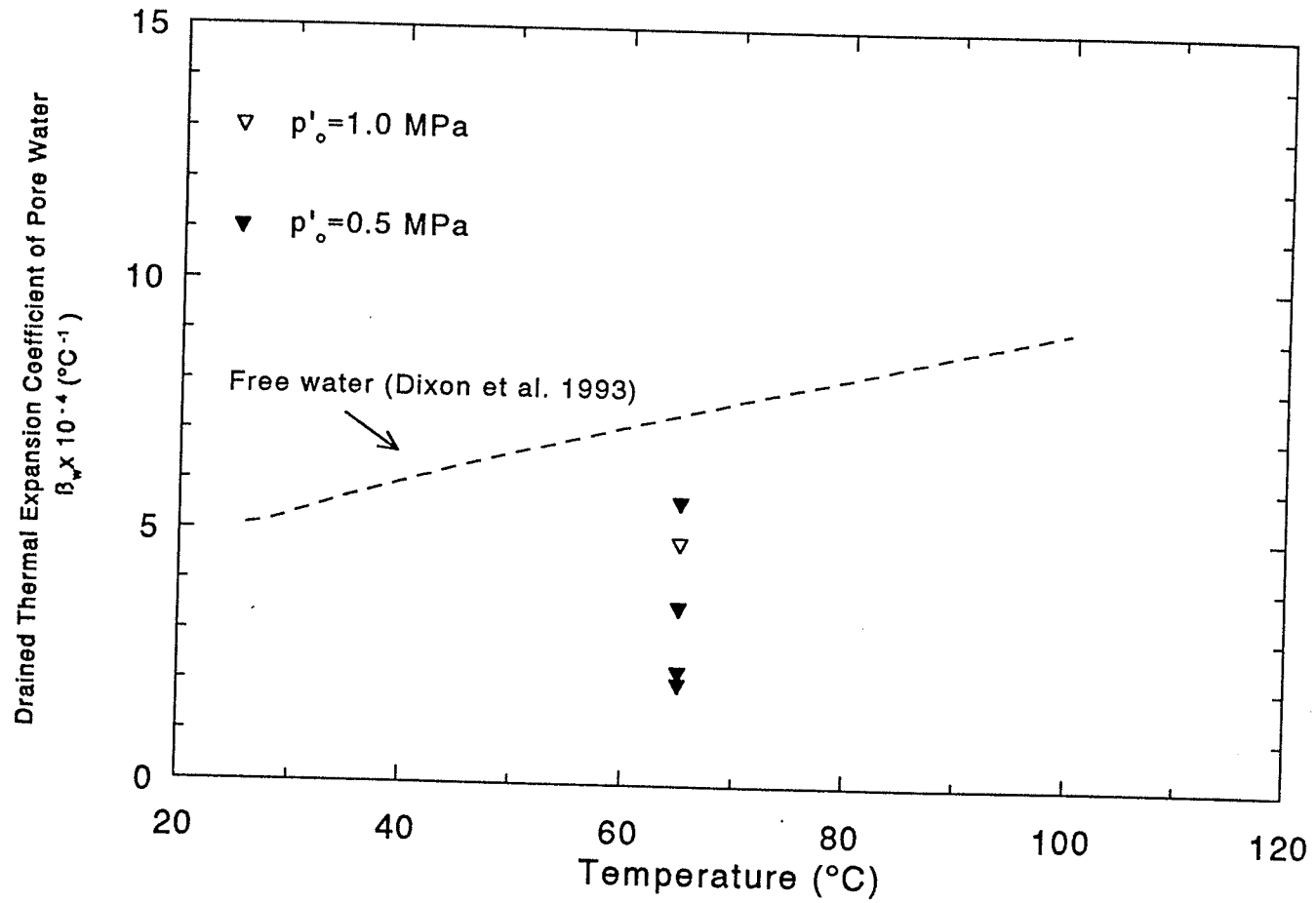
Figure 6.5   Drained thermal expansion coefficient of pore water: Compacted illite specimens at p'_o = 0.5 MPa and 1.0 MPa.
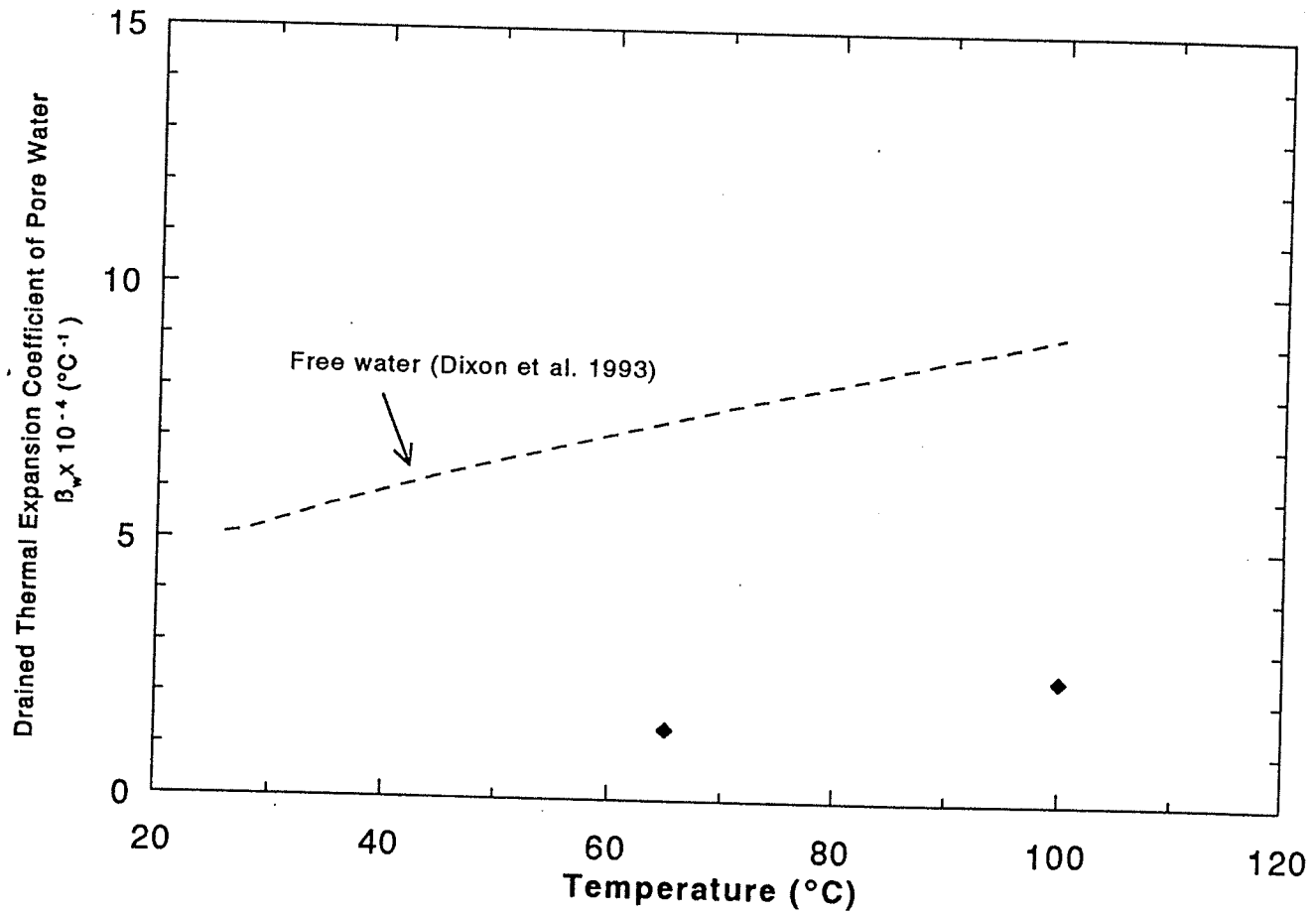
Figure 6.6   Drained thermal expansion coefficient of pore water: Compacted sand-bentonite mixture at $p_o' = 1.5$ MPa.
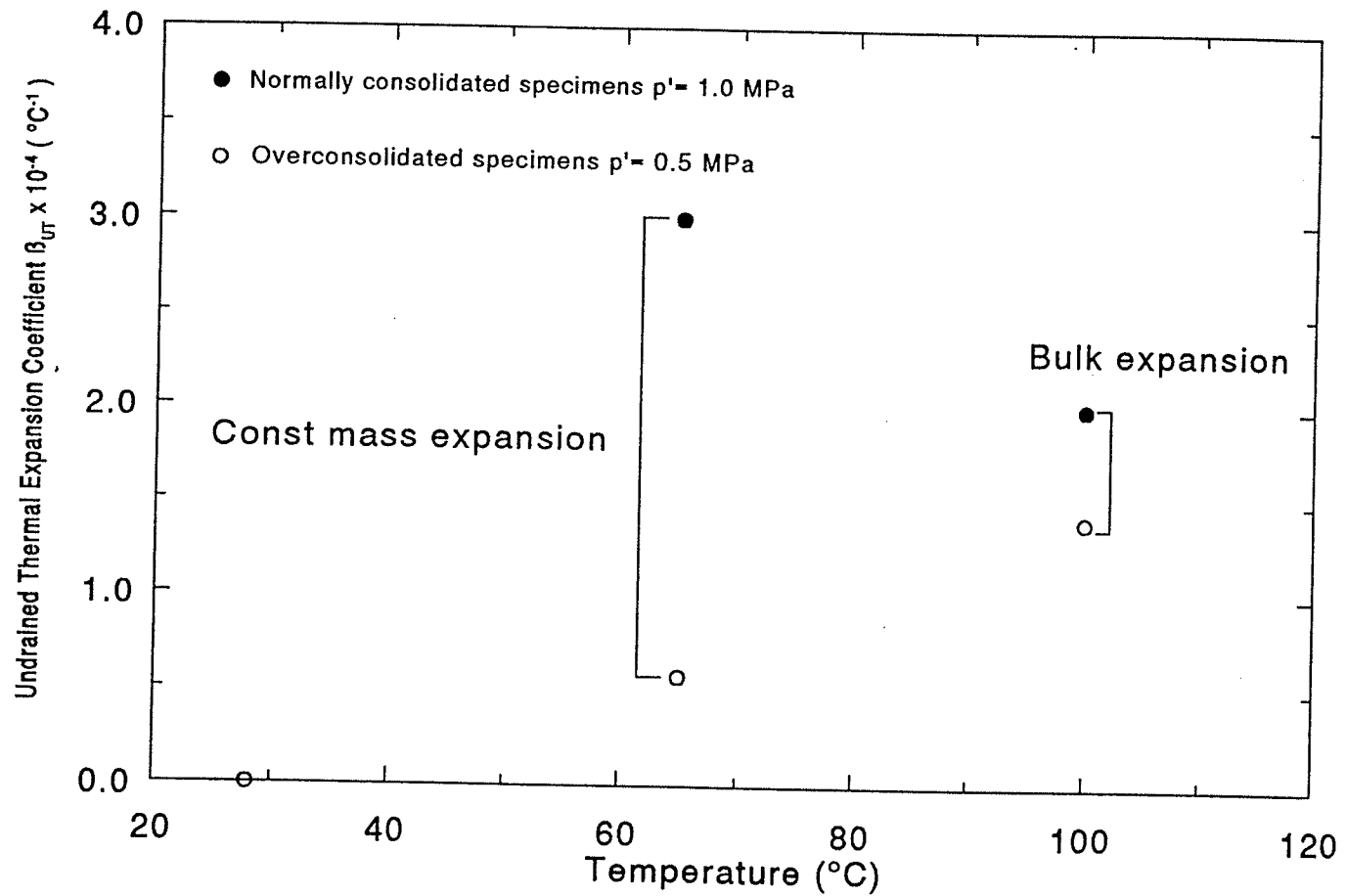
Figure 6.7 Undrained thermal expansion coefficient: Reconstituted illite (normally consolidated and overconsolidated specimens).
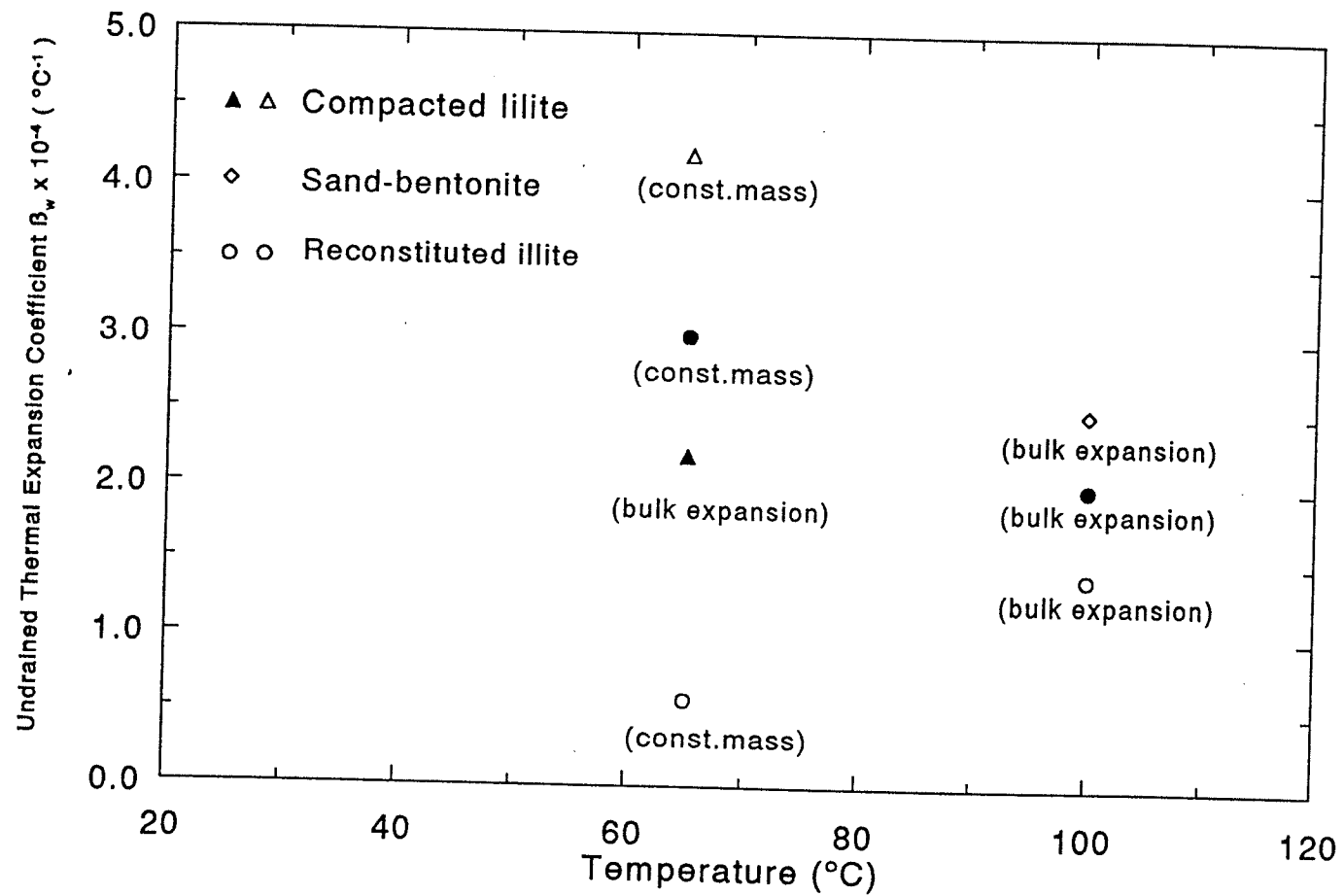
Figure 6.8 Undrained thermal expansion coefficient: Compacted illite and compacted sand-bentonite mixture.
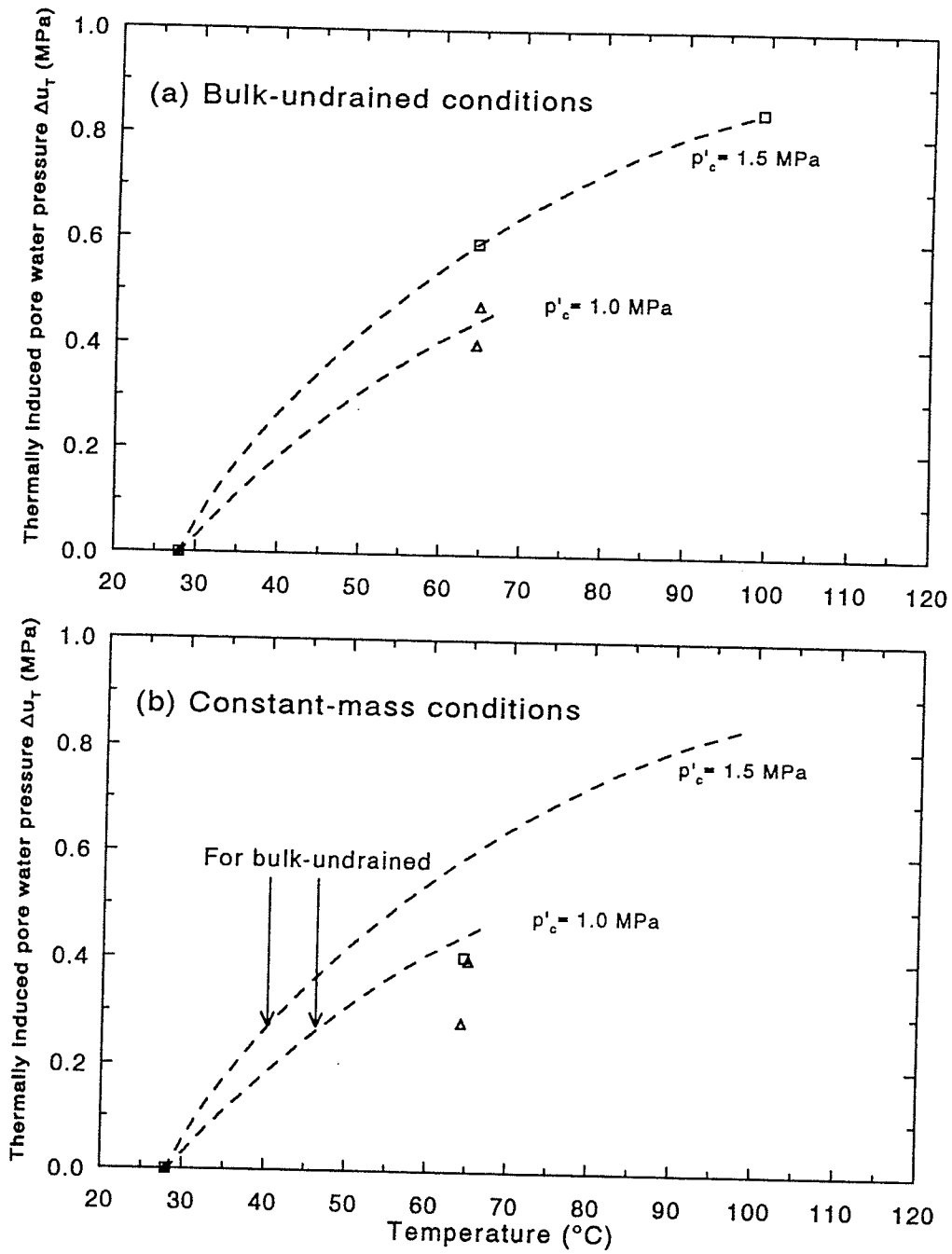
Figure 6.9 Thermally induced pore pressure: Reconstituted illite (normally consolidated specimens) (a) Bulk-undrained conditions, and (b) Constant-mass conditions.
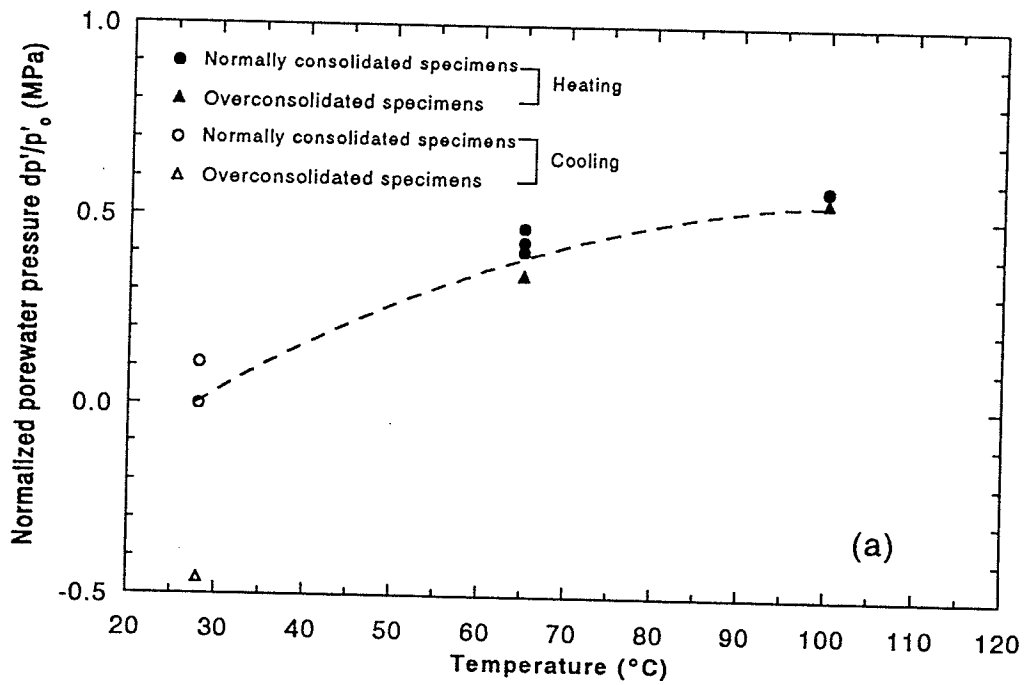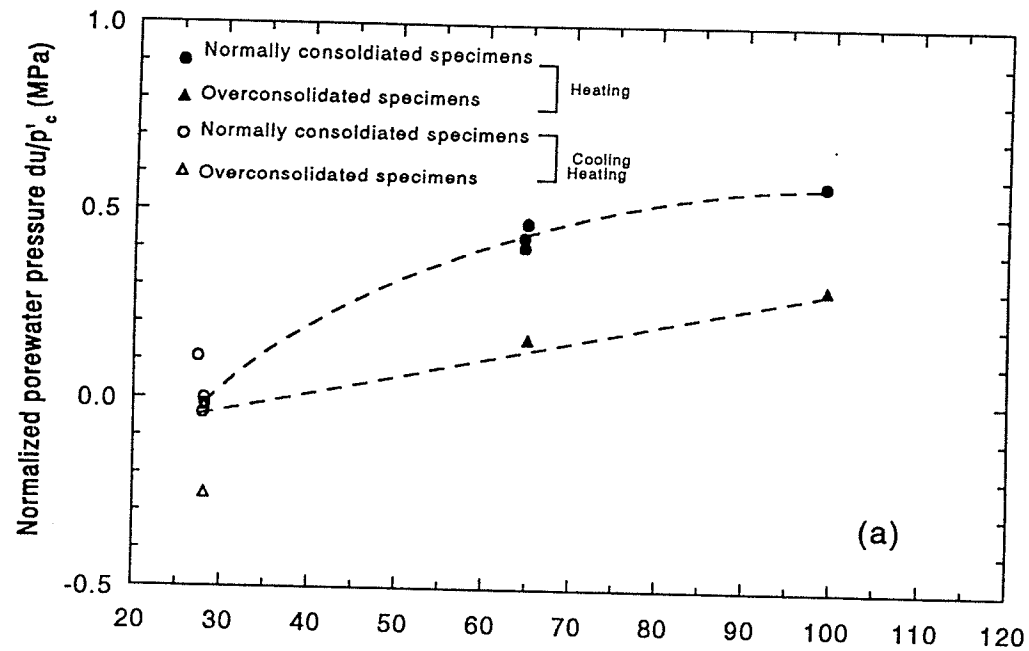
Figure 6.10 Thermally induced pore pressure: Reconstituted illite (a) Normalized by preconsolidation pressure p'_c, and (b) Normalized by consolidation pressure p'_o.
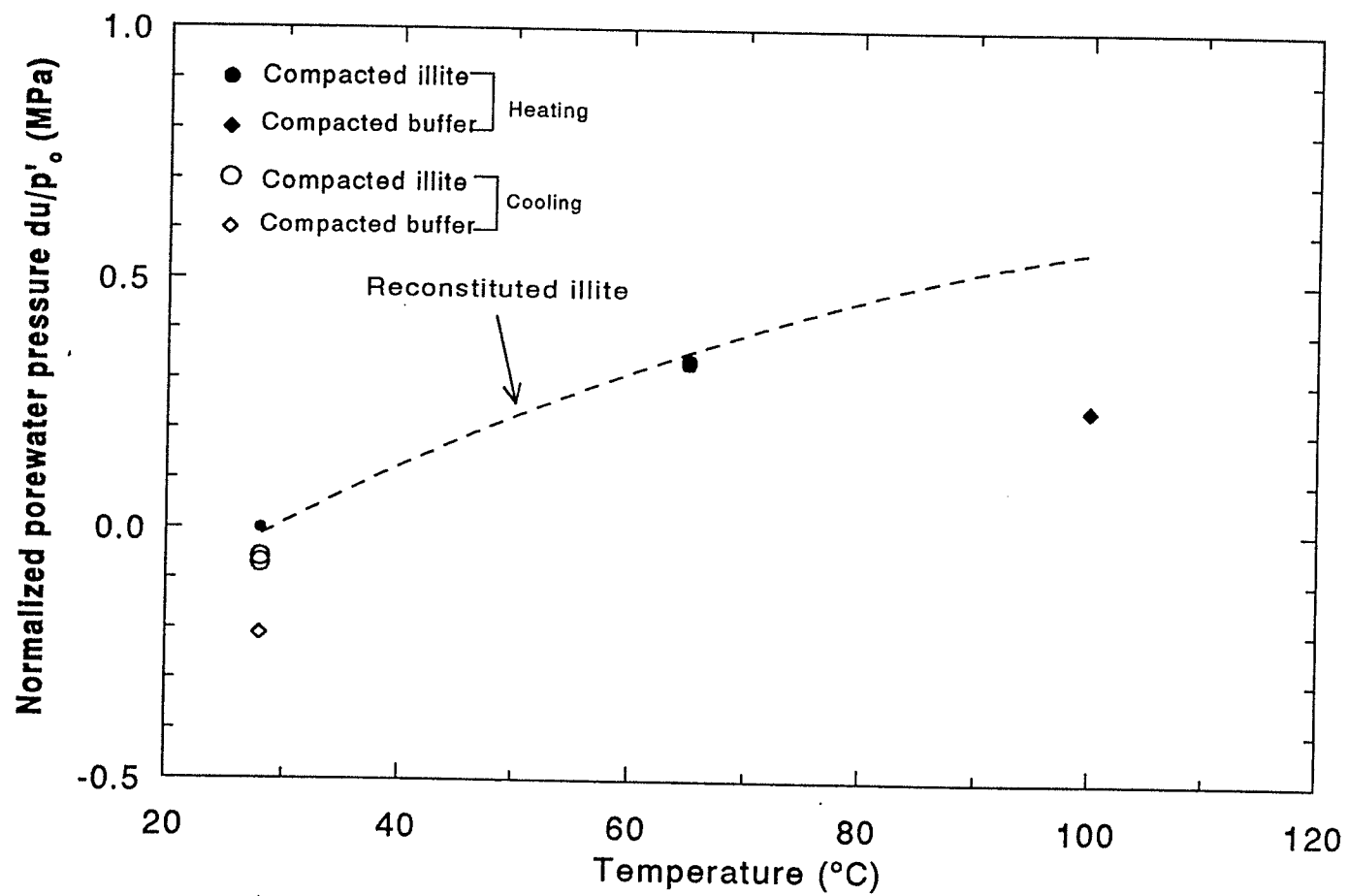
Figure 6.11 Thermally induced pore pressure normalized by p_o': Compacted illite and compacted sand-bentonite mixture.
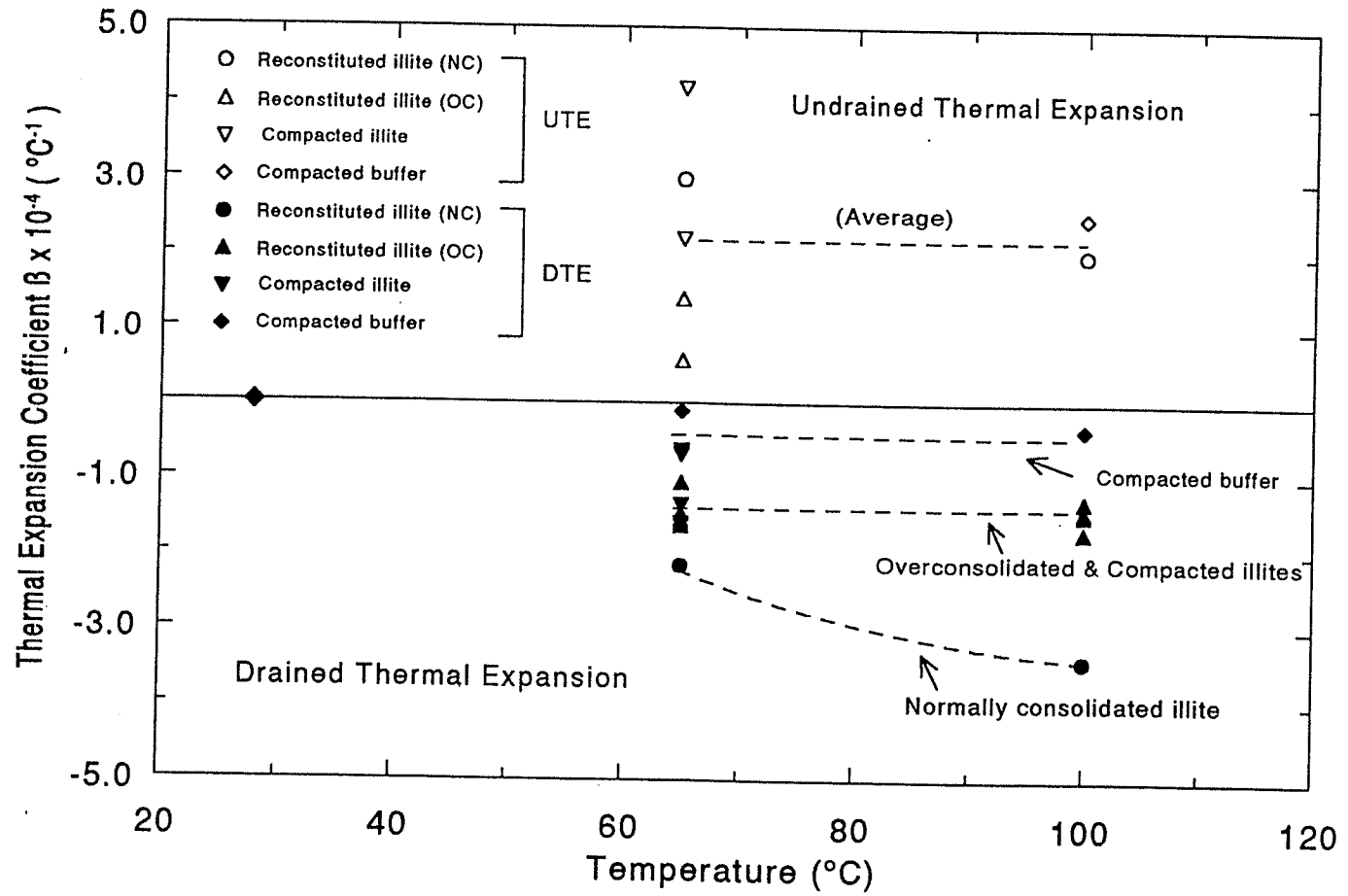
Figure 6.12 Summary of thermal expansion coefficients.
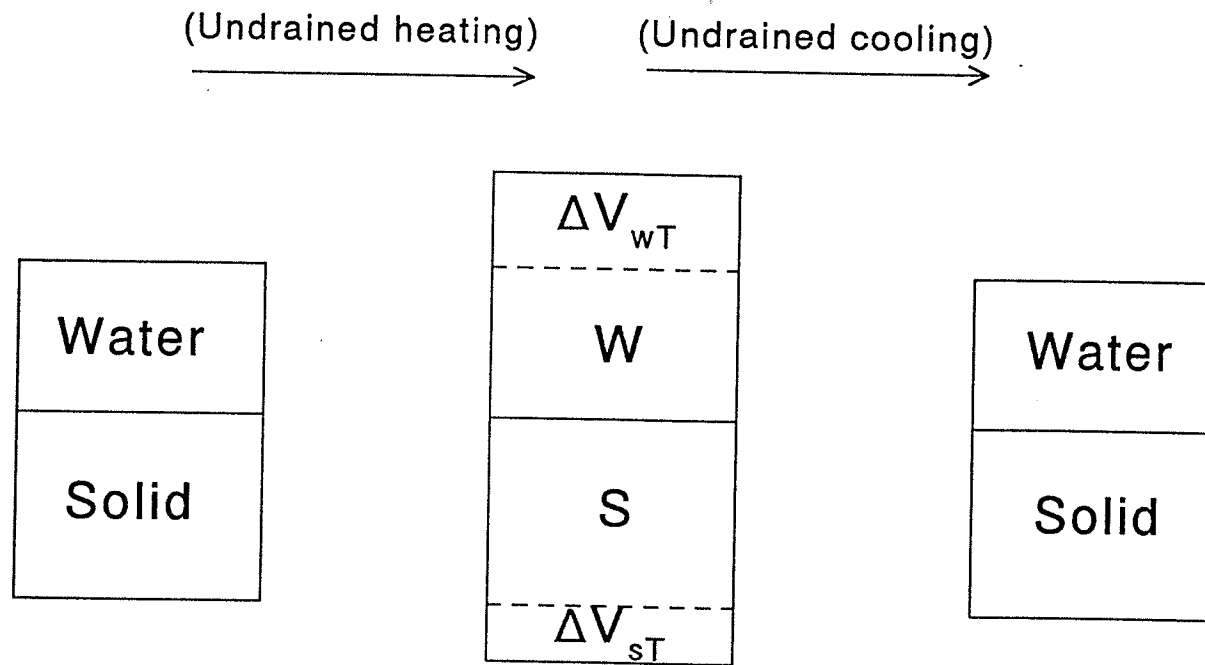
ΔV_{wT} : Thermal expansion of pore water volume

ΔV_{sT} : Thermal expansion of solid particle volume

Figure 6.13 Mechanism of undrained thermal expansion.
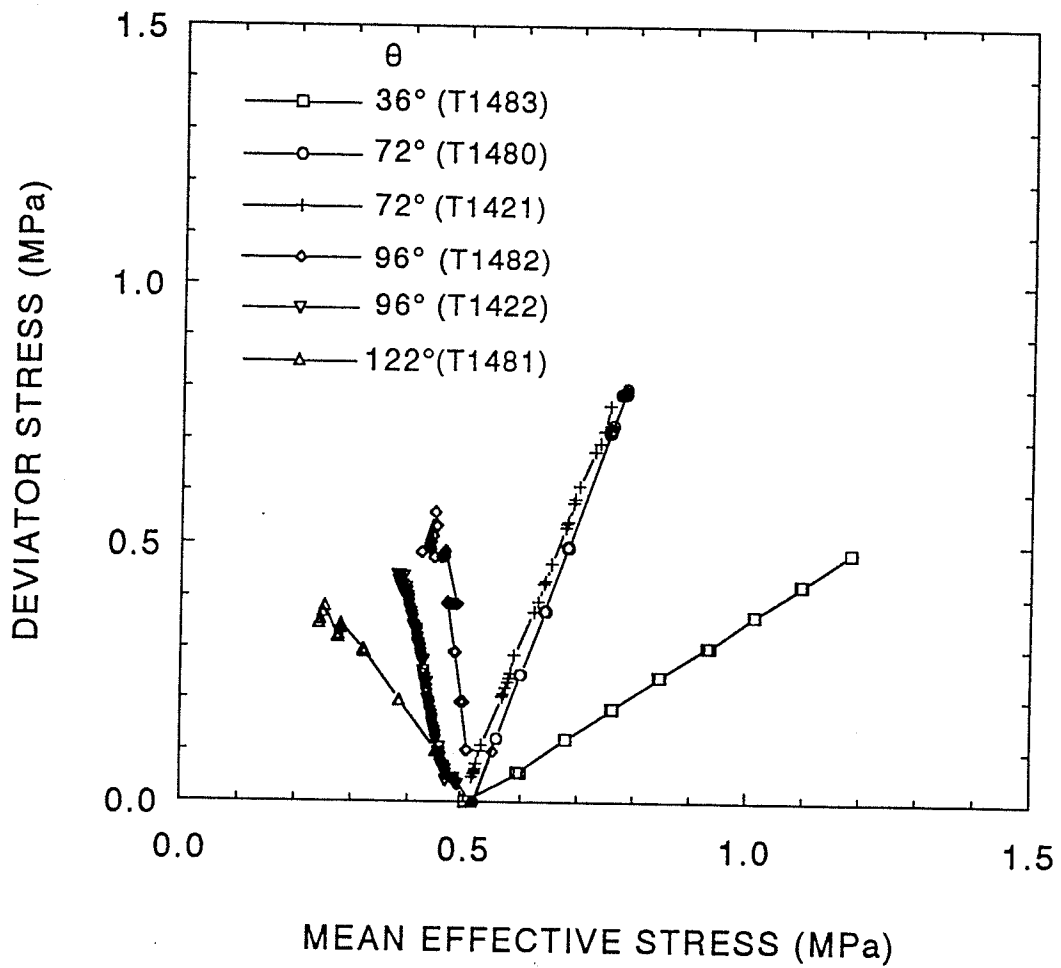
Figure 7.1 Stress   paths   for   drained   tests   at   28°C   for
reconstituted illite (OCR = 2).
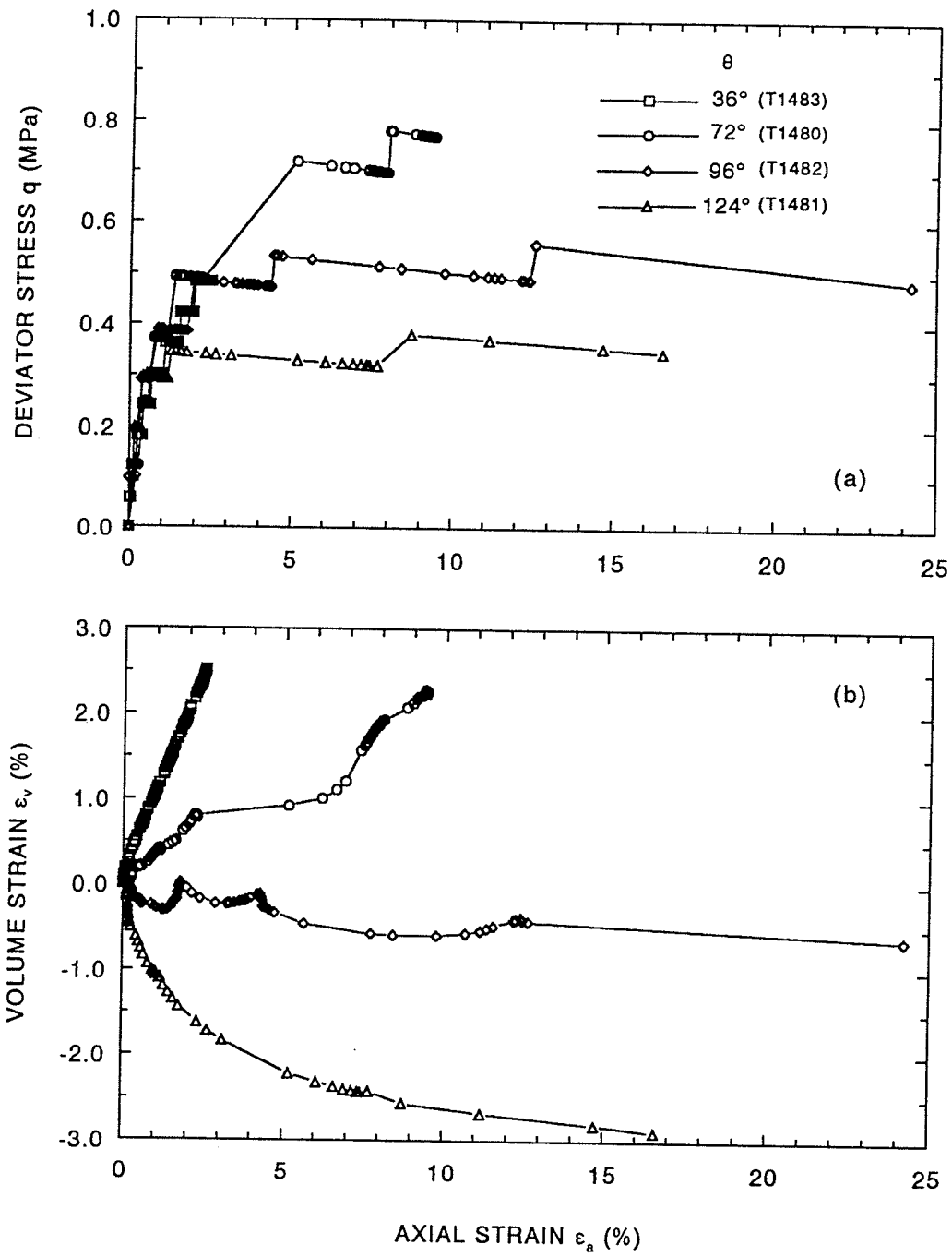
Figure 7.2 Stress-strain relationships in drained stress path tests on reconstituted illite at 28°C. (a) Deviator stress *vs.* axial strain. (b) Volumetric strain *vs.* axial strain.
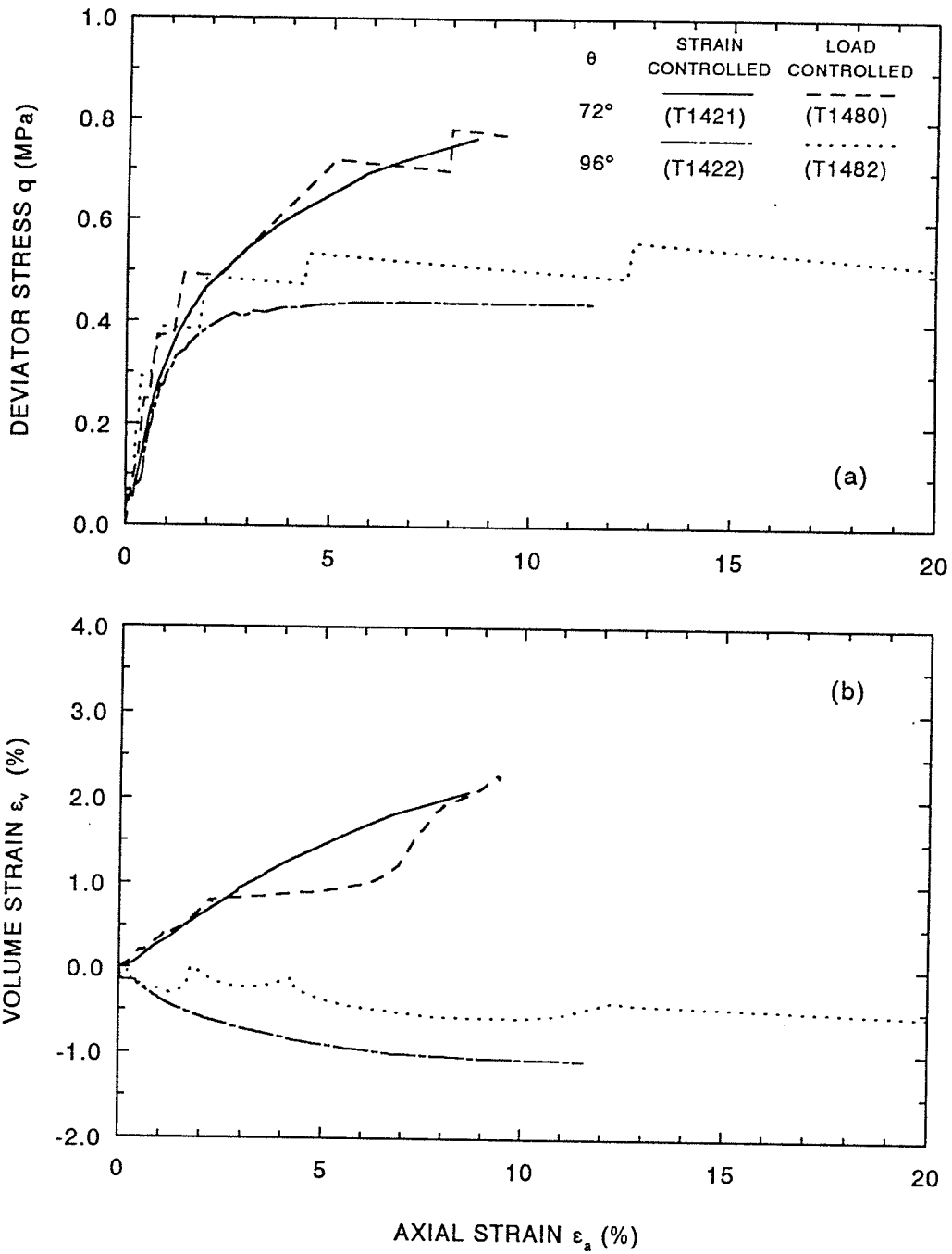
Figure 7.3 Comparison between strain-controlled and load-controlled tests for draned stress-path tests. (a) Deviator stress *vs.* axial strain. (b) Volumetric strain *vs.* axial strain.
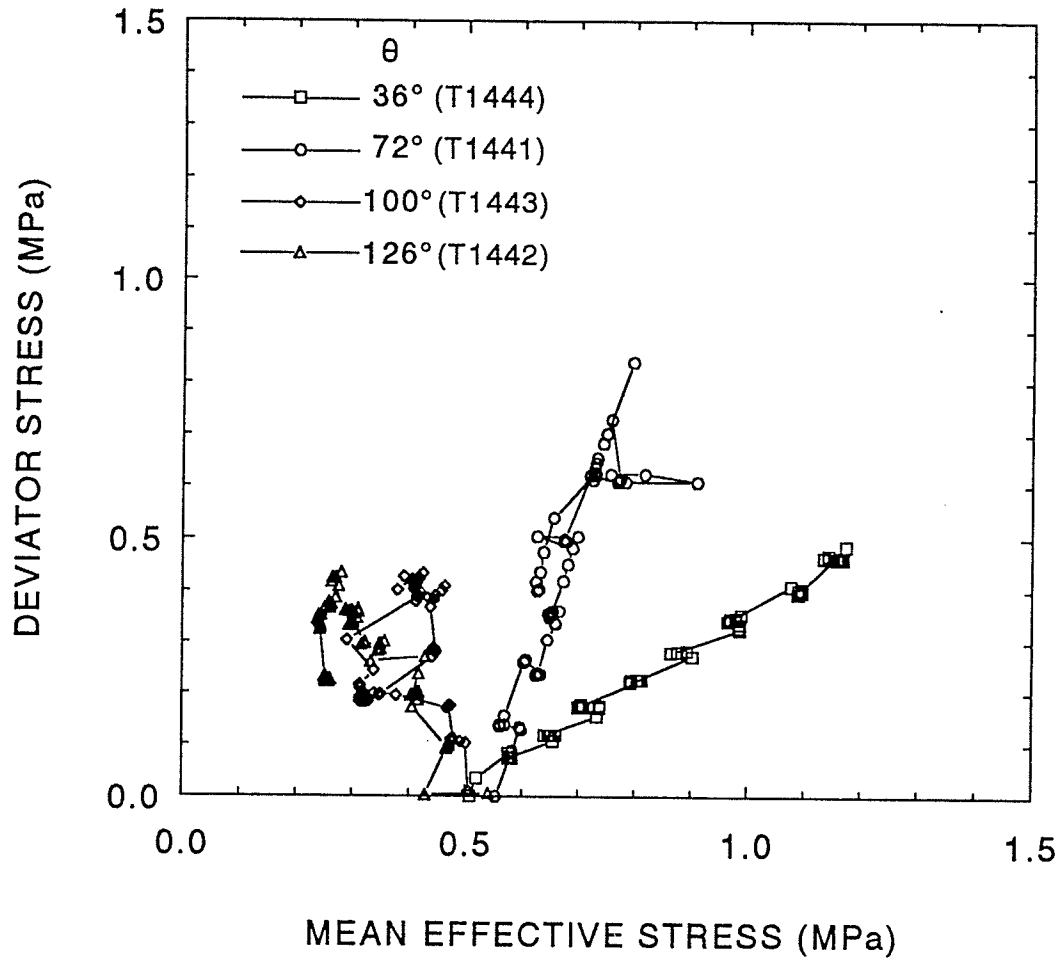
Figure 7.4 Stress paths for drained tests at 65°C for reconstituted illite (OCR = 2).
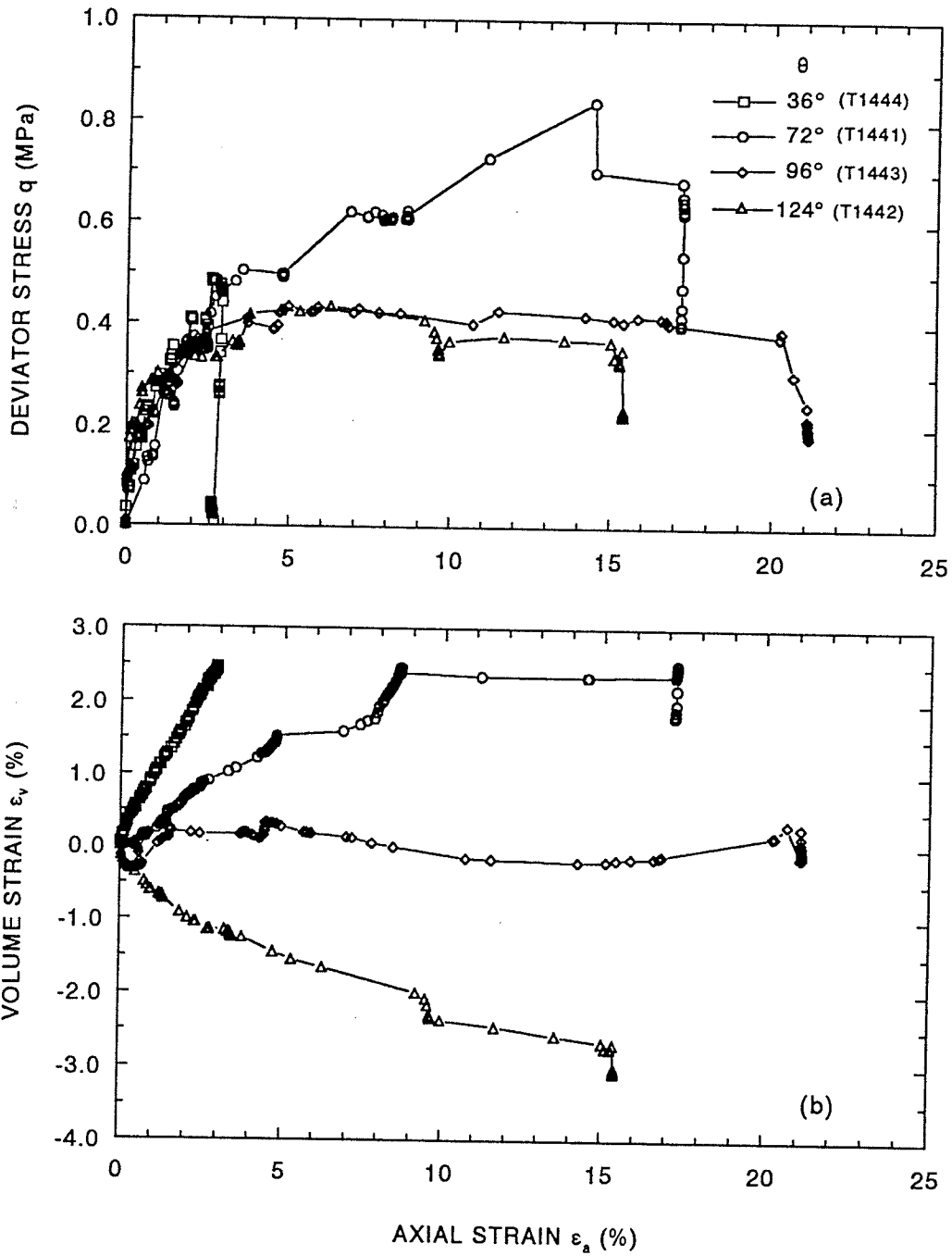
Figure 7.5 Stress-strain relationships in drained stress path tests on reconstituted illite at 65°C. (a) Deviator stress *vs.* axial strain. (b) Volumetric strain *vs.* axial strain.
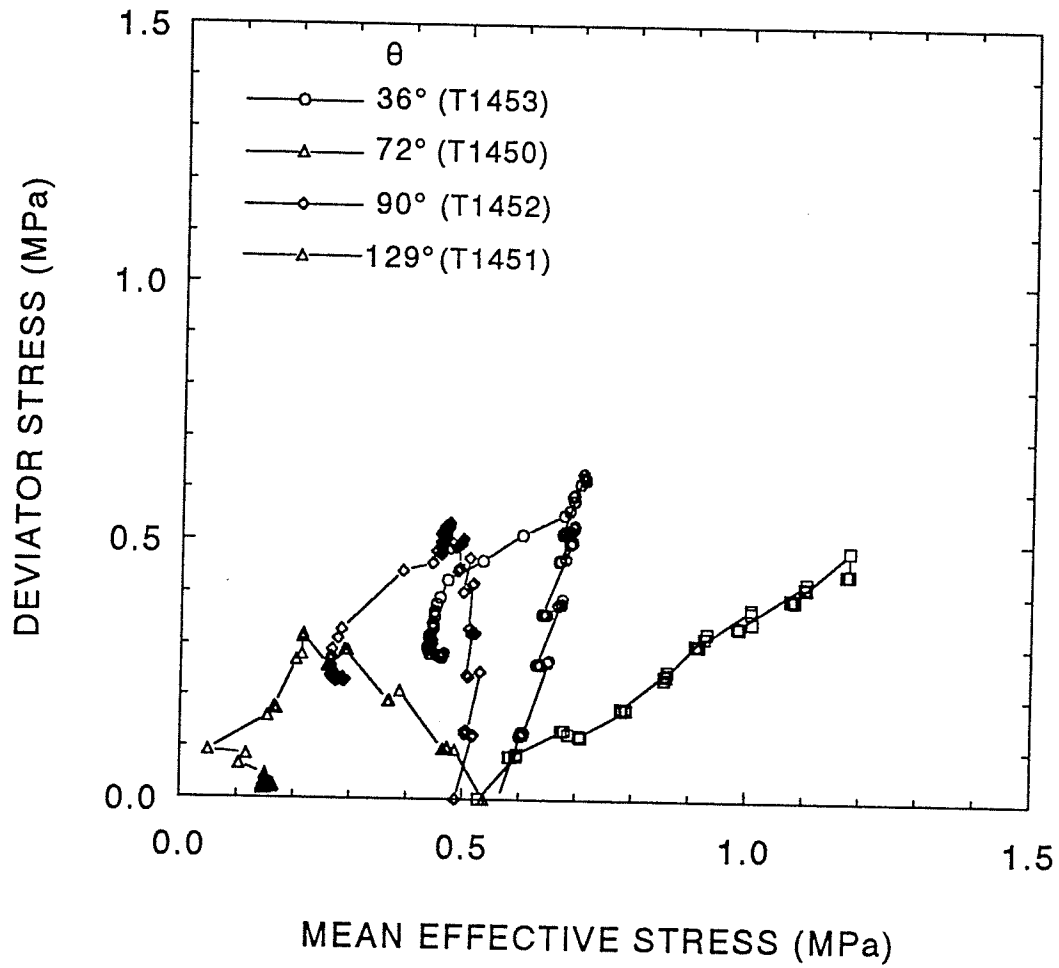
Figure 7.6 Stress paths for drained tests at 100°C for reconstituted illite (OCR = 2).
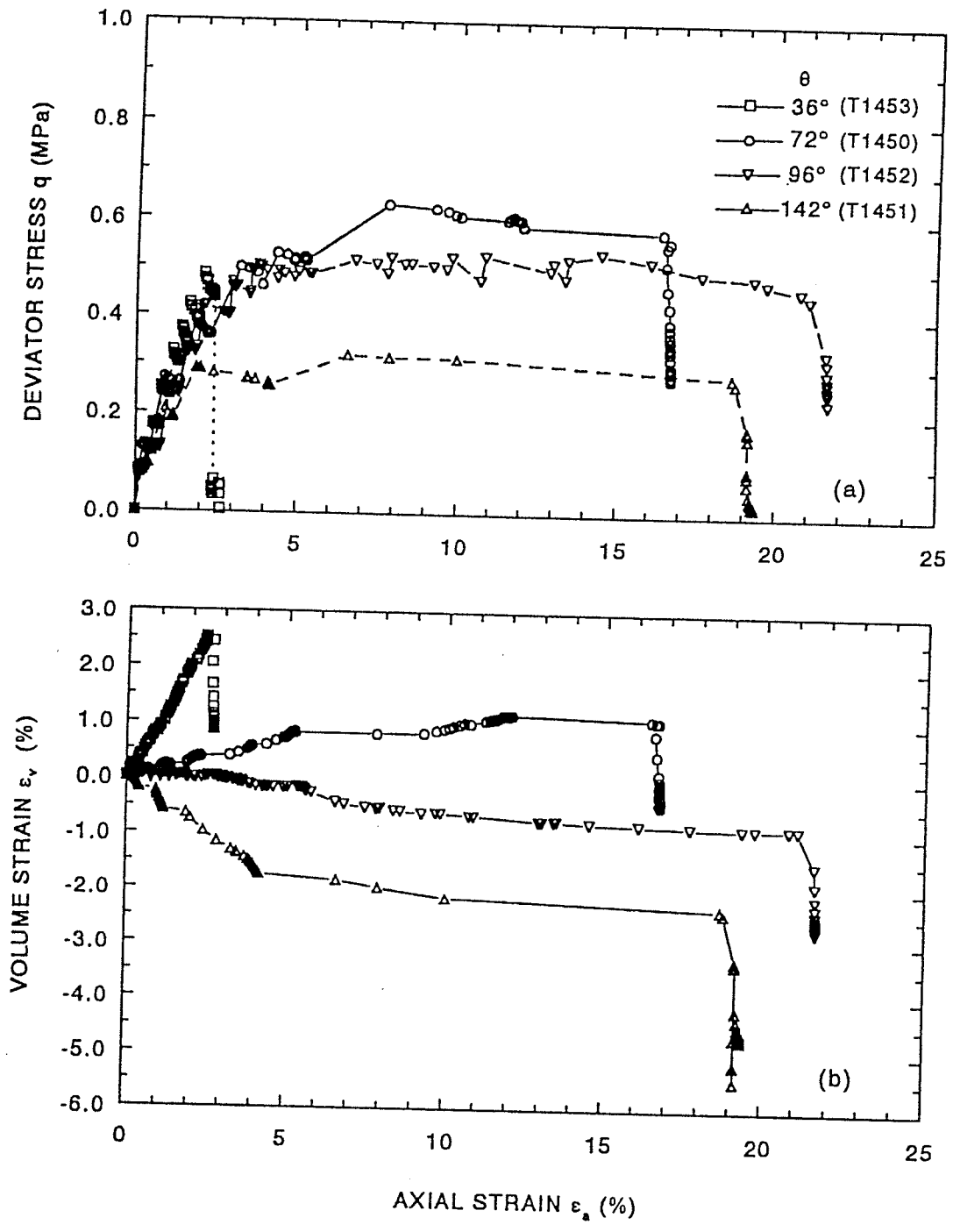
Figure 7.7 Stress-strain relationships in drained stress path tests on reconstituted illite at 100°C. (a) Deviator stress *vs*. axial strain. (b) Volumetric strain *vs*. axial strain.
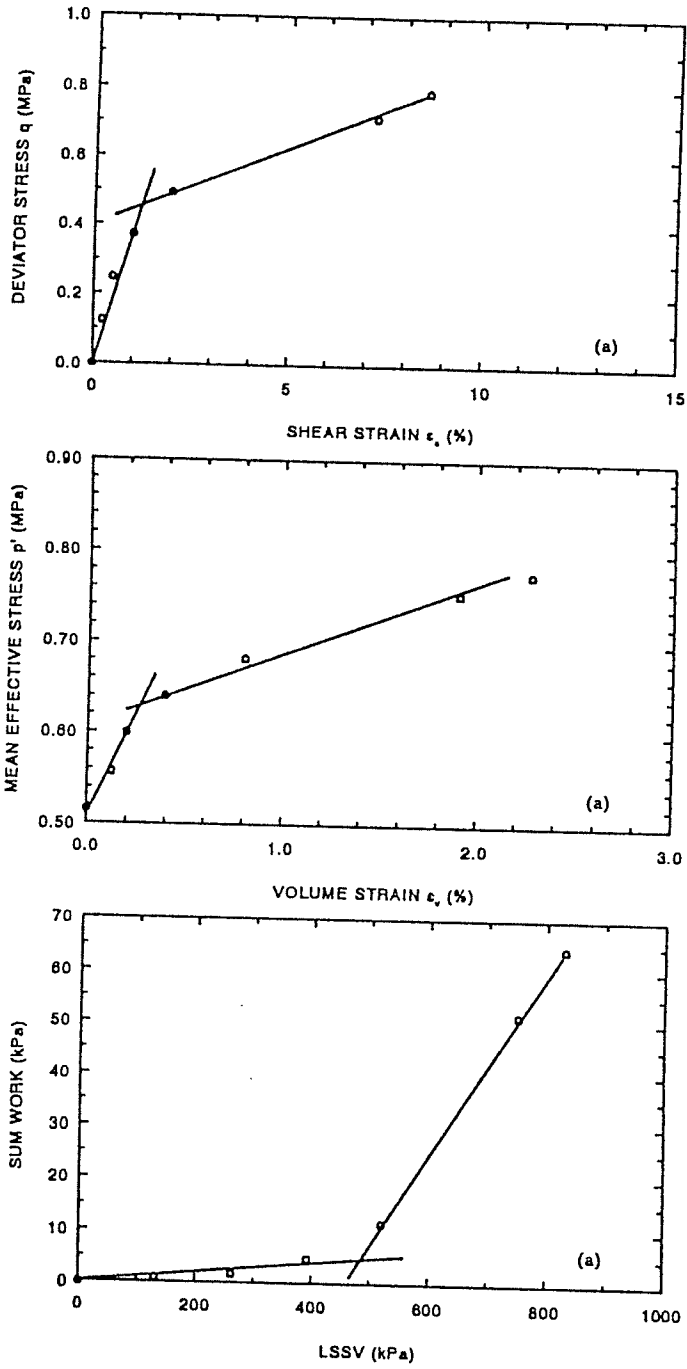
Figure 7.8 Determination of yield stresses. Test T1480 (28°C).
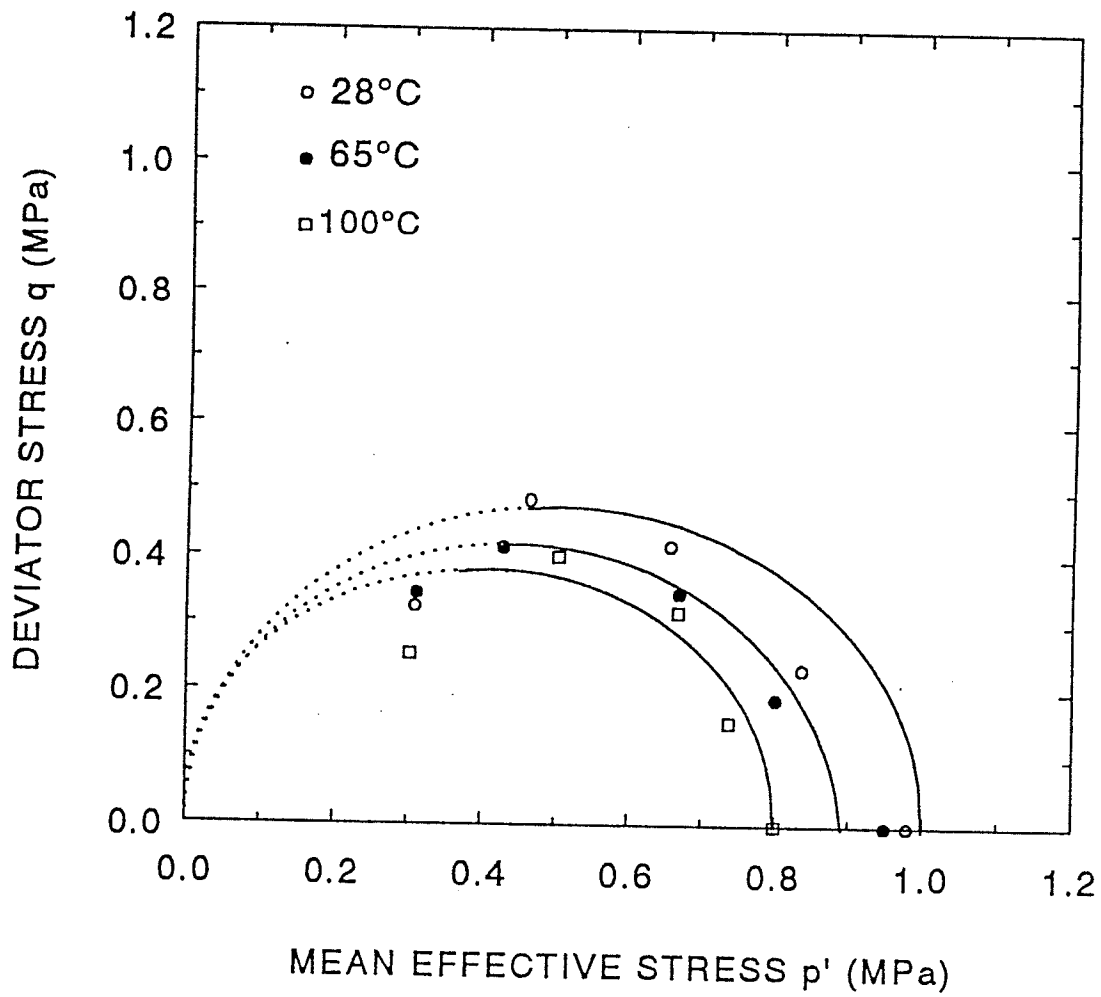
Figure 7.9   Yield loci at 28°C, 65°C, and 100°C on reconstituted
             illite.
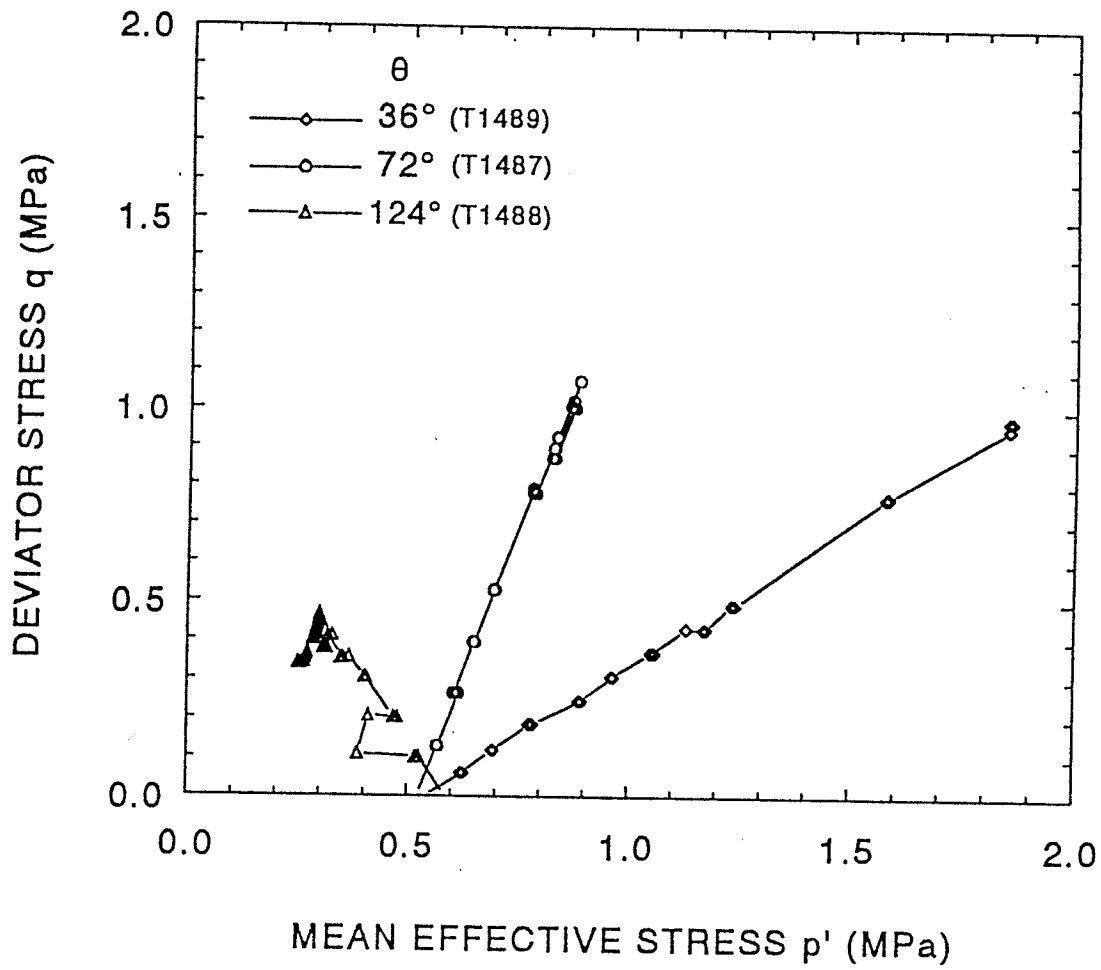
Figure 7.10 Stress paths for drained tests at 28°C for compacted
illite (p_o' = 0.5 MPa, p_o'/p_i' = 2)
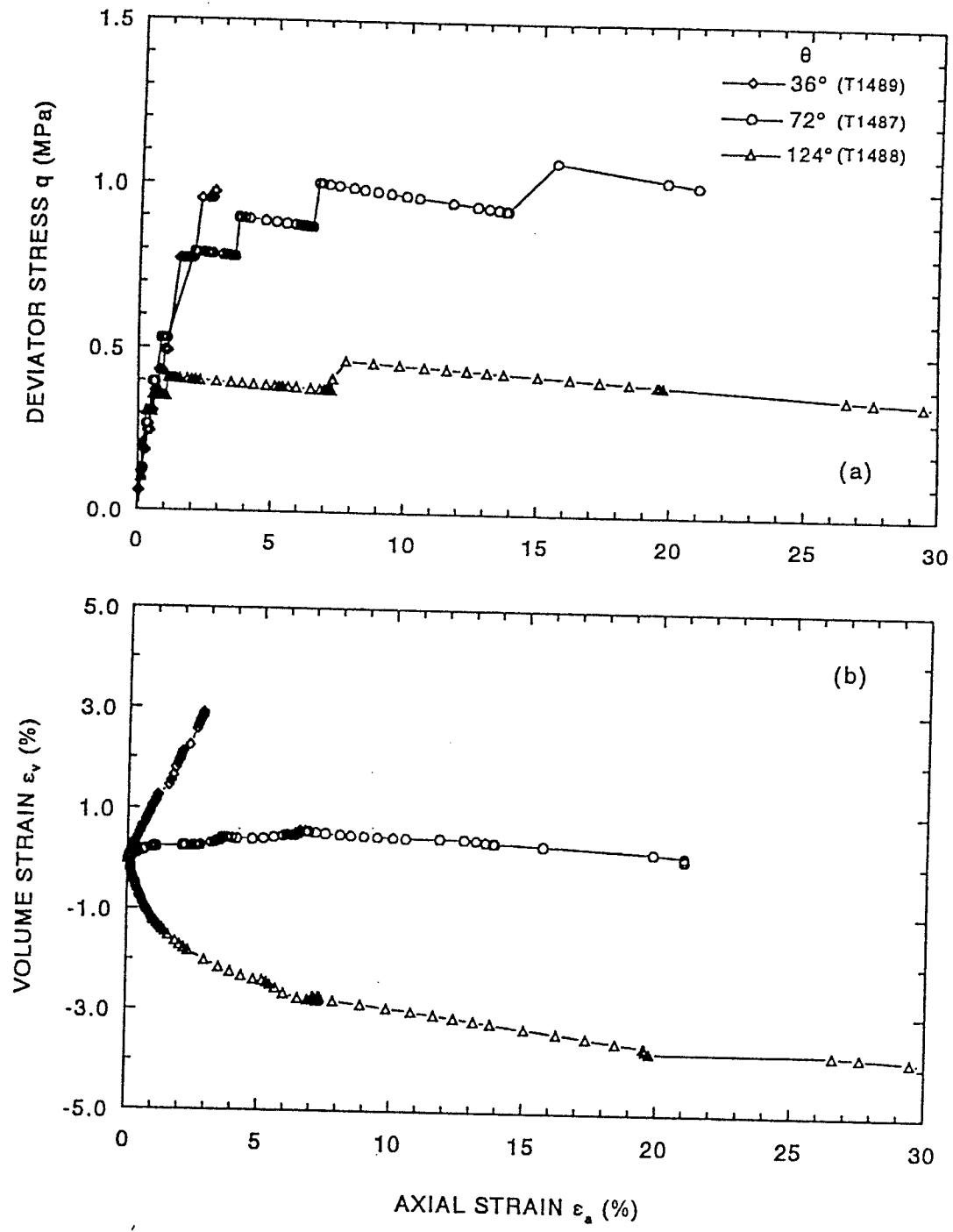
Figure 7.11 Stress-strain relationships in drained stress path tests on compacted illite at 28°C. (a) Deviator stress *vs*. axial strain. (b) Volumetric strain *vs*. axial strain.
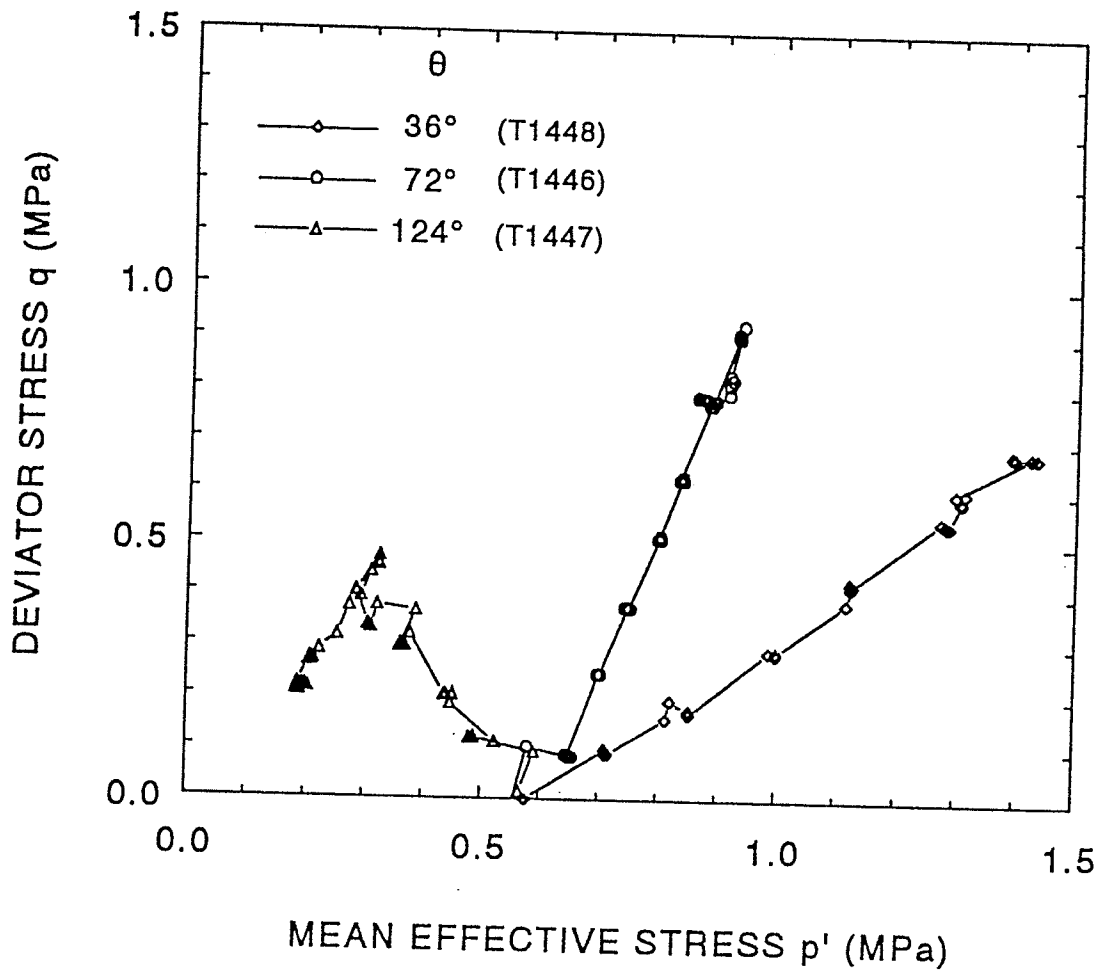
Figure 7.12 Stress paths for drained tests at 65°C for compacted illite ($p'_o = 0.5$ MPa, $p'_o/p'_i = 2$)
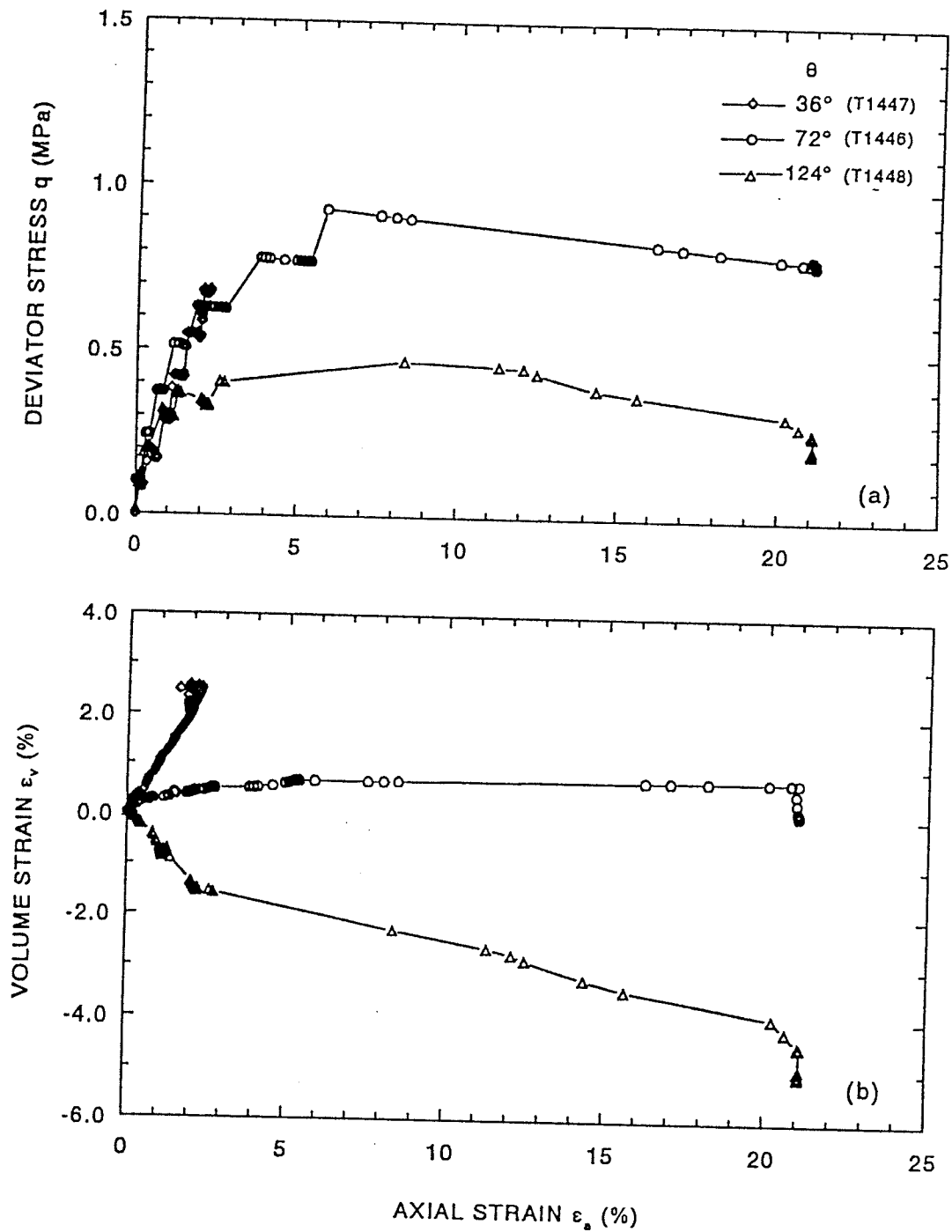
Figure 7.13 Stress-strain relationships in drained stress path tests on compacted illite at 65°C. (a) Deviator stress *vs*. axial strain. (b) Volumetric strain *vs*. axial strain.
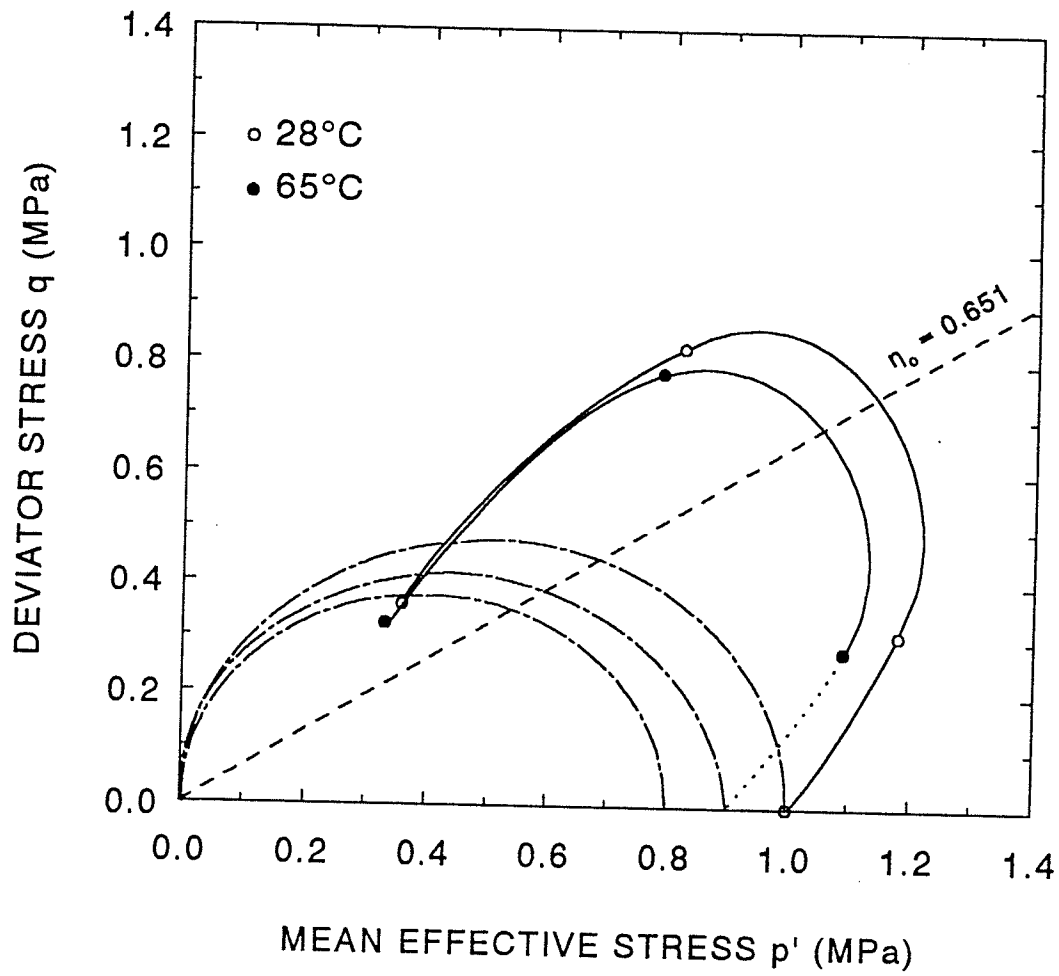
Figure 7.14   Yield loci at 28°C, and 65°C on compacted illite.
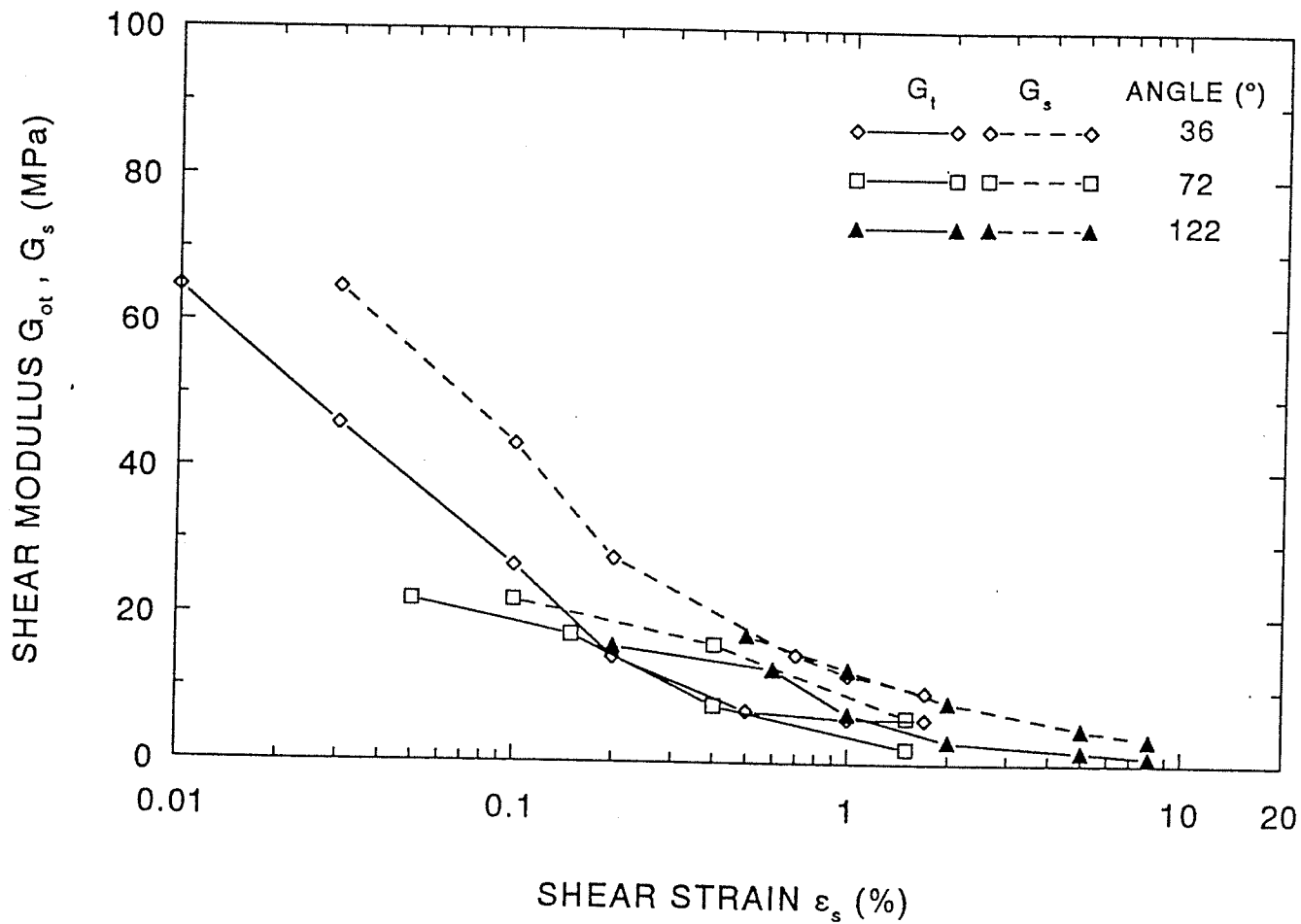
Figure 7.15 Tangent and secant moduli *vs.* shear strain. Reconstituted illite at 28°C.
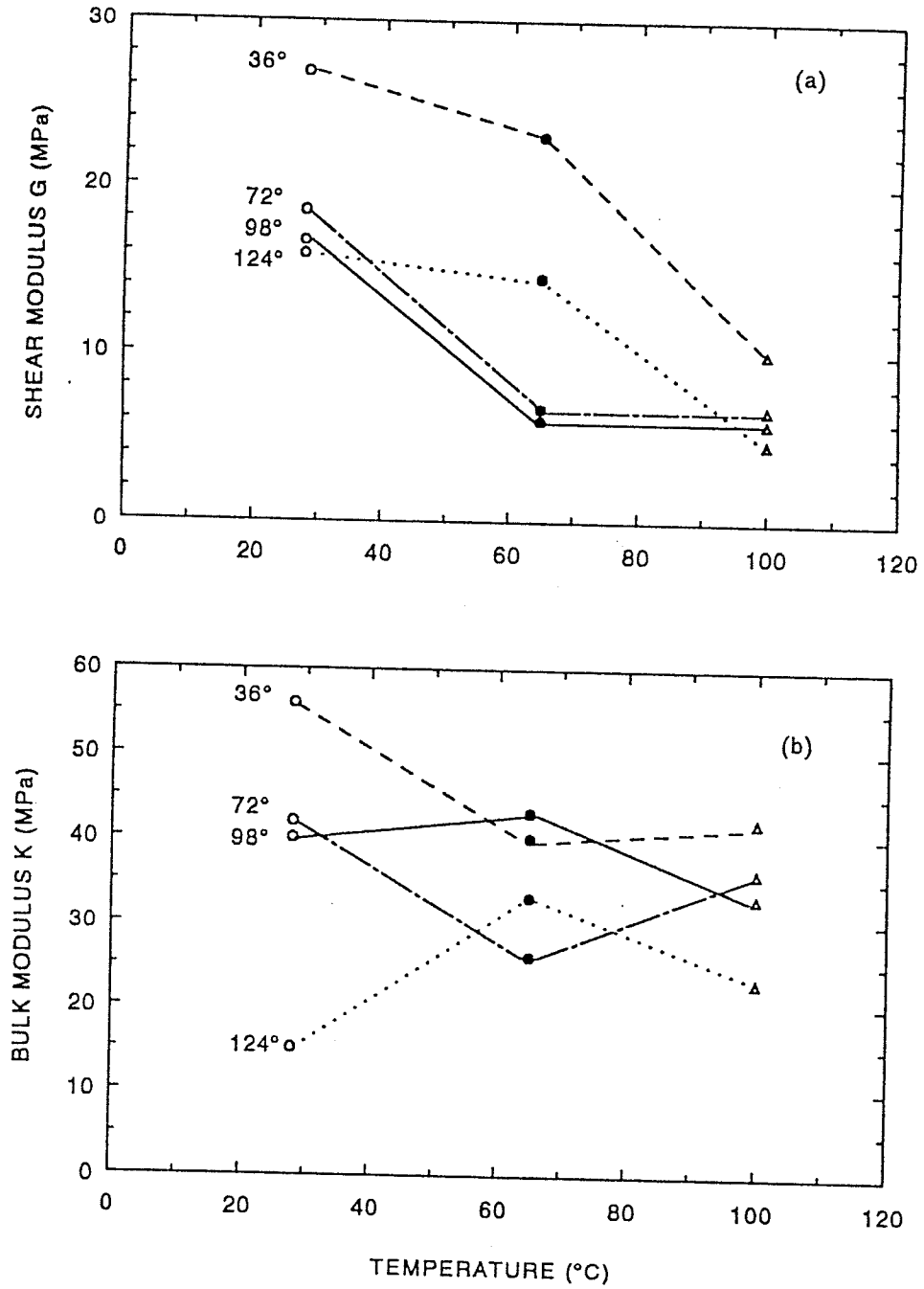
Figure 7.16 Elastic properties of reconstituted illite at 28°C, 65°C, and 100°C. (a) Shear modulus *vs*. temperature. (b) Bulk modulus *vs*. temperature.
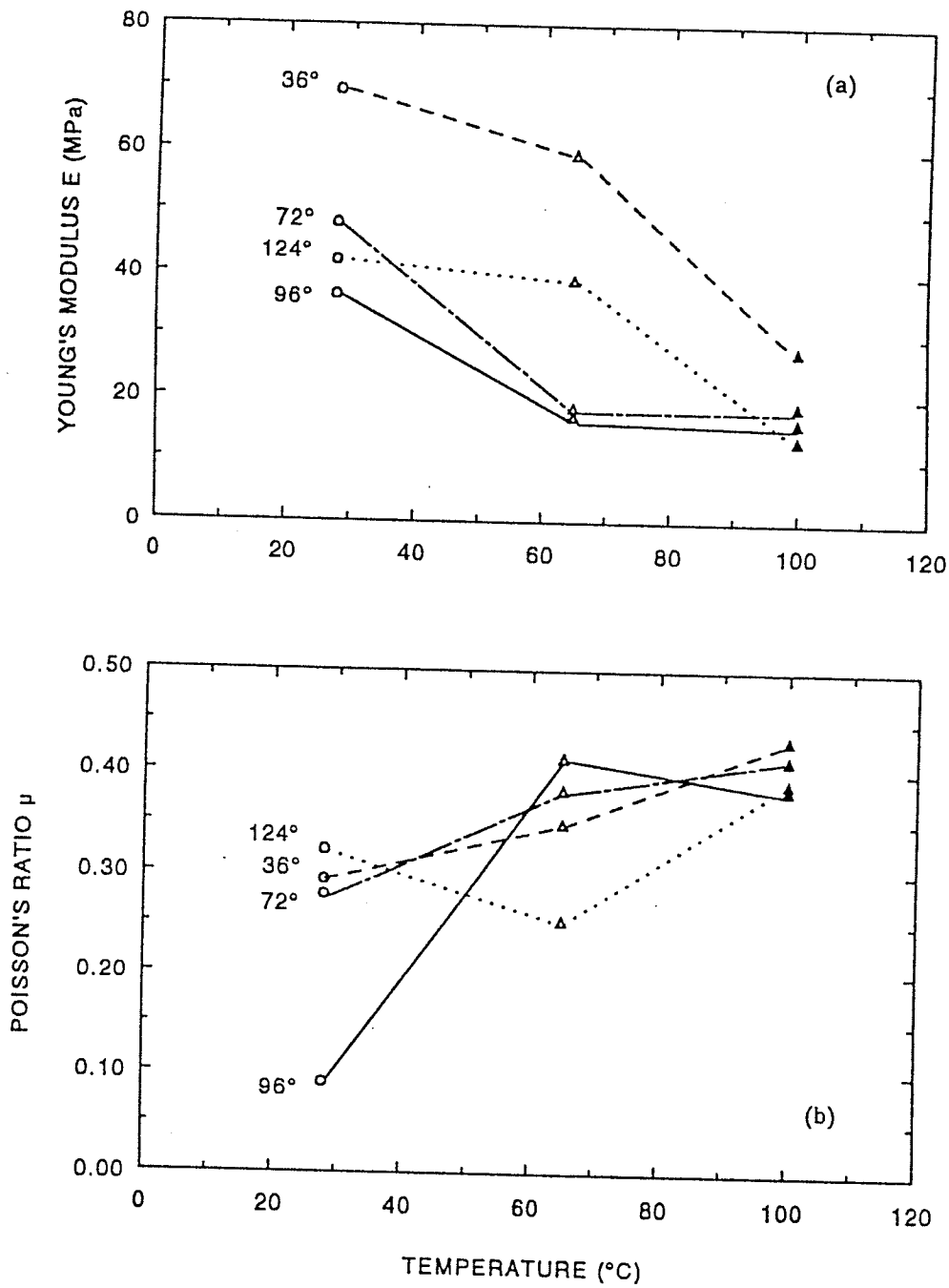
Figure 7.17 Elastic properties of reconstituted illite at 28°C, 65°C, and 100°C. (a) Young's modulus *vs.* temperature. (b) Poisson's ratio *vs.* temperature.
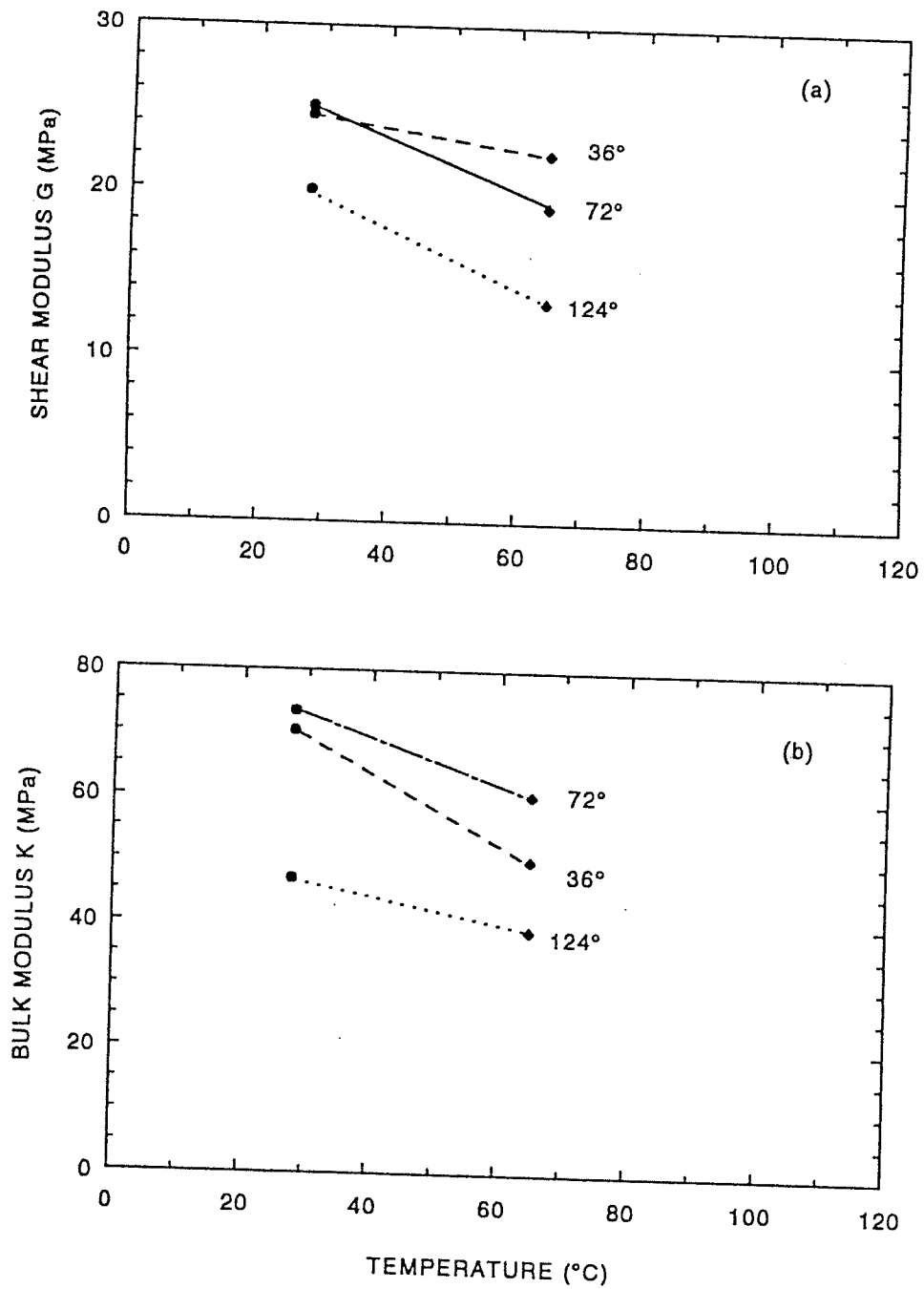
Figure 7.18 Elastic properties of compacted illite at 28°C and 65°C. (a) Shear modulus *vs.* temperature. (b) Bulk modulus *vs.* temperature.
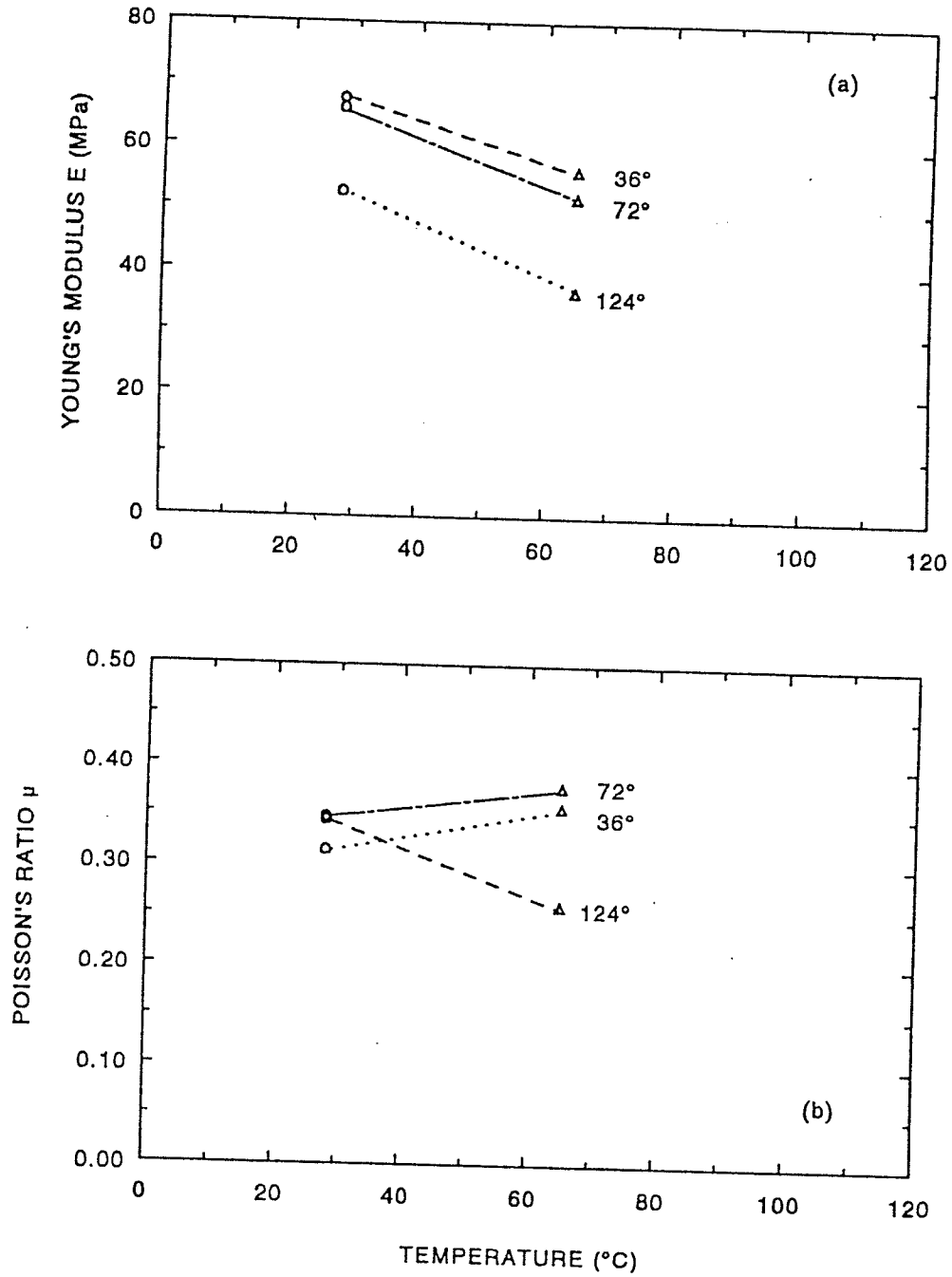
Figure 7.19   Elastic properties of compacted illite at 28°C and 65°C. (a) Young's modulus *vs.* temperature. (b) Poisson's ratio *vs.* temperature.
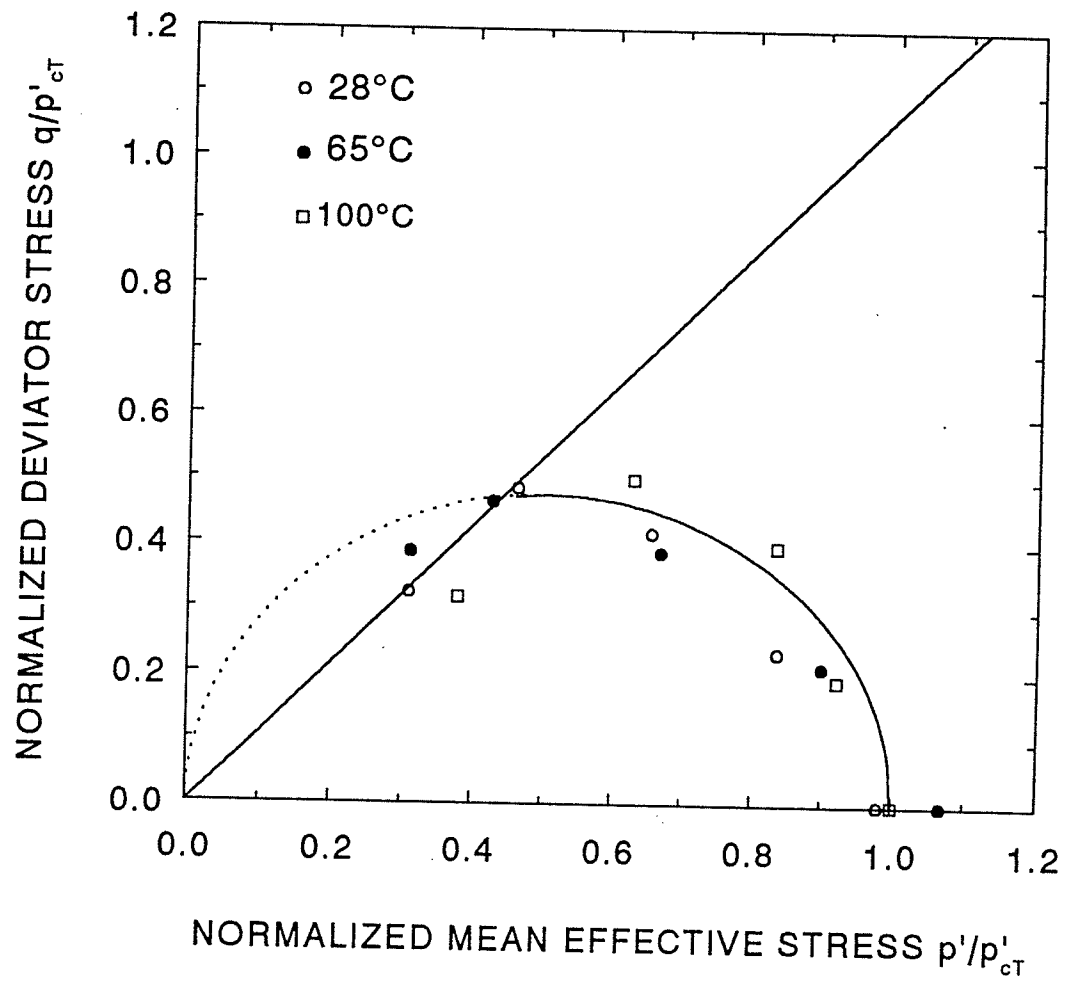
Figure 7.20 Normalized yield loci of reconstituted illite at
28°C, 65°C, and 100°C. Normalized pressure
p'_{cT} = isotropic yield pressure at temperature T.
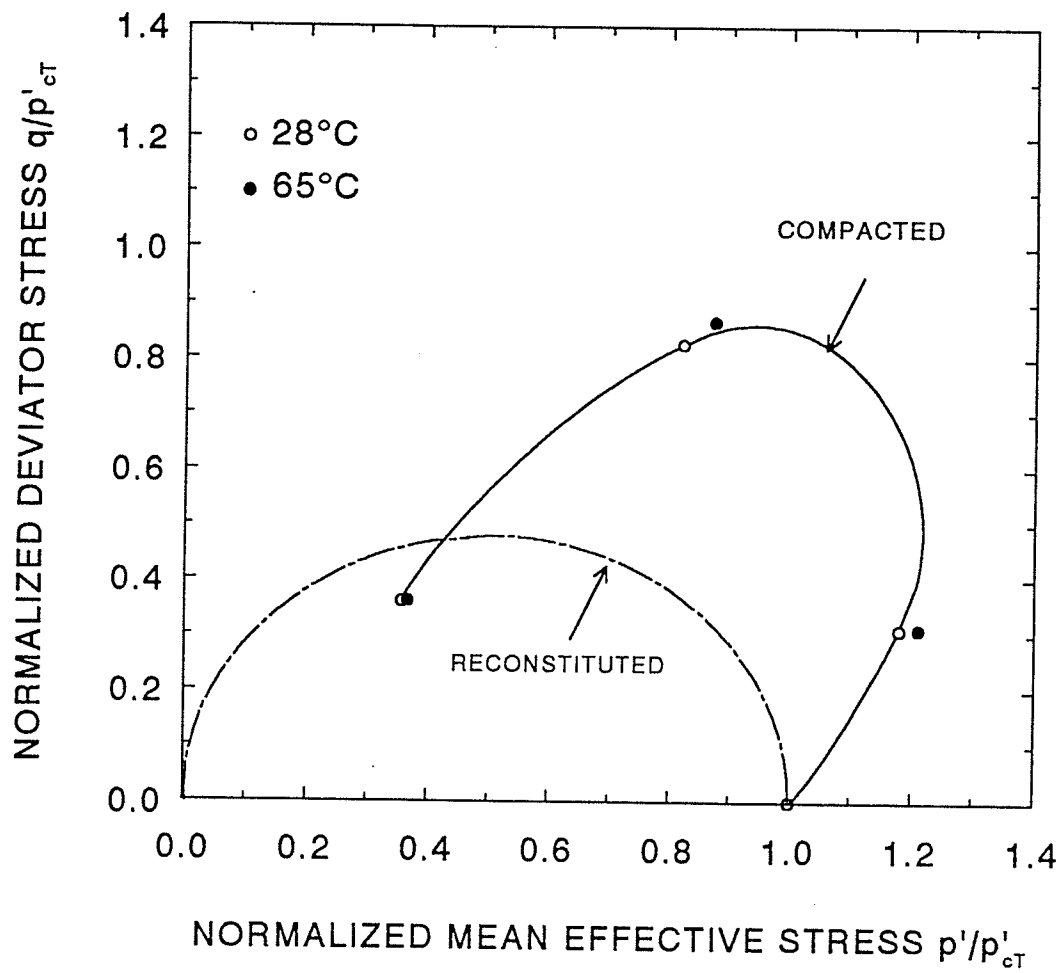
Figure 7.21 Normalized yield loci of compacted illite at 28°C and 65°C. Normalized pressure p'_{cT} = isotropic yield pressure at temperature T.
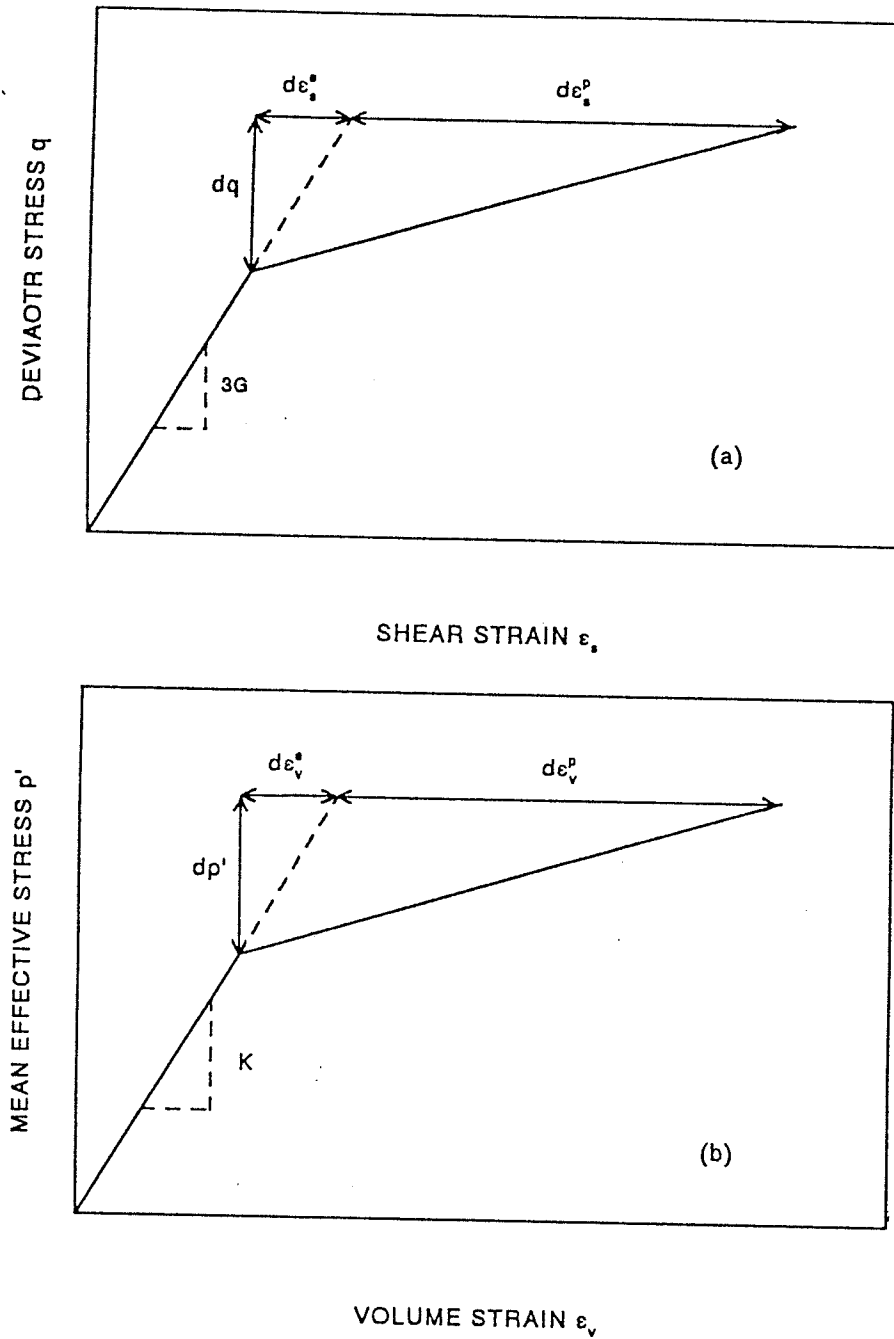
Figure 7.22 Descriptions of elastic and plastic components of strains.   (a) Shear strain components.   (b) Volumetric strain components.
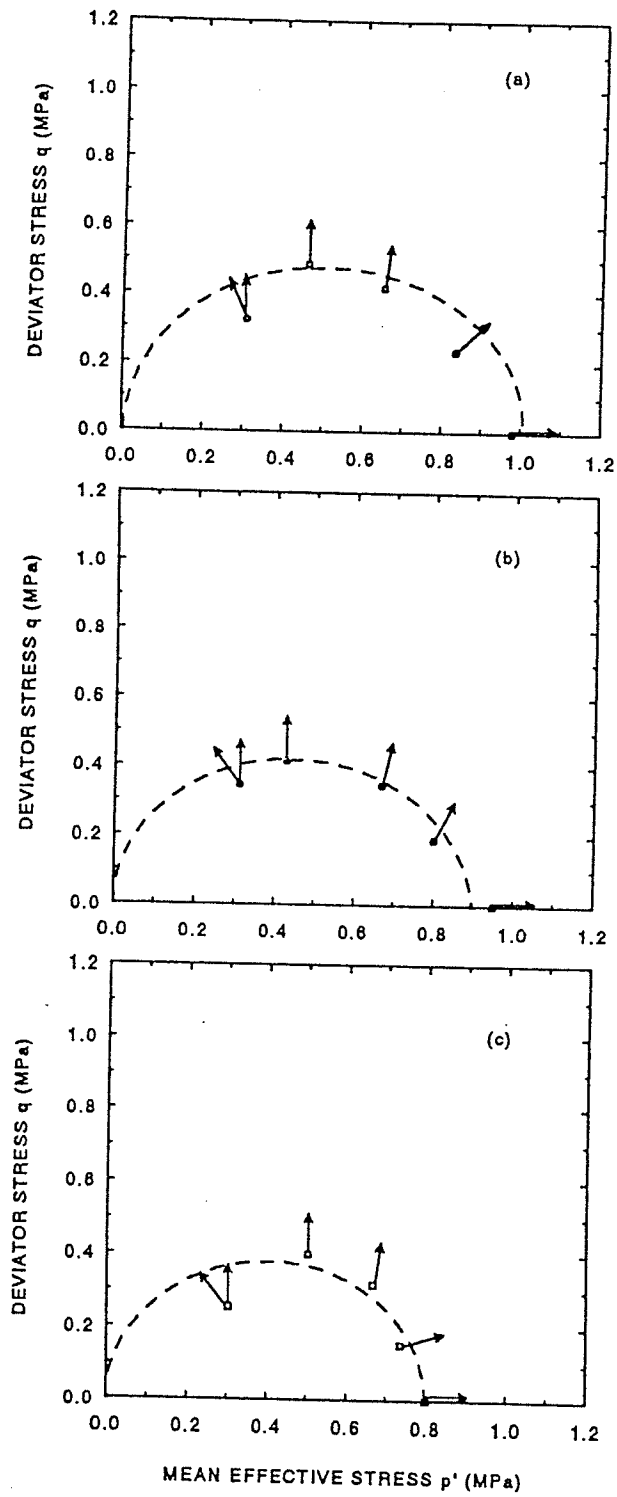
Figure 7.23 Plastic potentials of reconstituted illite. (a) 28°C. (b) 65°C. (c) 100°C.
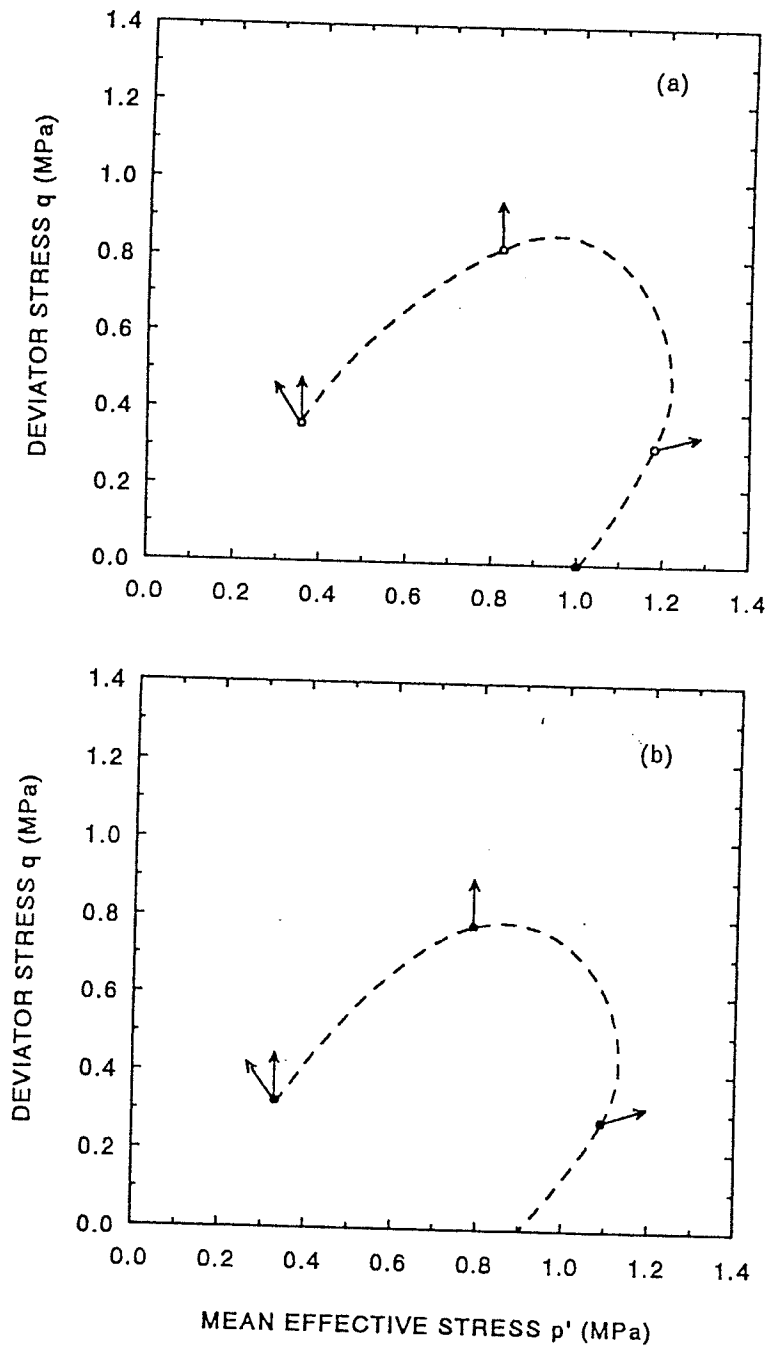
Figure 7.24 Plastic potentials of compacted illite. (a) 28°C.
(b) 65°C.
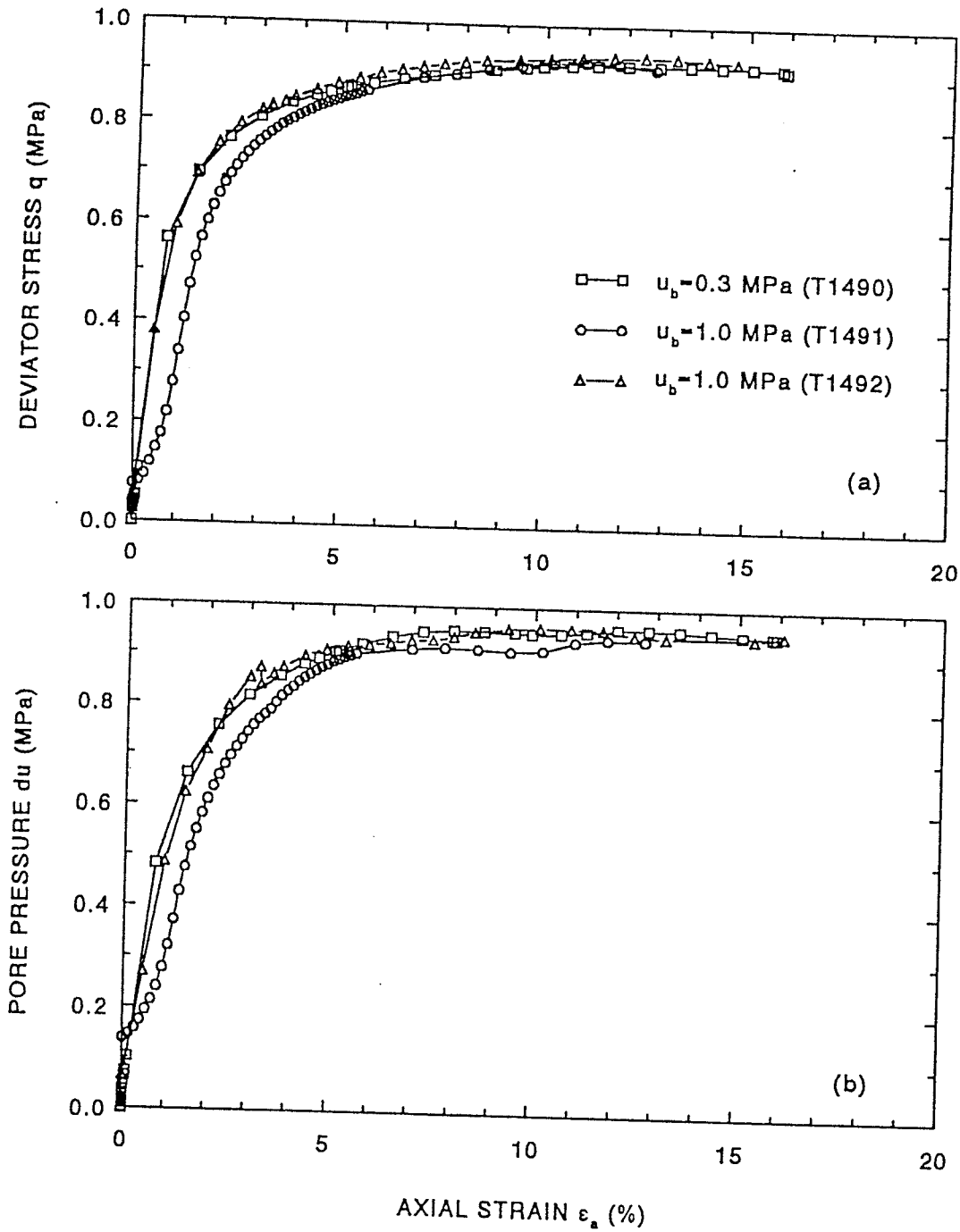
Figure 8.1 Effect of back pressure on stress-strain relationships
of normally consolidated reconstituted illite at 28°C.
(a) Deviator stress *vs.* axial strain.   (b) Pore
pressure *vs.* axial strain.
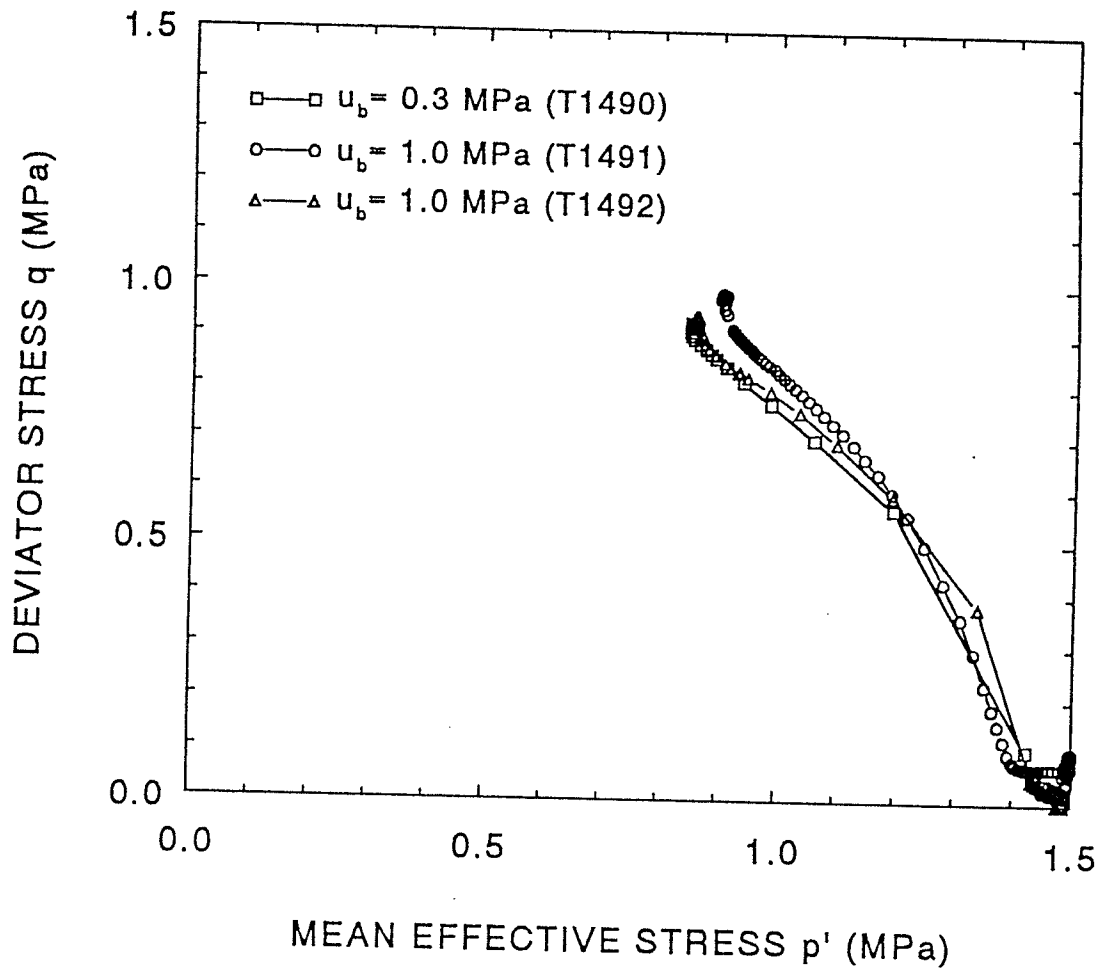
Figure 8.2 Effect of back pressure on stress paths of normally consolidated reconstituted illite at 28°C.
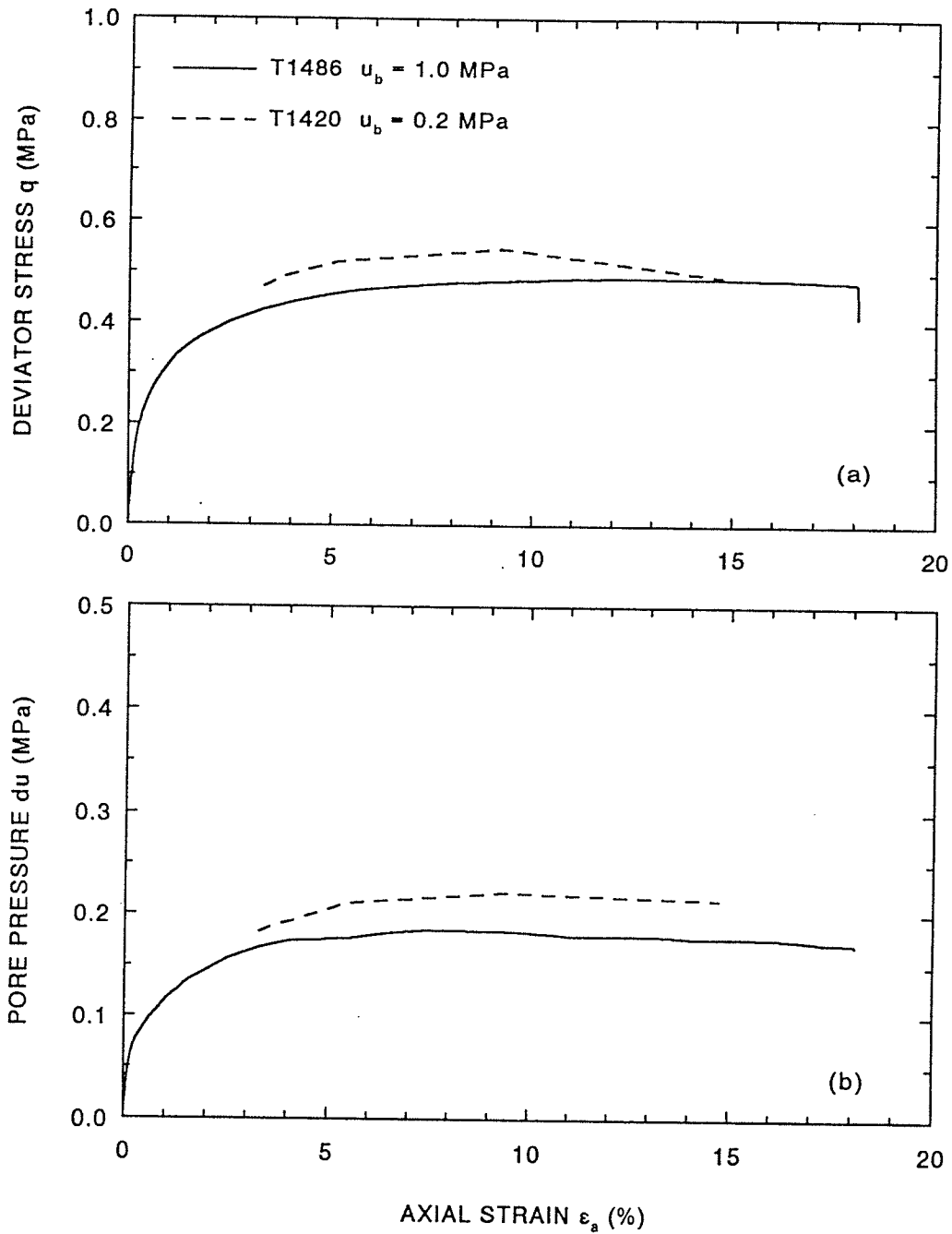
Figure 8.3 Effect of back pressure on stress-strain relationships of overconsolidated reconstituted illite at 28°C. (a) Deviator stress *vs.* axial strain. (b) Pore pressure *vs.* axial strain.
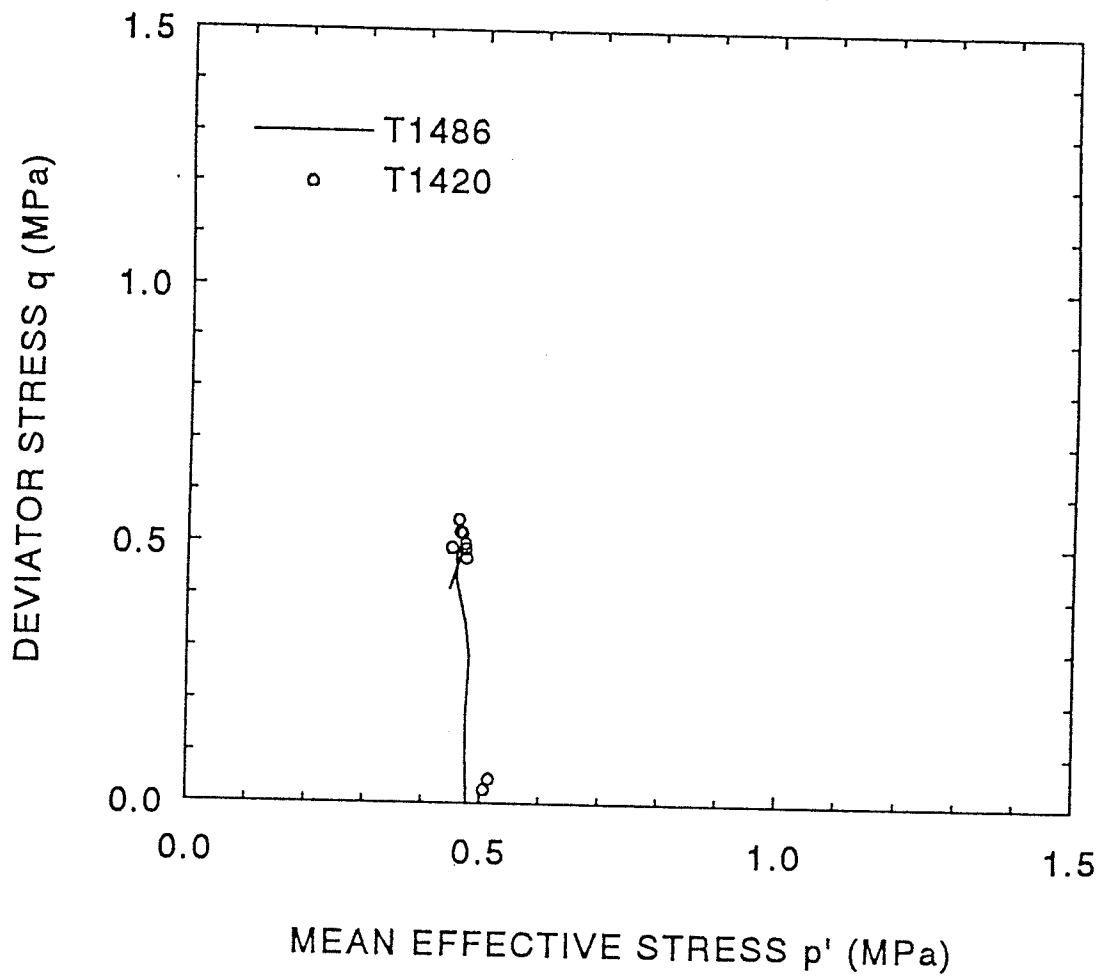
Figure 8.4 Effect of back pressure on stress paths of overconsolidated reconstituted illite at 28°C.
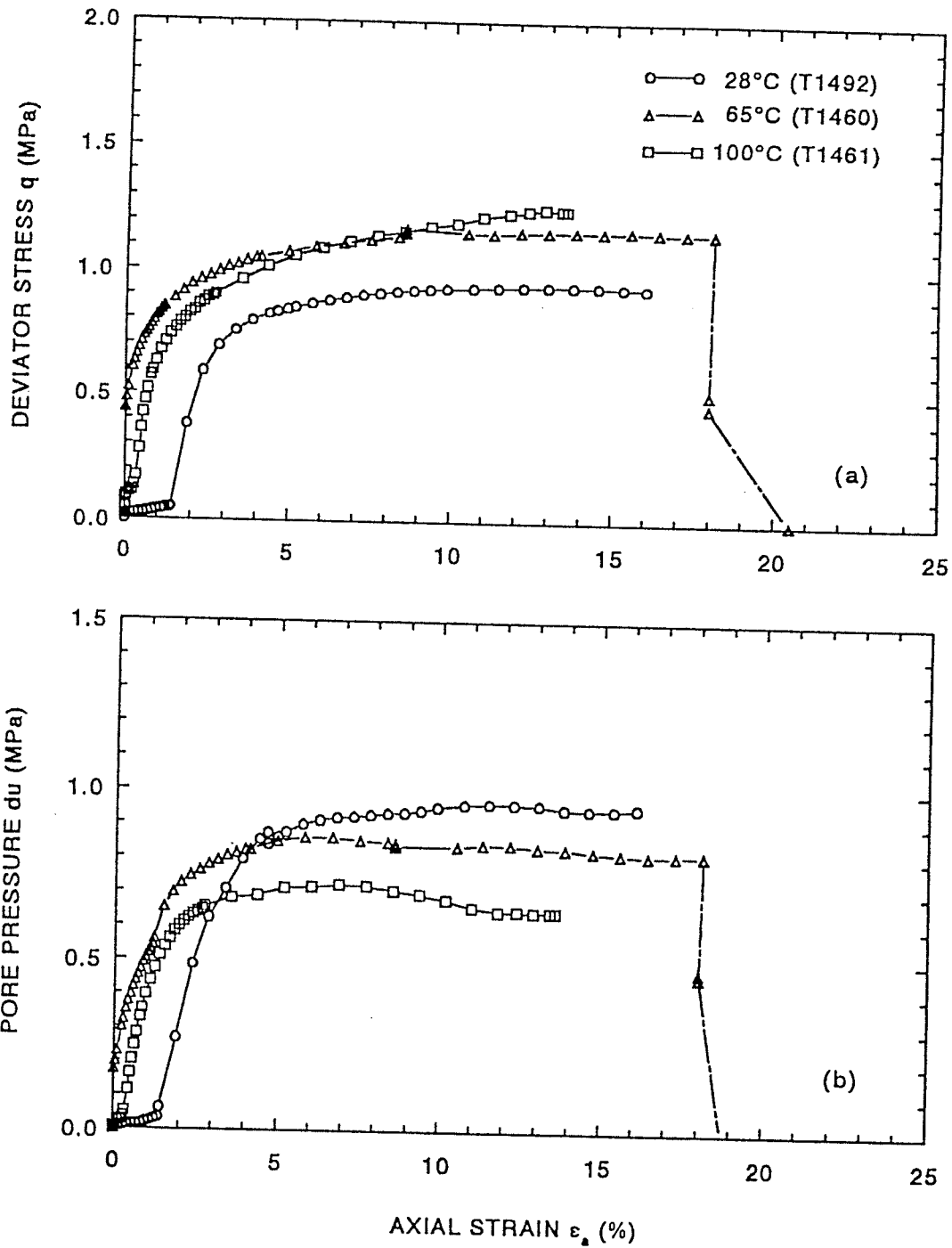
Figure 8.5 Effect of elevated temperature on stress-strain relationships of normally consolidated reconstituted illite. (a) Deviator stress *vs*. axial strain. (b) Volumetric strain *vs*. axial strain.
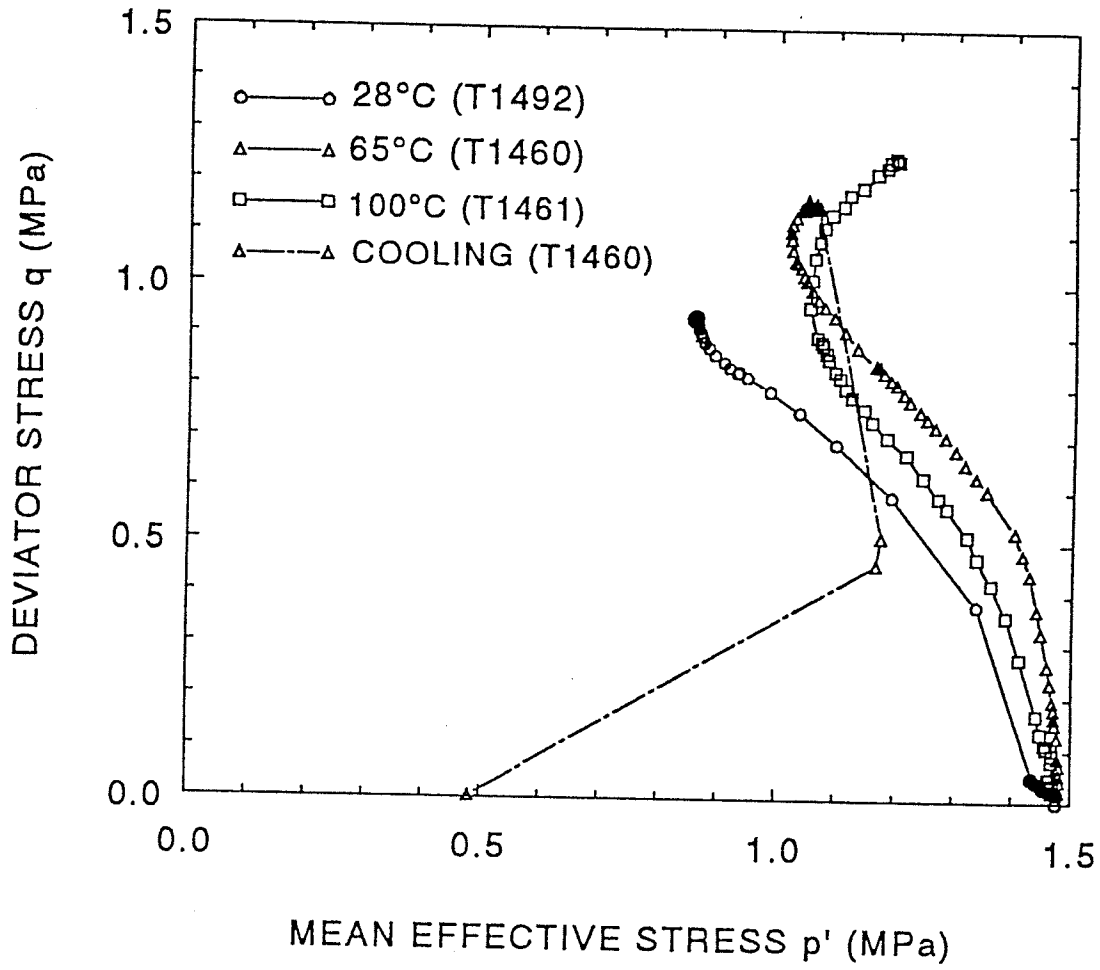
Figure 8.6 Effect of elevated temperature on stress paths of normally consolidated reconstituted illite.
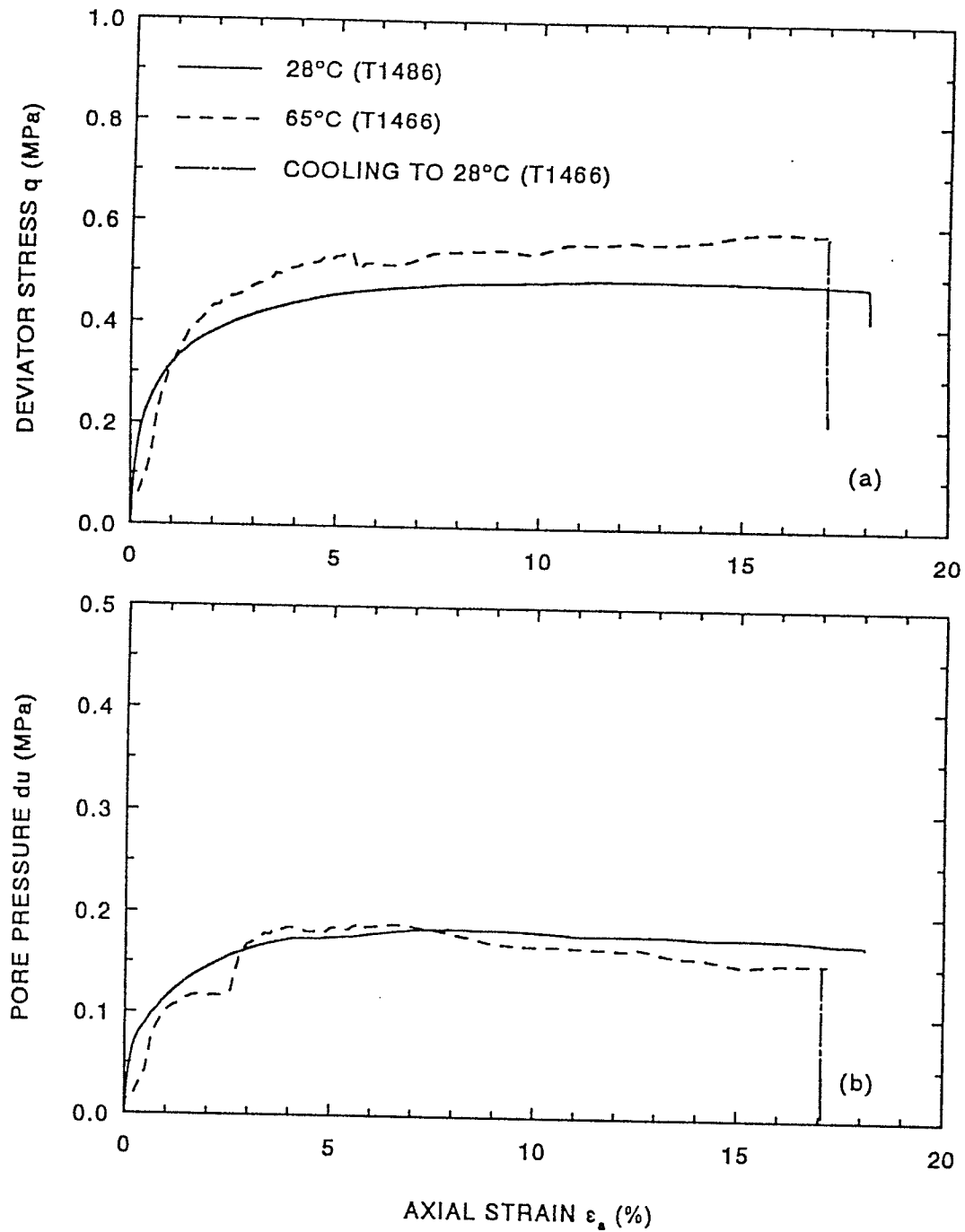
Figure 8.7 Effect of elevated temperature on stress-strain relationships of overconsolidated reconstituted illite. (a) Deviator stress *vs*. axial strain. (b) Volumetric strain *vs*. axial strain.
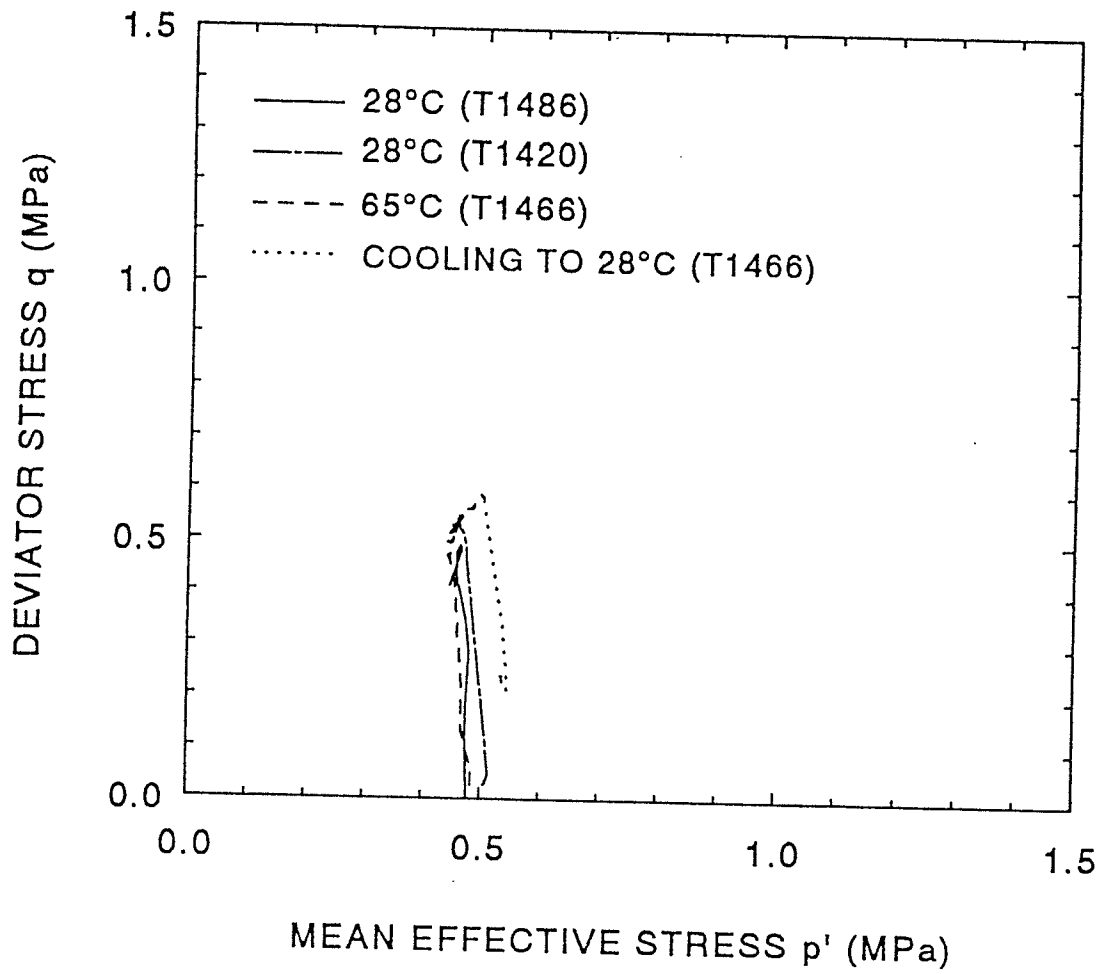
Figure 8.8 Effect of elevated temperature on stress paths of overconsolidated reconstituted illite.
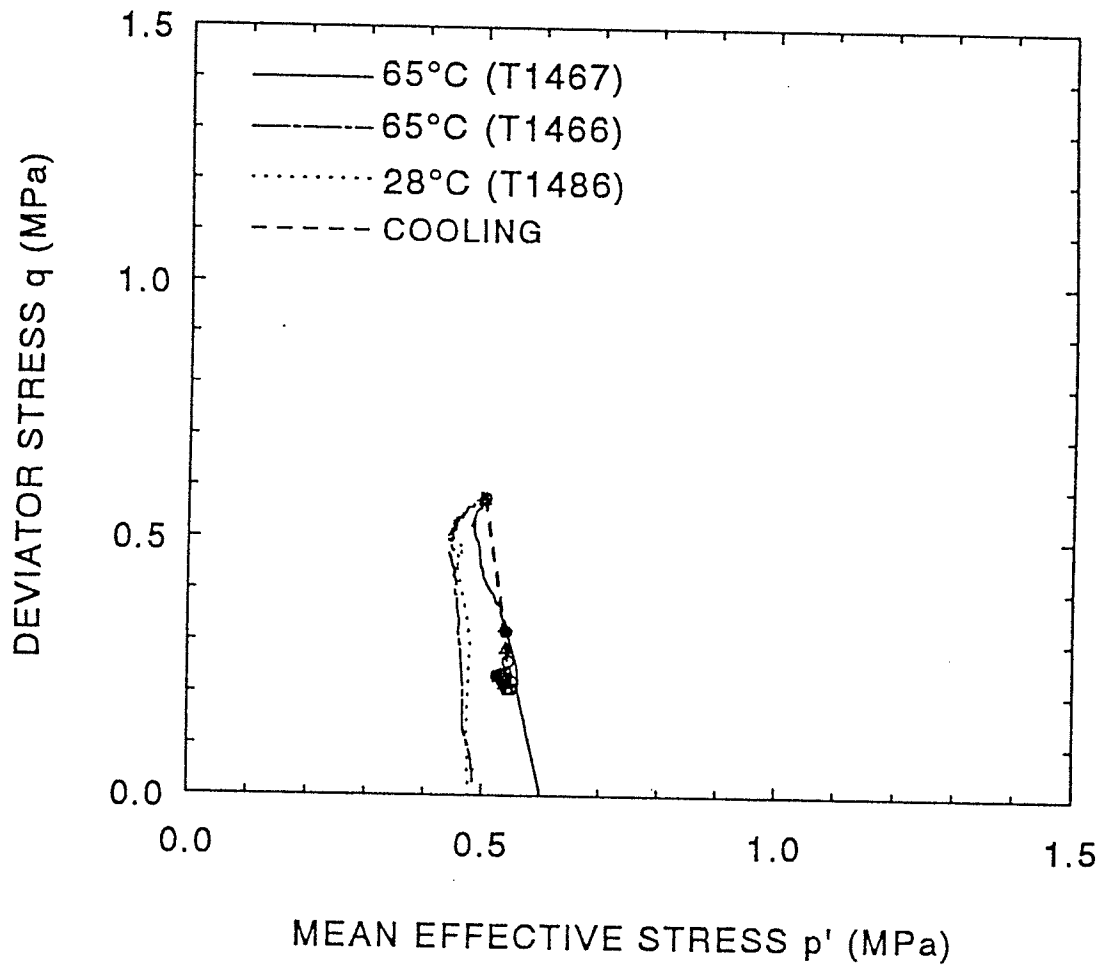
Figure 8.9 Effect of undrained heating in consolidation phase on stress paths of reconstituted illite.
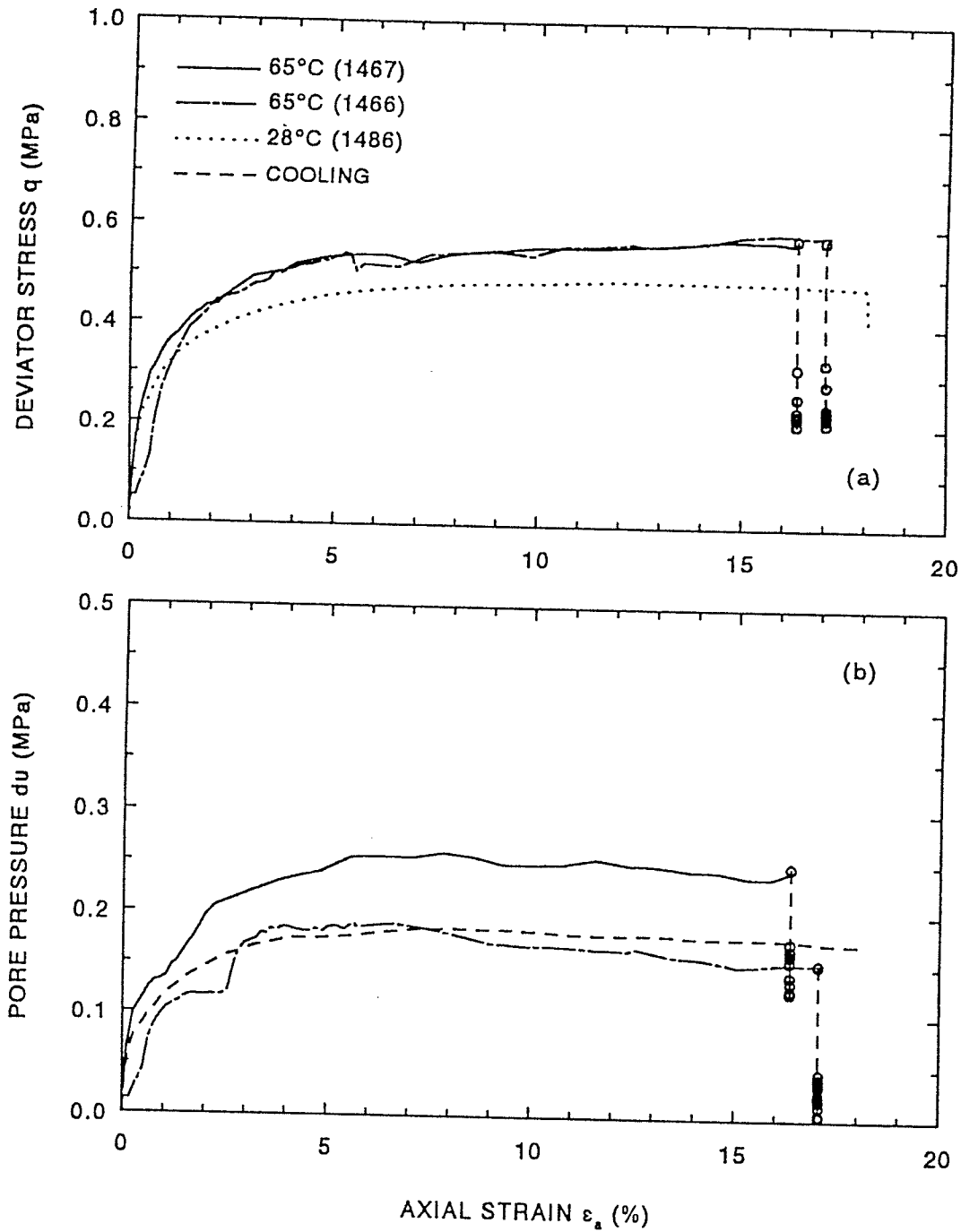
Figure 8.10 Effect of undrained heating in consolidation phase on stress-strain relationships of reconstituted illite. (a) Deviator stress *vs*. axial strain. (b) Volumetric strain *vs*. axial strain.
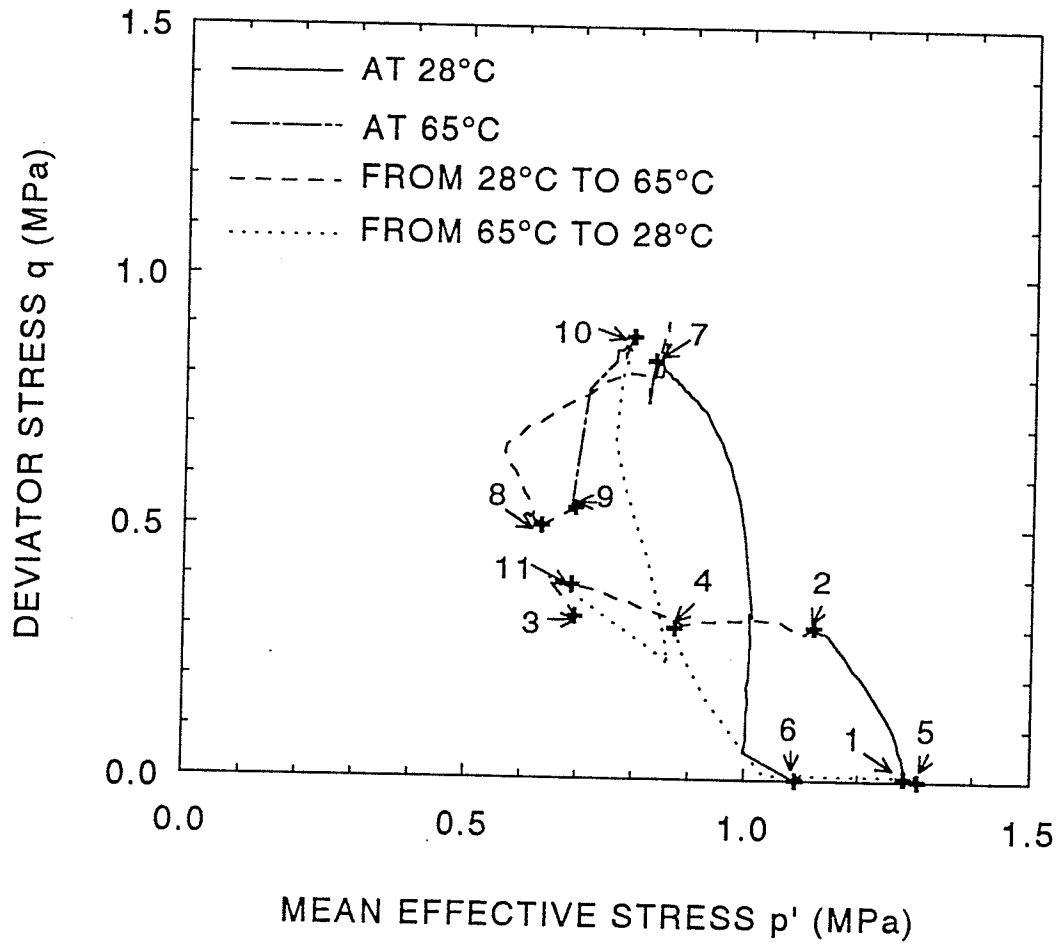
Figure 8.11 Stress paths for undrained heating (28°C to 65°C) test (T1464) on normally consolidated reconstituted illite under q = 0.3 MPa.
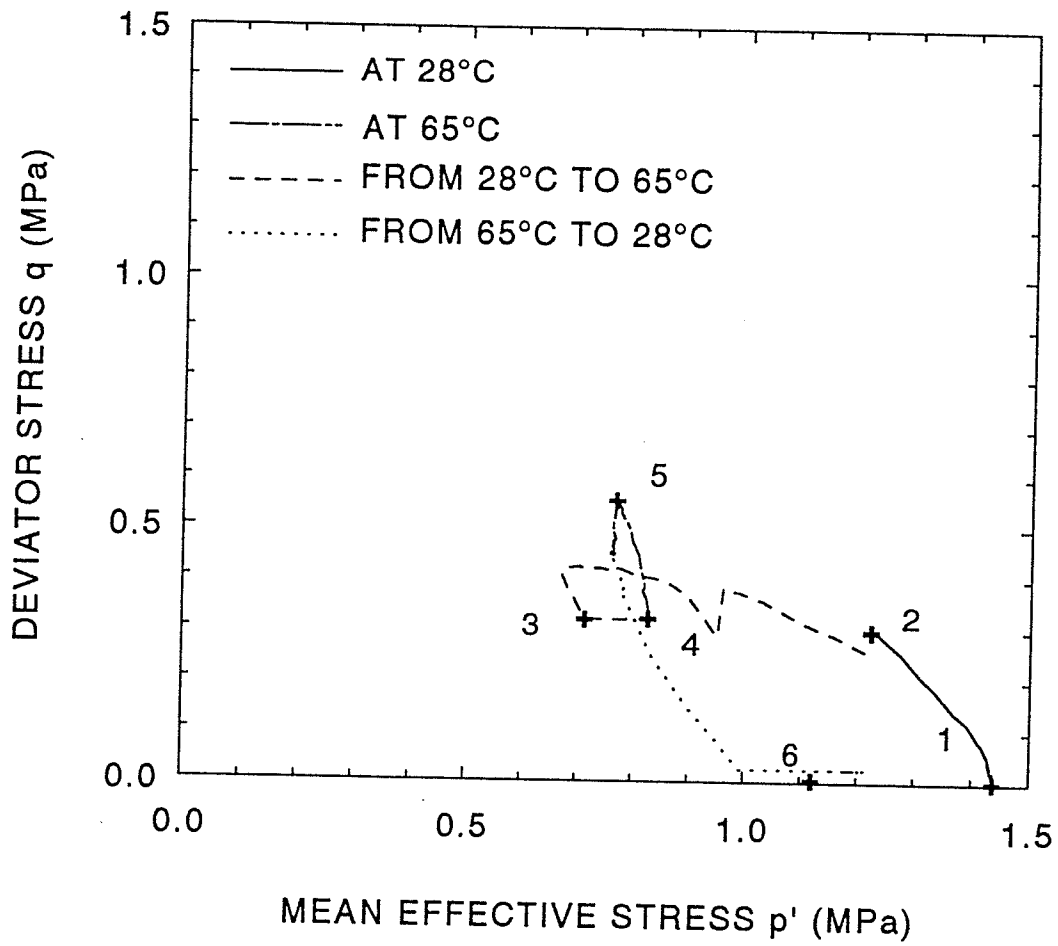
Figure 8.12   Stress path for undrained heating (28°C to 65°C) test
(T1468) on normally consolidated reconstituted illite
under q = 0.3 MPa.
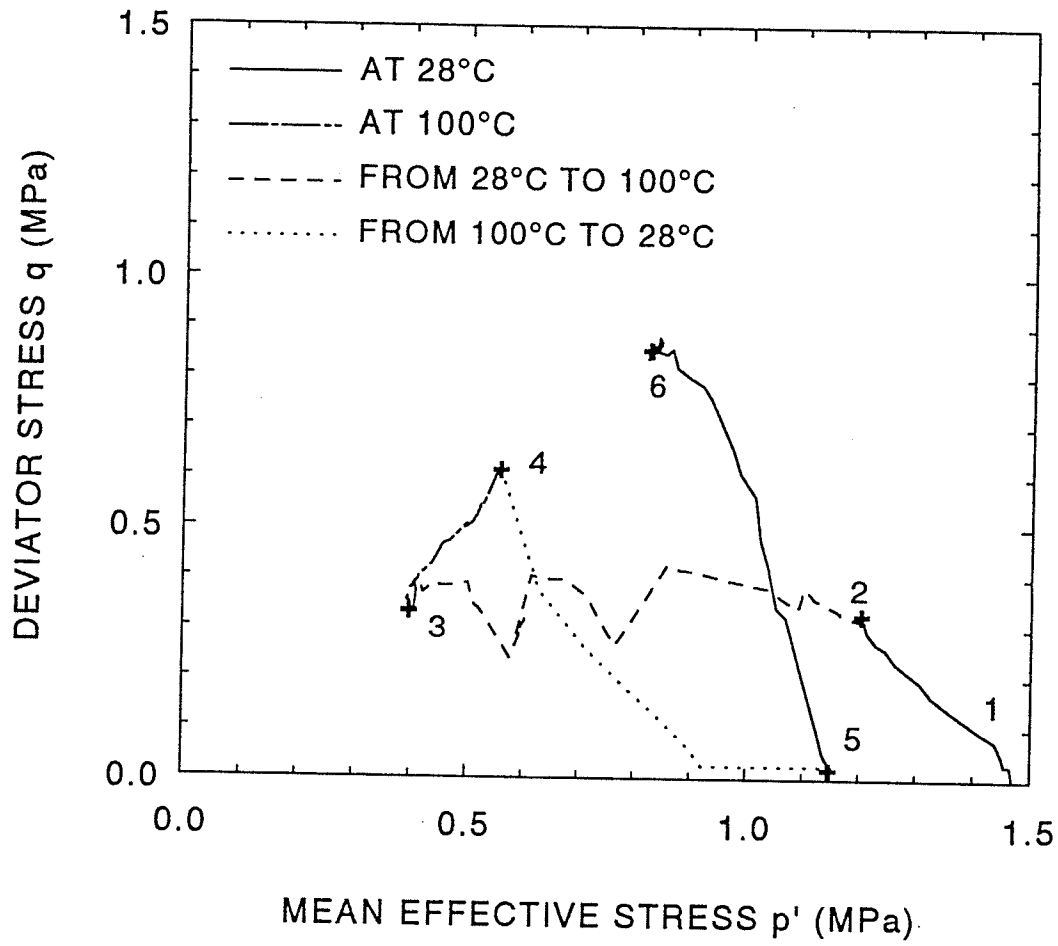
Figure 8.13 Stress paths for undrained heating (28°C to 100°C) test (T1472) on normally consolidated reconstituted illite under q = 0.3 MPa.
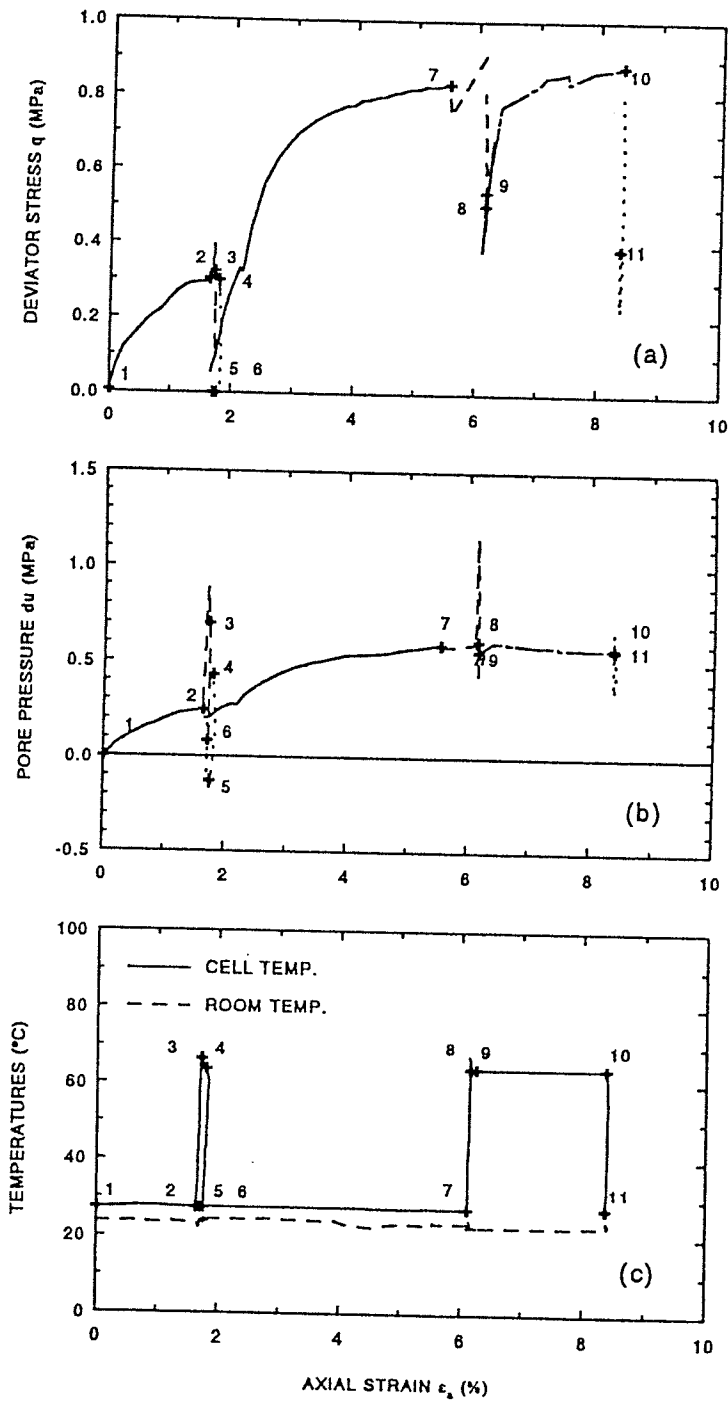
Figure 8.14 Stress-strain relationships in undrained heating (28°C to 65°C) test (T1464) on normally consolidated reconstituted illite. (a) Deviator stress *vs.* axial strain. (b) Pore pressure *vs.* axial strain. (c) Temperature *vs.* axial strain.
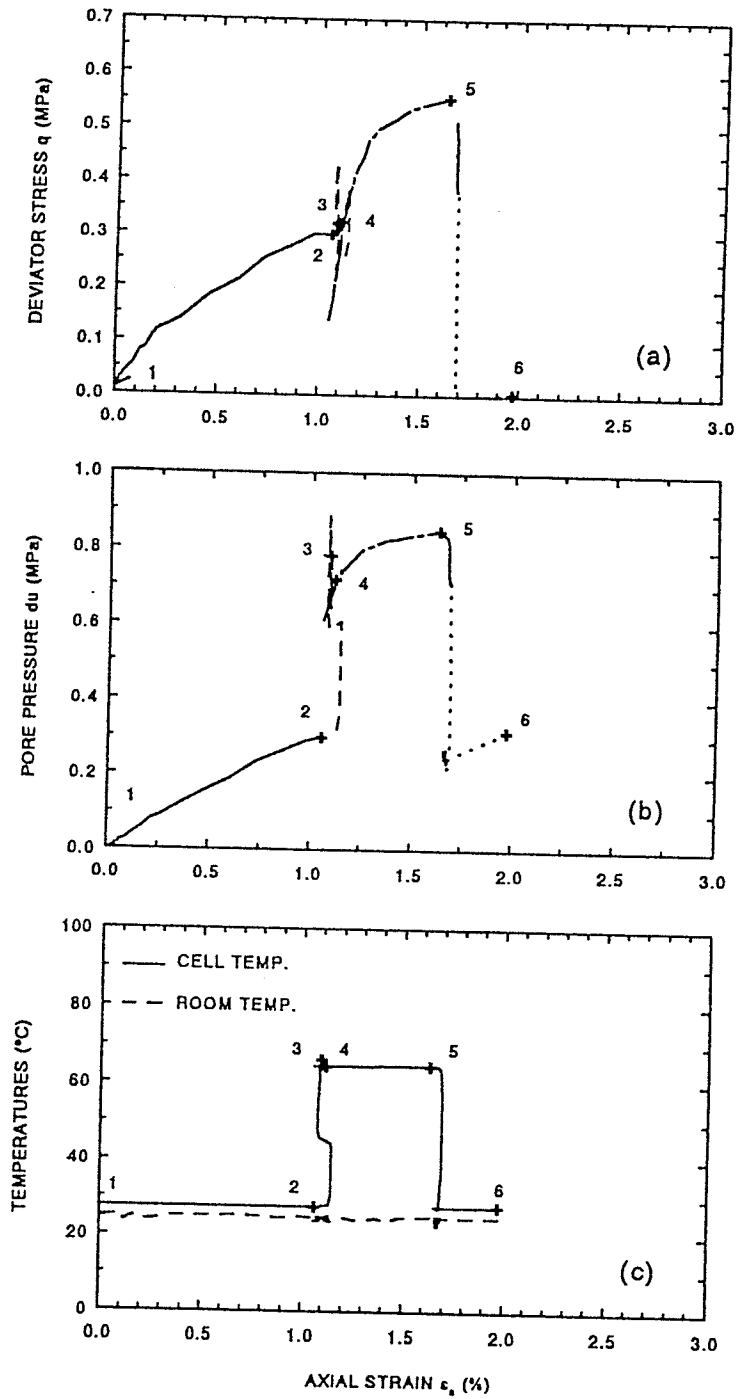
Figure 8.15   Stress-strain relationships in undrained heating
(28°C to 65°C) test (T1468) on normally consolidated
reconstituted illite.   (a) Deviator stress *vs.* axial
strain.   (b) Pore pressure *vs.* axial strain.   (c)
Temperature *vs.* axial strain.
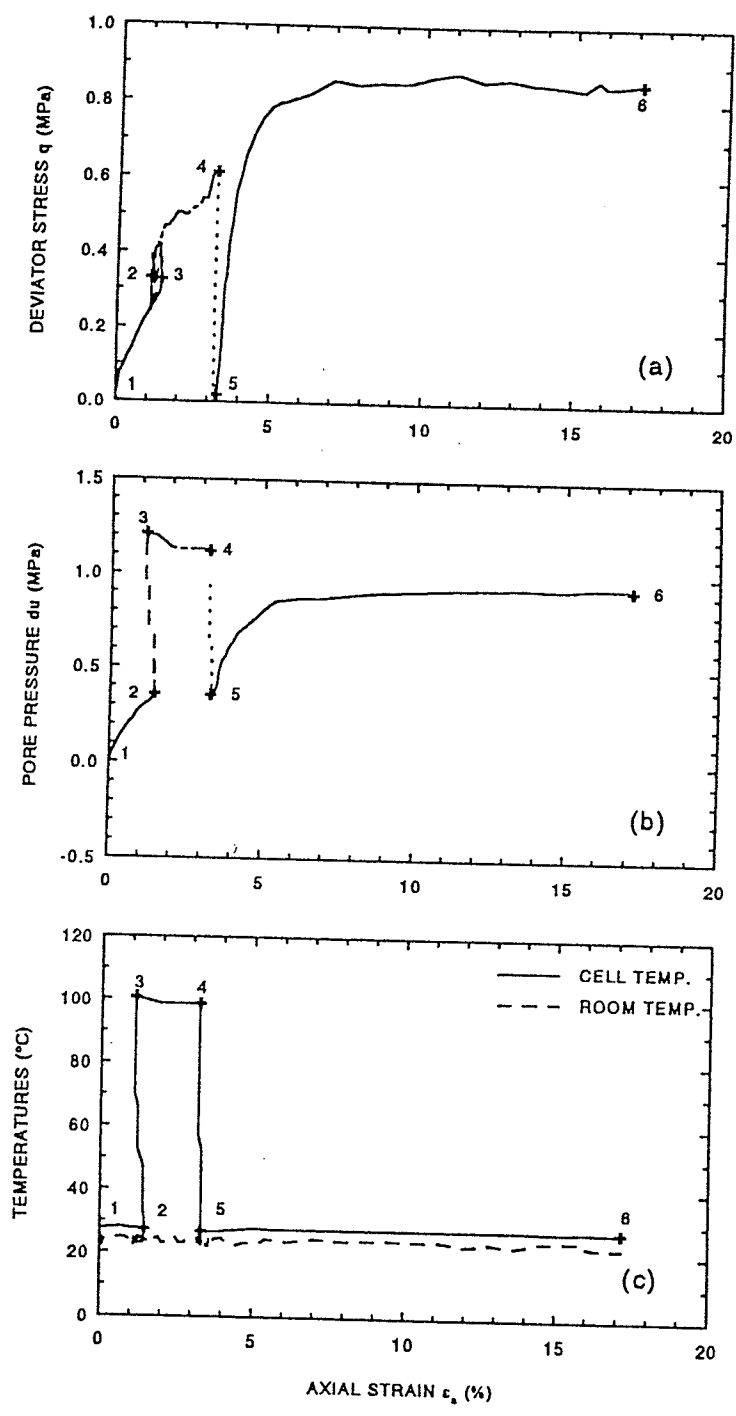
Figure 8.16   Stress-strain relationships in undrained heating
(28°C to 100°C) test (T1472) on normally consolidated
reconstituted illite.   (a) Deviator stress *vs.* axial
strain.   (b) Pore pressure *vs.* axial strain.   (c)
Temperature *vs.* axial strain.
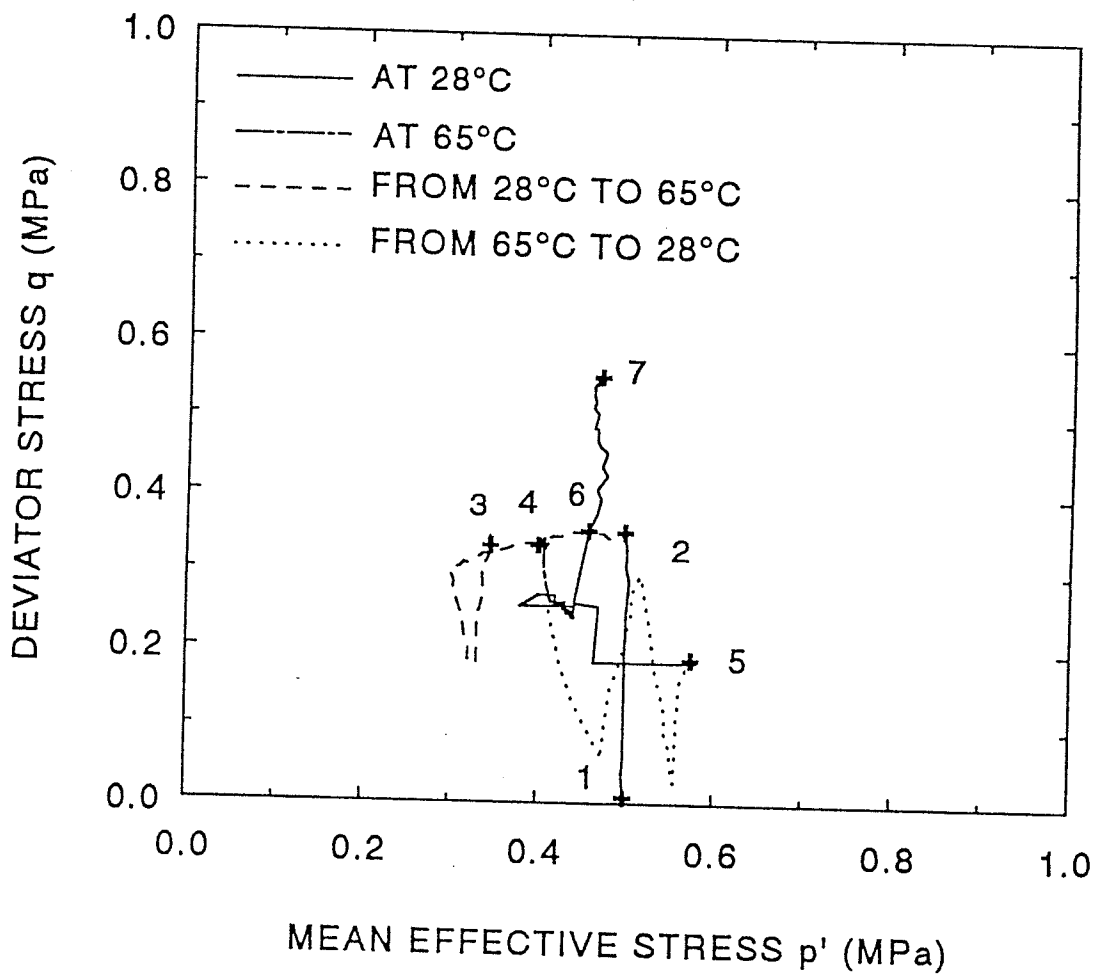
Figure 8.17 Stress paths for undrained heating (28°C to 65°C) test (T1465) on overconsolidated reconstituted illite q = 0.3 MPa.
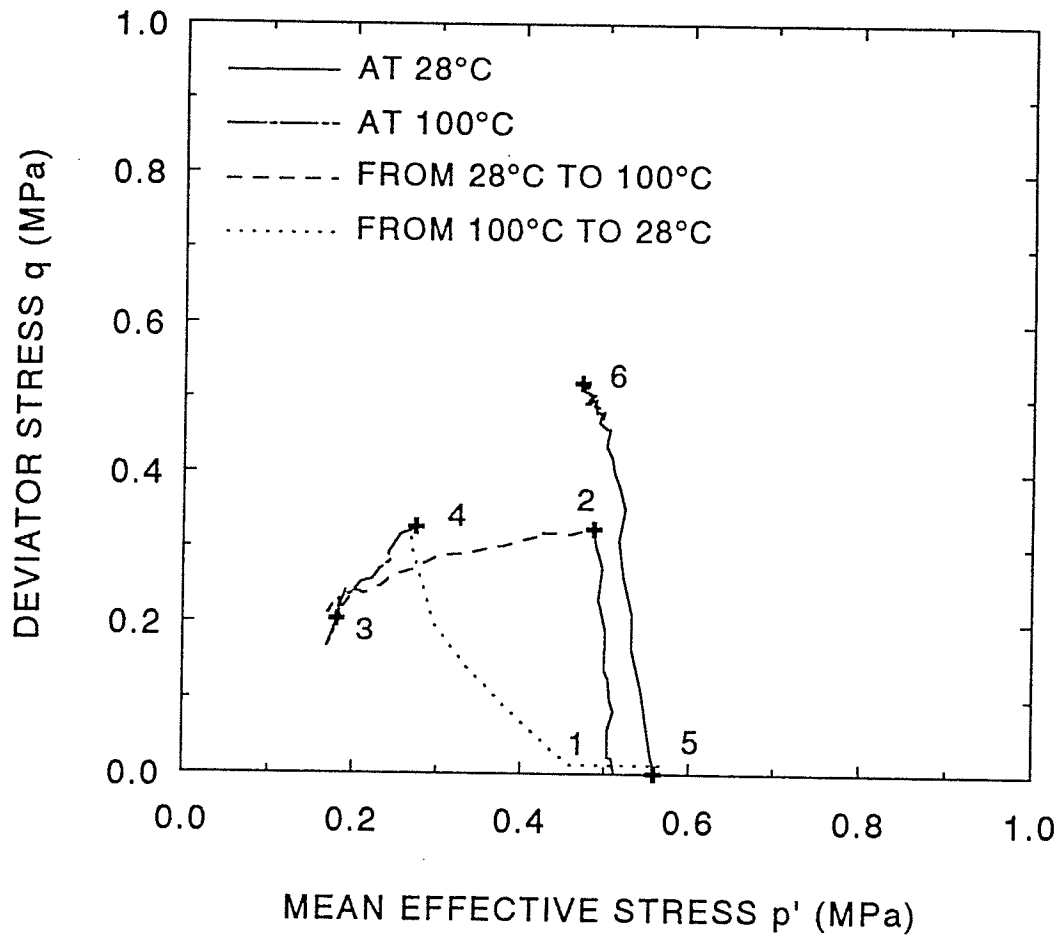
Figure 8.18 Stress paths for undrained heating (28°C to 100°C)
test (T1473) on overconsolidated reconstituted illite
under q = 0.3 MPa.
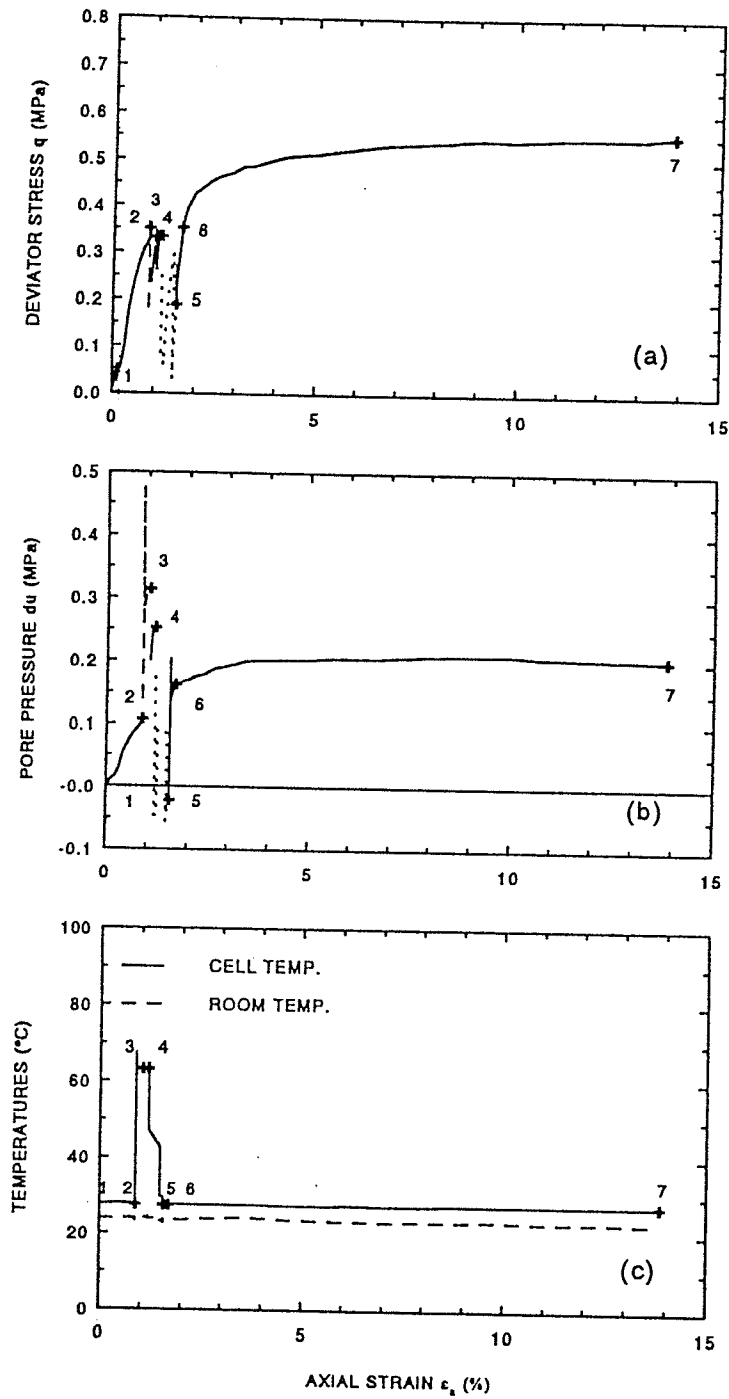
Figure 8.19 Stress-strain relationships in undrained heating (28°C to 65°C) test (T1465) on overconsolidated reconstituted illite. (a) Deviator stress *vs.* axial strain. (b) Pore pressure *vs.* axial strain. (c) Temperature *vs.* axial strain.
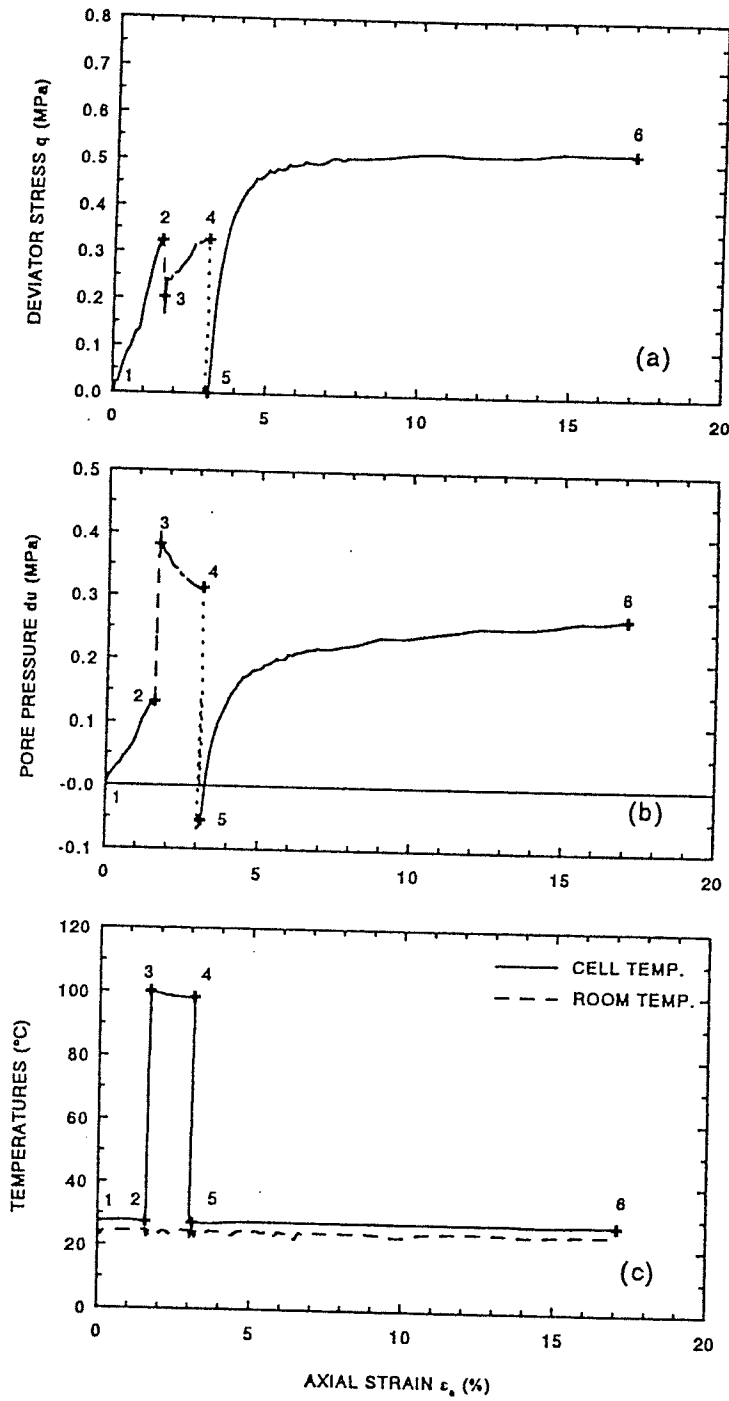
Figure 8.20 Stress-strain relationships in undrained heating
(28°C to 100°C) test (T1473) on overconsolidated
reconstituted illite. (a) Deviator stress *vs.* axial
strain. (b) Pore pressure *vs.* axial strain. (c)
Temperature *vs.* axial strain.
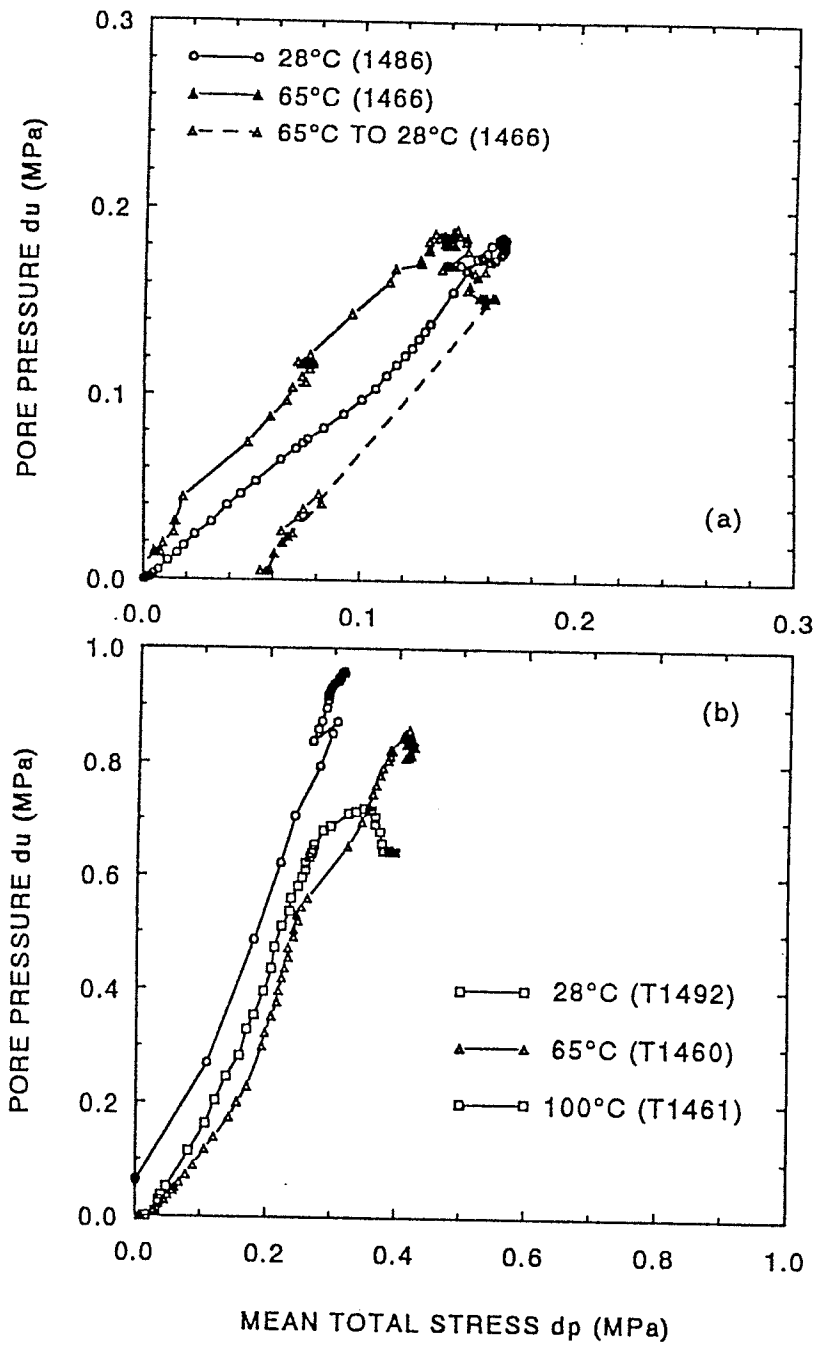
Figure 8.21 Pore pressure · *vs*. mean total stress at elevated
temperatures (a) Overconsolidated illite at 28°C and
65°C.   (b) Normally consolidated illite at 28°C,
65°C, and 100°C.
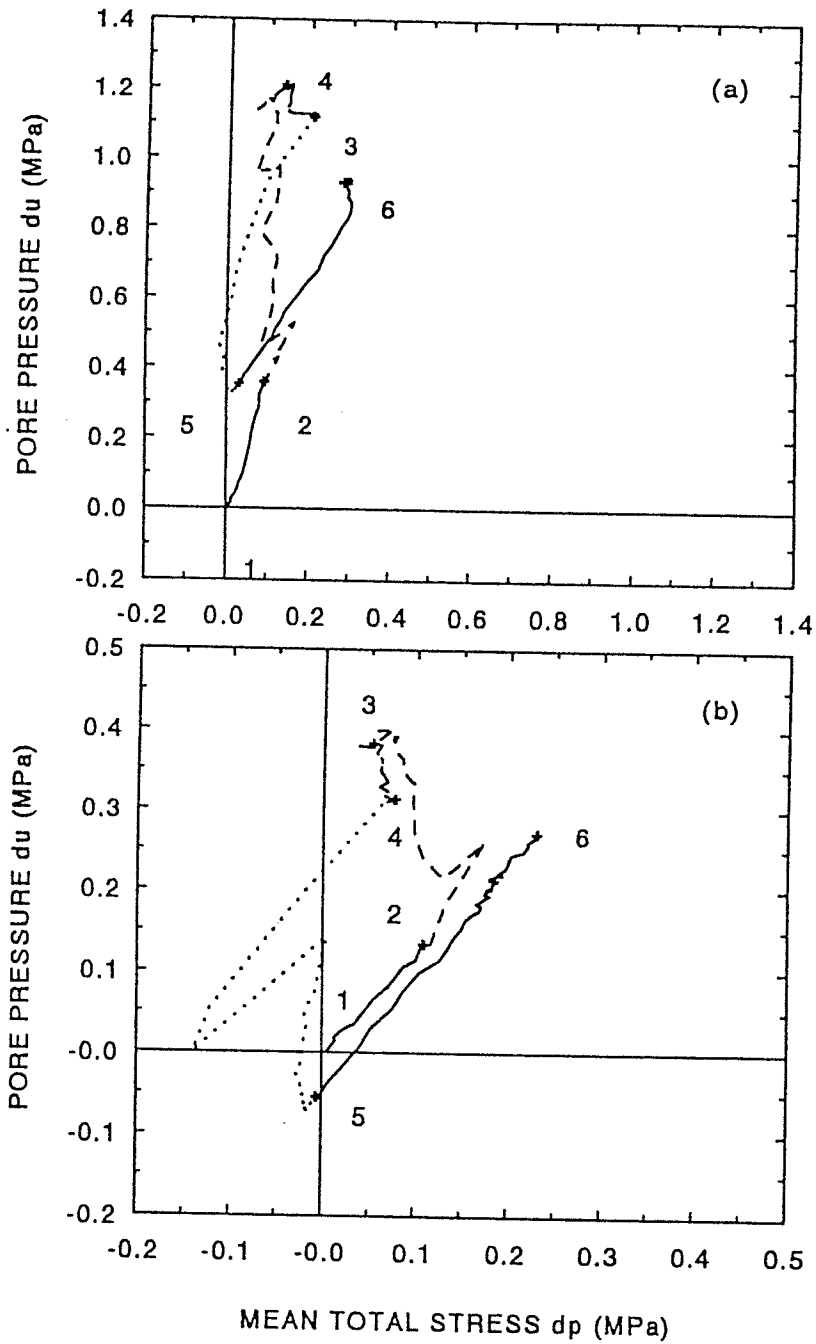
Figure 8.22 Pore pressure· *vs.* mean total stress at ramped temperatures. (a) Normally consolidated illite at 28°C (T1472). (b) Overconsolidated illite at 28°C (T1473).
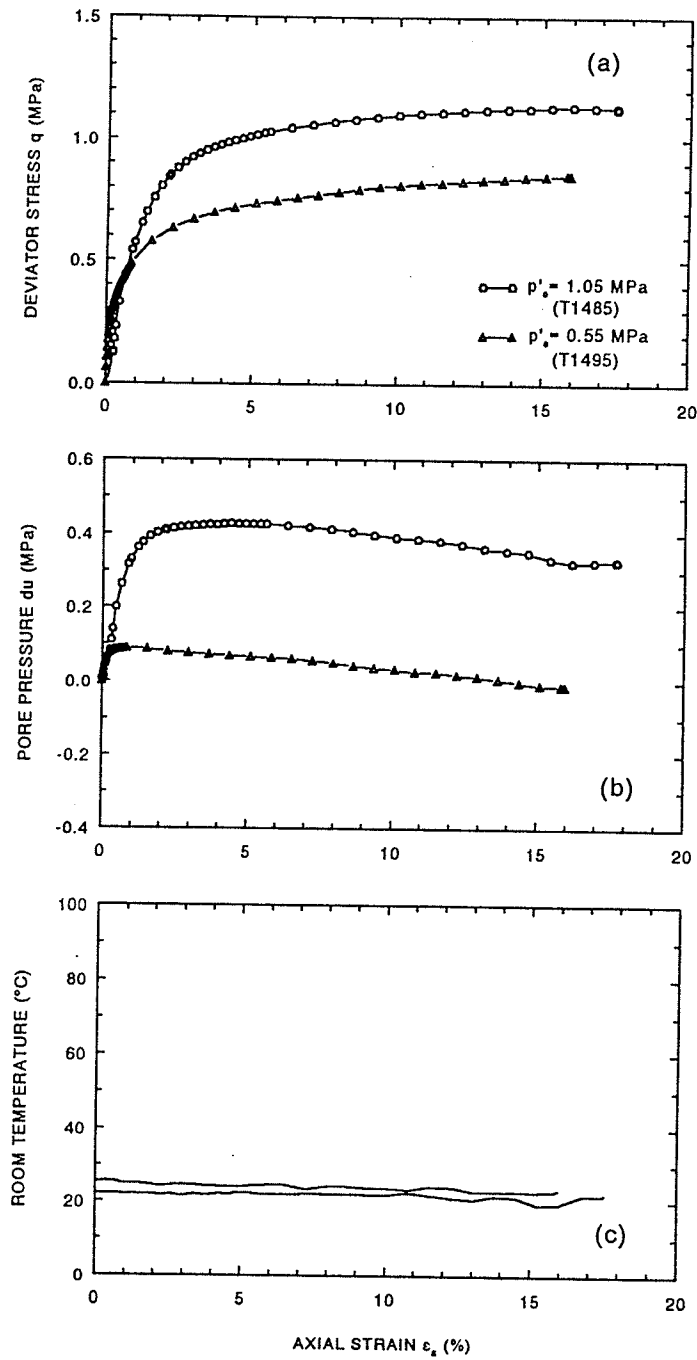
Figure 8.23 Stress-strain relationships on compacted illite at 28°C. (a) Deviator stress *vs.* axial strain. (b) Pore pressure *vs.* axial strain. (c) Temperature *vs.* axial strain.
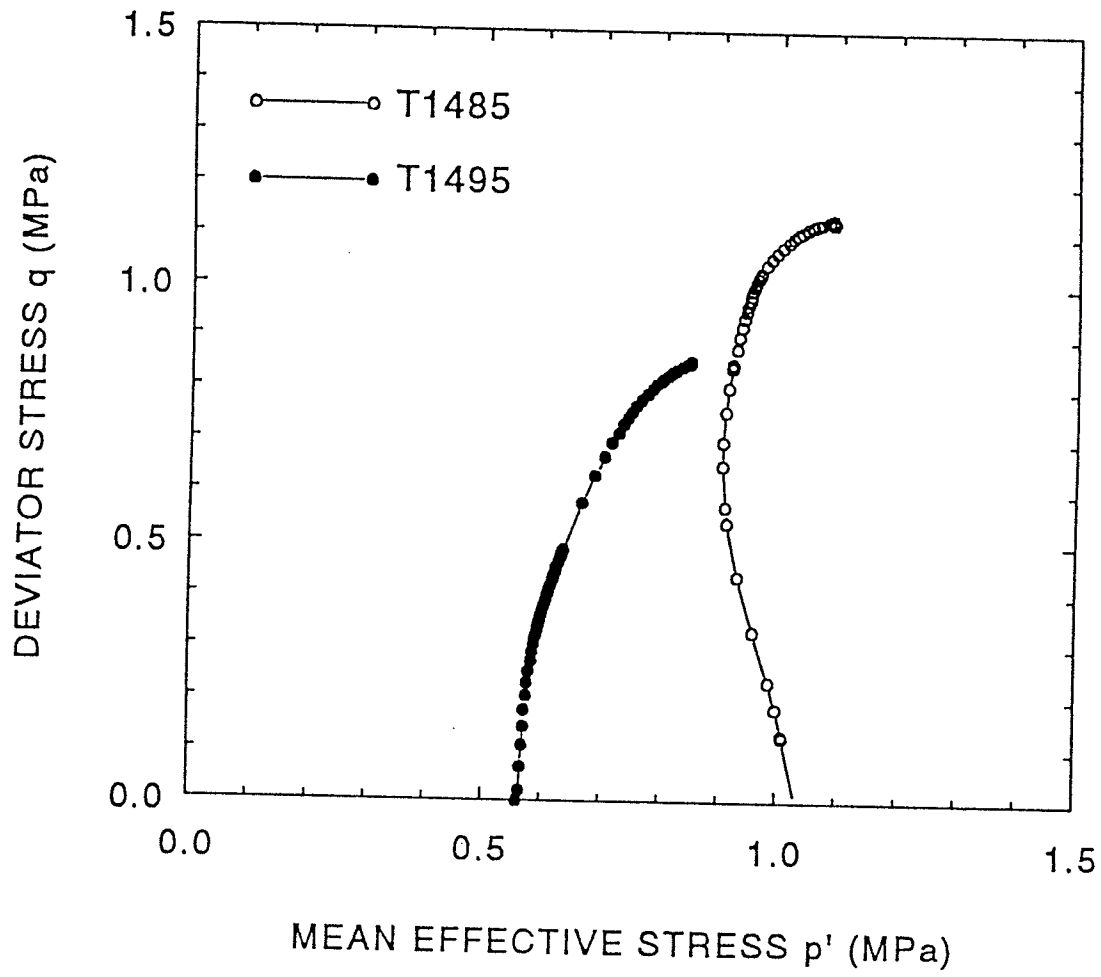
Figure 8.24 Stress paths for compacted illite at 28°C.
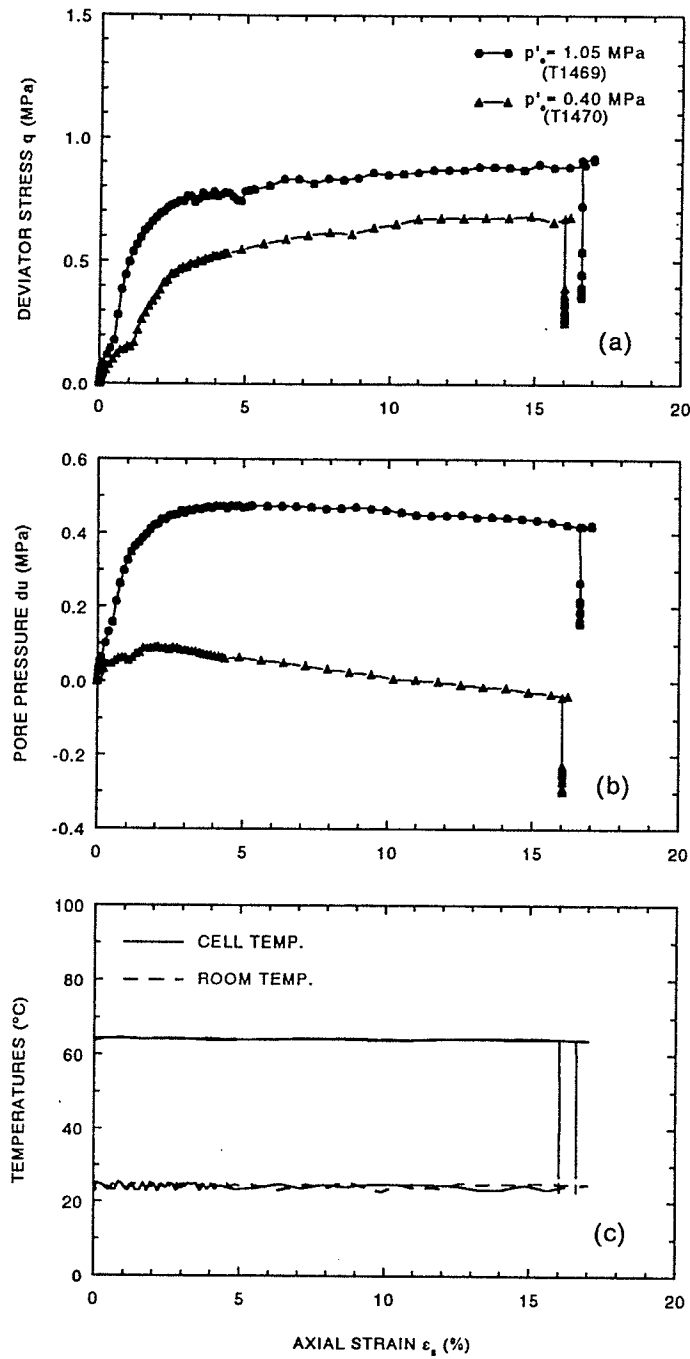
Figure 8.25   Stress-strain relationships on compacted illite at 65°C.   (a) Deviator stress *vs.* axial strain.   (b) Pore pressure *vs.* axial strain.   (c) Temperature *vs.* axial strain.
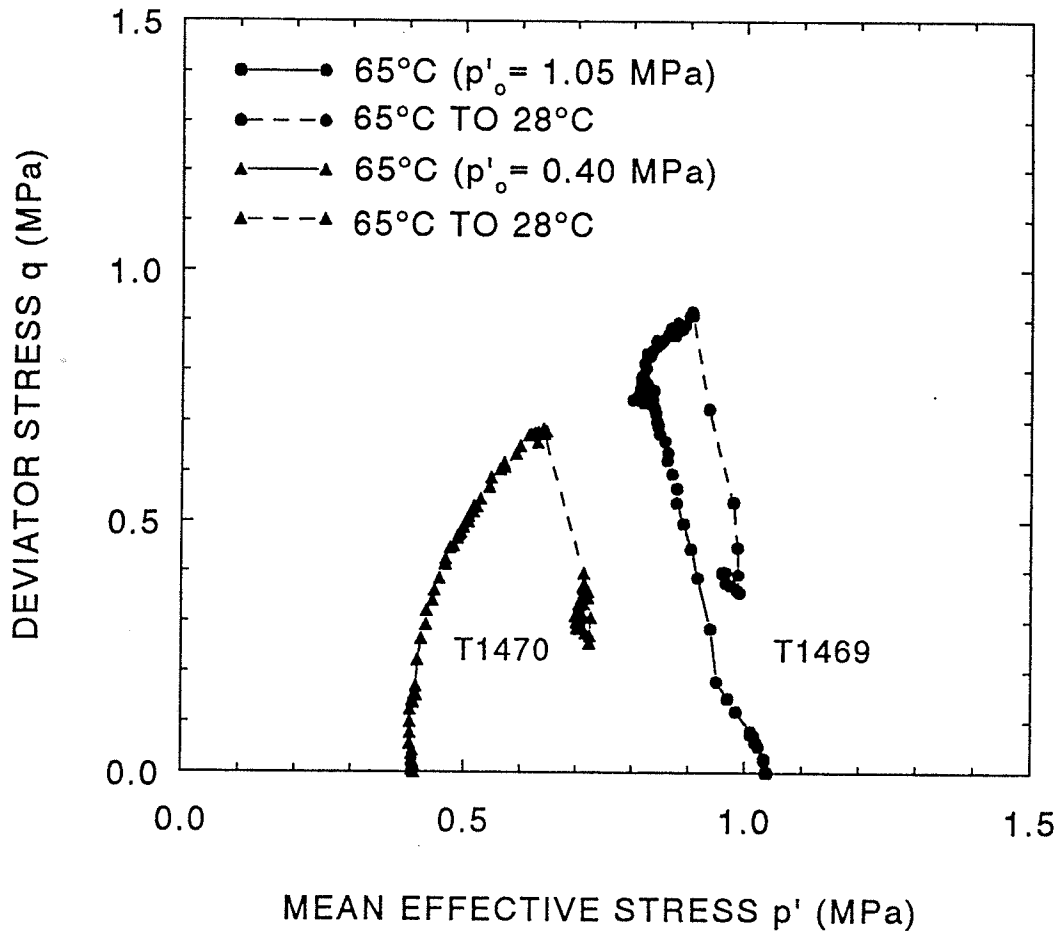
Figure 8.26 Stress paths for compacted illite at 65°C.
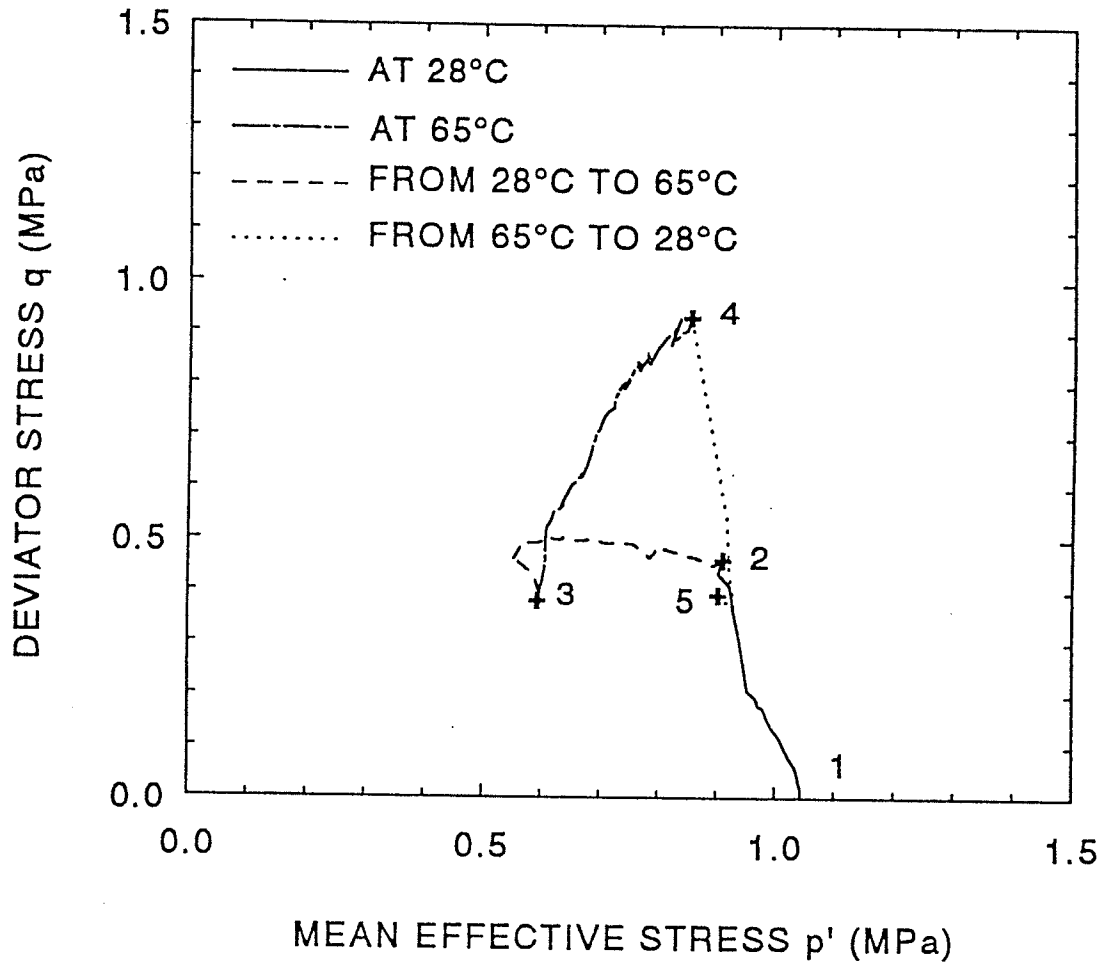
Figure 8.27   Stress paths for undrained heating (28°C to 65°C)
test (T1471) on compacted illite.
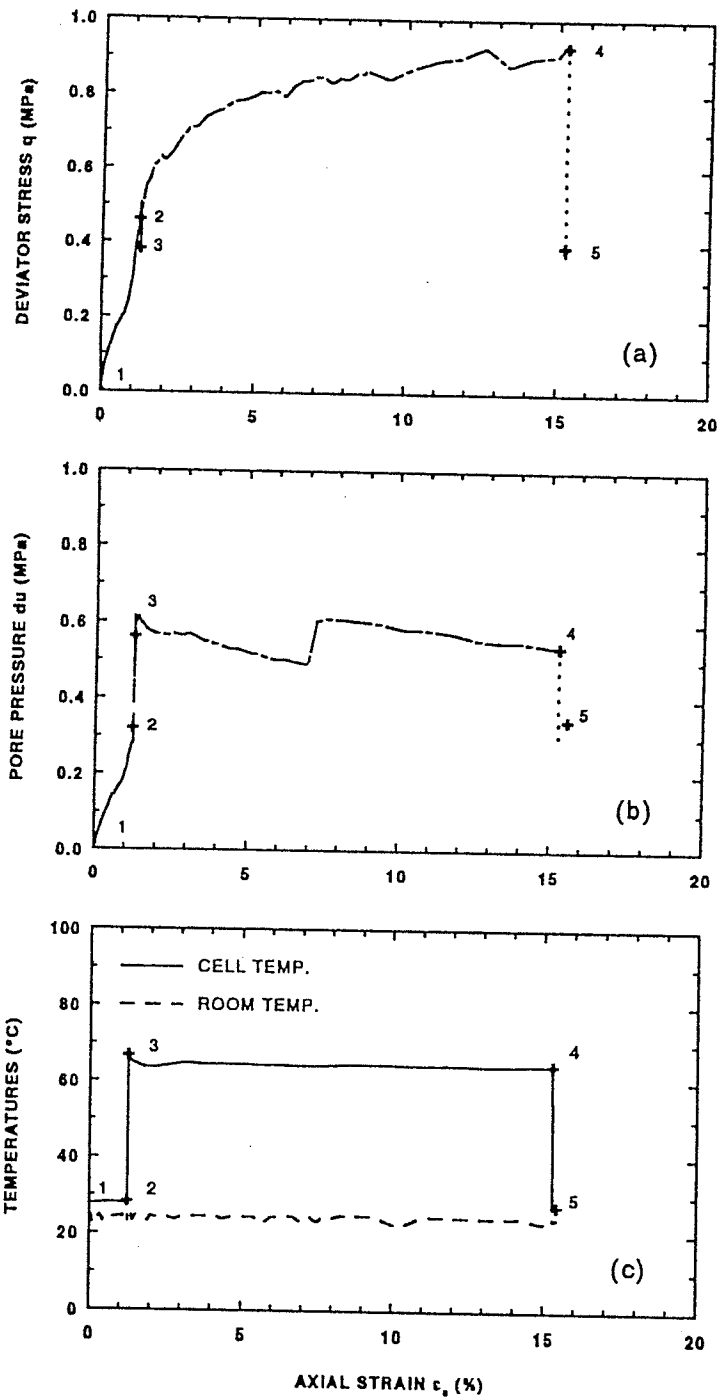
Figure 8.28   Stress-strain -relationships in undrained heating
(28°C to 65°C) test (T1471) on compacted illite. (a)
Deviator stress *vs*. axial strain. (b) Pore pressure
vs. axial strain. (c) Temperature *vs*. axial strain.
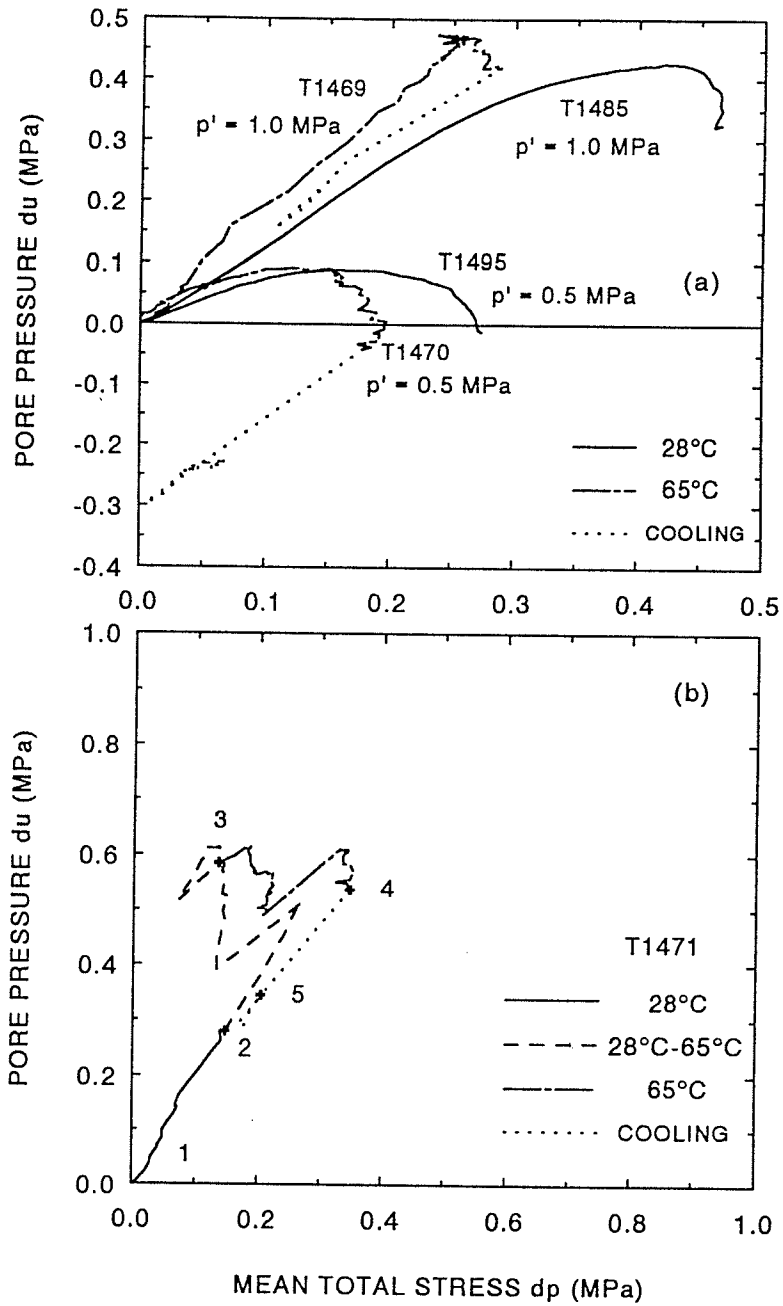
Figure 8.29   Pore pressure *vs.* mean total stress. (a) at elevated
temperature, and (b) at ramped temperatures on
compacted illite.
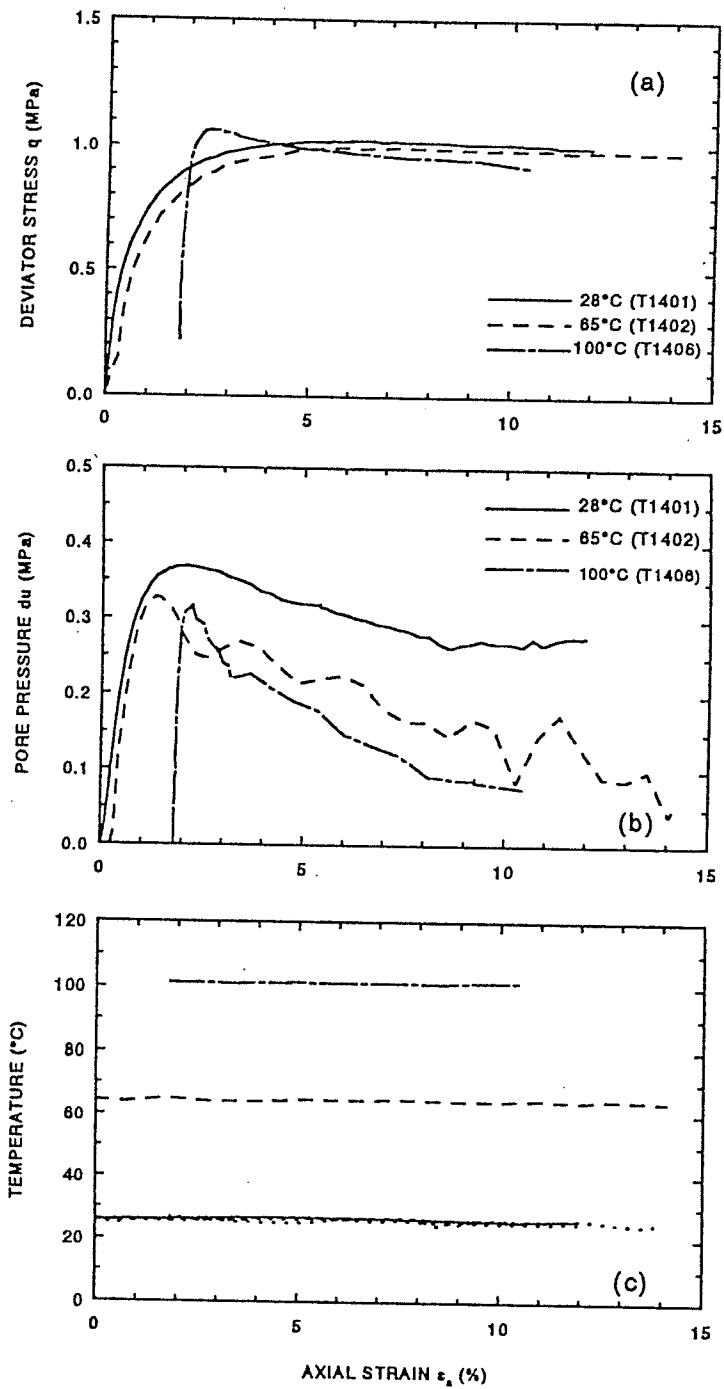
Figure 8.30 Effect of elevated temperature on stress-strain relationships of compacted sand-bentonite mixture. (a) Deviator stress *vs.* axial strain. (b) Pore pressure *vs.* axial strain. (c) Temperature *vs.* axial strain.
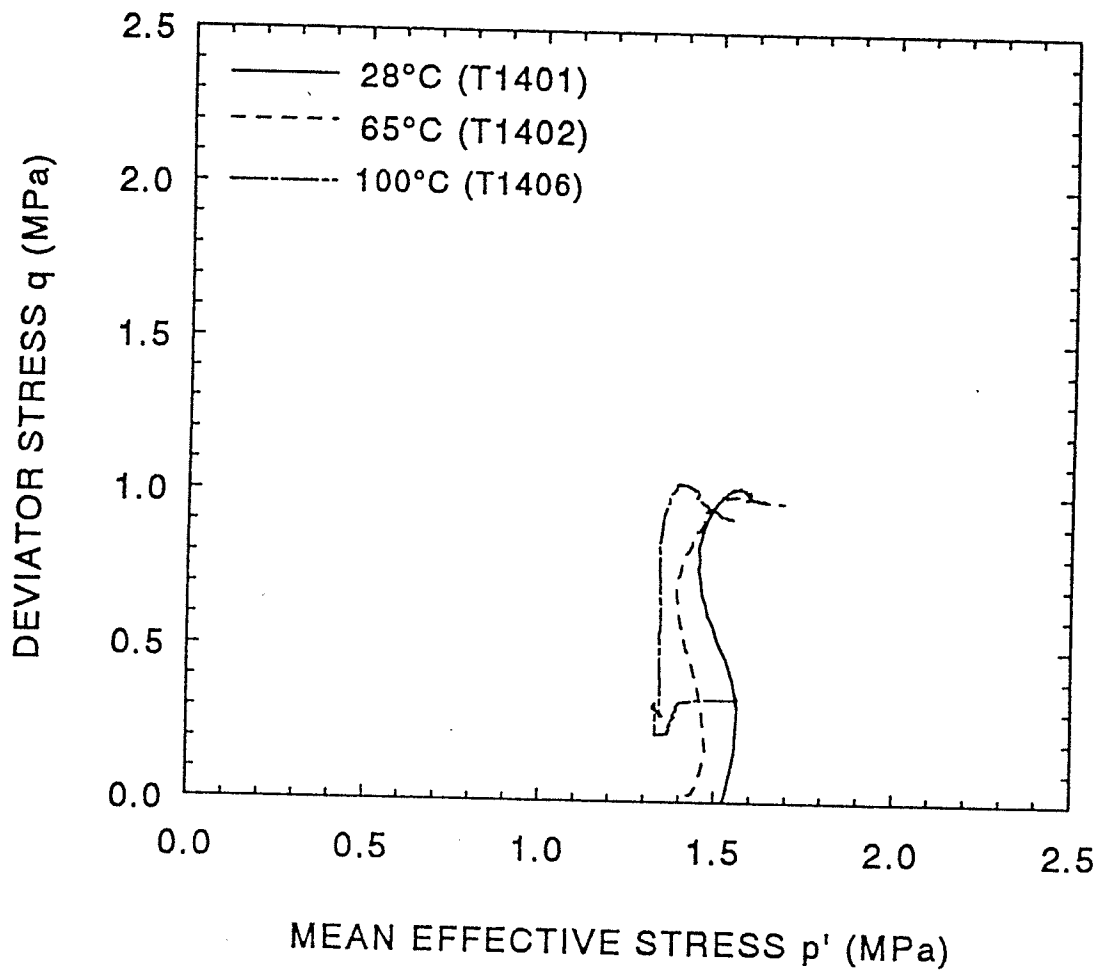
Figure 8.31   Effect of elevated temperature on stress paths of
compacted sand-bentonite mixture.
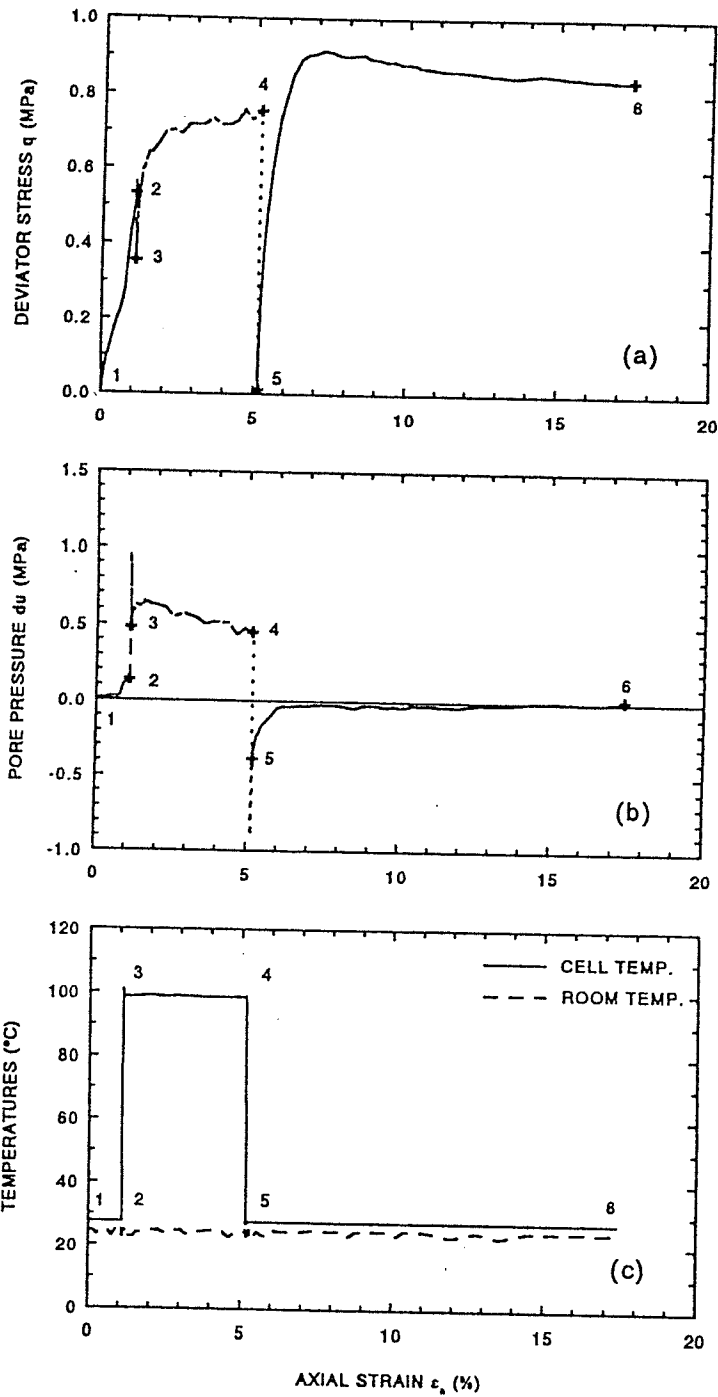
Figure 8.32 Effect of ramped temperatures on stress-strain relationships of compacted sand-bentonite mixture (T1475). (a) Deviator stress *vs.* axial strain. (b) Pore pressure *vs.* axial strain.
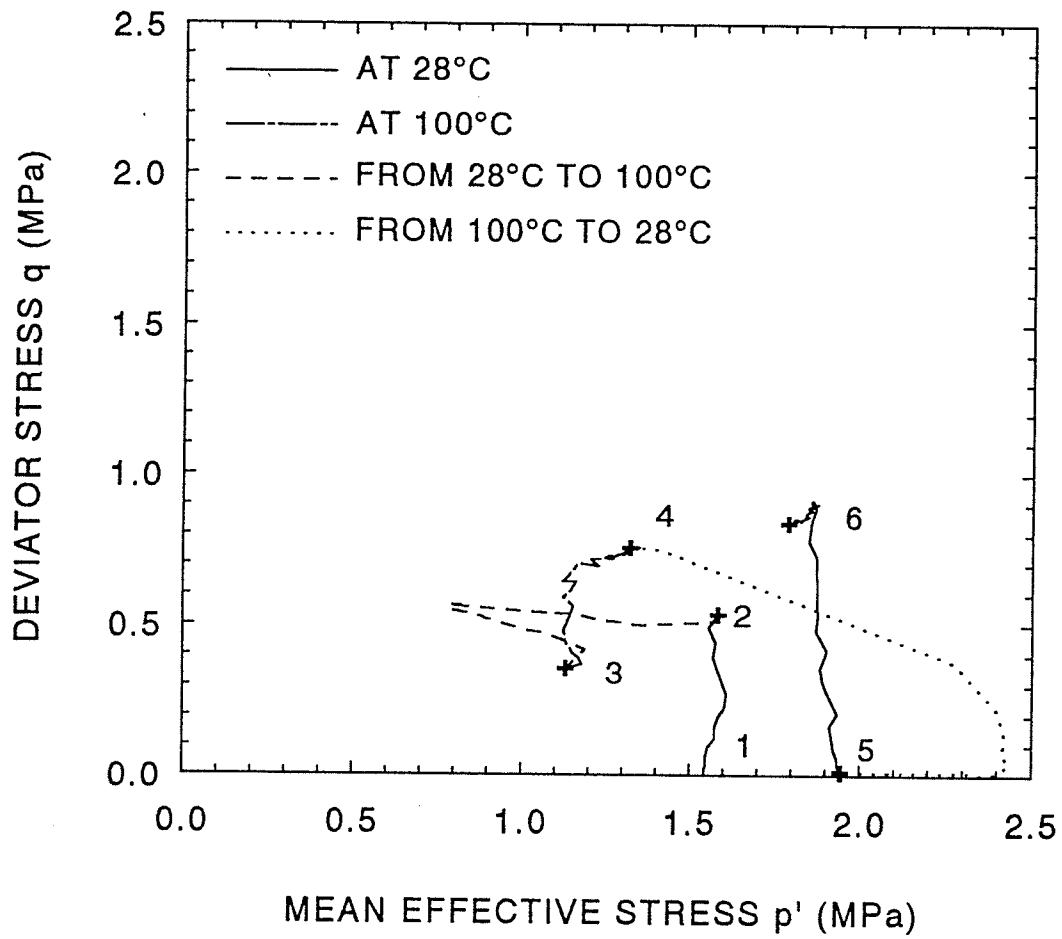
Figure 8.33 Effect of ramped temperatures on stress paths of compacted sand-bentonite mixture (T1475).
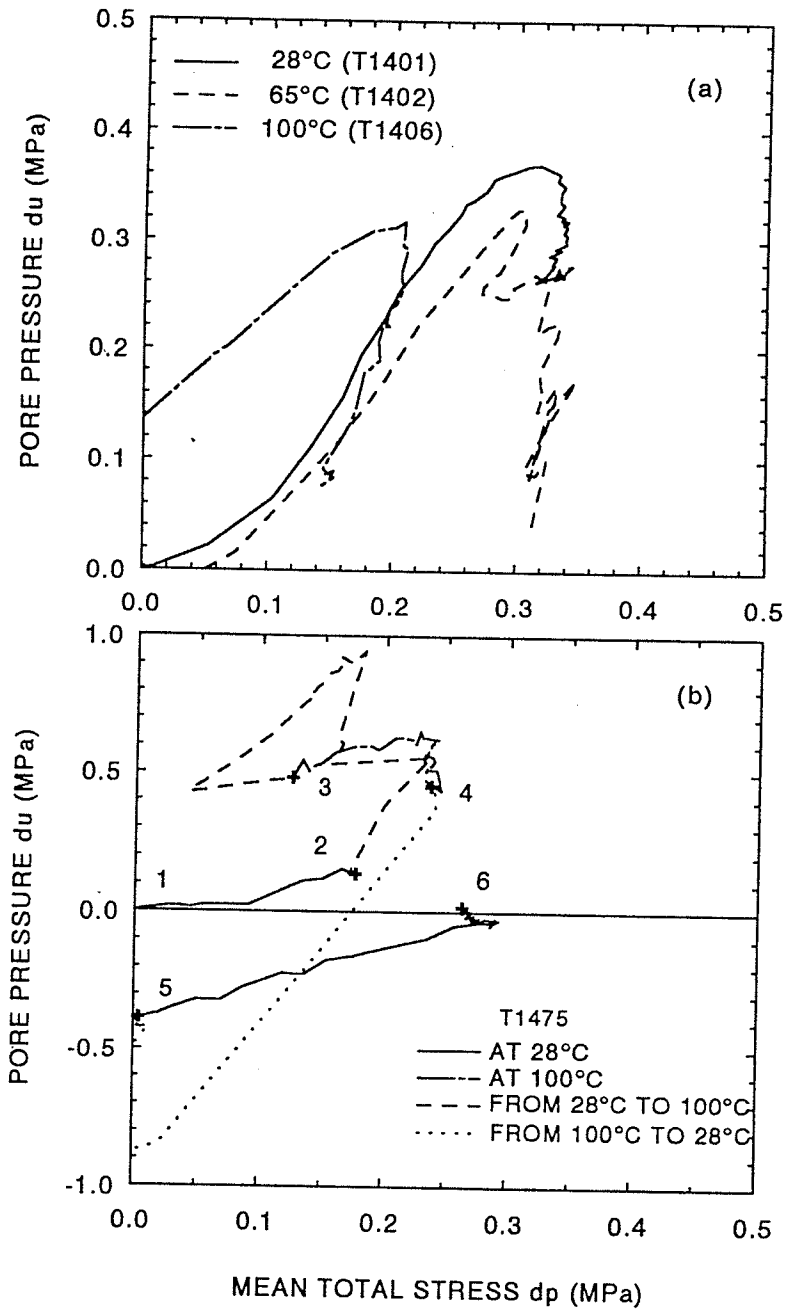
Figure 8.34 Pore pressure *vs.* mean total stress. (a) at elevated temperature, and (b) at ramped temperature.
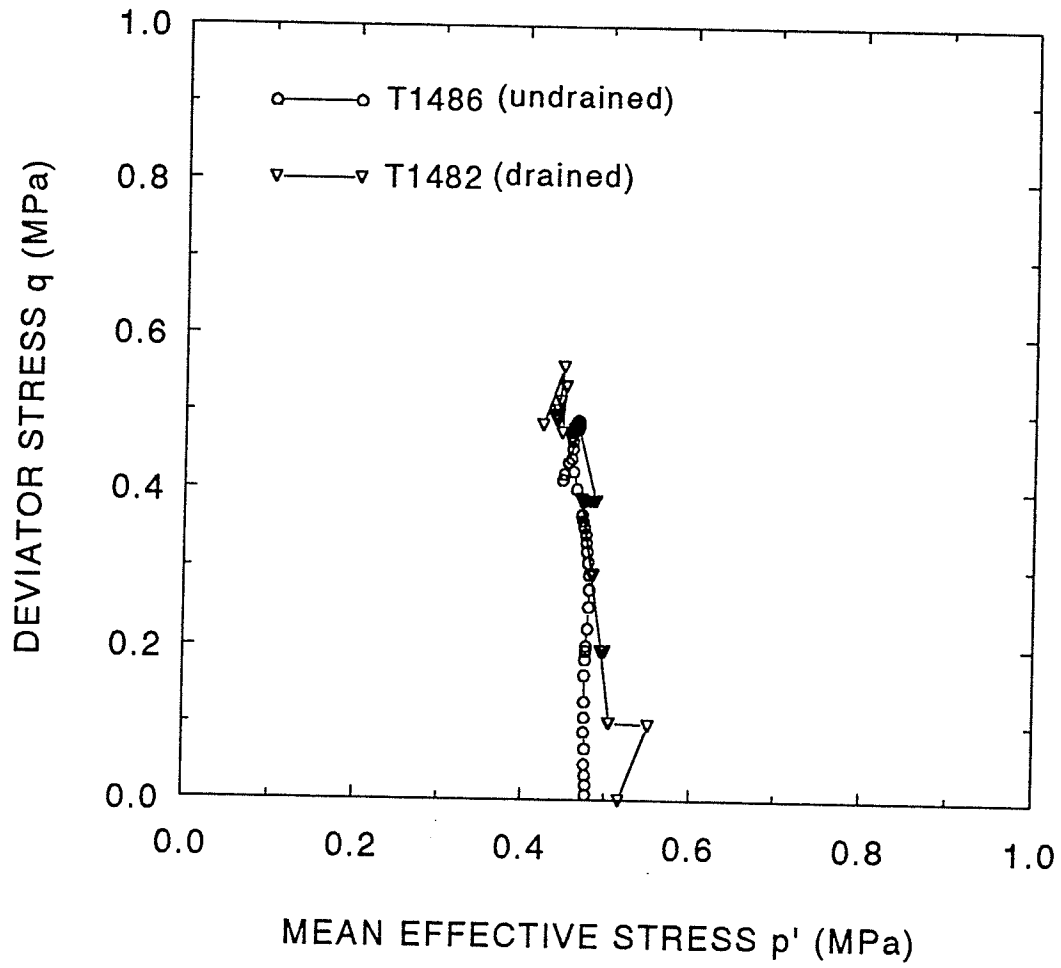
Figure 8.35 Stress paths for drained and undrained tests on overconsolidated illite specimens at 28°C.
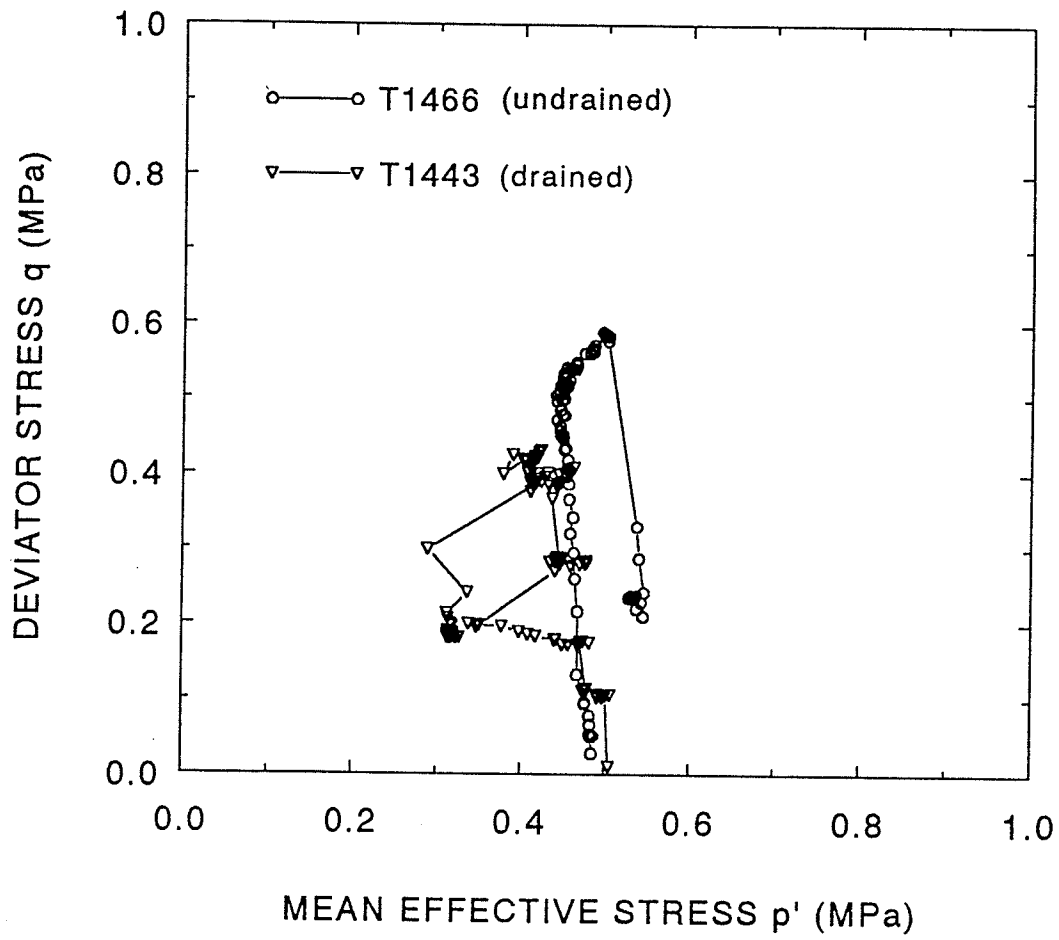
Figure 8.36   Stress paths for drained and undrained tests on overconsolidated illite specimens at 65°C.
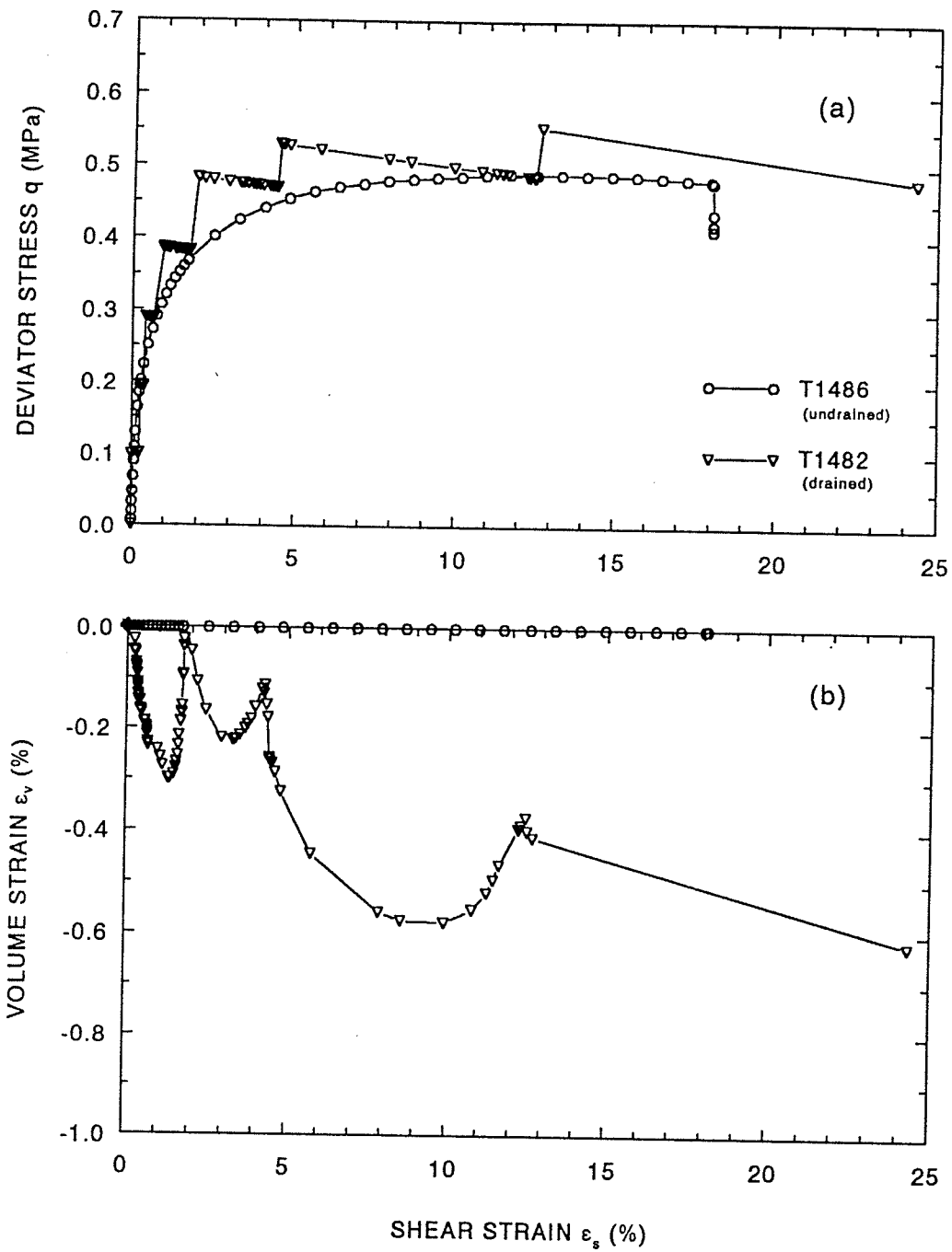
Figure 8.37   Stress-strain relationships for drained and undrained
tests on overconsolidated illite specimens at 28°C.
(a) Deviator stress *vs.* shear strain.   (b) Volume
strain *vs.* shear strain.
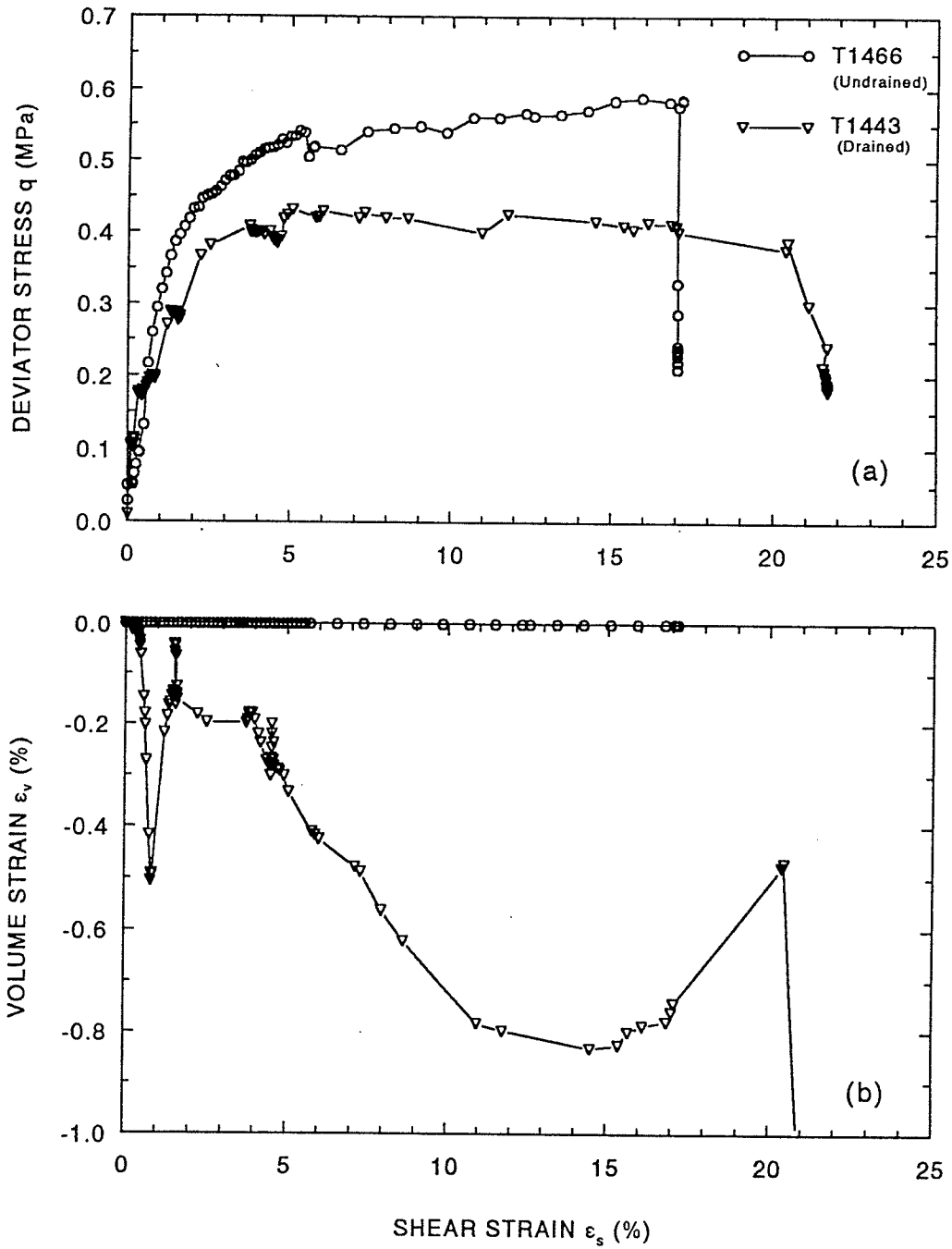
Figure 8.38   Stress-strain relationships for drained and undrained
tests on overconsolidated illite specimens at 65°C.
(a) Deviator stress *vs.* shear strain.   (b) Volume
strain *vs.* shear strain.
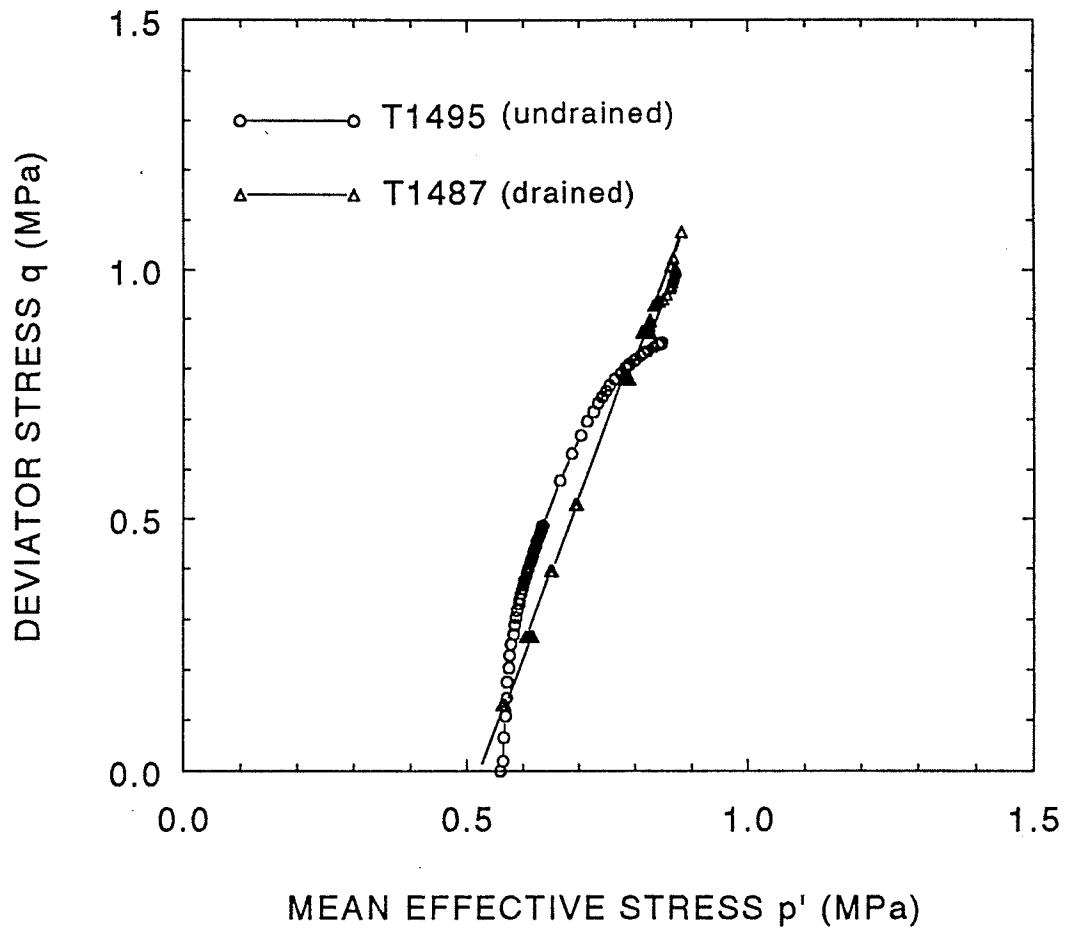
Figure 8.39 Stress paths for drained and undrained tests on compacted illite specimens at 28°C.
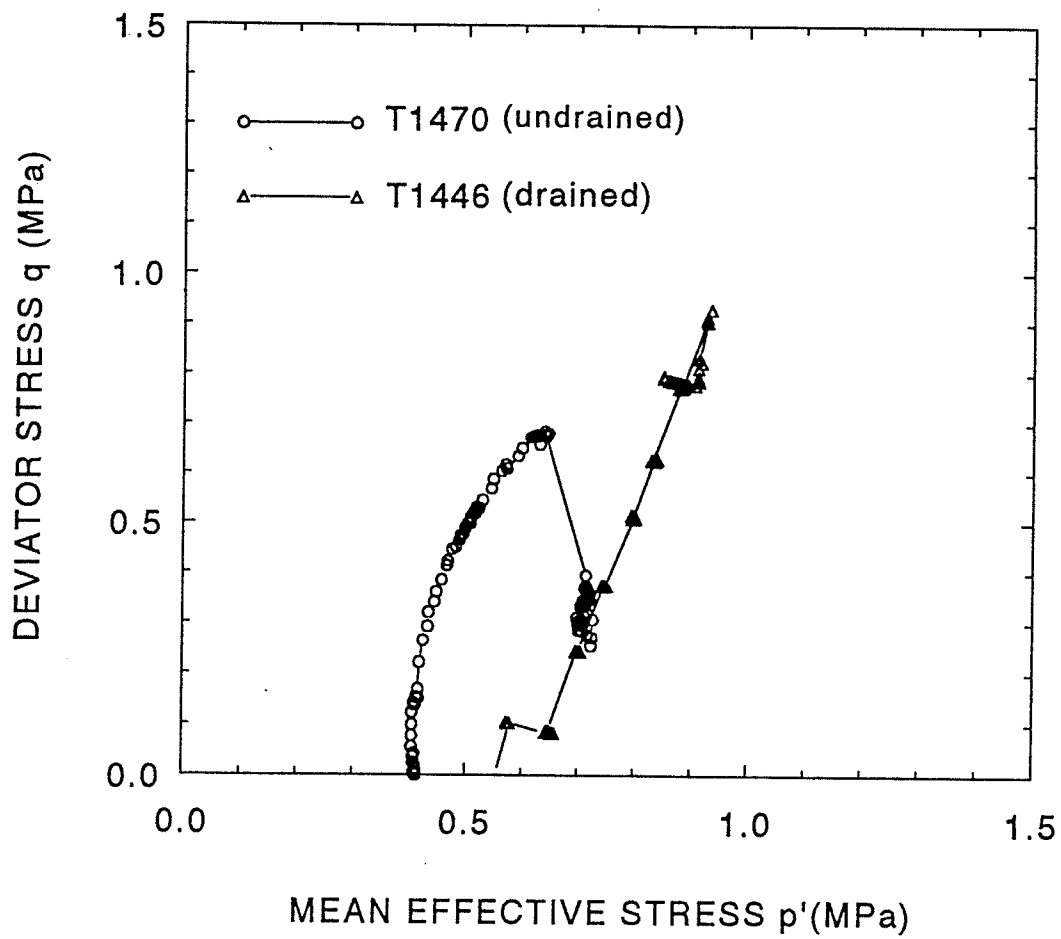
Figure 8.40 Stress paths for drained and undrained tests on compacted illite specimens at 65°C.
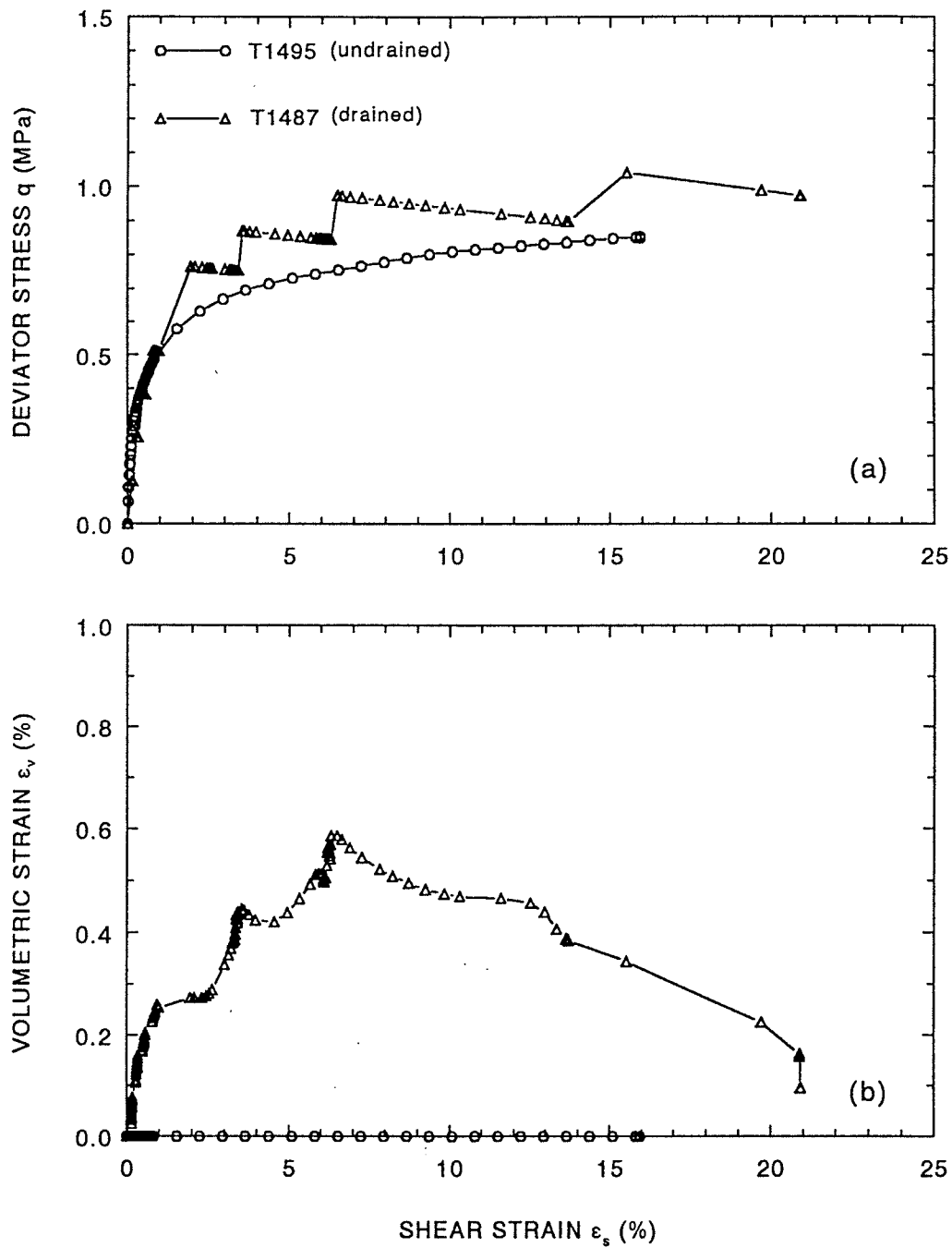
Figure 8.41 Stress-strain relationships for drained and undrained
tests on compacted illite specimens at 28°C. (a)
Deviator stress *vs.* shear strain. (b) Volume strain
vs. shear strain.
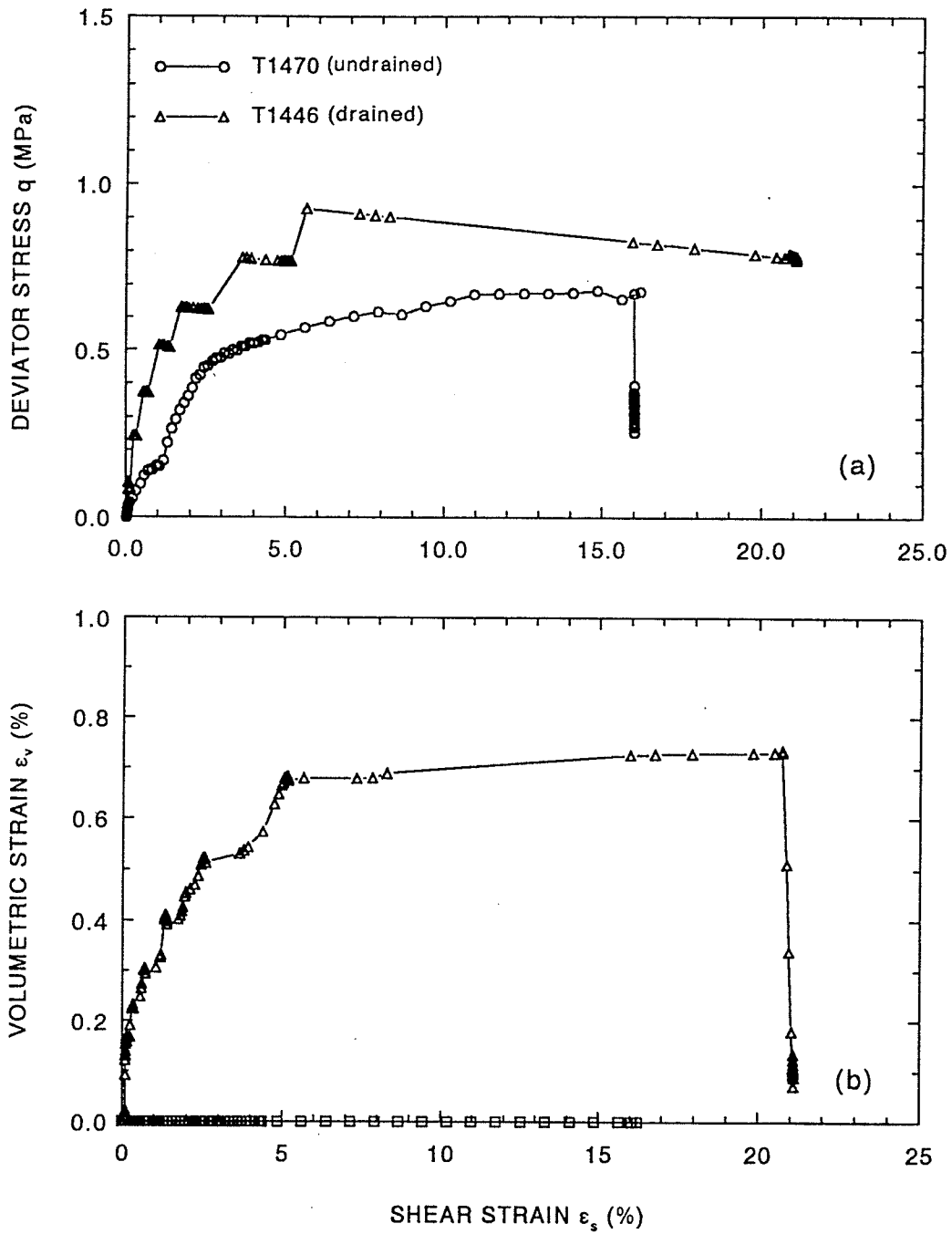
Figure 8.42   Stress-strain relationships for drained and undrained tests on compacted illite specimens at 65°C.   (a) Deviator stress *vs.* shear strain.   (b) Volume strain *vs.* shear strain.
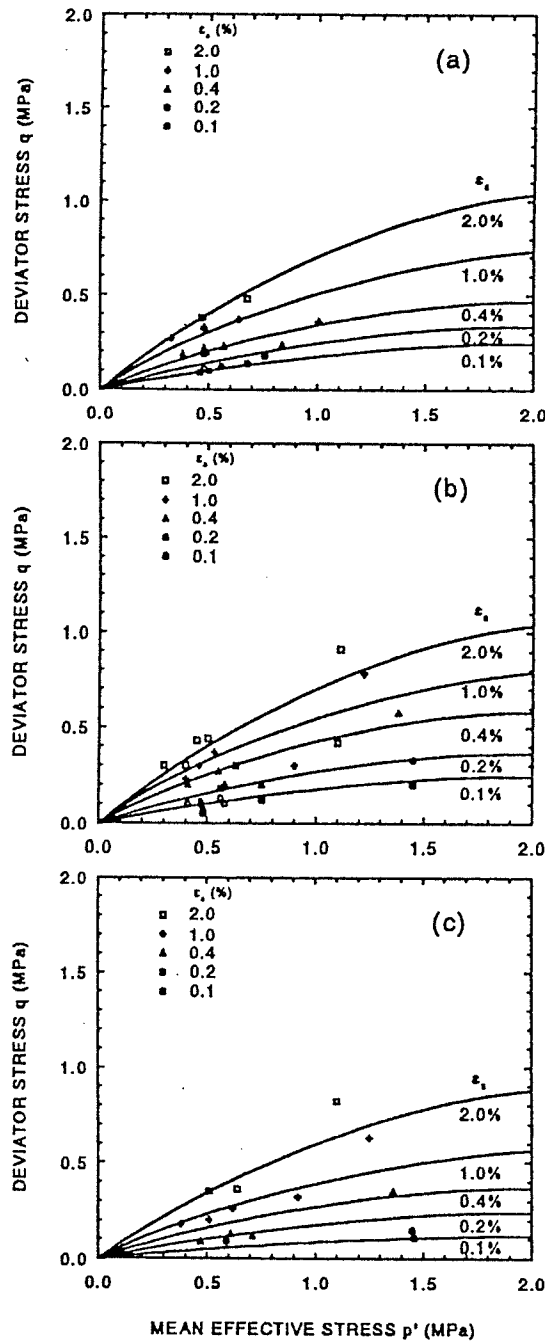
Figure 8.43 Shear strain contours in p'-q space for reconstituted illite. (a) 28°C. (b) 65°C. (c) 100°C.
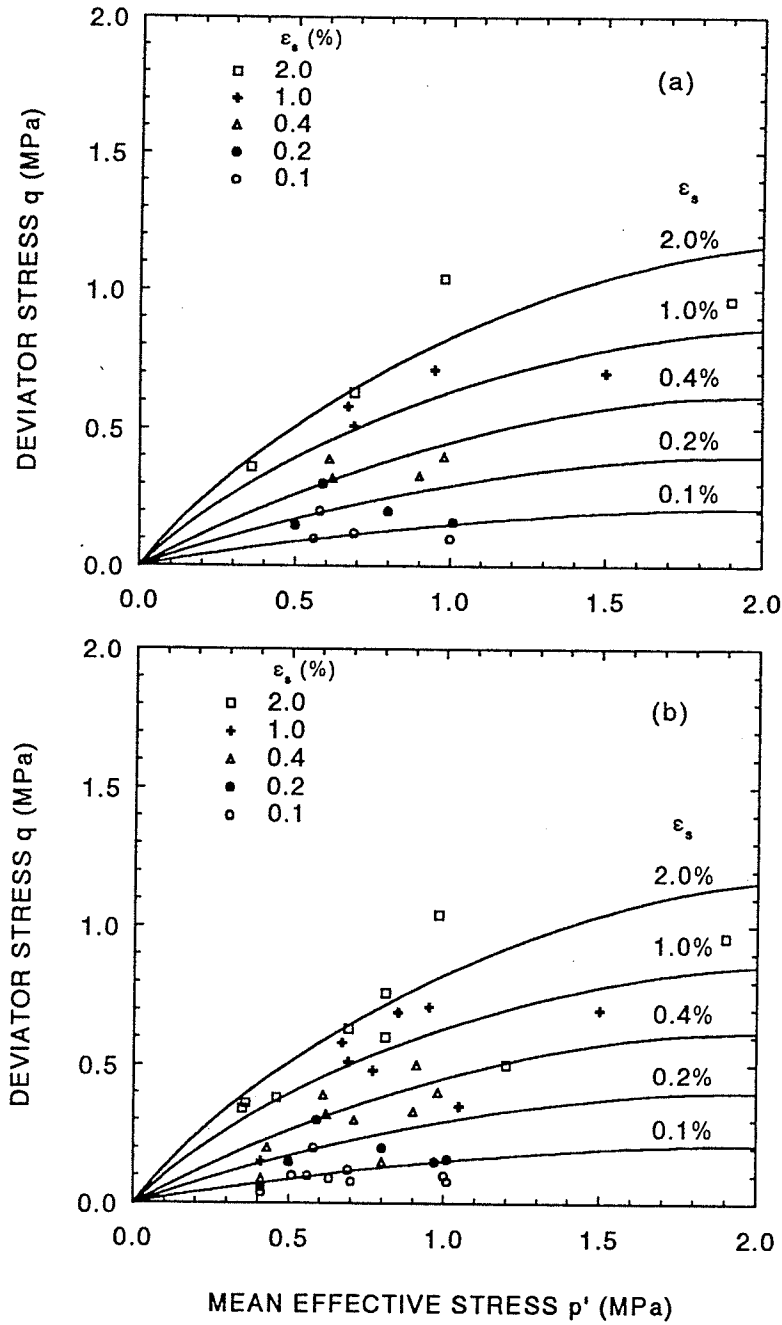
Figure 8.44   Shear strain contours in p′-q space for compacted
illite at (a) 28°C and (b) 65°C.
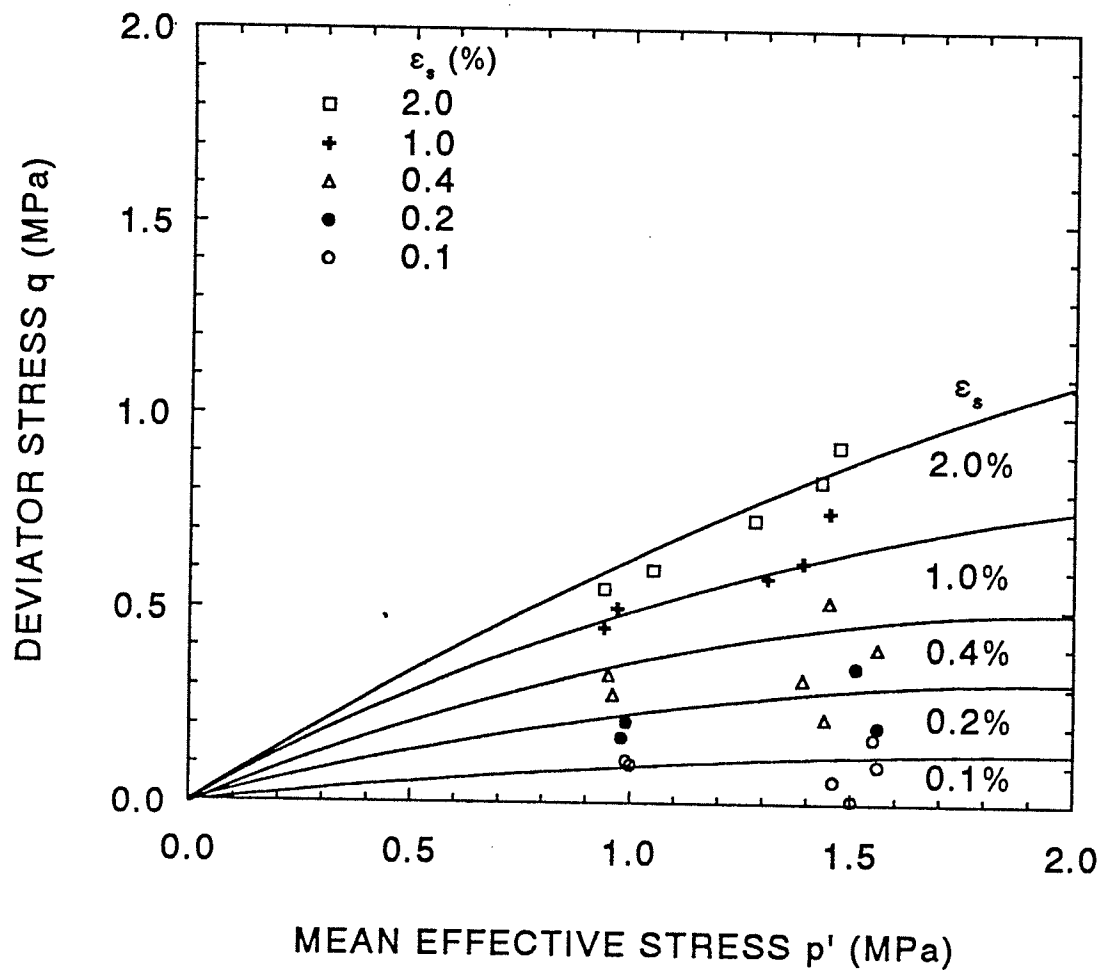
Figure 8.45 Shear strain contours in p'-q space for compacted sand-bentonite mixture at 28°C, 65°C, and 100°C.
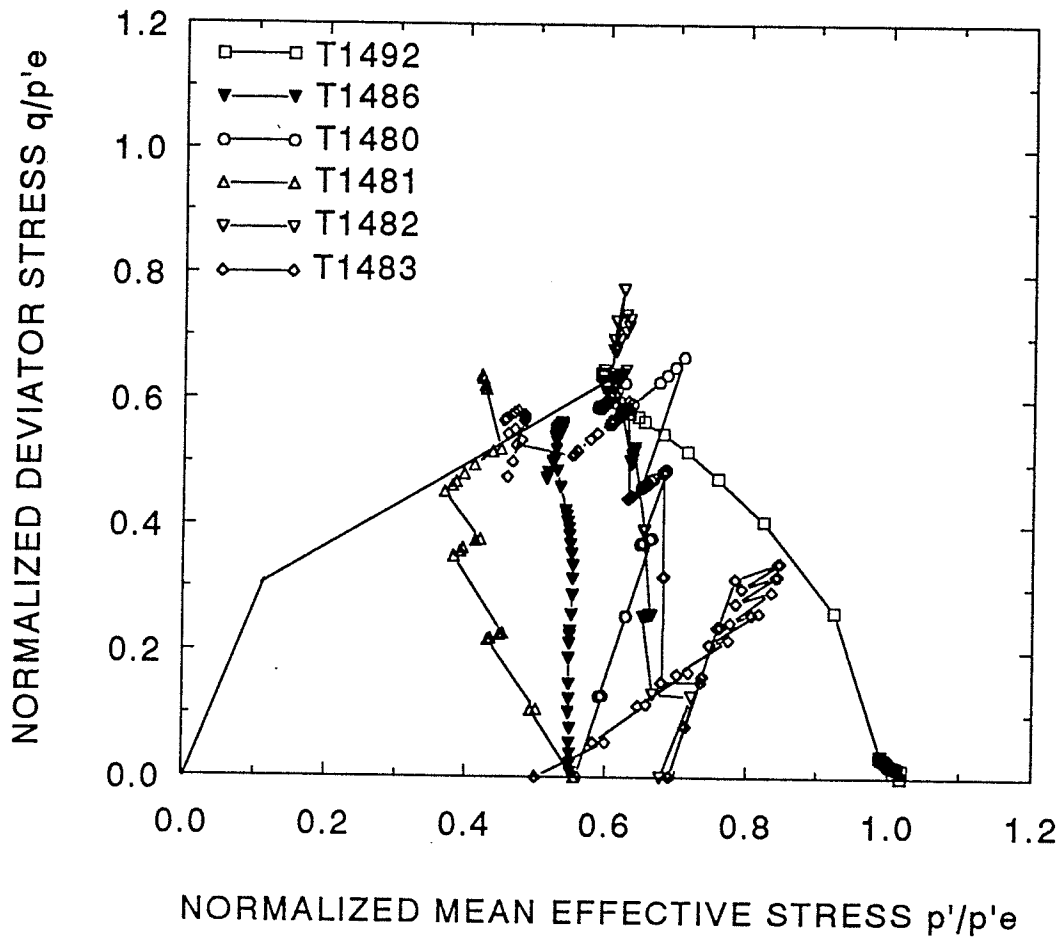
Figure 8.46 State boundary surface and stress paths for
reconstituted illite at 28°C.
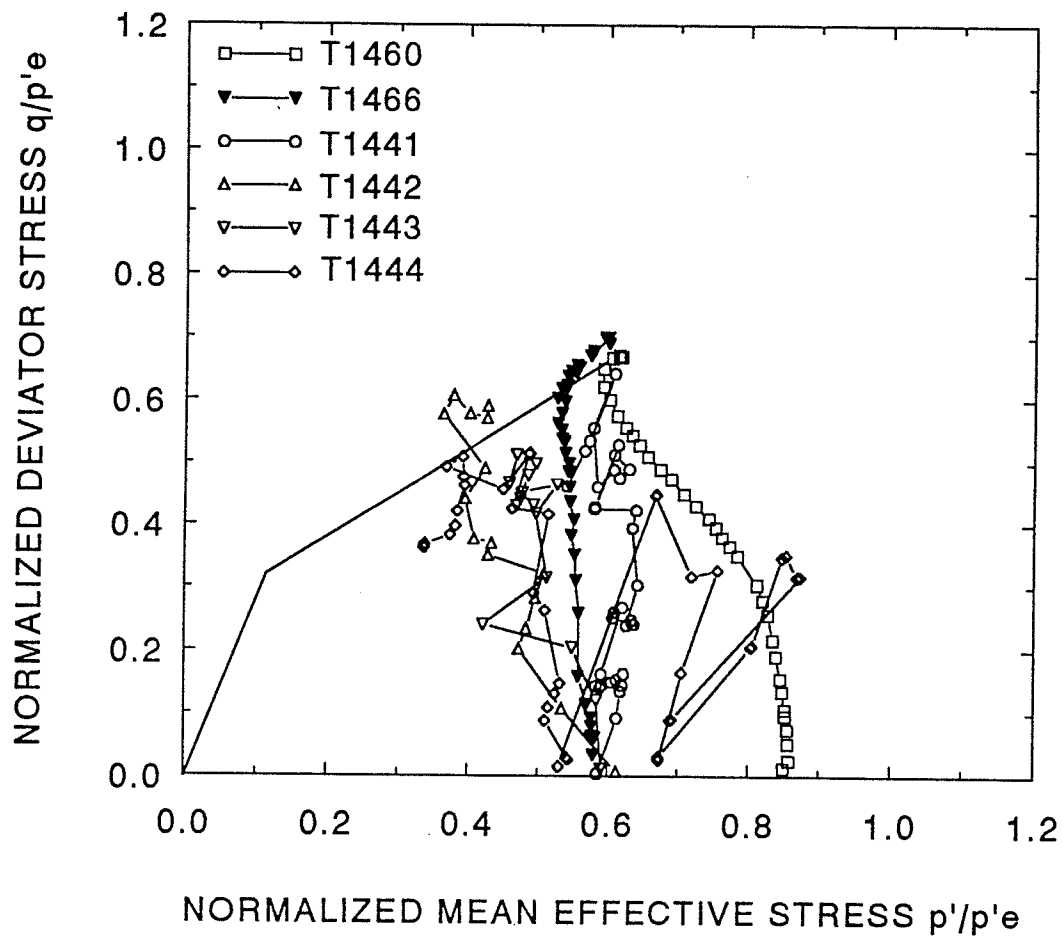
Figure 8.47   State   boundary   surface   and   stress   paths   for reconstituted illite at 65°C.
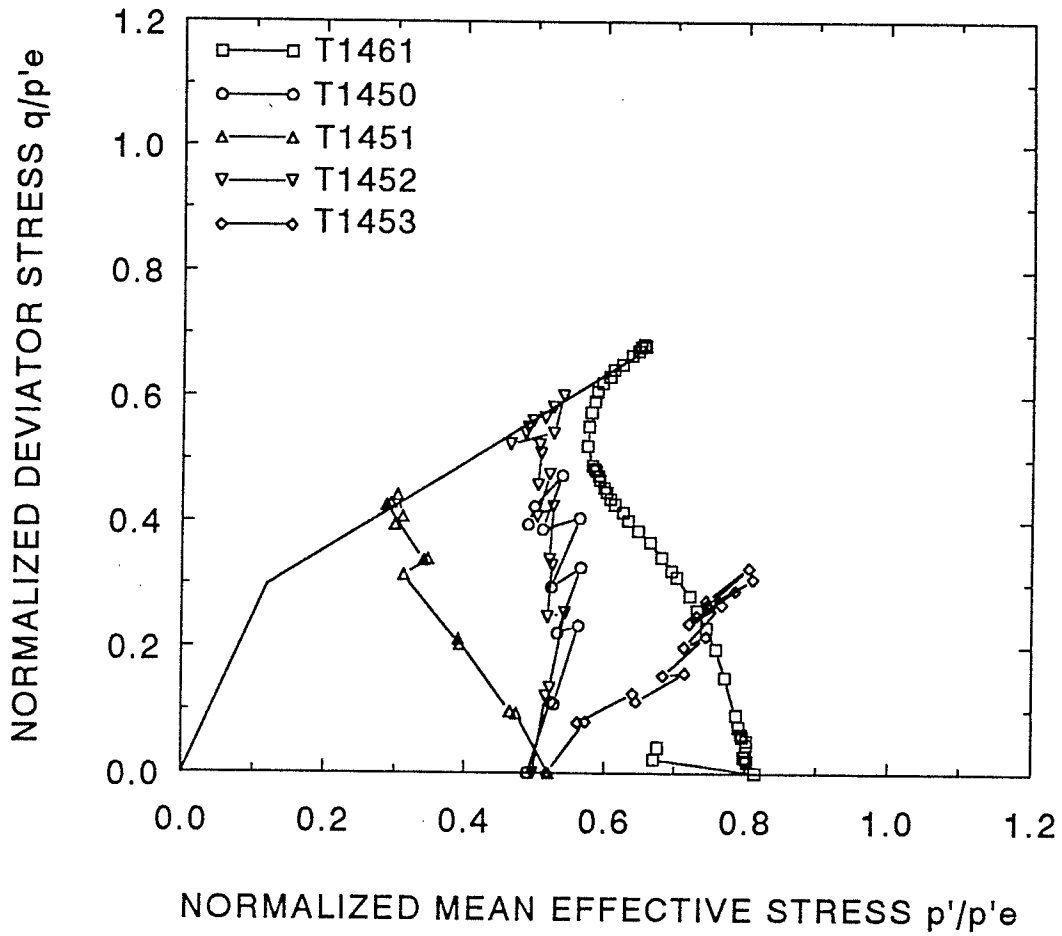
Figure 8.48   State   boundary   surface   and   stress   paths   for reconstituted illite at 100°C.
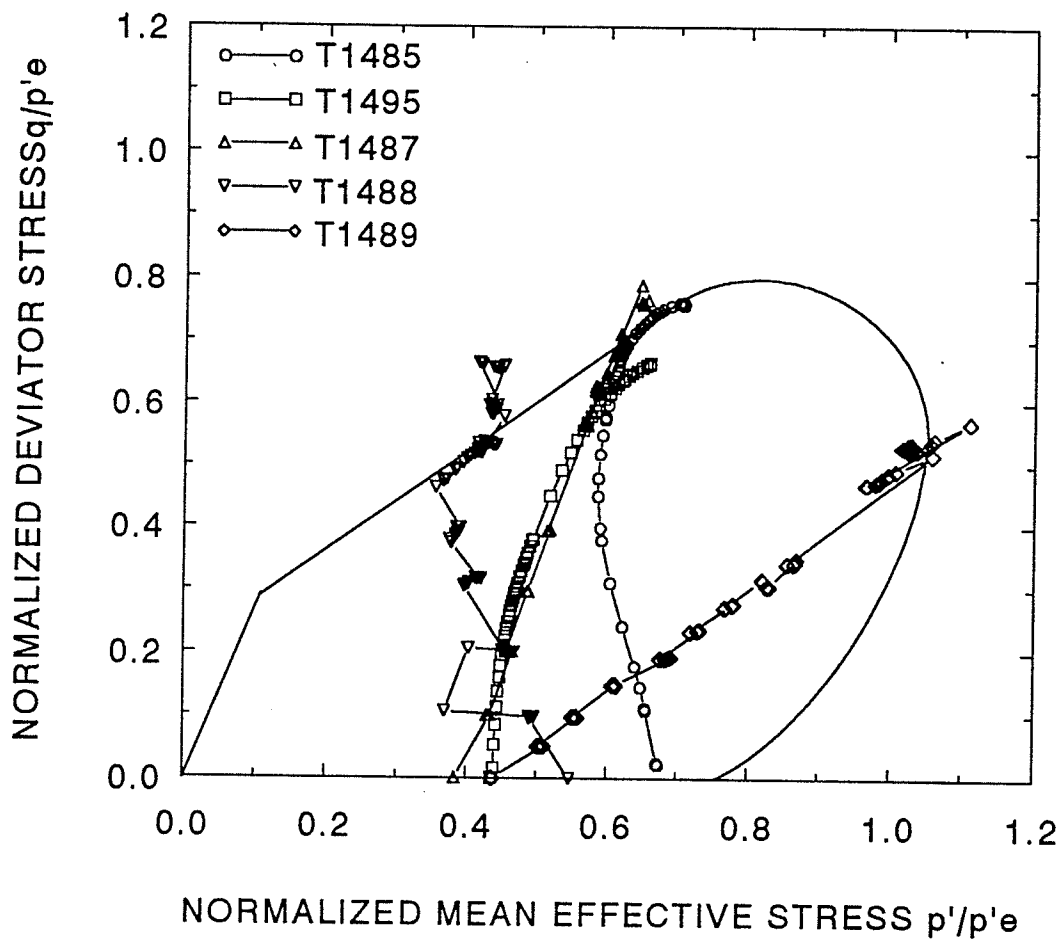
Figure 8.49 State boundary surface and stress paths for compacted illite at 28°C.
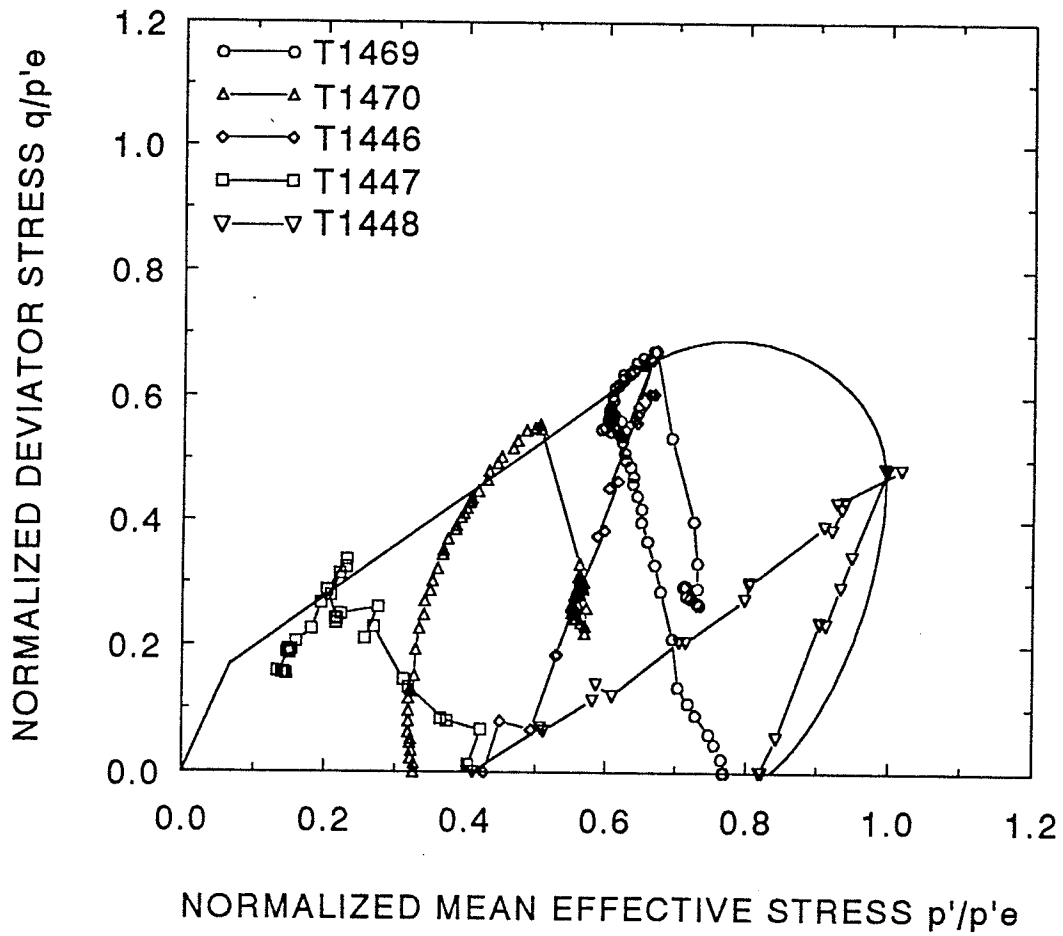
Figure 8.50 State boundary surface and stress paths for compacted
illite at 65°C.
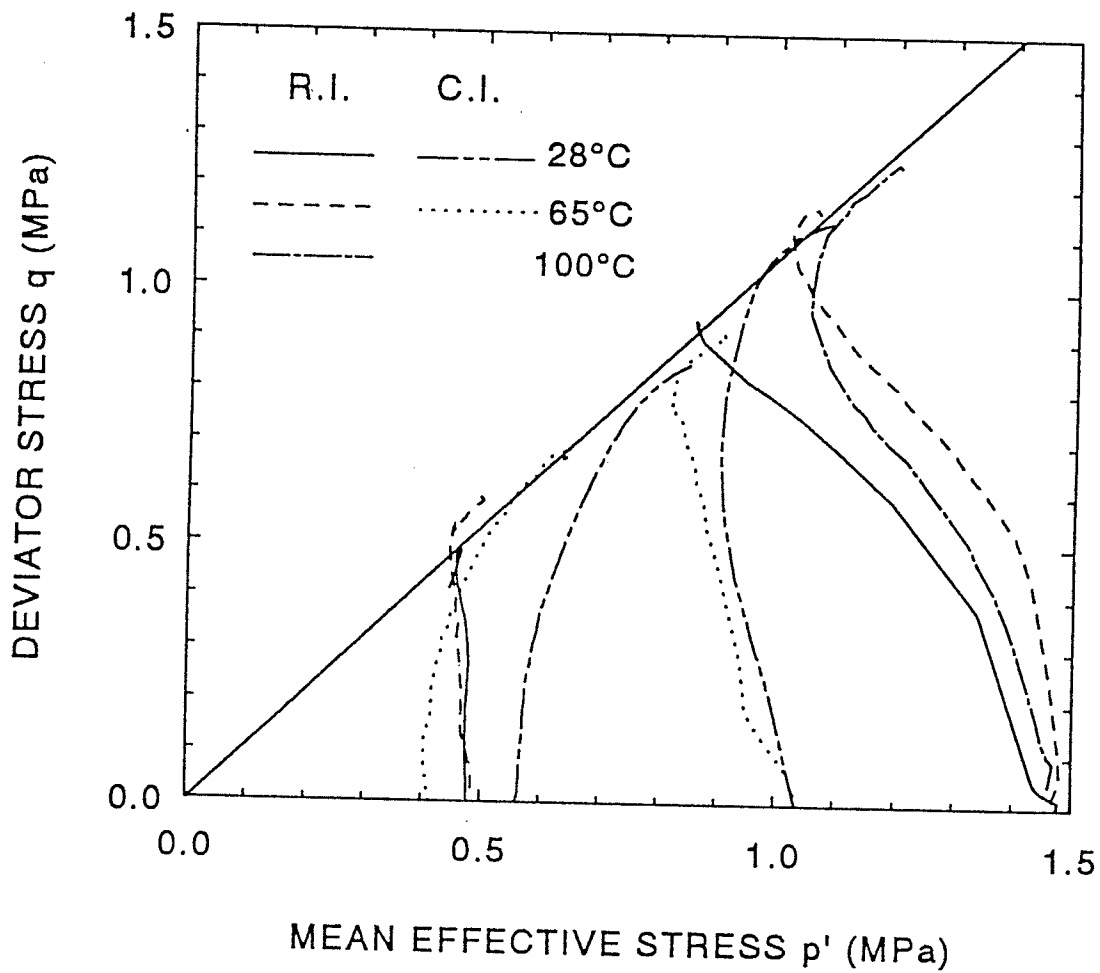
Figure 8.51   Failure strength envelopes at elevated temperatures
on illite.
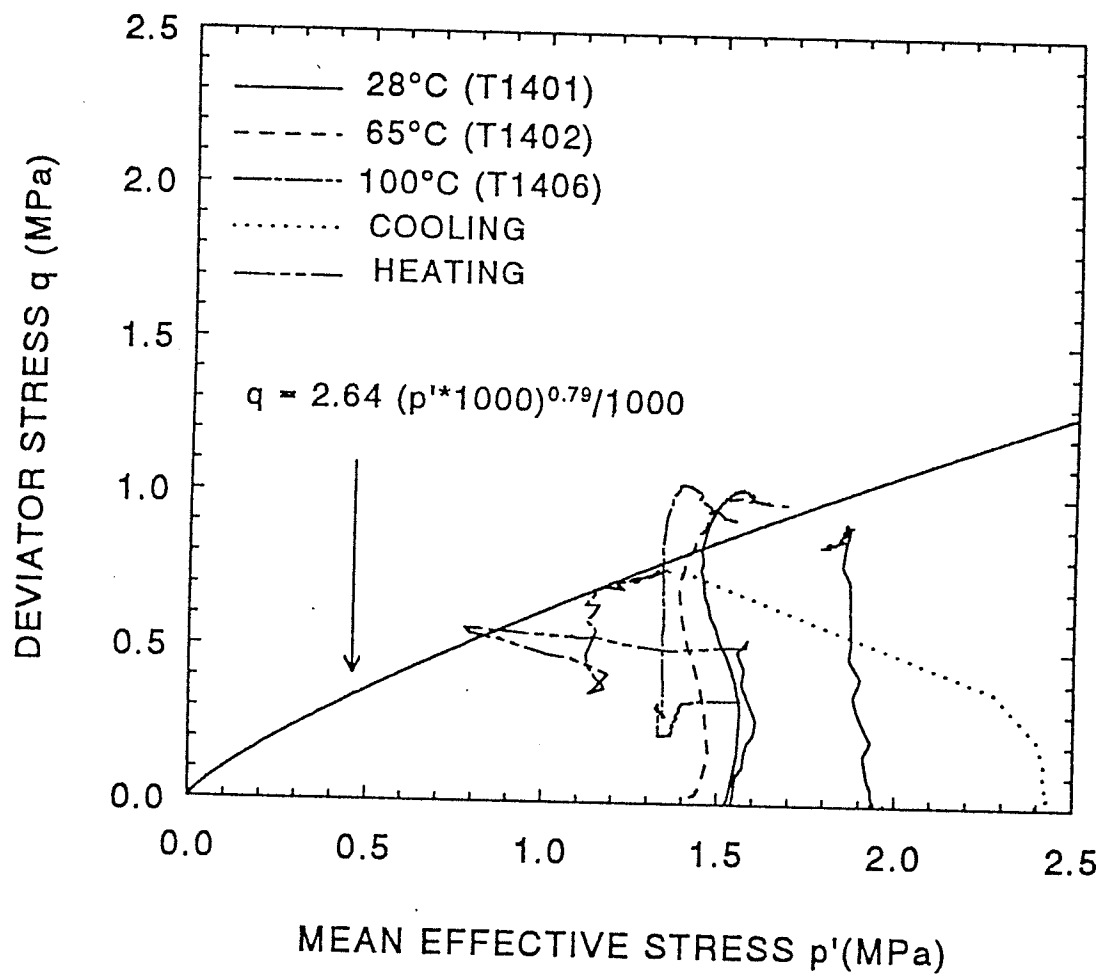
Figure 8.52 Failure envelopes at elevated temperatures on sand-
bentonite mixture.
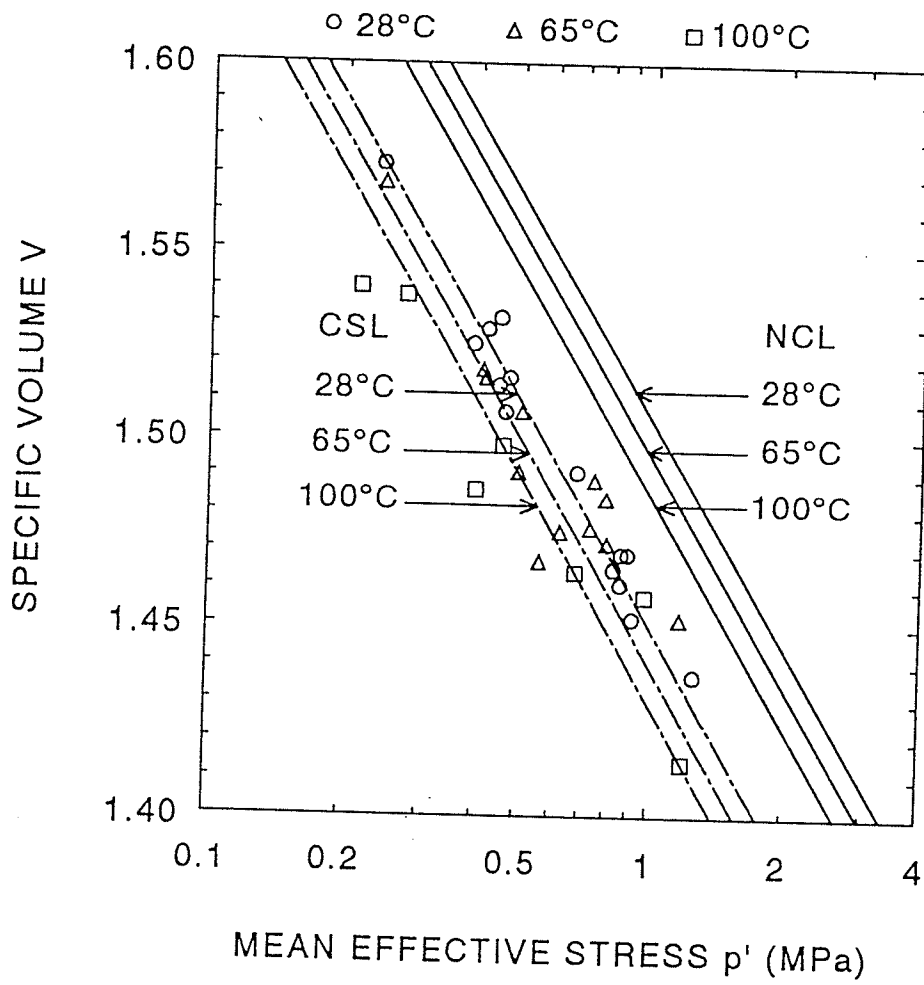
Figure 8.53 Critical state lines at 28°C, 65°C, and 100°C for reconstituted illite.
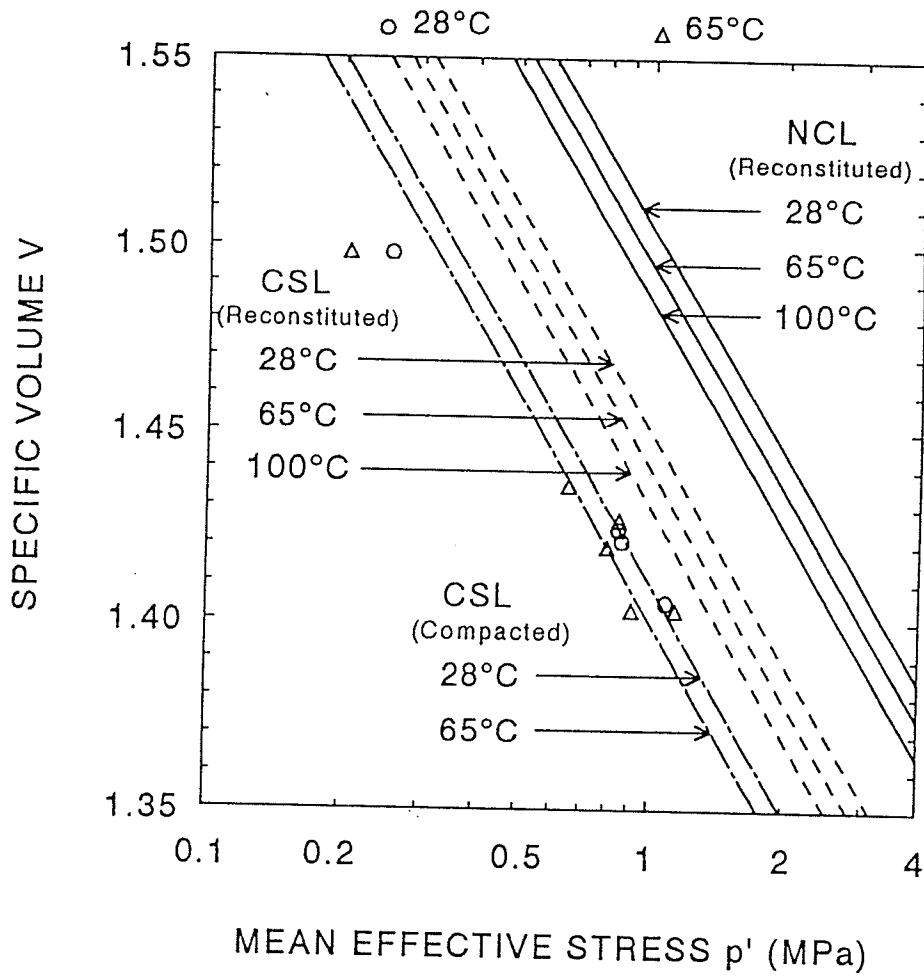
Figure 8.54 Critical state lines at 28°C and 65°C for compacted illite.
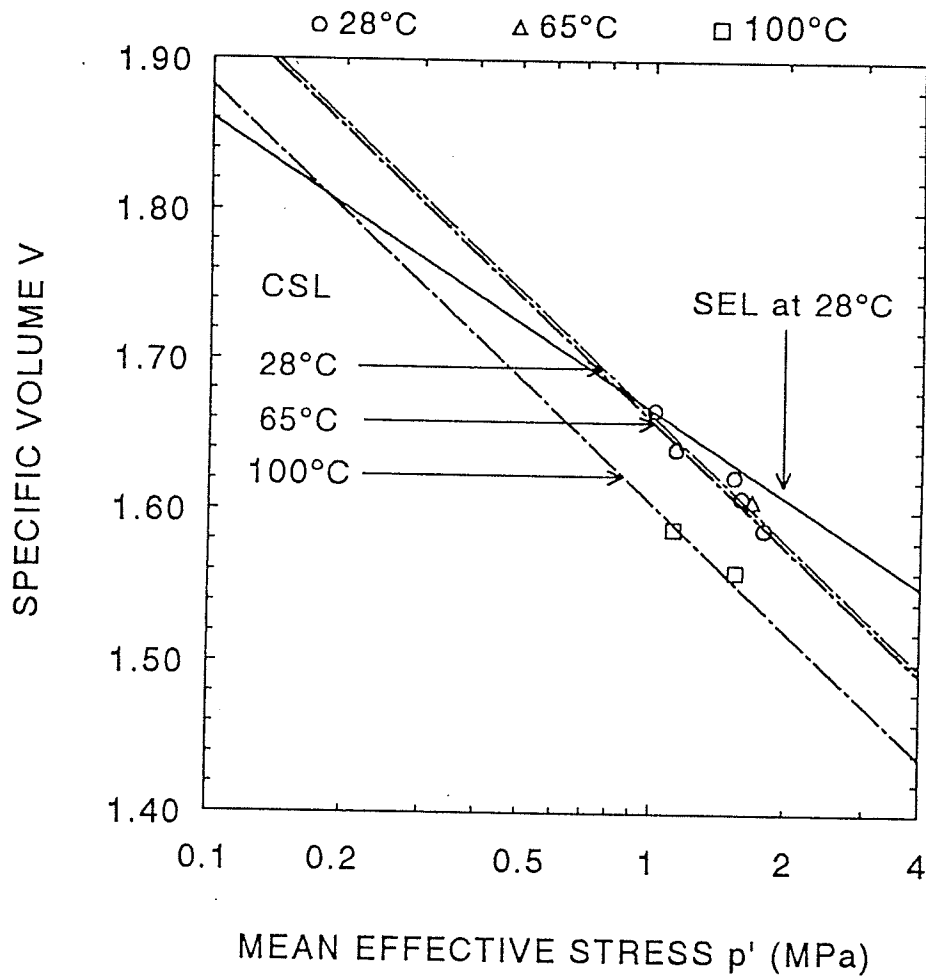
Figure 8.55 Critical state lines at 28°C, 65°C, and 100°C for compacted sand-bentonite mixture.
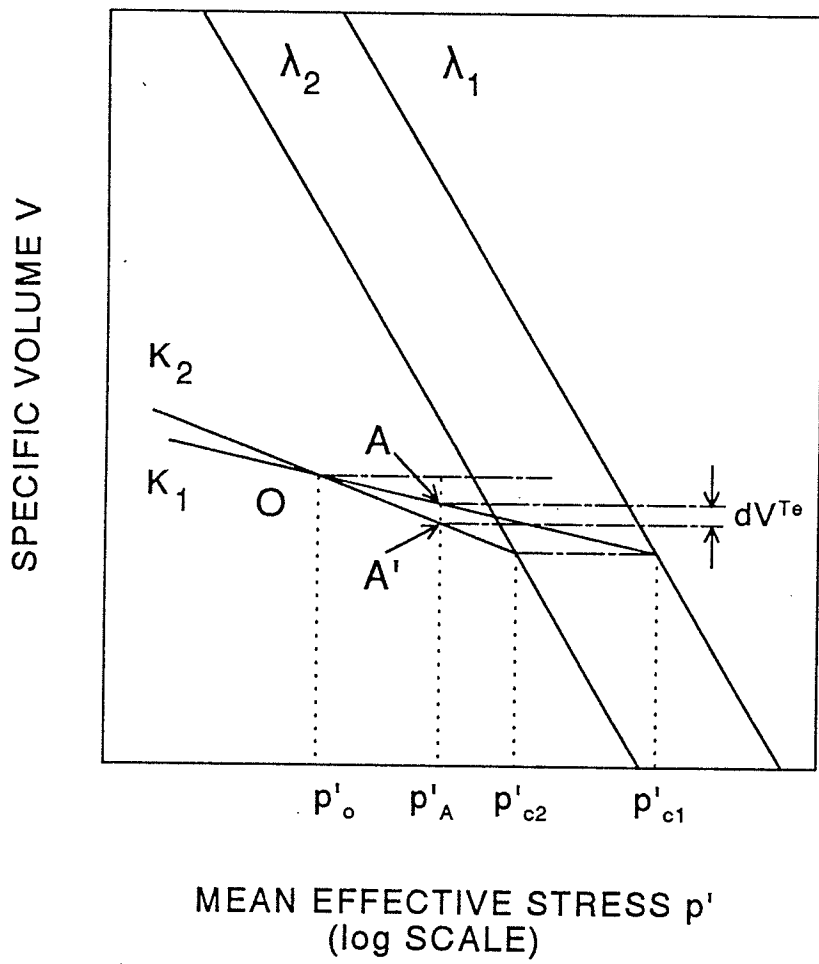
Figure 9.1   Schematic of thermally induced elastic volumetric
strain with mean effective pressure.
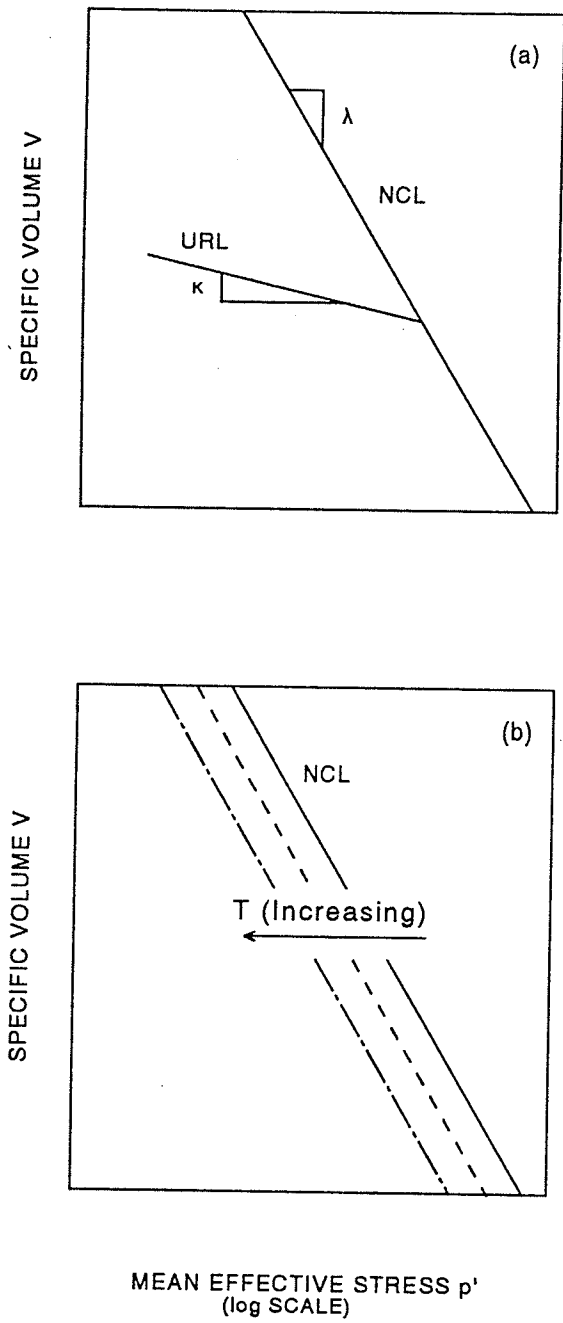
Figure 9.2 Schematic of consolidation behaviour. (a) Elastic and
plastic behaviour in consolidation. (b) Hardening
rule at elevated temperatures.
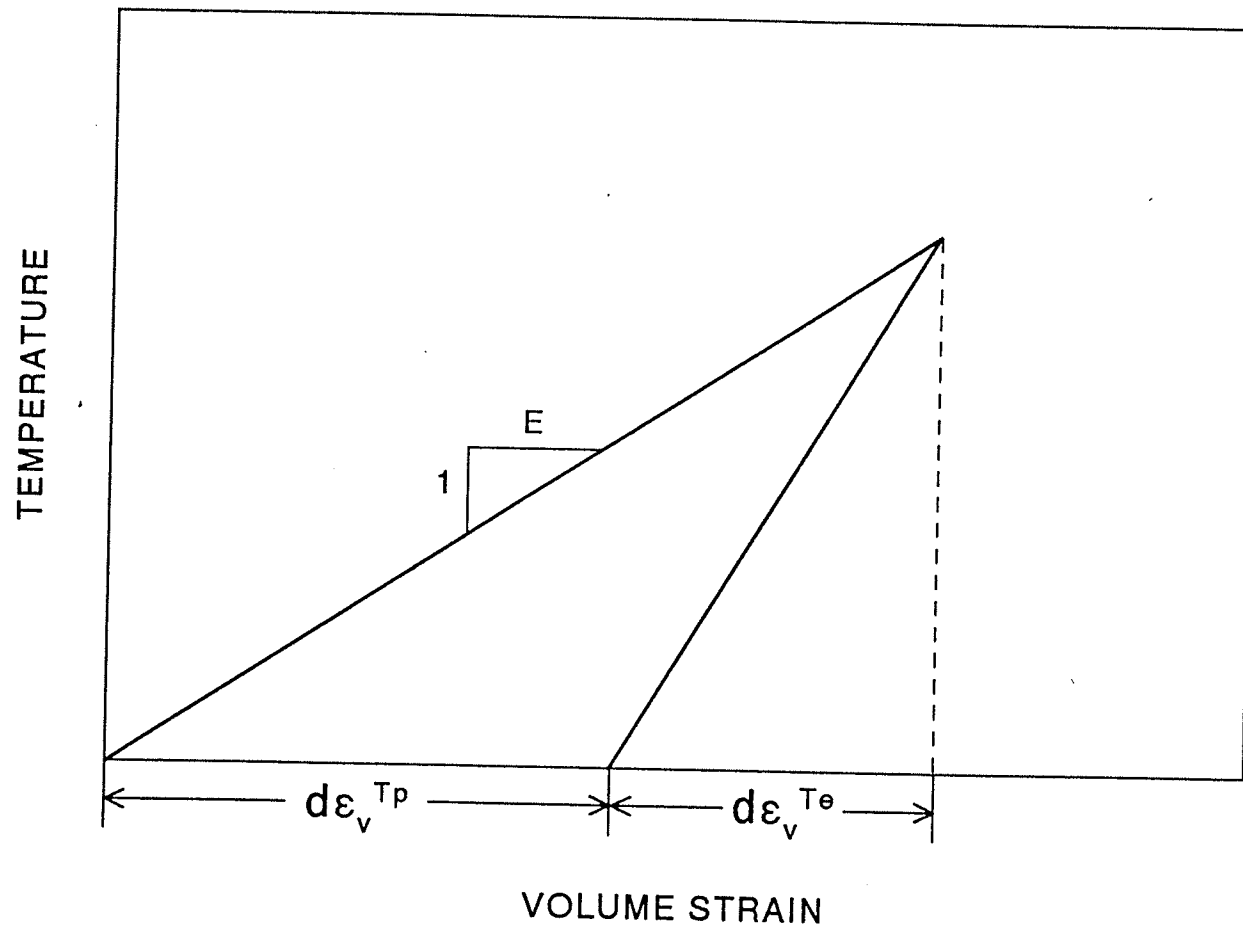
Figure 9.3 Schematic of thermally induced strains with temperature.
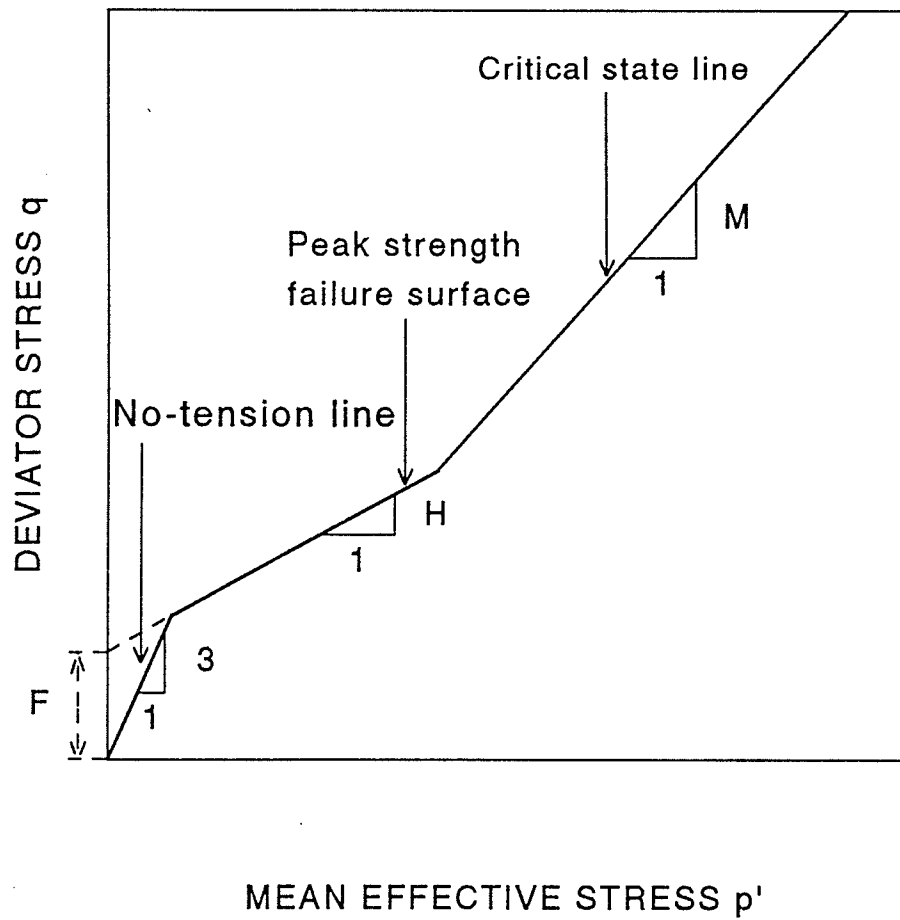
Figure 9.4 Schematic of peak strength and failure criteria at critical state.
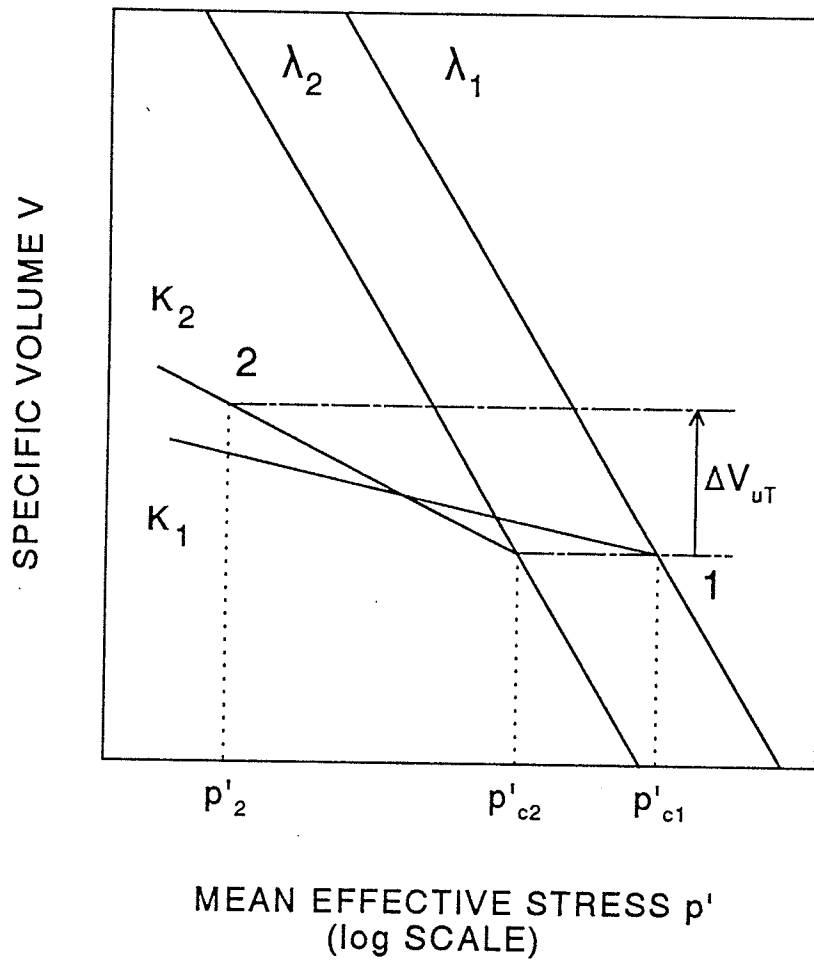
Figure 9.5   Schematic of volume change during undrained heating with pressure.
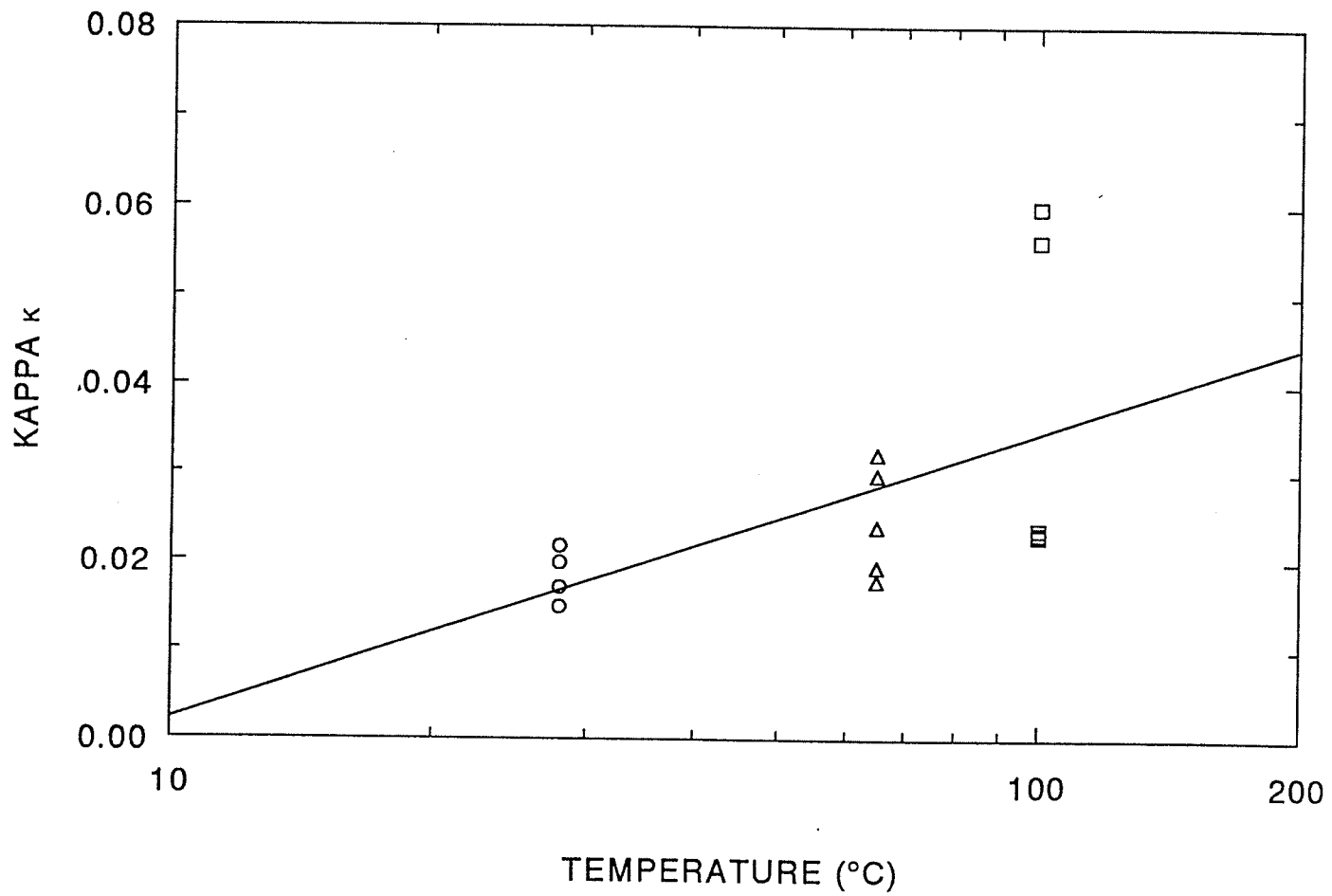
Figure 10.1   Relationship between slope of unload-reload line and temperature.
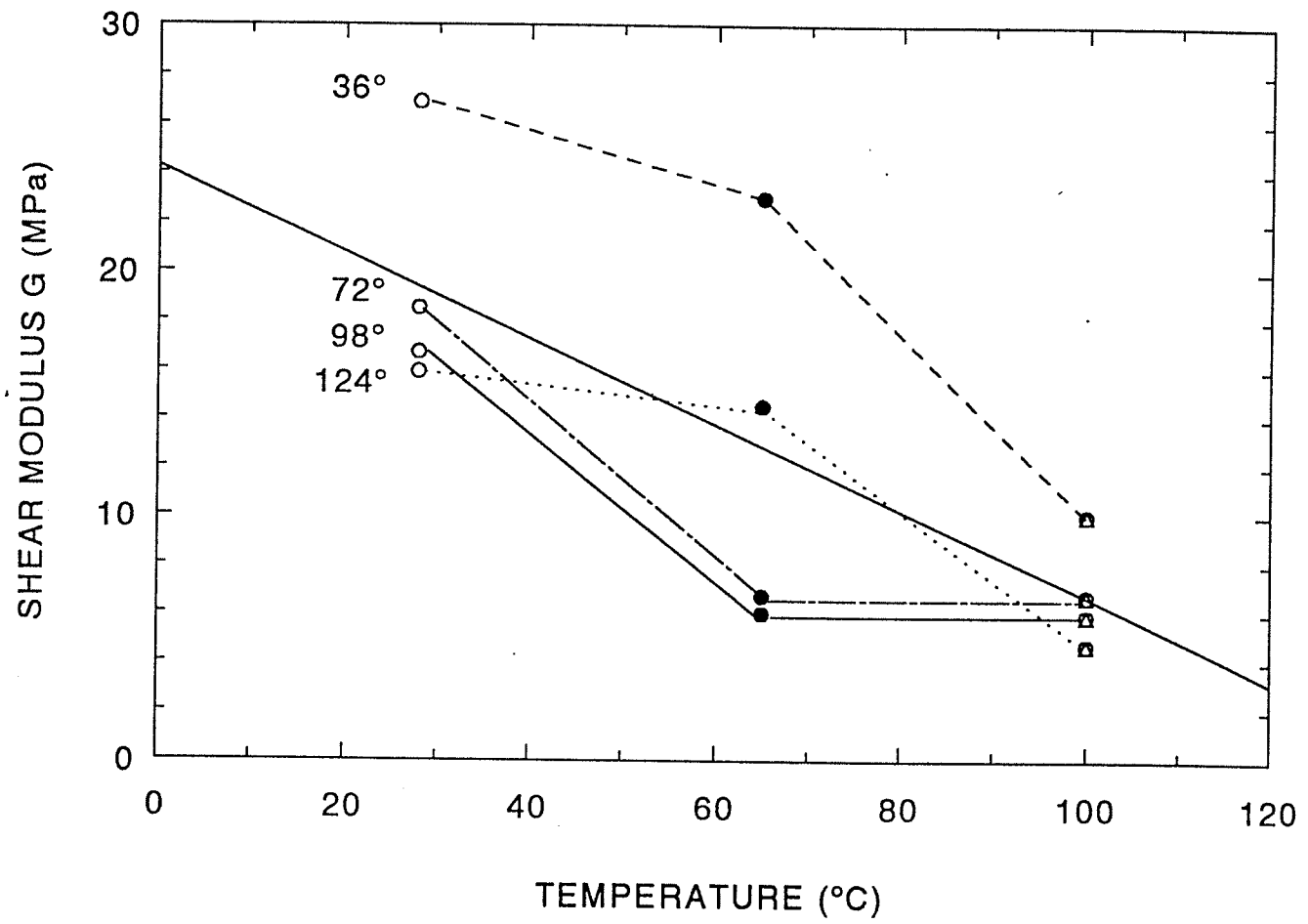
Figure 10.2 Relationship between shear modulus and temperature.
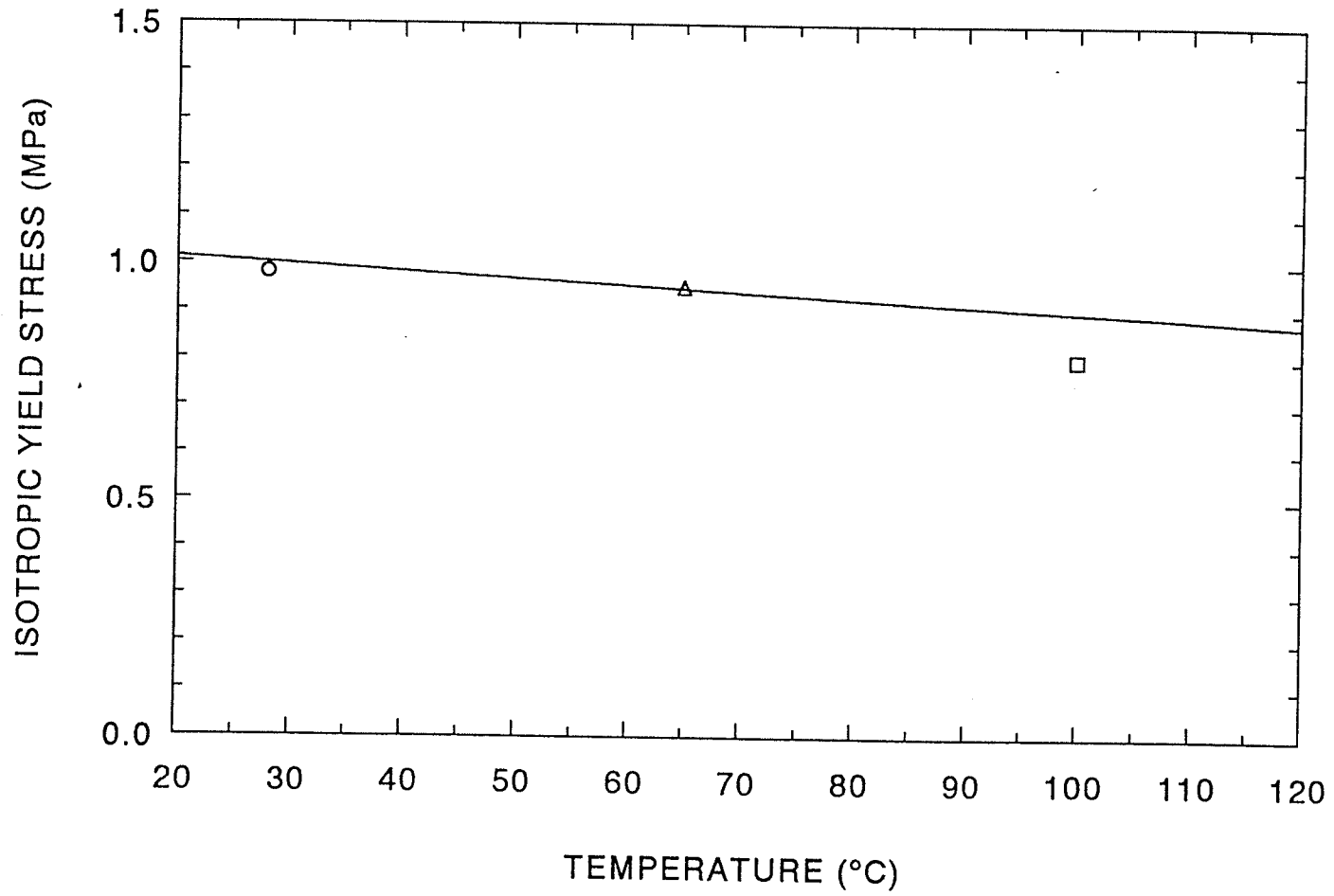
Figure 10.3 Comparison of predicted (line) and measured (data points) for isotropic yield stress.
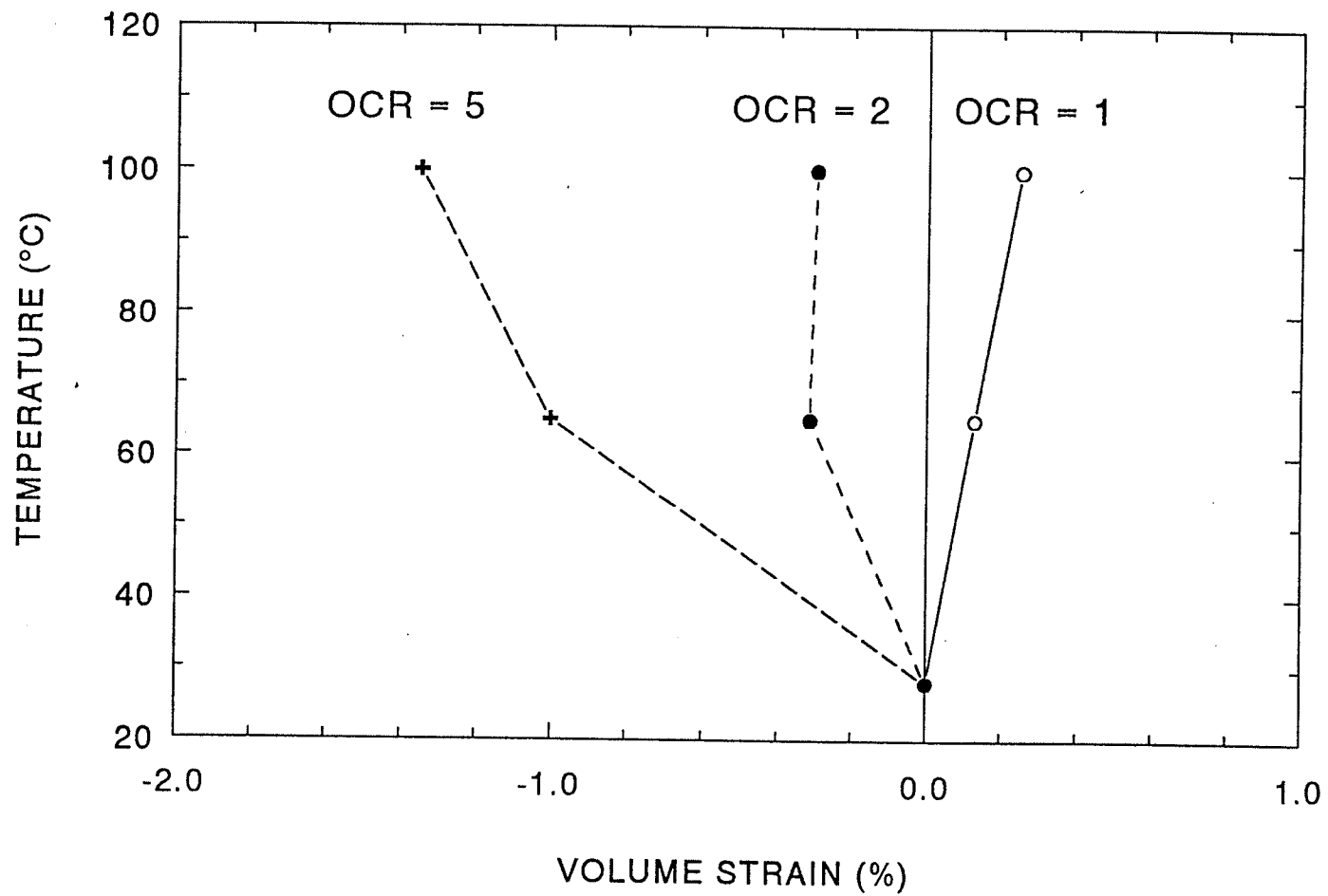
Figure 10.4   Prediction for volume strain.
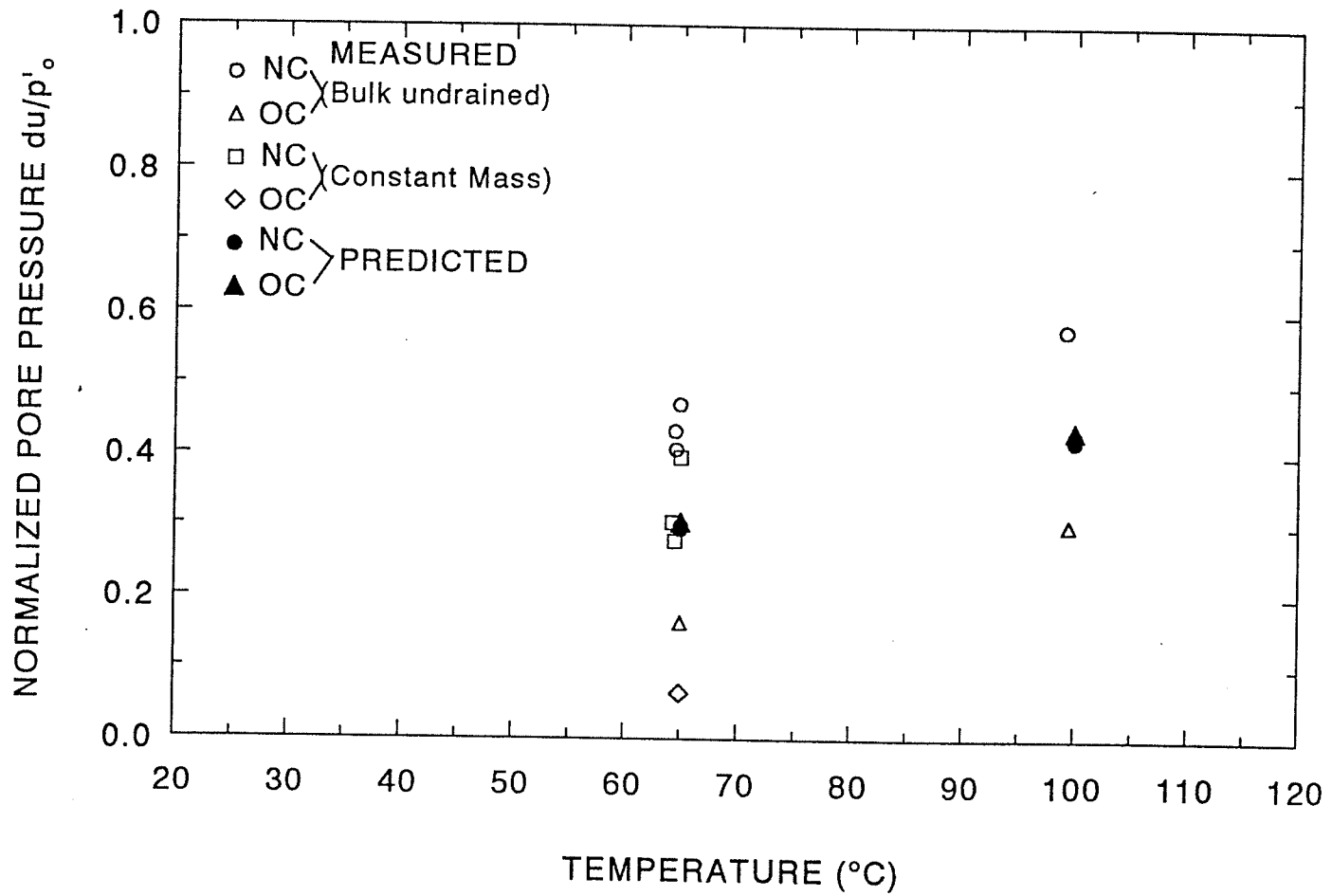
Figure 10.5 Prediction for normalized pore water pressure.
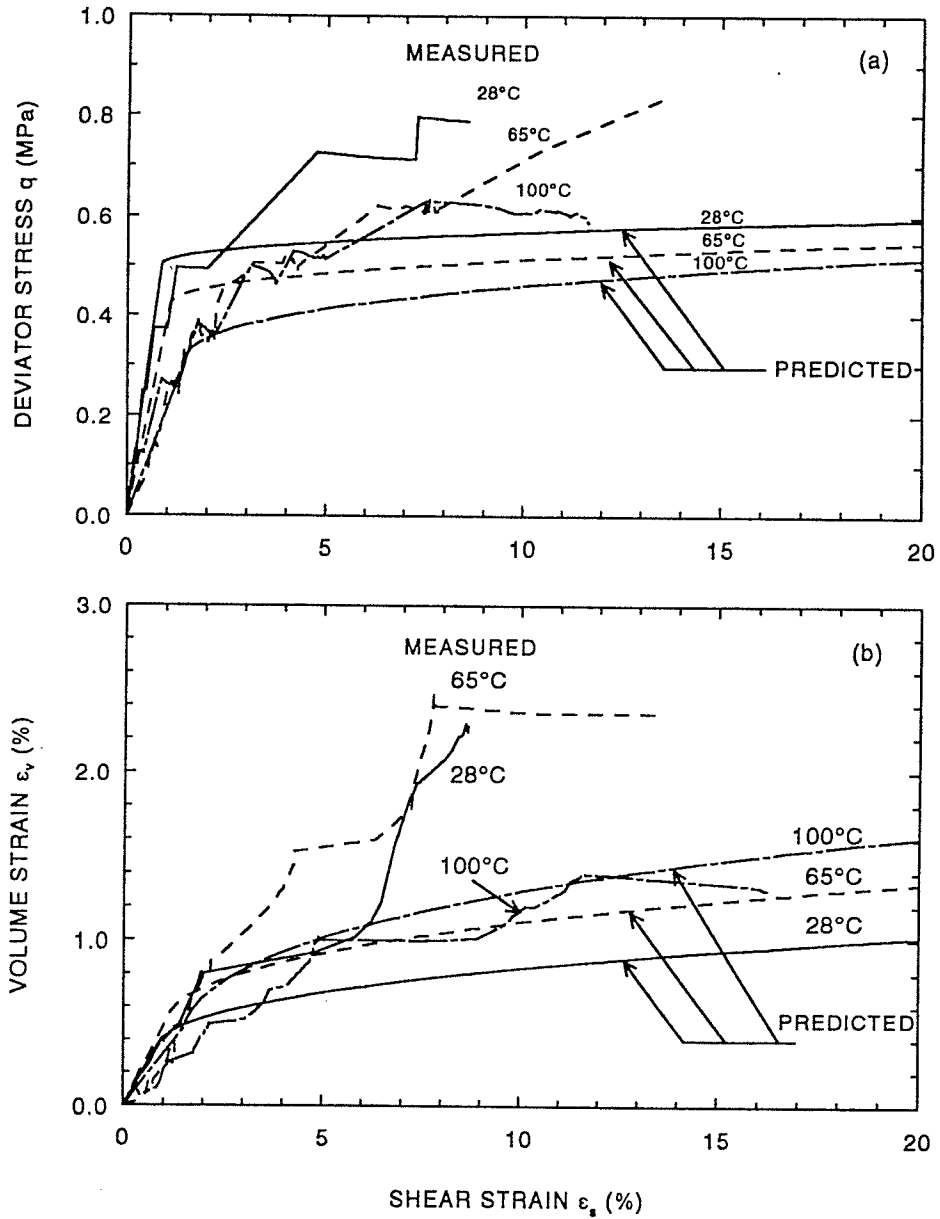
Figure 10.6 Prediction for stress-strain relationships for overconsolidated specimens (OCR=2) in drained shear at 28°C (T1480), 65°C (T1441), and 100°C (T1450). (a) deviator stress *vs.* shear strain, (b) volume strain *vs.* shear strain.
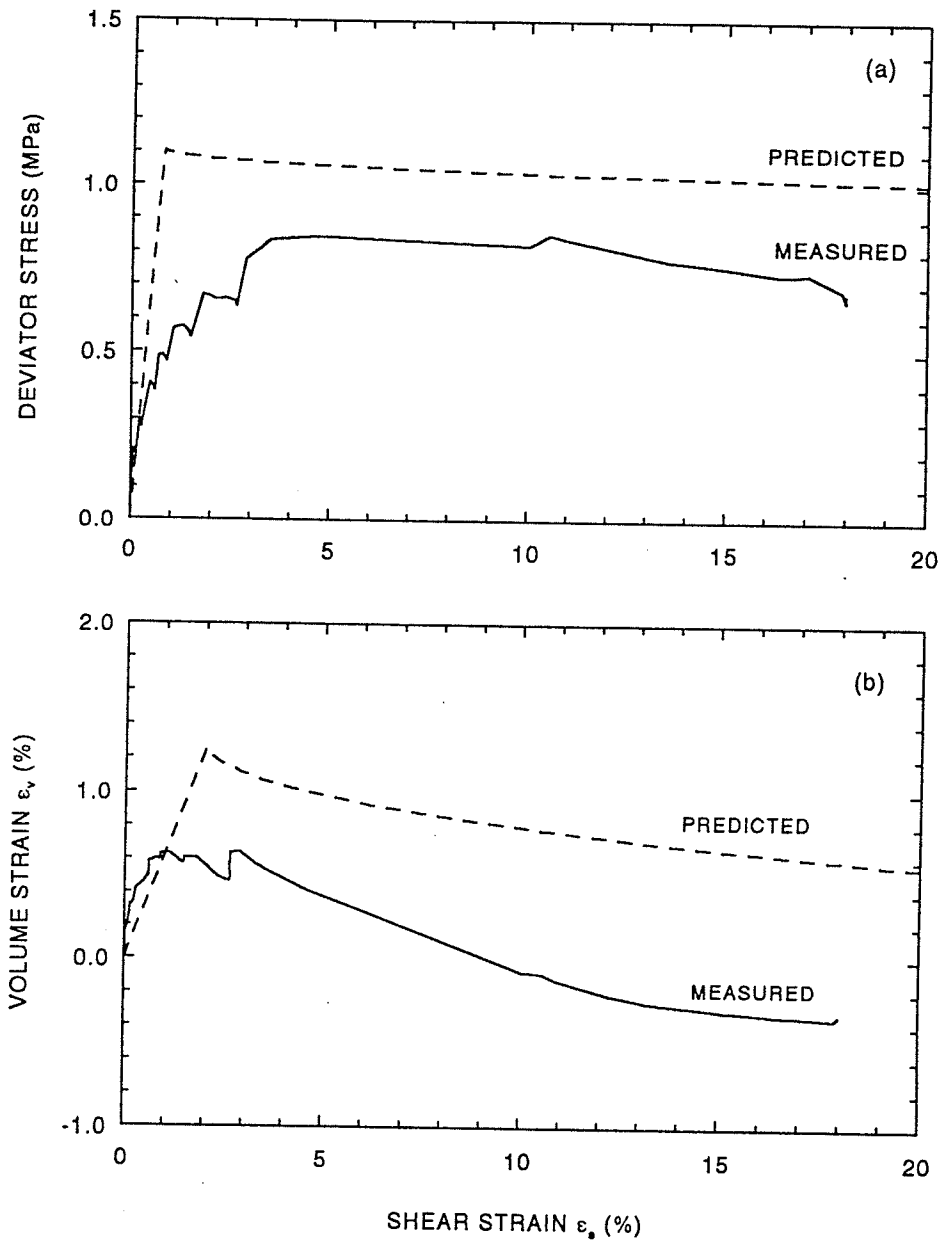
Figure 10.7 Prediction for stress-strain relationships for overconsolidated illite (OCR=7.5) in drained shear at 65°C (T1445). (a) deviator stress *vs.* shear strain, (b) volume strain *vs.* shear strain.
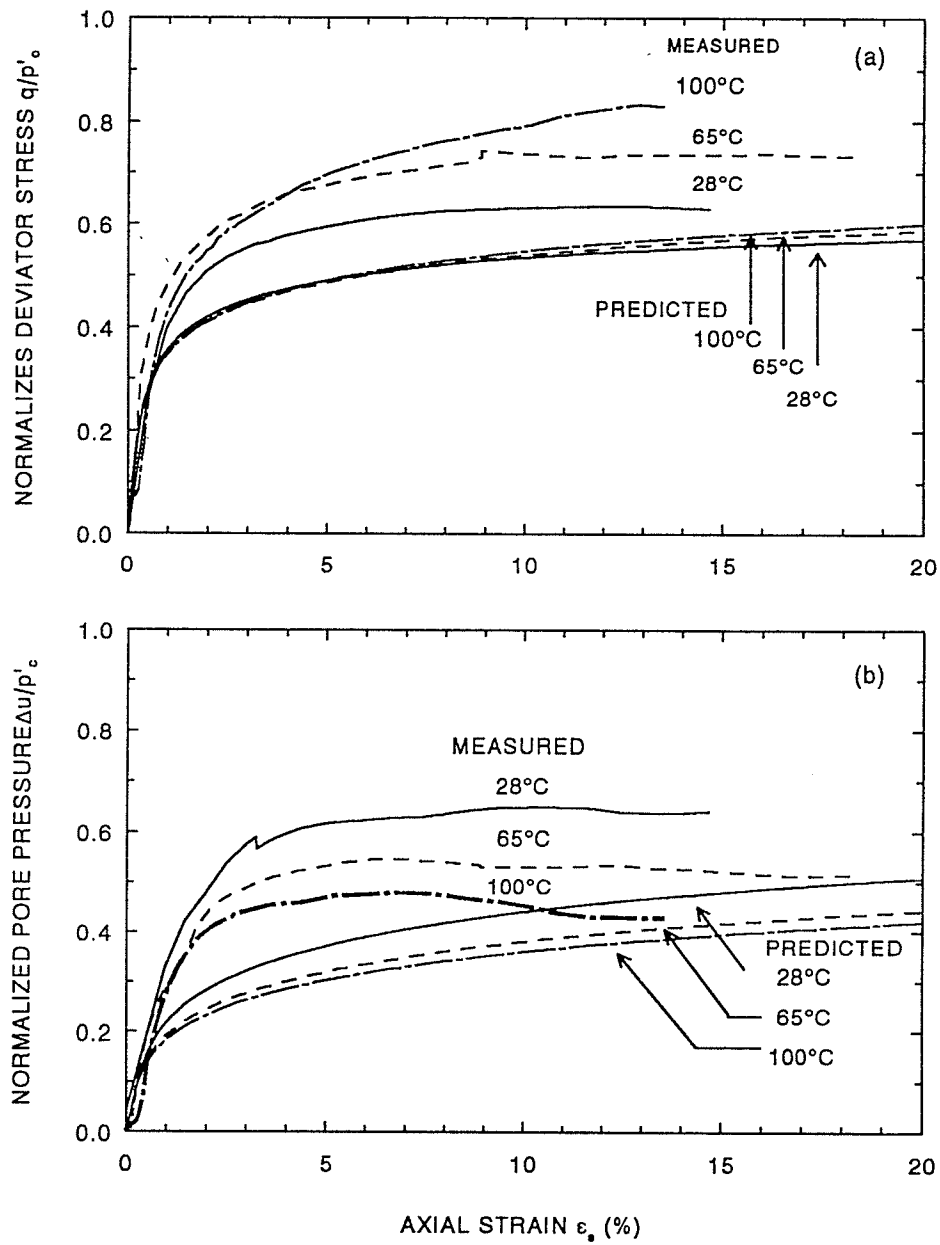
Figure 10.8 Prediction for normally consolidated specimens in undrained shear at 28°C (T1492), 65°C (T1460), and 100°C (T1461). (a) deviator stress *vs.* shear strain, (b) pore water pressure *vs.* shear strain.
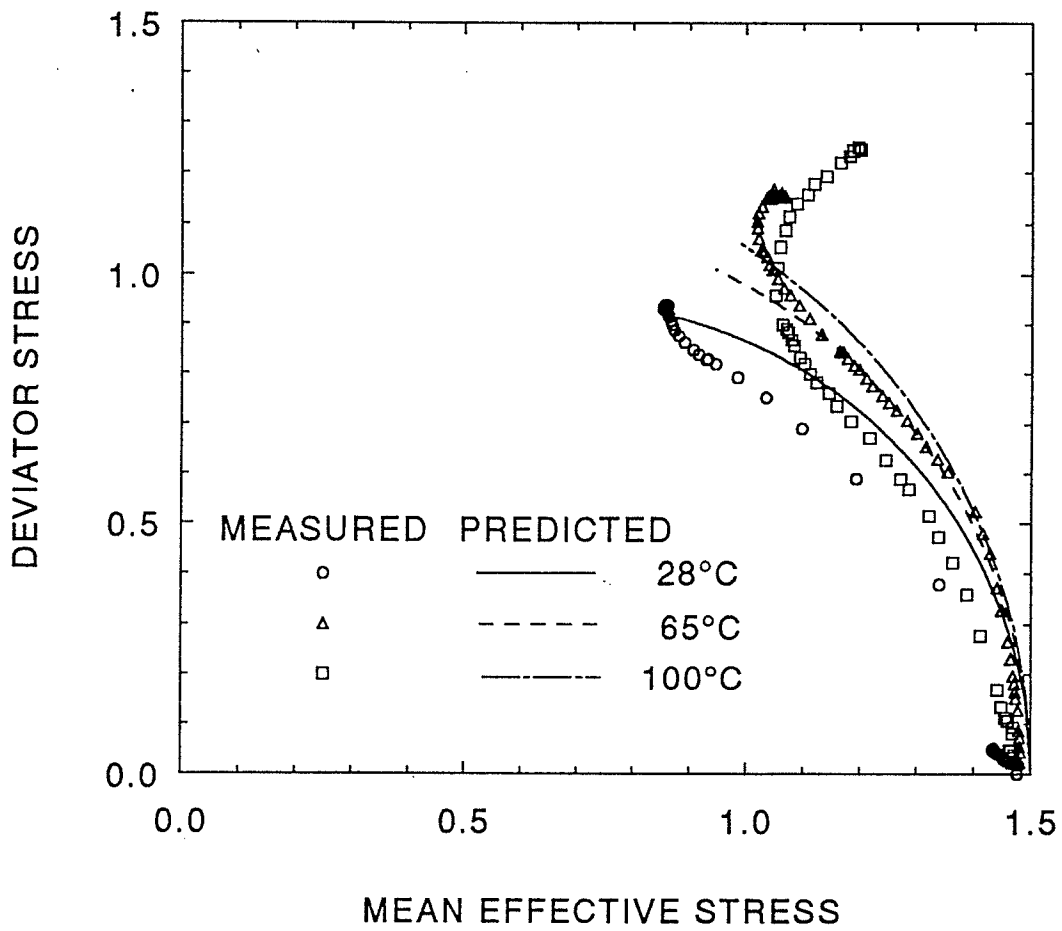
Figure 10.9 Prediction for stress path for normally consolidated
specimens in undrained tests at elevated temperatures
of 28°C (T1492), 65°C (T1460), and 100°C(T1461).
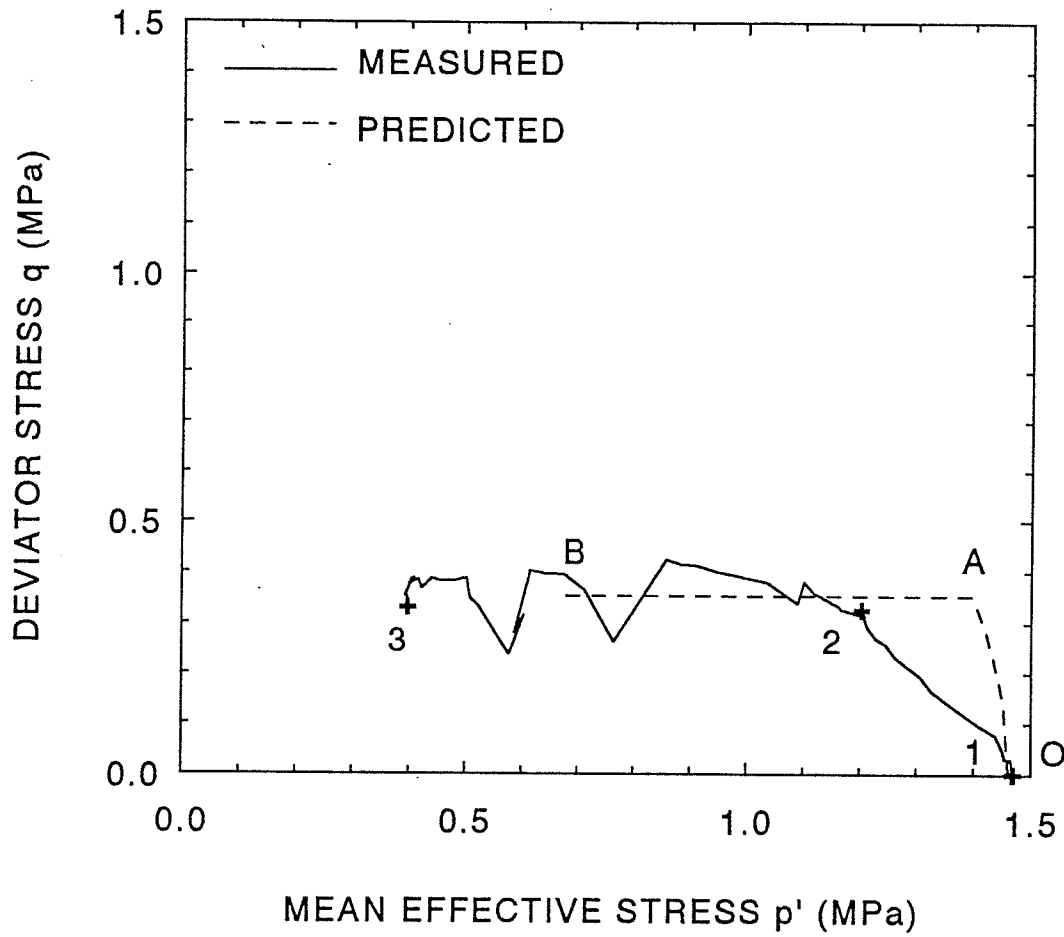
Figure 10.10 Prediction for stress path in undrained heating (T=28°C-100°C) for normally consolidated specimen (T1472) under a given deviator stress (q=0.35 MPa).
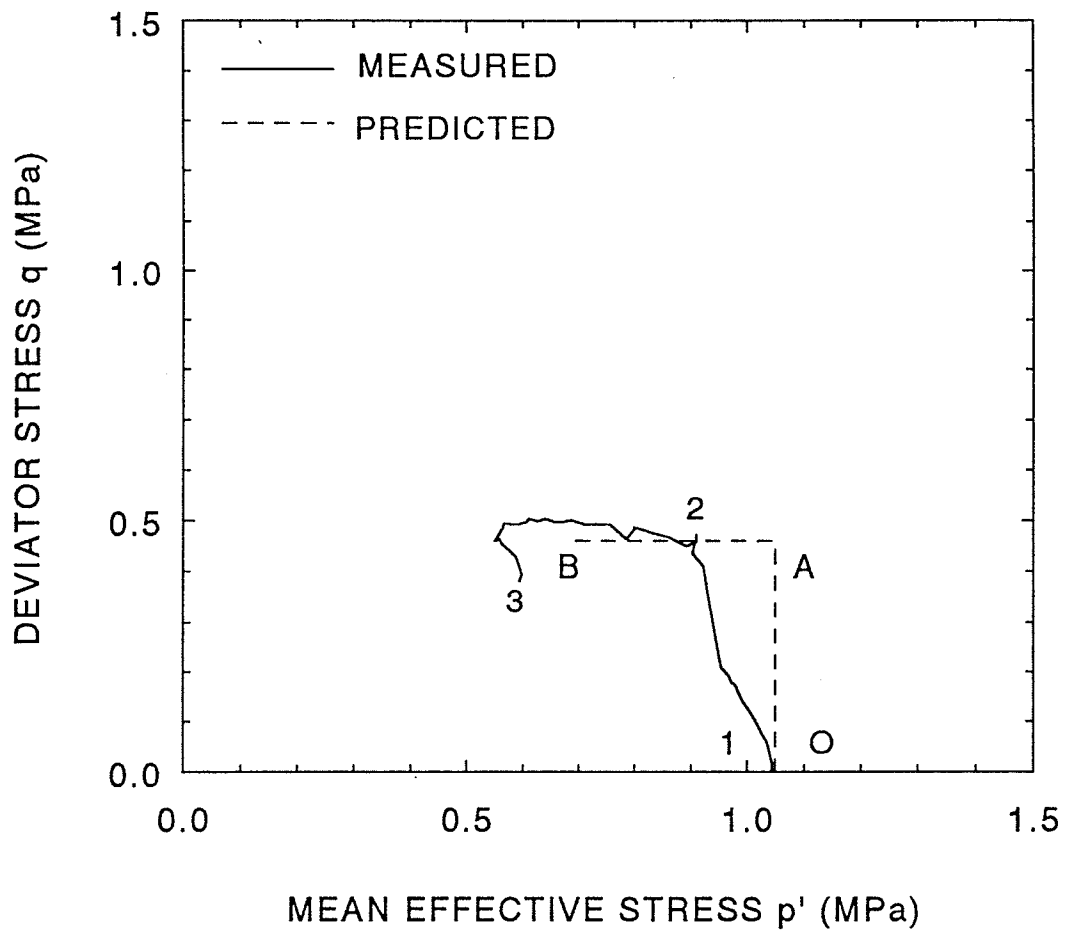
Figure 10.11 Prediction for stress path in undrained heating (T=28°C-65°C) for compacted illite specimen (T1472) under a given deviator stress (q=0.45 MPa).
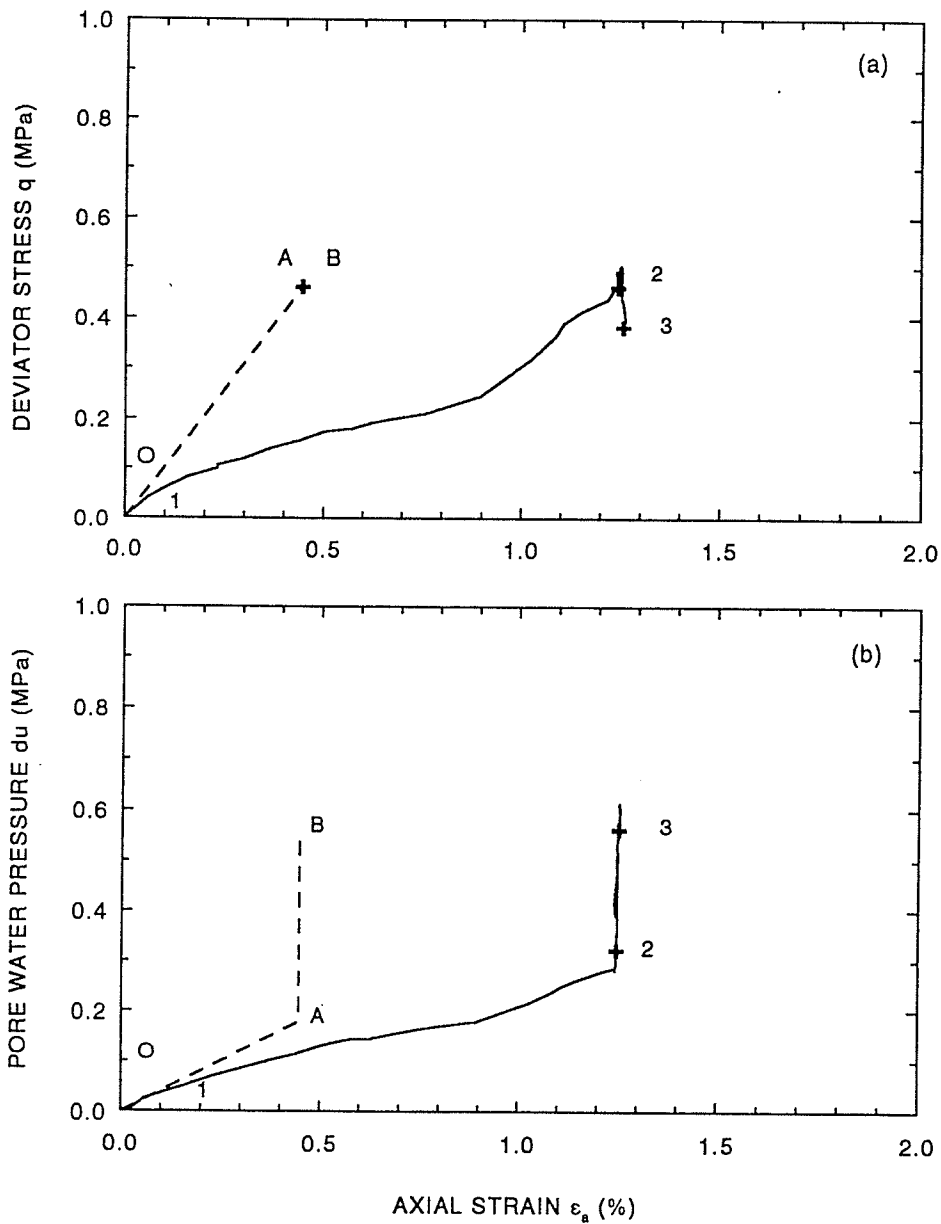
Figure 10.12   Prediction for stress-strain relationships in undrained heating (T=28°C-65°C) for compacted illite (T1471) under q=0.5MPa. (a) deviator stress *vs.* shear strain, (b) pore water pressure *vs.* shear strain.
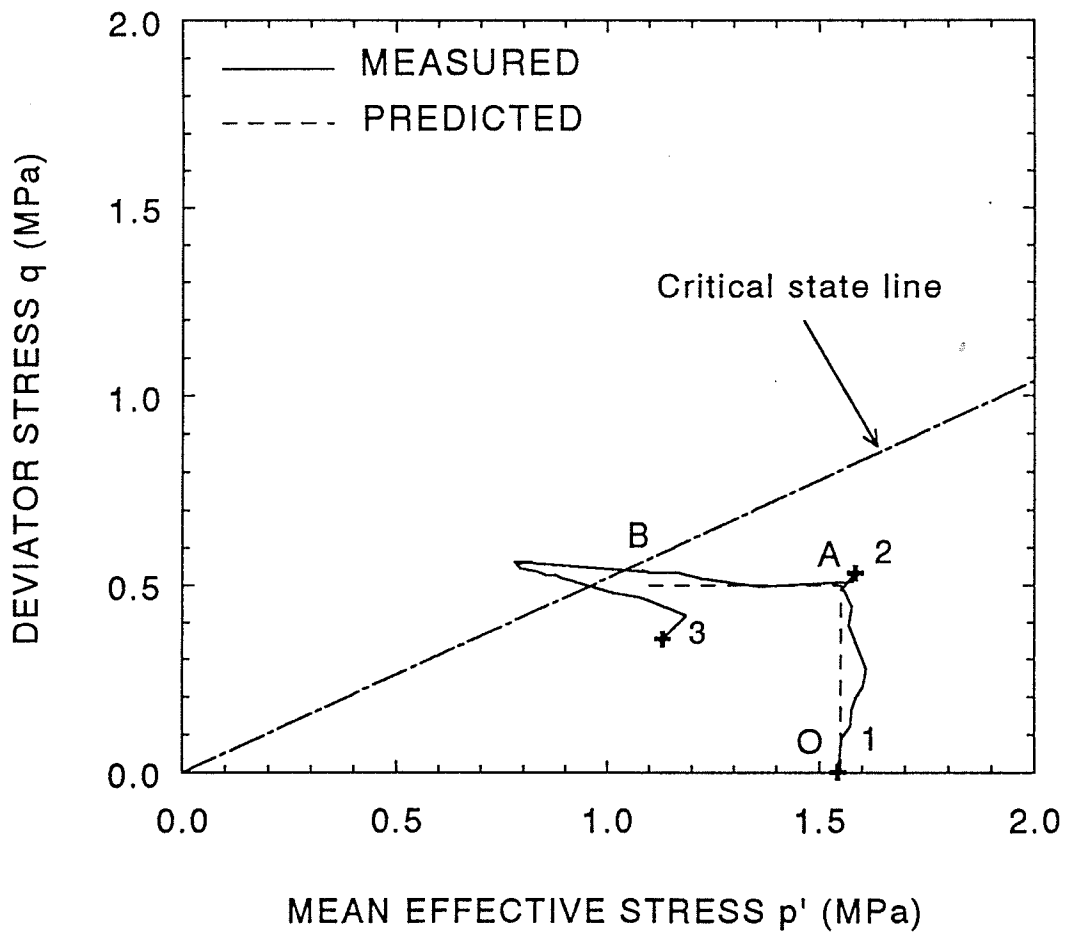
Figure 10.13 Prediction for stress path in undrained heating
(T=28°C-100°C) for compacted sand-bentonite specimen
(T1475) under a given deviator stress (q=0.5 MPa)
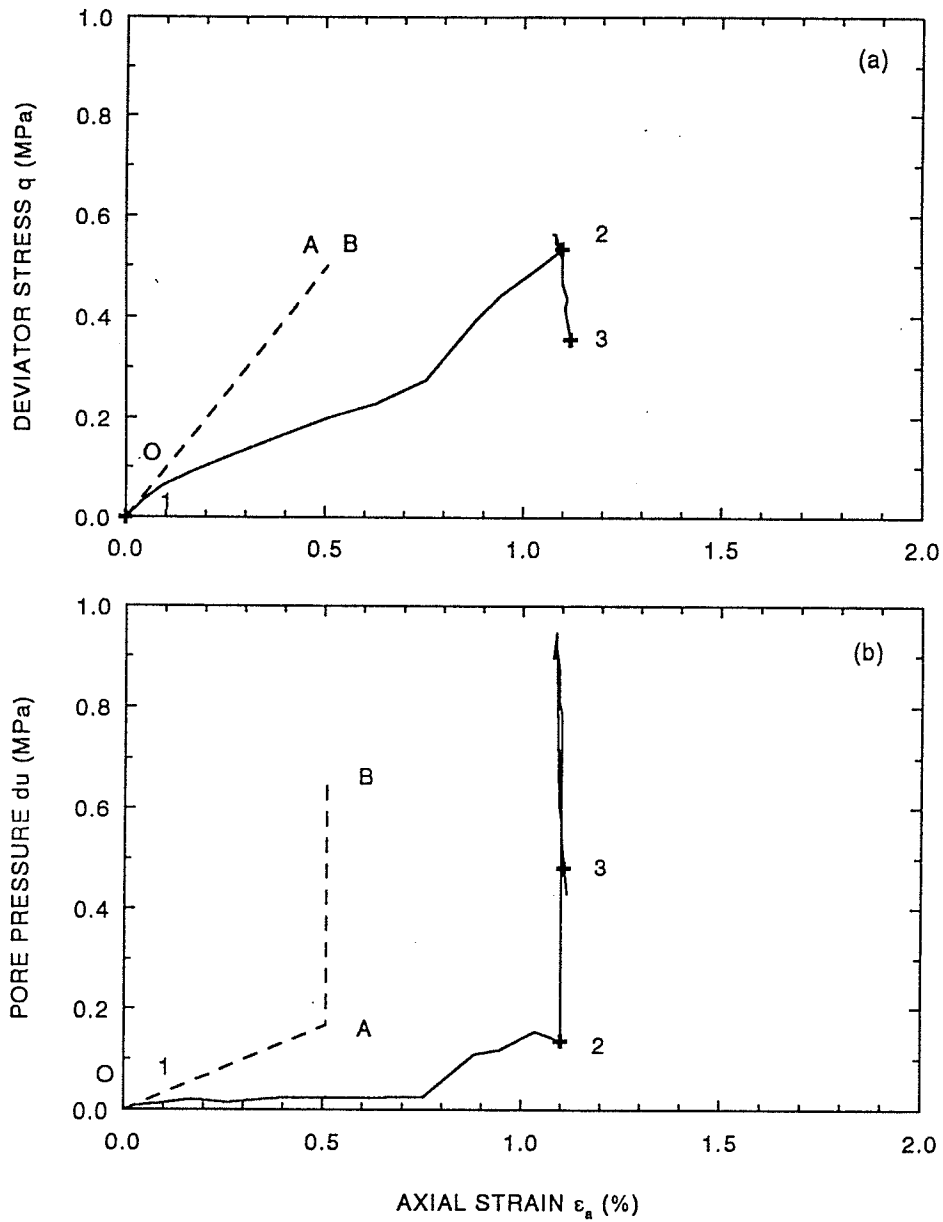
Figure 10.14 Prediction for stress-strain relationships in undrained heating (T=28°C-100°C) for compacted sand-bentonite specimen (T1475) under a given deviator stress (q=0.5 MPa). (a) deviator stress *vs.* shear strain, (b) pore water pressure *vs.* shear strain.